NEOTECTONICS, SEISMIC AND TSUNAMI HAZARDS, VITI LEVU, FIJI

A thesis submitted in fulfilment of
the requirements for the degree of

Doctor of Philosophy
in Engineering Geology

at the

University of Canterbury

by

TARIQ I. H. RAHIMAN

University of Canterbury
2006

ABSTRACT

Viti Levu, the main island of Fiji, is located in a seismically active area within the Fiji Platform – a remnant island arc that lies in a diffuse plate boundary zone between the Pacific and Australian tectonic plates in the southwest Pacific. The southeast coast of Viti Levu is a highly developed and populated part of Fiji and is vulnerable to the effects of large earthquakes that are expected to occur both onshore and offshore. The structural framework and the origin of seismicity within the Fiji Platform, as well as the seismic and tsunami hazards of central and southeast Viti Levu are investigated.

The upper crust of southeast Viti Levu is dissected by several intersecting fault/lineament zones. These are mapped from remote sensing imagery of the surface (topography, radar, and aerial photos) and of the basement (magnetic), and have been subject to rigorous statistical tests of reproducibility and verification with field mapped fault data. Lineaments on the various imagery correlate with faults mapped in the field and show spatial continuity between and beyond mapped faults, thereby providing a fuller coverage of regional structural patterns than previously known. Some fault/lineament zones extend beyond the coastline to the offshore area of southeast Viti Levu. Here high resolution SeaBAT 8160 multibeam bathymetry data and seismic reflection data show that the fault zones occur along, and exert control on the locations of a number of linear submarine canyons. The morpho-structural expression of these canyons are contiguous with fault controlled physiographic features mapped on the nearshore marginal shelf (rectilinear bays and peninsulas, reef passages) and on land (fault valleys, slope and drainage alignments forming lineaments). The canyons are considered to have developed from several cycles of downslope incising and infilling events, whilst their positions were still primarily controlled by zones of weakness created by the fault zones.

The principal fault sets in southeast Viti Levu represent generations of regional tectonic faulting that pervaded the Fiji Platform during and after disruption of the proto Fijian arc in the Middle to Late Miocene. These fault sets combine to form a complex network of interlocking faults creating a fault mesh that divides the upper crust into a number of fault blocks ranging from ~2 to 30 km. It is inferred that the fault mesh evolved throughout the Neogene as a response to the anticlockwise rotation of the Fiji Platform through progressive development of different fault sets and intervening crustal block rotations. Regional tectonic deformation is presently accommodated in a distributed manner through the entire fault mesh. Low magnitude earthquakes (<M4) occur regularly and may represent ruptures along short linking segments of the fault mesh, while infrequent larger earthquakes (>M4) may result from complex rupture propagation through several linking fault segments of the mesh that lie close to optimum stress orientations. This interpreted model of distributed deformation through the fault mesh for southeast Viti Levu is inferred to be characteristic of the style of active deformation that occurs throughout the entire Fiji Platform.

Seismic activity is primarily responsible for triggering submarine landslides that occur on the southeastern slope of Viti Levu. These slides typically occur on the outer barrier reef edge, as well as in submarine canyon heads and walls, and in the mid slope areas. They are characteristically translational and lack bathymetric evidence for displaced masses. Morphometric analysis and empirical modelling, show that slides triggered at shallow water

depths, within 5 km of the coastline, at the outer barrier reef edge and submarine canyon heads, produce the largest near-field tsunami amplitudes. Such slides are interpreted to represent a significant local tsunami hazard. A detailed case study of the destructive 1953 Suva tsunami that followed the M_s 6.75 Suva earthquake, reveals that the source of this tsunami was a 60 million cubic metre submarine landslide at the head of the Suva Canyon, 4 km to the WSW of Suva City. A test simulation of this tsunami using the Geowave tsunami generation, propagation and inundation model, closely replicates the wave heights and arrival times recorded in 1953. This simulation also reveals that high variability in tsunami impact over short coastal distances of southeast Viti Levu is attributable to the complex interplay of wave propagation with the barrier reef system, erratic lagoon bathymetry and the irregularly shaped coastline. A predictive simulation using Geowave, based on an incipient failure in the 1953 source area and on a potentially worse case scenario event at or near high-tide, is used to show a maximum vertical run up of at least 4 m and a maximum horizontal inundation level of at least 400 m at the Suva coast.

The seismic hazard of five sites on Viti Levu, including Suva City, Navua and Nausori Towns, and the Monsavu and Nadarivatu dam sites, is evaluated using a deterministic approach, and seven newly identified crustal fault earthquake source structures. The maximum magnitudes interpreted for these structures, estimated using empirical relationships, range from M_w 6.8 to 7.6. The Suva Canyon Fault, the Naqara Fault, the Mavuvu/Fault Lineament Zone and the Nasivi Fault provide the controlling maximum credible earthquakes (CMCE) at all the five sites. The CMCE peak ground acceleration values for Suva City range from 0.4g to 0.6g, for Nausori Town from 0.18g to 0.2g, for Navua Town from 0.27g to 0.32g, for Monasavu from 0.39g to 0.42g, and for Nadarivatu from 0.23g to 0.33g. The horizontal spectral accelerations at a period equal to 0.2 seconds, calculated using the CMCEs, are comparable to accelerations derived by probabilistic methods that have return periods between 50 and over 1000 years.

TABLE OF CONTENTS

page

page

page

page

APPENDICES

MAPS

LIST OF FIGURES

LIST OF TABLES

CHAPTER 1

INTRODUCTION

1.1 RATIONALE

The Fiji region lies in a tectonically complex area at the boundary of the Pacific and Australian plates in the southwest Pacific. In this region the plate boundary switches polarity from west directed subduction at the Tonga Trench to east directed subduction at the Vanuatu Trench, to the east and west of Fiji respectively. The main islands of the Fiji archipelago occur on the Fiji Platform, a shallow submarine plateau less than 2 km deep, in the zone of plate boundary overlap (Figure 1.1). The Fiji Platform occurs about midway between the opposite facing subduction zones and is separated from them by distances up to 1000 kilometres. Complex deformation by seafloor spreading and strike slip faulting occurs in back-arc basins between the Fiji Platform and the subduction zones. Despite the apparent remoteness of Fiji from the well defined plate boundary zones at the Tonga and Vanuatu Trenches, distributed seismic activity within and surrounding the Fiji Platform demonstrates the effect of intricate active tectonic deformation in the broad area separating the subduction zones. The rates of tectonic activity and seismicity in the Fiji region however, are lower than those at the neighbouring subduction zones. Even though they are infrequent, strong earthquakes have occurred in the Fiji region and their impact on society has been profound. The historical Suva Earthquake of 1953 is an example of a large near shore event very close to a highly populated area that brought about considerable losses, not only through the effects of severe ground shaking but also through a destructive local tsunami that followed soon after.

The research presented in this thesis has the overall aim of addressing challenges facing earthquake related hazard evaluations in Fiji and ultimately providing a new tectonic context and approach within which such work can be carried out in future. The problems facing earthquake related hazard assessments in Fiji are manifold and fundamentally concern the question about the seismotectonic setting of the islands. Other difficulties are related to undertaking scientific research in a tropical and marine environment, where onshore outcrop exposures are scarce and where investigations must extend to include the offshore

area. In addition, local issues such as the rapid expansion and development of coastal population centres require consideration of the specific hazards related to coastal settings.

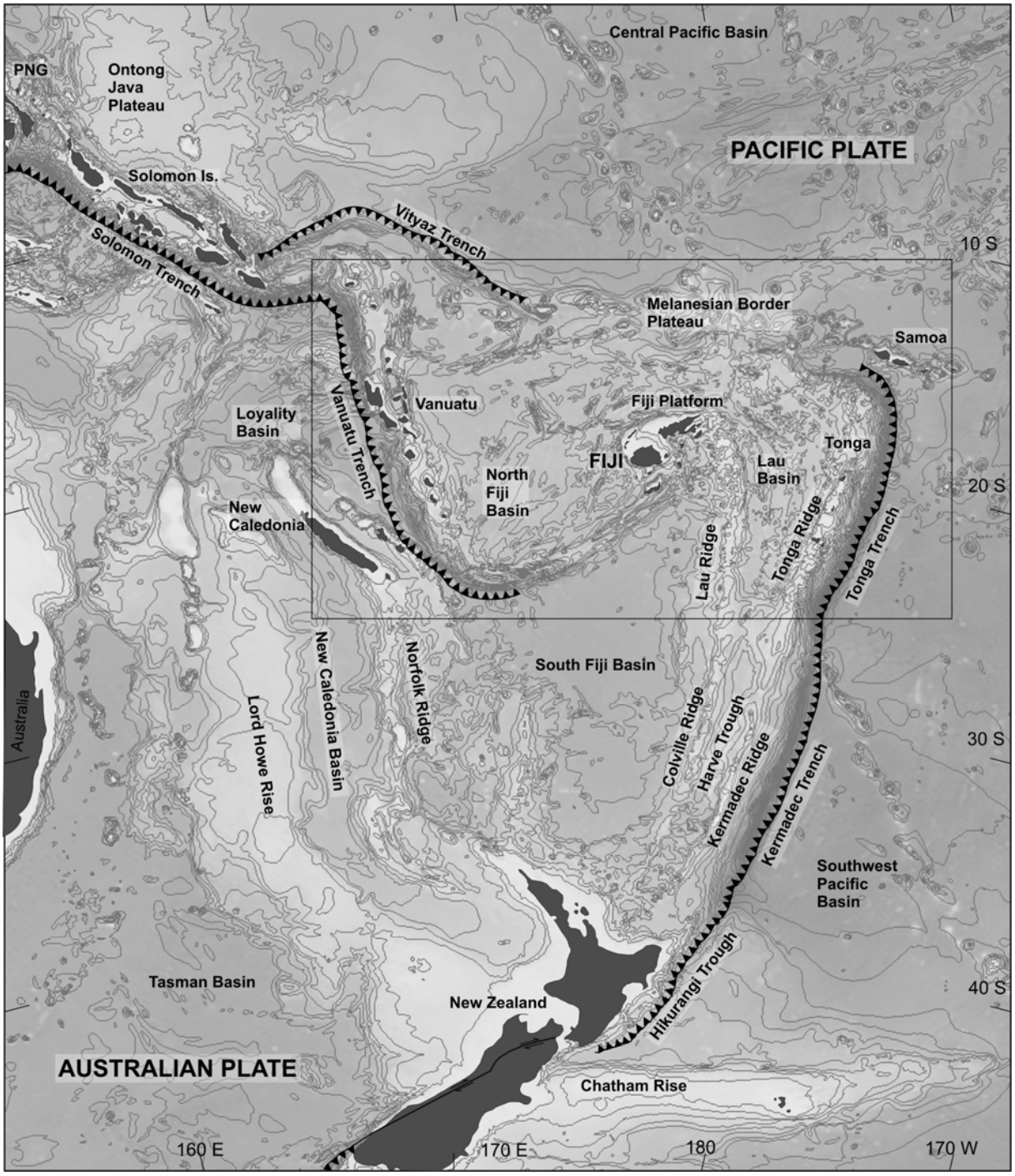

Figure 1.1: Regional tectonic and morphologic features of the Australia/Pacific plate boundary in the southwest Pacific. Detail of boxed area shown in Figure 2.7. (Isobath interval is 500 m, bathymetry is from SOPAC, www.sopac.org).

The spatial and temporal complexity of Fiji's tectonic setting imposes significant challenges on the understanding of tectonic stresses, characteristics of faulting, origin of earthquake

activity and, consequently performing seismic hazard evaluations in Fiji, compared to more well known and studied tectonically active interplate regions of the world. Very few previous studies have addressed the seismotectonic setting of the Fiji islands. A notable early investigation by Berryman (1979) was largely reconnaissance work of late Quaternary uplift of raised coastal features around Fiji. More recently, the influential work of Hamburger et al. (1988; 1990) was based on seismological observations from local network stations. Other studies have attempted to use detailed field geological observations to infer broader scale tectonic features and processes within the Fiji region (e.g. Shorten, 1990). No model however, has yet adequately explained the relationship between ongoing tectonic processes, existing geological structures and seismicity in the Fiji region. In this thesis, in light of new and comprehensive data on structural lineaments, a new seismotectonic model is proposed that attempts to explain the nature of tectonic deformation and origin of seismicity in the Fiji region.

High quality instrumental seismicity records of the Fiji region are incomplete, mainly because of dilapidation in local seismic network recordings over the last ten years. Existing seismicity data therefore, are not sufficient to make further contributions to the earlier work. It is not surprising that prior to this present study, there have been no other studies in Fiji that have attempted to investigate faults as earthquake sources or have considered them in the previous seismic hazard evaluations (e.g. Jones, 1998). With lower rates of tectonic and seismic activity, geologic and geomorphic evidence for earthquake source structures and tectonic deformation in general are scarce. This is compounded by the negative effects of the tropical climate in Fiji, such as deep weathering profiles, high erosion rates and near continuous vegetation cover, on exposing bedrock structure and preserving evidence of late Quaternary paleoseismic activity. Furthermore, because a large portion of Fiji is maritime, potential source structures of strong earthquakes are concealed by the ocean and locally by coastal deposits. Faults in Fiji are generally poorly exposed and incompletely mapped and the geometry and structural styles of deformation of regional faults, both onshore and offshore, have remained unclear. In regional geological mapping of the past, geologists were not distinguishing inactive faults from faults that have the potential for renewed movement and related earthquake activity. Very few data are available on the kinematics and the activity rates of faults. Nevertheless, data on faults as earthquake source structures are a key factor in recognising and quantifying the longer-term seismic hazard, and this thesis attempts, as a first

approach, to improve the knowledge base in Fiji for both the onshore and offshore earthquake source structures and their capability.

As most population centres in Fiji are in coastal settings, seismic hazards associated with the near-shore environment, such as submarine mass movements and ensuing local tsunamis, are a major threat, during large offshore earthquakes. Very few high quality data are available on the morphology and structure from offshore areas of Fiji and there is no comprehensive documentation on tsunami sources. In this thesis, bathymetry data of unprecedented quality are used to document potential sources for local tsunamis, and an innovative methodology is employed to evaluate the hazards they pose.

In light of the new data acquired in this study and utilisation of techniques not previously applied in Fiji, this thesis presents a comprehensive evaluation of seismic and tsunami hazards in southeast Viti Levu, the largest island of Fiji (Figure 1.2), as well as provides a new seismotectonic framework for appraising earthquake related hazards in Fiji.

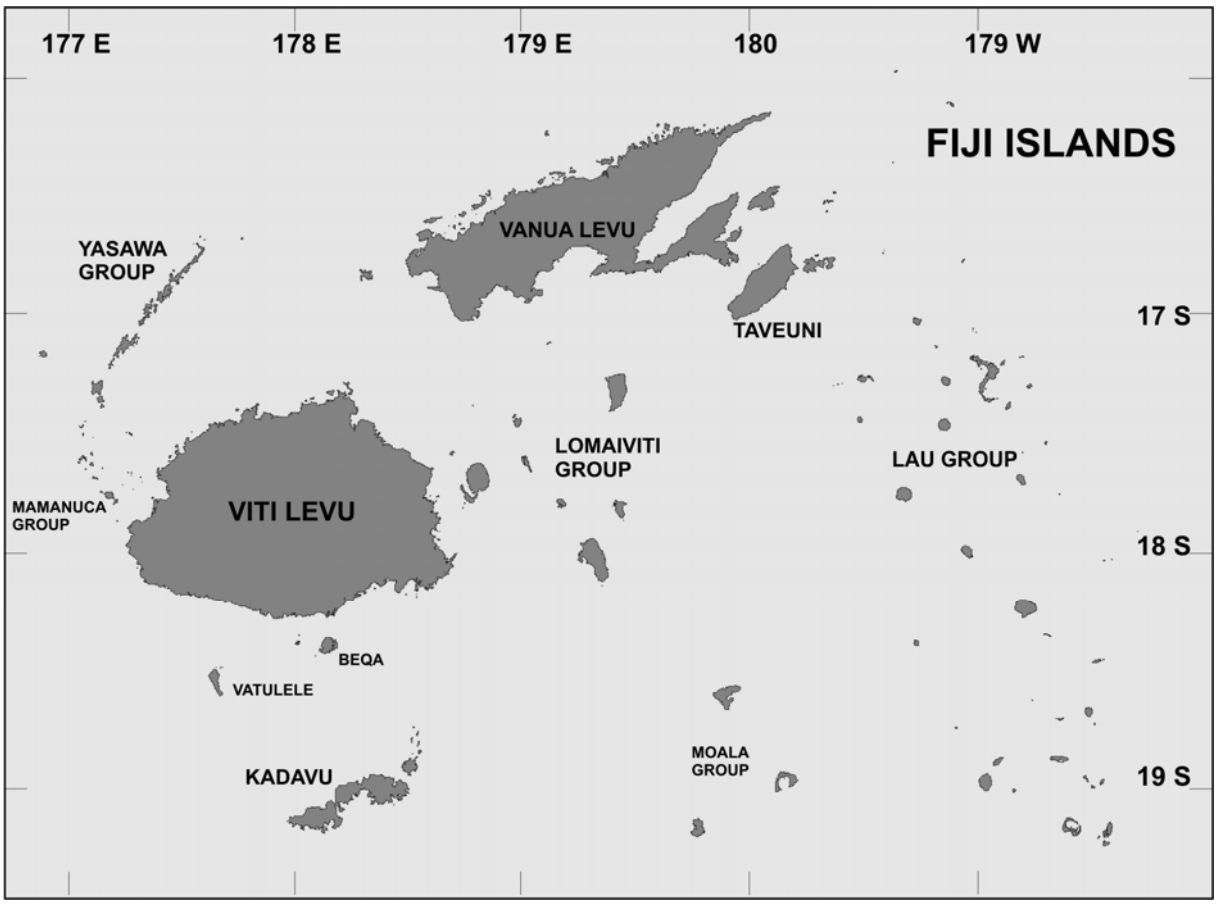

Figure 1.2: The main islands and island groups of the Fiji archipelago.

1.2 THE SCOPE AND CONTEXT FOR THIS RESEARCH

The work presented in this thesis was carried out in collaboration with the South Pacific Applied Geoscience Commission's (SOPAC) Reducing Vulnerability of Pacific ACP States Project, under the European Union EDF8 funding. The southern coast along Viti Levu was highlighted in the SOPAC Project as a critical area in Fiji, for having rapid population growth, significant investment and planned future investment in infrastructure, a dense tourism industry, important watersheds for agriculture and water resources, and for being an area susceptible to natural hazards. As a contribution to one of the key focal areas of the SOPAC Project in Fiji, entitled "Hazard Mitigation/Risk Assessment", this thesis presents the results of earthquake and tsunami hazard evaluation work focusing largely on, but not entirely confined to, the southeastern part of Viti Levu. More background information on southeast Viti Levu is presented in Chapter 3.

1.3 AIMS AND OBJECTIVES

The over-arching aims of this thesis are to identify earthquake and tsunami sources and quantify the hazard they pose in central and southeast Viti Levu, and to propose a seismotectonic framework for the Fiji region. This thesis attempts to achieve these aims through addressing a number of specific objectives. These objectives are listed below, together with the relevant chapters where they have been dealt with. The objectives of this thesis are to:

1. Review the tectonic history of Fiji to highlight key questions related to the present tectonic setting of Fiji, and identify southeast Viti Levu as a key area of study (Chapter 2, 3).

2. Develop an innovative methodology incorporating remotely sensed imagery, geographical information systems and field structural geology for identifying faults in areas of poor outcrop exposures (Chapter 4).

3. Employ high resolution offshore surveying techniques including multibeam swath bathymetric mapping and shallow marine seismic reflection profiling for mapping morpho-structure and locating offshore faults (Chapter 5).

4. Integrate onshore and offshore data to allow for corroborative interpretations of onshore and offshore structure and morphology spanning a coastal setting (Chapter 5).

5. Identify and document submarine landslides and evaluate their potential for generating submarine landslide tsunamis (Chapter 6).

6. Quantify inundation hazards by carrying out numerical simulations of tsunami generation, propagation and inundation (Chapter 7).

7. Use structural data to interpret active tectonic deformation and origin of seismicity in the region, leading to the proposal of a new seismotectonic model for the Fiji region (Chapter 8).

8. Document newly identified crustal fault seismic sources and evaluate their potential for generating strong ground motions through a deterministic seismic hazard analysis (Chapter 9).

The introductions of individual chapters contain more detailed objectives relevant to the specific studies presented therein.

1.3 THESIS ORGANISATION

This thesis is organised into ten chapters. The individual components and the overall structure of the thesis are presented in Figure 1.3. This chapter provides a general introduction to the thesis, oulines the scope, aims and objectives of the research, presents the thesis outline and introduces the methods and data sources used. Chapter 2 presents the tectonic and geological setting of the Fiji islands as well as a brief tectonic history of Fiji, which forms the basis on which structural data are interpreted and the seismotectonic model is developed in the following chapters. Chapter 3 introduces the southeastern Viti Levu area, where much of the fieldwork was carried out, both in the onshore and offshore areas. Chapter 4 presents a detailed quantitative analysis of onshore lineaments from a number of remote sensing imagery in southeast Viti Levu and shows how they are related to field mapped structural features. Chapter 5 examines and describes the morpho-structure of the offshore area of southeast Viti

Levu. Chapter 6 documents submarine landslides in southeast Viti Levu and evaluates their potential for generating tsunamis. Chapter 7 presents a detailed case study on a submarine landslide tsunami generating area in southeast Viti Levu and evaluates tsunami inundation hazards by numerical modelling. Chapter 8 synthesizes data from Chapters 2, 4, and 5 to present a new tectonic context for the Fiji region by proposing a new seismotectonic model of the Fiji Platform. Chapter 9 presents a deterministic seismic hazard study of the southeast and central Viti Levu areas by evaluating major seismic source zones in the Fiji region and seismic source structures on Viti Levu. Finally, Chapter 10 summaries the main conclusions of the thesis and provides recommendations for future research directions.

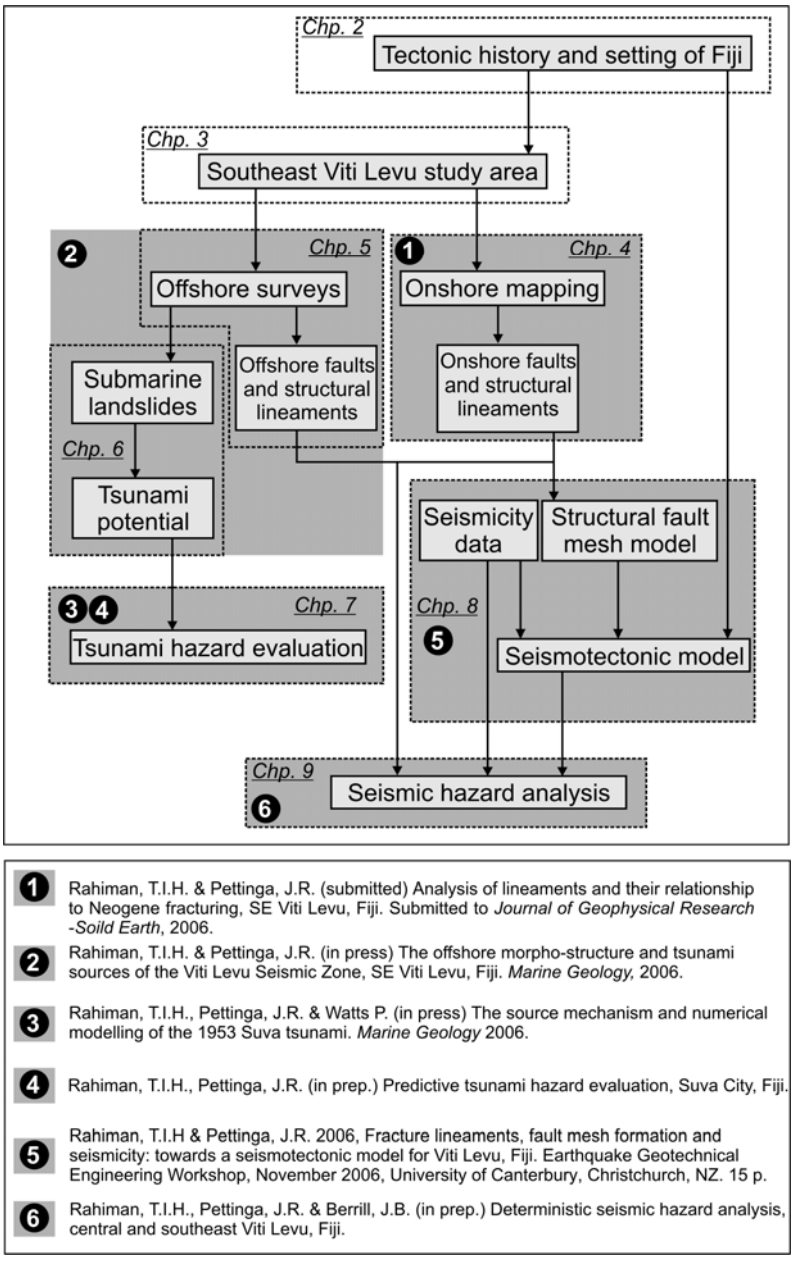

Figure 1.3: Overall structure of thesis and publication plan.

The eight main chapters of this thesis after the Introduction cover the six fundamental aspects of the research: 1) tectonic history and setting of Fiji; 2) onshore and offshore seismic sources; 3) submarine landslide tsunami sources; 4) tsunami hazard evaluation; 5) seismic hazard evaluation; and 6) seismotectonic model. Even though these aspects are covered primarily in separate chapters, some of the material they contain is interrelated and is not always in sequential order. Cross-referencing, therefore, is used to form links between chapters. The work that resulted from the early phases of this research, was originally compiled as three manuscripts that have now been submitted or accepted for publication (Figure 1.3). Chapters 4, 5, 6 and 7 contain material originally presented in these manuscripts that have been restructured to avoid repetition between the chapters. These chapters contain additional material not included in the manuscripts due to publication format restrictions. Chapters 8 and 9 are in the process of being modified into manuscript form for publication.

During the course of this research, attempts were made to obtain paleoseismic data from southeastern Viti Levu. Mapping of fault displacements of emerged late Quaternary coastal features were undertaken along the southern coast of Viti Levu. Geological and geomorphological mapping in the Namosi Gorge area (central southeastern Viti Levu) was conducted jointly with Michael Bonte (SOPAC). Several carbonate samples of emerged coastal features, as well as organic material in landslide and lake sediments from the Namosi Gorge area were collected for radiocarbon dating. The results of these studies, including the radiocarbon dates, are presented as separate reports in Appendix 1 and 2 and are cross-referenced in the main text of the thesis. Further appendices contain additional supporting data collected and compiled during this research. They also contain supporting calculations and methodologies relevant to the main body of this thesis.

1.4 INTRODUCTION TO METHODOLOGIES AND NEW DATA SETS

It was recognised early in this research that new data sets and innovative methods of dealing with specific problems would be required to address the main objectives of this research. A number of key methods and data sets utilised in this thesis are summarised below. A locality map showing the coverage of various spatial data sets is shown in Figure 1.4.

1. A multidisciplinary approach that combined field geology, remote sensing and geographical information systems (GIS) was used effectively to map regional

structural patterns in areas where outcrops were limited by vegetation cover and deep soil profiles.

2. Remote sensing data including aerial photos (1: 50 000 & 1: 15 000) and Side Looking Airborne Radar (SLAR) images were scanned, rectified and geo-referenced in a GIS. A 20 metre resolution digital terrain model (DTM) of Viti Levu and derivative shaded relief images were generated.

3. Lineament maps of aerial photos (1:50 000 scale), SLAR, DTM and first vertical derivative of total magnetic intensity images (1:150 000 scale) of southeast Viti Levu were produced.

4. Field structural data from over 100 localities in southeast Viti Levu were collected.

5. Offshore morpho-structure was mapped using the state of the art multibeam swath echo sounding system. The quality of bathymetric profiling from this method supersedes the resolution of all previous surveys in the area. Derivative data from the swath bathymetry including contour maps, shaded relief images with various sun-angles, cross sections, slope maps and morphological maps were produced.

6. Over 150 kilometres of high resolution shallow marine seismic reflection profiles were surveyed and continuous profiles of near shore sub-bottom geology to depths of up to 200 m below the sea floor were produced.

7. Onshore field mapping carried out in parallel with marine geophysical surveys allowed for corroborative interpretations of geological structure in both areas.

8. A combination of field geological mapping, offshore geophysical surveys, careful search and review of historical data was used to determine the source of the destructive 1953 Suva tsunami.

9. A numerical tsunami simulation model, validated with the 1953 Suva tsunami, was used to construct a predictive simulation of the future inundation hazards in Suva City.

10. Recent empirical equations were used for calculating Maximum Credible Earthquakes and updated attenuation relationships were used to quantify earthquake ground motion hazards.

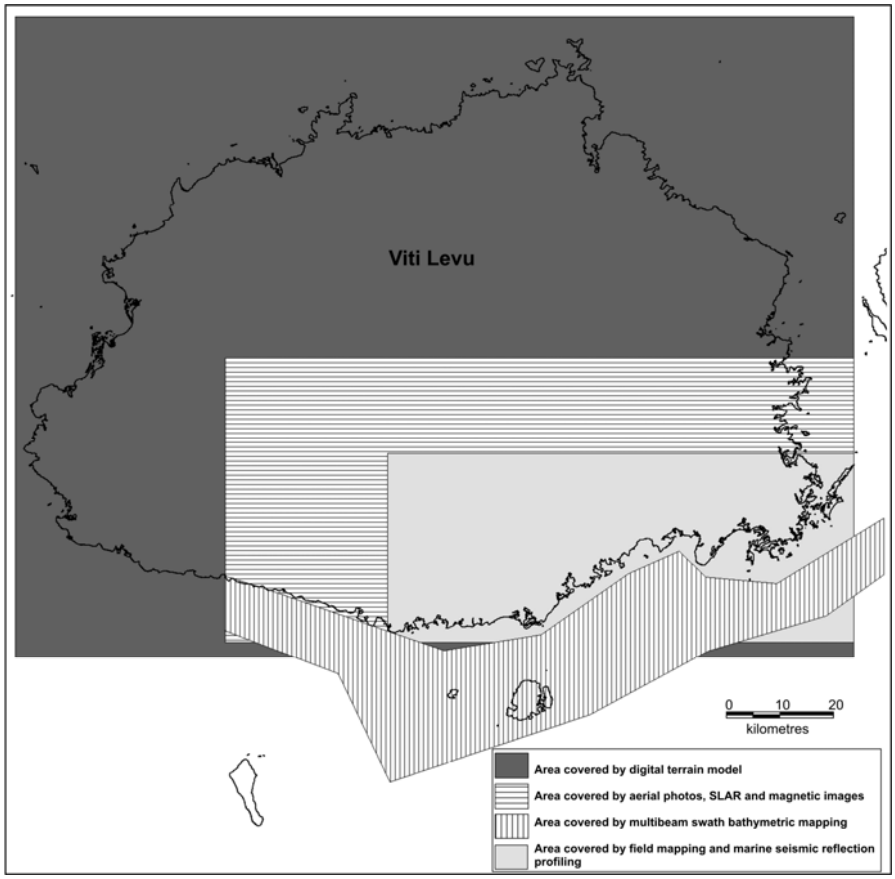

Figure 1.4: Spatial coverage of various datasets used in this thesis.

1.5 PRONUNCIATION OF FIJIAN PLACE NAMES

Throughout this thesis, references are made to field localities with Fijian place names. These names are written in the system of orthography used by indigenous Fijian people, now adopted by the Government of Fiji. A guide to correct pronunciation of five Fijian letters is given below:

B is pronounced MB, as in number
C is pronounced TH, as in that
D is pronounced ND, as in tinder
G is pronounced NG, as in singer
Q is pronounced NGG, as in finger

(from Rodda & Kroenke, 1984).

CHAPTER 2

TECTONIC EVOLUTION, SETTING AND SEISMICITY OF THE FIJI REGION

2.1 INTRODUCTION

Fiji has had a complex tectonic history and it currently occurs in an enigmatic position in relation to the major plate boundary features in the southwest Pacific. The origin of seismicity and the nature of tectonic deformation in Fiji, which accompanies the evolution of plate boundaries in the wider southwest Pacific region, are not well understood. In this chapter the tectonic and geological history of Fiji, and its present day tectonic setting and seismicity are reviewed. Some key questions are then posed in order to explore the relationship that may exist between seismicity observed in Fiji and the tectonic processes that are currently operating.

2.2 OVERVIEW

Over the last 30 years, a number of workers have contributed to the understanding of the tectonic and geologic evolution of the Fiji region through a variety of studies. Rodda (1967), Rodda & Band (1967) and Ibbotson & Coulson (1967), describe the geology of the main islands of Fiji - Viti Levu and Vanua Levu, from the compilation of early regional geological mapping carried out by the Geological Survey of Fiji. Dickinson (1967), Chase (1971) and Coulson et al. (1975) provide early insights into the structure and tectonic development of the Fiji Platform. Considerable work on the geochemical and petrological evolution of Fiji are contained in Gill (1970), Gill & Gorton (1973), Gill et al. (1984), Gill (1987), and Gill & Whelan (1989a). The early work on the seismicity of the Tonga-Fiji region is presented in Isacks et al. (1967), Isacks et al. (1969) and Sykes et al. (1969) and more recently in Hamburger & Isacks (1987), Hamburger & Isacks (1988) and Hamburger et al. (1988, 1990). Work on geometric plate tectonic reconstructions of the region and studies on the tectonic rotation of Fiji from palaeomagnetic studies are provided by Falvey (1975,1978), James & Falvey (1978), Cassie (1978), Malahoff et al. (1982a,b), Inokuchi et al. (1992) and Taylor et al. (2000). In recent years considerable work has focused on the offshore areas surrounding Fiji. The works by Brocher & Holmes (1985) and Johnson (1994) were primarily based on

exploration for hydrocarbon deposits, but they provide useful insights into the marine geology around Viti Levu. Other offshore studies along plate boundaries surrounding the Fiji Platform were carried out by Brocher (1985), Lafoy et al. (1990), Parson et al. (1990), Auzende et al. (1994), Auzende et al. (1995a), Pelletier & Auzende (1996), and Taylor et al. (1996). Together with the recent work on seismicity, the offshore work has considerably improved the understanding of current plate boundary features around the Fiji Platform. These separate pieces of work, with sometimes conflicting views, especially on the timing, location and mechanisms of the main tectonic episodes affecting Fiji, provide the framework for understanding the tectonic development of the Fiji Platform. An accepted working model for the tectonic evolution of the Fiji region, however, has been developed and updated over time (e.g. Chase, 1971; Gill & Gorton, 1973; Falvey, 1975; Hamburger & Isacks, 1987; Rodda, 1994).

2.3 TECTONIC AND GEOLOGIC HISTORY OF FIJI

The landmasses of Fiji are products of coalesced arc related volcanic, plutonic and volcaniclastic sedimentary rocks from a series of volcanic island arcs spanning the Cenozoic era. The geology is predominantly mapped as repeated sequences of volcanic lithostratigraphic units portraying lateral facies variations from coarse to fine volcaniclastics centered around remnant eruptive centres which have been characterised geomorphically or in more eroded terrain by the presence of volcanic stocks and sub-volcanic plutons. The rocks have undergone episodic periods of deformation attributable to, and controlled by regional tectonic processes. Tectonism has also, in part, controlled development of large intervolcanic sedimentary basins. Periods of emergence recorded in the stratigraphy are attributable to tectonic uplift or eustatic sea level changes or both. The magmatic and petrologic history of Fiji is reflective of primitive, mature, rift and post-subduction related episodes of Fiji's tectonic history. In the following section, the tectonic history of Fiji is reviewed and at the same time aspects of the tectonic episodes reflected in the geology of the islands are emphasised.

2.3.1 Yavuna Proto Arc and the South Fiji Basin (Eocene - Early Oligocene)

The details of the early history of the southwest Pacific region are speculative. Collective evidence suggests that Eocene convergence of the Pacific and Australian plates led to the

formation of a volcanic arc, the remnants of which form the basement of Fiji, Vanuatu and Tonga (Ewart & Bryan, 1972; Coleman & Packham, 1976; Carney & Macfarlane, 1978; Gill, 1987; Hathway & Colley, 1994; Tappin & Ballance, 1994) (Figure 2.1a). The Yavuna Block in southwest Viti Levu, Fiji, represents the remnant fragment of a forearc block of this terrain (Figure 2.1b), and is composed of reef limestones, arc tholeiitic, dacitic and transitional boninitic lavas, and the Yavuna (tonalite/trondhjemite) stock (Hathway & Colley, 1994; Wharton et al., 1995). Whelan et al. (1985) have obtained radiometric dates of 32 and 29 Ma from lavas of the Yavuna terrain and a date of 31 Ma for the Yavuna Stock. The intrusion of the Yavuna Stock represents the last magmatic event in the proto-arc before the opening of the South Fiji Basin in the Late Oligocene, during which the Yavuna arc is inferred to have migrated northeastward (Hathway & Colley, 1994).

Accompanying rifting and the opening of the South Fiji Basin, southwestward and westward directed subduction of the Pacific plate under the Australian plate and volcanism along the rifted southwestward margin of the Yavuna Block resulted in the Wainimala volcanic arc in Fiji (Hathway & Colley, 1994). A lull in volcanic activity in the early Wainimala arc rocks and late proto-arc rocks is marked by an unconformity which may reflect tectonism during rifting of the proto arc (Rodda & Kroenke, 1984; Wharton et al., 1995). The Wainimala arc formed part of the continuous Vityaz arc (or Outer Melanesian arc) comprising the ancestral Solomon, Vanuatu, Fiji/Lau, Tonga and Kermadec-Colville arc segments along the Tonga-Kermadec Trench and the now relict Vityaz Trench which lies to the north of Fiji's present position (Chase, 1971; Gill & Gorton, 1973; Falvey, 1975). This episode of subduction may have commenced in response to the northward movement of the Australian plate and change in direction of Pacific plate motion, which is exemplified by the bend in the Emperor-Hawaii seamount (hot spot) chain (Gill, 1987).

2.3.2 Vityaz (Wainimala) Arc (Early Oligocene - Late Miocene)

The Wainimala arc prevailed from Early Oligocene (23-28 Ma, Wharton et al., 1985) to Middle-Late Miocene or possibly the earliest Pliocene (Rodda, 1994) (Figure 2.2a). The youngest magmatic rocks of the Wainimala arc range from 10 to 14 Ma (Rodda, 1981; Whelan et al., 1985; Fanning, 1986). The rocks of the Wainimala arc are assigned to the Wainimala Group and Savura Volcanic Group and are found in southern Viti Levu, and some islands of the Yasawa/Mamanuca island chain and Lau island group, in the western and

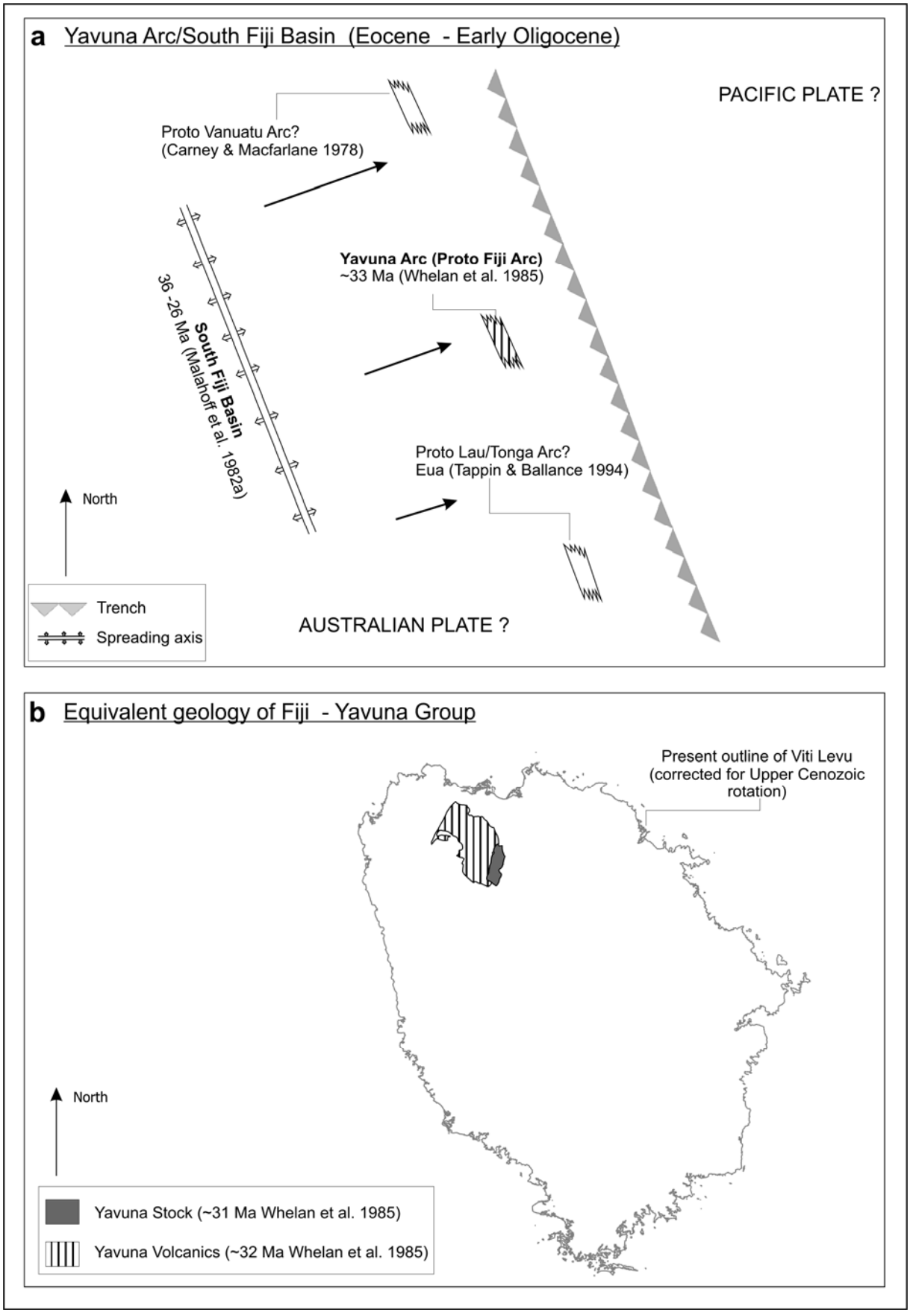

Figure 2.1: Schematic tectonic and geologic reconstruction of Fiji (Eocene - Oligocene).

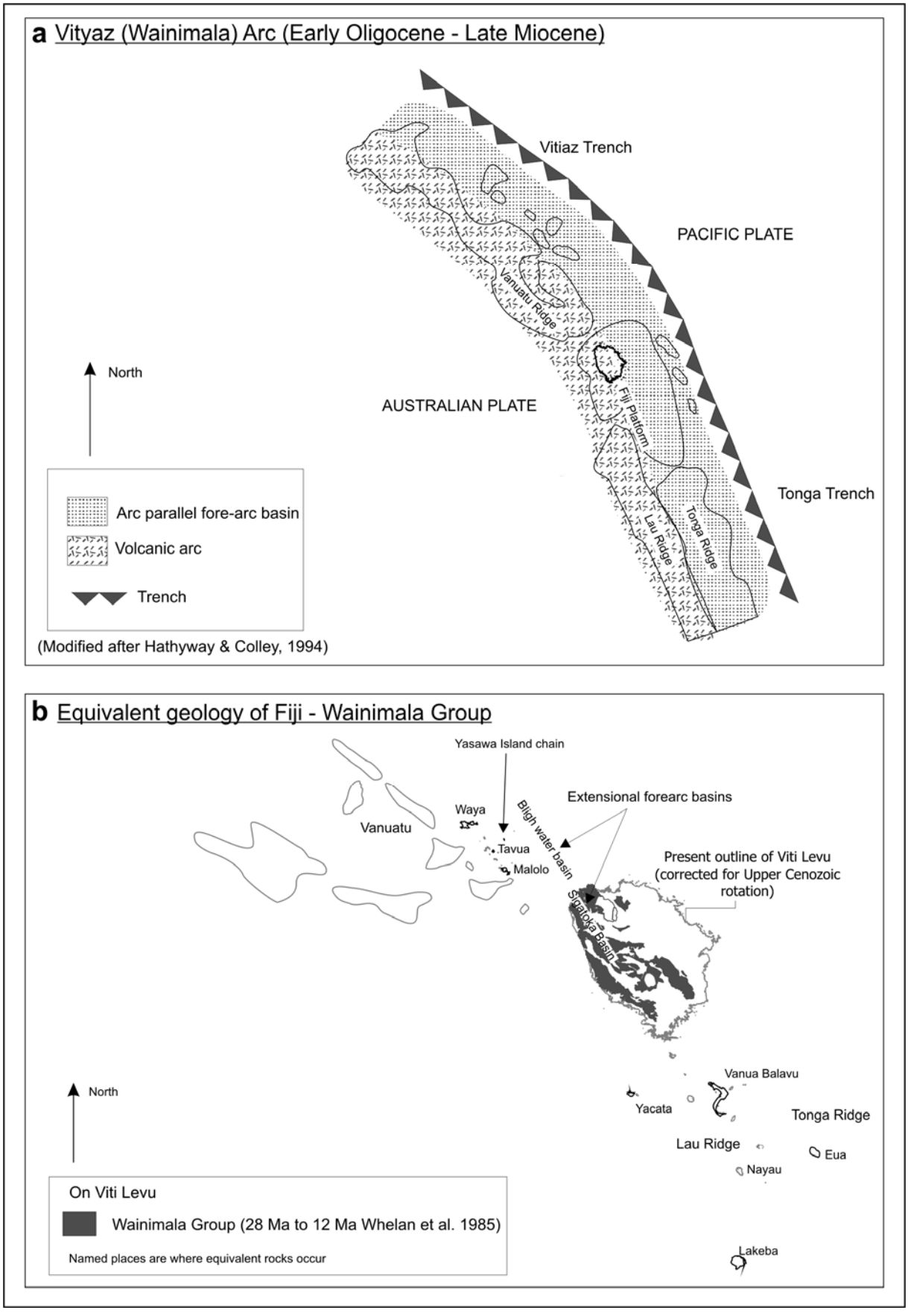

Figure 2.2: Schematic tectonic and geologic reconstruction of Fiji (Early Oligocene - Late Miocene).

eastern parts of Fiji respectively (Figure 2.2b). These rocks are massive, brecciated and pillowed basalt lavas, dacites, coarse to fine volcaniclastics, tuffs and pelagic limestone. Magamatic rocks have arc tholeiitic and transitional calc-alkaline affinities. These rocks are affected by greenschist facies regional metamorphism. The Bligh Water Basin in northwestern Fiji and the Sigatoka Basin in southwest Viti Levu originated as part of the fore-arc basin at this time bordering the Wainimala arc to the north (Hathway & Colley, 1994; Johnson, 1994).

A number of significant events are noted in the geological record towards the end of the deposition of Wainimala rocks at about Middle to Late Miocene times, including:

1. Widespread plutonism in southern Viti Levu from 12.5 Ma to about 7 Ma (Rodda, 1994). Colley & Greenbaum (1980) refer to this event as the Colo Orogeny, the only one of its kind seen in any of the archipelagos of the southwest Pacific. The plutons, ranging in composition from noritic gabbro to trondhjemite, occur in an elongated E-W belt in southern Viti Levu and are referred to as the Colo Plutonic Suite (Rodda & Kroenke, 1984).

2. Folding and faulting, with the formation of an anticlinorium enveloping the plutonic belt.

3. Extreme deformation in rocks post-dating the Colo Orogeny, notably those of the Tuva Group in southwest Viti Levu (Rodda, 1994).

4. Eruptions of sub-aerial basaltic lava along the Yasawa-Mamanuca chain of islands and eruption of dacitic/rhyolitic volcanoes in northeast Vanua Levu (Udu).

In the regional context, this deformation episode in the Middle to Late Miocene marks the onset of the break-up of the Vityaz arc, leading to the fragmented configuration seen today. This would require separation of Vanuatu and Fiji in the western sector, polarity reversal at the Vanuatu arc segment and its movement away from Fiji. It also requires the separation of Fiji and Tonga and the isolation of Fiji from the Vityaz and Tonga trenches. The exact timing and location of the initiation of fragmentation of the Vityaz arc are disputed, however, there is general agreement that separation occurred by clockwise rotation of Vanuatu and

anticlockwise rotation in the Fiji region. The effect of the anticlockwise rotation of the Fiji Platform is manifested in the spiral-like bathymetric contours around the Fiji Platform, the extreme bending of the Lau Ridge at its northern end (Figure 1.1), and also the swing in strike of the Wainimala and Colo rocks and the Yasawa island chain.

2.3.3 Disruption of Vityaz Arc (Middle - Late Miocene)

Subduction along the Vityaz arc was terminated as a result of collisions with Pacific plate oceanic plateaux. The Melanesian Border Plateau collided just north of Fiji and the Ontong-Java Plateau, further north near the Solomon Islands (Gill & Gorton, 1973; Falvey, 1975; Gill et al., 1984; Rodda, 1994) (Figure 1.1). Continued convergence between the Australian plate and Pacific plate led to the subduction polarity reversal on the Vanuatu arc segment and subsequent fragmentation of the Vityaz arc (Gill, 1987; Gill & Whelan, 1989a) (Figure 2.3a). Fragmentation of the Vityaz arc was facilitated by the opening of the North Fiji Basin at about 8 Ma (Malahoff et al., 1982a), probably as a back-arc basin to the reversed Vanuatu arc. Geological evidence shows that initial rifting may have occurred in the western sector of the Vityaz arc, between Vanuatu and the Yasawa islands. Age equivalent and similar types of rocks are found in both these places (Rodda & Lum, 1990) (Figure 2.3b). Voluminous rift related eruptions in the north of Fiji (Gill et al., 1984; Whelan et al., 1985) also occurred at this time of incipient arc fragmentation, probably on a sinistral transverse rift that later developed into the Fiji Fracture Zone. Extending northeastward from the reversed Vanuatu Trench, towards the Tonga Trench, another sinistral transverse rift, equivalent to the ancestral Hunter Fracture Zone (Rodda, 1994), separated the southern Viti Levu and Lau segments of the Wainimala arc (Figure 2.4a). Continued spreading in the North Fiji Basin and associated transcurrent faulting facilitated the rotations of the Vanuatu and Fiji arc segments (Figure 2.4b) following their initial separation.

2.3.3.1 ARC ROTATIONS (?LATE MIOCENE)

Following disruption of the Vityaz arc, the Vanuatu arc segment underwent clockwise rotation, as lithosphere was created along the spreading ridges of the North Fiji Basin (Figure 2.5a). At about the same time or soon thereafter, the area now known as the Fiji Platform, at the north end of the Lau Ridge, underwent anticlockwise rotation. The exact time of initiation of the rotations of arc segments remains uncertain, but is generally considered to have

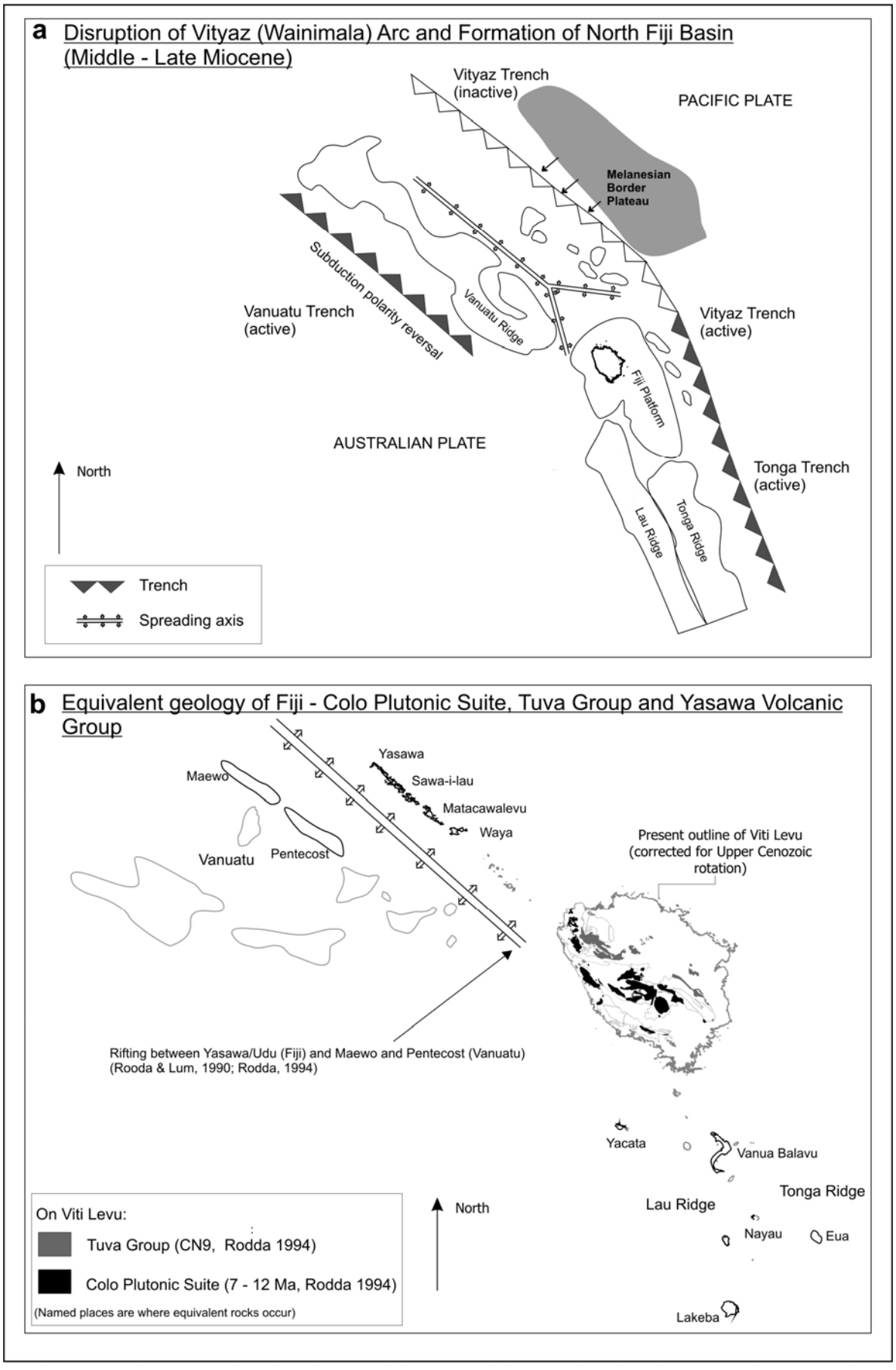

Figure 2.3: Schematic tectonic and geologic reconstruction of Fiji (Middle -Late Miocene).

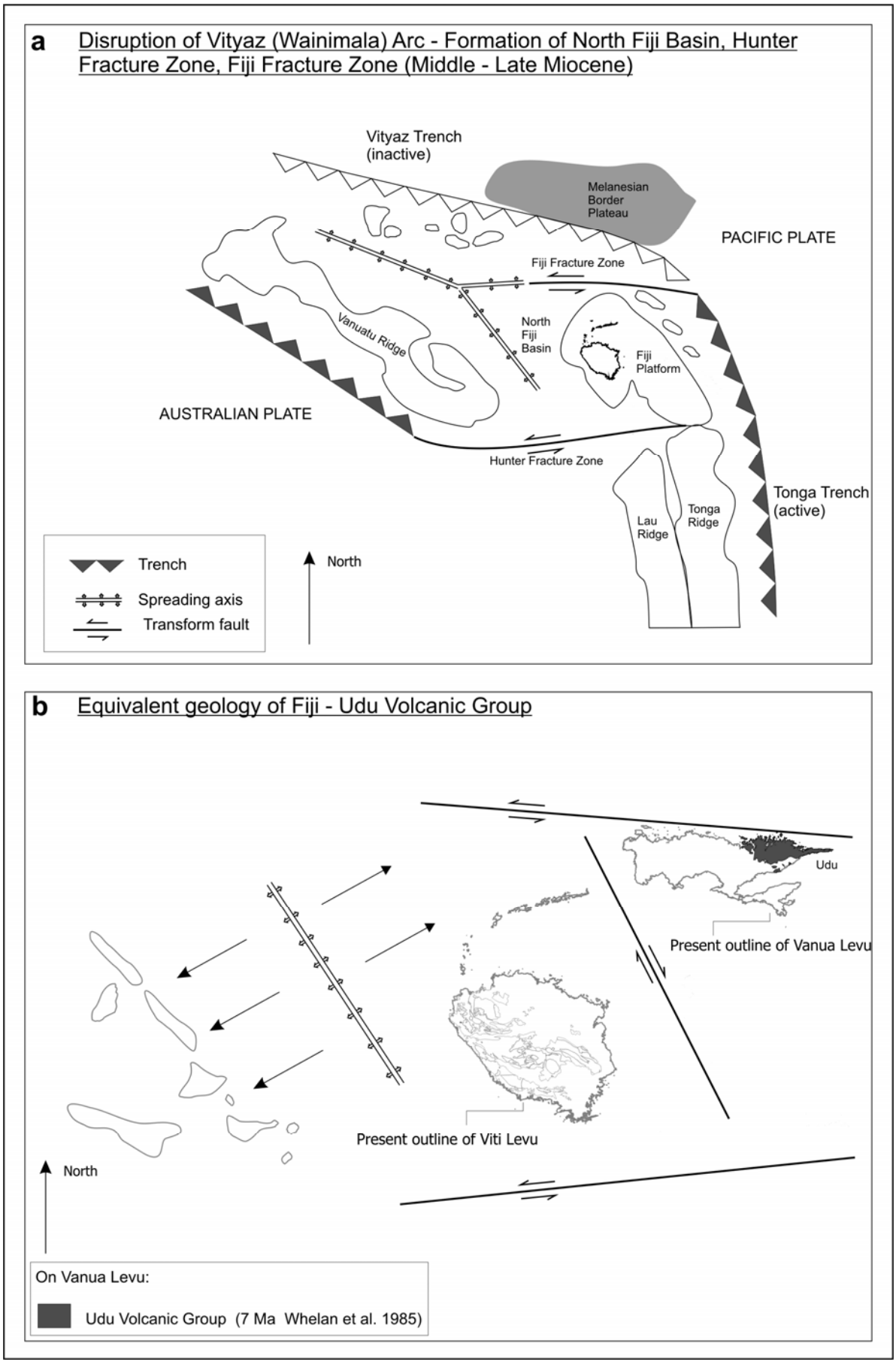

Figure 2.4: Schematic tectonic and geologic reconstruction of Fiji (Middle -Late Miocene).

commenced sometime between 5 Ma and 10 Ma (James & Falvey, 1978; Malahoff et al., 1982b; Gill et al., 1984; Whelan et al., 1985; Hamburger & Isacks, 1987; Auzende et al., 1988; Prichard, 1989; Inokuchi et al., 1992). The Vanuatu arc rotated clockwise by 30^{o} (Falvey, 1978) or 39^{o} (Musgrave & Firth, 1999). Regional paleomagnetic studies suggest anticlockwise rotation of the Fiji Platform by amounts ranging between 35^{o} and 114^{o} (Malahoff et al., 1982b; Prichard, 1989; Inokuchi et al., 1992; Taylor et al., 2000). In a more recent study, Taylor et al. (2000) used extensive paleomagnetic sampling to indicate that the Fiji Platform rotated 135^{o} anticlockwise from a N-S position in line with the Tonga Ridge commencing at or before 10 Ma, coincident with the onset of spreading on the major N-S aligned spreading centre of the North Fiji Basin. Although Taylor et al. (2000) put the cessation of rotation of the Fiji Platform at 3 Ma, this conclusion is based on a limited number of paleomagnetic samples, and it remains unclear whether the rotation of the Fiji Platform is ongoing today (Rodda, 1994). This is discussed further in Section 8.4.

2.3.3.2 Syn-disruption Arc Volcanism and Strike slip Basins (Late Miocene to Early Pliocene)

Following the episode of arc disruption and during the initial tectonic rotation, subduction at the Fiji segment of the Vityaz Trench continued to generate arc-like magmas to further develop the landmasses of Fiji (Gill et al., 1984; Rodda & Kroenke, 1984; Gill & Whelan, 1989a). From the Late Miocene onwards volcanism became more widespread (Rodda, 1994). From 5.5 to 3.0 Ma basalts were erupted from more than 30 centres around Fiji (Whelan et al., 1985). Primitive submarine boninitic lavas erupted in Cikobia, northeast of the Vanua Levu. Predominantly submarine arc tholeiitic and calc-alkaline lavas of the Macuadrove Super Group erupted in Vanua Levu, Rabi and Kioa, largely submarine calc-alkaline and shoshonitic lavas of the Koroimavua Volcanic Group and Ba Volcanic Group in northern Viti Levu, calc-alkaline lavas of the Medrausucu Group at Namosi (and Mau) and Nakobalevu in southeastern Viti Levu and calc-alkaline lavas of the Lau Volcanic Group in Lau. Structural control on volcanism during the rotation of Fiji is evident in the parallel alignment of late Miocene to Pliocene eruptive centres. These alignments are: 1) the ENE Viti Levu Lineament in northern Viti Levu; 2) the Namosi - Nakobalevu - Ovalau trend; 3) the ENE Vatulele to Beqa trend (Vatulele-Beqa Lineament) possibly including Gau island; 4) the ENE trend through to northern Vanua Levu; 5) the northeast Rabi, Kioa and Dakuniba trend in southeast Vanua Levu; 6) the NNW alignment of Pliocene eruptive centres and elongation

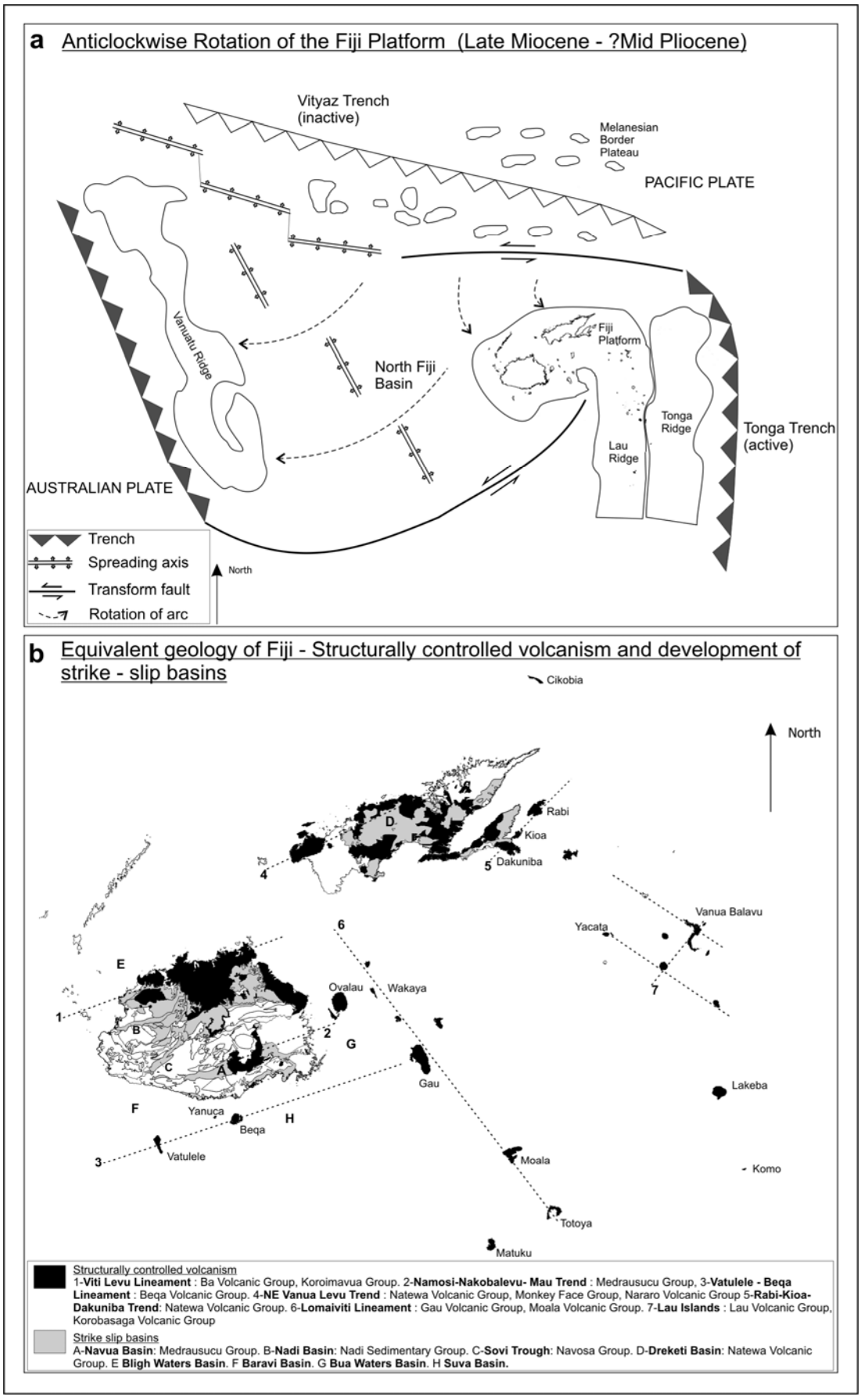

Figure 2.5: Schematic tectonic and geologic reconstruction of Fiji (Mid Miocene – ?Mid Pliocene).

of islands in Lomaiviti (the Lomaiviti Lineament); and 7) northeast and northwest alignments of islands in the Lau Group (Gill & Whelan, 1989a) (Figure 2.5b).

Contemporaneous with the Late Miocene volcanism was widespread sedimentation. These sediments occur in predominantly elongated basins, which formed as a result of strike-slip faulting following the disruption of the Vityaz arc (Hathway, 1993; Hathway & Colley, 1994; Johnson, 1994). The best onshore expression of these basins are the Nadi, Sovi and Navua basins on Viti Levu (Hathway, 1993). Offshore examples of the Late Miocene basins include the Bligh Water Basin to the north of Viti Levu, and the Bau Waters Basin in eastern Viti Levu (Johnson, 1994), the Baravi Basin off southwestern Viti Levu (Brocher & Holmes, 1985) and the Suva Basin to the southeast of Viti Levu (Holmes et al., 1985) (Figure 2.5b).

2.3.4 Lau Basin and Ocean Island Basalt Volcanism (Mid Pliocene - Quaternary)

Another phase of rifting saw the Fiji arc segment separate from the Tonga arc, with the opening of the Lau Basin, the backarc basin to the Tonga arc (Figure 2.6a). Dates for the opening of the Lau Basin are suggested as the Mid Pliocene (Colley & Hindle, 1984), 5 to 3 Ma (Whelan et al., 1985), from 5 Ma (Parson et al., 1990), from 4 Ma (Taylor et al., 1996) and as recent as 2.5 Ma (Malahoff et al., 1982a). The dates of around Early to Mid Pliocene from seafloor magnetic-anomaly studies and sediment cores seem the most accurate. This stage of rifting completely isolated the Fiji Platform from the Vityaz and Tonga trenches and marks the end of the eruptions of subduction-generated lavas on the Fiji Platform. Fiji became a remnant arc at ~3 Ma (Gill & Whelan, 1989b).

This period also marks the introduction of ocean-island-basalt eruptions in Fiji (Figure 2.6b). The oldest date for alkali-basalt lavas in Fiji is from a sample of the Seatura Volcano in western Vanua Levu dated at 3.35 Ma (Hindle & Colley, 1981). Alkali basalts also erupted on Koro (Lomaiviti Group), in islands of the Lau Group, on Taveuni, and on Galoa in the Kadavu Group. The youngest eruptions have occurred at Galoa (0.36 Ma - Whelan et al. 1985), Mago, Lau Group (0.28 Ma - Whelan et al. 1985) and in Taveuni in historical times (~1500 AD, Cronin et al. 2001).

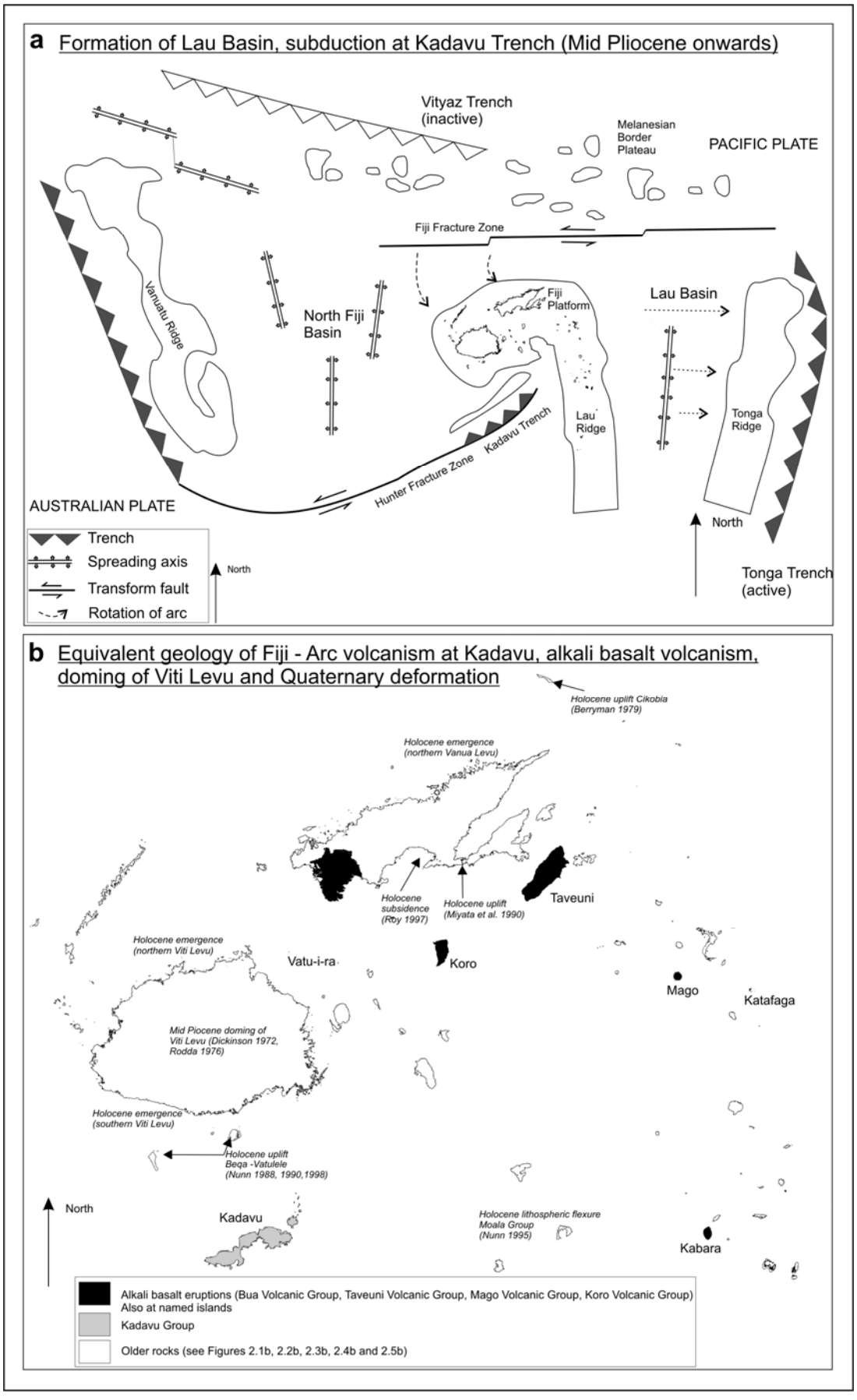

Figure 2.6: Schematic tectonic and geologic reconstruction of Fiji (Mid Pliocene onwards).

2.3.5 Kadavu Arc (Mid - Late Pliocene - Quaternary)

Anticlockwise rotation of Fiji is considered to have been partly accommodated by oblique subduction along the Kadavu Trench (Malahoff et al., 1982a; Gill et al., 1984; Whelan et al., 1985; Verbeeten et al., 1995) (Figure 2.6a). The arc volcanic rocks in the Kadavu island chain have been dated by Whelan et al. (1985) to 3.39 Ma to 0.48 million years old (Figure 2.6b). Quaternary volcanism (Rodda, 1994), earthquakes recorded landward (north) of the Hunter Fracture Zone (Hamburger et al., 1990), and lithosperic flexuring near the southern Lomaiviti islands (Nunn, 1995), suggest that convergence along the Kadavu Trench has taken place into the late Quaternary. Earthquake focal mechanisms near Kadavu show strike-slip and thrust movements (Sykes et al., 1969). Recently, Cronin et al. (2004) have dated Holocene eruptions on Kadavu at 2250, 1686 and 780 years BP and infer a historical event as recent as AD 1680.

2.3.6 Quaternary Deformation

Tectonic deformation on the Fiji Platform continued from the Neogene to the present day. Domical uplift of central Viti Levu placed Pliocene basaltic pillow lavas that erupted below sea level to over 1000 m above sea level on the southern sector of the Tavua Volcano in central Viti Levu (Rodda, 1976) (Figure 2.6b). The updoming also uplifted and tilted Quaternary erosional surfaces in western and southern Viti Levu (Dickinson, 1972; Rodda, 1993). Various coastal regions of the Fiji Platform also show evidence for late Quaternary tectonic uplift. Holocene emergence of coastal features occurred along the southern coast of Viti Levu (Dickinson, 1968; Berryman, 1979; Maeda et al., 1986; Sugimura et al., 1988; Rodda & Nunn, 1990; Shepherd, 1990), in Cikobia Island, northeast of Vanua Levu (Berryman, 1979), and in southeast Vanua Levu (Miyata et al. 1990). Differing ages and amounts of coastal emergence across the platform imply differential uplift across active faults (Rodda, 1994). For example, displaced shorelines across faults normal to the northeast trending Beqa-Vatulele Ridge to the south of Viti Levu, are indicative of recent tectonic activity in the area (Nunn, 1988;1990;1998). Faults which show activity in the Quaternary are also found in southeast Viti Levu (Rodda, 1992; Shorten, 1993a). Furthermore, in historical times, significant horizontal strain occurred in the southeast Viti Levu, as observed in comparisons of geodetic measurements made in 1909 and 1980 (Berryman, 1981).

2.4 TECTONIC SETTING OF THE FIJI PLATFORM

The main islands of Fiji including Viti Levu, Vanua Levu, the Yasawa and Mamanuca island groups, Taveuni, Lomaiviti Group and Beqa-Yanuca-Vatulele Group occur on the Fiji Platform, a broad and shallow submarine platform with an area of about 100 000 square kilometres. The Platform is defined by the 2 km bathymetric contour (Smith & Raicebe, 1984; Brocher & Holmes, 1985) (Figure 2.7). The Fiji Platform forms the northern end of the linear submarine Lau Ridge, on which the Lau islands occur. The islands of the Kadavu group occur separately on the Kadavu Ridge to the south of the Fiji Platform.

The Fiji Platform was originally considered a stable continental landmass (Chase, 1971; Green & Cullen, 1973). However, more recent studies reveal that the crustal thickness of the Fiji Platform is typical of island arcs, averaging about 15-20 km (Chase, 1971; Green & Cullen, 1973; Hamburger et al., 1988; Hamburger et al., 1990). Crustal velocity (P wave) is low, averaging 6 km/s, and the anomalously low upper-mantle velocity observed beneath the platform (7.55 km/s) is in the same range as that observed beneath the active back-arc basins and island arcs neighbouring Fiji (Hamburger et al., 1988). These factors, as well as Neogene to Quaternary volcanism and shallow seismicity, indicate that the Fiji Platform is actively involved in regional plate boundary deformation processes (Hamburger et al., 1988).

Plate boundaries around the Fiji Platform are defined by zones of seismicity and disrupted submarine topography. Convergent margins are located at the Tonga Trench to the east of Fiji, where the Pacific Plate is currently consumed, and at the Vanuatu Trench to the west, where the Australian Plate is being consumed. Divergent boundaries are at seafloor spreading ridges in back-arc basins, both the North Fiji Basin (Brocher & Holmes, 1985; Auzende et al., 1994; Auzende et al., 1995b) to the west of Fiji and the Lau Basin (Parson et al., 1990; Taylor et al., 1996) to the east of Fiji. These backarc basins separate Fiji from the active subduction at the Tonga and Vanuatu Trenches. Left lateral transcurrent boundaries are located at the Fiji Fracture Zone (Hughes Clarke et al., 1993; Jarvis et al., 1994; Pelletier et al., 2001) to the north of Fiji and the Hunter Fracture Zone (Malahoff et al., 1982a; Verbeeten et al., 1995; Pelletier et al., 1998) to the south. The Vityaz Trench lineament is what remains of the relict Oligocene to Miocene convergent plate boundary to the north of Fiji, extending westward from the Tonga Trench (Brocher, 1985).

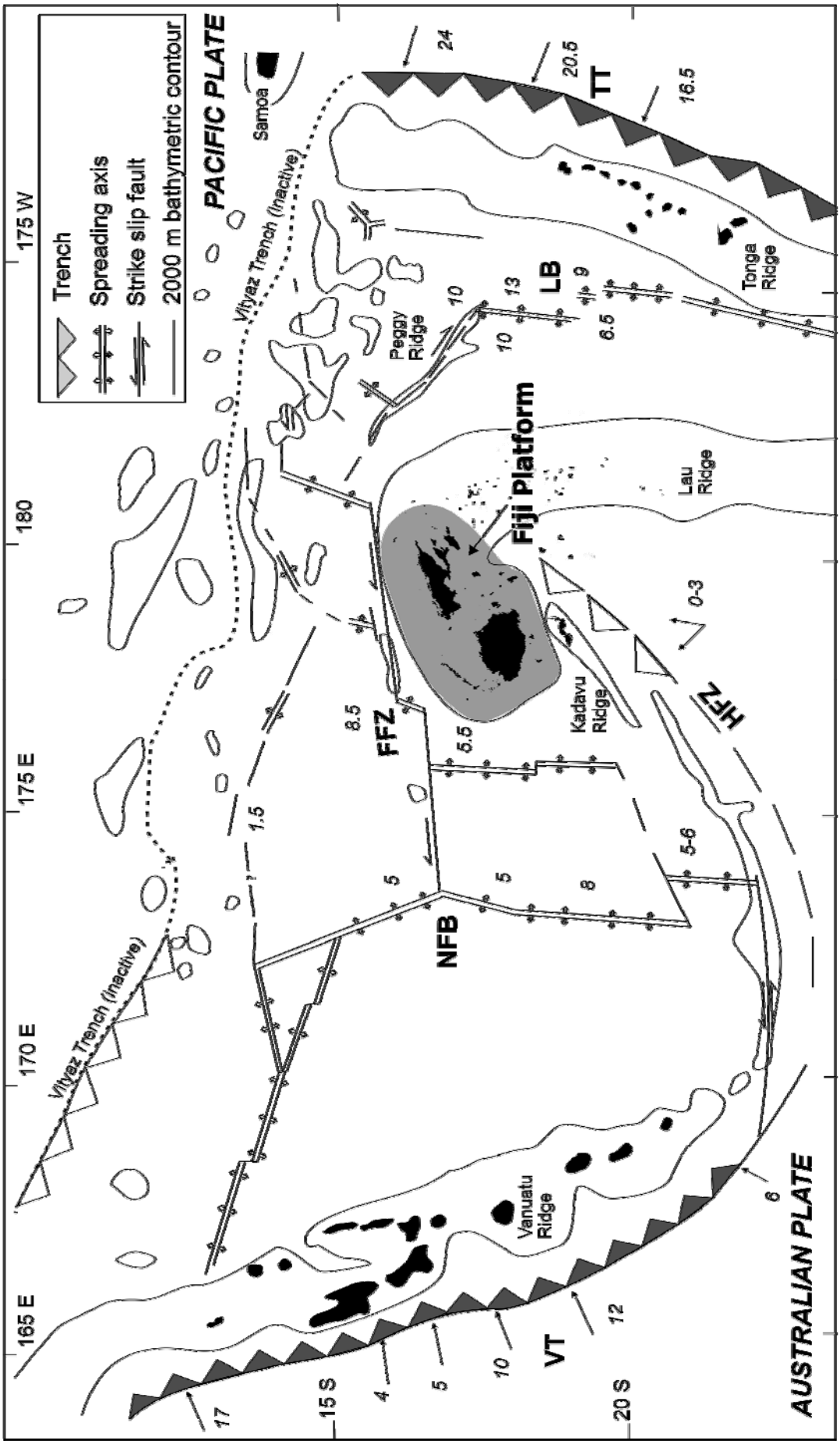

Figure 2.7: Tectonic setting of the Fiji region (modified from Hathway (1993), Auzende et al. (1995b), Hawkins (1995) and Pelletier et al.(2001)). The main tectonic features are (i) Vanuatu Trench (VT), (ii) Tonga Trench (TT), (iii) North Fiji Basin (NFB), (iv) Lau Basin (LB), Fiji Fracture Zone (FFZ), and (v) Hunter Fracture Zone (HFZ). The 2000 m isobath defines the Fiji Platform (shaded area) at the northern end of the Lau Ridge. Numbers in italics are rates of motions of plates (cm/yr), adopted from Pelletier et al. (1998).

The plate motions surrounding the Fiji Platform have been derived from magnetic anomalies on spreading centres, and from direct GPS measurements (Pelletier et al., 1998) (Figure 2.7). The full spreading rate of the Central Spreading Ridge of the North Fiji Basin varies from 50 to 80 mm per year (Auzende et al., 1995a). The spreading rate along the Central Lau Spreading Ridge of the Lau Basin is between 56 and 100 mm per year (Taylor et al., 1996). North of the Fiji Fracture Zone, the Pacific plate currently moves westward at a rate of 85 mm per year relative to the Australian plate (Pelletier et al., 2001). Along the Hunter Fracture Zone/Conway-Kadavu Lineament, 20 – 30 mm per year of convergence or sinistral strike slip motion occurs between the Australian plate and the Fiji Platform (Pelletier et al., 1998). The area surrounding Fiji, bound by the Fiji Fracture Zone in the north and the Hunter Fracture Zone in the south, including the Fiji Platform, can be viewed as a broad E-W trending sinistral transfer zone that is accommodating the divergence of the Vanuatu and Tonga Trenches by distributed strike-slip faulting and crustal accretion along irregular, short-lived spreading centres (Hamburger & Isacks, 1988).

2.5 SEISMICITY OF THE FIJI REGION

Ongoing seismic activity provides the clearest indication of ongoing tectonic deformation in the Fiji region. Shallow seismicity data of the Fiji region (depth < 80 km), determined from the global seismograph network, local network, and historical data for large earthquakes (Everingham, 1983a; Hamburger & Everingham, 1986; Everingham, 1988; Hamburger et al., 1990) are shown in Figure 2.8. There are no historical earthquakes in the Fiji region that have exceeded M_S 7.1 (Everingham, 1983b). Seismicity occurs along the boundaries of the Fiji Platform as well as within the Fiji Platform. Seismicity at the boundary of the Fiji Platform is characterised by a history of moderate to large earthquakes (M_S >5) and continuous activity at moderate magnitudes, whilst seismicity within the Fiji Platform is continuously active at low magnitudes (M_s <4), and characterised by sporadic moderate to large earthquakes separated by long periods (decades) of quiescence (Hamburger et al., 1990). Well-constrained earthquakes with reliable hypocentral depths show that seismicity in the Fiji Platform area is concentrated in the upper 15 to 20 km of the crust (Hamburger et al., 1990). Earthquake focal mechanisms show that NE-SW directed shortening dominates to the north of Fiji and may reflect the stress associated with sinistral slip on the Fiji Fracture Zone. However, within the Fiji Platform, north-south shortening and eastern-west extension on NE and NW trending strike slip faults are similar to those on the surrounding North Fiji Basin and Lau Basin

(Hamburger & Isacks, 1988). In addition, to shallow seismic activity, the Fiji region is also subject to deep earthquakes from the Tonga subduction interface, and these are among the world's deepest earthquakes, in excess of 600 km (Sykes et al., 1969; Hamburger & Isacks, 1987; Giardini, 1988). As these earthquakes are not important in terms of seismic hazards, they are not covered in detail in this thesis. More details on the shallow seismicity of the Fiji region is provided in Chapter 9.

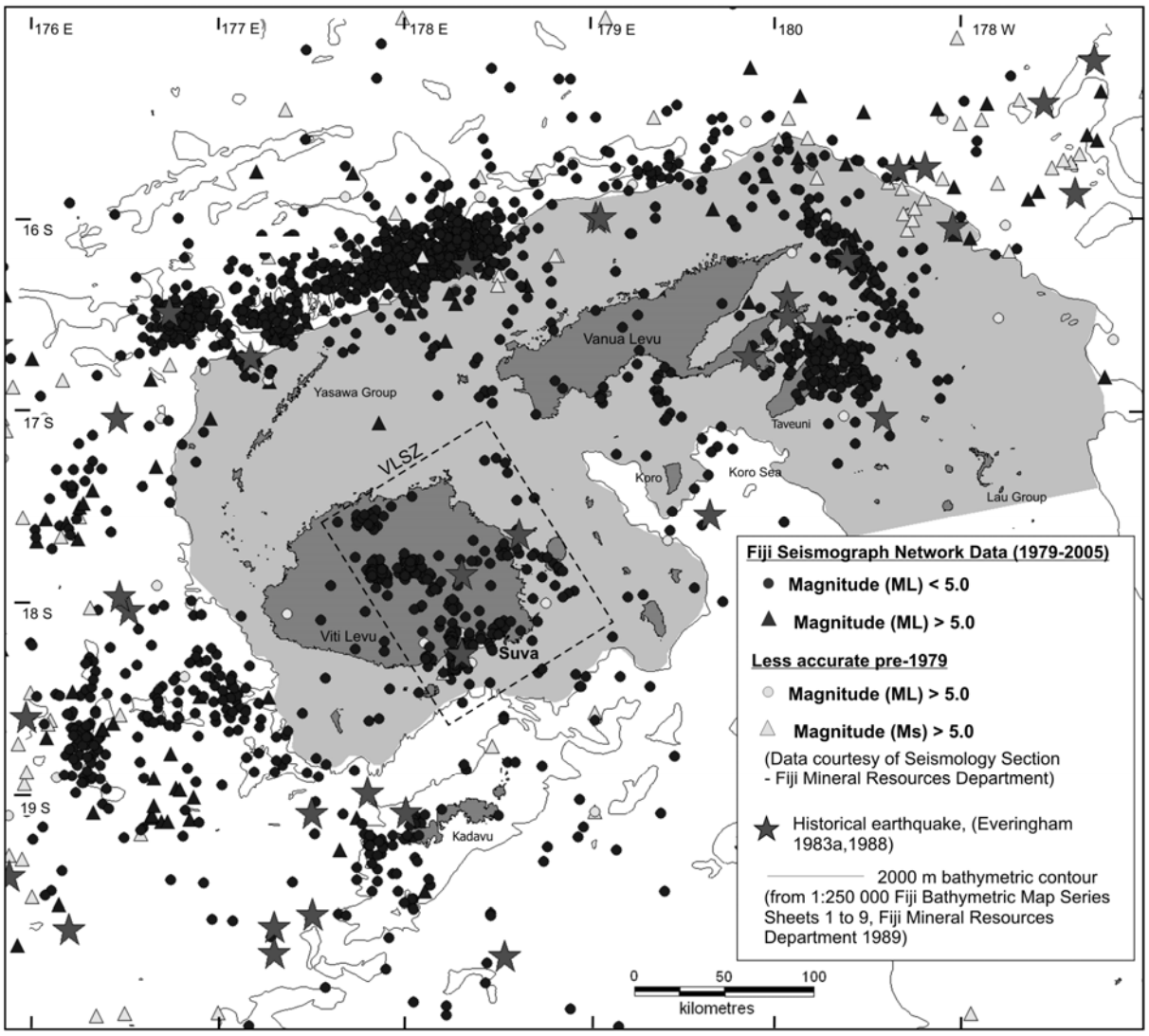

Figure 2.8: Seismicity within and around the Fiji Platform (shaded area). The boxed area shows the approximate location of the Viti Levu Seismic Zone (VLSZ).

2.6 SUMMARY AND KEY QUESTIONS

Fiji lies in the region of plate convergence between the Australian and Pacific plates in the southwest Pacific. Despite its apparent isolation from active subduction and rift zones, it is

still subject to the effects of intraplate and/or near plate boundary seismicity. It is widely agreed that Fiji has been tectonically active since at least the Late Eocene. During this time, the plate boundary near Fiji has undergone repeated reorganisation by various tectonic processes, which have repeatedly changed the tectonic setting of Fiji. The Fijian arc has faced episodes of subduction and rifting and has undergone arc fragmentation and arc rotation, and presently lies largely as a remnant arc in a broad, complex and highly deformed area between two opposing subduction zones. Current tectonic processes around Fiji can be summarised as follows; 1) subduction at the Vanuatu and Tonga Trenches, 2) accretion at spreading ridges defined in North Fiji Basin and Lau Basin, 3) transform movement along the Fiji Fracture Zone to the north and the Hunter Fracture Zone to the south, and 5) distributed extensional and shearing deformation in the area between the two transform zones, including the Fiji Platform, as result of divergence of the opposing arc-trench systems.

Paleomagnetic evidence, as well as physiographic and geological data proves that tectonic rotation has played a significant role in the development of Fiji's present tectonic configuration. This large and rapid rotation since about the Middle to Late Miocene is expected to be associated with severe deformation within the Fiji Platform. Scant geological evidence from work done within various parts of Fiji indicates that tectonic rotations may have induced significant internal disruptions within the Fiji Platform (e.g. Hathway, 1993; Begg & Gray, 2002). This deformation, however, is yet to be accounted for in a structural model for the Fiji Platform as a whole. Uncertainty on the timing of cessation of rotation of Fiji allows for the hypothesis that rotational/transcurrent stresses are still acting within the Fiji Platform today. This assumption is highly probable as current plate-motion vectors indicate that Fiji is situated within a large left-stepping transform zone between the opposing subduction zones (e.g. Hamburger & Isacks, 1988), which allows for the possibility of shear driven tectonic block rotations.

Some key questions that result from this synthesis are:

1) How is internal deformation within the Fiji Platform related to the large-scale tectonic rotation that have been observed from paleomagnetic studies?

2) Can the currently observed seismicity with the Fiji Platform be reconciled with deformation associated with the large-scale tectonic rotation?

The work presented in the following chapters of this thesis not only focuses on the assessment of seismic hazards in Viti Levu, but is also driven to address these broader and more intricate questions about the seismotectonic evolution and present-day setting of the Fiji region.

CHAPTER 3

SOUTHEAST VITI LEVU STUDY AREA

3.1 INTRODUCTION

This chapter presents a brief introduction to southeast Viti Levu, where most of the field work presented in this thesis was carried out. Viti Levu is the largest island of Fiji with an area of about 10 000 km^2. The southeast coast of Viti Levu is an important part of the country that currently serves a number of purposes nationally and internationally. Suva, the capital city of Fiji, located on the Suva Peninsula (Figure 3.1), is where the administrative, legal and commercial infrastructure of Fiji is located. Suva also accommodates a number of important regional trans-national institutions. The Port of Suva is an important trans-Pacific shipping link. The town of Nausori, 15 km to the east of Suva, is where the country's second international airport is located. A number of industries in Fiji are reliant on offshore resources and along the southeast coast of Viti Levu in particular, aggregate dredging, tourism, fishing and aqua cultural activities are quite common. The total population, which is mostly concentrated in urban areas around the Suva and Nausori metropolitan centres and the smaller towns of Lami, Navua and Pacific Harbour, and in dispersed rural settlements that fringe the southeast coast, is close to 200 000 (Fiji Census 1996). Southeast Viti Levu occurs within a seismically active area within the Fiji Platform that has experienced a number of destructive earthquakes in the past. From a societal perspective, the identification and characterisation of fault-specific earthquake sources, both onshore and offshore, and of potential tsunami generating zones offshore, will provide new insights into seismic and tsunami hazard analysis in this highly developed and populated part of the country. From a seismotectonic viewpoint, because of current seismicity in this area, it is the most promising region for exploring active tectonic deformation within the Fiji Platform.

3.2 SEISMICITY OF SOUTHEAST VITI LEVU

A broad anomalous zone of shallow seismicity occurs in southeast Viti Levu, and is referred to here as the Viti Levu Seismic Source Zone (VLSZ) (see Figure 2.8). Seismicity in this area is characterised by micro-earthquakes recorded by the Fiji Seismograph Network from a

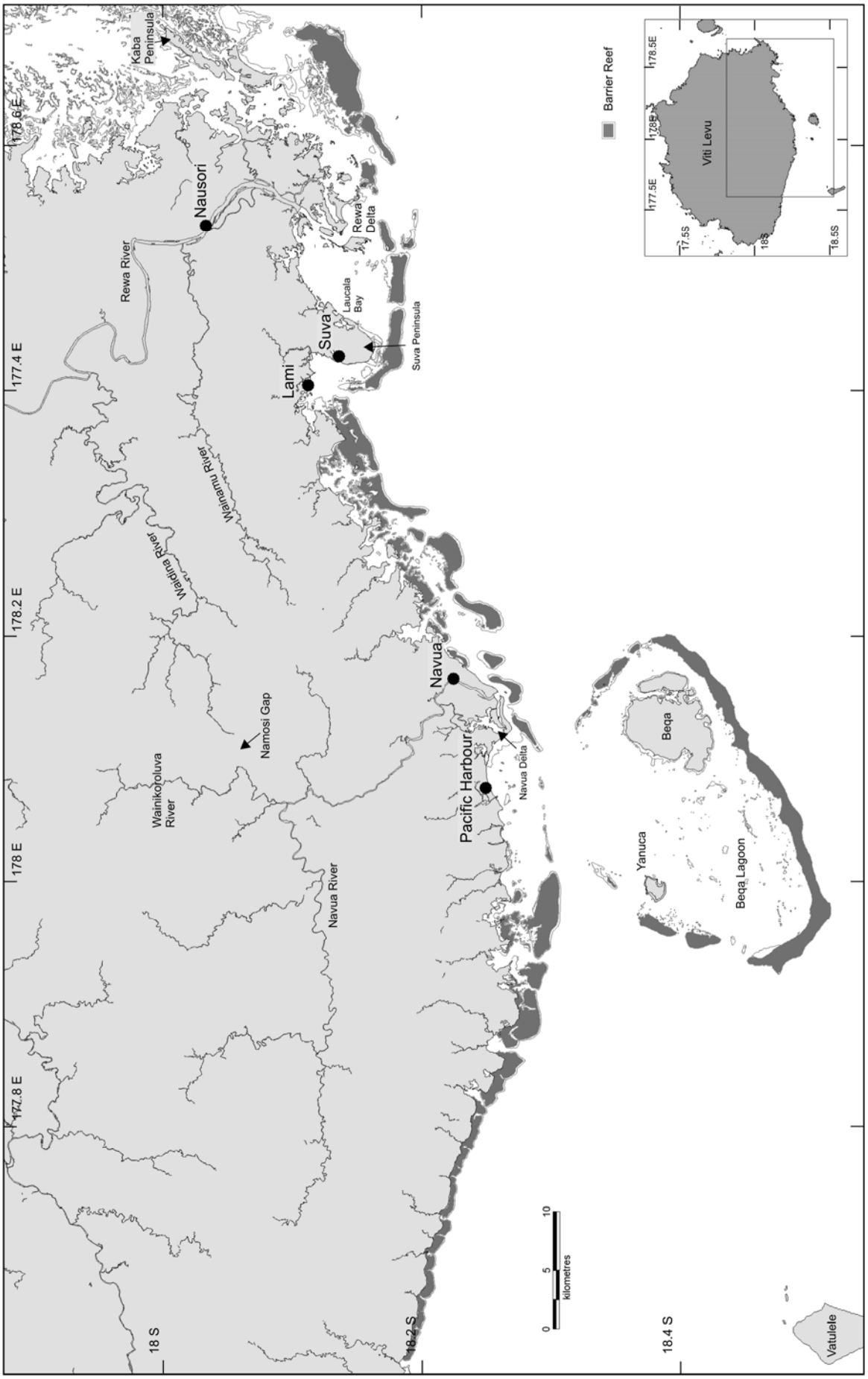

Figure 3.1: Locality map, southeast Viti Levu.

closely spaced network of stations and also larger magnitude events. All earthquakes are confined to within the top 20 km of crust, with most foci located at depths between 7 and 13 km (Hamburger et al., 1990). Southeastern Viti Levu is the location of the most destructive earthquake in Fiji's history, which occurred on the 24th of September in 1953 with magnitude M_s 6.75 (Houtz, 1962a). This earthquake induced a destructive tsunami, which had a maximum run up height of 2 m in Viti Levu. More details of this tsunami and the earthquake are given in Chapters 7 and 9 respectively. Other damaging earthquakes in southeastern Viti Levu have occurred in 1869 (M_s ~6.0), 1906 (M_s ~5.5) (Everingham, 1983a), in 1961 (M_S ~ 4.0 (Houtz, 1962b; Everingham, 1988), and another tsunami generating earthquake (M_S 5.2), which occurred about 50 km southeast of Suva in 1975 (Everingham, 1983c). The isoseismal maps of some of the major events in southeast Viti Levu are given in Figure 3.2. The future occurrence of a moderate to large offshore earthquake in this area, such as the one in 1953, will probably be associated with a tsunami attack, as well as strong ground shaking, and these pose significant hazards to the more intensively developed and populated coastal areas.

3.3 OVERVIEW OF THE GEOLOGY OF SOUTHEAST VITI LEVU

The basement rocks of southeastern Viti Levu are weakly metamorphosed (greenschist facies) lavas and volcanoclastic sedimentary rocks of the Lower Oligocene to Middle Miocene Wainimala Group and the Savura Volcanic Group (Band, 1968; Rodda, 1994) (Figure 3.3). The Wainimala rocks are intruded by Middle to Late Miocene tonalite and gabbro stocks of the Colo Plutonic Suite. Strata of the Mid to Late Miocene Tuva Group, considered to be the detritus of the Wainimala and Colo rocks, disconformably overlie the Wainimala rocks in southwestern Viti Levu (Hathway & Colley, 1994). A Late Miocene phase of deformation affects the Tuva Group and led to the pronounced arcuate ENE-striking anticlinal belt in the Wainimala strata along the axis of the Colo stocks (Band, 1968; Coulson et al., 1975). Deformation at this time is also characterised by a number of faults (Band, 1968) and development of fault-bounded NE and ENE elongated basins (Hathway, 1993).

Late Miocene to Late Pliocene volcanic and sedimentary rocks of the Medrausucu Group in the east, and Navosa Sedimentary Group in the west, overlie with a marked unconformity, or are partially downfaulted against, the Wainimala and Colo rocks (Band, 1968). The Medrausucu Group consists of volcanic rocks derived from the Namosi, Mau, Nakobalevu and Nasinu volcanoes (Rodda, 1982; Stratford & Rodda, 2000) and contemporaneous and

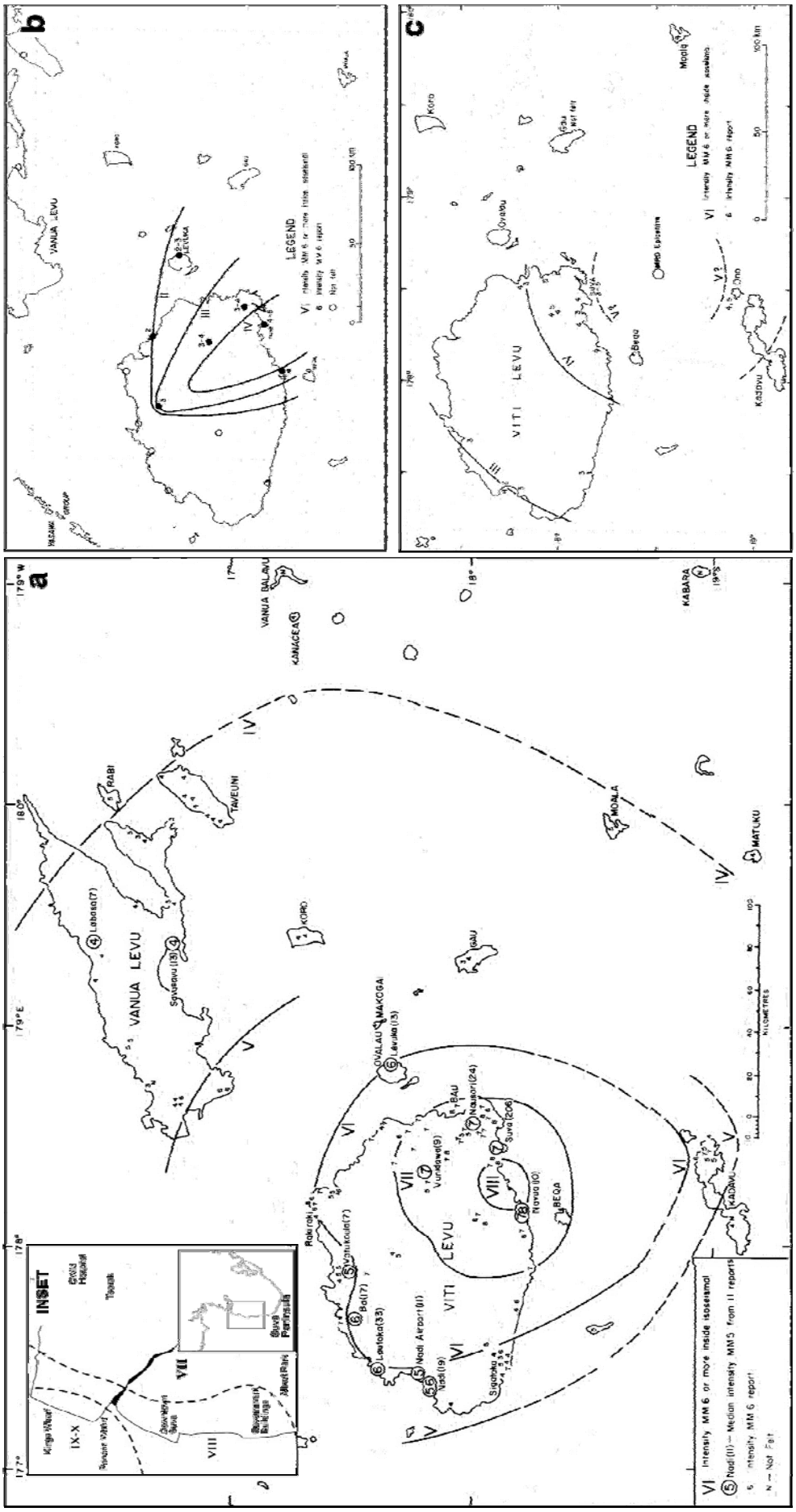

Figure 3.2: Isoseismal maps of significant earthquakes in southeast Viti Levu. All earthquake intensities are in Modified Mercalli (MM) Intensity units (see Appendix A4). (a) 1953 event, M_L 6.75 (from Everingham, 1988). Inset shows close up of isoseismal lines near Suva (from Rynn & Prasad in SPDRP, (2002). (b) 1961 event, M_L 4.0 (from Houtz, (1962b), (c) 1975 event, M_L5.2 (from Everingham, (1983c).

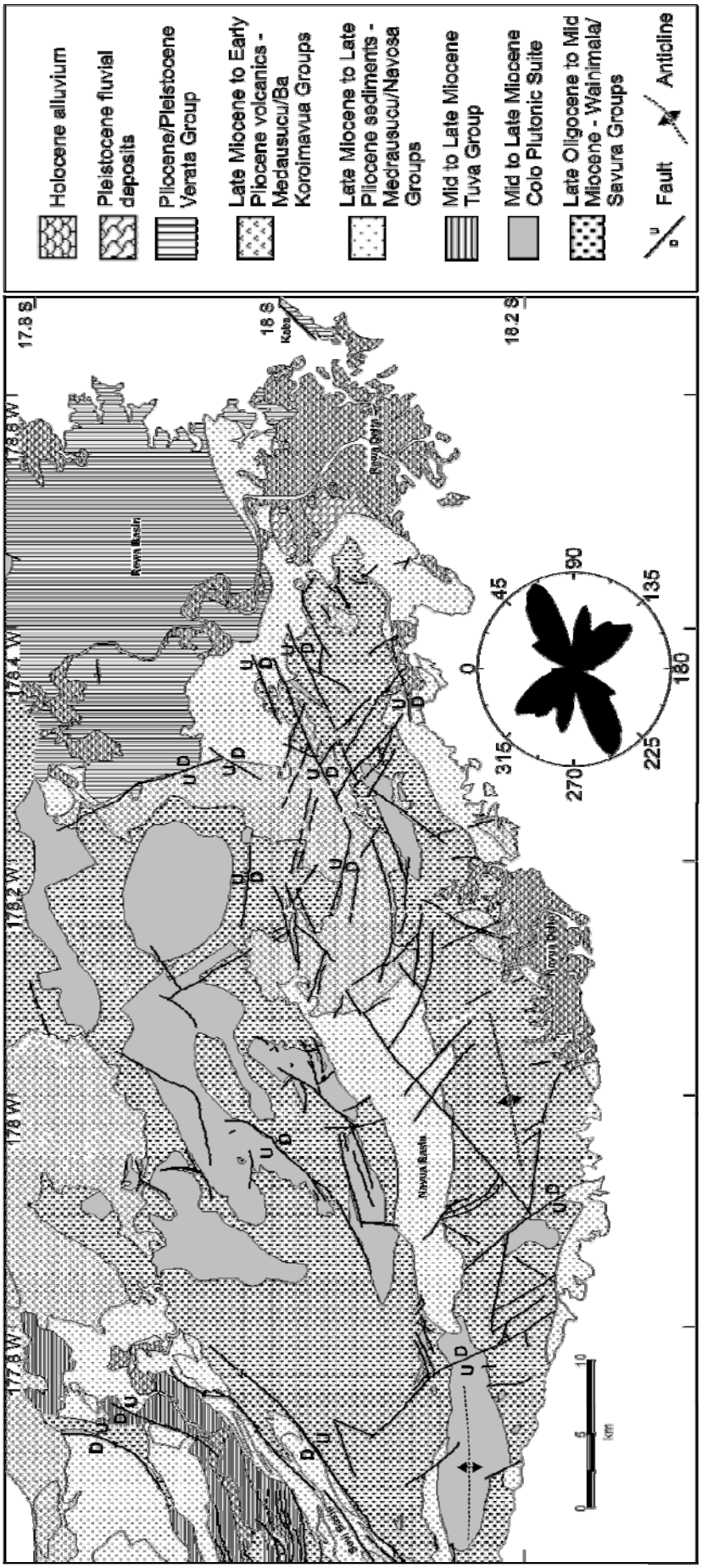

Figure 3.3: Geology of southeast Viti Levu (from Band, 1967abc; Hirst, 1966;1967; Houtz, 1960a; Houtz, 1962c; Ibbotson, 1960; Rodda, 1970; Rodda and Band, 1966). Rose diagram shows orientation of mapped faults.

younger marine sediments. The sedimentary rocks of this period occur predominantly in the down-faulted Sovi, Navua and Rewa basins in between the older basement rocks. Two other Late Miocene basins occur offshore from the southern coast of Viti Levu (Brocher & Holmes, 1985) (Figure 3.4). The ENE trending Suva Basin is located to the south and separates southern Viti Levu from the Kadavu Ridge. This basin is about 100 km wide and has maximum bathymetric depths of 2200 m. Seismic profiles in the Suva Basin reveal basin filling sediments reach over 4 kilometres in stratigraphic thickness (Larue et al., 1980; Brocher & Holmes, 1985; Holmes et al., 1985). These cover sediments overlie a faulted seismic basement, which is inferred to be equivalent to the onshore Wainimala Group. The thickness of this sediment cover decreases upslope across the basin margin toward the southeastern Viti Levu coast. The Baravi Basin is located southwest of Viti Levu and is separated from the Suva Basin by the ENE trending Beqa-Vatulele Ridge (lineament); along which occurs the Pliocene volcanic islands of Yanuca and Beqa (Band, 1968), and the predominantly limestone island of Vatulele where minor volcanic rocks of similar age occur (Whelan et al., 1985). Other Late Miocene to Pliocene calc-alkaline and shoshonitic volcanic rocks, of the Koroimavua and Ba Volcanic Groups, overlie all other rocks to the north of the study area. Late Miocene to Early Pliocene structure controlled arc volcanism and contemporaneous sedimentation in elongated basins are considered to have occurred following the disruption of the Wainimala arc and during the subsequent rotation of the Fiji arc segment (Gill & Whelan, 1989a; Hathway, 1993) (see Section 2.3.3.2).

Late Pliocene and possibly Early Pleistocene shallow-shelf strata of the Verata Sedimentary Group disconformably overlie strata of the Medrausucu Group in the Rewa Basin and other areas in the southeast (Rodda, 1982) (Figure 3.3). Pleistocene fluvial gravels unconformably overlie the Verata and older rocks along the western margin of the Rewa Delta (Rodda, 1994, 2003). Holocene alluvial and deltaic deposits occur in the Navua and Rewa river deltas. In the coastal lowland areas, several metres of Holocene inter-tidal deposits underlie alluvial cover deposits (Maeda et al., 1986).

Post-Early Pliocene deformation follows NW and NE structural trends (Band, 1968; Shorten, 1993a). NE trending faults along the coast of Kaba Peninsula, to the east of the Rewa Delta, have tilted strata of the Early Pleistocene Verata Sedimentary Group to the southeast (Rodda, 1992). A NW trending fault disrupts Holocene sediments in Suva Harbour (Shorten, 1993a).

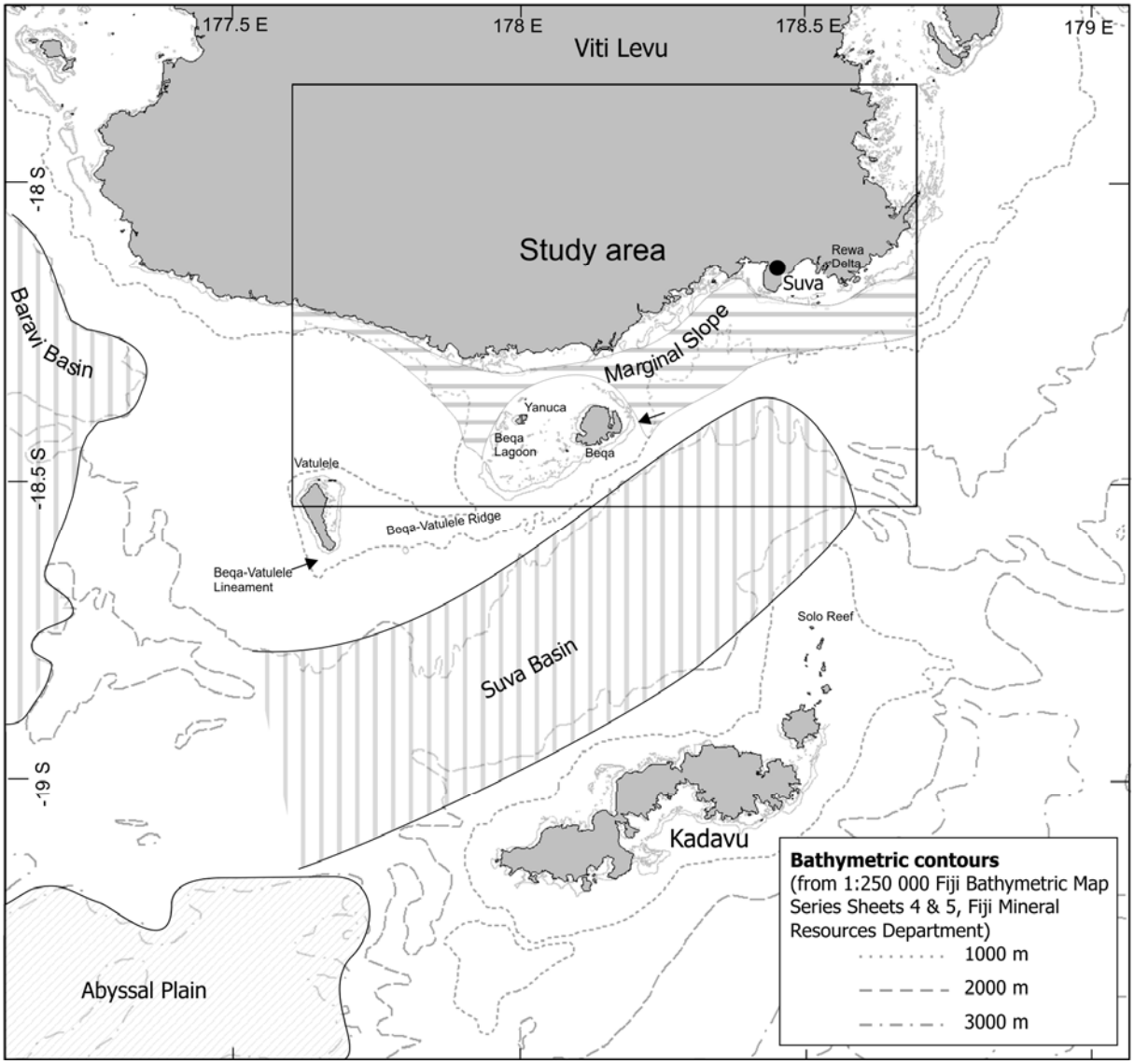

Figure 3.4: Regional bathymetric features of southern Viti Levu.

Shallow sediment cores collected in a north–south transect across the Suva Basin, from the Rewa Delta to Solo Reef in northern Kadavu (Figure 3.4), show that the surface sediments on the northern Suva basin slope and the basin floor are dominated by terrestrial-derived mud, sourced from the Rewa River (Pickering & Suda, 2003). Downslope transportation is indicated by several shallow-water species of ostracods in cores taken from the floor of the Suva Basin at water depths greater than 2000 m. The basin floor sediments also contain a significant proportion of carbonate sediments, composed of mainly planktonic forams. The slope, between the Suva barrier reefs and 500 m water depth, contains a high proportion of gravel size carbonate debris, mainly composed of benthic forams and mixed reef detritus. Gravel-sized mixtures of terrestrial and carbonate sediments occur in isolated patches at water depths greater than 1000 m indicating sediment mass flow transport from higher parts of the

slope (Pickering & Suda, 2003). At the top of the slope outside the fore reef, large coral fragments embedded in oozes indicate slumping of the outer reef flank (Schneider et al., 1995).

3.4 ONSHORE AND OFFSHORE PHYSIOGRAPHY OF SOUTHEAST VITI LEVU

The southeast coast of Viti Levu is on the windward side of the island. The highland parts of this side of the island experience between 4000 to 5000 mm of rainfall annually. Tropical rain forest is developed over the entire highland, while alluvium-covered valley floors support lighter vegetation, and mangroves flourish along much of the coast. The highland terrain, composed of the Wainimala and Colo rocks and volcanics of the Medrausucu Group, is topographically dissected almost everywhere, with creeks flowing in deeply incised valleys separated by narrow ridges with peaks over 1000 m amsl (Figure 3.5). The Navua Plateau, in the southwestern part of study area, is a broad surface eroded on various lithologies of the Wainimala, Colo and Medrausucu Groups at approximately 150 m amsl (Band, 1968). The coastal lowlands, rising to an elevation of no more than 100 m, comprise the coastal strip coming off the highlands and the plateau, include the Rewa Basin and the Rewa and Navua Deltas. The coastal strip, which includes the Suva and Muaivuso peninsulas and other, smaller peninsulas and small nearshore islands, is composed of rocks of the Medrausucu Group. The coastal plains, including the Rewa and Navua deltas, comprise Holocene landform features such as floodplains, beach ridges and peat bogs.

The marginal marine slope of southern Viti Levu is defined as the sloping seafloor between the shallow water marginal shelf and the Suva and Baravi marginal basins. The floors of these marginal basins are defined by the 2000 m bathymetric contour (Figure 3.4). Regional bathymetric maps (Smith, 1992a, b) show that the marginal slope of the Baravi Basin is steep initially for the first 10 km to depths of ~1500 m. Beyond this point it takes another 45 km to reach the basin floor edge at 2000 m depths. The marginal slope of the Suva Basin, by contrast, is more gradual. The base of this slope is reached within 25 km from the top of the slope. The seafloor gradually rises from the northern edges of the marginal basins to the southern coast of Viti Levu. The seafloor slope is locally steeper around the offshore islands of Beqa and Yanuca, south of Viti Levu. Detailed morphology descriptions of the marginal slopes of the coast of southern Viti Levu, shown in Figure 3.5, are given in Section 5.3.

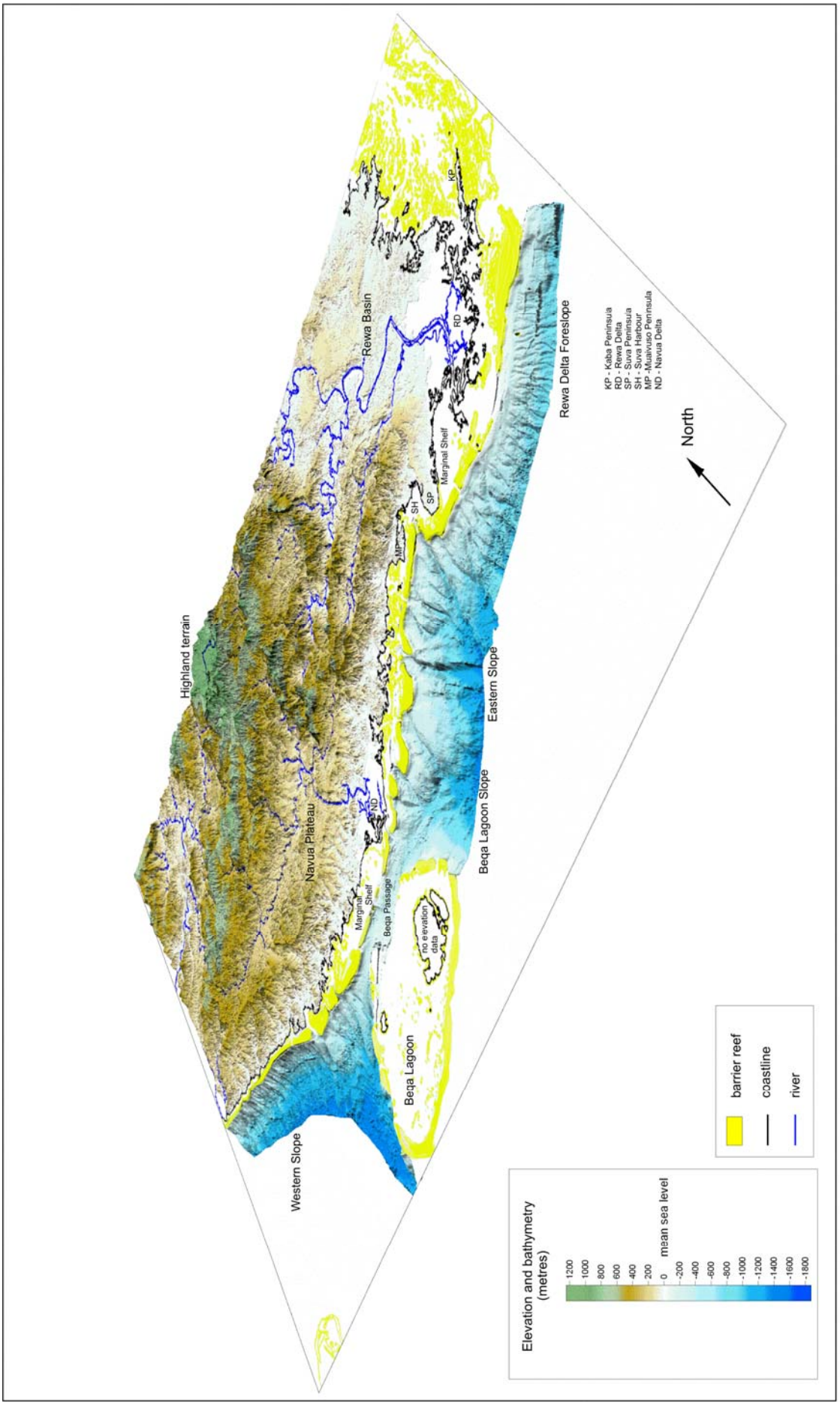

Figure 3.5: Combined onshore and near shore digital terrain model of southeast Viti Levu. The image has a X2 vertical exaggeration.

The coast of southern Viti Levu and the offshore islands are surrounded by Late Quaternary reef systems, which are built upon a shallow marginal shelf (Figure 3.5). A narrow fringing reef occurs along the southwestern coast of Viti Levu and a broader barrier reef, up to 5 km wide, occurs along the southeastern coast. The barrier reefs are sectioned by narrow deep-water passages. Beqa and Yanuca islands are enclosed within a single barrier reef system forming the Beqa Lagoon, the widest part of which reaches 30 km. As will be shown in Chapters 6 and 7, the barrier reef system plays an important role when it comes to the tsunami hazards in southeastern Viti Levu. Unstable reef front slopes contribute to tsunamigenic failures, however, the reef also acts as a natural breakwater protecting the coast from the approaching waves once the tsunami is generated.

CHAPTER 4

ONSHORE FRACTURE LINEAMENTS AND FAULTS

4.1 INTRODUCTION

A major problem with definitive field based studies of geological structure and tectonic deformation in Fiji, as well as in other tropical environments, is the lack of good bedrock exposures. Near continuous vegetation cover, deep weathering, rugged terrain and poor access all contribute to this problem. Most faults in Fiji are incompletely mapped, with isolated exposures limited to creeks in remote inland areas and to road cuts and excavations in civil construction sites in built up areas. The only places where extensive bedrock exposure can be found are on the coastal platforms at low tide. The coverage of faults and data on kinematics and chronology of fracturing are insufficient to discuss comprehensively the regional structural evolution of the islands. Over the last few years a number of high resolution remotely sensed images have been acquired for the main islands. This has presented the opportunity to investigate lineament and fracture patterns in southeast Viti Levu and to gain further insight into the regional structure and seismotectonic setting of the island.

In this chapter an innovative multidisciplinary approach is presented that combines remotely sensed imagery, geographical information systems (GIS) and geology for mapping structural lineaments. Remote sensing data is a powerful tool for mapping regional lineament patterns as they allow rapid coverage of large areas and compilations and interpretations of regional structural trends that would seldom be possible in field based studies alone. They also provide a relatively uniform coverage of data and are not restricted by exposures as is the case when collecting field structural data. Lineaments are considered to be naturally occurring, mappable linear topographic features on the Earth's surface, or linear forms at deeper levels of the crust discernible in aeromagnetic imagery (Boyer & McQueen, 1964; O'Leary et al., 1976). Mappable linear features on images of the Earth's surface are emphasised by topography, drainage, soil tones and vegetation. Lineaments on images of the magnetic basement rocks at depth can be due to covered geological contacts between rock material of different magnetic susceptibility or faults juxtaposing blocks of contrasting magnetic susceptibility. Lineaments are considered to be formed by fractures in the Earth’s crust that can be joints, faults or shear

zones (Boyer & McQueen, 1964; O'Leary et al., 1976). The characteristics of fracture systems contain fundamental information about deformational processes and can provide insights into the structural and tectonic evolution of a region (e.g. Braun, 1982; Wise et al., 1985; Cortes et al., 1998) and how ongoing deformation and seismicity may be related to tectonic setting and local structural features (e.g. Roy et al., 1993).

The use of lineament analysis in structural geology is not entirely clear of controversy. Such studies may suffer from the perception of subjectivity in the acquisition stage of lineament data (Siegal, 1977; Wise, 1982), engineering of data plots to suppress or develop components of the data to fit pre-defined descriptions, and also for lacking strictness in making inferences from the data (Wise, 1982; Wheeler & Wise, 1983). A number of methods are presented in the formally published literature that are used to overcome some elements of subjectivity, such as reproducibility tests from multiple trials, multiple observers and multiple images (Wheeler & Wise, 1983; Mabee et al., 1994). The use of running averages, standardised vertical scales and criteria for selecting peaks using statistical limits demonstrates the validity of lineament azimuth peaks in statistical plots (Wise, 1982; Wise & McCrory, 1982; Wise et al., 1985; Nemec, 1988; Fisher, 1989). There is also a need to firstly attempt to seek the origin of lineaments in the field before structural interpretation of lineaments is carried out (Mabee et al., 1994).

This chapter presents an approach for structural and tectonic analyses in a region where this is hindered by the paucity of exposures, through utilising the inference about lineaments (geomorphic and magnetic) identified from remote sensing imagery as two dimensional expressions of crustal structure. The key objectives are to map lineaments in the southeast of Viti Levu using multiple imagery and multiple trials, check their validity, and demonstrate that the most robust sets of lineaments identified are related to fractures mapped on the ground and are of tectonic origin. These features then allow for regional structural and tectonic interpretations and seismic hazard analyses, which will be addressed in later chapters.

4.2 METHODOLOGY

The lineament analysis procedure was carried out in four main steps that included: 1) the acquisition of lineament data from multiple imagery; 2) their analysis to select those that are significant; 3) their presentation as statistical and spatial plots; and 4) their comparison with

field fracture data. Each of the steps involved the use of clear definitions and strict statistical rules, which are outlined in the flow diagram presented here as Figure 4.1.

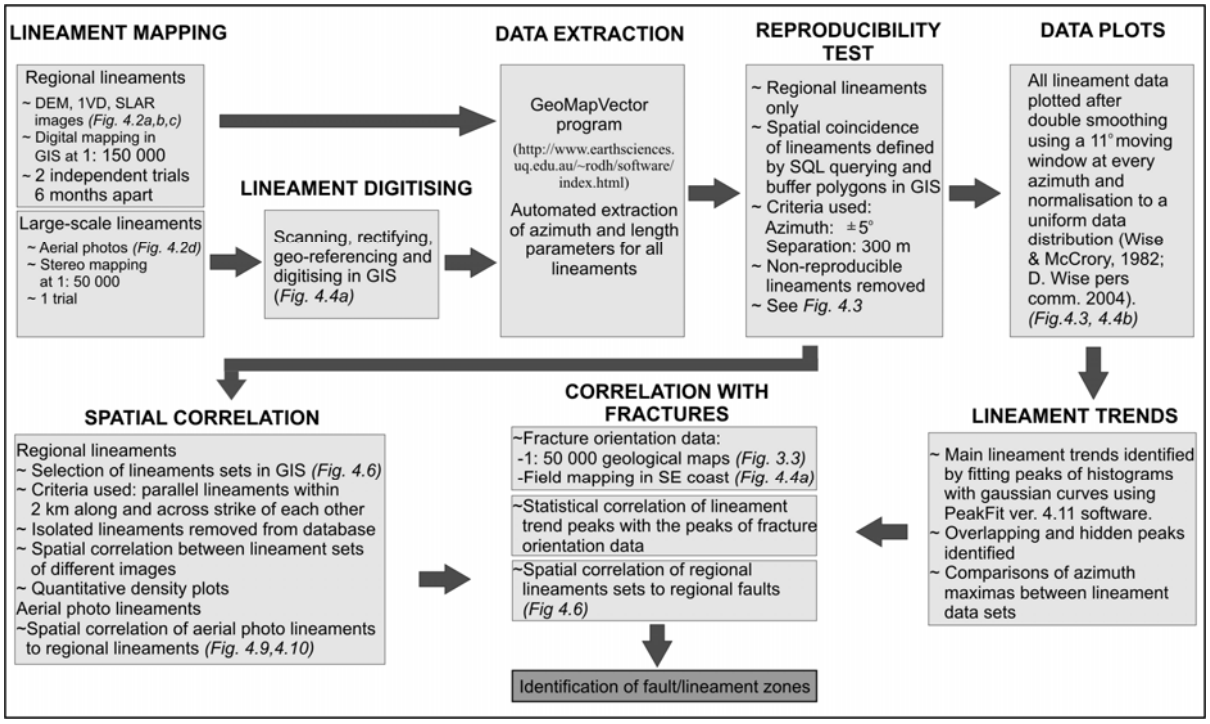

Figure 4.1: Flow diagram indicating the various steps used in the acquisition, statistical and spatial analyses of lineament data, their subsequent correlation to mapped fracture data and identification of fault/lineament zones.

4.2.1 Description of remote imagery

Shaded relief images of a digital terrain model (DTM), side-looking airborne radar (SLAR) images, an aeromagnetic image and aerial photographs were utilised to map lineaments (Figure 4.2). The DTM, SLAR and magnetic images have complete overlap with each other. Aerial photographic coverage includes the southeastern half of the area covered by the other images. The local Fiji Map Grid (FMG) (www.sopac.org.fj) was used as the reference coordinate system for all images and spatial data sets.

A digital terrain model for southeastern Viti Levu was prepared from 20 m topographic contours originally derived by photogrammetric methods and field surveys (Department of Lands and Surveys, Fiji). The contour lines from digital topographic maps were converted to points using automated software, and exported as an ASCII file with X and Y co-ordinates and heights values into the Surfer© program. The point data were gridded in Surfer© using ordinary point kriging method, with a linear variogram, search radius at 500 m with 8

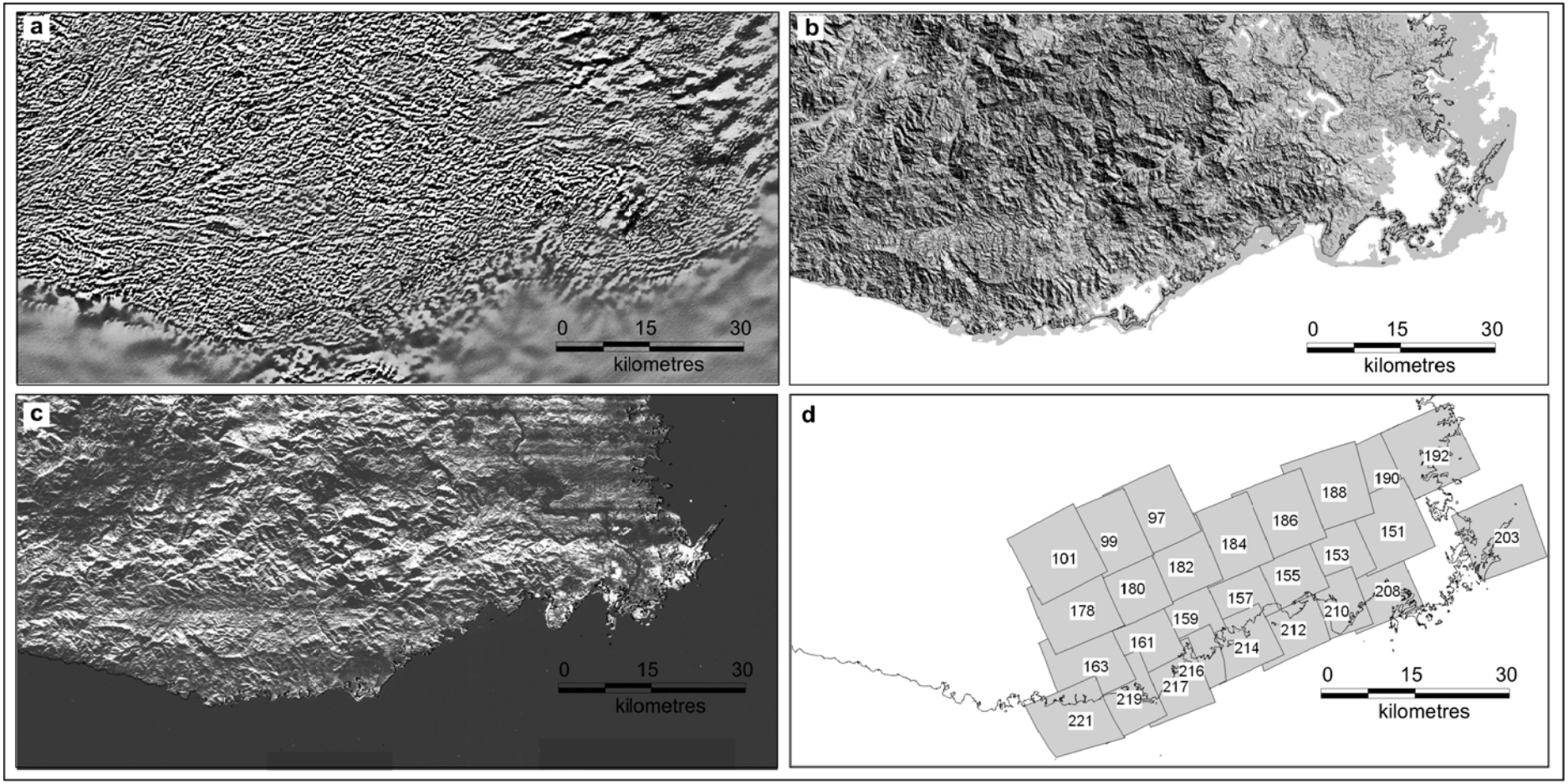

Figure 4.2: Remote sensing imagery used for mapping lineaments in southeast Viti Levu: (a) first vertical derivative of total magnetic intensity (1VD); (b) digital terrain model (DTM); (c) side looking airborne radar (SLAR); and (d) mosaic of aerial photo coverage.

minimum points and grid size set at 20 m.

SLAR images (north and south looking) for the two largest islands of the Fiji group were acquired in 1984 by Bercha Company, probably by a standard side-looking airborne system using K-band (wavelength about 1 cm) microwaves (Mallick & Habgood, 1987). The original hardcopy images (north and south look) for southeast Viti Levu, available at 1: 250 000 scale, were used in this study. The SLAR image is an image of the surface morphology. The main factors controlling the intensity of the radar signal are the incidence angle of the radar beam relative to the local topographic slope, roughness of the surface relative to the wavelength of the radar and electrical properties of the surface material. Maximum responses are from slopes perpendicular to the radar beam and in southern Viti Levu, where moisture content is high, penetration is minimal, reflection is therefore almost complete and thus represents the morphology of the rain forest canopy.

Aeromagnetic data were acquired by the Australian Geological Survey Organisation in 1997 at 80 m elevation, 400 m line spacing at 330 degrees from true North and tie lines at 4000 m spacing at 60 degrees from true North (Gunn et al., 1998). The first vertical derivative (1VD) of the total magnetic intensity reduced to the pole colour image (with north-south sun angle) was used to derive lineaments. The image by being reduced to the pole, corrects for the asymmetry of magnetic anomalies relative to their source. This asymmetry is caused by induction of the Earth's magnetic field, which has an inclination of 38.37 degrees over Fiji. The total magnetic intensity image produces broad anomalies due to interference between adjacent bodies and causes difficulties in delineating body boundaries. Also deeper strongly magnetic bodies mask the shallow less magnetic bodies in the total magnetic intensity image. The solution to this is to calculate the derivatives of the magnetic field. The anomalies shrink in width and it is more representative of the boundaries of the source body. The first vertical derivative image used in this study enhances fine detail, suppresses broad magnetic anomalies and suppresses the effects of deep magnetic intrusions and thereby allows easier mapping of near surface features.

A set of black and white vertical aerial photos of the Department of Lands and Surveys, Fiji, taken in 1994 at approximately 1:50 000 scale, along N70^{o} E trending flight lines were also used in this study.

4.2.2 Analyses of lineaments

4.2.2.1 INTERPRETATION OF REGIONAL LINEAMENTS

Regional lineaments were identified and mapped from the 1VD, DTM and SLAR images. Various shaded relief images of the DTM were produced using a variety of sun angles and azimuths at 1:150 000 scale. A first-pass lineament interpretation was then completed on hard copies using acetate overlays. The final interpretations were done by drawing the lineament lines onscreen in the Surfer© program with the aid of three-dimensional topographic models which could be rotated onscreen. Systematic application of lighting direction was used to create various illumination and shadow effects (shaded relief) from eight azimuths (0, 45, 90, 135, 180, 225, 270, 315) with source at 45^{o} to the horizontal. The digitised lineaments were directly imported into GIS using linear transformation. Hard copies of north- and south-looking SLAR images were scanned and geo-referenced using control points from 1:50 000 topographic maps. The geo-referencing process yielded positional errors of fewer than 12 pixels, which equate to about 200 m on the ground. Lineaments were then mapped at 1:150 000 and 1: 300 000 scales, largely based on morphological (textural) grounds; a few were recognised as tonal lineaments in areas of low relief and were not processed or recorded further. This was done on screen on a vector layer in GIS. Lineaments were then drawn ranging in length from 1 km to greater than 10 km, the lower limit arbitrarily chosen to include all lineaments considered to be of regional significance. Lineaments from the north and south looking SLAR data were then combined to produce a single SLAR lineament map. The 1VD image was available digitally in GIS, geo-referenced to FMG and lineaments were directly interpreted on a line vector layer at 1:150 000 and 1: 300 000 scales. Lineaments were drawn to show boundaries of areas with contrasting magnetic intensity. Lineaments from the DTM, SLAR and 1VD images were mapped again six months after production of the first set (trial 2), using the same procedure as outlined above, to produce a second (repeat) set of lineament maps.

4.2.2.2 INTERPRETATION OF AERIAL PHOTO LINEAMENTS

Large-scale lineaments were delineated from aerial photographic interpretations. This was done using a large wing-mirror stereoscope, by plotting linear geomorphic features such as drainage channels and scarps on acetate overlays marked with reference co-ordinates. The

lineaments were then digitised on screen in GIS after scanning, rectifying and geo-referencing the overlays using control points from 1:50 000 topographic maps. The rubber sheeting rectification process was applied to the overlays in AutoCAD© AutoDesk-Map Overlay software. An average of 10 ground control points was used in each 11 km X 11 km photo. Geo-referencing the overlays in MapInfo© GIS software resulted in pixel errors that were fewer than 10, ie. <40 m on the ground. Cultural features such as roads, fences and power lines were avoided when inspecting aerial photographs. No other images contained cultural or man-made linear features.

4.2.2.3 LINEAMENT DATA EXTRACTION

Large numbers of lineaments drawn from various data sets required the use of an automated program to extract azimuth and length parameters for all lineaments. The GeoMapVector program (http://www.earthsciences.uq.edu.au/~rodh/software/index.html) was used. This program generated a file that contained the trend of each line measured clockwise from the north and its length. The azimuth values were read to the nearest integer and the length of lineaments were read to the nearest metre. This technique did not allow for recording curvilinear features and as such, curvilinear lineaments with significant azimuthal deviations were digitised as segments with the minimum number of components possible, in order to preserve the original orientation of the lineament.

4.2.2.4 REPRODUCIBILITY TESTS

In this study the reproducibility of lineaments was tested by comparing spatial coincidences and statistical orientation peaks of lineaments datasets generated from multiple trials and multiple images. Spatial reproducibility tests were carried out by comparing lineaments between lineament maps generated from two independent trials of each regional image, by comparing lineaments in compilation maps generated from the various regional images, and by comparing regional lineaments maps to larger scale aerial photo lineaments maps. Azimuth peak reproducibility was examined by comparing orientations peaks of the various regional lineament datasets and the aerial photo lineament dataset. The spatial reproducibility tests were done by using specified criteria for spatial coincidence in GIS. Coincident lineaments were defined as those that have azimuths within $\pm 5^{o}$ and separation distances within 1 - 2 mm at the scale of drawing (Wise et al., 1985; Mabee et al., 1994). The spatial reproducibility tests

were done in MapInfo© GIS software using a combination of buffer analysis and Standard Query Language (SQL) querying technique (see Appendix 5).

4.2.2.5 DATA PLOTS

All data are presented as histograms of azimuth frequency on linear graphs or rose diagrams that were generated after double smoothing by applying an 11-degree moving-average window on every azimuth. The odd number for counting window width was chosen to avoid skewing the data. The value on the radius of the rose diagram and Y-scale on linear histograms are the data concentration factor - DCF (Wise & McCrory, 1982), which simply represents the number of times the data are concentrated beyond what is expected from an absolutely uniform data distribution. The linear curves graphs were drawn in such a way that one unit of the concentration factor along the vertical scale is always equal in length to 10 degrees of azimuth on the horizontal scale. The peaks of all lineament azimuth histograms curves were fitted with Gaussian curves using the PeakFit software (http://www.systat.com/). This program allowed the separation of overlapping peaks and recognition of peaks that are hidden on the histograms. The above procedures eliminate the vertical scale problem and binning problem in statistical plots, highlighted in “Rule 13” and “Rule 14” of Wise (1982).

4.3 MULTIPLE TRIAL REPRODUCIBILITY TESTS

More than 400 regional lineaments are mapped in each trial interpretation of the 1VD, SLAR and DEM images (Figure 4.3). Average lengths from all trials are generally from 2 km to 4 km. The longest lineaments are mapped from the 1VD image and are in the order of 25 to 35 km long. The longest DEM and SLAR lineaments are much shorter, around 10 to 13 km, although they appear to form part of continuous lineament sets. The results of the multiple-trial reproducibility tests show that the percentage of coincident lineaments ranges from 35 % to 43% for all images. The average lengths of reproducible lineaments from all images are higher than those from the individual trials. This shows that longer lineaments in all images had a higher degree of reproducibility than shorter ones. Non-reproducible regional lineaments were removed from the database.

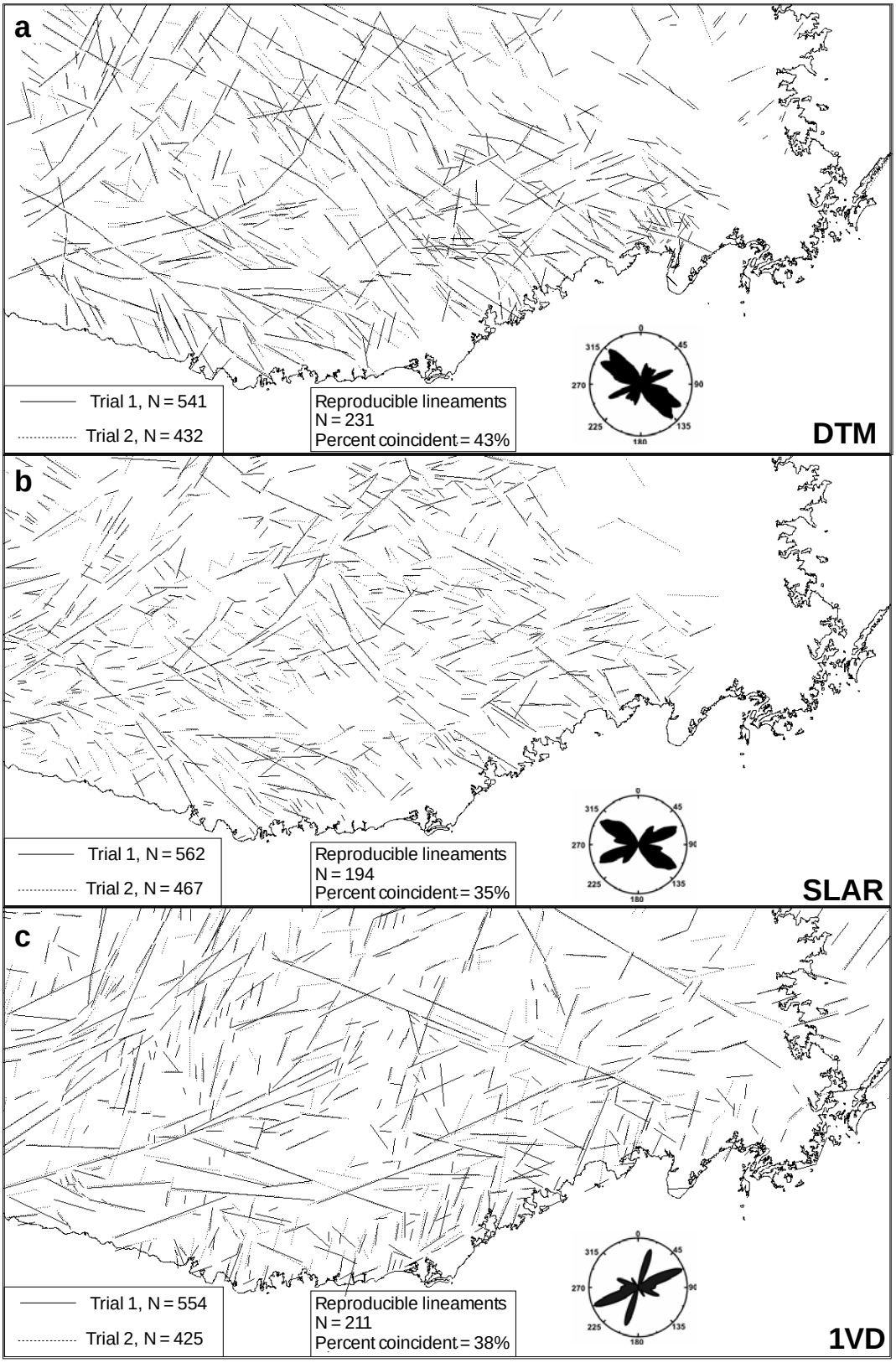

Figure 4.3: Interpreted regional lineament sets produced from two trials. Compilations are from (a) DTM image (b) SLAR images (c) 1VD image. Rose plots show the orientation peaks of reproducible lineaments from each of the data set. The number of lineaments in each trial and the number and percent of reproducible lineaments are also indicated.

A total of 4278 lineaments were mapped from aerial photographs (Figure 4.4a). Multiple-trial reproducibility tests were not performed on the aerial-photo lineaments as the first set was interpreted at a high level of detail. An indirect test was used to check for reliability of the data. Each aerial photo was interpreted independently of the others and the photos from the runs in the north, with numbers between 97 and 101, and 178 and 192 (see Figure 4.2d), were interpreted six months after the interpretation of the southern half. Subsequent merging of the data shows continuity of lineaments across the photo boundaries.

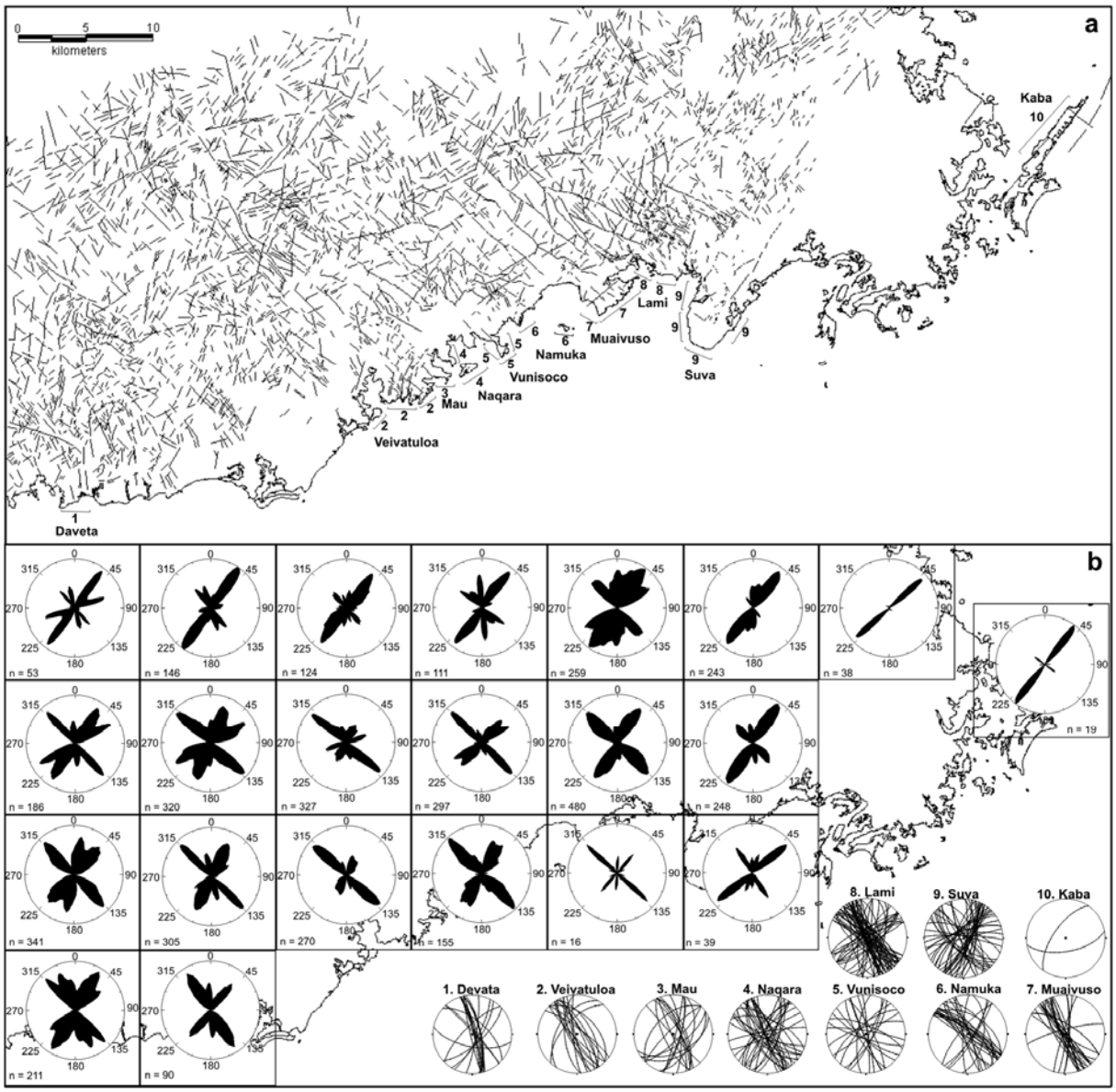

Figure 4.4: (a) Map of lineaments determined from aerial photo interpretations. (b) Rose plots show the orientation of lineaments in the cells of a 10 km x 10 km square grid of the lineament map. The number of lineaments in each cell is also indicated. Lower hemisphere stereonets show attitudes of representative fracture data collected at sites along the coast labelled in (a).

4.4 LINEAMENT TRENDS

4.4.1 Regional lineament trends

A quantitative analysis carried was out to determine the orientation patterns of reproducible regional lineaments. The major trends of regional lineaments were identified by checking for coincidences of azimuth peaks from the lineament azimuth histograms. Parameters of peaks were determined by deriving the mean azimuth, height and azimuthal width at half height of the Gaussian peaks. The coincidences of these peaks were checked by comparing the positions of the width at half peak height parameter to derive major trends. The peaks from one image coincided with or overlapped peaks from at least one other image. This result is another successful test of the reproducibility of regional lineaments, this time between multiple images. Three major regional lineament trends were identified. The trends are NW (280^o to 345^o), NE (10^o to 45^o) and ENE (55^o to 77^o) as shown in Figure 4.5. The broad azimuth ranges shown by the data are probably due to the curved nature of some continuous lineaments sets. A general summary of regional lineament trend characteristics is given in Table 4.1.

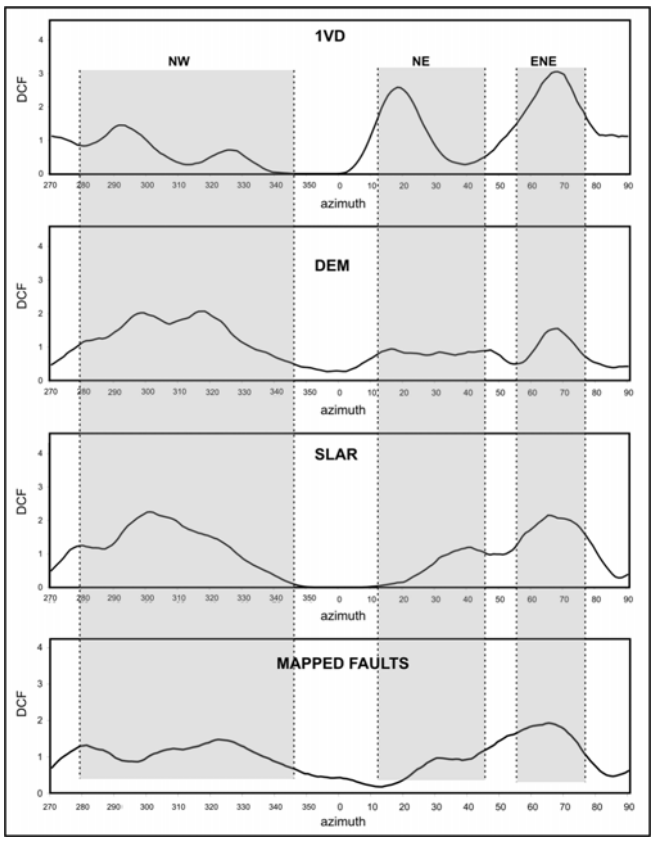

Figure 4.5: Linear histograms of azimuth frequency of reproducible regional lineaments and mapped regional faults, showing three major trends.

Table 4.1: Summary of reproducible regional lineament trend characteristics.

Trend	Azimuthal range	No. of Lineaments	%
NW	280 to 345	272	43
NE	10 to 45	119	19
ENE	55 to 77	149	23
Lineaments not belonging to any trend		96	15
Total		636	

The ENE trend occurs as a strong peak in all the images. The NW trend forms a broad peak in the DTM and SLAR images and covers a broad swath of azimuths ranging from NW to WNW. By comparison this trend on the 1VD image is subdued and shows only two small peaks at about NW and WNW. The 1VD lineament map indicates that even though the NW trend comprises a small number of lineaments, they are prominent and lengthy. The NE trend, however, forms small peaks in the DTM and SLAR images, but is quite prominent on the 1VD image. The prominence of this trend on the 1VD image may be partly attributed to a directional bias introduced during processing of this data. There is an absence of lineaments in the sector 45^o east and west of north on the SLAR image. Lineaments may be hidden in this sector by shadowing effects caused by the north and south sun angle used on the SLAR images. Lineaments are present within this sector in the DTM image where multiple sun-angle directions were applied. Overall there is a generally good correlation between the peak orientations of the surface SLAR and DTM lineaments and between peaks of these surface lineaments and the peaks of magnetic lineaments at depth.

4.4.2 Aerial photo lineament trends

Given the large number of aerial photo lineaments mapped, the area covered by these lineaments was subdivided into 22 ten-square-kilometre grid cells, and the azimuth frequency of lineaments within each cell was considered separately (Figure 4.4b). This was done to determine local azimuth peaks, which would have been hidden in the azimuth frequency histogram of the entire data set. This approach also allows for correlation between peaks of adjacent cells and the mapping of zonal distribution of lineaments with uniform azimuth. The major lineament trends shown by local azimuth peaks are NW (311^o to 340^o), NE (9^o to 48^o) and ENE (52^o to 72^o). A minor trend is also identified that has azimuth range 0^o to 7^o (N). The NW trend is prominent in all except the northernmost row of cells and represents continuous

NW trending lineaments in the southern half of the lineament map. NE lineaments form prominent peaks in almost all cells. The ENE trending lineaments are predominant in the cells in the northwestern sector of the mapped area. The minor N trend appear as small peaks in a few cells and do not appear to show any particular zonal distribution.

4.4.3 Comparison between regional lineament trends, aerial photo lineaments trends and fault/fracture trends

There is a good statistical correlation between the major trends of the regional lineaments and the aerial photo lineaments. The minor N trend of aerial photo lineaments do not appear in the regional data sets. This may be partly due to directional bias in the regional images. It is also possible that the N trend represents an older structural fabric in Viti Levu, as has been shown by field mapping in southeast Viti Levu (Shorten, 1990). These lineaments are probably disrupted by younger lineaments and do not appear as significant lineaments at regional scales.

The main trends of the mapped lineaments also show a good statistical correspondence with the main orientations of faults mapped in the field. The azimuthal ranges of the main NW, NE and ENE regional lineament trends are replicated in the linear histogram of the regional fault data (Figure 4.5). The fault orientation data used for this plot were compiled from published 1:50 000 geological map sheets of the Fiji Geological Survey mapped between 1960 and 1970. They include only those faults that have been confirmed by field mapping and do not include “inferred faults” that are commonly seen in regional geological maps.

The NE, NW, ENE and N trends of aerial photo lineaments also show a good correlation to fractures (faults, joints, shear zones) that were mapped in this study on the well exposed coastal platforms of southeast Viti Levu. Representative fracture data are presented in lower hemisphere stereonets in Figure 4.4b. The data on fractures were collected from over 70 coastal exposures, and close to 500 fractures planes were measured (see Figure 4.10). The majority of the fractures are joints, while others are faults with either lateral, oblique lateral or normal slip. Most of the fracture planes show steep dips ranging from vertical to ~60^{o}, consistent with the straight traces of lineaments over undulating topography. There are no prominent folds in bedrock along the southeast coast, and bedding generally dips less than 10^{o} to the SSE. There are many peninsulas present along this generally ENE trending section of

the coast (e.g. Suva, Muaivuso and Vunisoco). The total amount of exposure, therefore, is sufficient to remove any directional bias that may exist in collecting data along only one orientation of the coastline.

In summary there is generally a good statistical correlation between the trends of the lineaments and the trends of the mapped fault and fractures. In the next section I present an analysis of the spatial distribution of lineament sets, individual lineaments and mapped faults to further demonstrate this relationship.

4.5 SPATIAL DISTRIBUTION OF LINEAMENTS

The spatial distribution of regional lineaments appear to be even throughout the study area and independent of lithology, except for the areas coinciding with the Rewa Basin and Navua Delta, where there are relatively lower numbers of lineaments. This is due to the presence of Quaternary cover sediments in which the lineaments cannot be identified. As with the regional lineaments, the concentration of aerial-photo lineaments is low in the Rewa and Navua Deltas. There is a greater concentration of aerial photo lineaments in areas of volcanic rock such as those on the Savura Volcanic Group in the southeast and the Namosi Andesite in the central part of the mapped area (see Figure 3.3).

4.5.1 Regional lineaments sets

The most continuous and through-going sets of reproducible regional lineaments were selected from the database for each of the images (see criteria in Figure 4.1). Extraneous and isolated lineaments where removed. Six prominent lineament sets were identified from each of the images as shown in Figure 4.6a,b,c. The through going lineaments sets from the various images were then compared for spatial coincidence in GIS. The geographical extent of every lineament set from one image was found to have an excellent spatial correspondence with lineament sets from the other images over the same area. All images show i) a 10 to 15 km wide NE to NNE lineament set in the NW of the study area, ii) a 20 to 30 km wide NW to WNW set in the SW, iii) a continuous narrow zone of ENE to NE set passing from the SW through to the central north, iv) a broad ENE set in the central SE and a narrow ENE set in the central north, v) a broad continuous NW to WNW set extending from the SE coast to the NW, and vi) a weak NE set confined to the SE region.

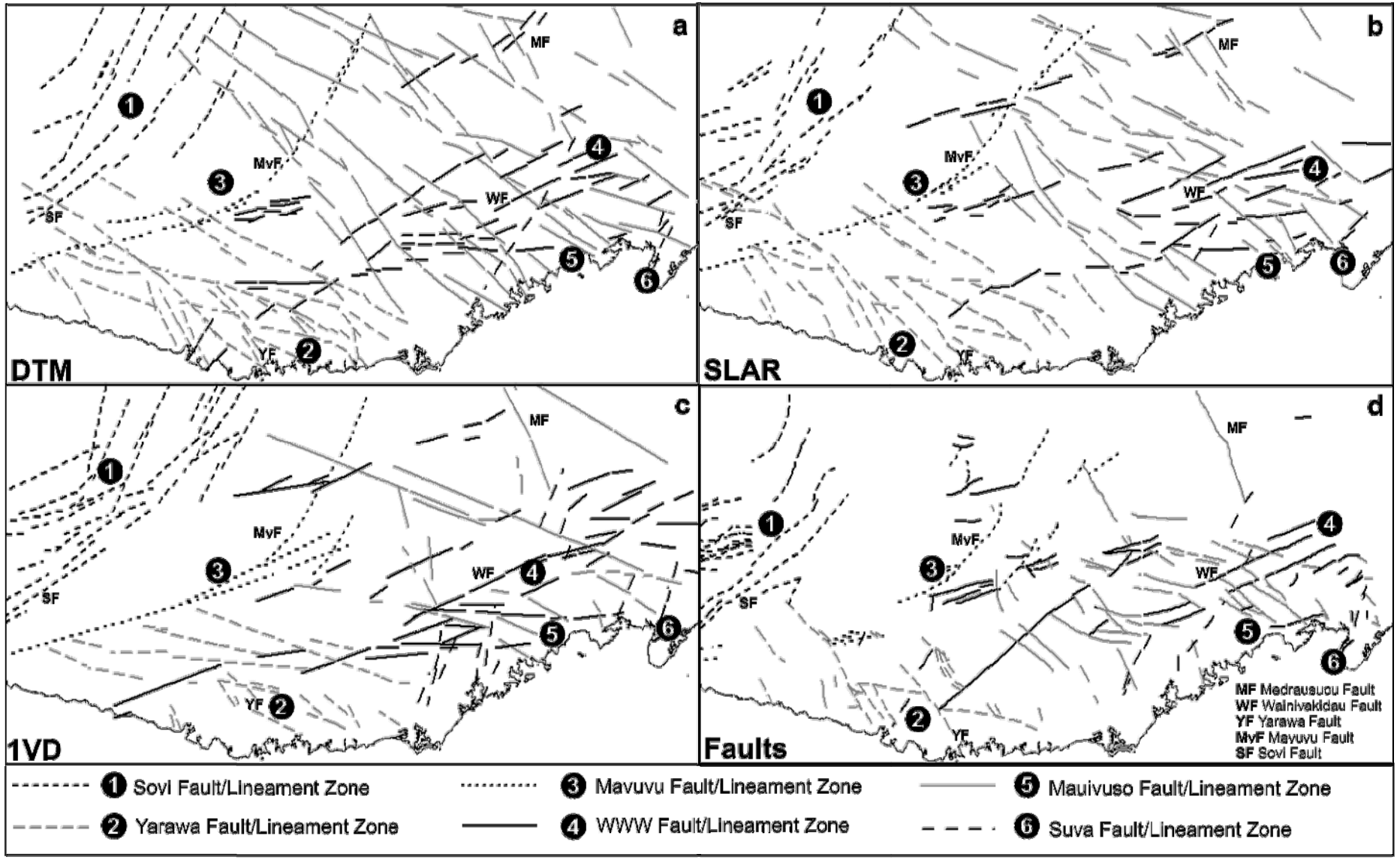

Figure 4.6: Spatial comparison of regional lineament set compilation maps of (a) DTM, (b) SLAR, (c) 1VD images and (d) field mapped regional faults. Six spatially coincident fault/lineament zones are labelled. Also labelled are individual faults that show excellent correlation between the datasets.

4.5.2 Quantitative density plots of regional lineaments

The spatial distributions of regional lineaments sets were checked quantitatively by plotting density contour maps. The reproducible lineaments from the 1VD, DEM and SLAR images were combined to create a single map of regional lineaments. Each of the lineaments in the combined set was assigned to one of the major trends defined by the regional lineaments statistics. If a lineament had an azimuth that fell within the range of the trend, it was assigned to the trend. Density contour maps were created using the density tool in the spatial analyst of ARC© GIS software. The density maps were created with a 4-km search radius at every 50 x 50 m cell of the study area. The numbers of lineaments falling in the search area were summed and divided by the search area to get each cell's density value. The kernel method was used whereby lineaments closer to the centre of the raster cell were weighted more heavily than those further away. The spatial distribution of the main trends of regional lineaments are shown in Figure 4.7. The shaded areas represent the density of two lineaments per 10 square kilometres and may define lineament swarms, which shows areas of closely spaced sub-parallel lineaments that appear to have geographic continuity. Most of the swarms have lengths which are of the order of tens of kilometres and their shapes are elongated parallel to the trend of the set. The density plots quantitatively replicate the distribution of the six major regional lineaments sets previously defined (see Figure 4.6).

4.5.3 Spatial correlation between regional lineaments and regional faults

The lineament sets were checked for spatial correlation with mapped faults (Figure 4.6d). It was found that the extent of each of the six lineament sets correlated either fully or in part with a major fault zone of similar orientation mapped in this part of Viti Levu. Fault zones on Viti Levu represent zones of shearing comprising multiple fault strands rather than a single structure. Careful checking revealed that the trajectories of some individual lineaments, which were fully or partly reproducible on all the images, corresponded with the exact location of a known fault mapped on the ground. This relationship is clearly shown by the corresponding lineaments of five mapped faults; the Wainivakidau Fault (WF), Medrarusucu Fault (MF), Mavuvu Fault (MvF), Yarawa Fault (YF) and the Sovi Fault (SF), and are labelled with abbreviations on all the maps in Figure 4.6. The close spatial correlation between the lineaments and mapped faults imply that the lineaments largely represent fractures in the bedrock and are of tectonic origin.

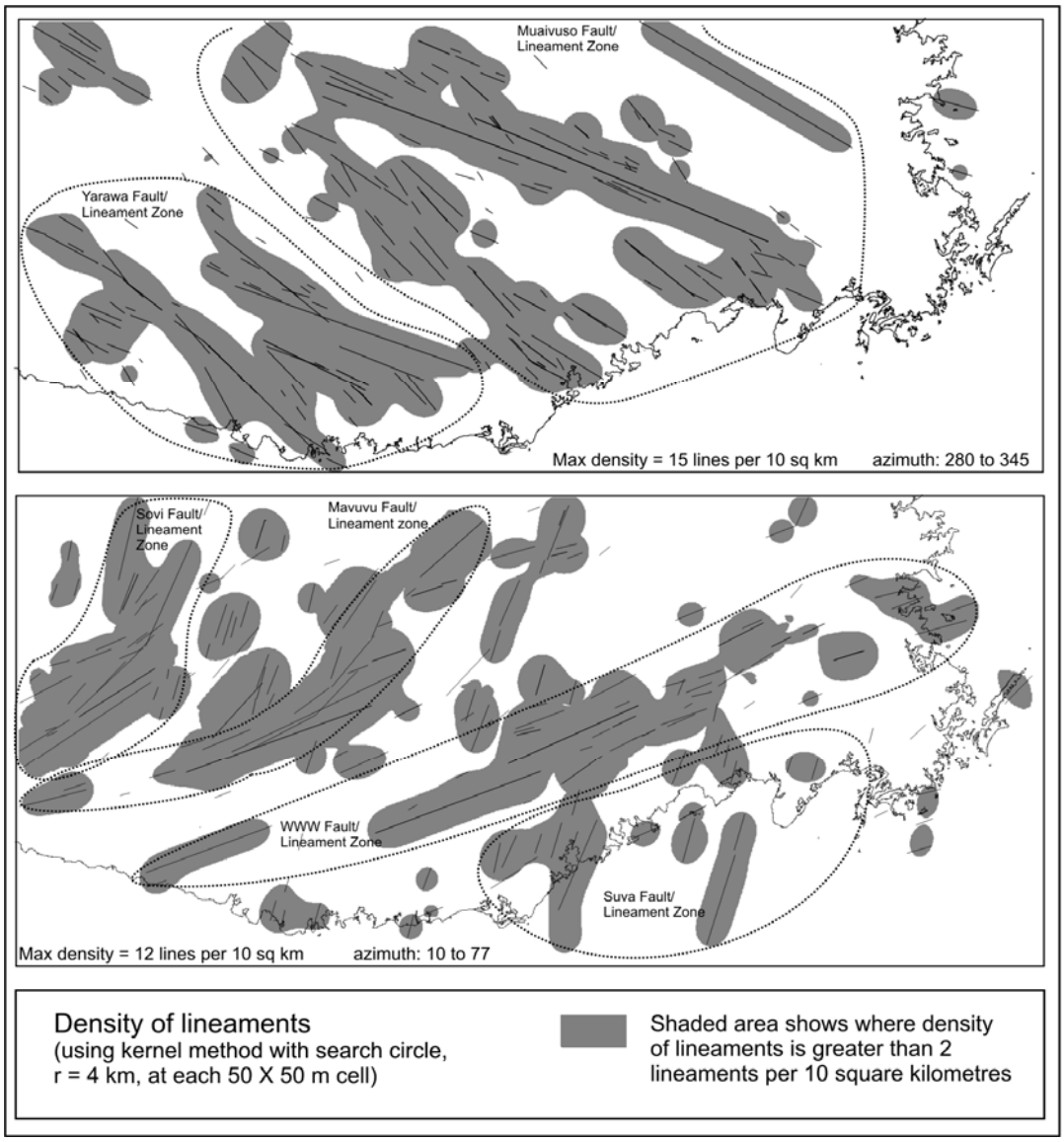

Figure 4.7: The spatial distribution of the main trends of regional lineaments shown as density maps. The high density areas correspond to the six major regional lineament sets.

4.6 GROUND EXPRESSION OF SURFACE LINEAMENTS

Using a small example area of southeast Viti Levu it is shown that individual reproducible (multi-trial) DTM lineaments correlate to larger scale aerial photo lineaments, and how both correspond in turn to structures mapped at a more detailed scale in outcrop exposures. By doing so, it is shown here very specifically the type of structures the lineaments represent on the ground.

A number of prominent NW, as well as NE, WNW and ENE trending topographic lineaments occur on the DTM image as shown in Figure 4.8. Over a subset area marked in the SE of this

figure, a number of lineaments seen on the DTM image are also well represented on aerial photos as tonal lineaments as shown in Figure 4.9. Correlation is possible almost on a lineament by lineament basis between the two images and corresponding lineaments are labelled with the same number on these two figures.

In order to establish a direct relationship between the origin of lineaments and geological elements, outcrop mapping was carried out along the trajectories of a number of lineaments seen on the DTM and aerial photos. In almost all cases, where an outcrop is found along a lineament, it reveals the presence of steep fractures sets and usually the dominant fracture set is always parallel to the lineament orientation. Examples of lineament outcrop maps are shown here to include lineaments from each of the major lineament trends in southeast Viti Levu. The majority of the NW lineaments project toward the coast where fracture sets are exposed on coastal platforms along the trajectories of these lineaments. This direct link between the lineaments and fractures sets can be found on the coastal platform fronting Namuka Island and Muaivuso Point (Figure 4.10a,b). The well exposed trace of a strong NE trending lineament occurs in the Tamavua Reservoir (Figure 4.11). Outcrop features of a prominent WNW lineament are exposed along a road cut batter at Sawani, orientated across the strike of the lineament (Figure 4.12). The fault associated with an ENE lineament is exposed at the Mudu Gorge along the Wainikoroluvu River (Figure 4.13).

Due to the variation in the scale of mapping, the traces of lineaments on the remote sensing images (0.5 to 1 mm thick) would require a wide zone of fracturing up to 50 m to 150 m wide on the ground surface. Detailed mapping on the coastal platform and in other outcrop exposures documents fracture zones as wide as 200 to 300 m, containing several individual fractures. The maximum intensity of fracturing across the strike of a fracture zone can be as high as 2 to 3 fractures per metre (Figure 4.10c, 4.12). The majority of these fractures are faults, which accommodate small offsets on the low dipping strata, most in the order of tens of centimetres (Figure 4.10d, 4.11, 4.12). Faults with the largest displacements, in the order to 20 m to 50 m, are associated with the highest intensity of fracturing and seem to occur toward the centre of the fracture zones.

In areas of high rainfall, deep incisions by streams are facilitated and controlled by the fracture zones in both weak and more competent bedrock (Figure 4.13, 4.14). As erodibility of bedrock increases with the degree and intensity of fracturing, erosional processes are

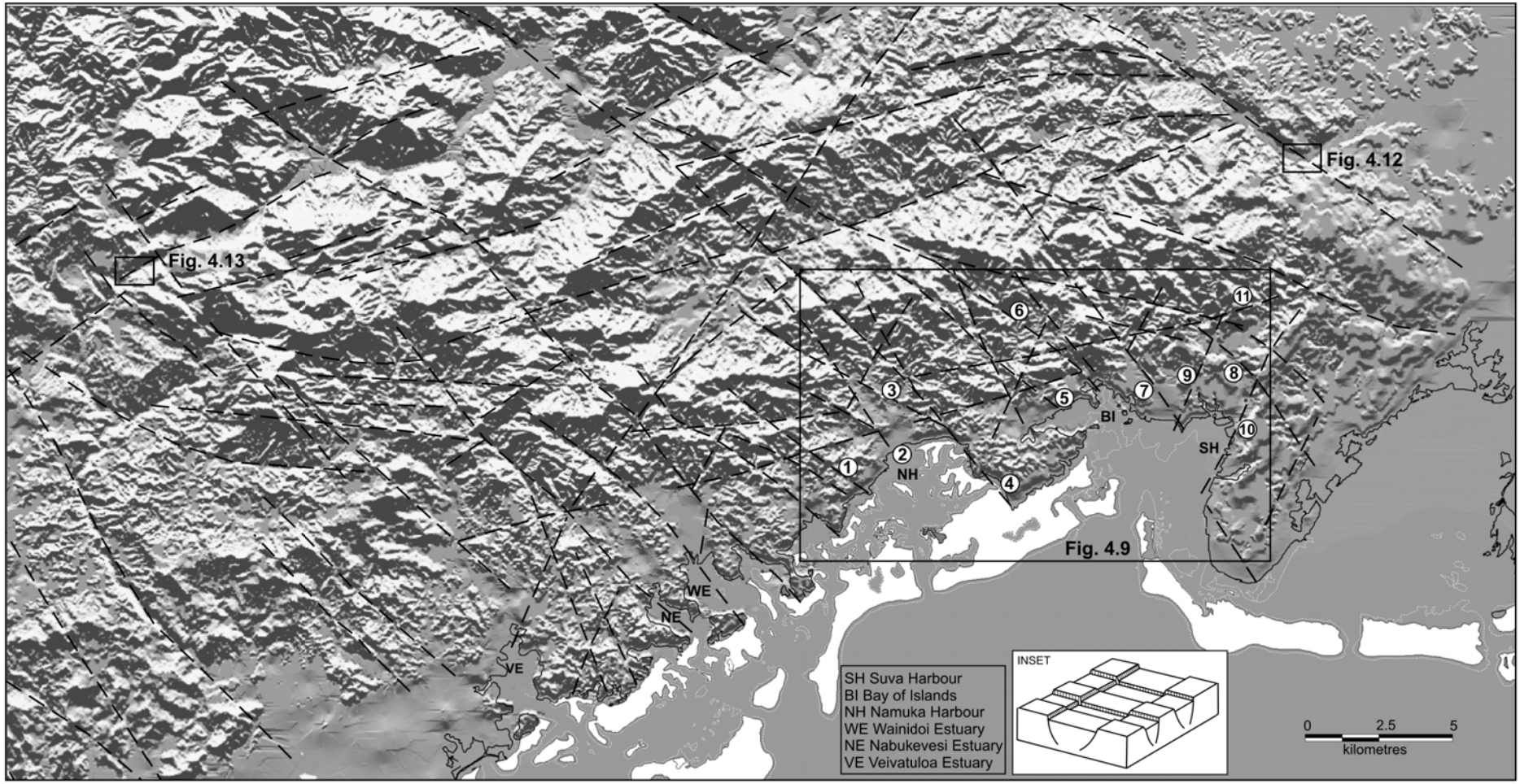

Figure 4.8: Regional DTM lineaments in a control area of southeast Viti Levu. Corresponding lineaments in aerial photos (Figure 4.9) are numbered. Labelled bays, harbours and estuaries correspond to intersecting coastal morphostructural grabens explained by the block diagram in the inset

Figure 4.9: Aerial photo lineaments in a subset area of Figure 4.8. Corresponding lineaments from the regional DTM image (previous page) are numbered.

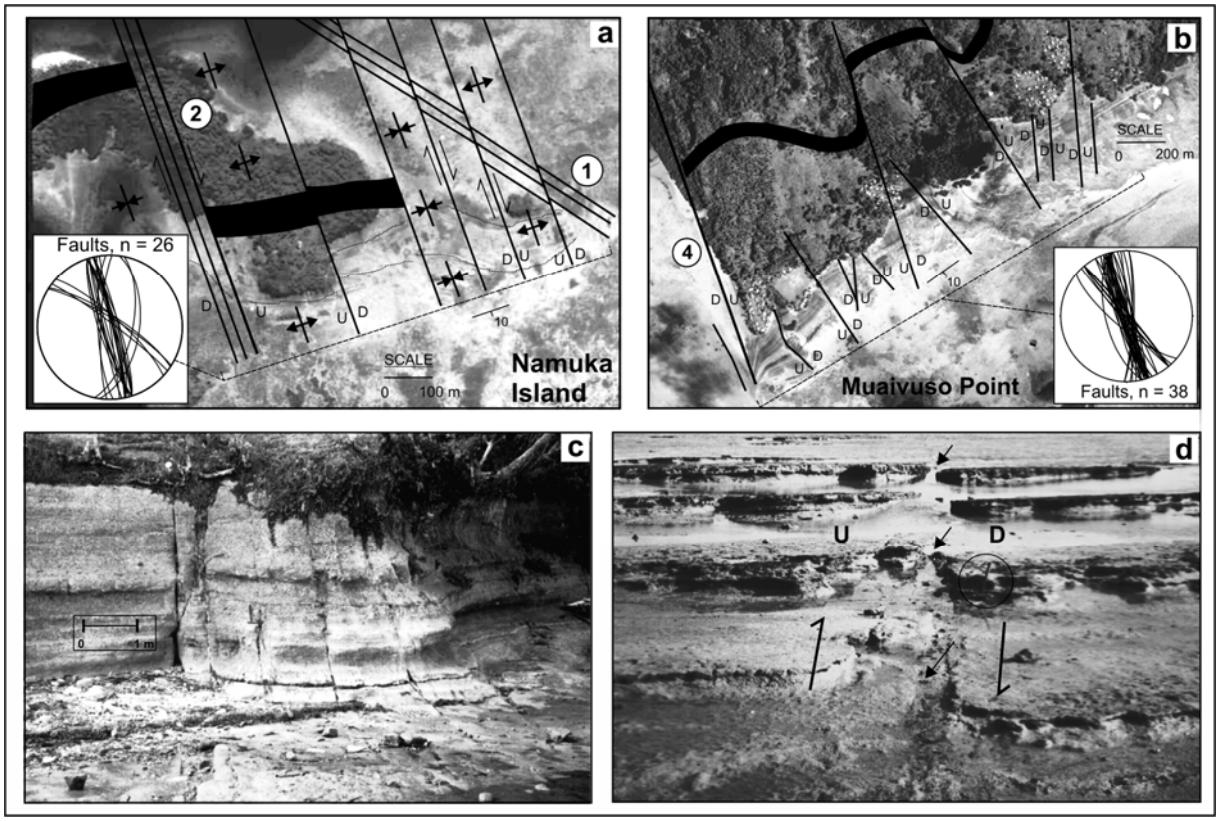

Figure 4.10: (a,b) Fault zones on the coastal platform along the trace of NW trending lineaments. Faults which correspond to lineaments in Figure 4.8 & 4.9 are labelled with the same number. See Figure 4.9 for location of maps. Lower hemisphere stereonets show attitudes of representative fracture data. Marker beds shown in black indicate relative offset by faults. (c) A steeply dipping fracture zone on a wave cut cliff and platform. (d) Small offset by an oblique slip fault on gently dipping strata on the coastal platform. The photo view is down dip. The circle shows hammer handle for scale.

enhanced towards the centre of the fracture zones. The expression this process imparts to the ground surface delineates the trajectories of the largest faults and allows their detection from topographic images (Figure 4.14). The correlation between lineaments and fracture zones clearly indicates that the topographic lineaments on the aerial photos and DTM images correspond to linear features that have developed as a result of preferential erosion along zones of fracturing.

4.7 STRUCTURAL CONTROL ON GEOMORPHOLOGY

In the final part of this lineament study I show through the use of topographic lineaments how the surface morphology of southeast Viti Levu is in part controlled by geological structure and how this can be used to infer aspects of the tectonic deformation. It is clear from the DTM image in Figure 4.8 that most lineaments have a close relationship with the geomorphology

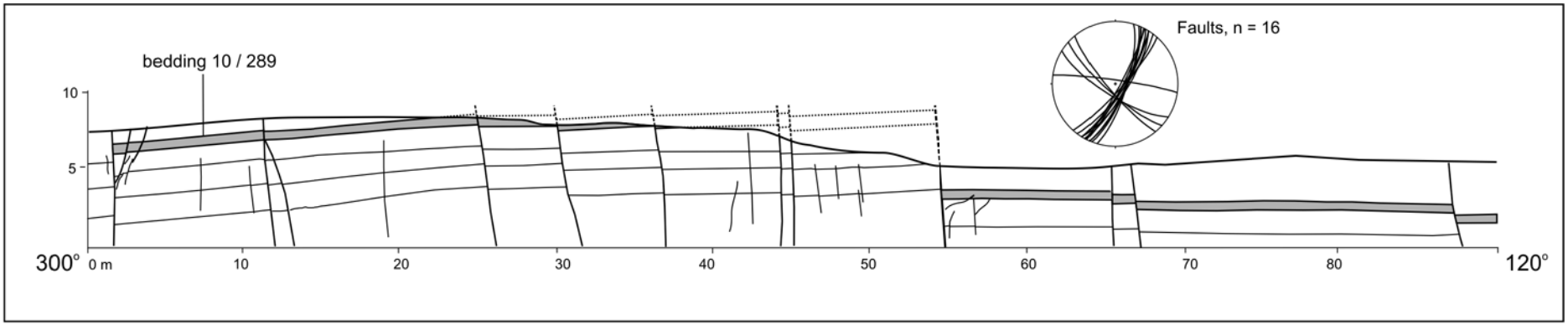

Figure 4.11: Fault zone exposed at the Tamavua Reservoir, Suva along the trace of a NE trending lineament (location of outcrop in Figure 4.9)

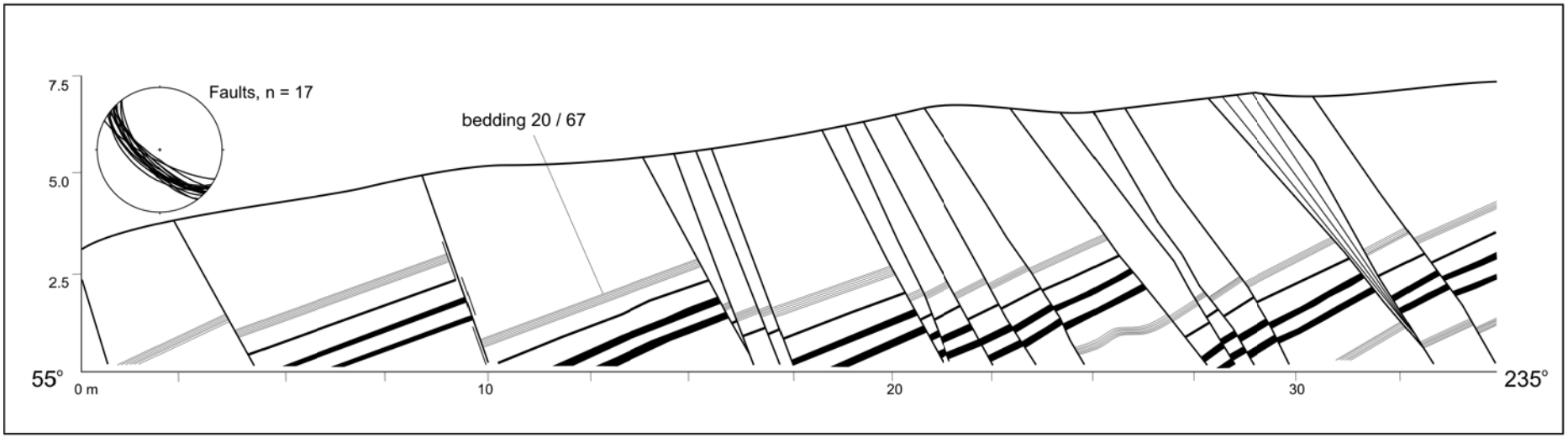

Figure 4.12: Fault zone exposed on a road cut batter along Princess Road, Sawani, across the trace of a WNW trending lineament (location of outcrop exposure is indicated in Figure 4.8)

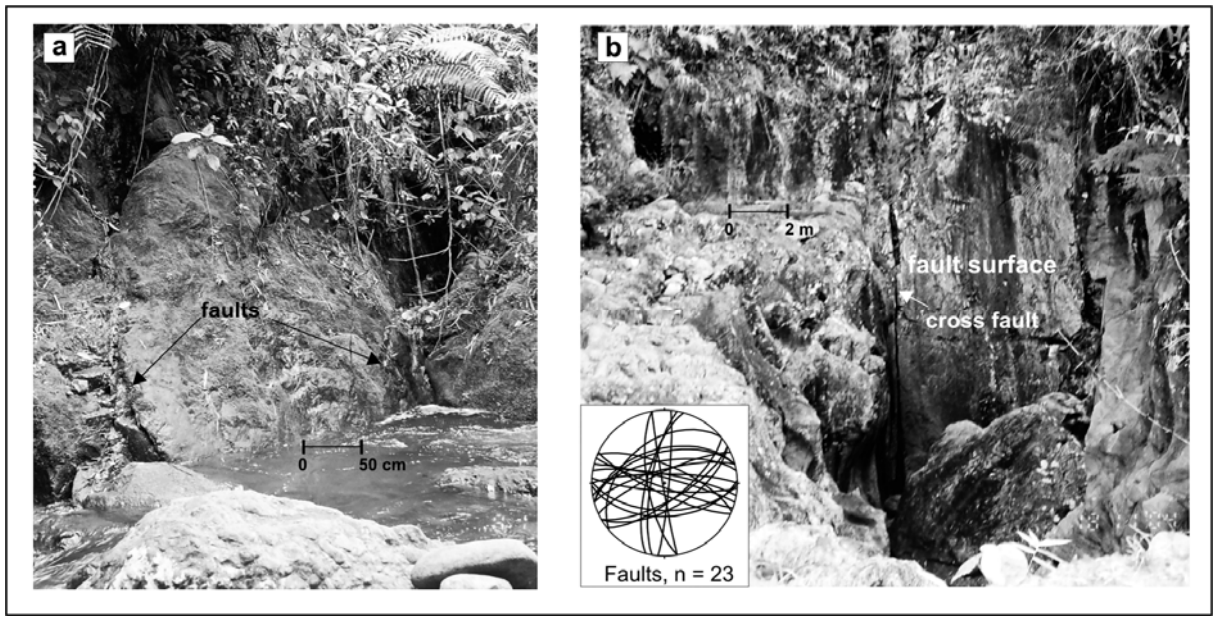

Figure 4.13: (a) Steeply dipping ENE fault zone exposed along the Wainikoroiluva River (see location of outcrops in Figure 4.8). Note in (b) how the deep incision of the river into massive andesite is controlled by the orthogonal fractures.

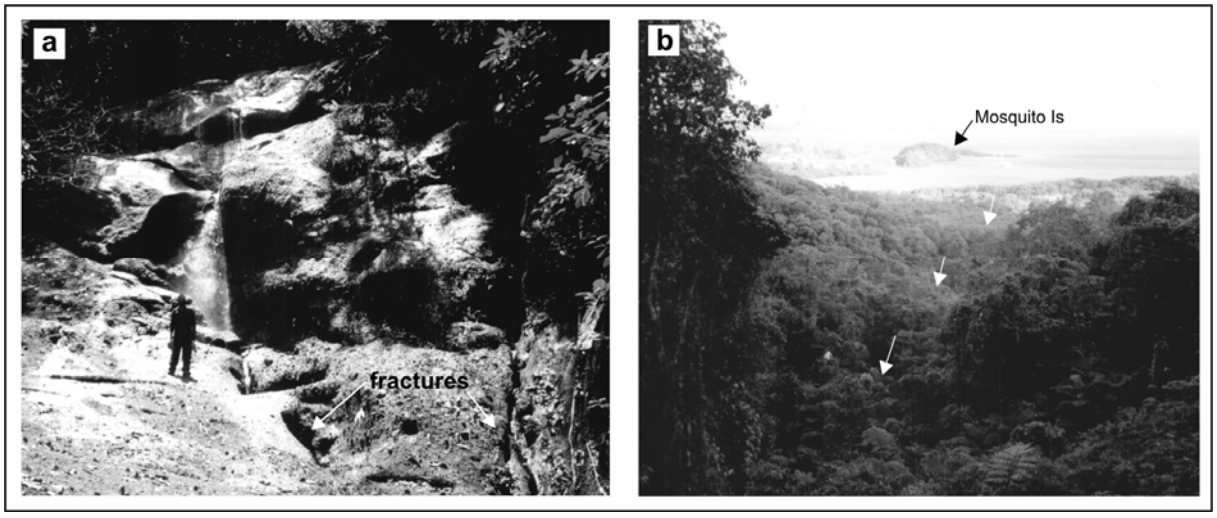

Figure 4.14: Lineament forming structures (north of the Bay of Islands, near Suva) (a) Erosion in bedrock by the stream is controlled by fractures. (b) The topographic expression of the stream delineates a lineament. (See Figure 4.9 for the trace of the lineament)

of the area. The lineament trajectories are seen to coincide with topographic slope alignments, drainage alignments, the boundaries of onland basins and particularly the rectilinear margins of peninsulas and bays that form the highly irregular coastline in this part of Viti Levu. The margins of most bays, harbours and estuaries along the southeast coast, appear to be controlled by intersecting lineaments. The prominent ENE trending lineament forms a range front that separates the rugged hinterland, from the coastal lowlands (Figure 4.8, lineament no. 11). Onshore mapping reveals that in most cases drainage has deeply incised along

fracture zones and that broader scale topographic changes are due to fault displacements across contrasting lithological units. The offshore continuation of the structural lineaments is revealed by offshore seismic reflection profiling and multibeam swath bathymetry (see Section 5.4.3). The complete pattern of onshore and offshore faulting indicates that the boxed geometries of the narrow valleys onland and rectilinear geometry of coastal bays and estuaries result from cross faulting and multistage overprinting by graben structures as illustrated by the block diagram in the inset of Figure 4.8. These observations indicate that erosion along structural lineaments, regional fault-generated mountain landscape, as well as narrow block faulting has played an important role in shaping the first-order geomorphic elements of the area.

4.8 DISCUSSION

4.8.1 Lineaments, fault geometry and fault kinematics

In this chapter the association of lineaments with faulting in bedrock is clearly demonstrated. The approach has focussed firstly on the analysis lineaments represented in a range of remotely sensed imagery, and secondly has linked these lineaments to faults and fault zones exposed at several selected outcrop exposure locations. By implication the occurrence of these lineaments may further provide insight into the structural geometries of the associated faults. A full structural analysis of all available fault data is beyond the scope of the present work.

Fault orientation and sense of shear data indicate that many major faults are steeply dipping to vertical, and in the field study area of southeast Viti Levu are shown to accommodate a range of motions, including strike slip, oblique-normal strike slip and normal offsets. Lateral fault separations of stratigraphic marker horizons are frequently observed in shore platform exposures (e.g. Figure 4.10a,b), and when combined with measurement of fault plane striations these commonly show this range of fault motions. Lateral offsets of streams (e.g. Waimanu River and Waidina River, see Figure 3.1) are inferred to be largely the result of fault displacement. While an exhaustive analysis of fault slip-sense with respect to the individual major lineaments is not possible, there exists sufficient data to be confident that the major lineaments are predominantly associated with strike-slip to oblique-normal strike-slip faulting.

In strike-slip, as well as normal-slip systems, fault zones in the near-surface may represent a zone of upward-diverging splays, which at depth merge into a single fault (e.g. Mandl, 1988; Sylvester, 1988). Such near-surface complexity is commonly linked to variations in fault plane geometry (e.g. fault segmentation; releasing and restraining bends and step-overs; fault relays etc), and also topographic loading over dipping faults. Such factors may in turn influence the partitioning of oblique fault slip into dip- and strike- parallel components. The occurrence of multiple, near-parallel, and closely spaced fault planes in outcrop exposures associated with the projected lineaments of southeast Viti Levu, and their variation in sense of slip data recorded, is therefore not inconsistent with the occurrence of major strike-slip faulting. Given the prominence of the lineaments, these faults are considered to represent an important indicator of the structural evolution of the Fiji Platform as a whole, reflected by the accommodation of significant crustal block rotation within the platform since Late Miocene times (Malahoff et al., 1982; Inokuchi et al., 1992; Taylor et al., 2000). This is discussed further in Chapter 8.

4.8.2 Reconciling topographic and 1VD magnetic lineaments

Mechanical models indicate that in strike slip shear zones, faults in the cover rocks above the primary basement fault develop progressively as precursor low angle synthetic and antithetic Riedel shears and P shears which form shear lenses and eventually an anatomosing pattern of shears (Naylor et al., 1986). This forms a zone of shearing on the surface that is much wider than the main fault in the basement. The closely spaced sets of sub-parallel fault splays, coincident with the topographic lineaments, are inferred to merge into singular uninterrupted faults at depth that may be represented in the 1VD data. Cumulative displacement on the merged fault arrays at depth would impart considerable offset on the (magnetic) basement, thus resulting in the observed magnetic lineaments. This may explain the fewer numbers and also the extensive nature of the regional 1VD lineaments in Figure 4.3c, relative to the surface lineaments shown in SLAR and DTM images in Figure 4.3a,b. This relationship between topography, magnetic signature and variation in the geometry of faults with depth that may exist in southeast Viti Levu is illustrated in the schematic diagram in Figure 4.15.

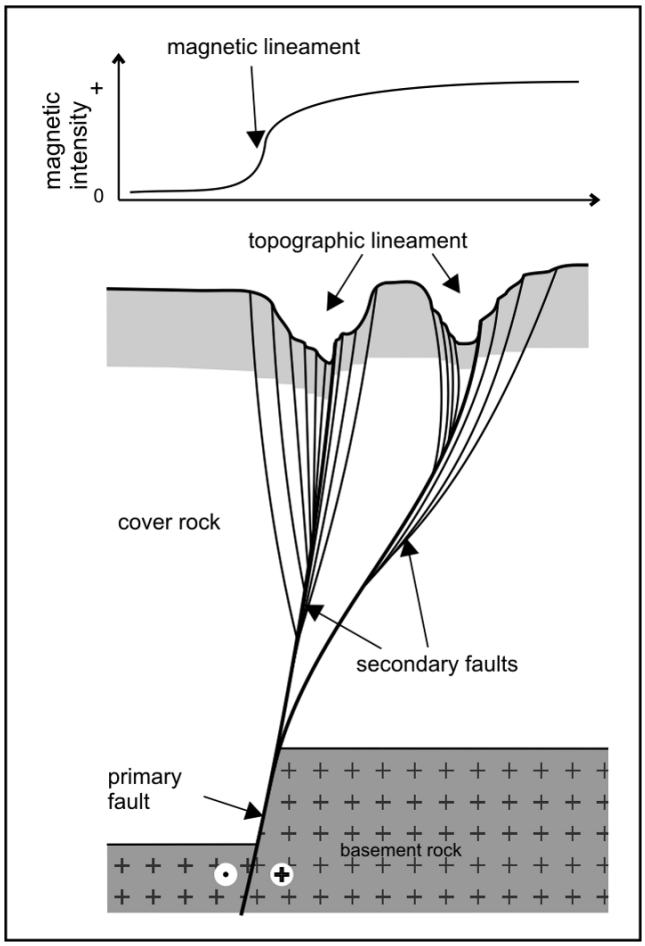

Figure 4.15: Schematic diagram showing the relationship between topographic lineaments, magnetic lineaments and faulting in southeast Viti Levu.

4.8.3 Fault/lineament zones

It is evident from the relationship established by spatial correlation between lineaments and faults that the faults may be under-represented in the existing regional geological maps. The along strike extent of most of the fault zones and individual faults are generally much less than those of the lineament sets. It is reasonable to expect that in regional geological maps the extent of coverage is restricted by exposures, and furthermore that the level of detail is controlled by the scale of mapping undertaken. Thus, only the most prominent faults, those that may impart considerable offset on geological boundaries will be captured on such maps. The lineament data, however, may portray the fuller extent of brittle deformation and include fractures with little or no displacements. The lineament sets in southeast Viti Levu indicate that brittle deformation extends beyond the limits of faults as presently shown on geological maps, possibly as zones of closely spaced, intense fracturing. The lineament sets identified

here, show that a number of small faults that are separated by distances of 5 to 15 km and previously remained unrelated, are actually segments of larger and more prominent faults zones (e.g. Mavuvu Fault/Lineament Zone, Figure 4.6). The lineament sets, therefore, delineate more significant structural patterns that can be used more effectively in regional structural synthesis than existing mapped faults represented on the published and unpublished geological maps for Viti Levu. The fault correlated lineament sets are used to define six fault lineament zones in southeast Viti Levu. These zones are 1) Sovi Fault/Lineament Zone, 2) Yarawa Fault/Lineament Zone, 3) Mavuvu Fault/Lineament Zone, 4) WWW Fault/Lineament Zone, 5) Muaivuso Fault/Lineament Zone and 6) Suva Fault/Lineament Zone (Figure 4.6). When combined, these fault/lineament zones form a complex network of intersecting faults.

4.8.4 Interpretations using fault/lineament zones

With the relationship between bedrock structure and lineaments established in this study, there is an opportunity to address the tectonic history and evolution of this sector of the Fiji Platform, and use this relationship to further perform hazard analyses. Cross-cutting relationships of lineaments (Hancock, 1985), stratigraphic distribution of lineaments sets (Cortes et al., 2003) and correlation of lineament domains to tectonic features (Wise et al., 1985; Roy et al., 1993) can be used to infer the chronology and evolution of fracturing and their tectonic significance. Structural control of the distribution of seismicity in the region can be defined by correlations between the earthquake epicentres and lineaments, which may in turn help define earthquake source structures and source zones for a regional seismic hazard analysis. The interpretation of mapped lineament patterns in the context of the tectonic evolution of Fiji through crustal block rotations and the insights they provide on Fiji's present seismotectonic setting are discussed in Chapter 8. The effective use of lineaments in delineating seismic source structures and their application in a deterministic seismic hazard analysis are presented in Chapters 9. The following chapter explores the relationship between the onshore and offshore structural features in southeast Viti Levu.

4.9 SUMMARY AND CONCLUSIONS

In this chapter, an approach to identifying and mapping structural lineaments in southeastern Viti Levu is developed as a first step to gaining further insight into the structural and tectonic evolution of the region, and identifying and characterising seismic sources in this part of the

island. Lineaments have been mapped using aerial photographs, digital terrain models, side looking airborne radar images and the first vertical derivative of total magnetic intensity image. The reliability of mapped lineaments has been improved by using systematic lineament-analysis procedures that have included multiple trial tests, multiple image tests, as well as comparison of lineaments at two different map scales. Comparisons of lineaments with regional faults and mapped fracture data have permitted the exploration of the link between lineaments and fractures observed on the ground.

The statistical orientation peaks, as well as the spatial extents of lineaments correlate well between the various lineaments data sets. Furthermore, these characteristics show a good correlation between the lineament data sets and field mapped fracture data. This supports the interpretation that the lineaments represent fractures inherent in the bedrock that are emphasized on the surface by topography, drainage, vegetation, and magnetic contrasts at depth. Surface lineaments correspond to broad zones of intense fracturing and they impart considerable control over the landform features of the area. Broad zones of surface lineaments may represent fracture splay zones that merge into discrete uninterrupted faults at depth that impart considerable offsets on the magnetic basement. Fault correlated lineament sets indicate that fault zones extend over greater geographical distances and they depict more complex regional structural patterns than previously known.

This study provides a new and viable approach to mapping fracture patterns using lineaments where outcrop is limited and where conventional field mapping techniques of structural geology are impractical. It highlights the benefits of mapping lineaments from multiple remote sensing images of the surface and basement and for mapping them at regional and larger scales. Lineament data derived using such an approach can be used effectively to characterise regional structural patterns, and can be used to provide new insights into the tectonic evolution and seismic hazards of the region.

CHAPTER 5

OFFSHORE MORPHO-STRUCTURE

5.1 INTRODUCTION

In recent years the development and use of the digital multibeam echo-sounding system has significantly enhanced the study of seafloor geomorphology of the shelf and slope environments. Numerous high resolution bathymetric datasets are now being generated which contribute to the better understanding of tectonically active coastal regions of the world (e.g. Eichhubl et al., 2002; Gazioglu et al., 2002; Greene et al., 2002). This chapter presents the results of high resolution multibeam swath bathymetry and shallow marine seismic reflection surveys carried out across the southern slope of Viti Levu. These acoustic data sets allow the relationship between the seafloor morphology and underlying tectonic structures of the area to be explored, significantly advancing our understanding of the various tectonic controls and active geological processes that are operating within this part of the Fiji Platform.

In southeast Viti Levu the Viti Levu Seismic Zone (VLSZ) (Section 3.2) spans the onshore and offshore area. The origin of seismicity in the VLSZ is not well understood. Tectonic deformation of the VLSZ has been previously characterised by indirect methods, such as seismicity and earthquake focal mechanisms (Hamburger et al., 1990). A study of the complex offshore morphology of the southeast Viti Levu slope provides a more direct approach to understanding active tectonic processes associated with the VLSZ. Linear submarine canyons that dissect the slope are inferred to be the surface traces of seismically active fault systems (Houtz, 1959; Shorten, 1993a). Integration of high resolution offshore morpho-structural data with onshore physiographic and structural analysis allow for a corroborative interpretation of onshore-offshore geomorphology and structure. These in turn will provide for more direct insights into the character of tectonic deformation of the VLSZ, as well as contribute to unravelling tectonism within the Fiji Platform as a whole.

The main objectives of this chapter are: i) to document the morphometry and discuss the origin of numerous linear submarine canyons in southeast Viti Levu, ii) investigate the hypothesised link between bedrock faulting and submarine canyons, and iii) integrate the

offshore morphostructural data with onshore structural data to produce a combined onshore-offshore structural map of southeast Viti Levu.

5.2 METHODOLOGY

5.2.1 Multibeam Echo Sounding

The multibeam bathymetry of southern Viti Levu were acquired using a Reson SeaBat 8160 Multibeam Echo Sounder system mounted on the chartered vessel *MV Turagalevu* (Gouldby et al., 2003) (Figure 5.1a,b). The survey area extended to 1500 and 1800 m depths on the Baravi Basin and Suva Basin slopes, respectively (Figure 3.4). The base of the marginal slope was not reached. The SeaBat 8160 system comprises 126 beams, operating at 50 kHz, and has a depth range of 2500 m. It has an angular coverage sector of 150^{o} below the survey vessel. The horizontal coverage of the beams is generally three times greater than the depth of the water column. Navigational control was provided by a TrimbleDSM12/212 real time differential global positioning system. Motion sensing data were acquired by a TSS Dynamic Sensor and sound velocity measurements were made using the SBE SeaCat 19+ CTD probe. The survey was carried out at an average speed of about 7 to 8 knots. The Navisoft Sweep software was used for survey planning, data logging, real time visualisation and post processing. Extensive post processing included removal of erroneous beams, noise filtering, processing of navigation data and corrections for tides and sound velocity (Gouldby et al., 2003). After post processing, XYZ coordinate data were converted to ASCII format and imported into the Surfer© version 8 software for gridding. The data was gridded using the ordinary point kriging method, with a linear variogram, search radius at 100 m with 8 minimum points and grid size set at 60 and 20 m. Digital terrain models, shaded relief images, contour maps, slope maps and transverse and longitudinal profiles were created from the gridded data in Surfer© version 8 software. Some persistent across track ribbing artefacts remain in some areas, despite the post processing, and have been treated with caution during the analysis.

5.2.2 Seismic Reflection Profiling

High resolution shallow marine seismic reflection data were acquired by continuous profiling using a Datasonics Bubble-Pulser SPR 1200 profiling unit on the Fiji Mineral Resources

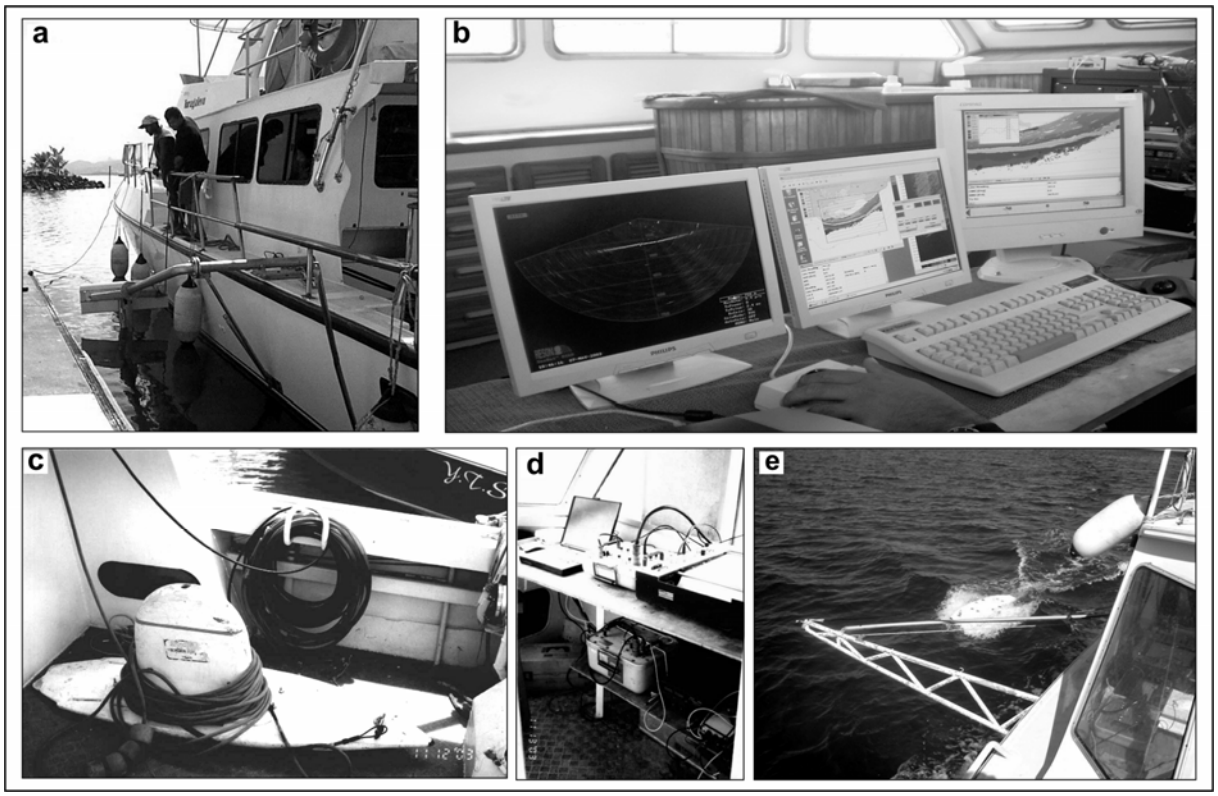

Figure 5.1: Geophysical equipment used for marine surveys. (a) Transducer of the swath mapper system mounted on the *MV Turagalevu*. (b) Control panel of the swath mapping system inside the vessel. (c) 400 Hz boomer seismic source and single channel streamer cable. (d) Analogue seismic receiver and processor, graphics recorder and GPS system. (E) Manifold arm on the *RV Yautalei* to keep the boomer surf-board and streamer cable away from the prop wash.

Department research vessel *RV Yautalei* (Figure 5.1c,d,e). The survey vessel is equipped with twin counter-revolution 150 hp outboard engines and a Del Norte 1009+ digital differential global positioning system. Real time differentially corrected GPS positions of survey fixes had positional errors of ± 1 m. The survey was carried out at speeds between 4 and 6 knots. The seismic source used was a boomer system, mounted on a surf-board sled, operating at 400 Hz. The seismic signal was recorded by a single channel, 7-metre long Datasonics BPH-540 Hydrophone Streamer cable with 10 hydrophone elements. A band pass filter with low cut frequency of 200 Hz and high cut frequency of 1000 Hz was used. The time variable gain (TVG) setting on the seismic processor was adjusted throughout the survey for the best possible signal. The profiles were recorded on a three channel EPC 4800 graphic recorder. Position fixes were manually annotated on the graphics recorder at 30 second or 60 second intervals. The profiles had seismic penetration of 125 to 200 ms two-way travel time (~90 and 150 m respectively, assuming interval velocity of ~1.5 km/s) (Shorten, 1993b). In deeper areas, sections were plotted with delays in 200 ms increments. The seismic profiles presented

here are unmigrated. Several acoustic artefacts of non-migrated seismic sections can be recognised. In particular, bubble pulse reverberations of prominent seismic reflectors, such as the seafloor, produce a couplet of reflectors 5 to 10 milliseconds apart. Other acoustic artefacts recorded include direct arrivals from source, hyperbolic diffraction patterns and bow tie effects, and reflection multiples. These spurious reflectors have been judiciously separated from true subbottom reflectors during interpretation.

5.3 THE MARGINAL SLOPE OF SOUTHERN VITI LEVU

The morphological character of the marginal slope varies across southern Viti Levu. Areas of sedimentation and erosion can be clearly distinguished. The structural complexity varies across the marginal slope and so does the density distribution of mass movement features. The marginal slope is subdivided into five distinct morphological units based on these distinctions. From west to east these units are: 1) the Western Slope; 2) the Beqa Passage; 3) the Beqa Lagoon Slope; 4) the Eastern Slope; and 5) the Rewa Delta Foreslope. These morphological units are shown on the shaded relief image* with 60 m grid resolution in Figure 5.2. Surface profiles across these units are shown in Figure 5.3. Descriptions of the seafloor morphology of these units are presented below.

(a) Western Slope:

The Western Slope occurs to the west of the Beqa Lagoon. The shelf break here is relatively straight and is demarcated by the outer edge of a narrow fringing reef parallel to the coastline. The fringing reef rests on a marginal shelf no more than a kilometre wide and 40 m deep (British Admiralty 1996). The slope of the seafloor outside the reef is relatively steep, with water depths increasing from 100 m to 1500 m within a distance of 10 km. Immediately outside the shelf break, the gradients are between 30 to 40 degrees. The gradient decreases gradually seaward to 10 degrees near the edge of the survey area. This low gradient area represents the top part of a broad submarine plain that slopes into the Baravi Basin. Apart from the relatively steep gradient and presence of numerous evenly spaced, shallow and linear erosional channels, this unit of the marginal slope is barren of pronounced morpho-structural features.

(b) Beqa Lagoon Slope:

The Beqa Lagoon Slope represents the seafloor outside the Beqa Lagoon. The seafloor here

* Fly-through over digital shaded relief images are given in Appendix 6.

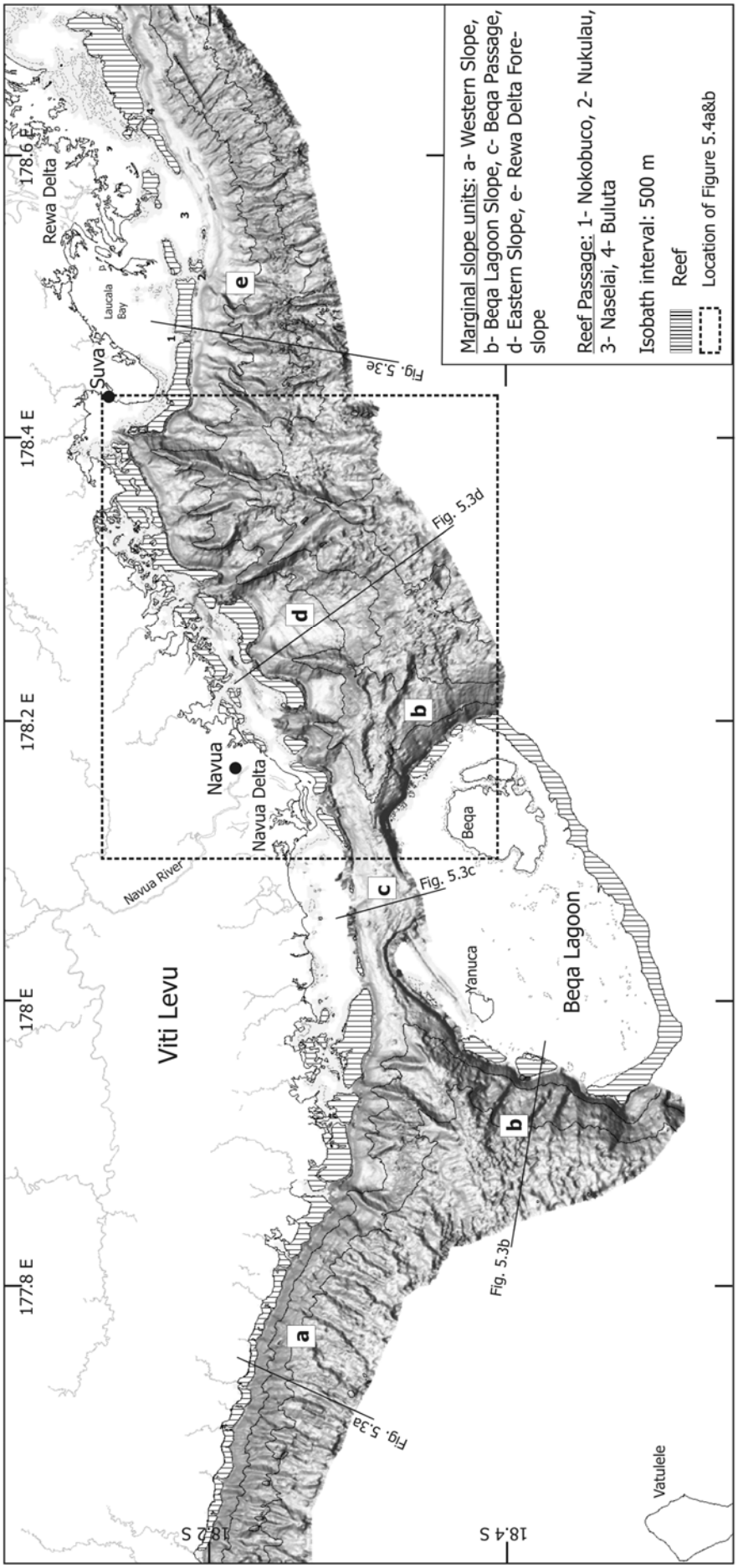

Figure 5.2: 60 m gridded bathymetric shaded relief image showing the main marginal slope units of southern Viti Levu. Sun illumination is from the south.

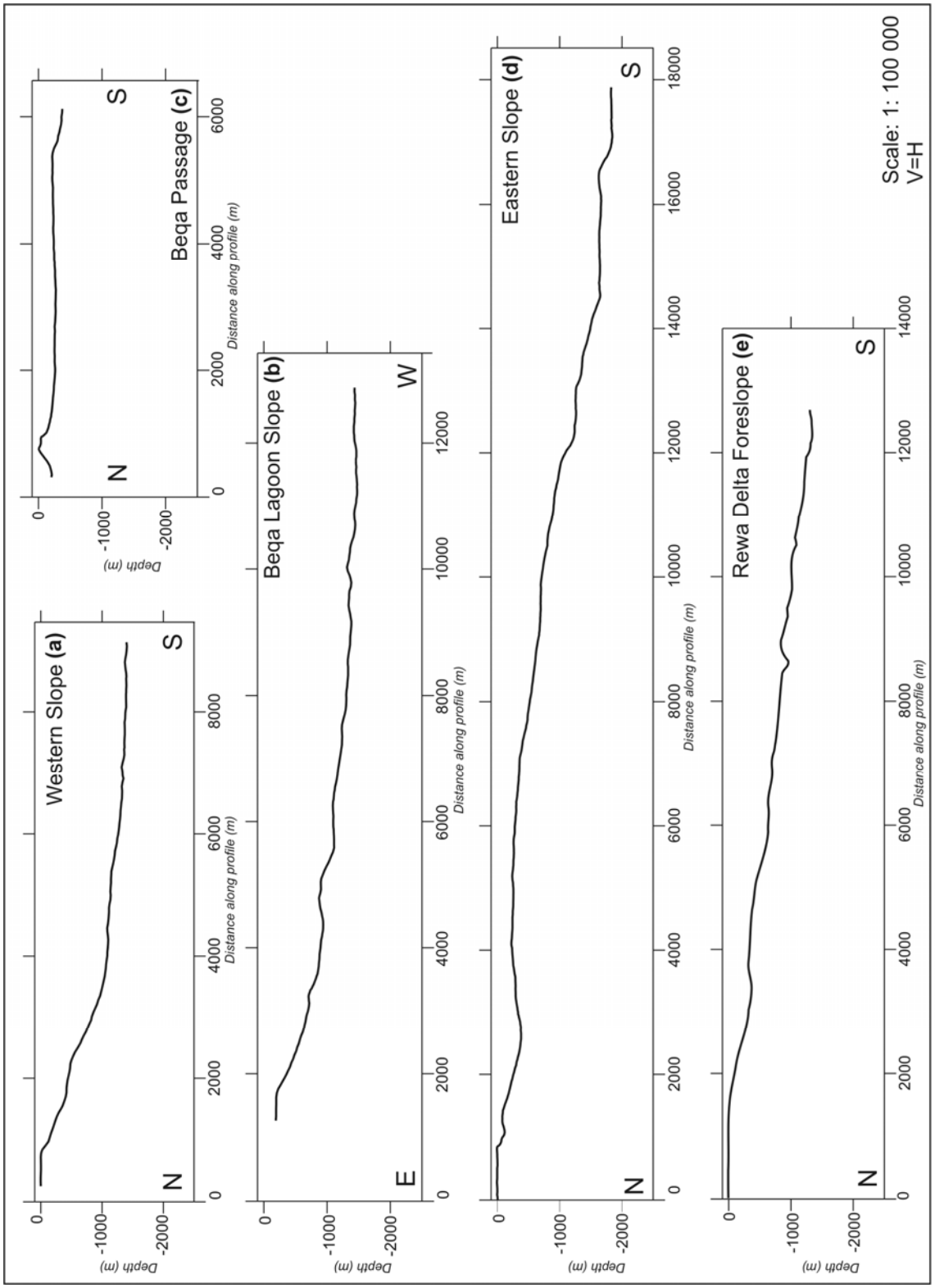

Figure 5.3: Surface profiles across the marginal slope units of southern Viti Levu based on the SeaBat 8160 bathymetry. There is no vertical scale exaggeration. See Figure 5.2 for profile locations.

slopes steeply and radially outwards from the exposed outer reef edge to water depths greater than 1500 m. The overall morphology of the slope is indicative of the flanks of an eroded submarine volcano. The slope gradient is highest (20^o to 30^o) closer to the reef edge, representing the steep fore reef slope. Beyond the fore reef slope, the gradient gradually decreases from 20 degrees to 10 degrees towards the deeper parts of the marginal slope. Several sets of narrowly spaced sub-parallel gullies, 50 to 100 m apart and 50 to 70 m deep, occur on the eastern sector of the Beqa Lagoon Slope. These gully sets define the runout paths of submarine landslides that have occurred on the reef fronts. The slides are described in more detail in the following chapter.

(c) Beqa Passage:

The Beqa Passage is a narrow and shallow passage between the Beqa Lagoon and the coast of Viti Levu and is interpreted to be a depositional setting of terrestrial sediments from the Navua Delta system (mean discharge 45 m^3/s and peak discharge 6000 m^3/s (Shepherd, 1990)). Terriginous sediments from the Navua Delta are transported westward by shallow currents generated by the prevailing southeasterly trade winds. The offshore extent of this sediment cover, can be clearly distinguished as a highly reflective smooth surface in the mutlibeam data (Figure 5.2). The Beqa Passage is 20 km long and on average 3 km wide; it is 1.5 km wide at its narrowest point. The sea floor in the central part of the Beqa Passage is smooth and gradients are less than 10 degrees. The gradients become higher, about 20 degrees, at the two ends of the passage, where it opens up to deeper parts of the marginal slope. West of the Navua Delta, the barrier reef is poorly developed due to the influx of fresh water. The lack of the barrier reef at this point allows for the inflow and deposition of terringenous sediments in the central part of the Beqa Passage where water depth is only 300 m. The water depth increases at the two ends of the passage to about 400 m.

(d) Eastern Slope:

The Eastern Slope unit occurs between the Beqa Lagoon and the Suva Peninsula, and in contrast to the other slope units, is the most morphologically complex and provides the best insights into the bedrock structural control of major seafloor features. A higher resolution (20 m grid) shaded relief map of the Eastern Slope is presented in Figure 5.4a. The interpreted bathymetric features of this area are presented in Figure 5.4b and show the complexity of the seafloor morphology. The top of the slope fronting Viti Levu is demarcated by the seaward edge of the barrier reefs. The fore reef slopes are cliff like features having gradients up to 40

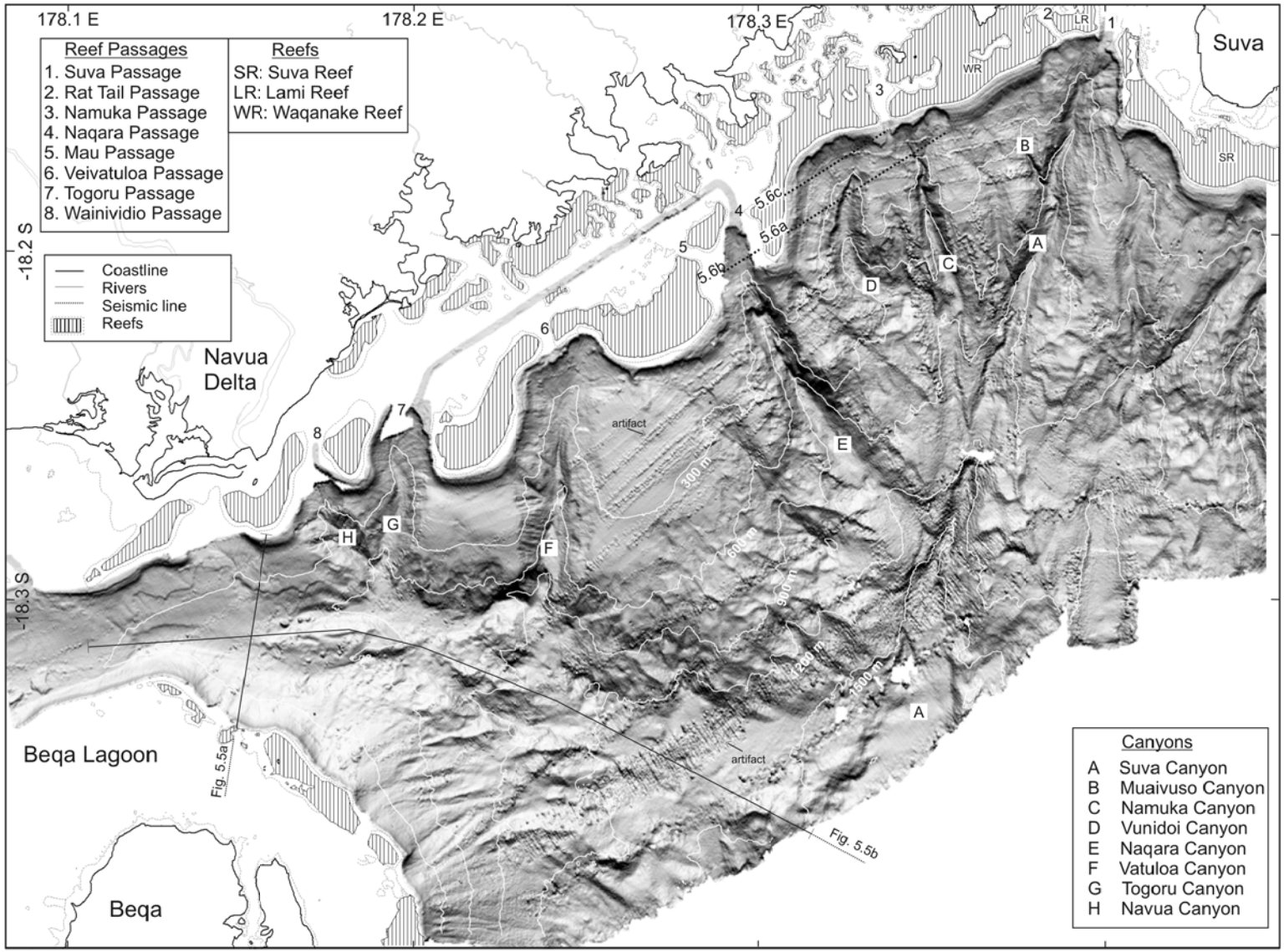

Figure 5.4a: Bathymetric shaded relief image (20 m grid) of the Eastern Slope of southeastern Viti Levu. Illumination is from the north. The isobath interval is 300 m.

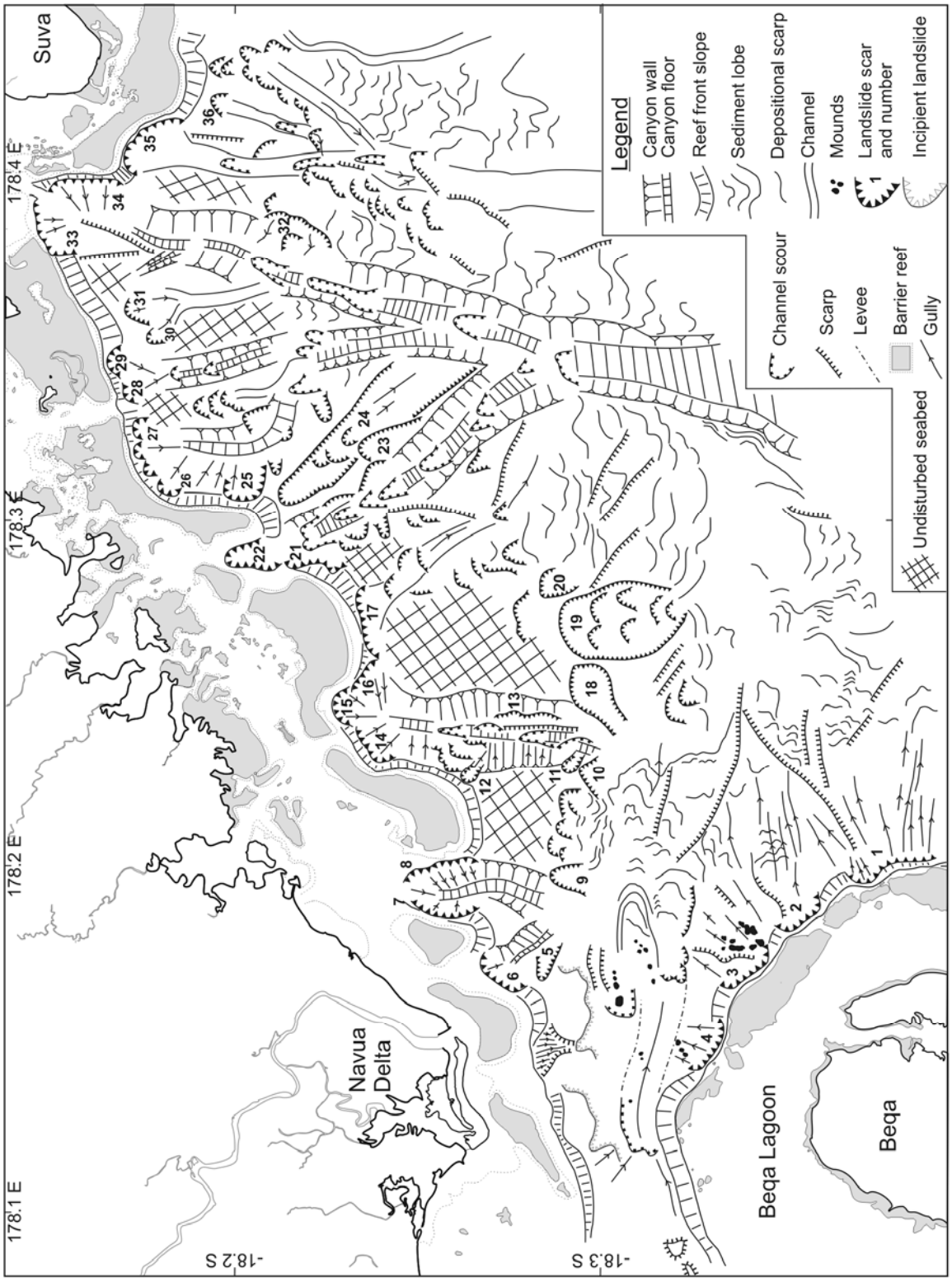

Figure 5.4b: Morpho-sedimentary and morpho-structural map of the Eastern Slope of southeastern Viti Levu.

degrees. For the first 4 to 5 km outside the barrier reef front (between the 100 and 400 m isobaths) there are broad areas of low gradient (about 10 degrees) and smooth (undisturbed) seafloor. The seafloor beyond the 400 m isobath is steeper and is disrupted from the effects of mass movements. Beyond the 1000 m isobath, sloping hummocky terrain with characteristics of sediment lobes, curved depositional scarps and pressure ridges, represents accumulated debris flow deposits derived from the upslope area. In the west, the Eastern Slope is separated from the Beqa Lagoon Slope by a wide WNW-ESE oriented valley, which originates at the eastern end of the Beqa Passage. The floor of this valley shows a levee channel and scour marks at the up slope end and mound like features towards the deeper end (Figure 5.4b, 5.5a). Small mounds, 60 to 100 m wide and 25 to 50 m high, occur near the head of a scour channel. These are interpreted as large blocks of landslide debris from the adjacent Beqa Lagoon slope. Alternatively they may represent the undulating surface of the basement rock around which cover sediments have been eroded away by mass flows/turbidity currents. Three larger mounds occur at the deeper end of the valley, shown in the long section in Figure 5.5b. These have not been studied in detail. They could either represent lobes of sediments deposited by turbidity currents generated near the Beqa Passage, possibly during episodic high sediment yielding flood events reported in the Navua River (Parry, 1981), or alternatively they could be large collapse features from the top of the Beqa Lagoon Slope. The surface of the central area of the Eastern Slope is scarred by a number of deep linear submarine canyons and mass movement features. Detailed descriptions of the submarine canyons of the Eastern Slope are presented in Section 5.4. Mass movement features of the Eastern Slope are documented in the next chapter.

(e) Rewa Delta Foreslope:

The protruding foreslope of the Rewa River Delta occurs to the east of the Suva Peninsula. The slope has a gradient of about 10 degrees and is dissected by several sinuous channels. The channels are up to 15 km in length. The morphology of this slope is indicative of a radiating sediment apron that is sourced from the main distributary channel of the Rewa Delta through passages in the barrier reef. Large amounts of sediments are interpreted to be actively discharged by the main distributary channel of the Rewa River (discharge range 50 m^3/s to 14 900 m^3/s (Morrison et al., 2001)) through the Naselai Passage and through the smaller Nukubuco, Nukulau and Buluta Passages. This is confirmed by the presence of terrigenous sand found in sea floor cores taken from the slope (Pickering & Suda, 2003; Narain et al., 2004).

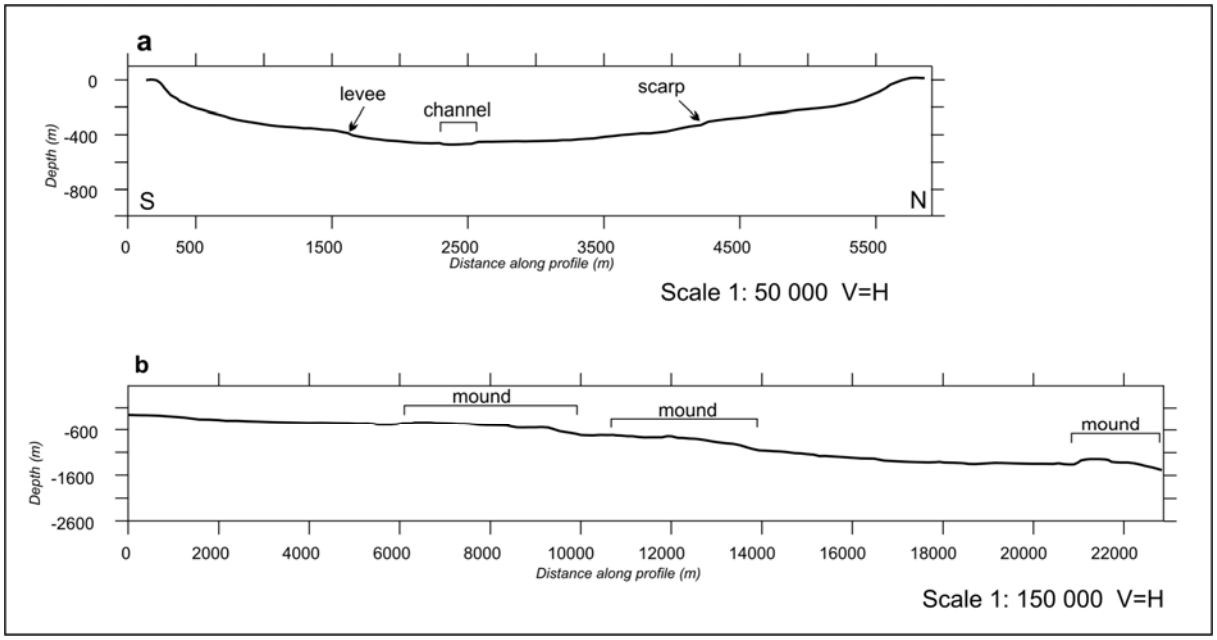

Figure 5.5: (a) Transverse and (b) longitudinal profiles through the eastern opening of the Beqa Passage. See Figure 5.4a for profile locations.

5.4 SUBMARINE CANYONS OF THE EASTERN SLOPE

The most distinctive morphological features of the Eastern Slope are the linear submarine canyons. These canyons, previously unnamed, are here named according to the nearest landmark features, and include the Suva Canyon, Muaivuso Canyon, Namuka Canyon, Vunidoi Canyon, Naqara Canyon, Togoru Canyon, Vatuloa Canyon and Navua Canyon (Figure 5.4a). For convenience in descriptions, submarine canyons are differentiated from other trough-like incisions on the marginal slope, including channels, and smaller rills and gullies. In this study, channels are defined as having shallow incisions (< 200 m) and are restricted to unconsolidated sediments; whereas canyons have deeper incisions (> 200 m), and dissect both bedrock and unconsolidated sediments.

5.4.1 Morphology of submarine canyons

The heads of all the canyons, except the Muaivuso Canyon, indent the marginal shelf. All shelf indenting canyons have corresponding deep water passages through the barrier reef at their heads as shown in Figure 5.4a. Subaerially, the canyon head indentations are represented as broad embayments on the barrier reef front. The amount of canyon head indentation, estimated from a projected position of the barrier reef front when embayments are removed,

ranges from 1 to 3 km. The longest and most prominent canyon is the Suva Canyon, which is traced southwestward for ~20 km to the southern limit of the survey area. The 100 m isobaths on the 1: 250 000 Bathymetry Map Sheet 5 (Smith, 1992a) indicate that this canyon may continue seaward for another 5 km and merge with the floor of the Suva Basin. The Muaivuso, Namuka and Naqara canyons are the western tributaries of the Suva Canyon. The Vunidoi Canyon is a western tributary of the Namuka Canyon. The Vatuloa, Togoru and Navua Canyons occur separately in the western part of the Eastern Slope and they drain into a WNW submarine valley east of the Beqa Lagoon. The morphometric data of all the canyons are summarized in Table 5.1, using the submarine canyon characteristics of Shepard & Dill (1966). Transverse and longitudinal profiles of submarine canyons are given in Figures 5.6a and 5.6b respectively.

All canyon heads have arcuate shaped and gullied head walls, which are 2 to 3 km wide. The canyon heads are much broader than the central canyon rims, which are on average 1000 to 1500 m wide. The canyon thalwegs or floors are on average 500 to 600 m wide. Transverse profiles across all the canyons (Figure 5.6a) show that the upper reaches of most of the canyons are narrower, with steep-sided walls, and V-shaped profiles. They progressively become broader with lower gradient walls (cross sectional) and U-shaped profiles downstream. The steep walls in the upper canyons have gradients between 40 and 60 degrees. The gentle sloping canyon walls in the lower (downstream) parts have gradients between 15 to 30 degrees. The consistent change in the shape of the canyon profiles from upslope to downslope may be attributable to accumulation and infilling of sediment debris derived from the marginal shelf and the upper parts of the canyons, by normal canyon sediment transport and deposition process. This feature is commonly recognized in submarine canyons elsewhere (Shepard & Dill, 1966; Herzer, 1979; Pratson & Coakley, 1996; Lewis & Barnes, 1999).

Even though the Suva Canyon has an overall linear appearance, closer inspection of the thalweg shows a number of tight bends. Going down-slope, left bends occur at axial distances of 1.1 and 3.5 km, and right bends occur at 8.5, 12 and 15.3 km. The longitudinal profile of the Suva Canyon (Figure 5.6b) shows a number of vertical steps in the canyon floor, which separate sections of uniform axial gradients. Vertical steps are also observed in the longitudinal profiles of the Namuka, Naqara, Vatuloa and Togoru canyons (Figure 5.6b), and similarly separate the canyon axes into sections that have uniform axial gradients. All canyons show a decrease in the axial gradient going downstream (Table 5.1; Figure 5.6b). A steep

Table 5.1: Dimensions of selected morphometric features of submarine canyons on the Eastern Slope, southeast Viti Levu.

Canyon	Length (km)	Overall orientation	*Width (m)	*Floor width (m)	[!]Wall height (max - min) (m)	*Axial gradient (deg)	*Wall gradient (deg)	*Transverse profile	Channel curvature	Indentation on shelf edge (km)
Suva Canyon	~25	NNE	1000 - 3000	350 - 2000	400 - 200	8 - 5 - 2 - <1	40 - 30	V - U	Straight with small kinks	2
Muaivuso Canyon	1.5	NW	300 - 500	100 - 200	200 - 150	22 - 6 - 15.	60 - 33	V - U	Straight	-
Namuka Canyon	9	NNW	700 - 1000	250 - 670	300 - 150	9 - 5.	60 - 30	V - U	Straight	1
Vunidoi Canyon	7	NW	1000 - 1500	320 - 500	300 - 200	10 - 5.	50 - 20	U	Slightly curved	3
Naqara Canyon	10.5	NW	1000 - 1500	500 - 650	400 - 200	6 - 8 - 3.5	55 - 15	U - V - U	Straight with small kinks	2
Vatuloa Canyon	7	NNE	2000	300 - 600	400 - 200	5 - 2.	65 - 15	V - U	Straight	3
Togoru Canyon	4	NNE	1700	300 - 450	400 - 250	4 - 3.5 - 1	30 - 22	U	Slightly curved	2
Navua Canyon	2.5	NW	1300	150 - 300	250 - 200	6 - 5.	17 - 23	V	Straight	1.5

* L to R represents progressive values from upstream to downstream

[!] L to R represented maximum and minimum values

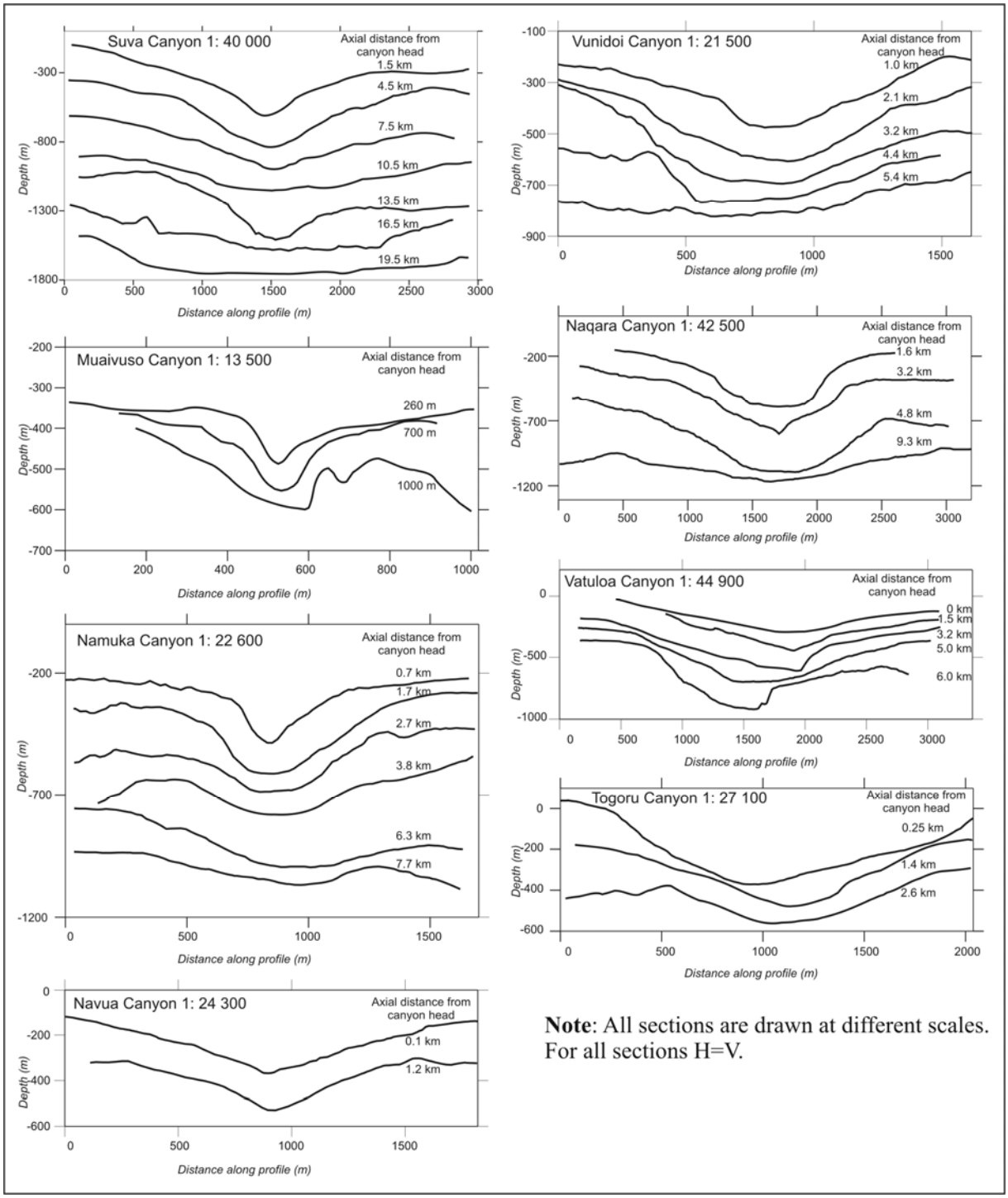

Figure 5.6a: Transverse profiles across the canyons of the Eastern Slope of Viti Levu.

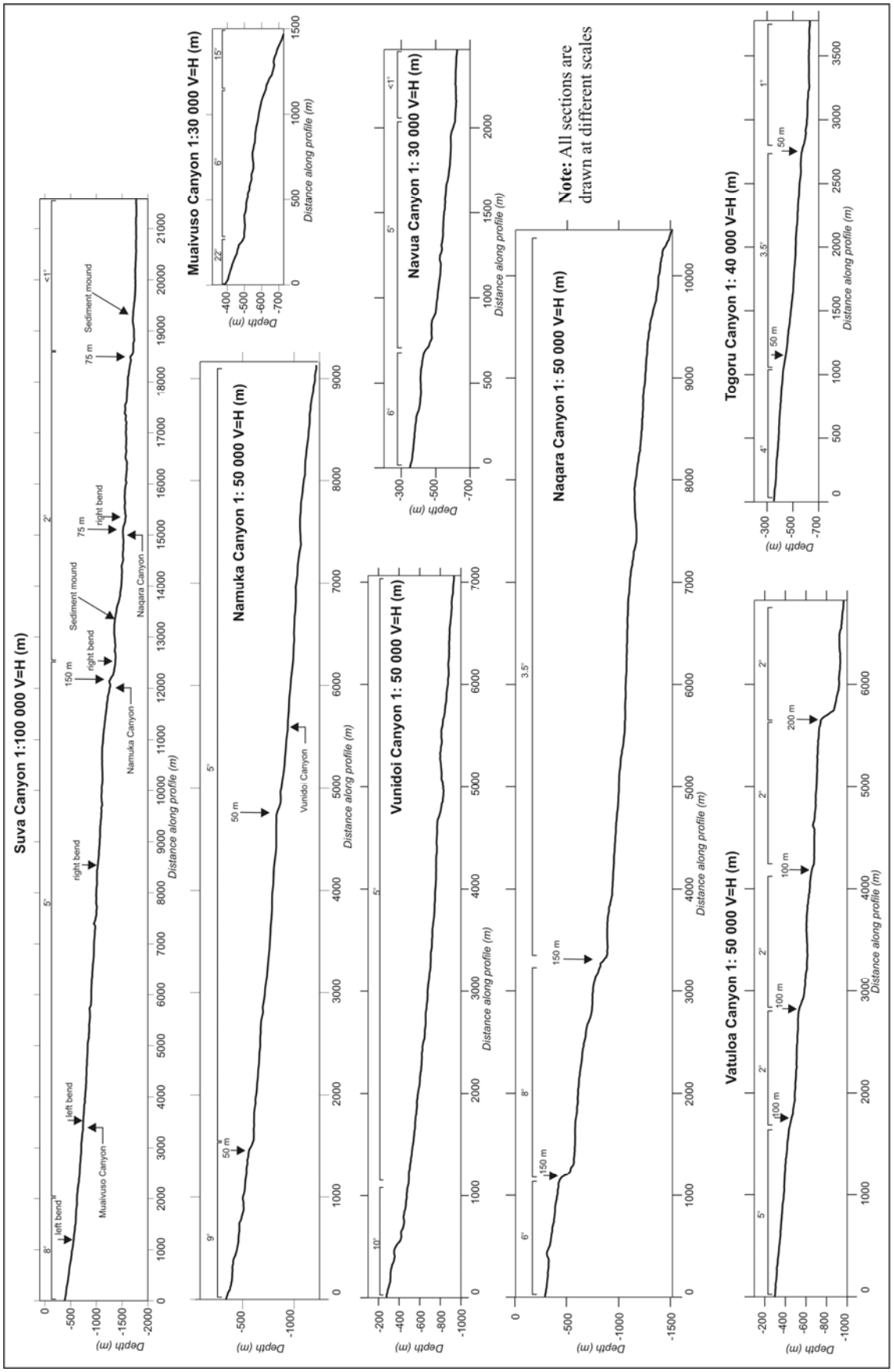

Figure 5.6b: Longitudinal profiles of the canyons on the Eastern Slope of Viti Levu. Also showing axial gradients and positions of confluences, lateral offsets and vertical drops (arrowed with heights).

drop in the floor of the Naqara Canyon to the floor of the Suva Canyon is observed, giving the Naqara Canyon the appearance of a “hanging valley”.

5.4.2 Seismic stratigraphy

The internal sedimentary structure of canyons is revealed by seismic reflection lines conducted across the heads of the submarine canyons (Figure 5.7a-c). Five distinct units are identified. The basal unit is lithified rock with well defined high amplitude internal parallel reflectors. This is interpreted to be the equivalent of the late Miocene to Pliocene Medrausucu Group rocks exposed along the coastline. A major erosional surface is identified, which forms 50 to 200 m deep V-shaped depressions in the bedrock unit below the present canyon floors. These depressions represent the buried axial traces of older canyons. The segment of the erosional surface that define the walls of these paleo-canyons, project upward to meet the present canyon walls on the surface, indicating episodes of infill followed by re-incisions along older canyon paths. Above the erosional surface, the canyons are filled with a weakly stratified canyon fill unit. The internal reflectors of this unit show an onlap relationship with the underlying erosional surface, while lensoidal reflectors occur higher up. An overlying cover unit is composed of weakly stratified to almost reflection free deposits and are characterised by a smooth seafloor surface. These together are interpreted to represent the hemipelagic cover. The fourth unit is a thin layer that forms broad mounds at the base of the canyon walls and on the canyon floors. This unit, characterised by chaotic internal reflections and hummocky surfaces, is interpreted to be deposits from failure of the canyon walls. Submarine landslides on the canyon walls are clearly recognised by the presence of rupture surfaces, displaced masses and headwall scarps (Figure 5.7b). The slide debris mounds overlie the canyon fill unit, partially blocking the thalwegs of the canyons. Holocene reefs, some of which are partially buried by the cover unit occur at the high points outside the rim of the canyons heads, directly above the basal unit.

5.4.3 Structural control of submarine canyons

The trend of the submarine canyons oblique to the coastline and oblique to the general slope of the seafloor of the Eastern Slope suggests that their formation and orientation is controlled by factors other than sedimentary or physical oceanographic processes. This inference is supported by the high degree of linearity and the general lack of sinuosity in most of the

Eastern Slope canyons. Unlike these canyons, high sinuosity is a distinct feature of submarine canyons elsewhere, for example, the Kaikoura Canyon and the Poverty Bay Canyon System in New Zealand (Lewis & Barnes, 1999; Lewis et al., 2001).

Submarine canyons in tectonically active settings can be controlled by local tectonic structures and zones of deformation (e.g. Scholl et al., 1970; Shepard, 1981; McHugh et al., 1998; Popescu et al., 2004). According to Shepard (1981), submarine fault valleys can be recognised by trough or V shaped floors, straight walls, hanging valley relationships with tributaries, and continuity with onland fault valleys. All these characteristics are common in the submarine canyons of the Eastern Slope.

5.4.3.1 SEISMIC STRUCTURE AND ONSHORE PROJECTION OF SUBMARINE CANYONS

Seismic reflection data across the upper parts of the submarine canyons reveal that they are bathymetric features, which are superimposed on structurally controlled depressions in the underlying rocks (Figure 5.7 a&c). Downthrow of the sub-seafloor rocks is shown to be accommodated by a number of normal faults facing the axes of these structural depressions. For example, a graben structure can be clearly seen in the seismic profile across the Vunidoi Canyon (Figure 5.7c). The graben-style faulting observed in the underlying rocks beneath the canyons is consistent with the style of deformation mapped onshore along the coastal areas of southeast Viti Levu and is also seen in seismic reflection profiles acquired on the marginal shelf. The structural grain of the submarine canyons extends landward as structural lineaments that are apparent in seismic reflection profiles on the marginal shelf, coastal and onshore morphology, and onshore geological structure (Figure 5.8 a,b,c,d).

Shelf indenting submarine canyons have clear near-shore morpho-structural expressions, which are defined by reef passages and elongated bays and estuaries bound by narrow peninsulas. The landward projection of the Naqara Canyon coincides with the Mau and Naqara Passages and the Nabukevesi and Wainidoi estuaries (Figure 5.8a); the Vatuloa Canyon by the Vatuloa Passage (Figure 5.8b), and the Namuka Canyon by the Namuka Passage and the Namuka Harbour (Figure 5.8c). The Suva Harbour is a morpho-structural graben (Shorten, 1993a), which occurs at the landward projection of the Suva Canyon. Field mapping and seismic reflection data indicate that the continuity of the NNE grain of the Suva Canyon with the Suva Harbour graben is disrupted and offset on the marginal shelf by a NW

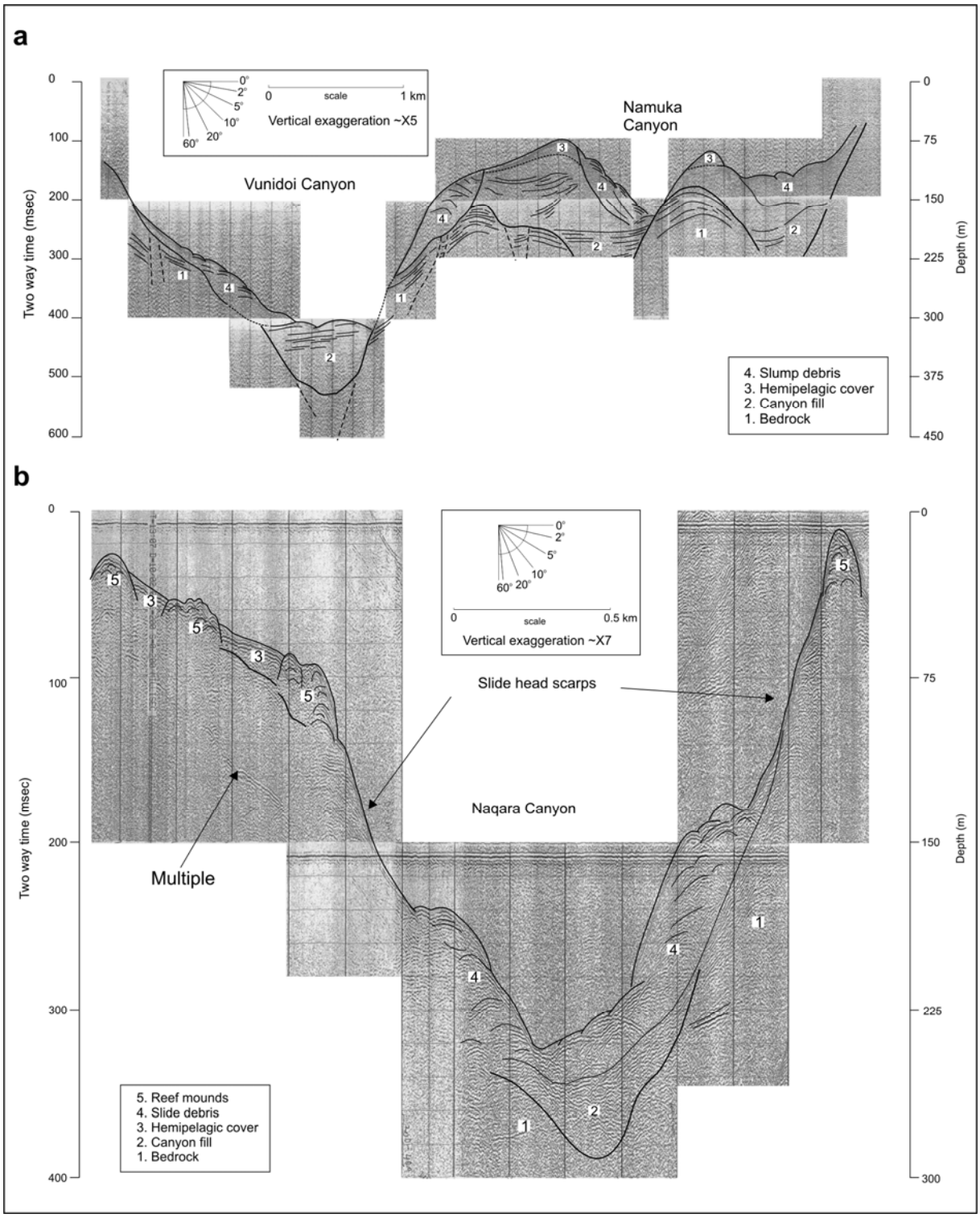

Figure 5.7: Single-channel seismic reflection profiles across the heads of the a) Vunidoi and Namuka Canyons and b) Naqara Canyon. Overlaid interpretations show the main sedimentary units across the canyons. See Figure 5.4a for location of profiles.

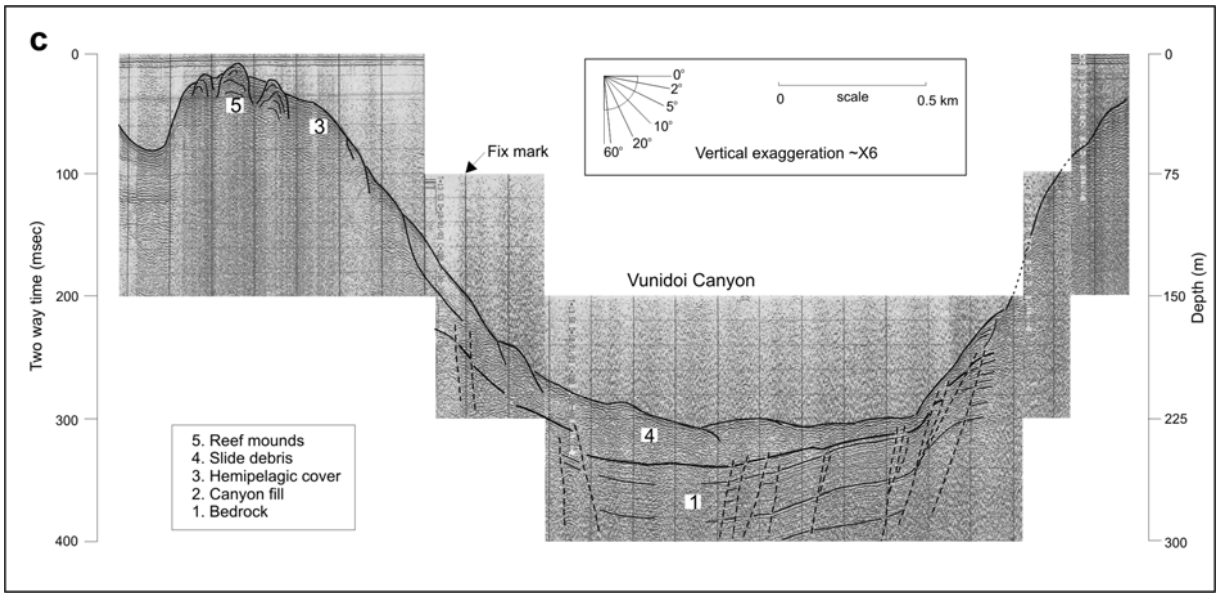

Figure 5.7c: Single-channel seismic reflection profiles across the head of the Vunidoi Canyon showing a graben structure. See Figure 5.4a for profile location.

trending fault zone. The NNE structure continues north of the Suva Harbour graben as the steep cliff bound valley along the Tamavua River (Figure 5.8d).

Seismic reflection profiles on the marginal shelf show monoclinal flexures and graben depressions in the underlying rocks directly along the landward projection of the submarine canyons. Examples of these features are shown in profiles across the landward projection of the Namuka, Vatuloa, Naqara canyons in Figures 5.9 a,b and c respectively. The seismic profiles show smooth, continuous and parallel reflectors in the underlying rocks across folds. Onshore mapping, however, such as near Namuka Island in this study (see Figure 4.10a) and on the Suva Peninsula by Shorten (1993a), show that folds develop along broad fault zones in which displacement is accommodated by many small faults that combine to form the flexures. A similar style of deformation is inferred to be present offshore. Their clear depiction however, appears to be limited by the resolution of the seismic data.

The profile across the Namuka Passage shows a drop in the level of the underlying rock (Suva Marl – Medrausucu Group) towards the west, which has been accommodated by a number of monoclinal folds that verge towards the centre of the passage (Figure 5.9a). The same set of structures are exposed on the shore platform fronting Namuka and Koronisako islands, a kilometre to the north, where pervasive faults are observed to

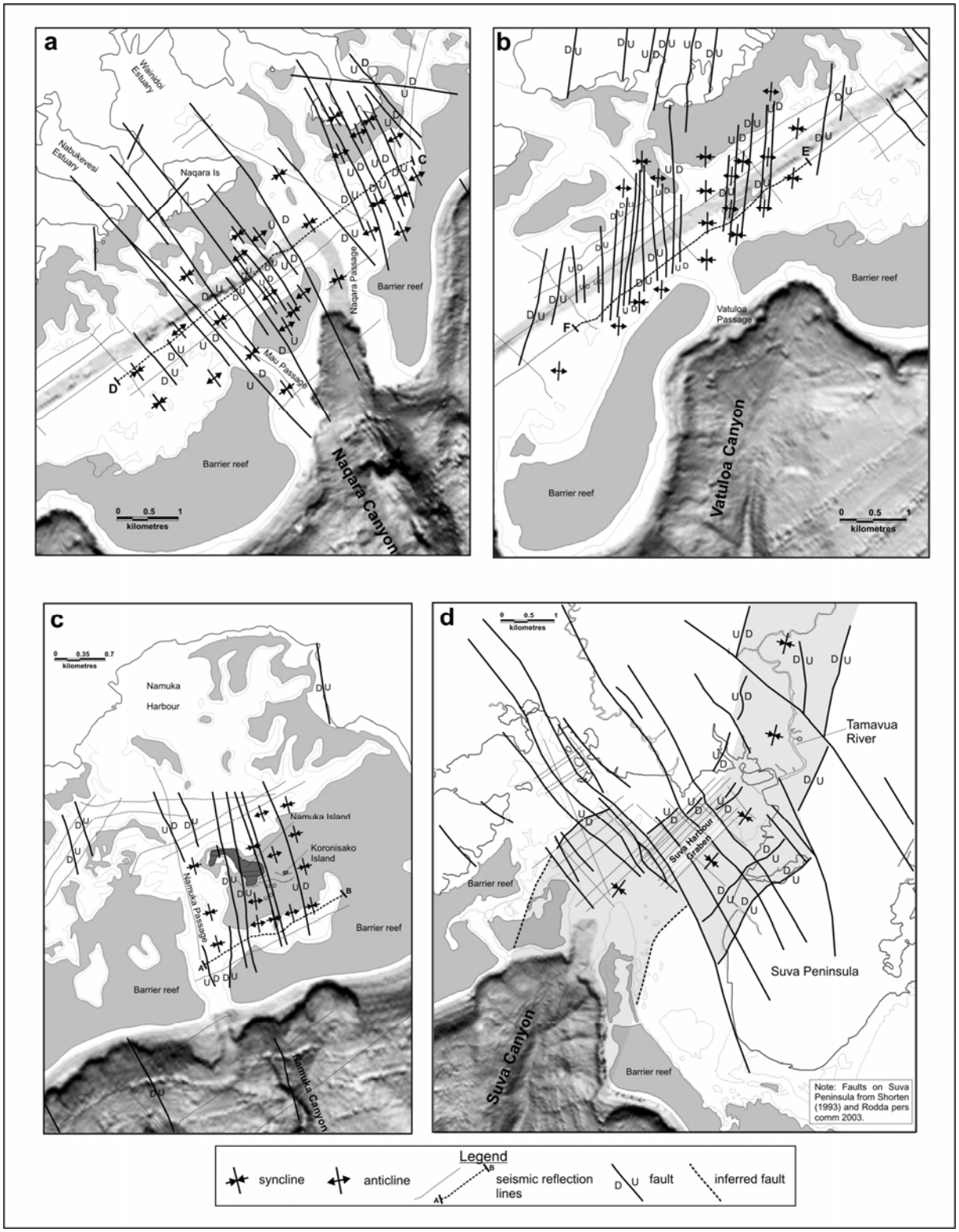

Figure 5.8: Projected onshore structural continuation of submarine canyons (a) Naqara Canyon (b) Vatuloa Canyon (c) Namuka Canyon (d) Suva Canyon. Labelled seismic lines in (a), (b), and (c) are presented in Figure 5.9. Shaded area in (d) shows the approximate onshore continuation of the Suva Canyon trend, having undergone disruptions by NW faults.

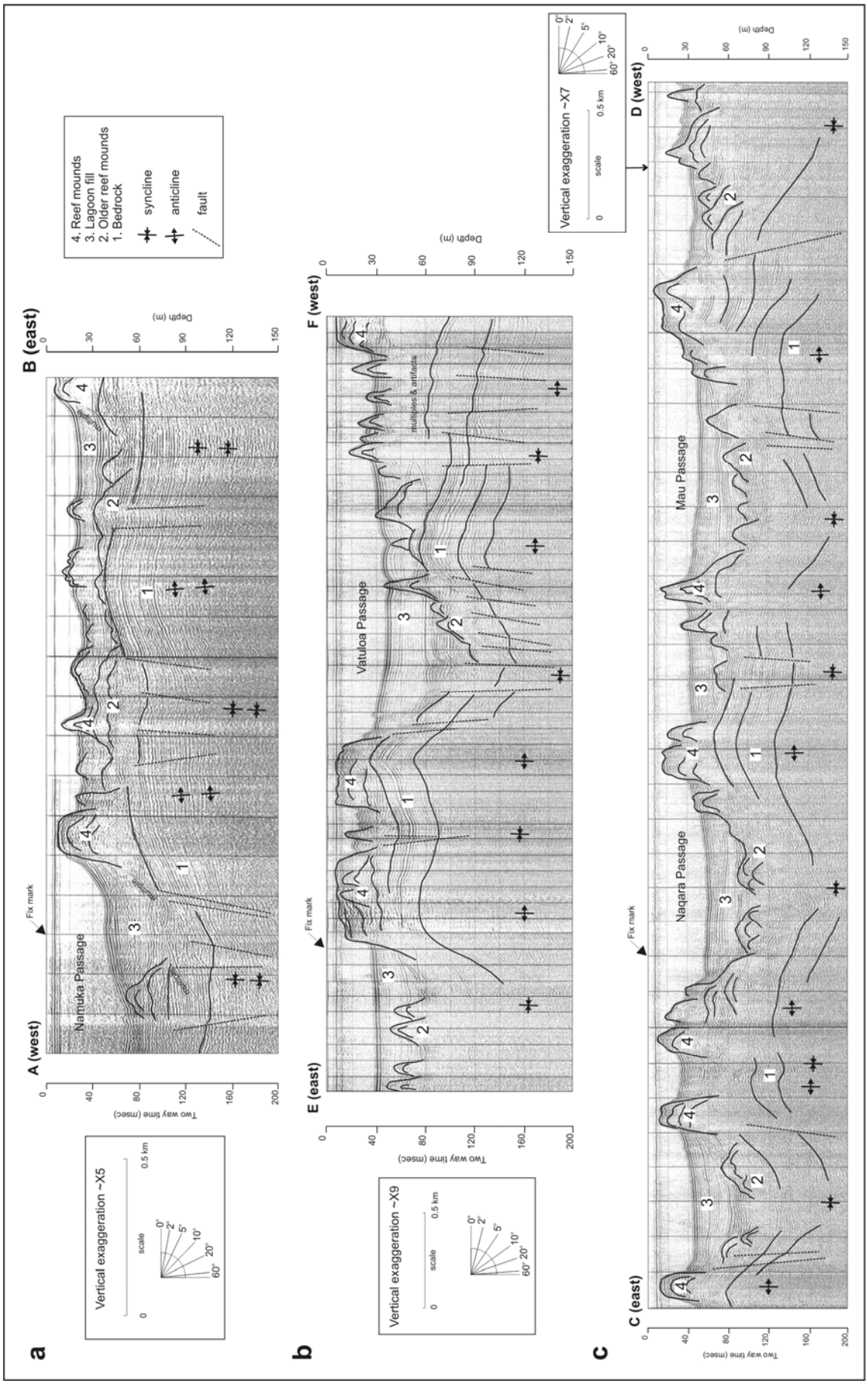

Figure 5.9: Interpreted seismic reflection profiles across the landward continuation of (a) Namuka Canyon (b) Vatuloa Canyon and (c) Naqara Canyon. See Figure 5.8 ab&c for profile locations.

accommodate displacement. In the west of the profile, the largest graben, below Namuka Passage, occurs directly in line with the northward projection of the Namuka Canyon thalweg (Figure 5.8c). Field measurements show that the base of the Suva Marl is downthrown 25 m in this graben, comparable to that observed in the seismic profile. A similar structural style is recognised in the seismic profile across the Vatuloa Passage, to the north of the Vatuloa Canyon. A large graben, a kilometre wide and accommodating a downthrow of approximately 60 m, coincides with the Vatuloa Passage and occurs along the projection of the Vatuloa Canyon thalweg (Figures 5.9b, 5.8b). Synclinal depressions are recognised below the Mau and Naqara Passages along the trajectory of the Naqara Canyon (Figures 5.9c, 5.8a). Low-angle slickensides are commonly seen in the onshore exposures of faults, indicating that there is probably a strike-slip component in the apparent normal displacements seen in seismic profiles.

5.4.3.2 REGIONAL ONSHORE-OFFSHORE STRUCTURAL LINEAMENTS

The continuity of structures between the onshore and offshore area was examined by mapping structural lineaments (Figure 5.10). Offshore lineaments of the Eastern Slope were mapped using the shaded relief image generated from the swath bathymetric data. On the Eastern Slope, lineaments represent all linear erosional features such as scarps, gullies and channels which may have a direct inheritance of basement structure. Linear depositional features such as channel levees have not been included in this set of lineaments. As such, the mapped lineaments show a clear distribution bias toward areas of steeper slope gradients, where erosion may be preferentially controlled by basement features. The offshore lineament data set also includes the canyon axes, which were mapped as linear segments.

Unique morphological characteristics are recognised in the submarine canyons at the intersections of offshore structural lineaments. These intersections correlate with the positions of the vertical steps and lateral offsets of the canyon axes, and coincides also with changes in the axial gradients of the canyons. For example, the intersection of two major structural lineaments at the confluence of the Namuka Canyon and Suva Canyon coincides with a 150 m vertical step, a slight right bend and a decrease in the axial gradient from 5^{o} to 2^{o} in the Suva Canyon (Figure 5.6b). Prominent vertical steps in the Vatuloa and Naqara Canyons also correlate with the positions of intersecting lineaments (Figure 5.10). These morphological features have not been studied in detail, however, they are interpreted to represent the surface

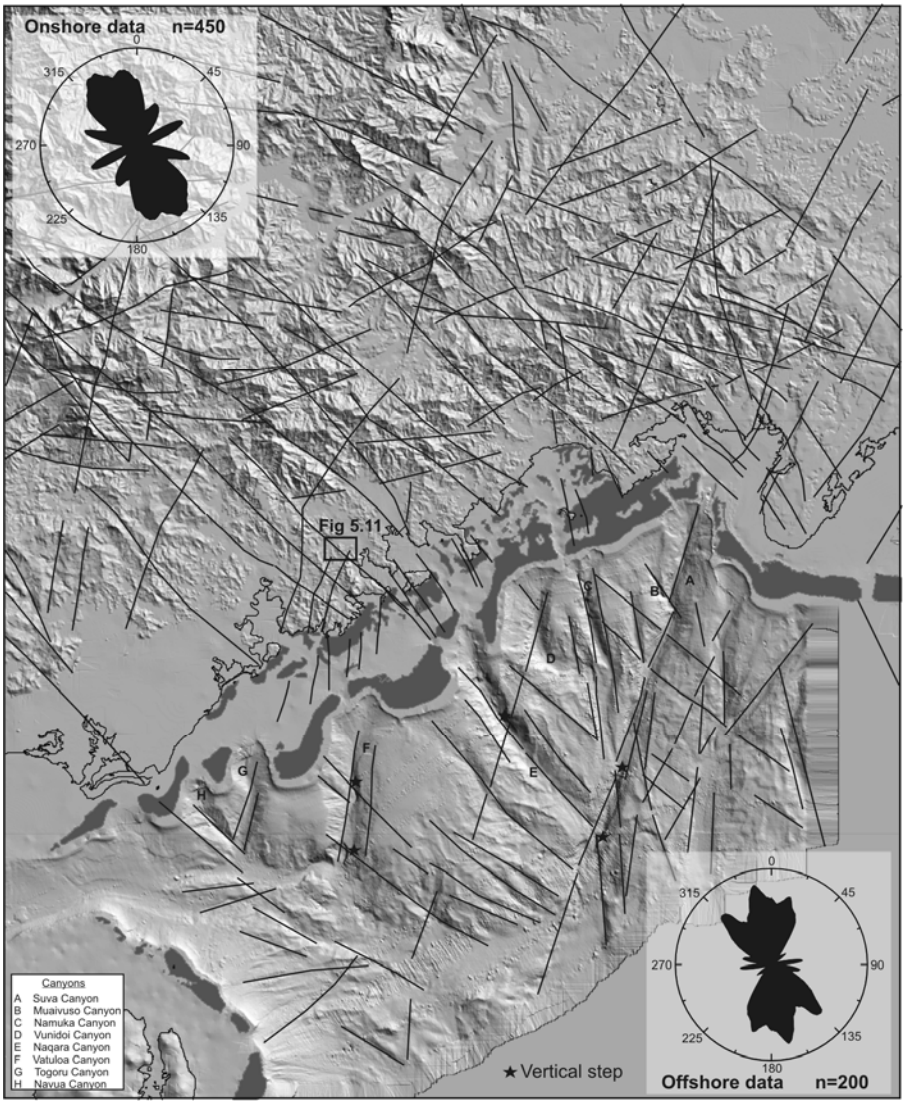

Figure 5.10: Simplified structural lineament map of the onshore-offshore area of southeast Viti Levu. Statistical rose plots of the entire onshore and offshore datasets show the main trends of the structural lineaments.

expression of fault displacements in the basement rock that have been modified by scouring effects along the canyons. A nearshore example of the intersection of two structural trends is shown along the landward projection of the Suva Canyon (see Figure 5.8d). The positions of the vertical steps are slightly upstream from the intersections of the lineaments, indicating that these steps are retreating upstream from their original position at the cross structure. Mound like features are noticeable downstream of the vertical steps along the Suva Canyon longitudinal profile (Figure 5.6b), which are interpreted as either accumulated sediments piles coming off the retreating cliff face, or alternatively may represent scour features associated with the hydraulic jump.

Onshore lineaments were mapped at 1: 50 000 scale and include: i) aerial photo lineaments; ii) fault data collected from new onshore mapping; iii) faults on the marginal shelf from seismic reflection profiles; iv) faults from published Fiji Geological Survey geological maps and; v) faults from Shorten (1993a), Armstrong (1993) and Rodda pers comm. (2004). A statistical analysis of 450 onshore and 200 offshore structural lineament orientations was carried out. The orientations of offshore and onshore structural lineaments are plotted separately on rose plots in Figure 5.10. All lineament azimuth data have been plotted after normalisation to a uniform data distribution (Wise & McCrory, 1982; D. Wise, pers comm. 2004). The offshore lineaments have the same peak orientations as the onshore lineaments, which are NW, NNW and NNE. The datasets also show WNW and ENE peaks, but the offshore peaks for these trends are distinctly subdued compared to the corresponding onshore peaks. It is possible that the offshore structures with these trends are buried and hidden by sedimentation. Another interpretation is that the WNW and ENE trends represent older faults and are not present offshore, as they are restricted to only Oligocene to Early Miocene Wainmala and Savura Group rocks onshore. The NW, NNW and NNE lineaments appear to represent younger faults, which are present in the Oligocene and Miocene rocks onshore, as well as in the younger offshore terrain of the post-Miocene rocks. The offshore lineaments with these trends show excellent continuity along strike with the onshore lineaments, defining a number of structures that are continuous through the onshore and offshore areas.

5.5 DISCUSSION

5.5.1 Submarine canyons as expressions of offshore faults

In the earlier sections of this chapter detailed information is presented from the upper slope areas of the Eastern Slope to show an apparent relationship between the morphology of submarine canyons and the underlying bedrock structure. The collective evidence presented provides a strong indication that the submarine canyons of southeast Viti Levu are the surface expression of concentrated zones of fracturing and faulting in the underlying bedrock. This evidence includes clear continuity of the canyon fabric in the physiography and bedrock structure along their nearshore and onshore trajectory, sharp bedrock undulations in the seismic reflection profiles taken directly across the canyons, and continuity of canyon trajectories with onshore structural lineaments. The morphology of the canyons can therefore be used to infer the positions of faults in the offshore area of southeast Viti Levu. The traces

of offshore lineaments mapped along the canyon axes can be used to depict the pattern of offshore faulting. The peculiar geometrical arrangement of the axes of submarine canyons on the Eastern Slope suggests that they may be related to a complex mesh-like pattern of faulting in the offshore area. A diffuse pattern of seismicty over the offshore area of southeast Viti Levu suggests that the fault zones underlying the canyons may be responsible for earthquakes that have occurred in this area and is consistent with this mesh style structural framework inferred for the area. A more detailed interpretation of the combined onshore and offshore structures of southeast Viti Levu in the context of tectonic setting and the origin of seismicity of the region is presented in Chapter 8.

The identification of submarine canyons as fault controlled submarine valleys and their correlation to onshore structure allow for the recognition of a number of continuous onshore-offshore faults in southeast Viti Levu that were previously unknown. For example, the trajectory of a NW trending fault zone passing through the Naqara Canyon, extends through the Mau Passage, Naqara Island and the Nabukevesi Estuary on the marginal shelf, and further inland as prominent lineaments on the onshore digital terrain model (Figure 5.10). The onshore segment of this structure outcrops as steeply dipping faults with low angle slickenslide lineations in some road cut batters along the Queens Highway between Nabukevesi and Lobau Settlements and on a side road to Qilai Settlement (Figure 5.11). High quality recordings of earthquake locations in the offshore area show alignment with the traces of some offshore faults, which indicates that some of these structures are seismically active (Figure 5.12). The continuity of onshore faults can now be traced through to the offshore area, and in turn can be used to define the absolute lengths of potential earthquake source structures in seismic hazard evaluations in southeast Viti Levu (Chapter 9).

5.5.2 Evolution of submarine canyons

It is now widely accepted that submarine canyons of the world form either by upslope erosion caused by retrogressive failures (Twichell & Roberts, 1982; Farre et al., 1983; Klaus & Taylor, 1991) and/or by downslope erosion caused by upslope (shelf) sourced sediment flows/turbidity currents (Daly, 1936; Scholl et al., 1970; Herzer, 1979; Pratson et al., 1994; Pratson & Coakley, 1996). Using data from different global localities Shepard (1981) concluded that submarine canyons are long-lived features that evolve over long periods of time by repeated infilling and re-incision events.

Figure 5.11: Faults mapped along the onshore trajectory of the Naqara Canyon at (a) Queens Highway and (b) Qilai Road. Lower hemisphere stereonets show attitudes of representative fault data collected at the sites. Locality of outcrops shown in Figure 5.10.

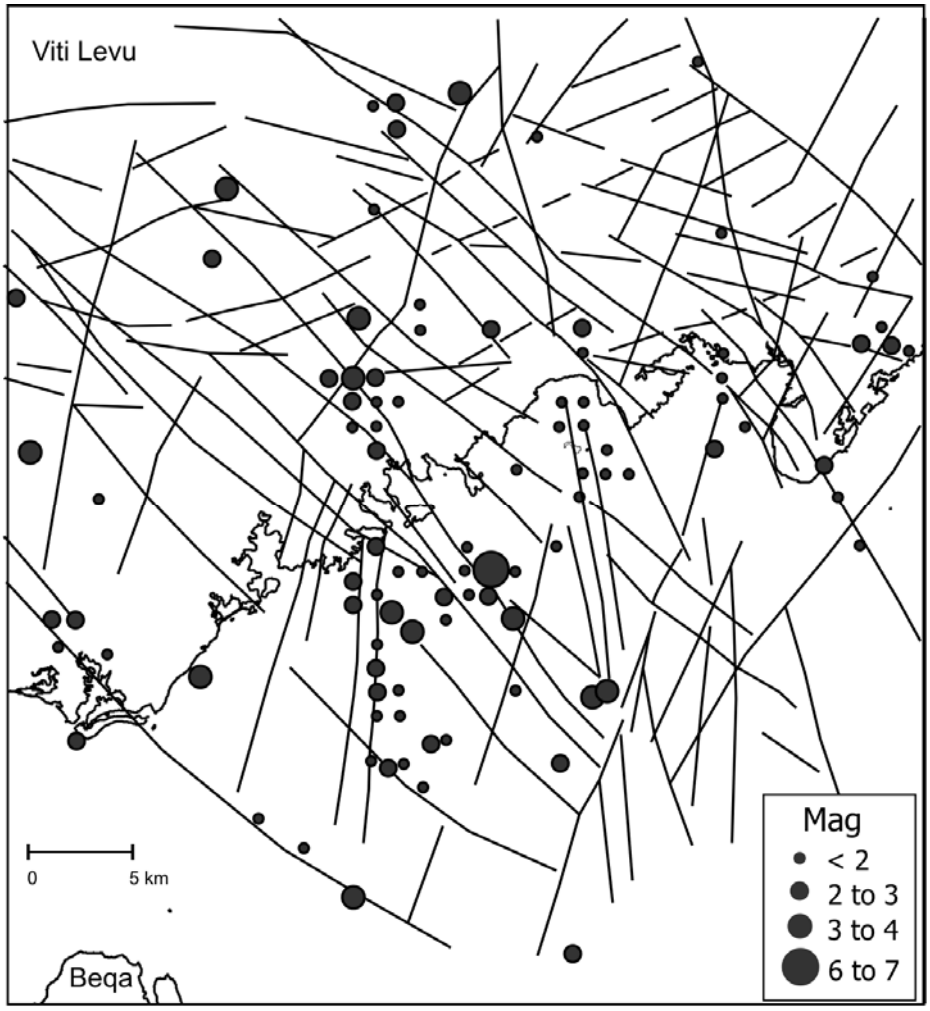

Figure 5.12: Earthquake epicentres in the southeast Viti Levu overlain on the mapped fault mesh. Discrete nests of epicentres occur along the traces of some fault segments within the fault mesh.

The initial carving of the submarine canyons of southeast Viti Levu would have preferentially exploited structural depressions and zones of weakness in bedrock created by the faults zones. This would have occurred sometime following proto-arc fragmentation and opening of the Suva Basin along with other offshore and presently onshore basins on the Fiji Platform (Brocher & Holmes, 1985; Hathway, 1993; Johnson, 1994). The submarine canyons, subsequently, may have been modified by numerous infilling and re-incision events coinciding with the Quaternary global glacio-eustatic sea-level changes, whilst their positions were still primarily controlled by the underlying structure.

Seismic reflection profiles show the buried axial traces of older canyons directly below the present canyon thalwegs (e.g. Figure 5.7a,b). It is postulated that this older incision, was coeval with the last low sea level stand of the late Pleistocene period (marine stage 2), about 21 000 years BP, when sea level was about 120 m below the present sea level (Lambeck & Chappell, 2001). The shoreline during this period was at the edge of the marginal shelf, about 120 m lower and about 5 km seaward of the present shoreline. Seismic reflection data on the marginal shelf show that bedrock levels below buried paleochannels are as much as 100 to 120 m below the present sea level (Figure 5.9a-c). These paleochannels represent the drainage system connecting the land valleys to the heads of the submarine canyons during this period of lowered sea level. Broad paleo-reef mounds are also seen in some seismic profiles (e.g. Figure 5.9a) in between the younger Holocene reefs and the underlying bedrock. These are interpreted as Pleistocene reefs eroded during the last and possibly earlier low-stand sea levels (Shorten, 1993b). Extensive erosion would have brought voluminous quantities of sediment through these paleochannels directly to the submarine canyon heads. Gravity driven sediment flows (turbidity currents) would have caused deep erosion along the canyons.

During marine transgression following the low-stand sea, a barrier reef system developed at the edge of the marginal shelf forming an inner lagoon and trapping most of the terrestrial sediment outflow. During the transgression, the sites of the paleochannels would have been unfavourable for reef development due to excessive sedimentation, water depth, and poor salinity (Shorten, 1993a). Deep-water passages developed at these sites and the connection of the submarine canyons to the inner lagoon would have been maintained as the reef continued to build in the surrounding high areas. Terrestrial sediment supply to the submarine canyons was maintained through the reef passages, albeit in reduced quantities, permitting sediment build up at the canyon heads and infilling in the upper parts of the canyon axes by

hemipelagic drape. Earlier similar cycles of lowered sea level and subsequent transgressions (e.g. marine stages 6, 8, 10, 12 etc.) would have had a similar effect in the evolution process of the canyons.

In the present high-stand, the submarine canyons of southeast Viti Levu continue to act as the end points of the coastal sediment transport system, similar to submarine canyons elsewhere, for example, Sepik River, PNG (Kineke et al., 2000), and the Eel Canyon, California (Mullenbach et al., 2004). At present, suspended sediment from the distributaries of the Rewa River are carried westward by the southeasterly trade winds and tidal currents and deposited in the Suva Harbour (Solomon & Kruger, 1996). Under the influence of wave and tidal currents on the shelf, the Suva Harbour sediments are fed to the head of the Suva Canyon through the Suva Passage.

The canyons of southeast Viti Levu are presently cutting into the marginal shelf and this is being achieved by the process of retrogressive failures at the heads of the canyons (see Section 6.3). The landward extension of the canyon fault zones appears to guiding the current headward erosion of the canyons into the marginal shelf. The process of retrogressive failures at the heads of the canyons and the resulting turbidity flows (e.g. Houtz and Wellman, 1962) are contributing a current phase of incision along the canyon axes that is partially re-excavating the older canyon positions.

5.6 SUMMARY AND CONCLUSIONS

The southern slopes of Viti Levu are subdivided into five morphological units based on surface morphological characteristics and structural complexity. These units are the Western Slope, Beqa Lagoon Slope, Beqa Passage, Eastern Slope and the Rewa Delta Foreslope. The Eastern Slope, an area bound by the coast between the Suva Peninsula and the Beqa Lagoon is the most structurally complex. The surface of the Eastern Slope is scarred by linear submarine canyons, which are the surface expressions of structurally controlled depressions in the underlying basement rock. The morpho-structurally defined submarine canyons are contiguous with physiographic and structural features on the marginal shelf and on land. The structural trend of submarine canyons continue onshore as fault zones and structural lineaments. The morpho-structural expression of the submarine canyons are therefore, inferred to represent offshore fault zones and they are used to collectively define continuous

onshore-offshore fault zones. The overall pattern of offshore faulting is that of a complex mesh of faults, and similar to that described for the onshore region of southeast Viti Levu (Chapter 4). This geometry of faulting is consistent with the overall diffused pattern of seismicity observed over this region. Closer examination of the seismicity pattern reveals that earthquakes follow the trace of submarine canyon fault segments, which indicates that some may be seismically active. Absolute lengths of continuous onshore–offshore faults can be used in seismic hazard evaluations of the coastal region. The submarine canyons are considered to have developed primarily by downslope erosional processes and may have experienced several episodes of re-incision and infilling events since initial carving along zones of weakness created by fault zones.

CHAPTER 6

SUBMARINE LANDSLIDE TSUNAMI SOURCES

6.1 INTRODUCTION

Local tsunamis occur occasionally in the Fiji region. Out of the eleven tsunamis reported in the Fiji region over the last 150 years, three have been locally generated (Everingham, 1987). The other eight events were from distal sources in Vanuatu, Tonga and South America. The local tsunamis, which followed medium to large local earthquakes, were recorded along the coastlines of northern Vanua Levu in 1881 and southeastern Viti Levu in 1953 and 1975 (Everingham, 1987). The 1881 event produced waves as high as 2 m and was inferred by Everingham (1987) to have originated from the highly seismically active Fiji Fracture Zone north of Vanua Levu. The 1953 tsunami caused several fatalities and considerable damage in Suva. This event is reviewed in more detail in the following chapter. The 1975 tsunami was a minor event with maximum estimated wave heights of 0.5 m in Suva. It followed an offshore earthquake with magnitude M_s 5.2 (Everingham 1983c).

Co-seismic fault ruptures and associated displacement of the seabed may not be a significant contributor to local tsunamis in the Fiji region. Close to fifty large earthquakes (M> 6) have occurred in Fiji over the past 150 years (see Section 9.3.1) and not all the large offshore events are associated with local tsunamis. For example, the destructive nearshore events in 1979 near Taveuni (M_s 6.9) and in 1932 near Koro (M_s 6.5) had no reports of unusual wave or tidal activity at nearby coasts. It is possible that earthquakes in Fiji do not have sufficient strength to cause dislocation of the seabed and generate tsunamis. The maximum magnitude of historical earthquakes in Fiji does not exceed M_s 7.1. In addition, mapping of faults (Chapter 4) and focal mechanism data (Figure 9.3) indicate that the predominant style of faulting in Fiji is strike slip, the mechanics of which are not conducive to generating large tsunamis. It is also seen that events as small as the 1975 Suva earthquake are associated with tsunamis that normally would not have been predicted based on the earthquake magnitude alone.

It is therefore considered likely that submarine landslides play an important role in the generation of local tsunamis in Fiji. Seismically triggered submarine landslides at the shelf break of southeast Viti Levu have been postulated as sources of local tsunamis and erosive turbidity currents by previous workers (Houtz, 1962a; Houtz & Wellman, 1962; Everingham, 1987). It is shown in the next chapter that numerical simulations of tsunami generation and propagation based on a submarine landslide source produce coastal wave heights and arrival times that are consistent with those recorded during the 1953 event. A simulation of an earthquake dislocation source is unable to reproduce the observed data of the 1953 event.

This chapter presents a study of submarine mass movement features in the offshore area of southeast Viti Levu and their capability for tsunami generation. Newly acquired high resolution multibeam bathymetry data reveals the morphology of the offshore area of southeast Viti Levu in unprecedented detail, which provides new insights into the active seabed processes and the evolution of the slope. The high quality images of youthful bathymetric features allow for the recognition of active and potentially hazardous mass movement processes. The main objectives of this chapter are to: i) to document the location, morphometry and possible triggering factors of submarine landslides on the southern slopes of Viti Levu; ii) evaluate their potential for tsunami generation; and iii) identify offshore zones that may have potential to generate submarine landslide tsunamis that may impact the adjacent coast of Viti Levu in the future.

6.2 METHODOLOGY

Newly acquired high resolution SeaBat 8160 multibeam bathymetry data, introduced in Chapter 5, were used to map submarine landslides on the southeast slopes of Viti Levu. The spatial resolution of this acoustic data set allow the morphological characteristics of recent mass movements to be depicted at an accuracy to within a few metres. Morphometric data on submarine landslides were measured using GIS directly from derivative shaded relief and contour maps, cross sections, and three dimensional images of the swath bathymetric data set.

A rapid method was used to assess the tsunami potential of all submarine landslides mapped in southeast Viti Levu. This method involves the calculation of the initial maximum tsunami amplitude above the slope failure as a proxy of the hazard at the coast. This method has been used in studies on the tsunami hazard potential of submarine landslides in continental margins

of the world, for example by Goldfinger et al. (2000), Bohannon & Gardner (2004), Locat et al. (2004) and McAdoo & Watts (2004). This method of assessing the tsunami hazard is a simplistic approximation only as wave propagation from the source area to the coast may undergo complex modifications. Wave focussing and shoaling effects due to shallow nearshore bathymetry features, complex interaction with irregular shoreline and wave front spreading may all affect the size of the waves striking the coast. Notwithstanding this limitation, this method is sufficient to provide an approximate indication of the relative tsunami hazard potential of a large number of widely distributed submarine landslides. The complex near shore effects associated with tsunami wave propagation in southeast Viti Levu and a more in depth assessment of the tsunami hazard using a specific case study are presented in the next chapter.

6.3 DESCRIPTION OF SUBMARINE LANDSLIDES

In southeast Viti Levu, the occurrence of mass movement features are recognised on the multibeam bathymetry data primarily from head wall scars left by submarine landslides. Mass movement features can be less commonly recognised by the occurrence of debris mounds, sediment lobes and depositional scarps. The failures are predominantly disintegrative, turning into mass flows, as most lack bathymetric evidence of displaced mass at or near the base of the scar. The Eastern Slope, an area between Suva Peninsula and Beqa Lagoon (see Chapter 5), contains the highest proportion of mass movement features on the slopes of southern Viti Levu. There is little evidence in the multibeam data of slope failures outside this zone. There are very few submarine landslides scars on the slopes immediately outside the outer margins of the Navua and Rewa River deltas. Here the sedimentation rates would exceed the rate of mass movements. There is a good correlation between the position of landslide headscarps and anomalously high slope gradients. This indicates that very high slope gradients are due to oversteepening by slides. Areas of high gradients, typically between 25^{o} to 30^{o}, occur in the canyon head walls at the edge of the marginal shelf. In the upper sections of the canyons, the lateral walls are locally as steep as 60^{o} (see Figure 5.6a). High gradients also occur on the barrier reef fronts, and are between 20^{o} to 40^{o}. These high gradients areas are indicative of unstable slopes, where slope failure is occurring and is likely to occur in the future.

Slope failures of the Eastern Slope were classified based on their specific location on the marginal slope. The four divisions recognised are: i) reef edge slides; ii) mid-slope slides; iii)

canyon wall slides; and iv) canyon head slides. The mid-slope slides refer to those slides on the marginal slope that do not occur in the first three categories. The spatial distribution of all significant slides mapped is shown in a three-dimensional image of the Eastern Slope in Figure 6.1. The slides are also shown on the morpho-sedimentary/morpho-structural interpretation map of the Eastern Slope in Figure 5.4b. The morphometric parameters of all slides are presented in Table 6.1.

All slides have thickness to length ratios less than 0.2 and therefore are classified as translational slides (Mulder & Cochonat, 1996). Canyon wall slides are typically the smallest by volume and appear to be the most frequently occurring type of failure on the Eastern Slope. Owing to their small size and abundance, only the largest are shown in Figure 6.1. They occur on steep canyon walls in the upper sections of the canyons and are clearly observed in seismic profiles, for example in Figure 5.7b. These slides appear to be youthful features which frequently result from undercutting by the erosive canyon turbidity flows.

Reef edge failures are the largest slides recognised on the Eastern Slope, with average surface areas of 6 km^2; the largest reef edge slide mapped has an area of ~14 km^2. Typical reef edge slides occur along the eastern edge of the Beqa Lagoon. Such slides have broad headscarps, 2 to 4 km wide, which form arcuate embayments on the outer barrier reef edge. Several sets of narrowly spaced sub-parallel to radiating gullies, define the runout paths of these slides, which overlap at the base of the slope. Angular mounds, 20 to 40 m high, on the seafloor immediately downslope of the headscarps are inferred to represent piles of slide debris derived from the headscarps (see Figure 5.4b). These are considered to be similar to blocky reef debris found by Schneider et al. (1995) from diving transects immediately outside the barrier reef fronts near Suva.

The mid-slope slides typically have narrow and elongated scars, 300 to 500 m wide. Occasionally they have multiple arcuate headscarps whose runout paths link down slope to form a single channelised chute. Minor headscarps occur downslope of the main headscarp. The largest slides have surface areas between 6 to 8 km^2. The geometry of these slides indicate that they may have formed as complex retrogressive failures, with the slide mass changing into debris flows that are “funnelled” downslope along channelised (erosional) chutes. Based purely on morphological characteristics it appears that mid-slope slides evolve

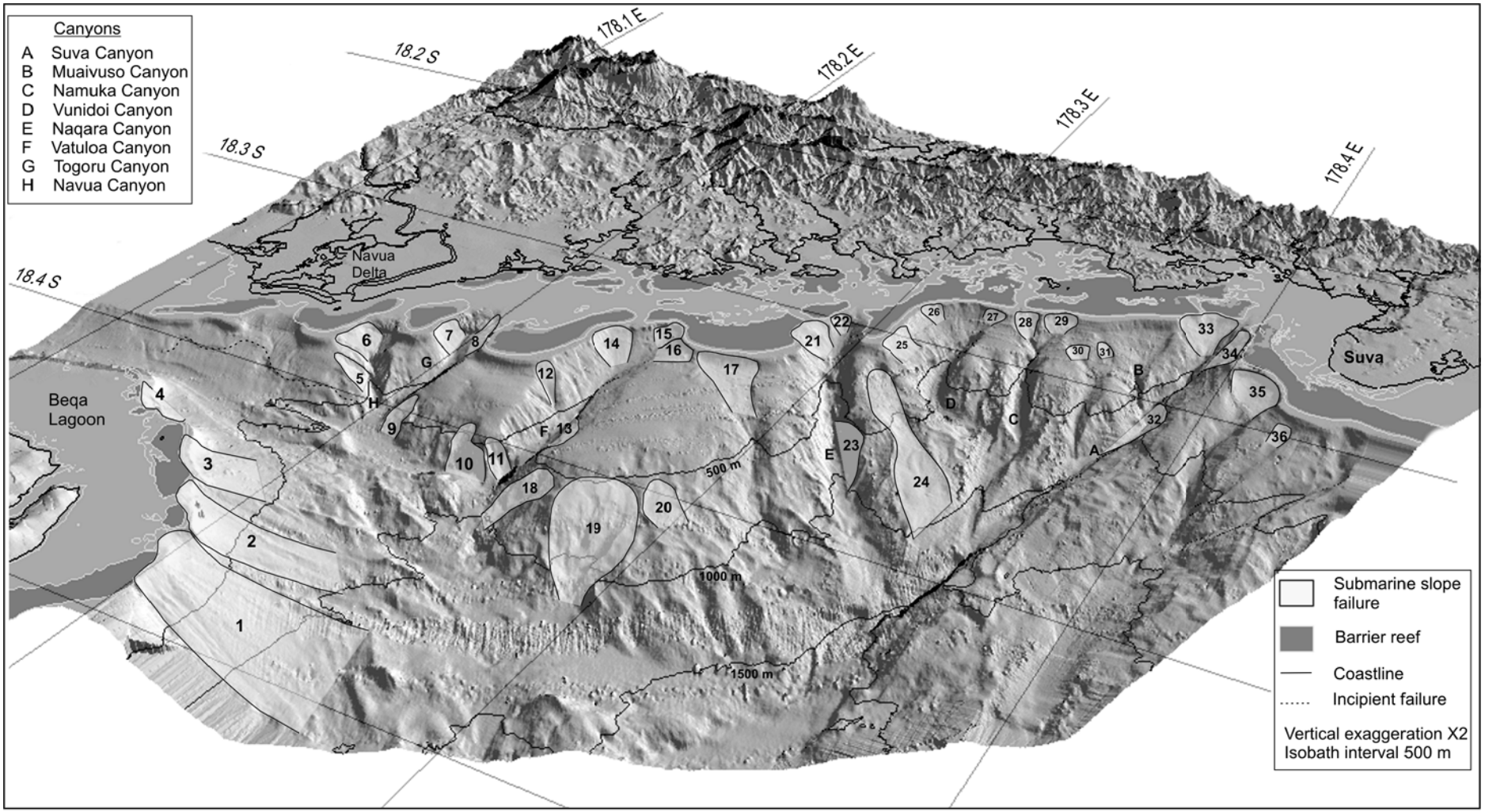

Figure 6.1: A three dimensional perspective image of the marginal slope between Beqa Lagoon and Suva Peninsula (Eastern Slope) showing the locations of submarine landslide scars (number 1-36: also refer to Table 6.1).

Table 6.1: Measured submarine landslide characteristics and their calculated near-field tsunami dimensions.

slide*	type	area (km^2)	θ (deg)	d (m)	b (m)	T (m)	w (m)	T/b	λ (m)	A (m)
1	reef edge slide	14	15	400	4000	25	3600	0.01	9622	4
2	reef edge slide	6	10	400	3500	50	1700	0.01	10989	2
3	reef edge slide	4	10	250	2500	40	1700	0.02	7342	3
4	reef edge slide	4	15	200	1500	20	2500	0.01	4167	3
5	canyon wall slide	1	15	300	1400	20	730	0.01	4930	1
6	canyon head slide	1.2	15	150	800	25	1500	0.03	2635	2
7	canyon head slide	1	30	150	800	30	1220	0.04	1896	6
8	canyon head slide	1.7	15	200	1120	25	1550	0.02	3600	2
9	mid slope slide	0.8	15	450	1400	25	550	0.02	6038	0.3
10	mid slope slide	0.6	30	650	670	50	850	0.07	3612	0.6
11	canyon wall slide	0.4	30	650	600	70	690	0.12	3418	0.7
12	canyon wall slide	0.7	15	300	1300	30	500	0.02	4751	1
13	canyon wall slide	1.3	20	550	760	25	1750	0.03	4278	0.5
14	canyon head slide	2	15	150	1300	35	1300	0.03	3359	5
15	canyon head slide	1.3	10	120	1300	35	1000	0.03	3668	3
16	canyon head slide	1	15	125	1600	55	600	0.03	3402	6
17	reef edge slide	4	12	200	2400	50	1500	0.02	5880	6
18	mid slope slide	2	13	750	1800	25	1160	0.01	9481	0.2
19	mid slope slide	8	15	900	3800	40	2000	0.01	14068	1
20	mid slope slide	1	10	550	1400	40	810	0.03	8149	0.2
21	canyon head slide	2	10	150	1200	20	1640	0.02	3940	2
22	canyon head slide	0.4	10	75	800	25	500	0.03	2275	2
23	canyon wall slide	1	30	650	1100	45	900	0.04	4628	1
24	mid slope slide	6	10	600	6300	50	1000	0.01	18056	1
25	canyon head slide	2	20	200	1740	50	1300	0.03	3904	8
26	canyon head slide	1.3	10	125	1600	30	800	0.02	4153	2
27	canyon head slide	0.7	17	130	1250	35	590	0.03	2885	4
28	canyon head slide	0.6	20	100	850	30	690	0.04	1929	5
29	canyon head slide	0.8	15	120	1000	50	770	0.05	2635	5
30	mid slope slide	0.7	10	225	960	20	680	0.02	4316	0.3
31	mid slope slide	0.6	5	275	1170	25	530	0.02	7436	0.1
32	canyon wall slide	3	7	675	1200	30	2300	0.03	9977	0.2
33	canyon head slide	3	25	200	1700	70	1500	0.04	3471	16
34	canyon head slide	2.7	20	175	1300	50	2100	0.04	3156	11
35	reef edge slide	3	15	200	1400	60	2100	0.04	4025	8
36	mid slope slide	0.8	10	200	1540	50	520	0.03	5154	1
						Mean Values				
	reef edge slide	6	13	275	2550	41	2183	0.02	7004	4
	mid slope slide	2	13	511	2116	36	900	0.03	8479	1
	canyon wall slide	1	20	521	1060	37	1145	0.04	5330	1
	canyon head slide	1	16	145	1224	38	1137	0.03	3127	5

Measured values are: slide area, pre-failure slope angle (θ), initial submergence depth at middle of slide (d), length of slide (b), slide thickness (T), slide width (w). The wavelength (λ) and near field tsunami amplitude (A) are calculated using predictive tsunami amplitude equations of McAdoo & Watts (2004)
* For locations of slides refer to Figure 6.1.

over time into deep mid-slope channels as a result of continued retrogression of headscarps and entrenchment of runout chutes. A further mid-slope slide type is recognized on the slope to the south of the Navua Delta. Here wavy lines sub-parallel to the isobaths represent 20 m

high headscarps of broad and shallow incipient bedding plane detachment failures that are occurring in unconsolidated terrigenous sediments rapidly accumulating on the foreslope of the Navua Delta (see Figure 5.4b).

Canyon head slides also occur at the reef edge but are confined to the heads of the shelf indenting canyons. They are shallow depth retrogressive slides that have comparatively smaller widths and lengths than the reef edge slides. They have surface areas that range from 0.5 to 2 km^2. In plan view these slides have well defined arcuate shaped headwall scarps that are up to 2 to 3 km wide and subaerially represented as curved indentations on the barrier reef fronts. The pattern of the headscarps indicate that some of the slides are composite features which have resulted from several smaller sliding events. The upper failure surfaces of these slides have a rotational scar, which narrows downslope and is of planar geometry, becoming progressively more channelised as they enter the canyons. This geometry is typical of submarine landslides, having shallow rotational movements in their upslope portion due to localised oversteepening, followed downslope by translational instability (Prior & Coleman, 1979). Displaced debris masses cannot be identified downslope of these slide headscarps. It is likely that the absence of displaced masses is due to their transportation further down-canyon by sedimentary mass-flow processes. Submarine landslides are known to undergo fluidization and change into debris flows and that eventually may develop into a turbidity current which can travel downstream for several tens of kilometres (Mulder & Cochonat, 1996). Dredge samples collected by Houtz & Wellman (1962) from the base of the Suva Canyon, where it debouches onto the Suva Basin floor (2000m depth), revealed a large deposit of sand. The sand was interpreted by these workers to be deposits of turbidity flows sourced from the Suva Canyon following failures at the canyon head triggered by the 1953 Suva earthquake. The turbidity currents were also implicated for damage to submarine cables that lay along the Suva Canyon. The headscarp of the canyon head slides are typically inclined at 25^o to 30^o. These oversteepened areas of the seafloor would be subject to further failures resulting in retrogression and enlargement of the slide scars.

6.4 EVALUATING POTENTIAL SUBMARINE LANDSLIDE TSUNAMI SOURCES

The characteristic near-field tsunami wave amplitude in the submarine slope failure source region can be calculated using predictive tsunami amplitude equations. There are several predictive equations available in literature that are based on analytical approximations and

used in scenario studies on continental margins. These approximations are related to the motion and geometry of the slope failure or transfer of slope failure energy to wave energy. The minimum surface depression above the middle of the initial slope failure position is taken as the characteristic near-field submarine mass failure tsunami amplitude (Watts et al., 2003).

The predictive tsunami amplitude equations require input parameters from the submarine landslide source, which can be derived from marine geology data. Commonly required parameters are the mean pre-failure slope angle θ, the initial submergence at the middle of the failure d, the failure length along the slope b, the thickness of failure perpendicular to the slope T, the width of failure w, the density of the slide ρ_s, the density of sea water ρ_w, and water depth at the end of the runout (base of slope) D_o. These parameters are depicted in a schematic cross sectional diagram in Figure 6.2. Three methods for estimating the near-field tsunami amplitude were considered for use in this study. They are described briefly below.

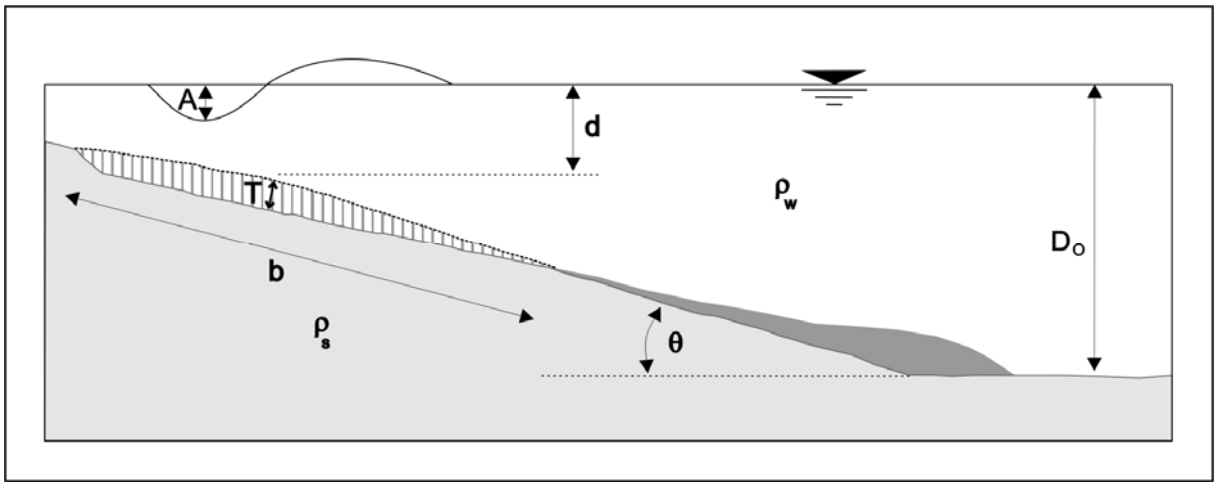

Figure 6.2: Geometric description of submarine slope failure parameters used in predictive tsunami amplitude equations. The various parameters are defined in the text.

- *Method 1:*

This method uses an analytical approximation in which the wave amplitude above a submarine slope failure is scaled with the centre of mass motion of the failure (Watts, 1998, 2000a). Here, tsunami generation is related to submarine landslide acceleration and deformation (Watts et al., 2003). Tsunami amplitude estimates are based on curve fits of numerical experiments on laboratory fluid dynamic simulations of wave generation (Grilli & Watts, 1999). Tsunami wavelength and 2D amplitude can be calculated for slope failures based on the morphology of the failure using empirical equations derived by Watts et al. (2003). Using an approximate ratio given in Watts (2004), the 2D equations can be related a

corresponding 3D tsunami amplitude as in McAdoo & Watts (2004). Since all the slope failures in southeast Viti Levu show characteristics of translational slides, the equations for linear slides only were considered here. The 3D predictive equations for linear slides from McAdoo & Watts (2004), with corrections based on De Lange and Moon (2004), W. De Lange (pers. comm. 2006) and P. Watts (pers. comm. 2006) are as follows:

For linear slides:
Wavelength:

$$\lambda = 3.87\ (bd/\sin\theta)^{0.5} \quad (1)$$

Amplitude:

$$A = 0.224\ T\ [w/(w + \lambda)]\ [(\sin\theta)^{1.29} - 0.746\ (\sin\theta)^{2.29} + 0.170\ (\sin\theta)^{3.29}]\ (b/d)^{1.25} \quad (2)$$

-Method 2:

A predictive tsunami amplitude equation derived by Bohannon & Gardner (2004) using the energy scaling relationship of Watts (2000a) is as follows:

$$A = [\eta(\rho_s - \rho_w)Tbh/\rho_w\lambda]^{0.5} \quad (3)$$

where h is the drop in height of the centre of mass of failure, η is the dimensionless energy efficient factor and λ is assumed to be ~10 000 m (Bohannon & Gardiner, 2004).

-Method 3:

The third method of estimating tsunami amplitude is based on a simple approximation of Striem & Miloh (1976), which has been used in case studies by Murty (1979) and Locat et al. (2004). This approximation calculates the height of a solitary wave above the submarine failure using the following equation:

$$A = 1/D\ [8(3)^{1/2}\ \mu bT\ (\{\rho_s/\rho_w\}-1)(D_o-d)]^{2/3} \quad (4)$$

where D is the local water depth (same as D_o) and μ is the fraction of the potential energy released by the slide that is transformed into wave energy and is assumed to be equal to 0.01, according to Murty (1979). The relation is valid provided that $d \leq D \leq D_o$.

The observed near-field wave amplitude of the 1953 Suva tsunami (up to 15 m, Houtz, 1962a) was used in a comparative study of all three methods using parameters of some reef edge and canyon head slides to select the best method for use in southeast Viti Levu (see Appendix 7). This study showed that Method 3 tended to overestimate the amplitude of tsunami waves. The results of Method 2 and Method 3 were quite similar. Method 1 however, was considered to be the best for estimating initial tsunami amplitudes in southeast Viti Levu. It is seen that all the parameters required in Method 1 can be accurately measured directly from the morphological features of the slides in the multibeam bathymetric data. Some parameters in the other two methods, were not available and needed to be estimated, possibly leading to large uncertainties in the tsunami amplitude values. For example, Method 3 requires the use of unknown quantities μ and ρ_s, and the since the exact runout paths are ill-defined in some slides due to the absence of displaced debris, the value of D_o has associated uncertainty. Similarly, in Method 2 the values of ρ_s, h and η are crucial unknown parameters, which had to be estimated. Method 1 provided the most reasonable comparison to the observed 1953 value and because all its required source parameters could be easily derived from the seafloor bathymetry alone, it was selected for use in this study to calculate the initial tsunami amplitudes for all slope failures mapped in southeast Viti Levu.

Most slides have no evidence of landslide mass in the run-out zones. For these slides the minimum run-out length was measured as the length of the run-out scar, delimited by the headscarp and the side walls, or the distance between the headscarp and the limit of disturbed/modified seafloor downslope of the headscarp. The gradient of the pre-failure slope was taken as the gradient of the slope adjacent to the failure. The value of T was extracted by determining the separation between the pre-failure and post failure seafloor surface. The pre-failure seafloor surface was estimated by extrapolating undisturbed isobaths outside the periphery of the failure across the disturbed area.

It is noted from the morphology data that the scars left by slope failures may be composite features. A detailed examination of individual scars is required to determine the prevalent size of failures. Such a detailed study of a selected individual slide is presented in the next chapter. In this study, since the geometry of entire scars were measured, the estimated tsunami amplitude value can be considered as upper bound values for each slide. The calculated near field tsunami dimensions are given in Table 6.1 (see Appendix 8 for full calculations).

The results of the calculations (Figure 6.3) indicate that the initial tsunami amplitudes range from 0.1 m to 16 m. Slides that produce initial amplitudes in the order of 10 to 15 m are considered to pose the greatest threat to the coast, as wave heights of a similar order were observed outside the barrier reef during the destructive 1953 Suva tsunami (Houtz, 1962a). This indicative analysis shows that slides at the heads of submarine canyons and the barrier reef fronts produce the largest initial tsunami wave amplitudes. The mid-slope failures and canyon wall failures produce relatively smaller amplitudes and are not considered to pose a significant tsunami hazard.

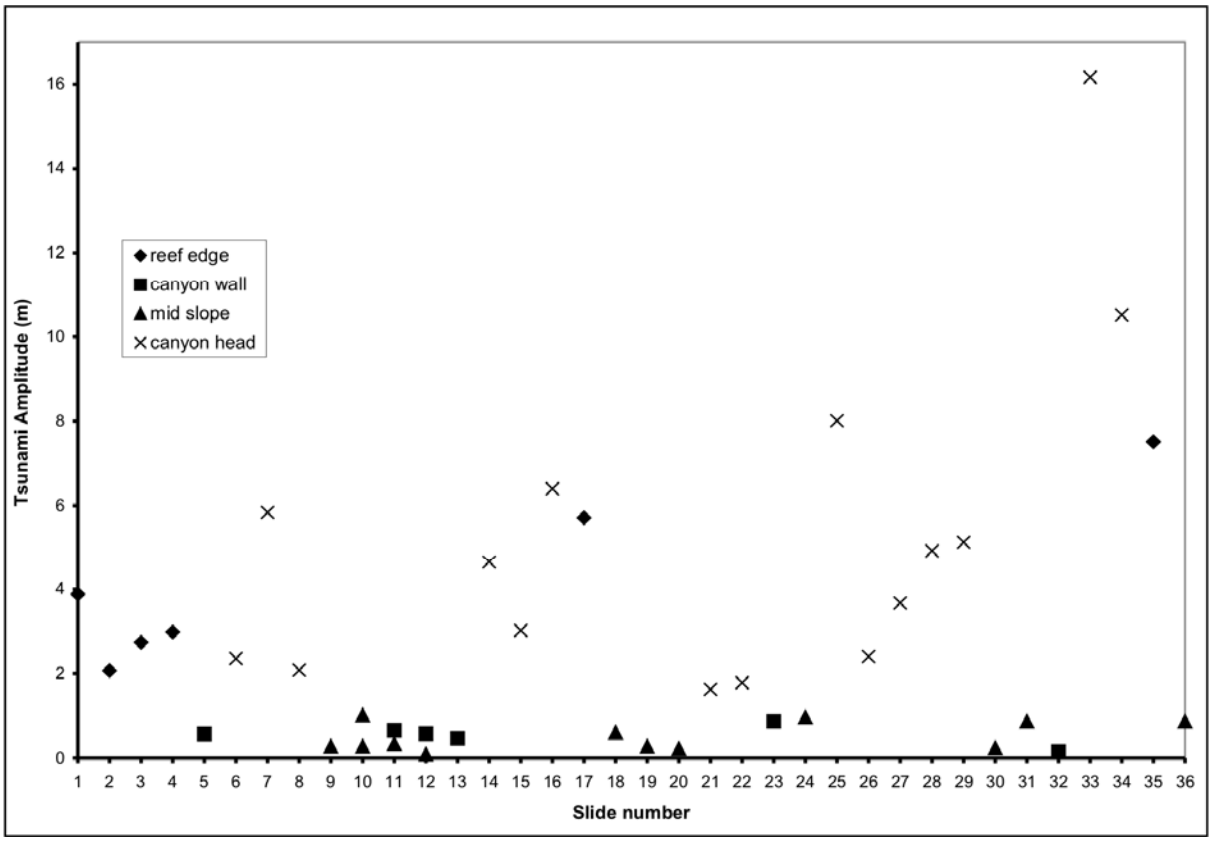

Figure 6.3: Plot of initial tsunami amplitude above various types of submarine landslide sources. Reef edge slide and canyon head slides generally show the highest amplitudes. Refer to Figure 6.1 for geographic locations of numbered slides.

6.5 DISCUSSION

6.5.1 Potential causes of submarine landslides in southeast Viti Levu

In submarine environments key contributing factors for slope failures include: i) earthquakes; ii) rapid sediment deposition; iii) undercutting by currents; iv) storm waves; and v) gas and

fluid expulsions in sediment (Prior & Coleman, 1984; Maltman, 1994; Hampton et al., 1996). A rigorous quantitative assessment of all causes of slope failure on the Eastern Slope is not possible as there are no geotechnical data available on the slope sediments. However, a qualitative evaluation of causative factors is provided here by using the known geological context.

Earthquakes are a key factor in triggering submarine landslides on the Eastern Slope of southeast Viti Levu. Earthquakes trigger submarine landslides because short-term strong seismic accelerations can repeatedly induce shear and normal stresses in the sediment and the cyclic loading can cause build up of pore pressures, so weakening the sediment (Prior & Coleman, 1984; Hampton et al., 1996). The Eastern Slope contains the highest proportion of documented slides relative to other offshore slope units of southern Viti Levu. This concentrated area of slope failures overlaps with the Viti Levu Seismic Zone. The absence of slides outside the zone of seismicity indicates that seismic loading may be an important factor for triggering slope failures on the Eastern Slope.

High concentrations of methane gas in Holocene organo-calcareous silts are found along nearshore areas of the marginal shelf (Shorten, 1993b). Seismic reflection surveys from inside the marginal shelf and at the tops of the marginal slopes show that acoustic turbidity in the seismic profiles, which is caused by gas overpressures (Wever & Fiedler, 1995; Whiticar, 2002), is restricted to the inner estuarine/lagoonal areas and is absent from sediments at the top of the marginal slopes. Therefore, pore gas generation is unlikely to be a major factor in triggering slope failures on the Eastern Slope.

Storm waves cause cyclic loading and associated pore pressure fluctuations of seafloor sediment within 150 m of the sea surface (Prior & Coleman, 1984). Mid-slope and canyon wall slides which generally occur below this depth are unlikely to be induced by storm waves. Storm waves are quite frequent in southeast Viti Levu (Krishna, 1983), but are unlikely to trigger large shallow depth failures at the reef edge or the canyon head, as these appear to be rarer events. Storm waves are more likely, however, to induce smaller failures at shallow depths, which appear to occur more frequently.

The top of the Eastern Slope is subject to the highest sedimentation rate, with a constant supply of sediment from the barrier reef fronts and tops, and terrestrial and lagoonal

sediments through reef passages. It is possible that high sedimentation rates at the top of the Eastern Slope are also a major contributing factor that has increased the susceptibility of sediment to failure. Long-term accumulation of sediments in the upper slope can lead to failure of oversteepened slopes. High sedimentation rates may also inhibit the capacity for pore-water drainage in sediments. This may locally induce excess pore pressures, producing underconsolidation, and so weakening the sediment pile (Prior & Coleman, 1984).

6.5.2 Submarine landslide tsunami generating zone

A submarine landslide tsunami generation zone exists at the top of the Eastern Slope, along the barrier reef front, and includes the heads of the submarine canyons that indent the marginal shelf. This zone occurs within 5 km of the coastline (Figure 6.4) and is identified as having the greatest potential for generating destructive local tsunamis. Canyon head slides and reef edge slides occur at very shallow water depths as shown by surface rupturing of their head scarps on the barrier reef fronts. The shallow water depths of these slides combined with relatively large slide thickness (40 - 70 m) produce large near field tsunami amplitudes. Production of large initial amplitudes by mid-slope and canyon wall slides on the other hand are constrained by their large water depths (400 – 900 m). Even though some mid-slope slides are quite large in size, their deep locations tend to produce minimal effects on the sea surface.

A variety of conditions exist at the shelf break of the Eastern Slope that provide optimum conditions conducive to tsunamigenic slope failures. During the late Pleistocene low-stand sea levels (e.g. at marine stages 2, 6, 8, 10, 12 etc), large quantities of sediment would have been deposited at the edge of the marginal shelf. The barrier reef fronts may be partially founded on these quasi-stable sediments. Instability of the shelf break is further increased by oversteepening and loading of the reef front slope by present day sedimentation. The reef fronts would be prone to deep-seated tsunamigenic failures during large earthquakes. As demonstrated by the 1953 Suva tsunami (see Chapter 7), the submarine canyon heads are also areas of potentially large seismically triggered tsunamigenic submarine landslides. At the shelf break, the canyon headwall slopes are exceptionally primed for large seismically triggered failures as the largest quantities of sediments are deposited here through the reef passages. The stability state of canyon head slopes is reduced as a result of sediment strength loss from rapid sedimentation, with accompanying increase in external stresses from slope oversteepening, as well as the added effect of canyon undercutting. Six potential canyon head

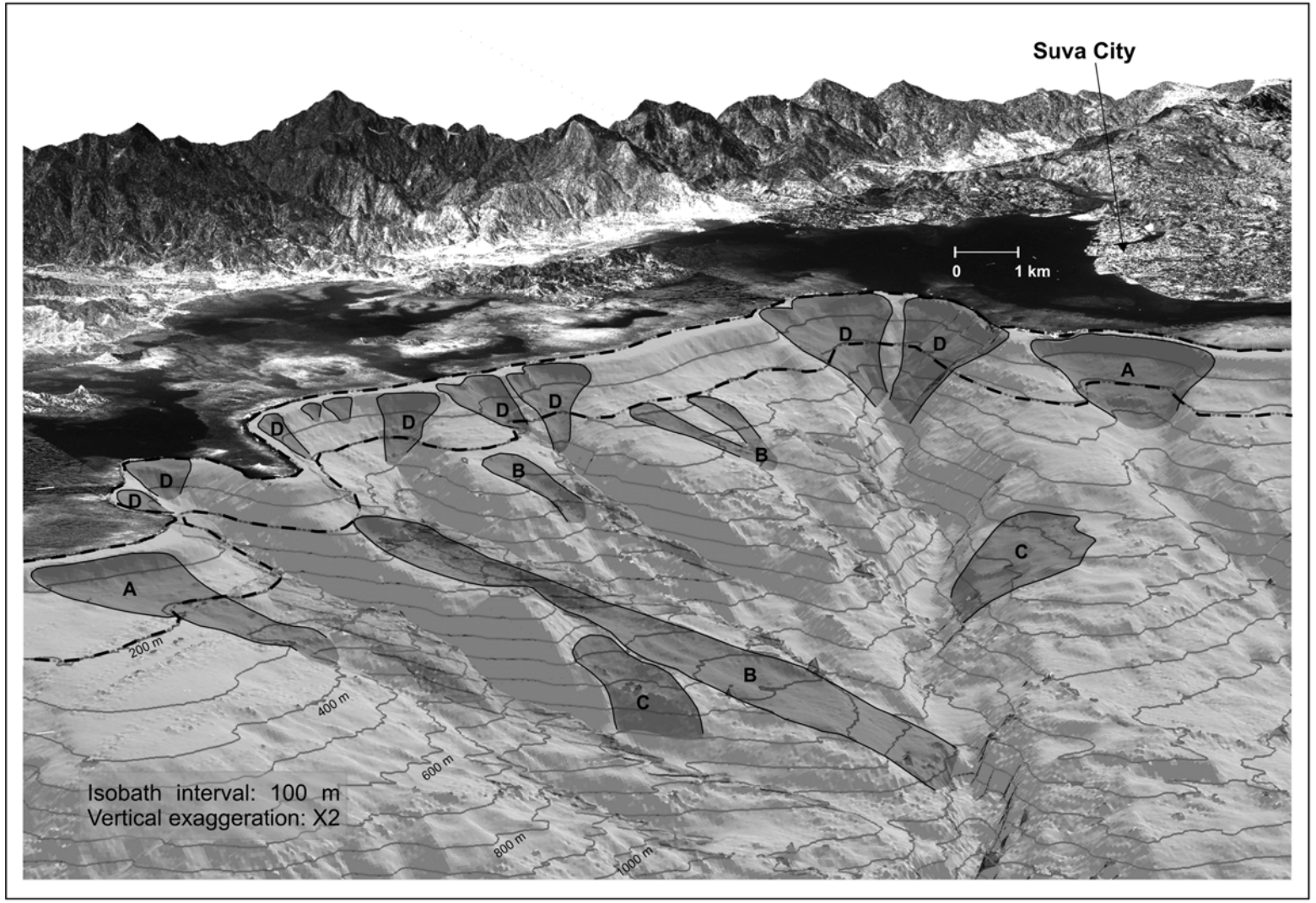

Figure 6.4: Tsunami generating zone, enclosed by dashed lines, shown on a three dimensional perspective image of the offshore-onshore area of southeast Viti Levu near Suva City. The view is towards the northeast. Note: scale varies with perspective. Labelled are various submarine landslide types of the Eastern Slope: (A) reef edge slide, (B) mid-slope slide, (C) canyon wall slide, (D) canyon head slide.

local tsunami source areas exist on the Eastern Slope of southeast Viti Levu.

6.6 SUMMARY AND CONCLUSIONS

High resolution multibeam swath bathymetric images were used to document the locations and morphometry of submarine landslides on the southern slopes of Viti Levu and then evaluate their capability for tsunami generation in order to identify potential tsunami generating zones. The highest concentration of submarine landslides occur on the Eastern Slope in the southeast of Viti Levu. Submarine landslides here occur on the barrier reef fronts, canyon heads and walls and in the mid-slope areas. They are typically translational and lack bathymetric evidence for displaced masses, implying transformation to debris flows and/or turbidity currents. Some slide scars may be composite features that were formed by several failure events. A qualitative analysis of causative factors suggests that slope instability may be primarily influenced by high sedimentation rates and earthquakes.

Using predictive tsunami amplitude equations and the morphometry of the slides, reef edge and canyon head slides at the shelf break were found to produce the largest near-field tsunami amplitudes. They have mean initial tsunami amplitudes of about 4 to 5 m, and are considered to pose the greatest threat to the coast. A variety of conditions at the barrier reef fronts and submarine canyon heads, which includes shallow water depths, weak foundations, slope oversteepening and loading by rapid sedimentation, and undercutting by canyon currents, makes these areas conducive to seismically triggered tsunamigenic failures. The shelf break at the top of the Eastern Slope, within 5 km of the coastline, is identified as a potential tsunami generating zone, from where submarine landslide generated tsunami events may pose a significant threat to the coast of southeast Viti Levu during large earthquakes in the future.

CHAPTER 7

TSUNAMI HAZARD ASSESSMENT

7.1 INTRODUCTION

The importance of submarine landslides as sources of destructive local tsunamis has recently come to the attention of marine geologists with the occurrence of catastrophic events in Flores Island, Indonesia in 1992 (Imamura et al., 1995), Skagway, Alaska in 1994 (Kulikov et al., 1996; Synolakis et al., 2002a; Watts et al., 2003), Sissano, Papua New Guinea in 1998 (Tappin et al., 2001; Synolakis et al., 2002b) and Izmit, Turkey in 1999 (Yalciner et al., 1999; Tinti et al., 2006). Large, highly focussed and devastating tsunamis that are associated with, but often not expected of distal or modest magnitude earthquakes, are now being attributed to local submarine landslide sources. Submarine landslide tsunamis are generated nearshore, provide very little warning time and are characterised by large localised peak run-ups along the adjacent coast (Synolakis et al., 2002b). This chapter presents a detailed case study of a submarine landslide triggered tsunami that struck Suva City in 1953. It also presents an evaluation of the hazard the city faces from a potential future tsunami that could be generated in the source area of the 1953 event.

An important aspect of tsunami hazard assessment and mitigation is to produce predictive numerical simulations of tsunami generation, propagation and run-up (Watts, 2000b). These simulations require accurate bathymetry data and tsunami source parameters. Predictive models used for simulations need to be tested and calibrated by running successful case studies. Some recently presented case studies of local tsunamis have suffered from lack of unequivocal historical accounts (e.g. California (Greene & Ward, 2003), Kaikoura (Walters et al., in press) or are complicated by mixed tectonic dislocation and submarine landslide sources (Borrero et al., 2001; Yalciner et al., 2002; Tinti et al., 2006). The controversy about the source mechanism (submarine landslide or earthquake dislocation) of the much publicised case study of the 1998 Sissano tsunami in Papua New Guinea remains (e.g. Matsuyama & Yeh, 2003).

The study presented in this chapter documents tsunami hazards in the Suva area, which are

attributed to seismically triggered submarine landslides and are well constrained by having a complete range of the critical datasets required for running predictive simulations. The destructive 1953 Suva tsunami is a well-documented event of a submarine landslide tsunami in the Suva area. Several historical documents provide informative accounts from witnesses of tsunami formation and the ensuing inundation along the coasts of southeast Viti Levu, near Suva, as well as Kadavu and other nearshore islands. In this study, coastal wave heights and arrival times from the 1953 event are used as a benchmark for a numerical tsunami simulation model. This model is then used for constructing a predictive local tsunami hazard scenario for Suva. High-resolution multibeam bathymetry recently acquired for the area off the Suva coast constrains the location and geometry of the source of the 1953 Suva tsunami and is also used to create an accurate simulation computational grid.

Previous tsunami modelling work based on the 1953 Suva tsunami was carried out by the Pacific Disaster Centre (www.pdc.org), using the Method of Splitting Tsunami (MOST) finite difference model. It is not known how the results of this simulation compared with observed values and arrival times of the 1953 event, or whether any validation work was attempted at all. This simulation, however, was based on a poorly constrained tsunami source (S. Goosby, pers comm. 2005) and low-resolution bathymetry. The data related to both these aspects of tsunami modelling in Suva have now been superseded by the results of new and more elaborate work presented in this chapter.

In this chapter, the 1953 Suva earthquake and tsunami are reviewed using data collated from various historical records. The potential source mechanisms of the 1953 Suva tsunami are evaluated and the submarine landslide responsible for the tsunami is accurately defined using marine geophysical data, historical records and field mapping. Using this source, the 1953 event is successfully simulated using the GEOWAVE tsunami initialization and propagation numerical model. An antecedent tsunamigenic event is recognised in the source area of the 1953 event and an attempt is made to date this event. An incipient failure in this source area is also identified. This is used to develop a potentially worse case scenario tsunami event in order to evaluate the threat it poses to Suva City.

7.2 DATA AND METHODS

7.2.1 Marine geophysical data

High resolution multibeam bathymetry and seismic reflection data outside the barrier reef of Suva were used to accurately define the source of the 1953 Suva tsunami. Details on the methods of acquisition, post-processing and preparation of bathymetric maps and images and seismic profiles are outlined in Section 5.2.

7.2.2 Historical data

The study of past tsunami events is important as it provides a comparison for numerical results with an actual observed event. In order to compile observational evidence on various aspects of the 1953 Suva tsunami, a number of historical documents were examined. An invaluable source of data was the Fiji Geological Survey 1953 Suva earthquake questionnaires kept in the Fiji Mineral Resources Department archives. Examination of printed material such as old newspapers, magazines, and Fiji Geological Survey administrative correspondence, articles, reports and publications also proved valuable for this purpose. Furthermore, eyewitnesses in several households and villages along the southeast coast of Viti Levu were interviewed during the present study.

7.2.3 Tsunami model

The use of numerical tsunami models is becoming a standard worldwide in tsunami hazard assessment, prediction and mitigation work. Models that are proven with past tsunami events provide a more credible basis for predicting future tsunami hazard scenarios. In this study, the Geowave tsunami generation, propagation, and inundation model is used.

The initial tsunami parameters (surface water profile and velocity) are computed with the Tsunami Open and Progressive Initial Conditions System (TOPICS) (Watts et al., 2003). TOPICS is able to produce tsunami sources for both earthquakes and submarine landslides, and each of these is further outlined as follows. In the case of earthquakes, TOPICS defines vertical coseismic displacements from the half-plane solution of an elastic dislocation

problem (Okada, 1985). A planar fault of length L and width W is divided into many small trapezoids and the point source solution of Okada (1985) is used to sum the contributions made by each trapezoid to vertical coseismic displacement, based on the actual depth of the trapezoid. The shear modulus μ can be specified based on the depth of the earthquake centroid as well as other seismic and geological descriptors. TOPICS outputs a characteristic wavelength λ_o that is the smaller of the fault dimensions L or W, and a characteristic tsunami amplitude η_o that is the minimum depression found from the coseismic displacement. The seismic moment M_o is proportional to, but slightly less than $\mu LW\Delta$, where Δ is the maximum slip, because a Gaussian slip distribution is assumed about the centroid.

The initial free surface elevation estimate above a submarine landslide source is based on semi-empirical curve fits of 2D (Grilli & Watts, 1999) and later 3D (Grilli & Watts, 2001; Grilli et al., 2002; Grilli & Watts, 2005; Watts et al., 2005) numerical experiments on laboratory fluid dynamics simulations of wave generation. The curve fits are presented as functions of non-dimensional quantities characterising the landslide (e.g density, geometry) and local bathymetry (e.g. slope, depth) based on the scaling laws of Watts (1998; 2000a). The duration of tsunami generation is equivalent to the duration of landslide acceleration t_o (Watts, 1998; Watts & Grilli, 2003). Thus, at time $t = t_o$, TOPICS provides a slide initial condition, as if results from the models of Grilli & Watts (1999) or Grilli et al. (2002) were being transferred directly to the tsunami propagation model at that instant of time. In this model, it is assumed that submarine landslide deformation has negligible effects on the tsunami generation for reasons given in Watts et al. (2003).

Tsunami propagation and inundation are simulated with the FUNWAVE code, a finite difference, Boussinesq water wave model developed at the University of Delaware (Wei & Kirby, 1995; Wei et al., 1995; Chen et al., 2000; Kennedy et al., 2000). FUNWAVE is fully nonlinear and is able to simulate a variety of wavelengths (Wei et al., 1995). FUNWAVE can also model dissipation from breaking waves and can simulate accurate vertical run-up and inundation of dry land in one simulation (Chen et al., 2000; Kennedy et al., 2000). Run-up is treated in FUNWAVE using the slot method (Watts et al., 2003).

The tsunami source predicted by TOPICS at time t_o is transferred as initial conditions into FUNWAVE, in a combined single model referred to as Geowave. In order to demonstrate

various aspects of a tsunami attack, Geowave has been designed to output numerical tide gauges, free surface snapshots, inundation limits, wave timing and water velocities (Watts et al. 2003). Geowave has been previously validated based on case studies of several submarine landslide generated tsunamis (Watts et al., 2003; Day et al., 2005; Ioualalen et al., submitted for publication).

7.2.4 Simulation grid

It is critical that the computational grid used for any simulations in Suva is able to resolve the intricate system of barrier reefs, reef passages and interconnected nearshore lagoons. To achieve this, the most accurate and comprehensive bathymetry/nearshore topography datasets were used in the construction of the computational grid. The bathymetry data used in the tsunami computational grid are from a number of data sources. Outside the barrier reef, the bathymetry from the upper slope of southeast Viti Levu is from the recently conducted Reson multibeam survey (20 m resolution). Data beyond the outer depth limit of this survey, from the Suva Basin and Kadavu slope, is from 1: 250 000 Lomaiviti Bathymetric Map Sheet 5 (Smith, 1992). The 100 m isobaths from this map were digitised and gridded for the purpose of this study. Bathymetry of the lagoon is from swath mapping surveys carried out by SOPAC and the Fiji Hydrographic Office, and from British Admiralty Charts: Suva Harbour 1660, Western Approaches to Suva Harbour 1673 and Beqa Passage and Lagoon 1682. The near-shore topography of Viti Levu, Beqa and Kadavu islands are from 20 m topographic contours derived from the Department of Lands and Surveys, Fiji 1:50 000 map sheets O29, N29, N30, N32 and O32. Higher resolution (2 m) height data for the Suva City area is from the Suva Pacific Cities data set (Biukoto et al., 2001). Coastal elevations from the Muaivuso Peninsula were derived from differential GPS field surveying conducted as part of this research project. The barrier reefs were mapped from 1:50 000 topographic maps sheets. The average height of the reefs at mean sea level was taken as 0.35 m (Solomon & Kruger, 1996). The final grid was re-compiled from these separate data sets with a grid cell size set at 100 m and with sea level set at mean sea level (MSL), 0.96m above the Fiji chart datum (Anon, 2004). For the 1953 simulation, special efforts had to be made to carefully adjust the grid for conditions that were prevalent in 1953. The grid was adjusted to remove reclaimed areas (see Appendix 9) and the sea level was set to mean low tide level, 0.7 m below MSL, to replicate the tide level at the time of the tsunami. The spring tidal range in this area is about 1.3 m (Anon, 2004).

7.2.5 Radiocarbon dating of tsunami deposit

A sample of coral was collected for radiocarbon dating from a coral limestone boulder in the older tsunami boulder zone on the Waqanake Reef (see Section 7.5.3). The dating was carried out by the University of Waikato, Radiocarbon Laboratory, New Zealand (see Appendix 3). The sample was crushed, tested for recrystallisation and aragonite was selected for dating. The conventional age is reported using the Libby half-life (5568 yr). The age was calibrated using the OxCal v3.9 program (C.B. Ramsey, http://www.rlaha.ox.ac.uk/O/oxcal.php) and the South Pacific Regional mean delta-R of 43 ± 23 marine reservoir correction (http://depts.washington.edu/qil/marine/). The 1-sigma range of the calibrated age is reported.

7.3 THE 1953 SUVA EARTHQUAKE AND TSUNAMI

The Suva earthquake of 1953 occurred on 14 September at 12.26 pm and has been the most destructive earthquake in Fiji's history (Houtz, 1962a). The earthquake killed three people and there were 20 cases of serious injuries. The Suva Wharf, bridges, buildings and water reticulation facilities in southeast Viti Levu suffered severe damage. The earthquake was a magnitude M_S 6.75 event, with the epicentre located offshore, about 15 km to the WSW of Suva City at a focal depth of 21 km (Houtz, 1962a; Sykes et al., 1969). The maximum felt intensities were [*]MMX along the coast of southeast Viti Levu (Rynn & Prasad in SPDRP (2002)). The duration of the main shock was 25 to 30 seconds long (The Fiji Times & Herald 1953a,b). The focal-mechanism solution of the earthquake indicates strike-slip faulting with a significant but poorly constrained dip-slip component, an east-west tension axis, and NW dextral and NE sinistral nodal planes (Hamburger et al., 1990). Onshore and offshore mapping shows no clear evidence for surface fault rupturing during this event and uncertainty remains about the source structure for this earthquake. A discussion about the possible source structure of this earthquake is presented in Section 9.3.2.4.

The 1953 Suva tsunami was witnessed by several hundred people in Suva, Kadavu and in the outer islands. A list of arrival times and wave heights from eyewitness reports from around Fiji is given in Table 7.1. The observational locations in southeast Viti Levu and in Kadavu are shown in Figure 7.1. Historical records indicate that the tsunami occurred during low tide, when sea level was about 0.7 m below mean sea level. The sea receded along the entire foreshore of the Suva coast below the lowest tide level soon after the main earthquake shock.

[*] Modified Mercalli Intensity (see Appendix 4)

Table 7.1: Observed tsunami run up and arrival times of the 1953 Suva tsunami.

Location	Initial receding of sea	Observed wave height (m)	Arrival time after earthquake	Distance from Suva Passage (km)	Additional notes
Suva Barrier Reef	-	3 to 15	-	0	[1,2]Upheaval and churning of sea (source area)
Walu Bay	> low tide	1 to 1.5	4-5 min	4.3	[3,4]Berthed ships badly damaged, 2 drownings in Suva Harbour
Suva City	-	1 to 1.5	4-5 min	4.3	[3,4]Damage to shops in CBD
Government Buidlings (Nasese)	> low tide	1.5	4-5 min	4.9	[1,3,4]Waves depositing mud and pebbles inland, 1 drowning
Lami	> low tide	1.5 to 2	-	4.5	[1,3,4]Sea wall smashed and reef boulders strewn on foreshore
MET Office (Laucala Bay)	-	1	15 min	15	Accurately timed first arrivals by L. Crowe of MET Office
Muaivuso Village	-	<5	-	3	[6]Village and school safe from waves
Makaluva and Nukulau (Nukubuco Reef)	-	2 to 3.5	-	16	[3,5]3 waves, all buidlings on islands destroyed
Nukui Village (Rewa Delta)	-	1.5	-	25	[3]Village almost completely destroyed
Naitonitoni (Navua Delta)	> low tide	0.5 to 1	10-15 min	30	[2,3]Preliminary small wave, 3 waves, last wave depositing debris inland
Deuba (Viti Levu)	observed	1 to 1.5	-	41	[2]Preliminary small wave
Rukua (Beqa)	-	1.5	15 min	44	[1]Preliminary small wave (0.3 m) 30 seconds after earthquake
Lomeri (Viti Levu)	> low tide	-	-	46	[2]Preliminary small wave, and 3 later waves in sucession
Korolevu (Viti Levu)	observed			77	[2]
Nakasaleka (Kadavu)	observed	4.5	12 min	90	[1,2] 3 waves, the second destroying 40 houses, 2 drownings
Vunisea (Kadavu)	-	< 1		105	[2]
Levuka (Ovalau)	-	< 1	30 min	96	[1,2]Waves flooding and receding in intertidal area for 30 min
Gau Island (Lomaiviti Group)	-	< 1	-	100	[2]Waves flooding and receding 3 times
Koro Island (Lomaiviti Group)	-	< 1	-	150	[2]Surprise wave reaching shore at low tide
Moala Island (Lau Group)	-	< 1	-	160	[2]Waves flooding lagoon at low tide
Kanacea (Lau Group))	-	< 1	1 hr	280	[2]Surprise wave reaching shore at low tide
Sawakasa (Viti Levu)	-	< 1	1.5 hr	98	[2]Waves flooding and receding intertidal area
Matavatucou (Viti Levu)	-	< 1	1.5 hr	100	[2]Waves flooding and receding intertidal area

References: [1]Houtz (1962a), [2]Fiji Geological Survey Suva earthquake questionaries (1953), [3]Usher (1987), The Fiji Times & Herald [4](1953a), [5](1953f), [6]Interview- this study

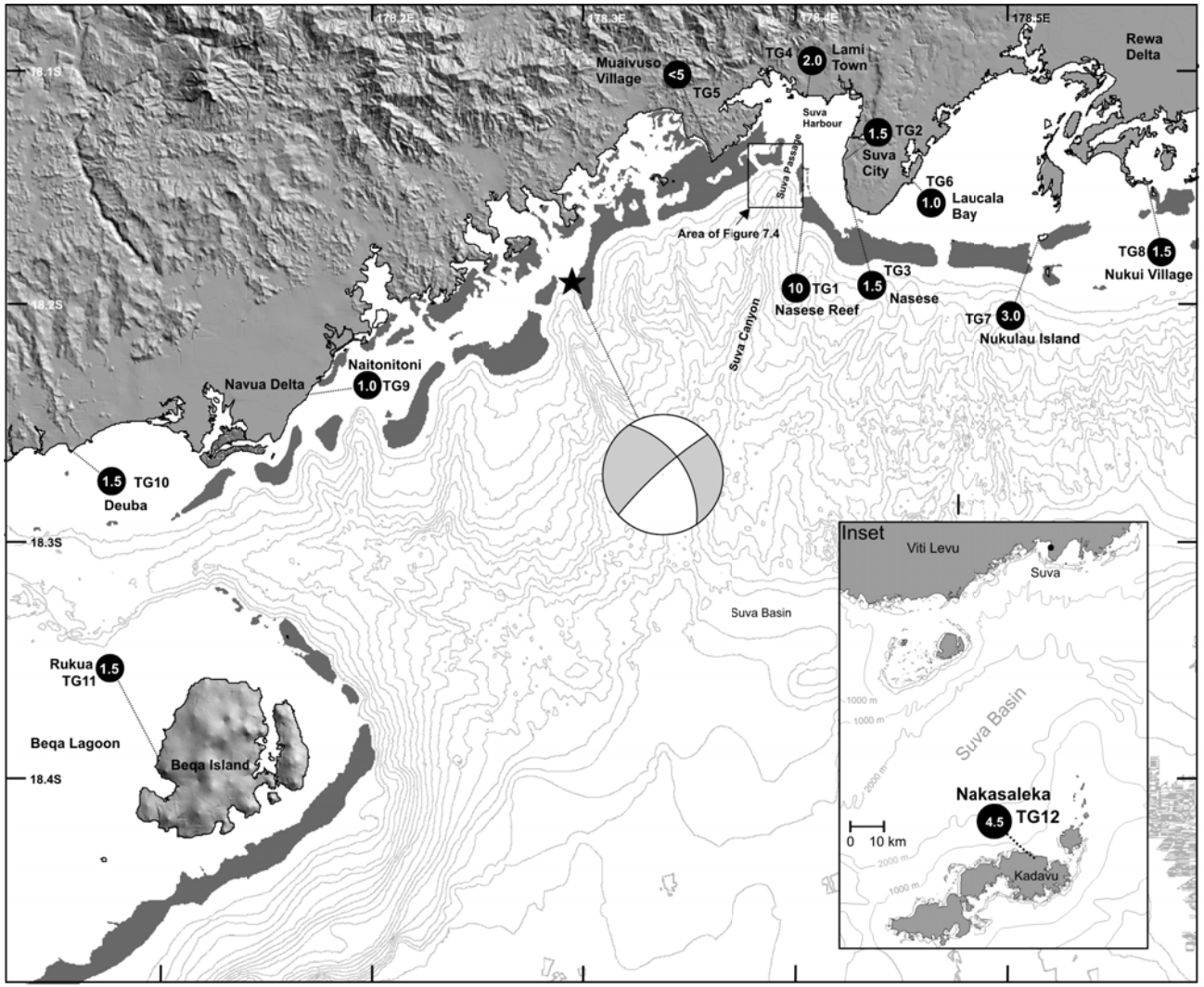

Figure 7.1: Observed wave heights of the 1953 Suva tsunami (in black circles). The numbers prefixed by TG refer to the numerical tide gauges used in the simulation model. Dark shaded areas represent the coral barrier reef. The bathymetric contour interval is 100 m. Also shown are the epicentre (star) and focal mechanism of the 1953 Suva earthquake, and the source area of the tsunami (area of Figure 7.4). The inset is a map of the Suva-Kadavu area showing the observed 1953 wave height and numerical tide gauge at Nakasaleka, Kadavu.

Parts of the seabed and submerged reefs were uncovered inside the lagoon near Lami (Usher 1987; Mrs Sharon Light pers. comm. 2003). The maximum height of the waves outside the Suva Reef was estimated by eyewitnesses to be 3 to 15 m high (Houtz, 1962a). The build up of these waves was fortunately broken by the barrier reefs. The waves crashed on the barrier reef front, dislodging reef blocks and throwing them on the reef crest. The hull of a sunken vessel was also thrown up on the reef flat by the waves. A reduced set of waves remained on passing over the barrier reef. These waves propagated across the harbour and firstly swept over the seawall and road at Nasese and penetrated to at least 100 m inland (Figure 7.2 a,b). They then proceeded to invade Suva City from the southern end with wave heights up to 1.5 m (The Fiji Times & Herald 1953a). Ships berthed at the Suva Wharf were badly damaged. The horizontal inundation distance in the city area was no greater than 50 m (The Fiji Times & Herald 1953a). A 1.5 to 2 m high wave was observed at the coast of Lami, which entered the harbour through the Suva Passage. At Muaivuso Point, the village and school built on a 5 m high marine terrace, were not affected by the waves. The first wave at Laucala Bay, on the east coast of the Suva Peninsula, arrived 15 minutes after the main earthquake shock. The rock breakwater of Laucala Bay airport had holes smashed through it by the waves. At Nakasaleka Village, on the northern coast of Kadavu, 100 km to the south of Suva, the first wave arrival was accurately timed to the nearest minute at 12 minutes after the earthquake (Figure 7.1, inset). The arrival times of the first waves at Deuba, Rukua in Beqa and at Naitonitoni on Navua Delta to the west of Suva, were about 10 to 15 minutes after the earthquake. Areas not protected by barrier reefs such as the islands of Nukulau and Makaluva on the Nukubuco Reef and Nukui Village on the Rewa Delta and Nakasaleka village on Kadavu were the most severely affected. Nakakasaleka and Nukui village were almost completely destroyed. Wooden structures on the islands of Nukulau and Makaluva were swept away or severely damaged (Usher, 1987). Outside the Suva Passage, telegraphic cables to Norfolk and Fanning Islands were broken by turbidity currents (Houtz & Wellman, 1962). A total of five people died from drowning; three in Suva and two in Nakasaleka.

7.4 TSUNAMI SOURCE: EARTHQUAKE VERSUS SUBMARINE LANDSLIDE

The 1953 Suva tsunami is closely associated with the Suva earthquake event. In this section the two triggering options for the tsunami i.e. earthquake and submarine landslide, are defined and evaluated.

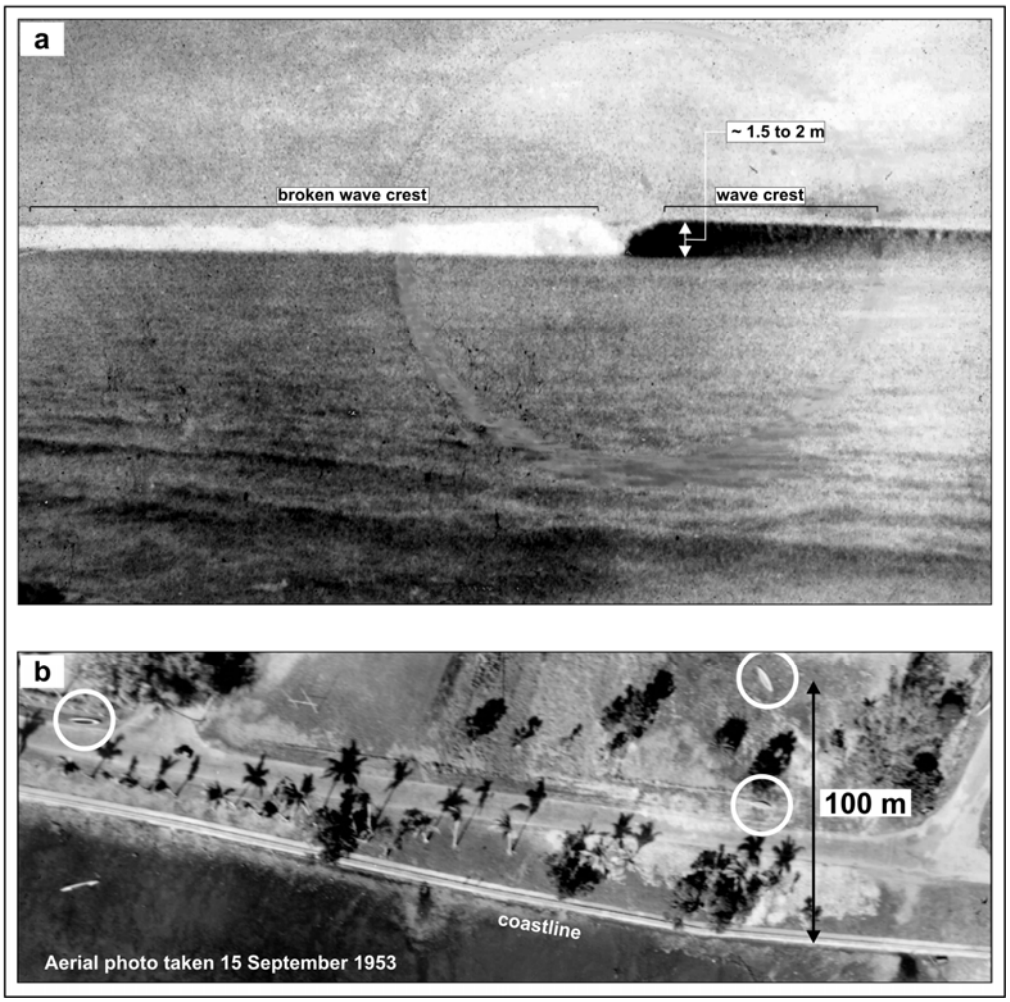

Figure 7.2: (a) Photograph taken by an eyewitness of the 1953 tsunami leading wave (bore) approaching the Suva coast (b) An aerial photograph of the Nasese coast taken by Adastra Airways for the Fiji Geological Survey a day after the 1953 Suva earthquake. The circles show boats that were carried inland by the tsunami waves, indicating inland penetration of at least 100 m at this location. (Photos used with permission from the Fiji Mineral Resources Department).

7.4.1 Earthquake tsunami

Following the earthquake there was no reported shoreline subsidence or uplift near the epicentre of the 1953 event. Field checks along the coast of southeast Viti Levu show no evidence for recent vertical displacements of shoreline features. These observations are consistent with the focal mechanism solutions for this earthquake, which indicate predominantly strike-slip faulting. Offshore swath bathymetric mapping also shows no evidence for recent surface deformation along faults. Statistical data on cosesimic surface rupturing show that earthquakes with magnitudes in the order of M_w 6 to 7 have a 40 to 80 % probability of producing surface rupturing (Lettis et al., 1997). Given the strike slip nature of

the 1953 earthquake source and lack of clear evidence for any coseismic surface deformation during this event, it is unlikely that any water waves were generated by the earthquake shock. If they were generated at all, the waves would have been insignificantly small compared to the much larger destructive waves actually observed by eyewitnesses.

The parameters of the 1953 earthquake source derived from focal mechanism, hypocentral and mapping data were used to quantitatively evaluate the tsunami caused by this earthquake using the Geowave model. The fault source parameters and the initial earthquake tsunami parameters derived from TOPICS are shown in Table 7.2. The fault source depth, width and dip are constrained by the earthquake hypocentral depth and focal mechanism data. The slip direction reflects the dominant orientation of slickenline lineations on NW trending fault planes measured in the epicentral area. The slip value was estimated using established relationships between the surface wave magnitude (M_s), seismic moment (M_o) and fault rupture parameters (Ekstrom & Dziewonski, 1988; Wells & Coppersmith, 1994). The fault rupture length was estimated using the length of a NW trending onshore-offshore structural lineament passing through the Navua Delta (see Section 9.2.3.4 and Figure 9.6).

The maximum amplitudes achieved at the coast by the simulated earthquake tsunami do not exceed 14 cm and would therefore not have contributed significantly to the observed destructive waves. In fact, the first arrivals of the simulated earthquake tsunami at numerical tide gauges in Beqa and Naitonitoni (Figure 7.1) fit eyewitness descriptions of a preliminary small wave arriving within a few seconds of the earthquake (Houtz, 1962a), followed several minutes later by the arrival of larger destructive waves. A previous suggestion as to the cause of this preliminary “warning” wave has been the impact of earthquake vibration of the reef on the sea (Houtz, 1962a). It is inferred here that the precursor “warning” wave was the effect of the earthquake tsunami, which was later followed by destructive submarine landslide initiated tsunami waves.

7.4.2 Submarine landslide source of the 1953 Suva tsunami

The location of the submarine landslide source of the 1953 Suva tsunami can be ascertained from descriptions in well documented eyewitness reports. The centre of the initial upheaval of the sea is consistently reported by eyewitnesses in Suva to be at the entrance of the Suva Passage about 4 km southwest of Suva. It is also consistently reported that the initial upheaval

Table 7.2: Earthquake tsunami source parameters.

Fault Characteristics	Quantities
X_o (longitude)	178.3
Y_o (latitude)	-18.2
d (km)	21
φ (degrees	146
λ (degrees)	121
δ (degrees)	50
Δ (metres)	1
L (km)	30
W (km)	27
μ (Pa)	4×10^{10}

Tsunami Source Characteristics	Quantities
M_o (J)	2.3×10^{19}
λ_o (km)	27
η_o (m)	-0.14

The inputs for TOPICS are, in descending order, the longitude of the earthquake centroid X_o, the latitude of the earthquake centroid Y_o, the centroid depth d, the fault strike clockwise from north φ, the fault slip direction clockwise from north λ, the fault dip δ, the maximum slip Δ, the fault length along rupture L, the fault width along rupture W, and the shear modulus μ. The output from TOPICS are the seismic moment M_o, the characteristic wavelength λ_o, and the characteristic tsunami amplitude η_o.

occurred no more than a minute after the end of the main earthquake (The Fiji Times & Herald 1953b,c). A remarkable account in The Fiji Times & Herald (1953d) of an inter-island boat captain who was on a southwest approach of the Suva Passage entrance at the time of the earthquake is as follows: "….the cutter Adi Tirisa was on its way to Suva….. beyond the reef some four to five miles southwest of Suva…….she was badly shaken and a little later three great spouts burst out of the sea, carrying mud, stones, and part of a long-wrecked vessel……". From this description, it can be clearly discerned that the captain had witnessed the formation of the tsunami.

The strongest evidence and most accurate location of the Suva Passage entrance source area is provided by Brother Hilary of St Felix College, Toorak, in the Fiji Geological Survey 1953 Suva earthquake questionnaire. He provides a well located sketch map showing the location of the initial area of upheaval of the sea to the west of the Suva Passage entrance. A copy of

Brother Hilary's sketch map is shown in Figure 7.3. The accounts of two other observers in the Suva earthquake questionnaires corroborate the specific location of the disturbance described by Brother Hilary.

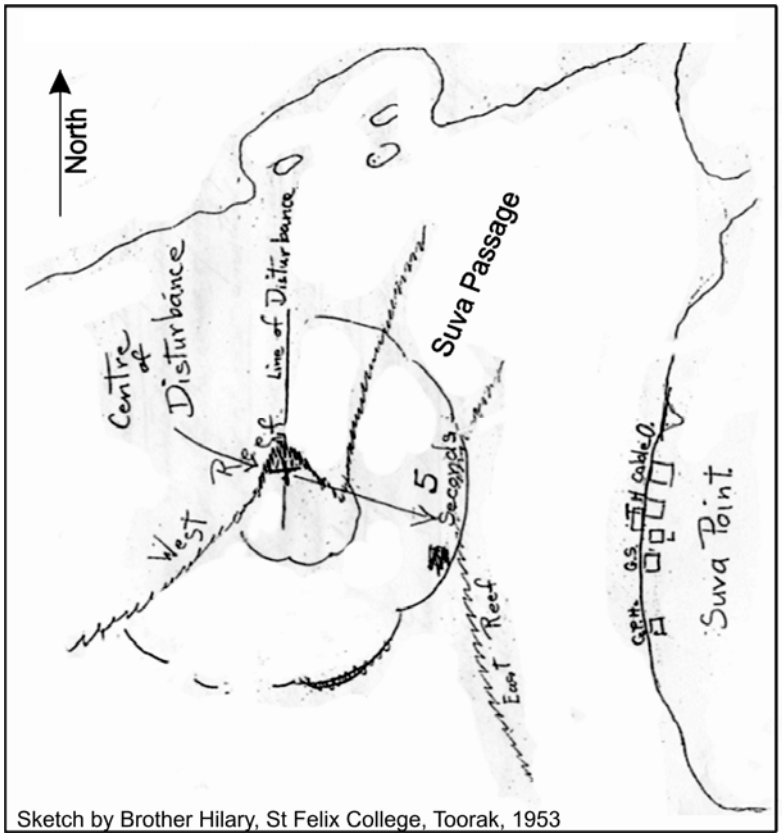

Figure 7.3: Eyewitness sketch map showing the exact location of the initial sea upheaval west of the Suva Passage entrance during the 1953 Suva tsunami (Fiji Geological Survey 1953 Suva Earthquake questionnaire).

High resolution multibeam bathymetry data reveal a large submarine landslide scar to the west of the Suva Passage entrance (Figure 7.4). The internal geometry of this scar shows that it is a composite feature composed of a number of successively smaller scars that occur adjacent to each other. The multibeam data clearly shows a well-defined smaller failure, the head scarp of which projects towards the barrier reef front between the Suva Passage entrance and the smaller Rat Tail Passage to the west (Figure 7.4). The head scarp of this slide had clearly breached the barrier reef front during the 1953 event. A survey of the reef front carried out by the Fiji Geological Survey a few days after the earthquake showed that fractures had developed in the reef front, along which sections of the reef front had slipped or were tilted seaward (The Fiji Times & Herald 1953c) (Figure 7.5). An aerial photo of the barrier reef

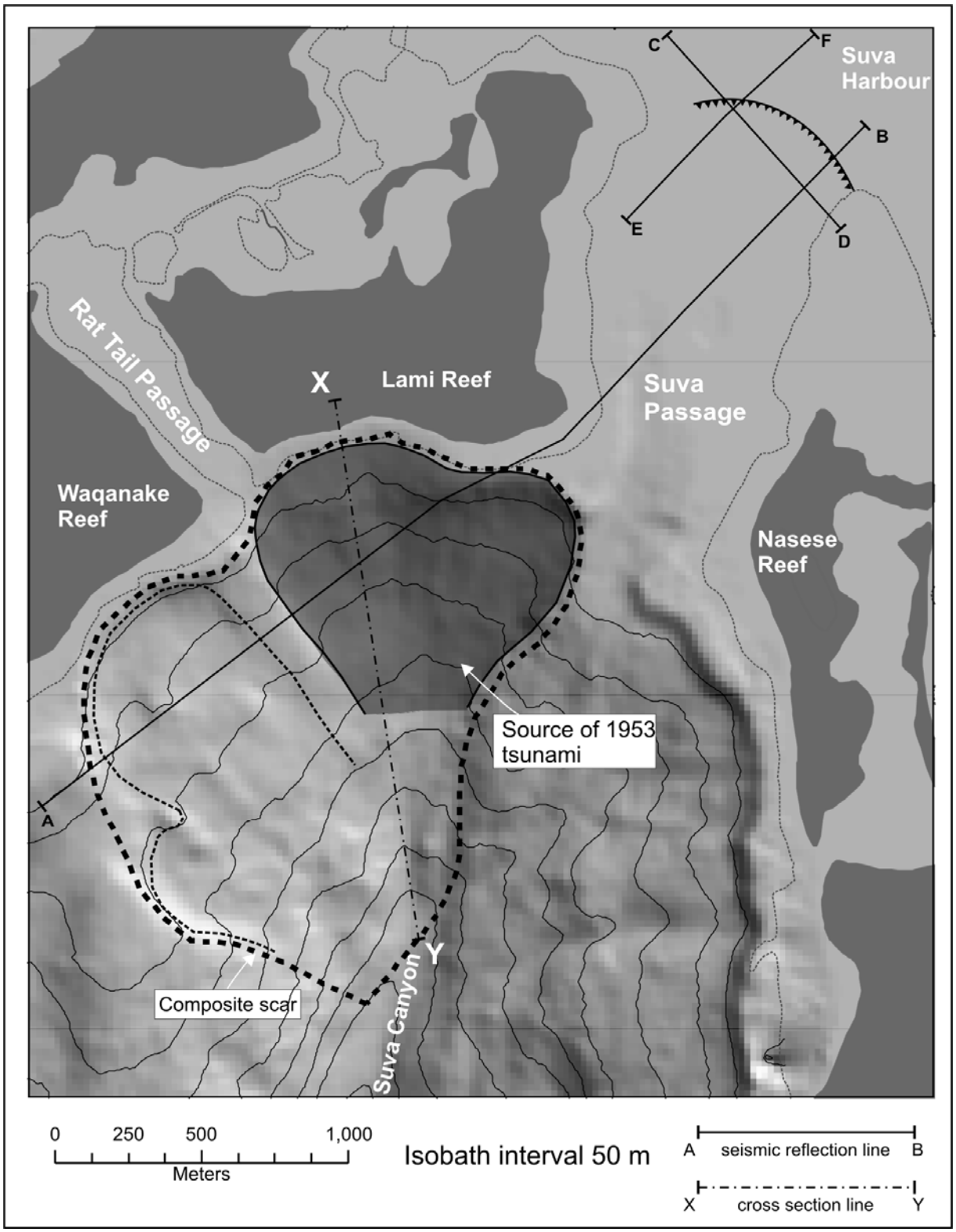

Figure 7.4: 20 m gridded multibeam bathymetric shaded relief image showing the location of the 1953 submarine landslide tsunami source within a large composite slide scar at the Suva Canyon head. Note that the bathymetry of the Suva Passage is not shown on this image.

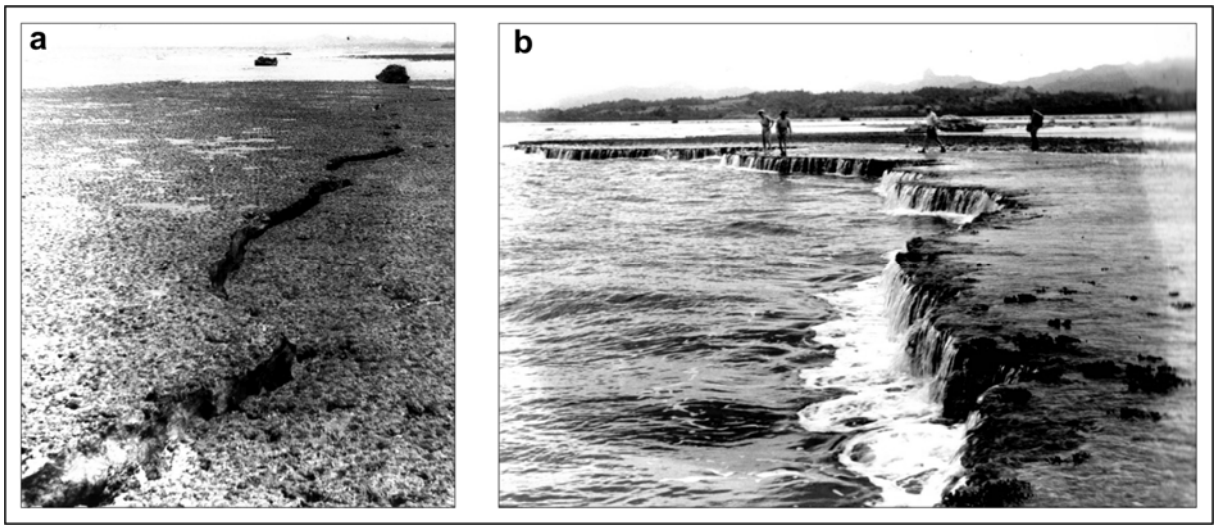

Figure 7.5: Barrier reef edge between Suva and Rat Tail Passages soon after the 1953 Suva earthquake. (a) Marginally stable reef front tilted seaward due to incipient failure (b) Total collapse of a section of the reef front. (Photos used with permission from the Fiji Mineral Resources Department).

front taken soon after the 1953 event clearly shows a 30 to 50 m wide section of missing reef overhang between Suva and Rat Tail Passages (Figure 7.6a). The slide between Suva and Rat Tail Passages occurs directly below the position of the initial sea disturbance shown by Brother Hillary's sketch and is implicated here to be the source of the 1953 Suva tsunami.

A seismic reflection survey conducted within and outside the Suva Passage provides a more detailed indication of the morphology of failure during the 1953 event. The survey line locations are shown in Figure 7.4. The NE trending seismic profile AB (Figure 7.7a) passes across the top of the composite slide scar and obliquely through the head scarp of the 1953 slide. The seabed expression of the composite scar from the seismic data agrees generally with that derived from the multibeam data. In the seismic data, the NE part of the composite scar is clear of surficial debris deposits, which are, however, present in the SW part of the scar. This confirms the recent occurrence of failure in the NE part of the composite scar. The seismic section shows a hanging ledge covered with reefs in the head scarp of the 1953 slide. This ledge appears to have slipped downwards from its original position near present day sea level. Seismic reflection profiles in the Suva Passage (see Figure 7.7a,b) show that the seafloor is relatively smooth close to the Suva Harbour end. However, there is a sudden drop in the level of the seafloor and it becomes hummocky in the area about 1.5 km from the Suva Passage entrance. The total drop of the seafloor, based on measurements on the seismic section using an interval velocity of 1500 m/s, ranges from 7 to 15 m. Complex internal reflections below the dropped uneven seafloor define a thin wedge of sediments disturbed by

mass movement. The drop in the level of the seafloor appears to represent the headscarp of a shallow failure that regressed up the Suva Passage from the main failure event outside the Suva Passage during the 1953 Suva earthquake.

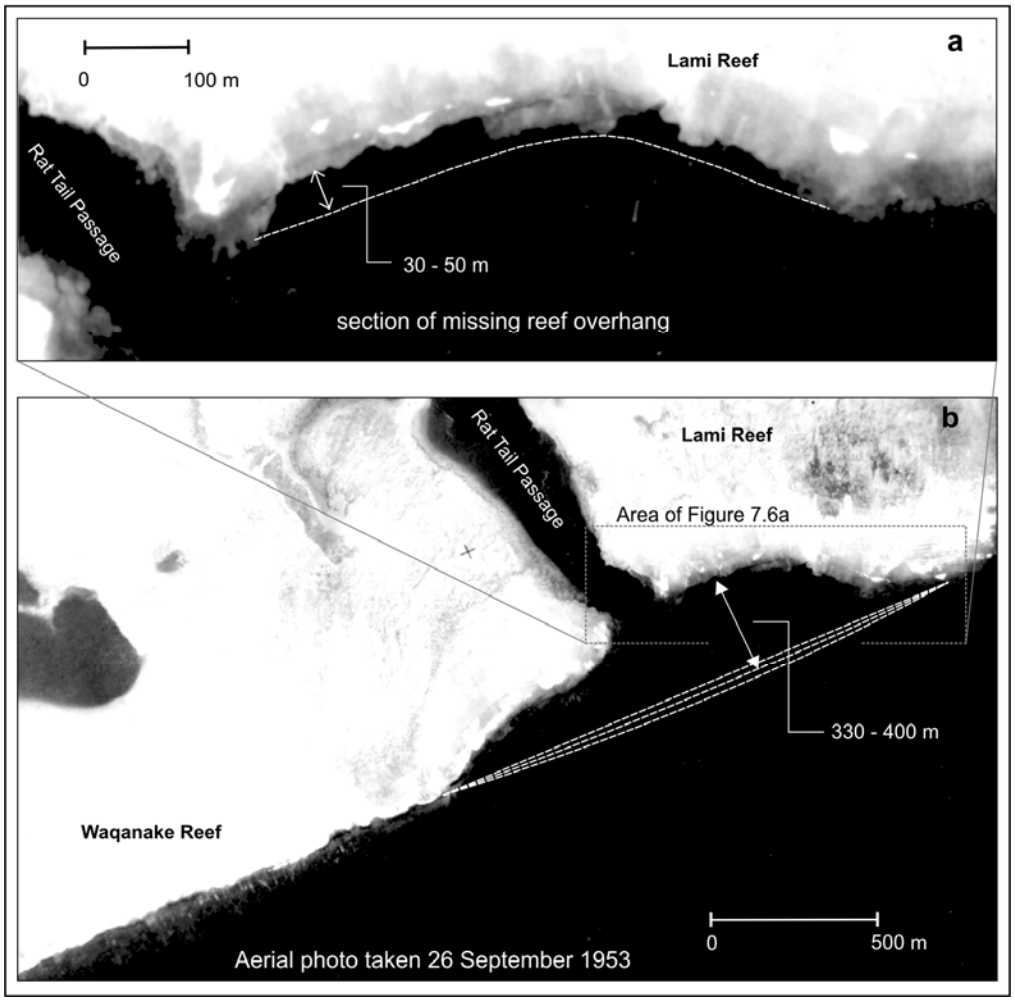

Figure 7.6: (a) Aerial photo showing reef front loss caused by the 1953 Suva tsunami east of Rat Tail Passage. (b) Composite indentation on the barrier reef fronts of Lami and Waqanake Reefs at the Suva Canyon head tsunami generating site. The aerial photograph was taken by Adastra Airways for the Fiji Geological Survey 12 days after the 1953 Suva Earthquake. (Photos used with permission from the Fiji Mineral Resources Department).

Previously the sea disturbance at the Suva Passage entrance has been attributed to the collision of two submarine landslides from opposite sides of the passage (Houtz, 1962a). However, the collective evidence presented here, including the eyewitness reports, new high resolution multibeam bathymetric and seismic reflection data, and mapping of reef edges, indicates that the main failure event occurred outside the barrier reef, between Suva Passage and Rat Tail Passage alone. The submarine landslide mapped in this area has an average width of 800 m and is approximately 950 m in length downslope. The long axis of the slide is

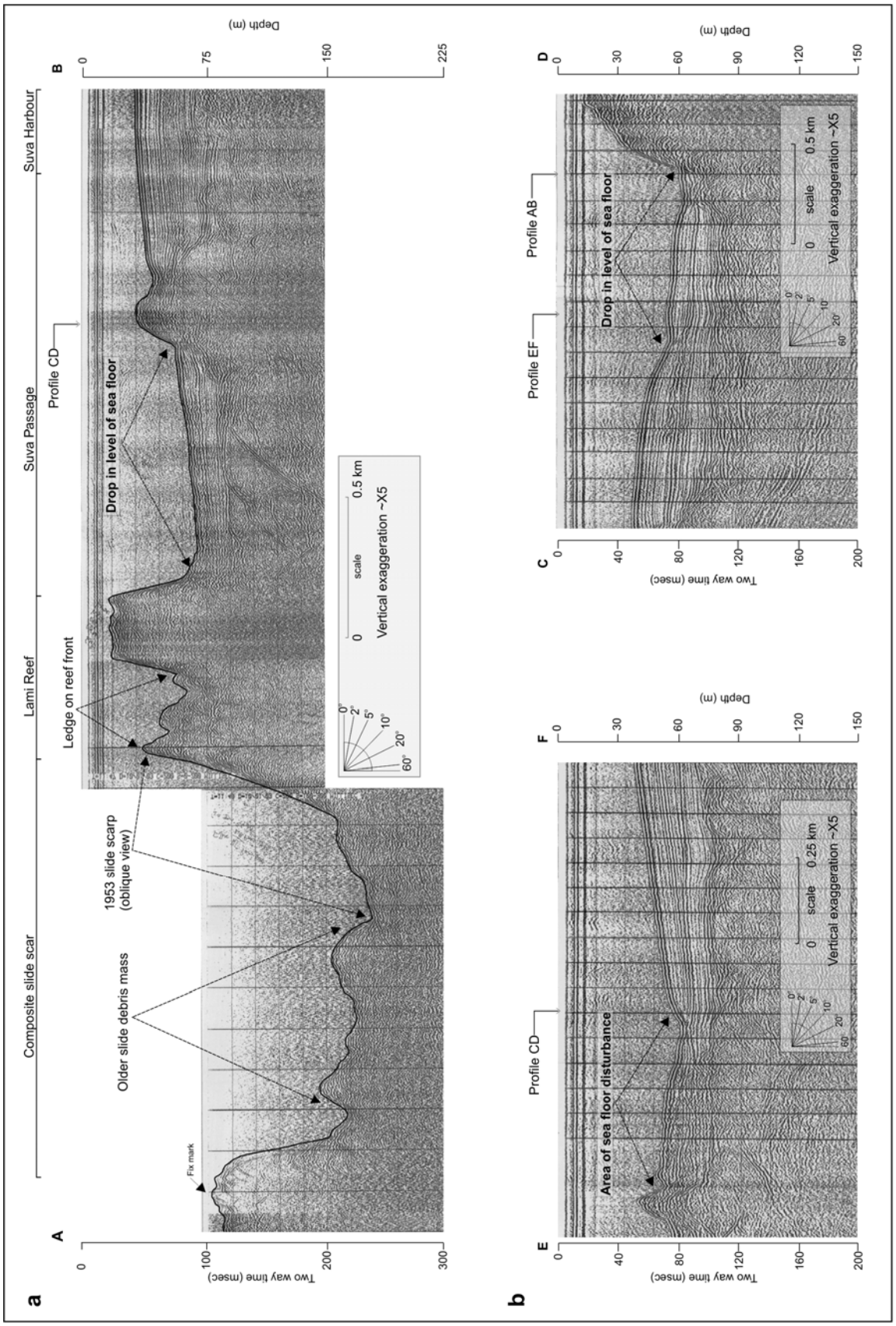

Figure 7.7: Seismic reflection profiles near the Suva Passage. Locations of survey lines are shown in Figure 7.4 (a) A profile along the Suva Passage and across the composite submarine landslide to the west of the Suva Passage entrance. (b) Profiles at the Suva Harbour end of the Suva Passage.

oriented at 180 degrees. The slip orientation on this slide is consistent with the initial drawdown witnessed in the Lami area directly behind the slide. A cross section through the slide (Figure 7.8) shows that the head scarp is inclined at 25^{o} to 30^{o}. The top of the failure has a concave upward slide plane. This is followed downslope by a more planar failure surface. The slide has incised about 80 m relative to the projected profile of the undisturbed seabed surface. The slide has an overall thickness to length ratio of 8.4% and can be classified as translational (Mulder & Cochonat, 1996). The runout path of this landslide is directly into the Suva Canyon. There is an absence of any displaced debris mass in the runout path of the slide and it is likely that the displaced material transformed into a debris flow and eventually a turbidity current, which travelled tens of kilometres downslope along the Suva Canyon. Turbidity currents in the Suva Canyon soon after the earthquake were responsible for submarine cable breakages and abrasion marks on retrieved cable pieces (Houtz & Wellman, 1962).

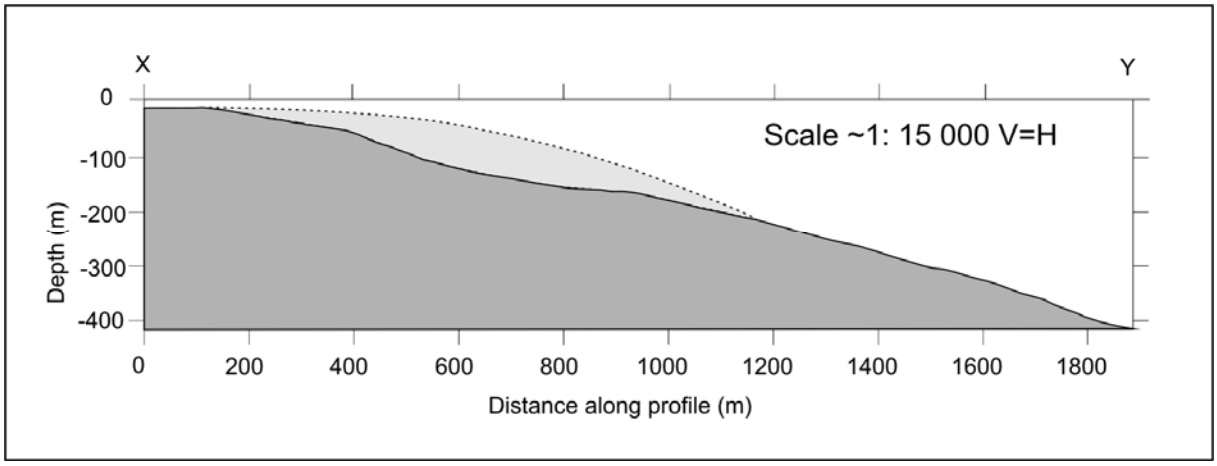

Figure 7.8: Cross section of the 1953 landslide showing thickness of up to 80 m determined from the level of pre-slide surface inferred from undisturbed contours adjacent to the slide. The volume of the slide mass is approximately 60 million cubic metres. (Location of profile shown in Figure 7.4).

7.5 SUVA CANYON HEAD TSUNAMI SOURCE ZONE

Further investigations in the 1953 tsunami source area at the Suva Canyon head reveal that other submarine landslides and associated local tsunamis may have occurred at this site in the past. The head scarp area also provides evidence for the possibility of further slides at this site in future.

7.5.1 Complex retrogressive failure system

The source area of the 1953 Suva tsunami can be classified as a complex retrogressive failure system (Hampton et al., 1996; Mulder & Cochonat, 1996). The multibeam bathymetry data indicates that the 1953 landslide is one of several adjacent failures that have combined to form the larger composite scar in the northwestern slope of the Suva Canyon head (Figure 7.4). At least one other scar is mapped in this composite scar. The composite scar is 1.8 km wide at the head scarp. The toe of the scar is located at the Suva Canyon floor axis, where it is 500 m wide and ~1.5 km from the head scarp. Over a period, successive slides in this failure system have formed and caused the upslope migration of the composite head scarp that is now represented subaerially by a broad and curved indentation in the fronts of the Lami and Waqanake reefs (Figure 7.6b). An interpolation of the reef front from outside the failed section indicates a total head scarp retreat of 330 to 400 m. Aerial photos over the last 50 years, since 1953, show that no further retreat of the reef front has taken place, implying that retrogressive failures may be periodic and may only accompany large earthquakes. Since the degree of total retreat of the composite head scarp is much larger compared to the amount of reef front loss caused by the 1953 failure (Figure 7.6a), other failures preceding the 1953 event would have contributed to the total reef front indentation as it exists at present.

7.5.2 Incipient failure at the Suva Canyon head

Two sets of tensions cracks have been mapped on the Lami and Waqanake reef crest behind the head scarp of the 1953 failure and they are highly indicative of further potentially tsunamigenic failures in this area (Figure 7.9a). The inner crack occurs within 50 to 60 m of the present head scarp and the outer crack occurs a further 60 to 80 m behind the inner crack. Both the fracture sets are curved and subparallel to the present head scarp. The outer crack is 1.2 km long and spans almost the entire crest of the Lami Reef. The tension cracks form an en echelon system of fractures. The individual fractures are up to 150 m in length, are highly irregular over a few metres and can be up to 10 cm wide (Figure 7.9b). The fractures are filled with carbonate cement and with reef organisms and show no evidence of recent or ongoing movement. They are likely to have developed in response to the removal of lateral support during previous failure events. Mechanical analysis of landslides shows that fractures near the head scarp are preceded by sliding at depth, implying that surface fractures represent a late stage of incipient landsliding and may be indicative of an imminent total failure (Martel,

2004). The cracks isolate sections of the reef front into marginally stable sheets or blocks. These are likely to fail completely under large earthquake loadings in future, forming the next generation of retrogressive tsunamigenic failures at this site.

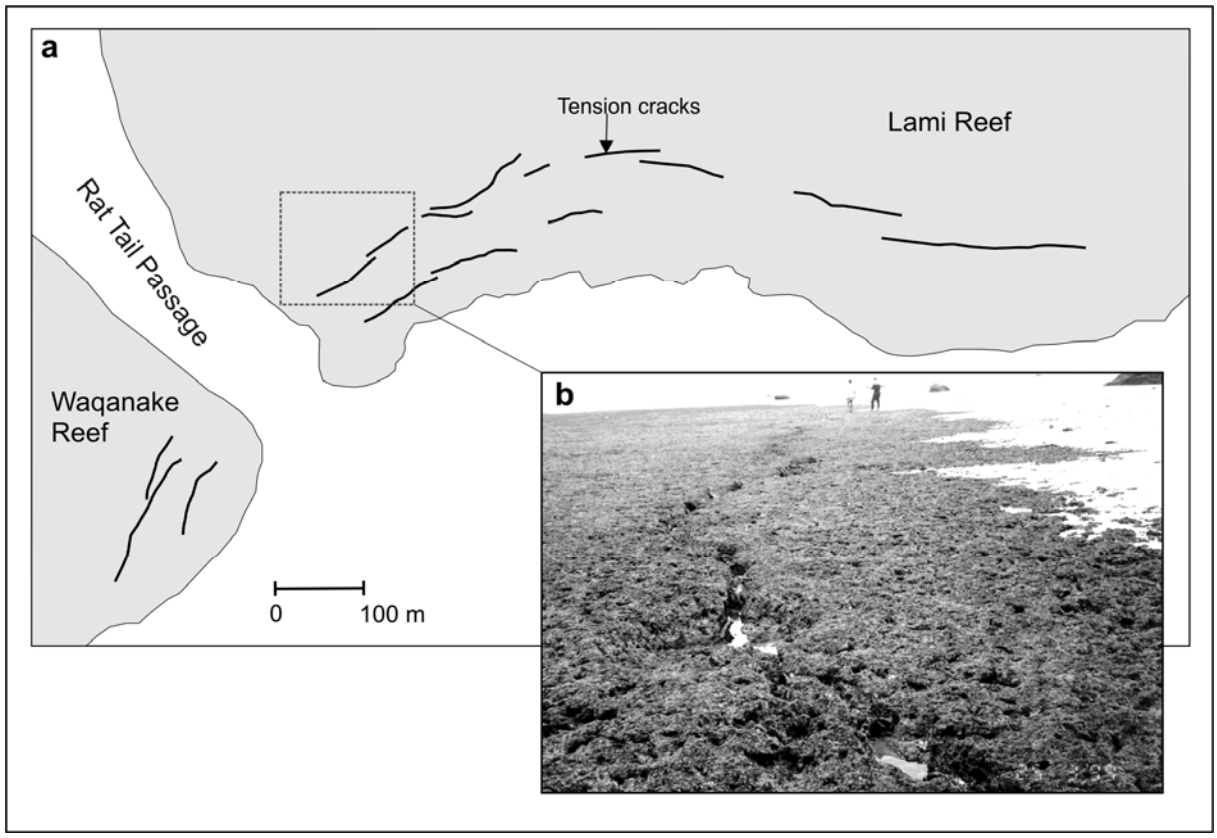

Figure 7.9: (a) Potential for further retrogressive failures at the Suva Canyon head source area defined by a curved set of tension cracks on the reef crest behind the present head scarp (b) An individual fracture on the Lami Reef crest.

7.5.3 Tsunami deposits

Local tsunamis generated by submarine landslides at the barrier reef fronts leave behind a deposit of reef edge derived coral limestone boulders on the reef crest in the vicinity of the source area. It is possible that this may be happening because sections of the reef edge are undermined immediately prior to the arrival of tsunami waves as a result of head scarp related fracturing of the tsunami causing failure. The deposits from the last two local tsunami events from the Suva Canyon head source zone have been identified and mapped on the Lami and Waqanake Reef crests. As described in Section 7.3, the waves from the 1953 tsunami dislodged sections of the barrier reef edge and deposited them on the reef flat. Eyewitnesses reported the presence of previously unseen boulders on the reef flats near the Suva Passage

soon after the 1953 tsunami (The Fiji Times & Herald 1953e). The dislodged reef limestone blocks are still present on the reef flat as boulder zones. Field measurements show that the largest of the coral limestone blocks deposited by the 1953 tsunami have volumes from 20 to 30 cubic metres and are estimated to weigh about 50 to 80 tons, if a specific gravity of 2600 kg/m^3 is assumed (Figure 7.10a). The corals in the boulders were identified as *Fungia scutaria, Acropora formosa, and Acropora echinata* that live at water depths between 1.5 and 6 m (Skiba, 1954). This indicates that the boulders were from the shallow parts of the reef edge, probably from overhanging coral.

The substantial size and congregated deposition of these boulders indicate that they are uniquely a feature of highly focussed and intense energy waves resulting from local tsunami events. Boulders are not known to be deposited on the reef flat during normal weather conditions (Holmes et al., 1987). Storm surges and cyclonic swells reach heights between 3 and 6.5 m above tide level in the Fiji waters (Krishna, 1983). A hurricane and a number of large tropical storms have occurred in southeast Viti Levu over the last century, yet there have been no apparent disturbances at the reef fronts or significant additions to the coral boulder zones as was experienced in the 1953 tsunami event. Weather driven waves would have a much more widespread impact on the reef and the resulting debris would be expected to have a much broader distribution, unlike the congregated deposits that presently occur on the reef flats. Overall, it is therefore unlikely that weather waves are capable of lifting boulders of the sizes that have been recorded and in the concentrations that have been mapped at the Suva Passage. The Suva Passage boulders are comparable in size to tsunami boulders mapped elsewhere, for example in southern Italy (Mastronuzzi & Sanso, 2000).

Soon after the 1953 tsunami a survey team from the Geological Survey of Fiji reported the presence of ‘older’ boulders which were deposited on the reef crest before the 1953 tsunami (The Fiji Times & Herald 1953c). These boulders were identified using 1951 aerial photographs and then retraced in the field using a GPS. This method formed the basis for distinguishing the older boulders from the 1953 boulders. The locations of the two boulder sets are shown in Figure 7.10b. The 1953 boulder zone occurs immediately behind and on average within 250 m of the head scarp. The older boulders are generally distributed outside the rear perimeter of the 1953 boulder field. The older boulders appear more weathered and are comparatively smaller in size than the 1953 boulders. Apart from the apparent shift towards the back reef of the older boulder zone, its pattern of distribution is generally similar

to that of the 1953 boulder zone. A well-traced older boulder now lies about 200 m landward of its position in 1951. It appears that a large contribution to this landward shift was caused by the 1953 tsunami waves. The parallel configuration of the older boulder zone implies that they were deposited by a local tsunami event generated at the Suva Canyon head source area, similar and prior to the 1953 tsunami. A radiocarbon date of a coral sample (WK15876) from an older boulder on the Waqanake Reef yielded an age of 1561 ± 30 yr BP with a calibrated age range of 830-940 AD.

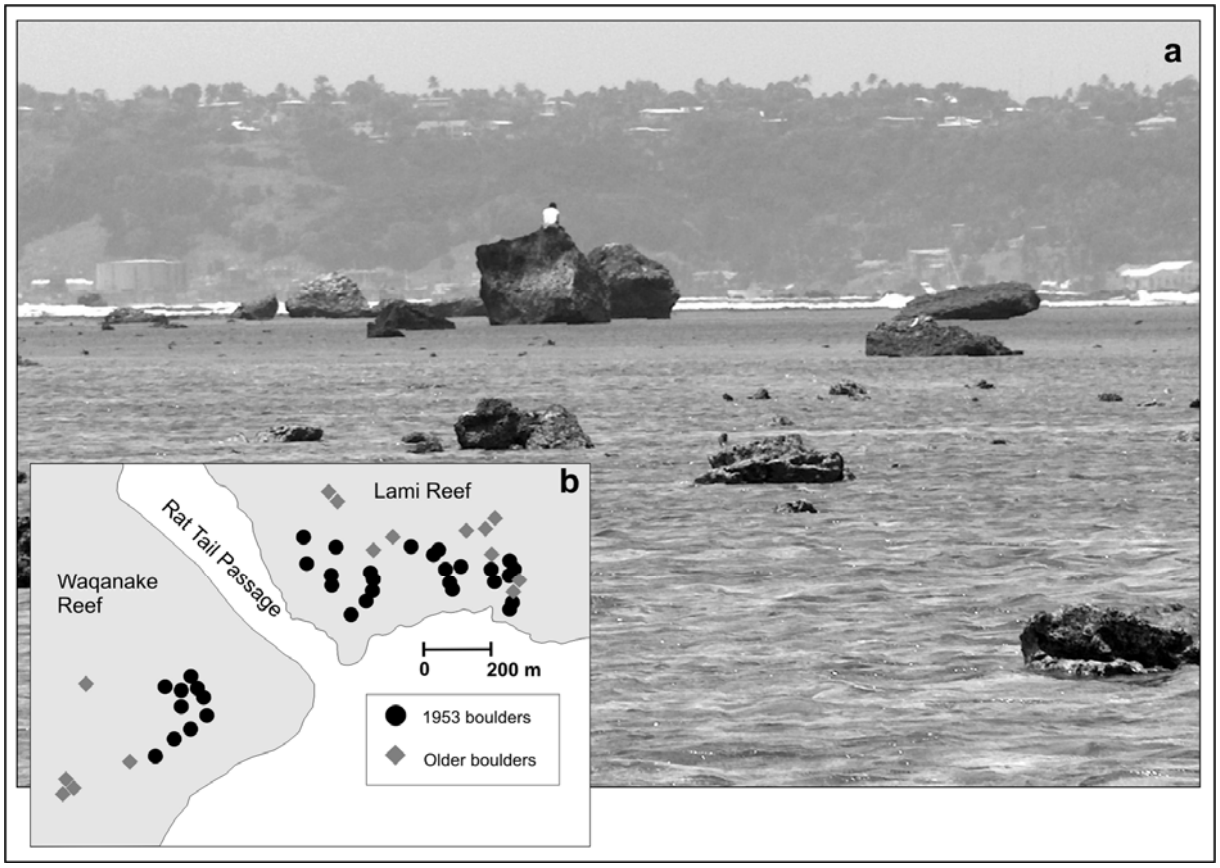

Figure 7.10: (a) Coral limestone boulders on the Waqanake Reef, 4 km southwest of Suva. Larger and more blocky boulders in the background were deposited by the 1953 Suva tsunami. An adult person is sitting on the largest boulder for scale. Comparatively smaller and more eroded boulders in the foreground were deposited by a preceding event. (b) Distribution of tsunami boulders on the Lami and Waqanake reef flats.

7.6 NUMERICAL TSUNAMI MODELLING

7.6.1 Simulation of the 1953 Suva tsunami

The initial sea surface conditions of the 1953 Suva tsunami were calculated using TOPICS and the parameters of the submarine landslide in the main failure area outside the barrier reef

as identified in Section 7.4.2. The submarine landslide source parameters and the initial tsunami conditions derived from TOPICS are shown in Table 7.3. The model calculates a surface wave above the slide, with trough amplitude of 41 m and peak amplitude of 11 m, 65 seconds after the failure initiation. The shaded contour map of this initial sea surface and subsequent snapshots of the sea surface elevation at time steps 2, 5 and 11 minutes are shown in Figure 7.11a, b, c and d respectively (for full simulation refer to Appendix 10). Twelve numerical tide gauges were placed in the simulation model to coincide with locations where eyewitness data were reported in 1953 (Figure 7.1). The wave profiles from selected tide gauges are shown in Figure 7.12. The amplitudes and arrival times of the largest elevation waves recorded by tide gauges are listed in Table 7.4 alongside observed values from 1953. Comparison of the two sets of data shows an excellent correspondence between the simulated and observed wave heights and arrival times.

Table 7.3: Submarine landslide tsunami source parameters.

Landslide Characteristics	Quantities
X_o (longitude)	178.39 E
Y_o (latitude)	18.15 S
ψ (orientation)	180^o
γ (kg/m^3)	1900
b (m)	950
T (m)	80
w (m)	800
d (m)	125
θ (degrees)	20

Tsunami Source Characteristics	Quantities
a_o (m/s^2)	1.003
u_{max} (m/s)	65.38
s_o (m)	4258
t_o (s)	65.14
λ_o (m)	2280.92
η_o (m)	-40.85

The inputs for TOPICS are, in descending order, the longitude of the initial slide centre X_o, the latitude of the initial slide centre Y_o, the clockwise orientation from north ψ, the specific density γ, the initial landslide length b, the maximum initial landslide thickness T, the maximum landslide width w, the mean initial landslide depth d, and mean initial incline angle θ. The outputs from TOPICS are the initial slide acceleration a_o, the theoretical maximum (terminal) slide velocity u_{max}, the characteristic time of the slide motion t_o, the characteristic wavelength λ_o, and the characteristic tsunami amplitude η_o from the depression at time $t = t_o$.

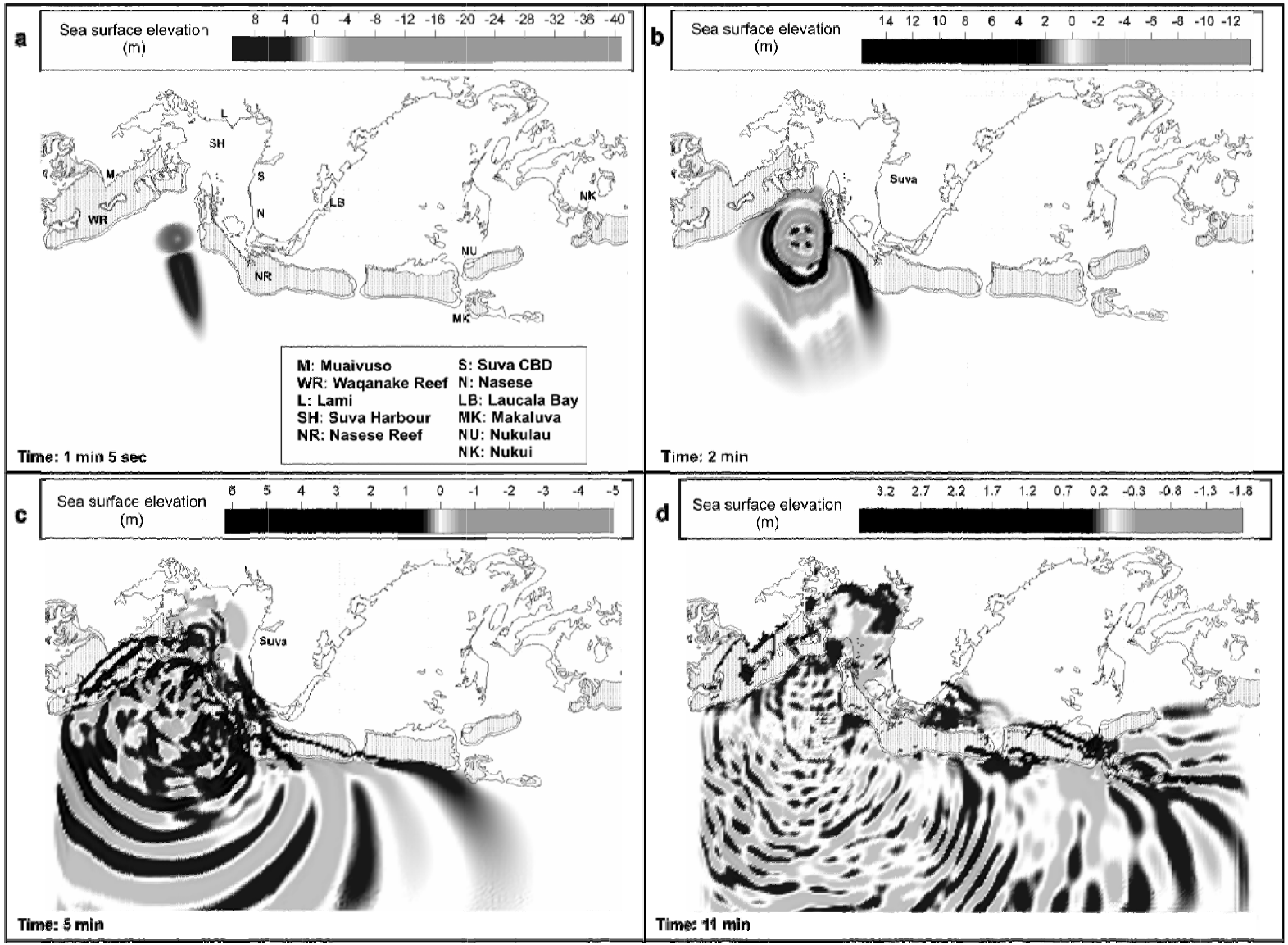

Figure 7.11: Simulated sea surface elevation of the 1953 Suva tsunami at times steps 1 min 5 sec, 2, 5 and 11 minutes of tsunami propagation from a submarine landslide source at the head of the Suva Canyon shown in Figure 7.4. For full simulation see Appendix 10.

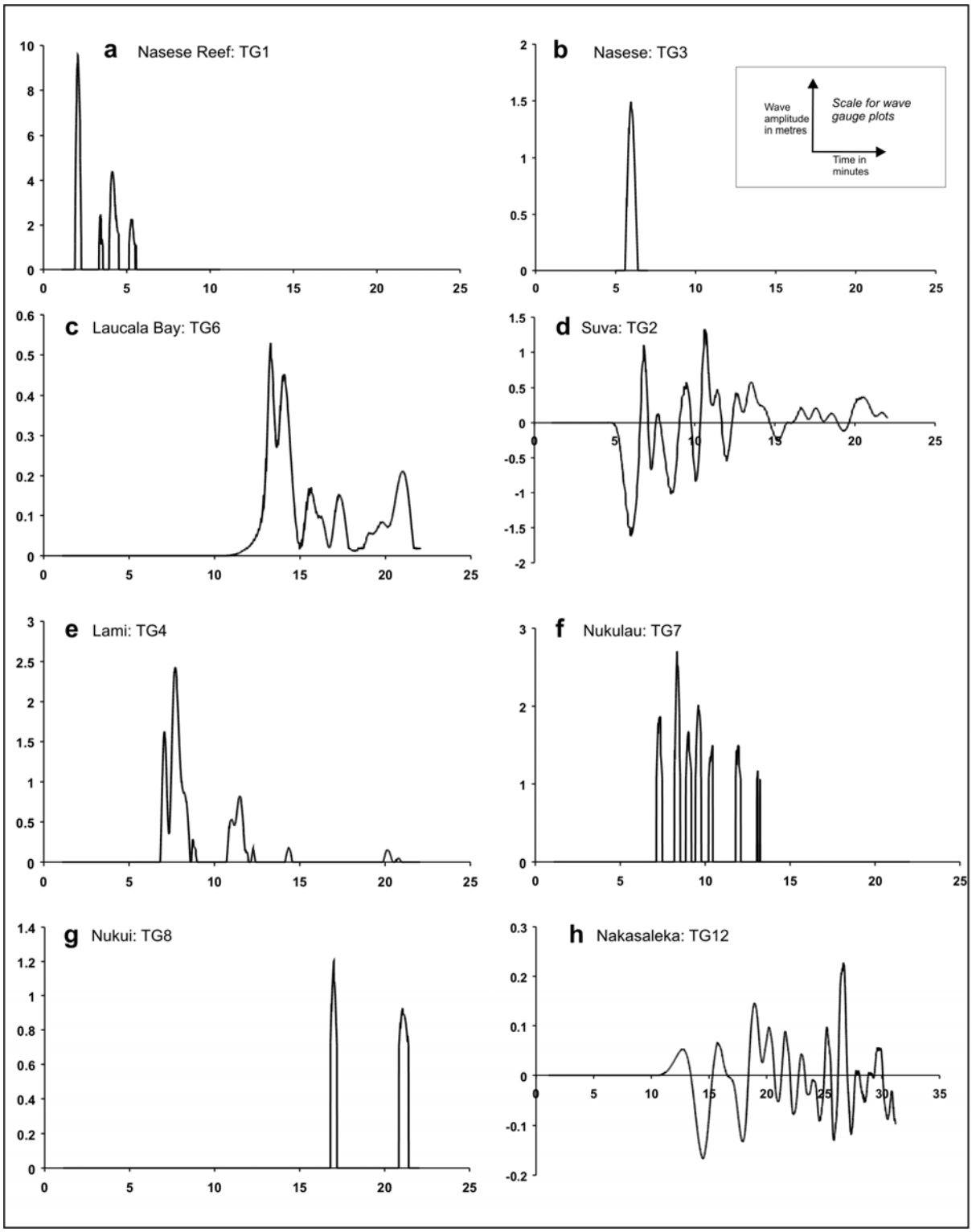

Figure 7.12: Simulated coastal wave profiles of the 1953 Suva tsunami. Location of numerical tides gauges are shown in Figure 7.1. Note vertical scales are different.

Table 7.4: Observed and simulated tsunami wave heights and arrival times of the 1953 Suva tsunami.

Location	Numerical tide gauge	Observed in 1953		Submarine landslide simulation of 1953	
		Wave height (m)	Arrival time# (min)	Wave height (m)	Arrival time* (min)
Suva Barrier Reef	TG1	3 to 15	-	8 to 10	2 min
Suva City	TG2	1 to 1.5	4-5	1.3 to 1.5	6 min
Nasese	TG3	1.5	4-5	1.3 to 1.5	6 min
Lami	TG4	1.5 to 2	-	2.4	7 min
Muaivuso Village	TG5	< 5	-	3.8	6 min
Laucala Bay	TG6	1	15	0.5	13 min
Nukulau Island	TG7	2 to 3.5	-	2.7	8 min
Nukui Village	TG8	1.5	-	1.2	17 min
Naitonitoni	TG9	0.5 to 1	10-15	0.5	10 min
Deuba	TG10	1.5	-	0.5	13 min
Rukua	TG11	1.5	15	0.5	15 min
Nakasaleka	TG12	4.5	12	0.3	12 min

#time after earthquake
*time after landslide initiation

The simulation shows that within a couple of minutes after slide generation, breaking of the leading elevation waves on the barrier reef fronts causes maximum positive amplitudes to be achieved (Figure 7.11b, Figure 7.12a). Edge waves are observed along the reef fronts, which collide into each other to produce larger amplitudes on the reef crests. On passing over the reef crests the wave heights are considerably reduced and waves that enter Suva Harbour are 4 to 5 times smaller. One set of positive leading waves passes over the Waqanake Reef and strikes the coast of Muaivuso (Figure 7.11c). The maximum simulated wave heights at Muaivuso are 3.5 to 4 m high and as reported are well below the level of the marine terrace at this location (Table 7.4). Another positive leading wave passes over the Nasese Reef and initially strikes the Suva Peninsula at Nasese with a solitary 1.5 m high elevation wave (Figure 7.11c, Figure 7.12b). The steep profile of this wave has the characteristics of a bore and resembles the approaching wave observed in the Suva Harbour (Figure 7.2a). After

striking Nasese this wave then propagates northwards and invades the Suva CBD area. This phase of the simulation is consistent with the sequence of events observed in 1953. Focussed wave effects in the Nasese area resulted in a relatively large area of inundation, inland sediment deposition, seawall damage and a person drowning. Inundation of the Suva CBD area was reported to have commenced from the southern end (The Fiji Times & Herald 1953a, Usher 1987). From Nasese, the simulated leading wave also travels southward along the coast and refracts around the Suva Peninsula before travelling north along the eastern coast of the peninsula (Figure 7.11d). At the Laucala Bay on the east coast, the simulated arrival time shows a close match to the observed arrival time (Figure 7.12c, Table 7.4).

The simulation correctly shows an initial drawdown in the Suva Harbour within 5 minutes (Figure 7.11c, 7.12d). This is due to the northward spreading of the initial depression wave through the Suva Passage. At around 7 minutes, the simulation shows an anomalous build up of positive amplitudes in the Lami foreshore area (Figure 7.11d). This effect is validated by descriptions in 1953 of focussed wave activity in the Lami area that led to seawall damage and deposition of reef boulders on the Lami foreshore (Usher, 1987).

A set of simulated leading elevation waves migrates eastward from the source area along the barrier reef front as edge waves (Figure 7.11c). These waves subsequently invade Nukulau and Makaluva islands (Figure 7.11d) with amplitudes as high as 2.5 m. They then proceed further through the reef passages and eventually strike Nukui Village. Here again a close correspondence is seen between the simulation and observations. Eyewitnesses on Nukulau island to the east of Suva described the approach of the waves from the west as a “great wave running along the reef” (The Fiji Times & Herald 1953f). The set of steep amplitude waves recorded by the tide gauge on Nukulau (Figure 7.12f) is consistent with the report of three waves sweeping away recreational facilities on Nukulau (Usher, 1987). Tide gauges located more than 30 km to the west of the tsunami source area, at Naitonitoni (TG9), Deuba (TG10), Rukua (TG11) and about 100 km to the south at Nakasaleka (TG12), show a good resemblance to observed tsunami arrival times. However, the simulated wave heights are generally lower than what was observed (Table 7.4).

A sensitivity analysis was carried out by varying the location of the source 200 m to the S, E and W of its defined position and varying the slide parameters by +/- 20 % of the measured values. For all the re-runs of the simulation, the location of the peak run-up positions occur

persistently at the Lami and Nasese. The arrival times of the first elevation wave at all tide gauges vary by only 1 to 8 %. The wave amplitudes generally vary by 15 to 20 %. As expected, larger dimensions of the slide geometry, higher slope angle and shallower water depths of the slide, produce larger amplitudes. The most sensitive parameters are the slide depth and the slide density. These parameters produce up to 35 % variation in the initial tsunami amplitudes and up to 40 to 70 % variation in wave amplitudes in some coastal tide gauges.

7.6.2 Simulation of a potential worse case scenario

Based on contemporary knowledge, Suva City is more vulnerable to local tsunami sourced from submarine landslides than any other source mechanism. Tsunamigenic submarine landslides can potentially occur at any of the submarine canyon heads of southeast Viti Levu (Figure 7.1). The Suva Canyon head is perceived to be the biggest threat considering the existence here of an incipient, potentially tsunamigenic failure and the occurrence of two previous tsunamigenic events. For a particular reason that is not entirely clear right now, the Suva Canyon head contains some specific geological condition that makes it conducive to large tsunamigenic failures. This condition is not present or may be subdued at the other submarine canyon heads of southeast Viti Levu. It is speculated that since the Suva Canyon is the largest on the marginal slope of southeast Viti Levu (see Section 5.4.1), active processes at the canyon head, which promote slope failure, such as rapid sediment deposition and canyon undercutting, are conceivably foremost at the Suva Canyon, restricting the largest failures to this site. It is also possible that the Suva Canyon lies along the trace of a seismically active fault (see Section 9.3.2.4), along which rupturing during large earthquakes creates instability at the Suva Canyon head.

A potentially worse case scenario event is constructed using the Suva Canyon head source area in order to evaluate the hazard that might be posed to Suva City. In this scenario it is assumed that the next tsunamigenic failure will nucleate along the inner line of tension fractures described in Section 7.5.2 and that its size and geometry will be similar to the 1953 failure. The degree of inundation in Suva City will be dependent upon the state of the tide. A high tide level (0.7 m AMSL) is assumed to replicate a worse case scenario. Calculations using tidal predictive tables (Anon, 2004) show that sea level in the Suva Harbour is above 75% of peak spring or neap high tide level for a period of about 8.5 hours a day

(encompassing two tide cycles). If a tsunami were to strike Suva, there is a about a 35% probability that it will occur during a period of high tide. Based on this scenario, a predictive simulation tsunami was done using the Geowave model.

The predictive simulation indicates that the waves will strike the Suva and Lami coasts within 5 to 7 minutes of slide generation and the wave heights at the coastline will range from 1.5 to 3.5 m (Figure 7.13a). Individual tsunami wave crests striking Suva will persist for up to 3 minutes. The entire period of wave effect at the Suva and Lami coasts is expected to last up to 10 minutes. Nearshore and overland water velocities are estimated to be in the order of 2 to 3.5 m/s. The maximum vertical run up at the Suva CBD area will be 4 m above tide level. The maximum horizontal inundation will be 400 m, and this will be in the area between the Nasese and the Suva CBD area (Figure 7.13b).

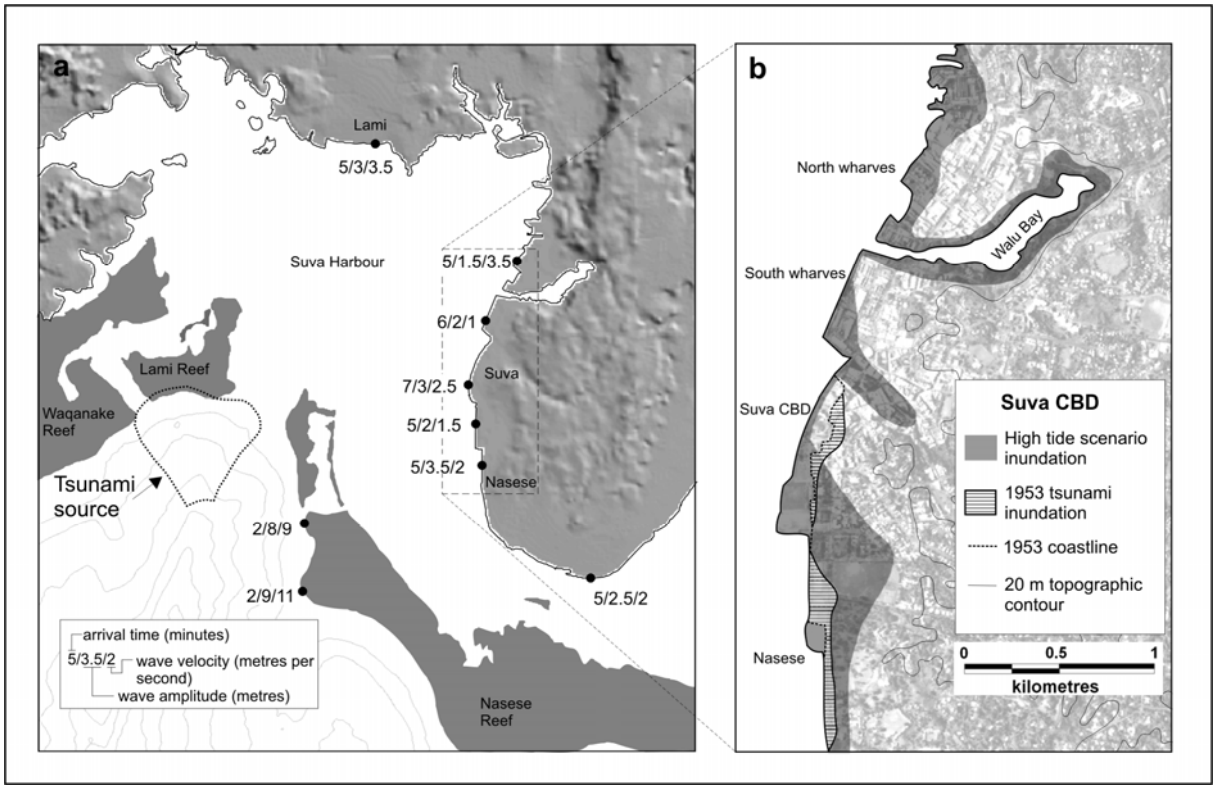

Figure 7.13: (a) Tsunami arrival times, wave heights and wave velocity around the Suva Harbour based on predictive simulation of a potentially worse case scenario (b) Worse case scenario inundation level in the Suva CBD area. Shown for comparison is the simulated 1953 tsunami inundation level based on the pre-reclamation 1953 coastline.

7.7 DISCUSSION

7.7.1 Single source for the 1953 Suva tsunami

Irreconcilable arrival times led Houtz (1962a) to suggest multiple submarine landslide sources for the 1953 Suva tsunami. Using the arrival times Houtz defined the source area as a locus of points along the barrier reef fronts between Suva and Beqa (see Figure 7.1). However, the results of the numerical simulation of the 1953 Suva tsunami presented in this study indicate that multiple submarine landslide sources are not required to reconcile near-field arrival times that were observed in 1953, but rather that a single source area at the Suva Canyon head is sufficient. Accurate simulation of arrival times of waves from the Suva Canyon head source area at distal locations to the west of Suva and at Kadavu further counteract the possibility of multiple submarine landslide sources along the barrier reef front of southeast Viti Levu. The possibility of the earthquake tsunami as the source of the preliminary "warning" wave observed at a number of locations however, is not ruled out.

Additional evidence contradicting multiple submarine landslide tsunami sources of the 1953 tsunami is provided by the distribution of tsunami boulders on the barrier reef crests. An aerial survey of the barrier reefs of southern Viti Levu conducted by the Geological Survey of Fiji in 1983 (Holmes et al., 1987) shows that the largest concentration of boulders occurs on the Waqanake, Lami and Nasese Reefs surrounding the Suva Passage entrance. In this survey, considerably smaller boulders were found randomly scattered on other parts of the barrier reef in southern Viti Levu and are likely to have been deposited by storm surges or cyclonic driven wind waves. None was found to be as densely distributed as those at the entrance of the Suva Passage. The exclusiveness of dense boulder distribution at the Suva Passage entrance is yet another assertion that this site alone was the source area of the 1953 tsunami and that no other tsunamigenic reef edge failures of similar or larger size have occurred elsewhere along the southern coast of Viti Levu in the recent past.

7.7.2 Antecedent tsunami event at the Suva Canyon head source area

Based on current data it is difficult to ascertain whether previous retrogressive failures in the Suva Canyon head source zone have been tsunamigenic. By implication, failures comparable to the 1953 slide would have been tsunamigenic and the internal morphology of the composite

scar shows one other slide of similar size to the 1953 slide (Figure 7.4). Evidence for at least one tsunamigenic event preceding the 1953 event in this source zone is offered by the older boulder zone mapped on the reef flat. The radiocarbon date from this deposit provides an upper age limit for this earlier event. The dated sample of coral was taken from a boulder composed of reef framestone derived from a section of dead reef and therefore is not necessarily the age of the tsunami event but of when the coral died during normal reef building processes. Nevertheless, this date constrains the age of occurrence of the antecedent event to within the last 1000 years.

There are no historical records of other local tsunami events comparable in size to the 1953 tsunami since written records began in Fiji towards the end of the 19th century (Everingham, 1987). There is, however, a well known local legend from this part of Fiji called “Dakuwaqa” (Reed & Hames, 1967), which describes aspects akin to the effects of a local tsunami. A part of the legend describes “great waves” at the mouth of the Rewa River and “flooding of valleys for many miles inland”. Out of the several tele-tsunamis that have hit the Pacific coastlines, only two from South America in 1877 and 1960 have been recorded in Fiji, but neither caused inundation (Everingham, 1987). It therefore seems more likely that the legend describes a local tsunami. A speculative proposition is that the legend may correspond to the event responsible for the “older” boulders at the Suva Canyon head. Events described by the legend at the Rewa River mouth, a place inhabited for many centuries, appears analogous to what was experienced at Nukui Village in 1953. Fijian legends are known to survive, for approximately 400 to 500 years from their inception (Cronin et al. 2004, P. Geraghty pers comm. 2005). This time period indicates, by conjecture, a more recent age for the previous Suva Canyon head tsunami event.

An estimate of the time frame between previous tsunamigenic events at the Suva Canyon head can be derived from the rate of head scarp retreat of the barrier reef front within the indented area of the composite head scarp. The original position of the reef front in the indented area can be taken as a 4000 to 4500 yrs BP timeline, a time the bulk configuration of the barrier reef system was attained when eustatic sea level stopped rising in southern Viti Levu in the mid-Holocene (Maeda et al., 1986; Shepherd, 1990; Shorten, 1993). If the amount of retreat caused by the 1953 event is taken to be typical of tsunamigenic failures at this site, then using the total retreat of the reef front (Section 7.5.1), the time frame between events is

estimated as 300 to 600 years. This timeframe shows an apparent consistency with the estimated age of the antecedent event.

7.7.3 Tsunami wave propagation

The simulations of wave propagation from the source area to the coastline show how tremendously variable wave dynamics and resulting coastal wave heights can be over very short longshore distances in the Suva area. To a large extent, this is due to the presence of a system of intervening barrier reefs and deep water passages, and a highly irregular coastline. Highly variable bathymetry of the shallow lagoon, due to underlying bedrock structure and reef growth, also contributes to a diverse range of wave effects. The important role of the barrier reef system as a natural breakwater to approaching tsunami waves is highlighted by all the simulations. Most of the wave energy is dissipated while breaking on the barrier reef front. Wave amplitude and velocity were reduced by up to 80% on passing over the barrier reefs.

Wave focusing in the Lami and Nasese areas is shown in simulations and its effects can be clearly discerned from observations during the 1953 tsunami. The wave heights at the Lami coast are 3 times greater than waves 800 m offshore. The build up of waves in the Lami area is attributed to shoaling and wave convergence on the shallow protruding reef platform that fronts the Lami foreshore. The seabed rises gradually at a gradient of 2 degrees to the shallow reef platform. Gradual shoaling and convergence causes an increase in tsunami amplitude. Peak amplitudes occur at Nasese as it is the closest area on the Suva Peninsula in the azimuthal direction of the slide failure and lies close to the direct path of wave radiation. It is possible that another factor contributing to focussing effects at Nasese is wave convergence around the seaward convex shape of the Nasese Reef.

Lower simulated wave heights at distal tide gauges are attributed to poor quality nearshore bathymetry data. As a result the model is unable to precisely simulate shoaling and wave focussing effects expected at these locations. The bathymetry at distal tide gauges to the west of Suva is from spot depth recordings only and at Nakasaleka (Kadavu Island) from 100 m isobaths. The effect of poor quality bathymetry is clearly highlighted at Nakasaleka. The tsunami arrival time at Nakasaleka tide gauge is remarkably consistent with the recording in 1953, however, the simulated wave height is only 0.25 m compared to the observed value of 4.5 m (Figure 7.12h). Nakasaleka Village is located at the head of a small bay, which is 800 m

long and narrows from 600 m near the mouth to 200 m at the head. Waves that enter a narrowing bay are confined, which forces waves to build in amplitude. It is likely that elevated waves experienced here in 1953 would have been subjected to this process. The 100 isobaths used in the simulation grid are too coarse to resolve the bathymetry of this bay. Wave focussing at Nakasaleka is consistent with the fact that other villages on straighter sections of the northern coast of Kadavu received only very small waves and were not damaged at all.

7.7.4 Predicted hazard for Suva City

The predictive simulation of the worse case scenario event is expected to be an accurate representation, given the success of the Geowave model in replicating the near field features of the 1953 event. With predicted coastal wave heights 1 to 2 m higher than what was experienced in 1953, the expected damage and losses in Suva are expected to be much greater. The vulnerability of Suva to the predicted event is further compounded by a four-fold population increase and considerable coastal infrastructure development since 1953.

There is an inherent shortfall in the predicted inundation levels of the Suva CBD area. The simulation grid does not take into account the existence of buildings, seawall and vegetation in the inundation area. It is expected that the interaction of these features with wave propagation will produce slightly different inundation levels and run-ups. Seawalls are expected to deflect the approaching waves, but since the high tide water level approaches the top of most seawalls around Suva, the effect of the seawall is considered minimal. Vegetation is expected to retard the waves slightly. The presence of buildings in the inundation area is expected to induce significant channelling effect on the waves that would contribute to greater run-ups. The final inundation level predicted for the worse case scenario, therefore is expected to be greater than what was simulated by the model.

Notwithstanding the discrepancy, Lami and the area between Nasese and the Suva CBD are expected to suffer the greatest impact of the waves with peak coastal amplitudes up to 3.5 m. These areas are likely to be subject to conditions that were experienced in Nukulau in 1953 that led to the more devastating consequences on the island (Usher, 1987). Experiences elsewhere, for example in Japan (Shuto, 1993), indicate that damage to property may occur when run-up heights exceed 2 m. Overland wave velocity is also an important damaging factor (Titov & Synolakis, 1997). Even though the predicted wave heights at the northern

wharves of Suva are only 1.5 m, this area is also expected to face relatively heavy damage, with inundation flow velocities as high as 3.5 m/s. A quantitative assessment of the full economic impact of this scenario is beyond the scope of this study. However, the hazard to Suva predicted in this study has the potential to underpin the implementation of mitigating strategies that can focus on measures such as raising public awareness, developing evacuation maps and land use zoning, and designing of protective structures at high impact sites such as Nasese and Lami.

7.8 SUMMARY AND CONCLUSIONS

A well constrained case study is presented on the tsunami hazard of a submarine landslide tsunami source zone along the morphologically complex and densely populated coastline of Suva City. Using high resolution bathymetric and seismic reflection data, historical records, and field mapping in the source area and of tsunami deposits, the source of the 1953 Suva tsunami is defined as a 60 million cubic metre submarine landslide at the head of the Suva Canyon within 4 km of Suva City. Using the parameters of this slide and the Geowave tsunami generation, propagation, and inundation model, the observed wave heights and arrival times of the 1953 tsunami are successfully simulated at eight near-field localities. The simulation shows that highly variable observations of coastal wave heights and arrival times in 1953 are the result of complex wave dynamic effects influenced by the barrier reef system, uneven nearshore bathymetry and the irregular coastline, and not multiple submarine landslide tsunami sources as previously thought. The earthquake tsunami, however, may have been responsible for the observed preliminary “warning” wave.

The 1953 submarine landslide is one of several failures at the Suva Canyon head forming part of a larger retrogressive failure system that is inferred to have produce tsunamigenic failures in the past. It is estimated that an event similar to the 1953 event occurred in this source area within the last 1000 years prior to 1953, possibly as recently as 400 to 500 years before. A system of tension cracks behind the present head scarp defines the next generation of retrogressive failures that will occur at this site. A numerical simulation, based on the next retrogressive failure and on a potentially worse case scenario event, is used to predict the level of inundation and flow velocities at the Suva coast.

CHAPTER 8

TECTONIC ROTATION AND FAULT MESH FORMATION: TOWARDS A SEISMOTECTONIC MODEL FOR THE FIJI PLATFORM

8.1 INTRODUCTION

Seismotectonics deals with tectonic plate boundary interactions and the resulting crustal deformation, seismicity and their spatial and temporal evolution. The progressive build up of tectonically induced elastic strain in the crust is released suddenly by earthquakes, primarily along faults. There is, therefore, a direct link between plate tectonic processes, crustal deformation and seismicity. Based on this relationship, earthquakes can provide direct insights into active tectonic processes; while, on the other hand, investigations of tectonic deformation can be used to understand the earthquake generating process and can be utilised in seismic hazard evaluations. Seismotectonic studies permit the identification and quantification of seismic hazards within the framework of regional tectonics. The development of a seismotectonic model for an area or region allows for the separation of the Earth's crust into seismic source zones that have distinctive geologic, tectonic and seismogenic properties, and that exhibit a similar earthquake potential throughout (Reiter, 1990).

Present day seismicity within the Fiji Platform provides direct evidence of active tectonic processes operating in this area (Hamburger et al., 1988). However, the origin of this seismicity in the context of Fiji's tectonic setting and structural evolution has remained poorly understood. No detailed work has been previously done on the seismotectonics of the islands, in terms of correlating the observed seismicity with identifiable structural geological features along which tectonic deformation is accommodated. A review of Fiji's tectonic history and present tectonic setting led to the proposing of questions implying a hypothetical relationship between tectonic rotation, internal deformation and present day seismicity of the Fiji Platform (Chapter 2). The work carried out during the present research on structural lineaments, especially in southeast Viti Levu, has allowed further investigations of this hypothesis.

It is shown in Chapter 4 that lineaments mapped over a wide area of southeast Viti Levu in a

variety of remote sensing imagery, of both the surface and sub-surface, are expressions of fault and fracture zones in the bedrock. Additionally, based on detailed work done in the offshore and near-shore areas of southeast Viti Levu (Chapter 5), it is shown that submarine canyon lineaments represent fault zones that are continuous with the onshore fault zones. The mapping of lineaments has allowed for the identification of new fault zones and has provided a vast coverage of and comprehensive information on two dimensional fracturing in southeast Viti Levu, that until now was insufficiently known for a seismotectonic analysis. The system of fractures mapped is fundamentally related to the crustal brittle deformational processes and thus provides insights into the structural and tectonic evolution, as well as allowing for the interpretation of seismicity of the area. The results of these investigations are used in the present chapter to provide a new perspective on active tectonic deformation within the Fiji Platform through a demonstrated correlation between seismicity and localising structural geological features within the platform.

In this chapter, the fracture lineament data are used to infer the structural framework for southeast Viti Levu in terms of a complex fault mesh. The development of this fault mesh is explained through complex internal deformation during the rotation of the Fiji Platform in the Neogene and Quaternary. Through the use of accurate seismicity data, it is shown how an active mesh style of faulting may be related to the seismicty in southeast Viti Levu. Finally, the fault mesh style model of deformation is used to interpret the seismotectonics of the entire Fiji Platform.

8.2 STRUCTURAL FAULT MESH OF SOUTHEAST VITI LEVU

In Chapter 4, detailed analyses of lineaments and faults were used to map six prominent and continuous fault lineament zones in southeast Viti Levu. The fault lineament zones are shown to be composed of parallel fractures sets with lengths in the order of a few kilometres to tens of kilometers, which follow the principal orientations of NNW to NW, NNE to NE, WNW and ENE. The structural pattern in the onshore and offshore areas of southeast Viti Levu that emerges when these fractures sets are superimposed is one of a complex fault mesh. The geometry of this fault mesh is provided by the combined fracture density map of all the principal fracture sets mapped in southeast Viti Levu, as shown in Figure 8.1. Individual density maps of the principal fracture sets were created using a detailed quantitative statistical analysis of fracture lineaments in the onshore area of southeast Viti Levu (Section 4.5.2). The

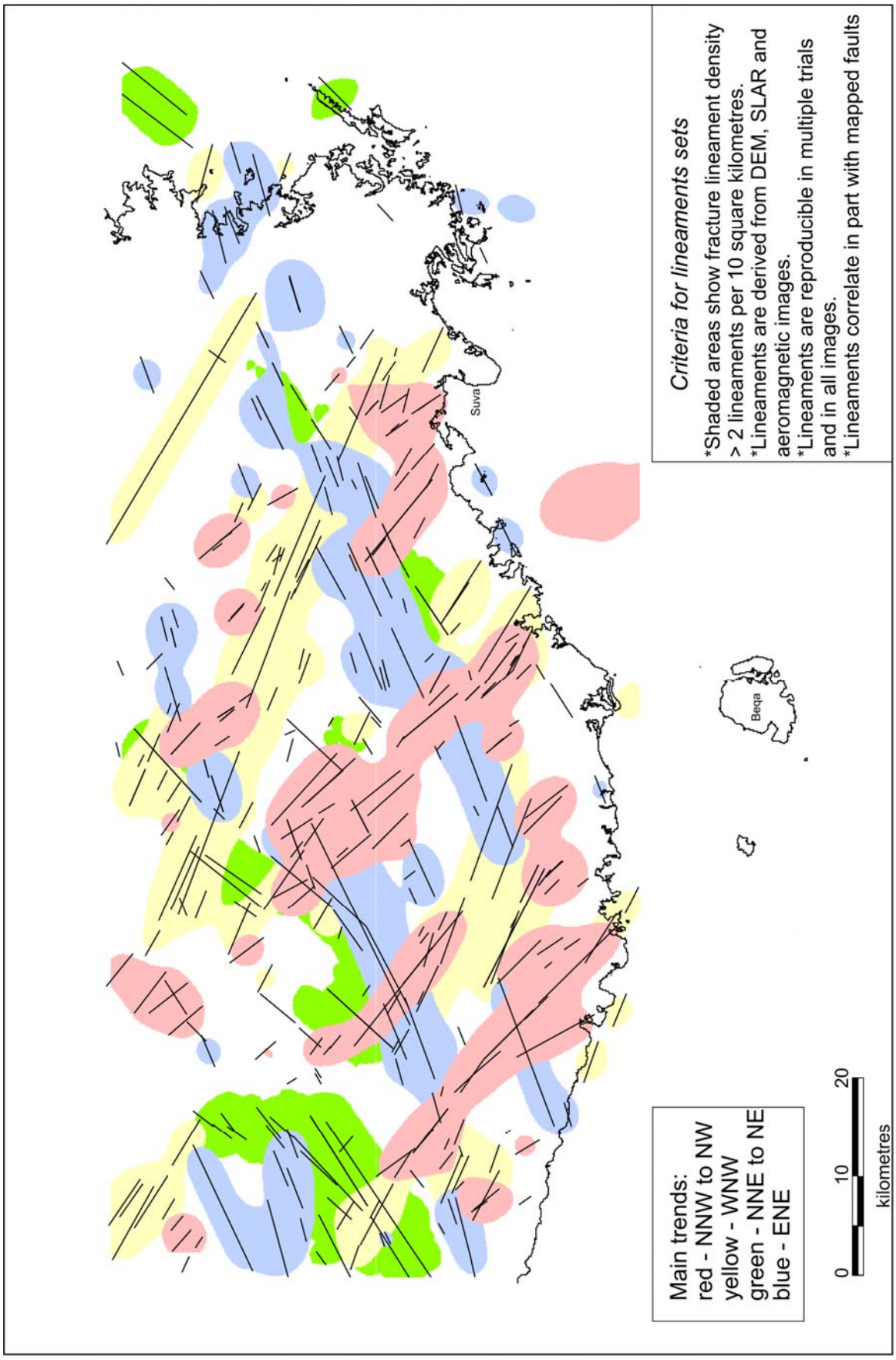

Figure 8.1: Result of a quantitative lineament analysis showing fracture lineament sets forming a complex fault mesh in southeast Viti Levu.

high density zones shown in these maps enclose elongate regions where there are concentrations of sub-parallel and possibly linked fractures. The combined density map shows that within the fault mesh, fracture sets terminate against, or are offset by each other. High concentrations of fractures occur at the intersection of fracture sets and large areas (blocks), which internally have very little fracturing, are enclosed by intersecting fracture sets of a number of orientations. It appears that the upper crust of southeast Viti Levu is subdivided into a number of upper crustal blocks that typically range from ~2 to 30 km across, by a network of interlocking fault sets that follow the principal orientations defined in this study. Other representations of the fault mesh are given in the regional lineament set compilation maps presented in Figure 4.6. A conceptual model of the structural fault mesh of southeast Viti Levu is shown in Figure 8.2.

The fault mesh represents the superposition of several generations of fracture sets. It is possible that some of the fracture sets in the fault mesh may have developed as conjugate or orthogonal sets. However, due to lack of clear age control on most of the fracture sets, this suggestion is difficult to prove or disprove. It is possible, however, to provide some general constraints on the age of the fracture sets with respect to the mapped geology and geomorphology, and also from cross cutting relationships. The ENE and WNW trends appear to represent older faults as they are restricted to the older terrain of the Oligocene to Late Miocene Wainimala and Savura Groups. They control the margins of the post Late Miocene Suva and Navua sedimentary basins in southeast Viti Levu, but are rarely found to occur in the younger rocks within the basins. On large-scale lineament maps, the ENE and WNW fractures are discontinuous and also appear to have undergone disruption and offset along younger generations of fractures (e.g. Figure 4.8). The NNW to NW and NNE to NE fractures appear to be younger than the WNW and ENE fractures, as they cut across the fabric of the older ENE and WNW trends. While the older ENE and WNW fractures appear to control the margins of the larger post Late Miocene basins, the NNW to NW and NNE to NE trends correlate with smaller structural features that have better defined and more youthful geomorphic expression. These fracture sets impart significant control on the geomorphic expression of bays, peninsulas and nearshore islands of the southeast Viti Levu coast (Figure 4.8, Section 4.7). By doing so, they disrupt the general ENE trend of this stretch of coastline. For example, NNW to NW fractures control the margin of the Bay of Islands and the Namuka Harbour, and the NNE to NE fractures, the trends of the Suva Peninsula and the Suva Harbour. Furthermore, as discussed in Section 5.4.3.2, these younger fractures impart strong

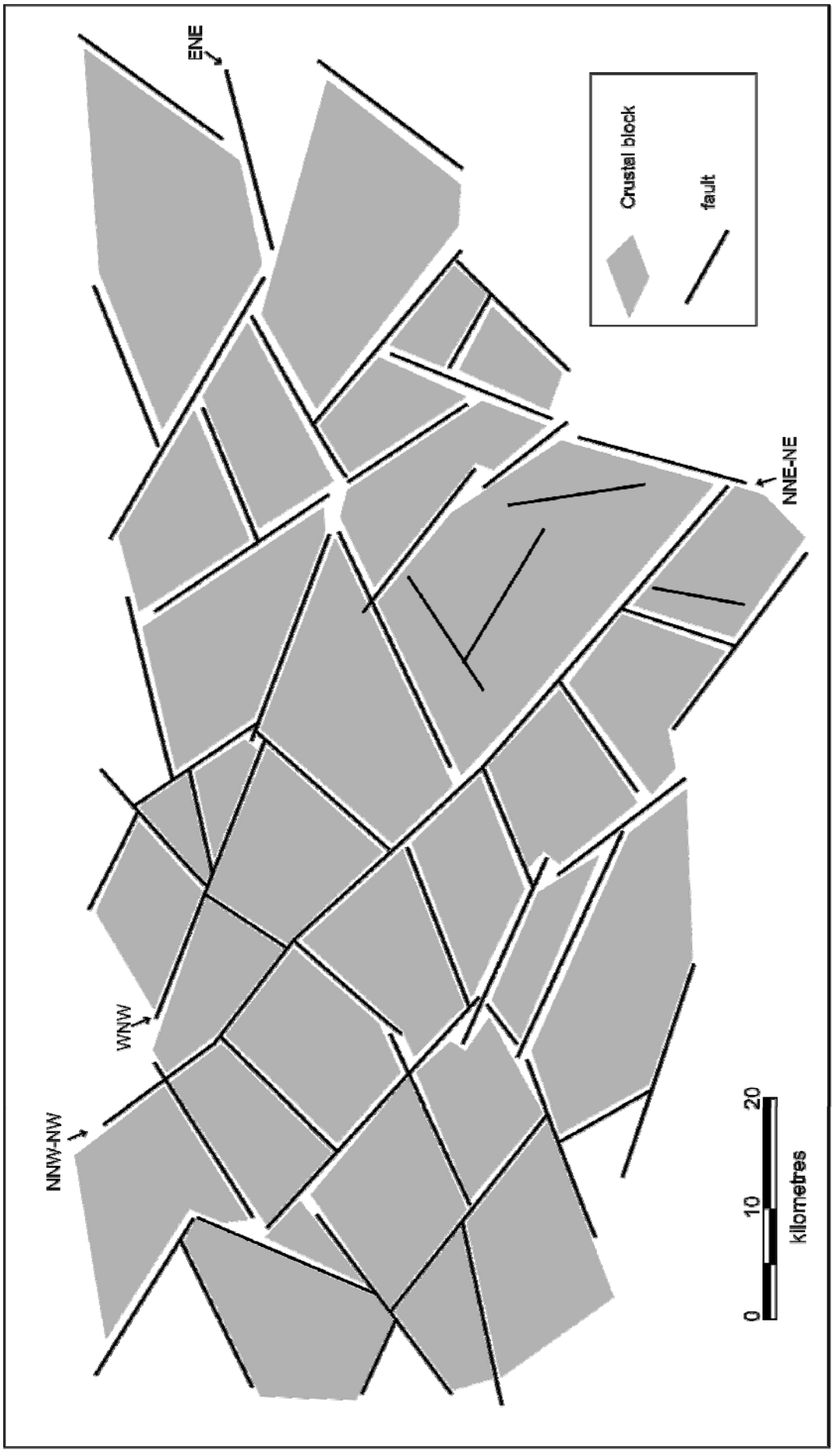

Figure 8.2: Conceptual model of structural fault mesh of southeast Viti Levu.

control on the offshore terrain of the Suva Basin that is underlain by post Late Miocene rocks. Here the fractures with these trends form narrow morpho-structural grabens along the mapped submarine canyons.

The main orientations of the mapped fractures in the structural fault mesh of southeast Viti Levu are parallel to major structural features elsewhere on the Fiji Platform (Figure 8.3):

- The ENE and WNW trends are parallel to the two main strike directions of the Wainimala oroclinal flexure, the most pronounced structural feature on Viti Levu. The Wainimala oroclinal flexure is an anticlinal belt formed in the Oligocene to Late Miocene Wainimala Group rocks, the core of which is intruded by rocks of the Colo Plutonic Suite (Chapter 2). The strike of the belt, defined by the line of the Colo stocks changes from ENE strike in eastern and south-central Viti Levu, to a WNW strike in the southwest.

- The ENE trend is parallel to faults that control the margins of the other post Late Miocene sedimentary basins in Viti Levu, such as the Nadi Basin in western Viti Levu (Hathway, 1993).

- The ENE trend is seen to control the location of Late Miocene to Mid Pliocene volcanic centres along the Viti Levu Lineament in onshore and offshore northern Viti Levu and along the Beqa-Vatulele Lineament to the south of Viti Levu.

- Three major sets of WNW trending faults subdivide Vanua Levu into large structural blocks (Gunn et al., 1998) (Figure 8.3). These fault sets cut across the strong ENE orientation of the island. The basement rocks on Vanua Levu are of Late Miocene age, and are much younger than the basement units on Viti Levu.

- The NW trend is parallel to the Lomaiviti Lineament that controls the location of Pliocene to Quaternary volcanic islands of the Lomaiviti Group. This lineament is a prominent regional structure that separates Viti Levu and Vanua Levu.

- In the northeast part of the Fiji Platform, the NE trend correlates with the strike of the Quaternary Savusavu Bay basin in southeast Vanua Levu (Roy, 1997) and the axis of

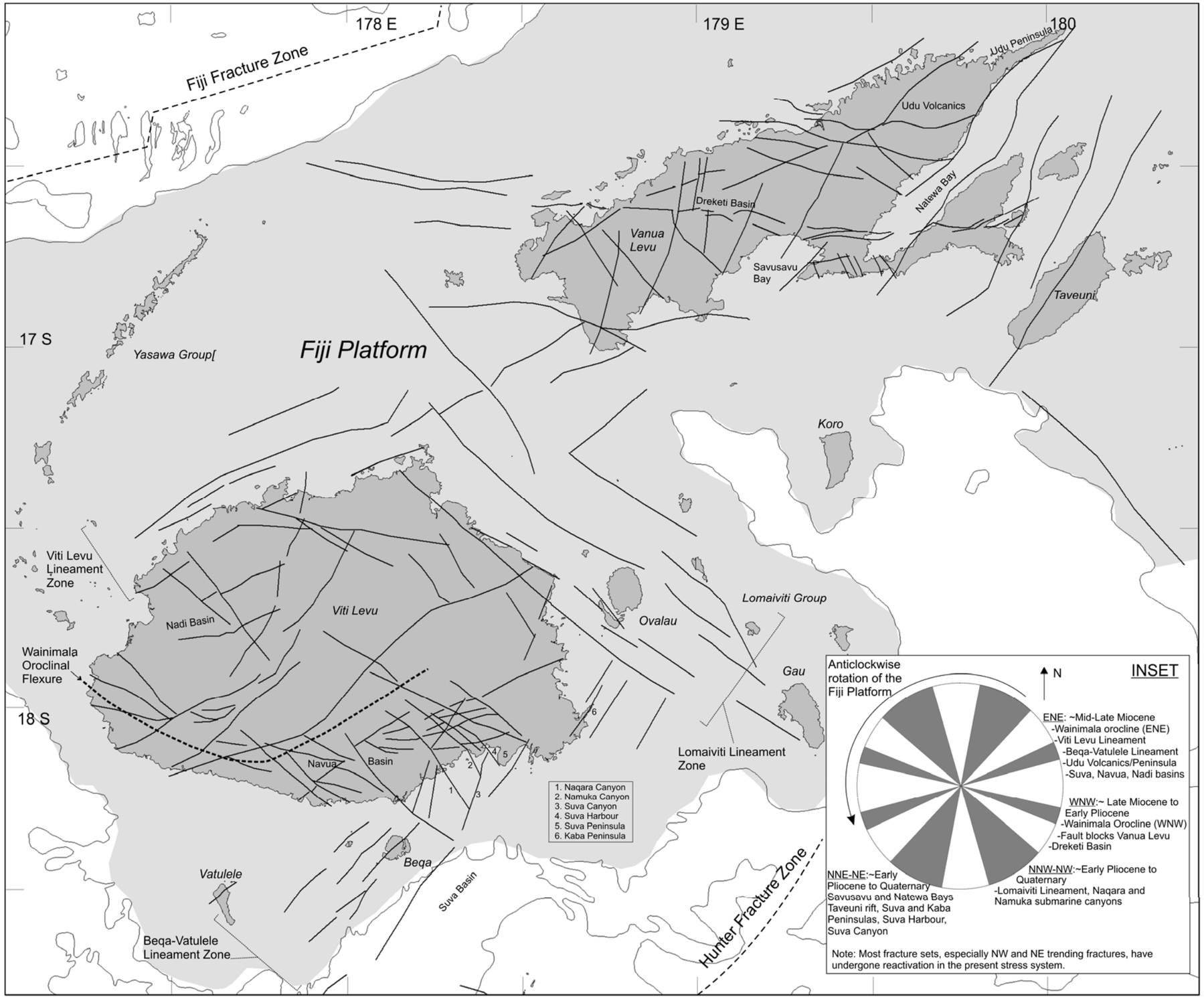

Figure 8.3: Synoptic structural lineament map of the Fiji Platform, based largely on interpretation of aeromagnetic data (after Gunn et al. 1998) and DTM lineaments on Viti Levu (see Section 9.3.2.1). Inset: A diagrammatic summary of the present orientations of structural features on the Fiji Platform and their inferred relation to anticlockwise rotation of the Fiji Platform.

Quaternary volcanism on nearby Taveuni island (Cronin et al., 2001).

The principal fracture sets in southeast Viti Levu are inferred to represent generations of regional tectonic faults, which have pervaded the Fiji Platform during and after disruption of the proto Fijian arc.

8.3 EVOLUTION OF THE STRUCTURAL FAULT MESH

It is proposed that the structural fault mesh of southeast Viti Levu has progressively evolved as the brittle deformational response to the upper Cenozoic anticlockwise tectonic rotation of the Fiji Platform. Regional paleomagnetic declinations reveal the anticlockwise rotation of the Fiji Platform about a vertical axis, apparently as a coherent mass, since the late Miocene (10 Ma), by amounts ranging as high as 75^{o} to 135^{o} (Malahoff et al., 1982b; Prichard, 1989; Inokuchi et al., 1992; Taylor et al., 2000).

The role of smaller tectonic block rotations and internal deformation during the rotation of the Fiji Platform is down-played in past paleomagnetic studies on Fiji. For example, Taylor et al. (2000) conclude that despite the large tectonic rotation of Fiji, Viti Levu has not suffered internal disruptions by strike slip faulting causing localized block rotations from 5 Ma onwards. Their conclusion is based on consistent results of paleomagnetic data from two sites in Viti Levu, one from Pliocene volcanics in northern Viti Levu and the other from Pliocene tuffs in Medruasucu Group sediments (Suva Marl) in southeast Viti Levu. They provide further evidence from younger (3 Ma) samples from Kadavu and Vanua Levu that show similar results. It is suggested here, however, that the results of Taylor et al. (2000), are not unequivocally indicative of the absence of internal deformation and accompanying block rotations within the Fiji Platform. It is possible that the two sets of consistent results are from separate structural blocks that had undergone similar amounts of rotations, accommodated by strike slip faulting. Furthermore, high dispersions in the results from another paleomagnetic study in Fiji by Prichard (1989) do not preclude the possibility of considerable internal deformation and smaller block rotations within the Fiji Platform. The work of Prichard (1989) also shows that Viti Levu has rotated at a faster rate than Vanua Levu. The degree of Neogene brittle deformation in southeast Viti Levu, as shown by the fault mesh documented in this study, suggests considerable internal deformation contemporaneous with the period of arc rotation.

Crustal block rotations about vertical axes between parallel fault sets are widely recognized in regions of strike slip tectonics (e.g. Jackson & Molnar, 1990; Luyendyk, 1991; Little & Roberts, 1997). Rotations of blocks are accommodated by displacements on block bounding faults, which themselves need to rotate. Mechanical consideration of faults require that large rotations (>45^{o}) need to be progressively accommodated by the development and rupturing of new faults across the blocks as older faults move out of optimal positions of slip (Nur et al., 1989). The amount of rotation that can be accommodated by only one set of parallel faults, under the same stress field is limited to 25^{o} to 45^{o} (Nur et al., 1989).

A simple model for accommodating block rotations within the Fiji Platform is proposed here, and is consistent with the development of the observed fault mesh pattern. In the Middle to Late Miocene, following the collision of the east-facing proto Fiji arc with oceanic plateaux (Ontong Java and Melansian Border Plateau) (Falvey, 1975), arc fragmentation and a flip of subduction polarity along the proto-Vanuatu arc segment, left the Fiji Platform isolated in the area of overlap between the diverging Tonga and Vanuatu subduction zones. Counterclockwise rotation of the Fiji Platform was initiated as a result of distributed left lateral wrenching which developed across the zone of overlap between the two subduction zones, due to the opposing plate motions to the north and south (Figure 8.4a). Assuming that the regional stress orientations in the Fiji Platform have remained constant after the Middle Miocene (e.g. Begg & Gray, 2002), an early set of faults, now ENE trending, developed presumably as N to NNE trending dextral riedel faults to accommodate the anticlockwise rotation in response to the distributed left lateral shear (Figure 8.4a). These early faults caused intense deformation within the Fiji Platform, dividing the terrain into elongate crustal block slivers. A transtensional component on these faults, as a result of widening of the overlap zone (Luyendyk, 1991) from back-arc extension would have led to development of elongate sedimentary basins within the older Oligocene to Early Miocene Wainimala terrain, throughout the Fiji Platform (Hathway, 1993; Johnson, 1994). These faults formed zones of weakness in the crust that would have also imparted structural control on the distribution of arc volcanism, with the platform still close to the two subduction zones (Gill & Whelan, 1989a). The mapped regional structural geology of southeast Viti Levu in particular, is consistent with this interpretation. Horst blocks comprising the basement (elevated) Wainimala and Colo rocks are separated by younger post late Miocene to Pliocene basins (e.g. Navua and Suva basins) and volcanic centres (e.g. Namosi, Mau, Nakobalevu and Beqa volcanoes) (see Figure 2.5b, 3.3).

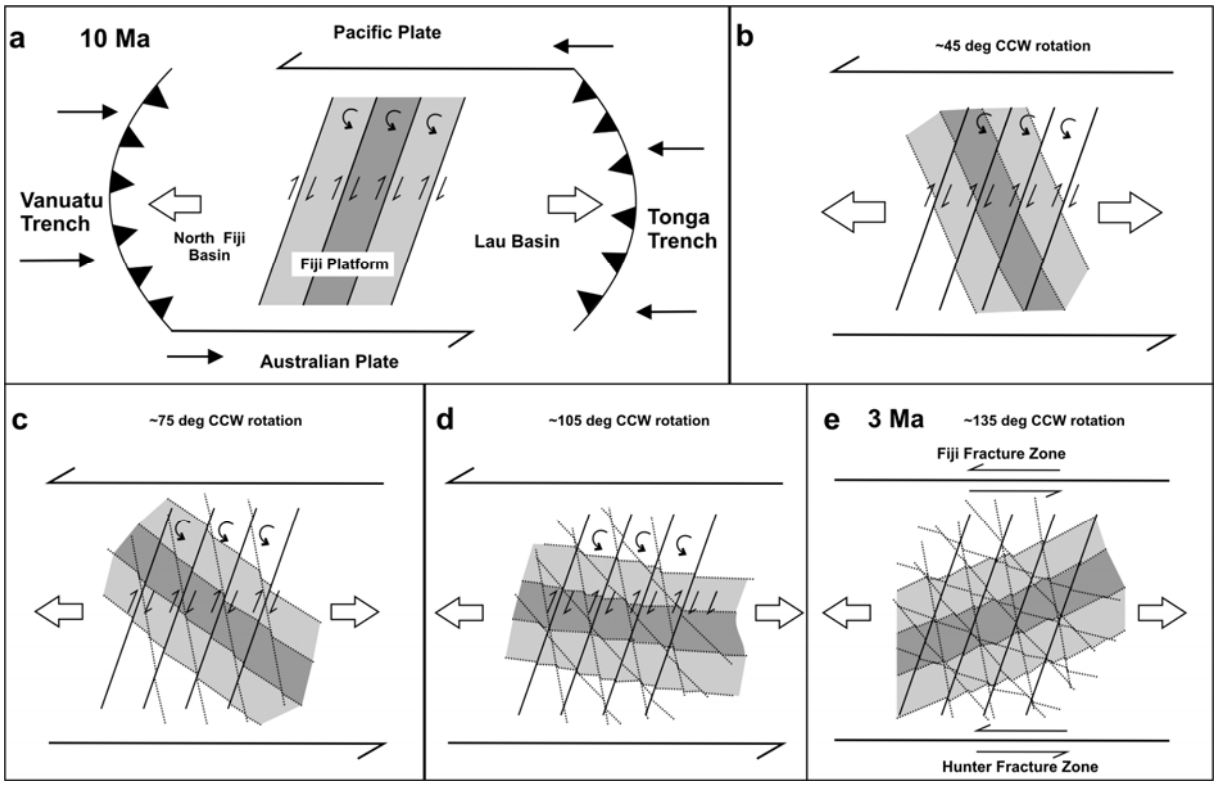

Figure 8.4: Schematic diagram showing progressive development of a complex fault mesh by fault and block rotations within the Fiji Platform in the Neogene.

With the counter-clockwise rotation of these blocks approaching close to 45^{o}, misorientation of these early faults with respect to the inferred regional stress field led to the propagation of new faults to accommodate further rotation (Figure 8.4b). These new generation faults are today represented as the WNW trending faults. As rotation progressed further, successive misorientations of older fault sets, and rupture of new optimally oriented transtensional faults after rotation intervals of 25^{o} to 30^{o} produced NW, NNW, NNE trending faults sets, that now occur as narrow morpho-structural grabens and form the later stages of fault mesh development (Figure 8.4c,d,e). The total amount of rotation recorded by these successive faults sets amounts to ~120^{o} - 135^{o}, in close agreement with the total amount of rotation of the Fiji Platform obtained from the recent paleomagnetic study (Taylor et al., 2000). The arcuate and fanning nature of some fractures are particularly evident in southwest and southeast Viti Levu, and across the length of the southern coast of Vanua Levu (Figure 8.3). These may reflect the constant readjustment of the positions of faults as block rotation took place, and fault relays evolved.

It is possible that the formation of block bounding faults may have been more complicated than represented in this simplistic model, such as through the formation of conjugate sets.

Nevertheless, as demonstrated by this evolutionary model, during the initial stages of the rotation there would have been fewer fractures on the Fiji Platform. As rotation progressed, more fractures developed on new orientations further building the fault mesh. It is possible that with the increase in the density of fractures, the deformational strain imposed on the Fiji Platform would become more distributed through the fault mesh. With the increase in distributed deformation, rupture of new block bounding faulting would become more complex and as a result the rotation of blocks more inefficient. The overall rotation of the Fiji Platform, therefore may have waned through time to the present day. It is also possible that the overall rotation could have decreased with the establishment of the Fiji Fracture Zone and the Hunter Fracture Zone as major left lateral transform faults to the north and south of the platform respectively (Figure 8.4e). These regional structures presently accommodate a large component of left lateral shear in the Fiji region. A decrease in the rotation rate of the Fiji Platform is implied by some paleomagnetic results (e.g. Prichard, 1989; Rodda, 1994).

8.4 CESSATION OF ROTATION OF THE FIJI PLATFORM?

Taylor et al. (2000) suggest that rotation of the Fiji Platform ceased abruptly at 3 Ma. They report that samples collected from Kadavu and Vanua Levu, with maximum ages of 3 Ma, do not show paleomagnetic directions different from the present direction. It is argued here that this age of cessation of rotation based on the given data cannot be applied to all parts of the Fiji Platform. Samples taken by Taylor et al. (2000) from Vanua Levu are from the Seatura Volcano of the Bua Volcanic Group in the eastern part of Vanua Levu (see Figure 2.6b). Mapping of fractures shows that the Bua Volcanic Group is part of at least three detached crustal blocks in eastern Vanua Levu. Therefore, it is possible that other parts of the Fiji Platform may still have undergone rotation after 3 Ma. For example, rocks on Viti Levu dated at 3 Ma have paleomagnetic directions that are rotated 30 degrees from the true north (Prichard, 1989), indicating significant rotations since 3 Ma. It is further argued here, that the Kadavu paleomagnetic direction of Taylor et al. (2000) is not indicative of the conditions on the Fiji Platform as a whole. Kadavu island occurs along the southeast margin of the Fiji Platform, on the Kadavu Ridge along the Hunter Facture Zone, and does not occur strictly within the Fiji Platform. Kadavu has had a tectonic history that is unique compared to the rest of the Fiji Platform, and therefore may not have undergone rotation at all. Even if it were subjected to the same rotational strain, the Kadavu Ridge may have acted as a detached crustal block separated from other parts of the Fiji Platform by fracture zones along the Beqa-

Vatulele Lineament and others similar to those mapped on the marginal slope south of Viti Levu (Chapter 5). Following on from this viewpoint, it is postulated that tectonic deformation continues to be accommodated within the Fiji Platform. This, however, occurs in a distributed manner and is accommodated through the fault mesh. It is possible that some minor localized rotations of internal crustal blocks may still be occurring as a result of strike slip faulting within this fault mesh. The role of localized structural features as identified in the present study, therefore, needs to be considered when interpreting the results of the earlier paleomagnetic data.

8.5 STRUCTURAL FAULT MESH AND THE ORIGIN OF SEISMICITY

Supporting evidence for distributed tectonic deformation through activity of the structural fault mesh is provided by seismicity data in Viti Levu. Seismicity data was recorded from the closely spaced and well-calibrated telemetered Fiji Seismograph Network between 1979 and 1994 (Jones, 1998). High-quality recordings of earthquakes on Viti Levu are mostly from the period between 1979 and 1985 (Hamburger et al., 1990), when the network comprised up to 12 seismograph stations operating on Viti Levu, Beqa and Ovalau (Figure 2, Appendix 11). The close array of seismographs in Viti Levu (less than 30 km separation) allowed for recordings of reliable epicentral locations to within 1 to 3 km and sensitive recordings of small to micro-earthquakes (M_L 4 to -1) (Hamburger et al., 1990). The accuracy of seismicity data for Viti Levu and the detailed level of work done on the mapping of faults in the onshore and offshore area of southeast Viti Levu permit the evaluation of the relationship between seismicity and present day deformation within the context of the interpreted structural fault mesh.

Seismicity is concentrated in the eastern half of Viti Levu (Viti Levu Seismic Zone), and the pattern of seismicity within this zone, from a regional perspective, appears as broadly disseminated (Figure 2.8). Closer examination of the seismicity pattern, however, reveals discrete clusters of earthquake epicentres, most of which can be correlated to fault segments that form the structural fault mesh (Figure 8.5). This correlation of earthquake clusters suggests that the active structures are short fault segments within the fault mesh. These fault segments follow a range of orientations without showing a preference for a particular trend. The correlation of earthquake clusters to mapped faults is shown in Figure 8.5 and described below:

- In the area between Viti Levu and Ovalau two linear clusters of epicentres occur along the southern continuation of the Nakorotubu Fault/Lineament Zone (Section 9.3.2.3) (part of the Lomaiviti Lineament Zone). Aeromagnetic data over the offshore area shows that these linear clusters of earthquakes occur on well-defined NW trending faults along the southern trajectories of the Nakorotubu Fault/Lineament Zone. An earthquake focal mechanism from within each of the two clusters shows a nodal plane that is NW trending (Everingham, 1983d), and is comparable with the strike of the mapped fault/lineaments.

- Along the southeast coast of Viti Levu, there are several elongate epicentral clusters that correlate to NE, NNW and NW trending faults that have been mapped spanning the onshore and offshore areas. A prominent linear cluster occurs along the NW trending Naqara Fault (Section 9.3.2.3). This cluster contains the epicentres of the damaging historical earthquakes of 1953 and 1961 (Houtz, 1962a,b). The NW trending nodal plane of the 1953 earthquake coincides with the strike of the Naqara Fault.

- Several other epicentral clusters in Viti Levu correlate closely with the mapped traces of fault/lineament zones. A broad, ENE elongated cluster extends from the middle of the island to the eastern coast, north of Ovalau. The strong historical earthquakes of 1869 (M_s ~6.0) and 1906 (M_s ~5.5) can be grouped into this cluster. This cluster occurs along the trace of the ENE trending Dawasamu Fault, the northeastern segment of the prominent Mavuvu Fault Lineament Zone (Section 9.3.2.3).

- A cluster of epicentres in the northern part of Viti Levu, between Ba and Tavua townships, occurred as a sequence of events between 1999 and 2001, with the largest event recorded measuring M_s 4.2 (Rahiman et al., 2001). This earthquake sequence occurred in an area that was previously considered aseismic. This cluster correlates with the northern end of the WNW trending faults of the Nasivi Fault/Lineament Zone (Section 9.3.2.3).

There is a cluster of very shallow earthquakes (< 4 km) in central Viti Levu that surrounds the Monasavu Dam. These are not related to tectonic activity of the fault mesh, as they are shown to be reservoir-induced seismic activity associated with water impoundment (Everingham, 1983e; Singh, 1996).

Reliable hypocentral depths of earthquakes indicate seismic activity in Viti Levu is generally confined to the top 20 km of the crust, with most activity between 7 and 13 km (Hamburger et al., 1990). The occurrence of linear clusters of earthquakes coincident with the mapped fault/lineament traces is indicative of steeply dipping faults and is in agreement with the steep dips on fault planes measured in outcrop exposures in southeast Viti Levu (Section 4.4.3). The distribution of hypocentres outlines the three dimensional geometry of the crustal fault blocks and provides constraints on the depth limits of fault mesh activity.

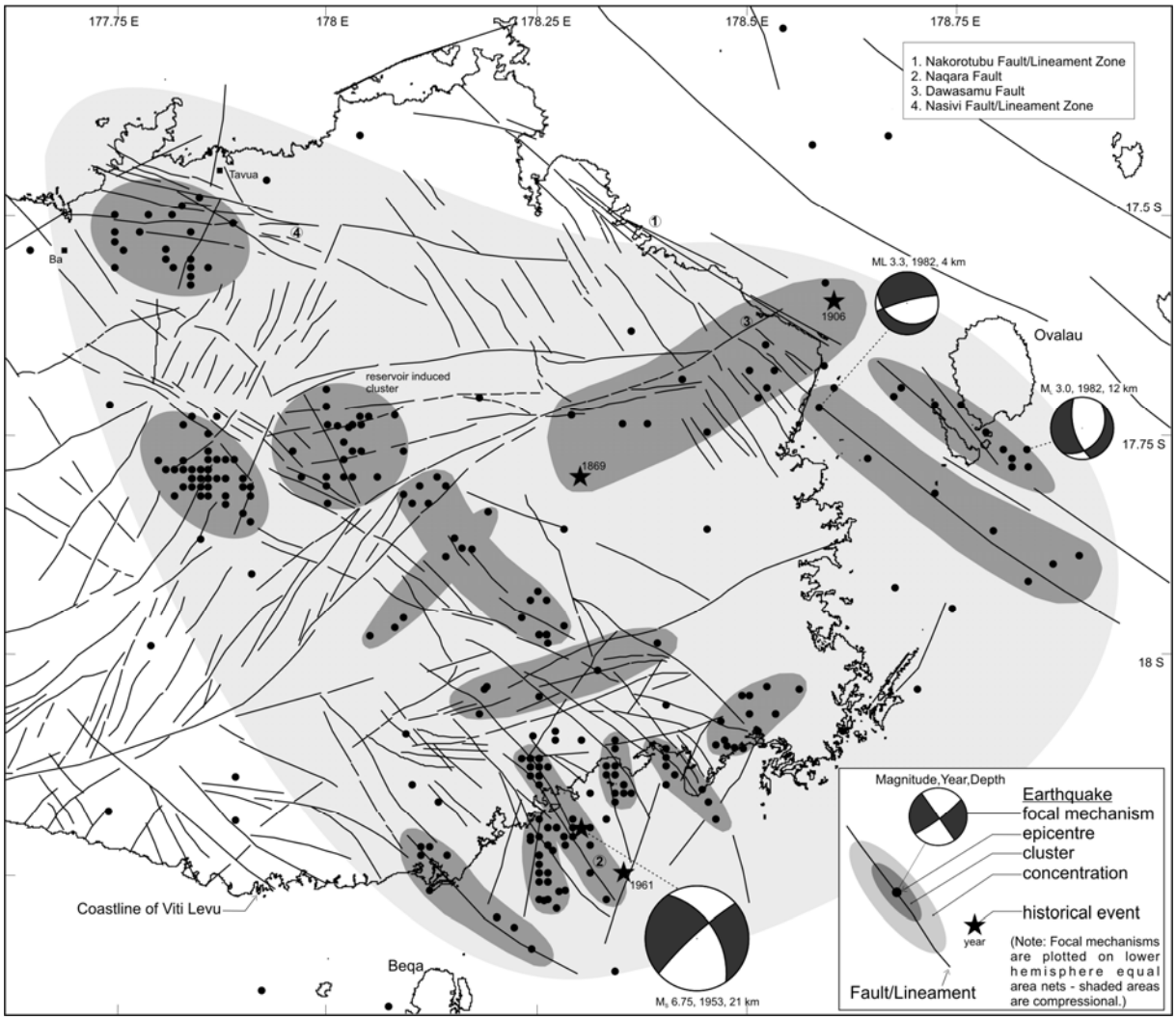

Figure 8.5: Map of eastern Viti Levu showing the geographical correlation between the location of earthquakes and the structural fault mesh model.

The seismicity data indicates the rupturing of fault segments over a range of azimuthal orientations. The activity occurring on multiple fault segments indicates that tectonic strain may be accommodated by the entire structural fault mesh in a distributed manner. The fault mesh presently functions as a network of interlocking and linked faults that accommodate this tectonic deformation. This probably occurs by a process that involves complex mesh style coseismic faulting, whereby ruptures propagate through short linking fault segments that form the fault mesh. These ruptures may occur along reactivated older linking faults, or may occur along newly created faults associated with continued rotation of some crustal blocks. Small earthquakes on linking faults may be the result of ongoing stress-driven instabilities in parts of the fault mesh which are constantly reacting to the regional stress field. It is possible that due to stress build-up in a particular part of the mesh, a set of linking fault segments, which are optimally oriented with respect to the regional stress field, will sometimes combine to rupture as a large earthquake, accommodating a larger fraction of the deformation. The following cycle of stress build-up leading to the next large earthquake may begin at some other location of the fault mesh, following the continued partial release of strain energy through lower magnitude earthquakes on linking faults of the fault mesh.

It has been suggested by Hamburger et al. (1990) that the Fiji Platform is currently deforming under the same stress field as the neighbouring North Fiji and Lau back-arc basins in which N-S contraction and E-W extension are accommodated by NE and NW strike-slip faults. The focal mechanism of the Suva 1953 event (M_s 6.75) has nodal planes that show these orientations. It is inferred that large earthquakes in Viti Levu are primarily the result of rupturing on either NW and NE trending faults, which lie in the optimum stress field orientation for slip within the fault mesh. Fault rupturing during these large earthquakes, however, may be occurring in a complex manner through the fault mesh, utilising the zones of weakness along older previously locked faults, that now lie close to favourable orientations for slip. This concept is shown diagrammatical in Figure 8.6. The results of this inferred process are the large through-going faults on the Fiji Platform that overall may show a complex sigmoidal form such as, for example, the Mavuvu Fault/Lineament zone. The complex geometry of these through-going faults may exert a topographic response in releasing and restraining bends and/or step-overs. For example, the elongate ridge of the Mt Gordon Highlands (Band, 1968) may be due to a restraining bend in between the Mavuvu Fault/Lineament Zone and the Sovi Fault, both inferred to be sinistral strike-slip faults (see Section 9.3.2.3 and Map 3).

The complex mesh style coseismic faulting postulated for southeast Viti Levu is consistent with the historically low occurrence of large earthquakes. Numerous small to moderate magnitudes earthquakes (M 3 to 4) have been recorded in this zone over the last 25 years by the Fiji Seismograph Network. However, only one earthquake with magnitude >M6 has been reported in the last 150 years within this zone (Everingham, 1983a; Everingham, 1988). Due to the complex interactions between faults, the fault mesh is rarely able to sustain rupture along a single fault of sufficient length to produce large earthquake magnitudes (>M7). There are no clear indications of large, late Holocene surface ruptures along any of the onshore or offshore faults. This observation is consistent with the prediction of complex spatial and temporal rupture propagation through the fault mesh in which coseismic surface displacements are likely to be limited, due to near surface partitioning of the fault slip through the mesh.

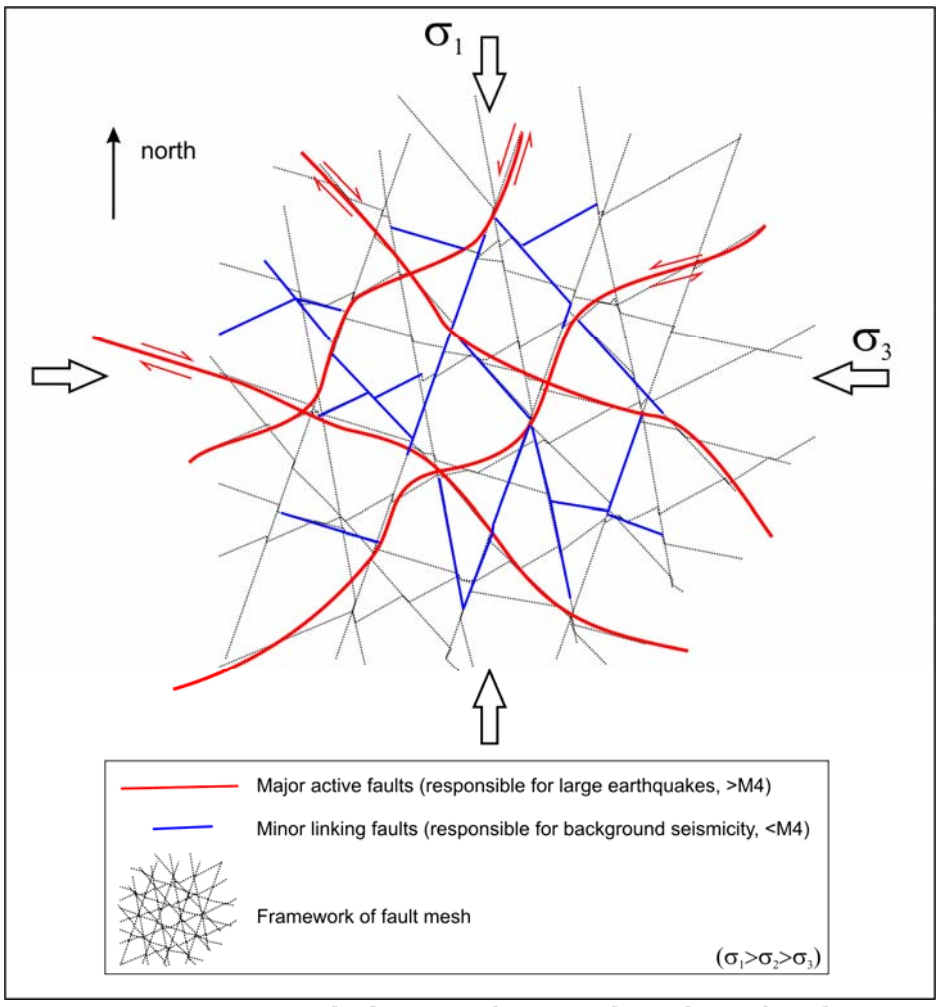

Figure 8.6: Conceptual diagram showing the relationship between seismicity (both large and small earthquakes), and active linking fault segments and major through-going faults within the structural fault mesh.

8.6 SEISMOTECTONICS OF THE FIJI PLATFORM

It is inferred that the seismotectonic model proposed for southeast Viti Levu is applicable to the entire Fiji Platform. The principal fracture orientations as seen in southeast Viti Levu are also recognised in other parts of the Fiji Platform especially on Vanua Levu (see Figure 8.3). The structure of large offshore areas of the Fiji Platform, however, remains unknown. The geometry of regional scale faults mapped in other parts of the Fiji Platform may reflect, on a more local scale, internal structural breaks quite similar to the fault mesh mapped in southeast Viti Levu and may similarly control the seismicity in those areas.

It remains unclear at this stage why earthquakes occur in only two areas of the Fiji Platform, that is, eastern Viti Levu and northeast Vanua Levu (Figure 2.8). This distribution, however, may be a reflection of the short period of available recordings of instrumental seismicity data. The longer-term seismicity distribution is inferred to be more widespread throughout the Fiji Platform. Large historical events, such as the Koro earthquake of 1932, have occurred well outside these two main areas of concentrated seismicity. A recent series of earthquakes between 1999 and 2002, in northern Viti Levu, occurred in an area of no known previous seismic activity.

It is possible that the two areas of seismicity within the Fiji Platform represent the presently active zones of the fault mesh accommodating deformation within the Fiji Platform. These areas probably represent zones of weakness that may be presently localising deformation within the Fiji Platform fault mesh. Possible changes in the geometry of the active fault mesh, due to continued internal deformation, may lead to a shift in the position of the accommodation zone. It is inferred that the spatial and temporal distribution of seismicity within the Fiji Platform varies as the fault mesh reacts to the tectonic stress field by continually shifting the locus of the deformation zone to other parts of the Fiji Platform. Based on this interpretation, earthquakes are expected to occur anywhere within the Fiji Platform. Eastern Viti Levu and northeast Vanua Levu, however, continue to largely remain the presently active areas.

The seismotectonic model proposed here is an attempt to address the origin and distribution of seismicity within the Fiji Platform. As in other parts of the world, the cause of seismicity in areas distal from well defined tectonic plate boundary zones is a question that cannot be

answered unequivocally. The structural fault mesh model and the explanation provided for its control on the characteristics of seismicity within the Fiji Platform are presented here as a hypothesis to be more thoroughly tested as new seismicity data, GPS/geodetic data and structural data on faults within the Fiji Platform become available in the future.

8.7 SUMMARY AND CONCLUSIONS

Fault lineaments mapped in the onshore and offshore area of southeast Viti Levu are used to define a structural model of Neogene brittle deformation, the context of which is then used to interpret the seismicity of the area and the sesimotectonics of the entire Fiji Platform. The principal sets of fault/lineaments mapped on remotely sensed images, bathymetric and seismic reflection data, and verified with field mapped structures, follow the orientations of NNW-NW, NNE-NE, WNW and ENE. These fracture sets combine to form a complex fault mesh, which divides the upper crust of southeast Viti Levu into a number of crustal blocks ranging from ~2 to 30 km wide.

The structural fault mesh is a composite feature that is the product of the superposition of several generations of faults that pervaded the Fiji Platform during and after disruption of the proto Fijian arc. The ENE and WNW faults correlate to the earliest sets of larger scale structural features on the Fiji Platform, while the NNW-NW and NNE to NE faults are younger fault sets that are associated with more recently formed (Pliocene-Quaternary) structural features that have clearer geomorphic expressions. It is interpreted that the fault mesh formed as a result of progressive tectonic deformation of the Fiji Platform, during the Neogene, by distributed faulting and associated crustal block rotations.

The fault mesh is used to explain the origin of seismicity in southeast Viti Levu, including both large earthquakes (>M4) and low magnitude earthquakes (<M4). The correlation of seismicity data to short fault segments of the structural fault mesh suggests that regional tectonic deformation is presently being accommodated in a distributed manner within the entire fault mesh. This may be occurring by a process that involves complex coseismic faulting throughout the mesh. Ongoing tectonic deformation is expressed by low magnitude earthquakes, probably following ruptures on short linking faults, and larger earthquakes when several linking faults combine at optimum stress field orientations forming longer ruptures in a complex manner. Low occurrence of large earthquakes and the diffused pattern of

seismicity currently observed in southeast Viti Levu reflect a complex mesh-style coseismic faulting. Distributed deformation through the structural fault mesh in southeast Viti Levu is inferred to be characteristic of the type of deformation that occurs within the entire Fiji Platform.

CHAPTER 9

SEISMIC HAZARD EVALUATION

9.1 INTRODUCTION

Newly identified crustal faults representing earthquake source structures are used to evaluate the seismic hazard on Viti Levu in order to improve the understanding of the hazard and to facilitate the reduction of impact on communities and critical facilities at risk. Along the southeast coast of Viti Levu, Suva City and the towns of Nausori and Navua are major population centres, and where important infrastructures are located (see Chapter 3). The Monsavu hydroelectric dam, in central Viti Levu, is considered to be the single most vulnerable structure on Viti Levu in terms of earthquake risk. This 82 m high earthfill dam, with lake capacity of 133 million cubic metres and power capacity of 80 MW supplies 70% of the country's electricity. The Qaliwana area, 15 km NW of the Monasavu Dam, is the site being developed for the new 45-55 MW Nadarivatu hydroelectric dam. These critical structures, as well as the population centres along the southeast coast of Viti Levu are vulnerable to the effects of damaging earthquakes from the various seismic source zones located in the Fiji region. Of particular relevance in this study is a region of high seismicity that covers the southeast and central sectors of Viti Levu.

Past regional seismic hazard studies in Fiji have relied solely on available instrumental seismicity data and historical records of earthquakes (Everingham, 1983b, 1986; Singh, 1996; Jones, 1998; Shorten et al., 2001). A summary of past seismic hazard analyses in Fiji is given in Appendix 11. One of the limitations of using this data uniquely is that historical and instrumental records of seismicity are incomplete with respect to much longer repeat times of large earthquakes on major faults. The recurrence period of major earthquakes within the Fiji Platform are inferred to be hundreds or even thousands of years (Hamburger & Everingham, 1986). Furthermore, the absence of instrumental or historical seismicity data in a particular area is not an assurance that the area has not been subject to earthquakes in the past or that it will not be subject to earthquakes in future. Indications are that significant historical events in the past 150 years in Fiji have occurred in areas that have been classified as aseismic by instrumental data (Hamburger & Everingham, 1986). Recent swarms of earthquake activity

have occurred in places that were not known to be seismically active from instrumental records a few decades before. Based on the proposed model of tectonic deformation of the Fiji Platform (Chapter 8), which indicates that deformation may be distributed throughout the platform, it is possible that a large earthquake could occur anywhere on the Fiji platform in the future. Therefore, it is imperative to identify and consider all seismic source structures on the Fiji Platform capable of generating large earthquakes in seismic hazard evaluations in Fiji.

It is assumed that the predominant form of earthquake source structures in Fiji are faults. Detailed work on faults as potential earthquake source structures in Fiji is very rare. Faults are incompletely mapped on geological maps (see Chapter 4) and their potential for generating large earthquakes is unknown. Factors that hinder the identification of active faults are continuous and dense vegetation cover and probably high erosion and deposition rates compared to fault slip rates. The absence of data on surface rupturing during recent earthquakes, probably because of deep hypocentres, incompetent overburden, offshore location, or slip partitioning through fault mesh (Section 8.5), contributes to deficiency in knowledge of earthquake source characteristics. Until the present study, there was no data available on the number or the activity of faults, as well as the application of appropriate fault parameters in seismic hazard evaluations in Fiji. As shown in the approach in Chapter 4, the use of lineaments mapped from remotely sensed imagery can be used effectively to delineate faults in southeast Viti Levu. The offshore continuation of onshore faults is clearly defined by work on offshore morpho-structure presented in Chapter 5 and is essential for a complete assessment of the seismic hazard of a coastal setting like southeast Viti Levu. The combined work has allowed for the recognition of a number of potential onshore-offshore earthquake sources in southeast Viti Levu.

This chapter presents the results of a study aimed primarily at improving seismic hazard evaluations in Viti Levu by identifying and attempting to characterize the major onshore and offshore earthquake source structures within and surrounding Viti Levu. A secondary aim is to carry out a comprehensive deterministic seismic hazard analysis using the earthquakes sources identified as capable of generating large ground motions at five sites of interest, including the populations centres of Suva, Nausori and Navua, as well as the Monasavu and the Nadarivatu dam sites. The results of this study are compared with probabilistic seismic hazard studies carried out in the past to check the probability of occurrence of the deterministic events.

Specifically, the objectives addressed in this chapter are:

- to identify principal seismotectonic features 500 km around Viti Levu;
- to prepare a high resolution Digital Terrain Model (DTM) for Viti Levu;
- to prepare a comprehensive fault/lineament map for Viti Levu using published mapped fault data, new fault mapping data and major DTM lineaments;
- to combine the onshore fault/lineament data with offshore fault/lineament data from southeast Viti Levu
- to compile and tabulate all available existing information on onshore and offshore faults in Viti Levu;
- to classify activity of faults using seismicity distribution and existing information on activity of faults in Viti Levu;
- to estimate maximum magnitude earthquakes of active faults and calculate their minimum distances to the site of interest;
- to provide a quantitative estimation of ground motion at the five sites of interest: Suva City, Nausori and Navua Towns; the Monasavu Dam and the Nadarivatu dam site, using recently updated attenuation relationships and a deterministic approach.

9.2 METHODOLOGY

One of the principal goals of a seismic hazard analysis is to produce quantitative estimates of earthquake shaking at a particular site in such a way that it can be considered in the engineering design of structures. The hazard can be quantified using a deterministic or a probabilistic approach. The deterministic method involves evaluating and quantifying seismic hazards based on the development of earthquake scenarios. The scenarios assume the occurrence of the largest single earthquake event of known magnitude that appears conceivable on each fault recognised in the region, regarded as the maximum credible earthquake (MCE). The effects of MCEs are compared by calculating ground motions at the site of interest using attenuation relations and the source to site distances. The controlling MCE earthquake or earthquakes (CMCE) are those that produce the worst-case or most severe ground motions and are selected as the design earthquake. This method is time invariant and does not provide the likelihood of the event occurring over a finite period of time. The

probabilistic method on the other hand, considers all possible earthquakes that are capable of affecting the site of interest by using all combinations of magnitudes and distances possible. It also takes into account the likelihood of occurrence of different magnitudes of earthquakes by using the frequency magnitude relationship to develop a seismicity model. It produces an estimate of the probability of exceedance of specified levels of earthquake ground motions at the site of interest within reference time intervals. The design values of motion are selected as those that have the specified design probability of exceedance. Uncertainties in the rate of occurrence of earthquakes, the size and location of earthquakes and the variability they produce in site-specific ground motions are also quantitatively evaluated in this approach. Useful reviews of probabilistic and deterministic methods are given in (Cornell, 1968; Reiter, 1990; Krinitzsky, 1995; Kramer, 1996; McGuire, 2001; Bommer, 2002; Mualchin, 2005).

This seismic hazard study is based on fault specific hazard characterisation, an approach that has not been used in Fiji before. There are not enough seismicity data available yet on individual faults for fault specific frequency magnitude relationships to be determined. Moreover, fault slips rates, recurrence intervals, displacement per event data are not yet known for many faults and therefore data on characteristic earthquakes (Schwartz et al., 1984) are not sufficient for combining with instrumental records in order to develop better recurrence models and provide recurrence rates for use in a probabilistic study. Large earthquakes have occurred in southeast Viti Levu, but they are infrequent. Data on recurrence rates of large damaging earthquakes in this region are almost non-existent, and this is a significant deficiency for a probabilistic approach. The deterministic method remains the most viable considering the availability of data from this region at present. This method was used to evaluate the seismic hazard in four main steps as shown in Figure 9.1. The results of this study are compared with the results of probabilistic analyses done in the past and is discussed in Section 9.5.4.

9.3 SEISMIC SOURCE CHARACTERISATION

The first step in any form of seismic hazard analysis is the identification and characterisation of earthquake sources. All possible sources of earthquakes must be identified and their potential for generating strong ground motions at the site concerned must be evaluated. These sources can be seismotectonic source zones or specific earthquake source structures (faults)

activated by tectonic processes. The principal seismotectonic source zones are first identified and evaluated for the Fiji region.

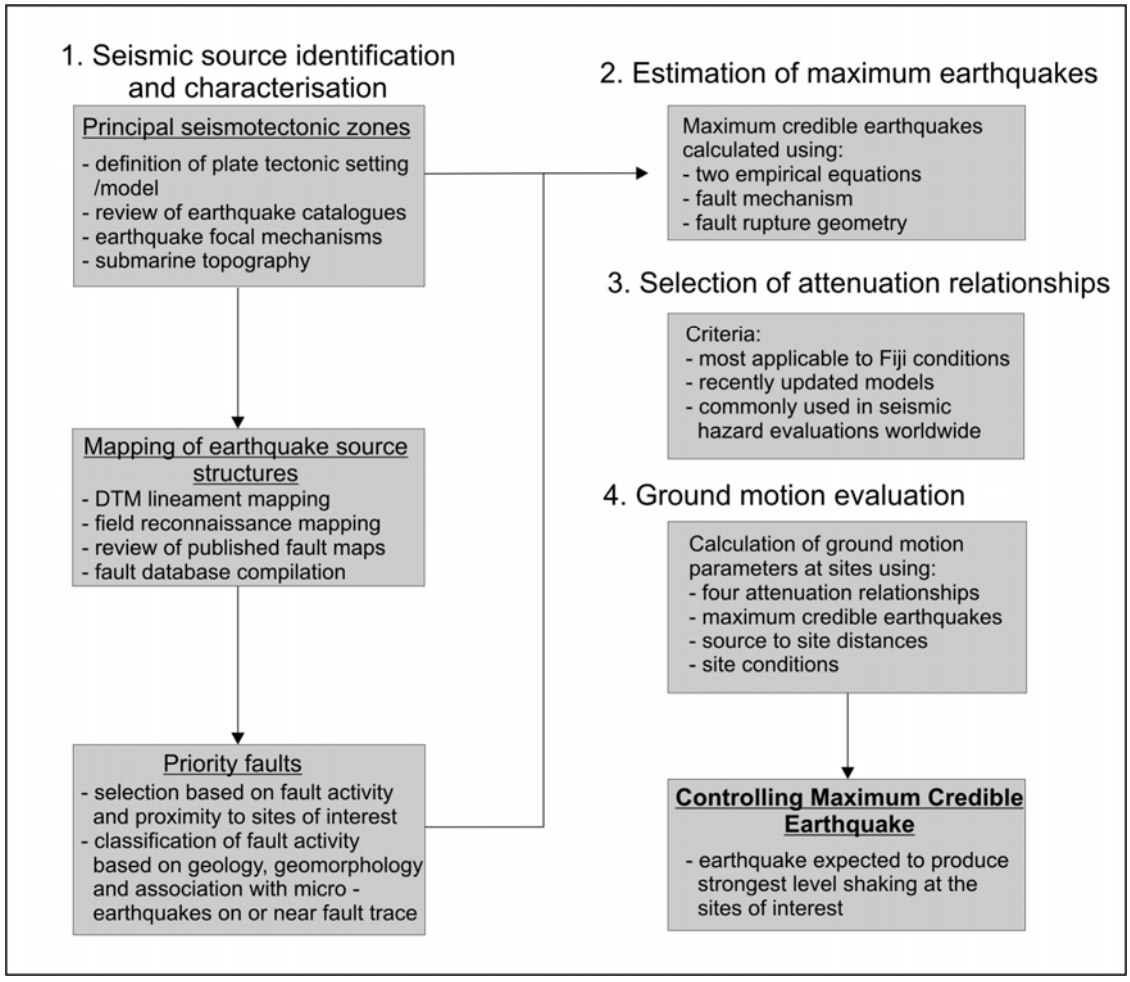

Figure 9.1: Flow chart showing the main steps of the deterministic seismic hazard evaluation approach used in this study.

9.3.1 Principal Seismotectonic Source Zones

Several seismic source zones in the Fiji region have been defined in previous studies (see Appendix 11). In the present study, updated seismicity data, as well as focal mechanisms and submarine topography, and the newly proposed tectonic model of the Fiji Platform (Chapter 8) are used to define five principal seismotectonic source zones within 500 km of Viti Levu Figure 9.2. The principal seismotectonic source zones identified in this study are: 1) Fiji Fracture Zone; 2) West Viti Levu Seismic Zone; 3) Peggy Ridge Seismic Zone; 4) Kadavu/Hunter Fracture Zone; and 5) the Fiji Platform. The main characteristics of these source zones are summarised in Table 9.1 and described in the following section. The focal mechanisms of earthquakes recorded within these zones over the last 50 years are shown in

Figure 9.3. These zones are generally similar to those identified in previous studies, however, the boundaries have been revised to reflect the present state of understanding of the tectonic setting. Having Viti Levu as the primary site of interest in this evaluation is another factor that has influenced the selection of the source zones. Four of the zones established in this study are associated with fracture zones/spreading ridges at the margins of the Fiji Platform, while the fifth represents a diffuse source zone within the Fiji Platform itself.

A deep seismic source zone to the east of Fiji is represented by intermediate and deep earthquakes along the dipping subduction interface of the Pacific plate at the Tonga trench. The deepest earthquakes at the western end of this source zone occur directly beneath the eastern parts of Fiji at depths of 550 to 700 km (Sykes et al., 1969; Hamburger & Isacks, 1987; Giardini, 1988). Deep earthquakes are quite common in the Fiji region, but because of their depth, are considered insignificant in terms of their contribution to the seismic hazard in Fiji. Large events from this zone with magnitude > 7.0 and depth > 500 km produce felt intensities of no more than MMII-III in Viti Levu. This deep earthquake source zone is not covered any further in this study. All further discussions about seismicity are restricted to shallow earthquake sources (< 80 km depth).

9.3.1.1 FIJI FRACTURE ZONE (SOURCE ZONE 1)

The ENE trending Fiji Fracture Zone (FFZ), also known as the Fiji Transform Fault, is the most seismically active area in the Fiji region (Figure 9.2). It is a broad belt of seismicity coinciding with a series of en-echelon submarine ridges and troughs along the northern margin of the Fiji Platform. The entire fracture zone extends for over 1500 km westward from the northern end of the Tonga Trench, in the northern Lau Basin, to the central spreading centre in the North Fiji Basin, where it forms one arm of the North Fiji Basin triple junction (Ridge-Ridge-Fault) (Hughes Clarke et al., 1993; Jarvis et al., 1994; Pelletier et al., 2001). Earthquake focal mechanisms show an overall left-lateral movement on the structure (Eguchi, 1984; Hamburger et al., 1990) (Figure 9.3). North of the FFZ, the Pacific Plate currently moves westward at a rate of 8.5 cm per year relative to the Australian plate (Pelletier et al., 2001).

The FFZ is segmented by a series of extensional and contractional relays (Hughes Clarke et

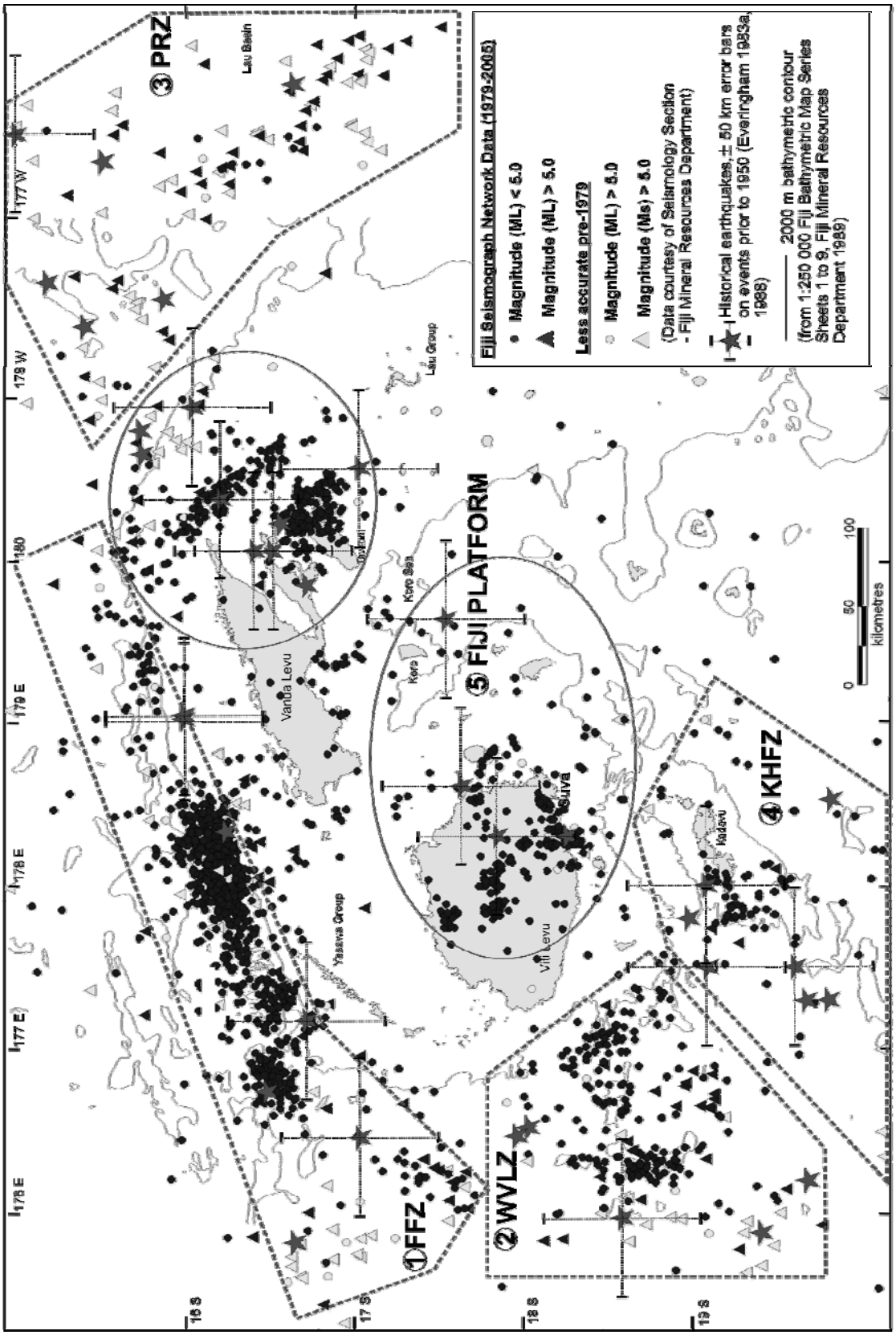

Figure 9.2: Five principal seismotectonic source zones in the Fiji region: 1) Fiji Fracture Zone (FFZ); 2) West Viti Levu Zone (WVLZ); 3) Peggy Ridge Zone (PRZ); 4) Kadavu/Hunter Fracture Zone (KHFZ) and 5) Fiji Platform, delineated by shallow seismicity (> 80 km depth) and bathymetry.

Table 9.1: Summary of principal earthquake source zones

Seismotectonic Feature		Type	Instrumental Seismicity (1979 to 2005)	Largest historical event	Distance to Suva	Distance to Central Viti Levu	Felt Intensity in Viti Levu from large events in this zone*
Fiji Platform Margins	1.Fiji Fracture Zone	ENE sinistral transform fault	continuously active, max recorded ML 5.9	MS 7.0? (1881)[2]	200 km	175 km	MMVI(1902)[2] MMV(1921)[2] MMIV(1956)[3] MMIV(1957)[3]
	2.West Viti Levu Zone	? Rift Zone ? NW dextral transform fault	continuously active, max recorded M_L 5.7	MS 6.6 (1954)[1]	150 km	130 km	No felt records
	3.Peggy Ridge Zone	NW dextral transform fault	max recorded M_S 6.5	M_S 7.0 (1943)[1]	450 km	470 km	No felt records
	4.Kadavu/Hunter Fracture Zone	Hybrid NE sinistral transform fault/ subduction system	clusters of activity, max recorded M_L 5.3	MS 6.6 (1963)[3]	130 km	160 km	MMIV(1918)[2] MMIII(1935)[2] MMIV(1950)[3]
4.Fiji Platform	Central (Viti Levu-Ovalau)	NW (and NE?) transform faults	clusters of activity, max recorded ML 4.3	MS 6.75 (1953)[4]	within 100 km	within 100 km	MMVII(1869)[2] MMV(1906)[2] MMIV(1932)[2] MMX(1953)[5] MMV(1961)[3] MMV(1975)[3]
	NE (Taveuni)	NE (and NW?) transform faults	clusters of activity, max recorded MS 6.9	MS 7.1 (1949)[1]	250 km	260 km	MMIII(1919)[2] MMIII(1928)[2] MMII(1979)[3]
Deep source zone	Tonga Subduction Zone	Thrust?	M_w 7.5 (USGS)	~	500 to 700 km depth		MII-III

References: [1]Everingham (1983b), [2]Everingham (1983a), [3]Everingham (1988), [4]Houtz (1962a), [5]SPDRP(2002)
* Based on Modified Mercalli Intensity scale (see Appendix 4)

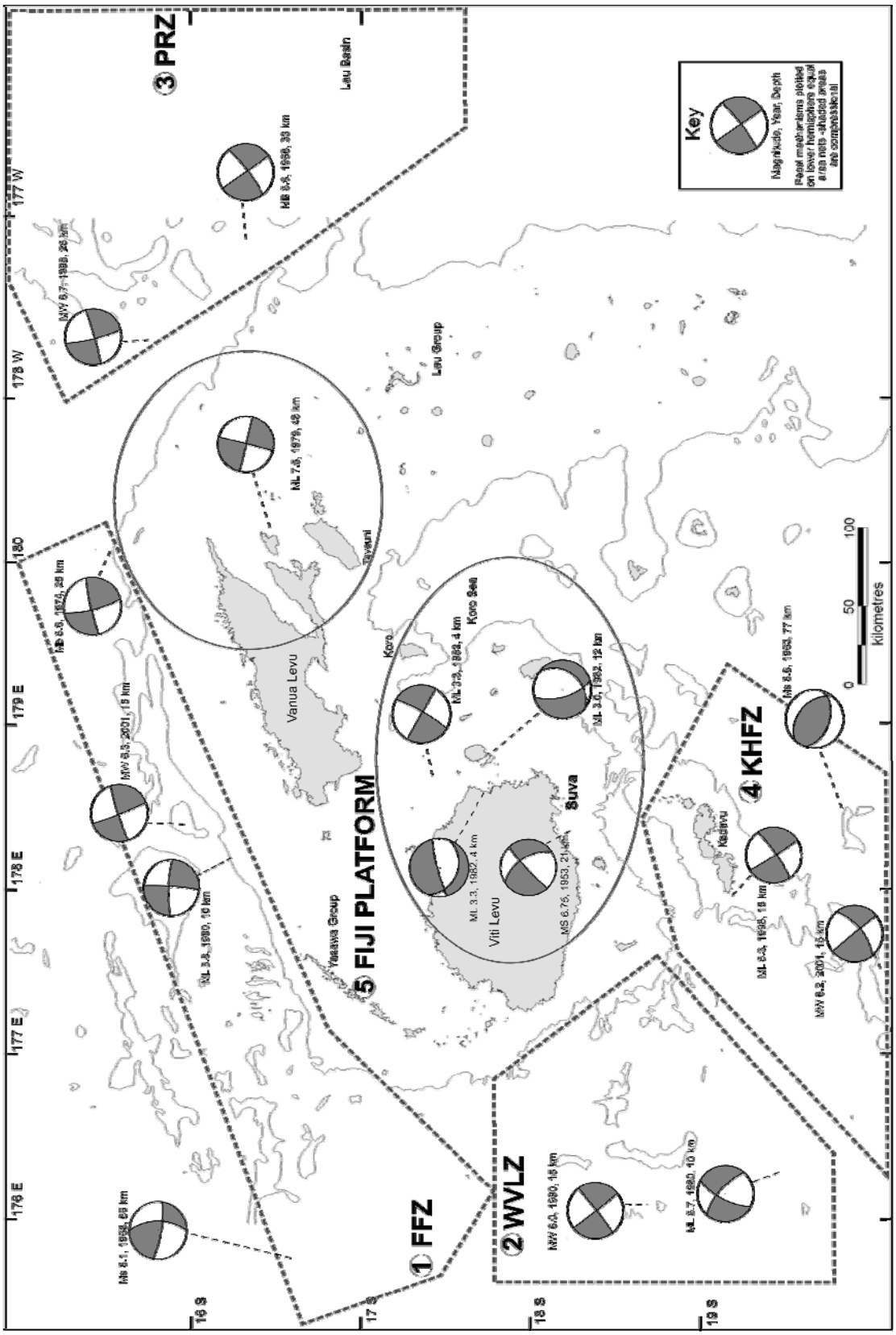

Figure 9.3: Focal mechanism solutions of large earthquakes in the principal seismotectonic source zones. Focal mechanisms are adopted from Sykes et al. (1969), Isacks et al. (1969), Johnson & Molnar (1972), Everingham (1983d), Eguchi (1984), Hamburger et al. (1990) and the National Earthquake Information Centre, USGS.

al., 1993; Johnson, 1994; Pelletier et al., 2001). Presently, the most seismically active segment of the FFZ is located in the area known on bathymetric maps as the Yadau Trough (Figure 9.4). The Yadau Trough is an ENE trending elongated basin with maximum bathymetric depth of ~4000 m. The length of this active segment, estimated from the length of the Yadau Trough is approximately 100 km. It lies approximately 200 km directly north of Suva. Historical seismicity data indicates that this segment of the FFZ has been continuously active over the last 150 years. The other segments of the FFZ to the east and west, show comparatively lower levels of recent seismicity. Historical records however, indicate that the quieter segments have experienced significant earthquakes in the past (pre-1979) (Everingham, 1983a; Everingham, 1988). Large historical earthquakes along the eastern segment of FFZ, along the Sau Sau Ridge, occurred in 1881 and 1884 (M_s ~6.8-7.0). The western segment, approximately 120 km in length, occurs along the Yasawa Trough, where historical events occurred in 1921 (M_s ~6.7) and 1968 (M_s ~6.1). In the presently active segment, moderate to large historical events occurred in 1902 (M_s ~6.8), 1956 (M_s ~6.0) and 1957 (M_s ~6.5). More recently, two significant earthquake sequences occurred in the active segment in 1980 and 1984, with main shocks measuring M_L 5.8 and 5.9 respectively (Hamburger et al., 1990). The maximum felt intensities in Viti Levu from large events in this source zone have been in the range MMIV-VI.

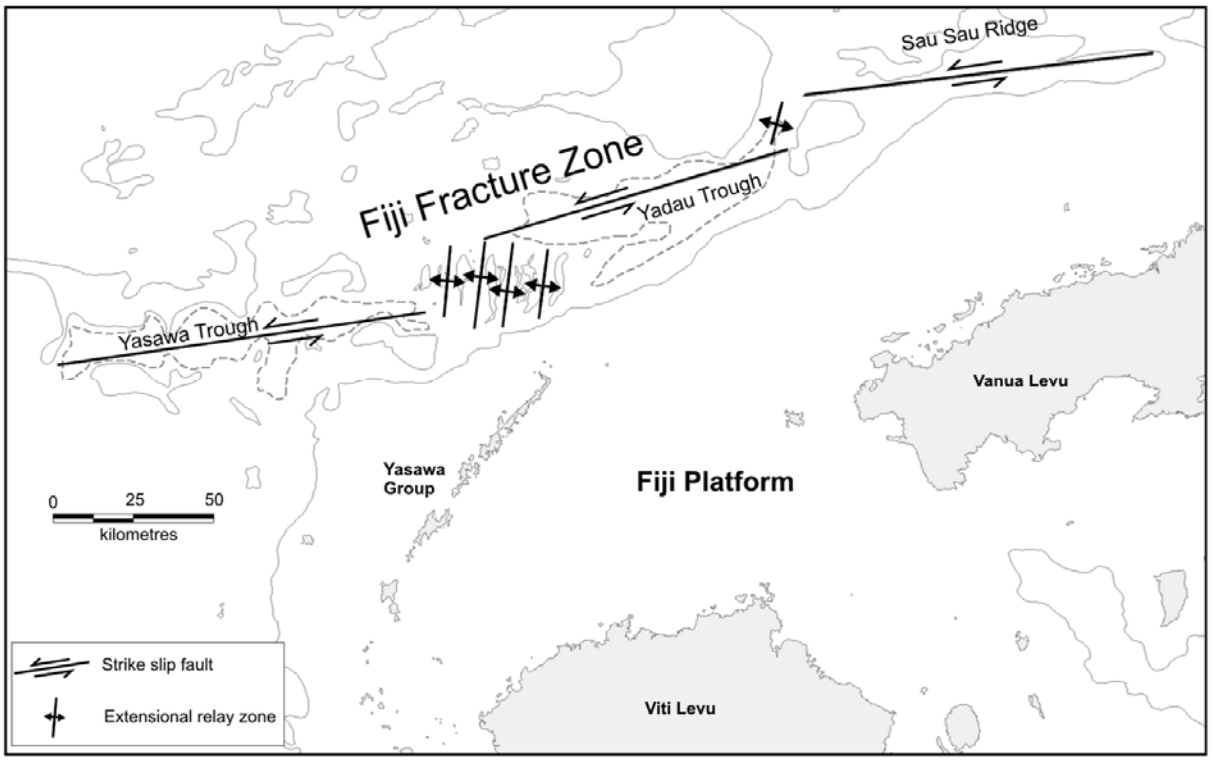

Figure 9.4: The main segments of the Fiji Fracture Zone close to the Fiji Platform.

9.3.1.2 WEST VITI LEVU ZONE (SOURCE ZONE 2)

The West Viti Levu source zone is an area of ongoing active earth deformation in the North Fiji Basin to the west of Viti Levu, and 150 km west of the Suva. Two clusters of earthquakes representing two separate seismogenic structures are recognised within this source zone. The cluster to the west coincides with the West Fiji Ridge (WFR), which represents the eastern, north-south elongated spreading centre of the North Fiji Basin. The WFR spreading centre is currently propagating southward (Brocher & Holmes, 1985; Auzende et al., 1994; Auzende et al., 1995). The axis of the spreading centre is offset by a series of NW trending transform faults (Brocher & Holmes, 1985). The cluster of seismic activity, located to the east of the ridge, originates from activity along an active NW trending transform fault (Brocher & Holmes, 1985). This transform structure controls the southwestern edge of the Baravi Basin and is delineated by the 2000 m isobath. Based on the distribution of seismicity, the maximum length of the WFR is ~200 km, and that of the transform fault is 130 km. Historical records indicate that seismicity in this area is represented by continuous activity. An earthquake sequence in 1980 was associated with M_L 5.7 main event. Earthquake focal mechanisms define a horizontal east-west tension axis and represent either a NE sinistral or a NW dextral strike slip fault (Figure 9.3). This zone has also been the source of strong historical earthquakes (M_s 6.0-6.6) experienced in 1934, 1953, 1954 and 1963 (Everingham, 1983a; Everingham, 1988). There are no records of felt intensities in Viti Levu from large events on this source zone.

9.3.1.3 PEGGY RIDGE ZONE (SOURCE ZONE 3)

The Peggy Ridge Zone is defined as a possible seismic source zone in the far northeast of Fiji in an area outside the northeast boundary of the Fiji Platform and at the northwest end of the Lau Basin (Figure 9.2). The boundary of the Fiji Platform is defined here by the 2000 m bathymetric contour. This source area is differentiated from the active area at the eastern end of the FFZ (Section 9.3.1.1) and the active area well inside the Fiji Platform in the northeast of Vanua Levu (Section 9.3.1.4, NE Fiji Platform). The Peggy Ridge Zone probably represents a complex zone of NW trending dextral strike-slip faults sub-parallel to the Peggy Ridge in the Lau Basin (Eguchi, 1984; Hamburger & Everingham, 1986; Hughes Clarke et al., 1993) (Figure 9.3).

The Peggy Ridge Zone contains a dispersed NW trending belt of earthquakes and appears to have been continuously active over the last 150 years. Twenty large earthquakes have been recorded in this zone between 1923 and 1993 with magnitudes M_s 6.0-7.0. Some large historical earthquakes have occurred close to the northeast margin of the Fiji Platform and because of uncertainties inherent in the locations of these events, it is unclear whether they originated from the inside the Fiji Platform or from the Peggy Ridge Zone. The Peggy Ridge Zone is 450 km northeast of Suva. There are no records of felt effects in Viti Levu from large events in this zone.

9.3.1.4 KADAVU/HUNTER FRACTURE ZONE (SOURCE ZONE 4)

A cluster of seismic activity occurs to the southwest of the Fiji Platform (Figure 9.2). This area of seismicity probably represents the continuation of the Hunter Fracture Zone (HFZ) through the Fiji region. The HFZ is a hybrid left-lateral transform fault/thrust (subduction) system to the southwest of the Fiji Platform (Malahoff et al., 1982; Pelletier et al., 1998). Abrupt truncation of magnetic anomalies of the South Fiji Basin along the HFZ, and bathymetry data from this area, which show a northeast-trending double ridge/trough morphology, have been used to defined a remnant trench and forearc complex associated with oblique, north-directed subduction at the HFZ (Chase, 1971; Malahoff et al., 1982; Brocher & Holmes, 1985). Subduction here may have ceased only recently as there is an absence of an inclined seismic (Benioff) zone (Hamburger & Everingham, 1986). Obliquely convergent sinistral strike slip motion has been shown to occur between the Australian plate and the Fiji Platform along the HFZ at a rate of 20-30 mm per year (Pelletier et al., 1998). The continuation of the HFZ in the Fiji region is marked by bathymetric troughs between Kadavu and the Koro Sea.

Isolated large shallow earthquakes occur along the northeast extension of the HFZ especially on the Kadavu Ridge near Kadavu. Significant historical earthquakes occurred in this area in 1850 (MMVIII Kadavu), 1918 (M_s 5.5), 1935 (M_s 6.0), 1950 (M_s 6.5) and 1963 (M_s 6.6) (Everingham, 1983a; Everingham, 1988). Swarms of earthquakes occurred recently near Kadavu in 1983 (Hamburger & Qiolevu, 1983) and in 1998 (Rao, 1998). The largest earthquakes of these swarms had magnitudes M_L 5.1 and M_L 5.3 respectively. The earthquakes in this area have been interpreted with thrust and left-lateral focal mechanism solutions on NE trending faults (Sykes et al., 1969; Johnson & Molnar, 1972) (Figure 9.3).

Faults with a similar trend have been mapped by Cronin et al. (2004) at the western end of Kadavu. Active deformation in this area is further corroborated by (Quaternary) lithospheric flexure associated with the Kadavu Trench (Nunn, 1995), Quaternary volcanism (Cronin et al., 2004), and tectonic uplift in the western part of Kadavu (Nunn & Omura, 1999).

The maximum felt intensities in Suva from large events in this source zone range from MMIII-IV. A large earthquake with a magnitude M_w 7.6 earthquake and an associated swarm of low magnitude events occurred on the 3 March 1990 along the HFZ 500 km southwest of Suva well outside the Kadavu Ridge (Jones, 1998). Another more recent but smaller earthquake (M_L5.2) recorded in this area by the Fiji Seismograph Network in 2001 produced felt intensities of MMII-III in Suva.

9.3.1.5 FIJI PLATFORM (SOURCE ZONE 5)

The Fiji Platform represents a broad and diffused seismic source zone delineated approximately by the 2000 m bathymetric contour. The temporal and spatial distribution of seismicity within this source zone is generally quite irregular and the seismicity record cannot be used to demarcate the boundaries of separate source areas with enough confidence. It is more likely, however, that the entire Fiji Platform represents a seismotectonic province as a whole, which may be undergoing tectonic deformation in a unique style due to interactions with neighbouring plate boundary features (see Chapter 8). The Fiji Platform can be considered as a geographical region with the same geological and seismological characteristics, independent of neighbouring regions, so that it possesses a uniform earthquake potential throughout, and in which earthquakes can occur randomly anywhere along localising source structures. Large earthquakes within the Fiji Platform are more sporadic than those which occur at the margins of the platform. The platform margins have continuous activity of moderate to large magnitude earthquakes (M_S >5), whilst seismicity within the Fiji Platform is continuously active at low magnitudes (Hamburger et al., 1990). There are no historical earthquakes (post 1850) in the Fiji region that have exceeded M_S 7.1. Everingham (1983b) inferred that the large b factor in the magnitude/frequency relationship indicated that earthquakes in Fiji occurred in zones of low stress, where the crust and upper mantle were weak and highly plastic, which prevented the accumulation of strain of sufficient energy to produce large earthquakes. The temporal distribution of major earthquakes and earthquakes sequences recorded within the Fiji Platform and other source zones over the last 150 years are

shown in Figure 9.5. The existing record of seismicity shows two areas of earthquake clustering within the Fiji Platform. They are however, not considered to signify the complete distribution of longer-term earthquake source areas and it is likely that large earthquakes may not be confined to these areas in future. Seismicity in these two areas of clustering within the Fiji Platform is described in the following sections.

-NE Fiji Platform (Taveuni):

A cluster of earthquakes, comprising both large historical events and micro-earthquakes is centered near Taveuni Island in the northeast part of the Fiji Platform. Large historical events have occurred in this area in 1919 (M_s 6.75), 1921 (M_s 5.7), 1928 (M_s 7.0), 1932 (M_s 6.5), 1957 (M_s 5.0), 1960 (M_s 5.9) (Everingham, 1983a; Everingham, 1988). The largest known shallow earthquake in Fiji (M_S 7.1) occurred close to the margin of the Fiji Platform in this region in 1949. Another large and damaging earthquake occurred in the southeast of Vanua Levu, near Taveuni on the 16 November 1979 (M_s 6.9). A swarm of earthquakes centred on the northeastern tip of Taveuni represents the aftershocks of the 1979 Taveuni event. Another sequence of earthquakes in this zone occurred in 1980, with three events > M_L 5 and nine events between M_L 4 and 5. The apparent NW trend of this cluster is simply an artefact of poor constraints on station arrival times (Hamburger et al., 1990). The maximum felt intensities in Suva from the large events in this area are in the range MMII-III. The focal mechanisms of the 1979 earthquake showed pure strike motion on faults trending N-S and E-W (Figure 9.3). These faults planes do not coincide with the trend of mapped geological features in the area. However, the NE-SW orientation of the compression axis and NW-SE orientation of the tension axis are in agreement with the direction of rifting along the Taveuni Volcano and the trends of morpho-structural horst and graben features that are defined by elongated bays and peninsulas in southeast Vanua Levu. Active tectonic deformation in this part of the Fiji Platform is further defined by Holocene uplift along sections of the southeastern coast of Vanua Levu (Miyata et al., 1990) and Quaternary uplift on Cikobia Island at the far northeast of the Fiji Platform (Berryman, 1979).

-Central Fiji Platform (Viti Levu-Ovalau):

A broad collection of micro-earthquakes and larger historical earthquakes occur in the central part of the Fiji Platform in the vicinity of Viti Levu and the Koro Sea. Most of the micro-earthquakes are centred on Viti Levu (referred to as the Viti Levu Seismic Zone in previous chapters) and may arguably be the effect of an inherent bias in the data in Viti Levu due to a

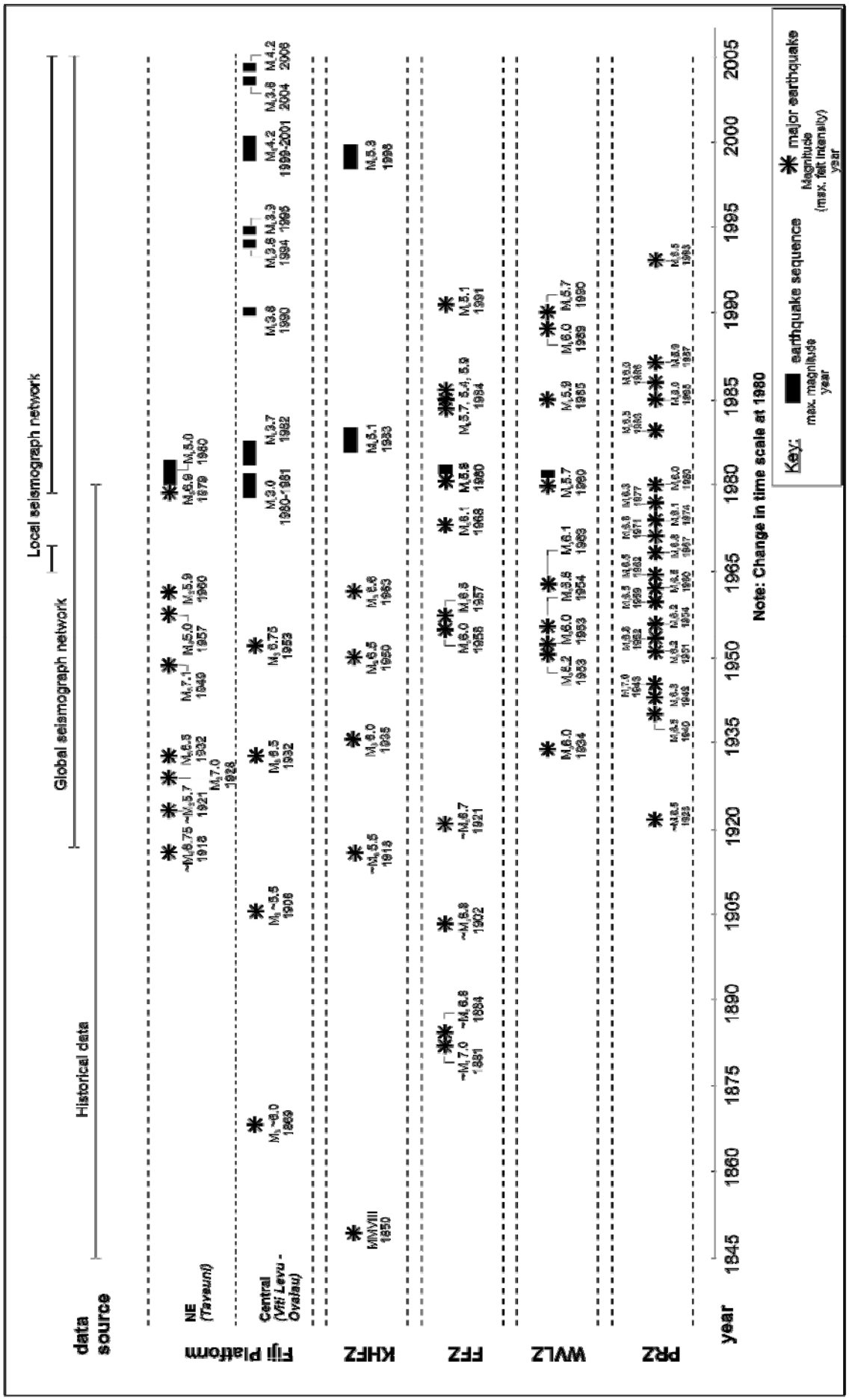

Figure 9.5: Major earthquakes and earthquake sequences within the principal seismotectonic source zones in the Fiji region.

more closely spaced network deployment in this area during the period 1979 to 1994. Nevertheless, the occurrence of several large historical earthquakes within and outside Viti Levu attests to the longer-term active nature of this region. The microsesimcity of the area has been described in detail in Section 8.5. Large historical earthquakes occurred in this region in 1869 in central south Viti Levu (M_s ~6.0), near Ovalau in 1906 (M_s ~5.5), near Koro in 1932 (M_s 6.5), and offshore southeast of Viti Levu in 1953 (M_s 6.75) (Houtz, 1962a; Everingham, 1983a; Everingham, 1988). The tsunami-generating Suva Earthquake of 1953 is the most destructive in Fiji's modern history (Chapter 7). The focal-mechanism solution of the 1953 earthquake indicates strike-slip faulting with a significant but poorly constrained dip-slip component, an east-west tension axis with NW dextral and NE sinistral nodal planes (Hamburger et al., 1990) (Figure 9.3). More recent damaging earthquakes in this area occurred in 1961 (M_S ~ 4.0, MMVI Suva), which originated in the epicentral region of the 1953 earthquake (Houtz, 1962b), and another tsunami-generating earthquake (M_S 5.2, MMVI Suva), which occurred about 50 km south-southeast of Suva in 1975 (Everingham, 1983c). Other notable small to moderate events close to Suva occurred in 1990 (M_L 3.8), 1995 (M_L 3.9), 2000 (M_L 4.3), 2004 (M_L 3.6) and 2006 (M_L 4.2). The maximum felt intensities in Suva over the last 150 years are from the 1953 Suva Earthquake, and they range from MMVIII-X.

9.3.1.6 SUMMARY

In summary, the principal seismotectonic source zones within 500 km of Viti Levu were reviewed in the previous sections and qualitatively evaluated in order to identify those that pose the most significant hazard to Viti Levu. Due to its close proximity, the central Fiji Platform region is considered to be the most important in terms of relevance to strong earthquake shaking in Viti Levu. Earthquakes in the central region of the Fiji Platform have generated intensities up to MMX in Suva and up to MMVII in central Viti Levu. Individual source structures from Viti Levu and offshore of southeast Viti Levu are examined further in the next section to provide the basis for a quantitative evaluation of seismic hazard posed by the central active region of the Fiji Platform. The other source zone that is considered critical to shaking on Viti Levu is the FFZ. This structure has produced intensities of shaking of up to MMVI in Viti Levu and is evaluated further in the following sections. Historical data indicates the shaking intensities in Viti Levu from earthquakes in the other principal source zones at the margins of the Fiji Platform and the seismically active region in the northeast of the Fiji Platform do not exceed MMIV and are therefore not considered any further.

9.3.2 Identification of potential earthquake sources in Viti Levu

9.3.2.1 FAULT AND LINEAMENT MAPPING

A fault/lineament map was compiled for Viti Levu in order to identify potential earthquake source structures. All faults on published 1: 50 000 scale geological maps of Viti Levu of the Geological Survey of Fiji/Mineral Resources Department, as well as fault data from recent mapping in southeastern Viti Levu (Chapter 4) are included in this compilation.

Most of the faults on the published geological maps are based on few limited outcrop exposures in creeks/rivers. Exposure elsewhere is generally very limited because of thick soil/regolith/colluvial cover and dense vegetation. Thus, it is generally not possible to trace an individual fault/shear zone for long distances along strike in the field. As shown in the fracture lineament study of southeastern Viti Levu (Chapter 4), fracture lineaments identified from analysis of remote sensing imagery can be used to infer/identify and quantify the extents of fault/shear zones. Faults zones are often associated with closely spaced and intense fracturing at the Earth's surface, and such fractures are preferentially more prone to erosion than the surrounding unfractured country rock. The lineaments appear as mappable linear topographic features, especially in shaded digital terrain models.

Owing to limitations of the existing fault database, a more comprehensive fault/lineament map was prepared. This integrates previously published fault data and new fault mapping data from this study with the lineament data interpreted from a high resolution Digital Terrain Model (DTM) of Viti Levu. The DTM for Viti Levu was prepared from 20 m topographic contours derived from the Department of Lands and Surveys, Fiji, 1: 50 000 topographic map sheets O27, O28, O29, N26, N27, N28, N29, M26, M27, M28, M29, L26, L27, L28 and L29. The topographic data was combined with bathymetric data for the offshore area of southeastern Viti Levu (Chapter 5) and gridded in Surfer© version 8 software using ordinary point kriging method, with a linear variogram, search radius at 1500 m with 8 minimum points and grid-size set at 20 m. A shaded relief map of the combined onshore and offshore DTM, with north sun-angle, is presented in this thesis as Map 1 at 1: 250 000 scale (see map pocket).

Lineaments were mapped using a selection of shaded relief images of the DTM produced using a variety of sun angles and azimuths at 1:250 000 scale. The main objective of the interpretation was to identify major continuous lineament structures as far as they could be resolved on the DTM without uncertainty. Two independently generated sets of interpretations were compared and only the reproducible lineaments were integrated with mapped fault data to prepare the final fault/lineament zone map, enclosed here as Map 2. Faults which were mapped previously and confirmed in the field are shown as heavy continuous lines on the map sheet. Lineaments that show continuity with and extend beyond the mapped faults, or are very strong lineaments sub-parallel to mapped faults, are classified as inferred faults and are shown by heavy broken lines. Weaker lineaments which do not correspond with faults and may represent other linear features (e.g. geological boundaries) are classified as undifferentiated lineaments, and are shown as thin continuous lines. Continuity between lineaments with the same strike are shown with thin broken lines and are classified as projected lineaments. A map of fault/lineament zones overlain on the shaded relief image is enclosed as Map 3. Twelve fault/lineament zones and a total of forty-seven major faults, ranging from confirmed to inferred categories, are identified and named. The fault/lineament zones have comparable orientations, widths and lengths as fault/lineament zones that were defined by detailed quantitative statistical analysis in southeastern Viti Levu (Chapter 4). If one were to extrapolate the relationship between lineaments and faults established in southeast Viti Levu to these island wide lineament zones, they offer a synoptic view of the regional faulting patterns on Viti Levu. The fault/lineament zones, associated individual fault strands, and their known characteristics are listed in Table 9.2.

9.3.2.2 CLASSIFICATION OF FAULT ACTIVITY

Under the fault mesh model of the Fiji Platform presented in Chapter 8, most faults within the Fiji Platform can be defined as neotectonic faults, that is, faults that are accommodating current plate boundary stresses (Machette, 2000). It was shown that certain groups of faults, whose orientations are NE or NW trending, are favourably oriented to accommodate the regional stress field and are associated with the largest earthquakes. Faults with these orientations on the Fiji Platform can be defined as capable faults. There is generally a lack of sufficient existing data to identify comprehensively the activity of faults in Viti Levu. The are no historical records of coseismic surface fault rupture in Viti Levu. Paleoseismic data concerning average fault slip rates, surface faulting earthquake recurrence intervals,

magnitudes associated with past surface ruptures and the time of the last coseismic surface rupture are not available. All the mapped faults are widely recognised to disrupt Oligocene to Pliocene strata onland. In most cases, overlying younger strata above these basement rocks either are hidden by vegetation, removed by erosion or have poor stratigraphic age control. For most faults, the most recent activity is not constrained geologically. It is conceivable that activity of many faults may have continued into the Quaternary. The close association of well located shallow earthquakes (<20 km depth) along the surface traces of some faults indicates renewed (or continued) rupture may be occurring. It is perceived that the main reason for the deficiency in fault activity data is the fact that there have rarely been field investigations in the past that focussed primarily on obtaining such data on faults, and not because the evidence of activity does not exist. Despite the current limitations in field data, an attempt is made in this study to classify the activity on the faults based on a number of indirect observations.

The classification scheme for fault activity used in this study is based on Cluff et al. (1972). The definitions of the activity categories of Cluff et al. (1972) however, have been modified slightly to fit the available data on fault activity in Fiji. The classification is based on geographic association of faults with microseismicity and strong earthquakes, and where available, age limiting geological and geomorphological data. Inferred structural relationships between groups of faults based on proximity and orientation are also used in the classification. This classification scheme has four categories of fault activity, which are: a) active fault; b) potentially active fault; c) tentatively active fault and d) inactive fault. Active faults are defined as those faults that have a history of strong earthquakes and surface rupturing defined by historical data, clear geological/geomorphological data, as well as geodetic indication of movement. Potentially active faults have not ruptured historically, but are known to displace recent (Quaternary) geological deposits and geomorphological features, as well as having an alignment of epicentres on the fault trace. Tentatively active faults either show displacement of recent (Quaternary) geological deposits and geomorphological features or have alignment of epicentres of fault trace. Inactive faults have neither geological/geomorphological evidence nor seismological evidence of recent activity. Owing to the lack of proven evidence, none of the faults of Viti Levu can be classified as active faults. Further studies, when completed in future, can supplement and refine the characteristics of faults that have been identified and categorised in this study. More detailed studies may lead to subsequent revision of categories assigned to the faults and possibly lead to identification of other faults that were not known to exist. A map of the fault/lineament zones with overlain seismicity distribution is enclosed as

Map 4. The categories into which all identified faults in Viti Levu fall, and the criteria on which those categories are assigned are listed in Table 9.2.

9.3.2.3 POTENTIALLY AND TENTATIVELY ACTIVE FAULT/LINEAMENT ZONES

Six priority fault/lineaments zones are identified in Viti Levu that comprise potentially active and tentatively active faults. They were investigated further to determine their potential for generating strong ground motions in Viti Levu. They are described in the following sections, followed by a discussion of the possible source structure of the destructive 1953 Suva Earthquake.

- *Mavuvu Fault/Lineament Zone:*

The NE trending left lateral Mavuvu Fault/Lineament Zone is the most prominent fault/lineament zone in Viti Levu. This structure is characterised by strong, single and through-going faults that span the entire island, with a total onshore length of 132 km. It comprises three main fault segments; the Mavuvu Fault (SE), Vatubuso Fault (central) and the Dawasamu Fault (NE). The Nailenga Fault forms a short E-W branch off the Dawasamu Fault. The main faults segments are separated by small step-overs. In the step-over zones the faults segments overlap by as much as 20 km, are parallel to and are separated by cross-strike distances of less than 5 km. With such a geometry, rupture is likely to propagate through the step-overs according to the criteria of Harris & Day (1993) and Scholz & Gupta (2000) and the entire Mavuvu Fault/Lineament Zone is inferred to be capable of rupturing as a single through going event.

In southwestern Viti Levu, an offset in the level of emerged Quaternary reefs (Berryman, 1979) occurs across the coastal projection of the Mavuvu Fault. This offset also occurs along the coastal projection of the Sovi Fault (Sovi Fault/Lineament Zone - see below). It is not known whether this displacement is caused by only one of the faults or both. In this study both faults are classified as tentatively active. A linear cluster of microearthquakes occur along the Dawasamu Fault. This fault occurs at the northern margin of the Plio-Pleistocene Rewa Basin. Two large historical earthquakes in 1869 and 1906, with estimated magnitudes M_s 6.0 (± 0.5) and M_s 5.5 (± 0.5) respectively, have occurred in the vicinity of the Dawasamu Fault and may have been associated with rupturing of this fault.

Table 9.2: Classification of faults in Viti Levu (refer to Maps 2 to 4).

Fault/Lineament Zone	Fault Number	Fault name	Strike	Interpreted Dip	Fault Type*	Known offset	Classification of Activity	Criteria
Muaivuso Fault/Lineament	1	Naqara Fault	NW	70	strike slip (dextral?)		Potentially Active	Microseismicity, Geology, Strong earthquakes
Zone	2	Naboro Fault	NW	75	strike slip (sinistral?)		Tentatively Active	Microseismicity
	3	Namuka Fault	NNW	80	strike slip (dextral?)	500 m right lateral(?)	Tentatively Active	Microseismicty
	4	Muaivuso Fault	NW	80	strike slip (dextral?)		Tentatively Active	Microseismicity
	5	Bay of Islands Fault	NW	70	strike slip (dextral?)		Potentially Active	Microseismicity, Geology, Geomorphic features, possibe surface rupture
	6	Walu Bay Fault	NW		strike slip (dextral?)		Tentatively Active	Microseismicity
	7	Nauluvatu Fault	NW	70	strike slip (dextral?)		Potentially Active	Microseismicity, Geology
	8	Bay View Heights Fault	NW		strike slip (dextral?)		Tentatively Active	Microseismicity
	9	Sawani Fault	NW	65	strike slip (sinistral?)		Tentatively Active	Microseismicity
	10	Medrausucu Fault	NNW	steep to E	normal		Tentatively Active	Proximity to potentially active faults
	11	Naitaradamu Fault	NW		?		Tentatively Active	Proximity to potentially active faults
Mavuvu Fault/Lineament	12	Mavuvu Fault	ENE		strike slip (sinstral?)		Tentatively Active	Geomorphic features
Zone	13	Vatubuso Fault	NE		strike slip (sinstral?)		Tentatively Active	Structural relationship to Mavuavu and Dawasamu Faults
	14	Dawasamu Fault	ENE		strike slip (sinstral?)	10 km(?) left lateral	Tentatively Active	Microseismicity, Strong earthquakes
	15	Nailenga Fault	E	N	normal?		Tentatively Active	Microseismicity
Sovi Fault/Lineament	16	Sovi Fault	NE	NW	oblique sinistral	7 km left lateral, 1 km vertical	Tentatively Active	Geomorphic features
Zone	17	Yalavou Fault	NE		?		Tentatively Active	Proximity to Sovi Fault
	18	Nasovatava Fault	ENE		oblique sinistral	7 km left lateral	Inactive	No geomorphic features, No eathquake epicentres
Nasivi Fault/Lineament	19	Nasivi Fault	WNW	steep to N	strike slip (sinistral)		Tentatively Active	Microseismicity
Zone	20	Koromakawa Fault			?		Tentatively Active	Microseismicity
	21	Shatter Fault	WNW	steep to N	?		Tentatively Active	Microseismicity
	22	Homeward Bound Fault	WNW	steep to N	?		Tentatively Active	Microseismicity
Yaloku Fault/Lineament	23	Yaloku Fault	NNE		?	900 m	Inactive	No geomorphic features, No earthquake epicentres
Zone	24	Nasaucoko Fault	NNE		?		Inactive	No geomorphic features, No earthquake epicentres
	25	Wainamau Fault	N		reverse?		Inactive	No geomorphic features, No earthquake epicentres
Naweidamu Fault/Lineament	26	Naweidamu Fault	ENE	N	oblique sinistral	60 m	Inactive	No geomorphic features, No earthquake epicentres
Zone	27	Nagado Fault	ENE		?		Inactive	No geomorphic features, No earthquake epicentres
Nakorotubu Fault/Lineament	28	Nakorotubu Fault	NW	W	strike slip (dextral?)		Tentatively Active	Microseismicity
Zone	29	Tonga Fault	NW	W	strike slip (dextral?)	90 m (vertical)	Tentatively Active	Microseismicity
	30	Navucu-Lawaki Fault	NW		strike slip (dextral?)	30-60 m (vertical)	Inactive	No geomorphic features, No earthquake epicentres
Yarawa Fault/Lineament	31	Yarawa Fault	NW	70	dextral		Inactive	No geomorphic features, No earthquake epicentres
Zone	32	Rewarani Fault	NW		dextral		Inactive	No geomorphic features, No earthquake epicentres
	33	Mindra Fault	NW		dextral	2 km right lateral	Inactive	No geomorphic features, No earthquake epicentres
Yavoli Fault/Lineament	34	Yavoli-Malakau Fault	NW	NE	strike slip (dextral?)		Inactive	No geomorphic features, No earthquake epicentres
Zone	35	Vagadra Fault	NW	NE	strike slip (dextral?)		Inactive	No geomorphic features, No earthquake epicentres
	36	Nabu Fault	NW	NE	strike slip (dextral?)		Inactive	No geomorphic features, No earthquake epicentres
	37	Koroqele Fault	arcuate - E-W				Inactive	No geomorphic features, No earthquake epicentres
Suva Fault/Lineament	38	Suva Canyon Fault	NE	75	strike slip (sinistral?)		Tentatively Active	Microseismicty, Strong earthquakes
Zone	39	Laucala Fault	NE		?		Tentatively Active	Microseismicity
	40	Kaba Fault	NE	60	?		Tentatively Active	Geology, geomorphic features
	41	Vatuloa Canyon Fault	NE		?		Tentatively Active	Microseismicity
WWW Fault/Lineament	42	Wailekutu Fault	ENE	S	?		Inactive	No geomorphic features, No earthquake epicentres
Zone	43	Waimanu Fault	ENE		?		Inactive	No geomorphic features, No earthquake epicentres
	44	Wainivakidau Fault	ENE		?		Inactive	No geomorphic features, No earthquake epicentres
	45	Wainiveisolekau Fault	ENE		?		Inactive	No geomorphic features, No earthquake epicentres
	46	Wainikoroluva Fault	ENE	70	?		Inactive	No geomorphic features, No earthquake epicentres
Koroyanitu Fault/Lineament Zone	47	Koroyanitu Fault	NW	?	?		Inactive	No geomorphic features, No earthquake epicentres

* All strike slip faults appear to have a normal component

The onshore length of the Mavuvu Fault/Lineament Zone is considered to be the minimum length, as continuity of this structure offshore is highly probable. Onshore faults on Viti Levu are likely to continue offshore. This is clearly shown by detailed offshore studies done in southeastern Viti Levu (Chapter 5), which confirm the offshore extension of the Muaivuso and Suva Fault/Lineament Zones. A limited area of multibeam bathymetric data at the southwestern end of the Mavuvu Fault/Lineament Zone shows submarine channels that have a trend parallel to the fault zone. The trend of the channels is oblique to the maximum gradient of the marginal sea slope at this location, indicating that they may be structurally controlled by the offshore extension of the fault zone. It is possible that the Mavuvu Fault/Lineament Zone may continue further southwest for another 50 km and terminate against the NW trending transform faults associated with the West Viti Levu Zone. In the northeast, the Mavuvu Fault/Lineament Zone either terminates against the Nakorotubu Fault/Lineament Zone or extends further northeast for 30 km and terminates against the aseismic Lomaiviti Lineament (Gunn et al., 1998).

- *Muaivuso Fault/Lineament Zone:*

The Muaivuso Fault/Lineament Zone consists of eleven individual NW trending fault strands in southeastern Viti Levu. These faults occur in an en echelon pattern, and most extend southeast into the offshore area. Some of the faults can be subdivided into fault segments that are separated by step-over zones that have cross strike widths of up to 2 km. Earthquake ruptures along these fault segments are likely to jump over these step over zones (Harris & Day, 1993; Scholz & Gupta, 2000). The Muaivuso Fault/Lineament Zone is 30 km wide at the southeast end. The grain of this fault/lineament zone continues northwestward as a series of discontinuous sub-parallel lineaments to near the northern coast of the island.

The faults classified as potentially active in the Muaivuso Fault/Lineament Zone are the Naqara Fault, Bay of Islands Fault and the Nauluvatu Fault. The Naqara Fault has two fault segments. The northern segment is 30 km long and the southern segment, which is mostly offshore, is approximately 23 km long. They overlap near Naqara Island where detailed onshore and offshore mapping (see Figure 5.8a) indicates that the two segments may be structurally linked and could rupture as a single unit. The epicentral region of the Suva Earthquake of 1953 (M_s 6.75) is centred on the trace of the southern segment of the Naqara Fault. The Bay of Islands Fault also consists of two segments, each about 18 km in length. The southern segment occurs mostly offshore. Offshore seismic reflection data shows that this

segment, which passes close to the Lami Beacon, displaces Holocene sediments in Suva Harbour (Shorten, 1993a). The southern segment also displaces the level of tectonically uplifted and emergent Holocene shoreline features (see Appendix 1). The Nauluvatu Fault is 11 km long, and is associated with grabens that are infilled with Holocene colluvium (Shorten, 1993a), indicating recent activity. Within the Muaivuso Fault Zone, the Naboro, Namuka, Muaivuso, Walu Bay, Bay View Heights and Sawani Faults are associated with microseismicity and are classified as tentatively active faults.

- *Sovi Fault/Lineament Zone:*

The Sovi Fault/Lineament Zone occurs in southwestern Viti Levu and includes the Sovi, Yalavou and Nasovatava Faults. The Sovi Fault is a NE trending sinistral strike slip fault with 7 km of left lateral and 1 km of vertical displacement (Houtz, 1960b; Evans, 1997). The Sovi and Yalavou Faults appear to be structurally related. The step-over zone between the two faults contains short fault segments with similar orientation to the main faults. These short segments may act as linking fractures to the main faults. The combined length of the Yalavou and Sovi Faults is 37 km. The Nasovatava Fault occurs 11 km to the northwest of the Sovi Fault. The Nasovatava Fault is also NE trending and shows sinistral strike slip movement (Hathway & Colley, 1994). There are two E-W trending fault offshoots of the Nasovatava Fault. There is no evidence of seismicity associated with the Sovi Fault/Lineament Zone. However, as mentioned earlier, the Quaternary displacement of coastal features in southwestern Viti Levu may be due to the Sovi Fault and therefore it is classified as tentatively active. With probable structural continuity between the Sovi and Yalavou Faults, the Yalavou Fault is also classified as tentatively active.

- *Nasivi Fault/Lineament Zone:*

The Nasivi Fault/Lineament Zone occurs in the central northern part of Viti Levu. It consists of four main NW to WNW trending fault strands. The main fault strands are the Nasivi, Koromakawa, Shatter and Homeward Bound Faults. These faults occur within the Tavua Caldera and some are exposed in the Emperor Mine workings. These faults correspond to a family of clear sub-parallel lineaments on the DTM. The entire Nasivi Fault/Lineament Zone is 7 km wide. Oblique sinistral strike slip movement occurs on the Nasivi Fault (Setterfield et al., 1991).

A cluster of earthquakes in northern Viti Levu that occurred between 1999 and 2001 appears

to be associated with activity at the western end of the Nasivi Fault Zone. The largest recorded event in this cluster had a magnitude of M_s 4.2. The epicentre, revised after considering macroseismic data, occurs midway between the Koromakawa and Shatter Faults. This earthquake had a maximum felt intensity of MMV, 3 km from the epicentre. The main fault strands of the Nasivi Fault Zone that are exposed underground in the Emperor Mine have not been monitored for movements (Fiji Mineral Resources Department, pers comm. 2005).

- *Suva Fault/Lineament Zone:*

The Suva Fault/Lineament Zone occurs in southeastern Viti Levu and consists of the NE trending Suva Canyon Fault, Laucala Bay Fault, Kaba Fault and the Vatuloa Canyon Fault. This fault zone controls the morphology of the southeastern corner of Viti Levu, including the Suva and Laucala Bays and the Suva and Kaba Peninsulas. The Suva Canyon Fault, Laucala Bay Fault and the Vatuloa Canyon Fault are largely offshore structures. The trace of the Suva Canyon Fault occurs along the Suva Canyon (see Chapter 5). It extends onshore as structures mapped along the margins of the Suva Harbour (Shorten, 1993a). The Suva Canyon and Kaba Faults are associated with faulting and folding of the Pleistocene Nakasi Beds. However, Holocene strata overlying the Nakasi Beds are not deformed by these faults (Armstrong, 1993; Shorten, 1993a). The Laucala Bay and Vatuloa Canyon Faults are associated with microseismicity. All four faults are classified as tentatively active.

- *Nakorotubu Fault/Lineament Zone:*

The Nakorotubu Fault/Lineament Zone occurs in the northwest part of Viti Levu and controls the northwest margin of the island. This fault zone comprises a set of faults that occur sub-parallel to the rift axis and dykes associated with the Pliocene Nakorotubu Volcano and controls the topography and drainage of the area (Hirst, 1965). These faults are probably Tertiary faults that were reactivated during the Plio-Pleistocene, when block faulting led to the downthrow of the western flank of the Nakorotubu volcano and tilting of the eastern flanks to the southeast. There are some offsets in strata that suggest dextral slip. Micro-earthquakes occur along the southern end of the Nakorotubu Fault. Aeromagnetic data indicate that this fault continues offshore as a lineament between Viti Levu and Ovalau. The trace of the offshore lineament occurs along a linear cluster of epicentres. The epicentres of this cluster are the aftershock sequence of a magnitude M_L 3.0 earthquake that occurred here in 1982. The focal mechanism of this and other events in the area shows NW trending nodal planes, consistent with the trend of the fault zone (Everingham, 1983d).

Due to the association of microseismicity, the Nakorotubu Fault is classified as tentatively active.

9.3.2.4 THE SOURCE OF THE 1953 SUVA EARTHQUAKE ?

The effects of the earthquake that occurred near Suva on the 14th of September 1953 are the most severe that have ever been recorded in the country. A future event of equal or higher magnitude and from the same source area can be considered as a significant threat to the communities and infrastructure in southeast Viti Levu.

The question about the source of the Suva 1953 earthquake has been a topic of much controversy (Shorten, 1990). Much uncertainty exists due to the lack of a clear surface rupture during this event and also due to poor quality instrumental data constraining the exact location of the epicentre. Evaluation of macroseismic data by Houtz (1962a), Everingham (1988) and more recently by Rynn & Prasad in SPDRP (2002) places the epicentral region along the coast of southeast Viti Levu, between Nausori and Navua. The epicentre of Houtz (1962a) at 16 km WSW of Suva City (178.30 E, 18.30 S) has an error range of 8 km and is based on re-determination of US Coast and Geodetic Survey instrumental data and by an evaluation of macroseismic activity. The choice of this epicentral region is further corroborated by the occurrence of more recent and well located micro-earthquakes in southeast Viti Levu (Hamburger et al., 1990). The best estimate of the focal depth of this event, determined by Sykes et al. (1969) of 21 km, is also corroborated by the hypocentres of well located micro-earthquakes of Hamburger et al. (1990). The focal mechanism of this event was initially obtained by Hodgson (1958), giving a dextral transcurrent plane striking 331^{o} and a sinistral transcurrent plane striking 061^{o}. A revised and improved calculation by Hamburger et al. (1990) using data from over 40 worldwide stations, indicates oblique normal strike slip faulting. The fault plane solutions show a NW trending plane (*50^{o}/56^{o}) with dextral slip and a NE trending plane (81^{o}/318^{o}) with sinistral fault slip.

Re-examination of macroseismic data indicates that Houtz's choice of the epicentre is not unequivocal, and is correctly demonstrated in his choice of the error limit. Spatially unbiased macroseismic information, such as damage to bridges on the highway running along the coast and landslides on terrain of similar slope, indicate that the intensity of shaking may have the same between Nausori and Navua, and the epicentre could have been anywhere within this

*dip/dip direction

region. Houtz's choice of the offshore epicentre appears to have been primarily influenced by the discovery at that time of a submarine canyon at the Naqara Passage, inferred to be fault controlled (Houtz, 1959), and the occurrence of the tsunami. Several other structure controlled submarine canyons have now been identified in southeast Viti Levu (Chapter 5). The source of the tsunami as shown unequivocally in Chapter 7, was a submarine landslide, and does require the source of the earthquake that triggered the failure to be offshore. A more plausible conclusion of the epicentre using newly available data is that it could have occurred anywhere between Nausori and Navua, either onshore or offshore, or spans both areas.

New mapping in the epicentral area, indicates that there are a number of faults, both in the onshore and offshore area of southeast Viti Levu (Chapter 5). Micro-earthquakes in this region indicate activity on a number of these faults (Chapter 8), thus the recent patterns of micro-earthquake clustering alone cannot be used to pin point the source of the 1953 event. A combination of instrumental records, observed historical data and new mapping have been used to constrain four faults as potential source structures of the earthquake and they are discussed below and shown in Figure 9.6.

The dips of the two fault plane solutions of the earthquake focal mechanism and the hypocentral depth of the earthquake can be used to calculate the location of where the rupture plane would have projected to intersect the ground surface. If the epicentre is taken to be at the centre of the epicentral zone – midway between Nausori and Navua, about the same position as Houtz's choice of location, then the surface projection of the NW trending nodal plane occurs along the line of an onshore-offshore lineament that passes through the Navua Delta and forms a prominent scarp at the base of Beqa Lagoon Slope. There is no evidence of this structure onland, however the morphology of the offshore scarp is quite indicative of a linear fault rupture trace. In this choice of fault plane, it is possible that due to thick and weak superficial deposits on the Navua Delta, the rupture did not reach the surface. This lineament is parallel to active (Holocene) faults along the eastern section of the Beqa-Vatulele Ridge, south of Navua, that have displaced the level of emerged Holocene shorelines features (Nunn, 1990). The surface projection of the NE trending nodal plane occurs within the vicinity of the trace of the Suva Canyon Fault. Seismically triggered tsunami generating failures are shown to be a unique feature of the head of the Suva Canyon compared to other submarine canyons in southeast Viti Levu (Chapter 7). This may be due to the near-field effects of the active fault plane along the Suva Canyon and corroborates the suggestion of rupturing along this

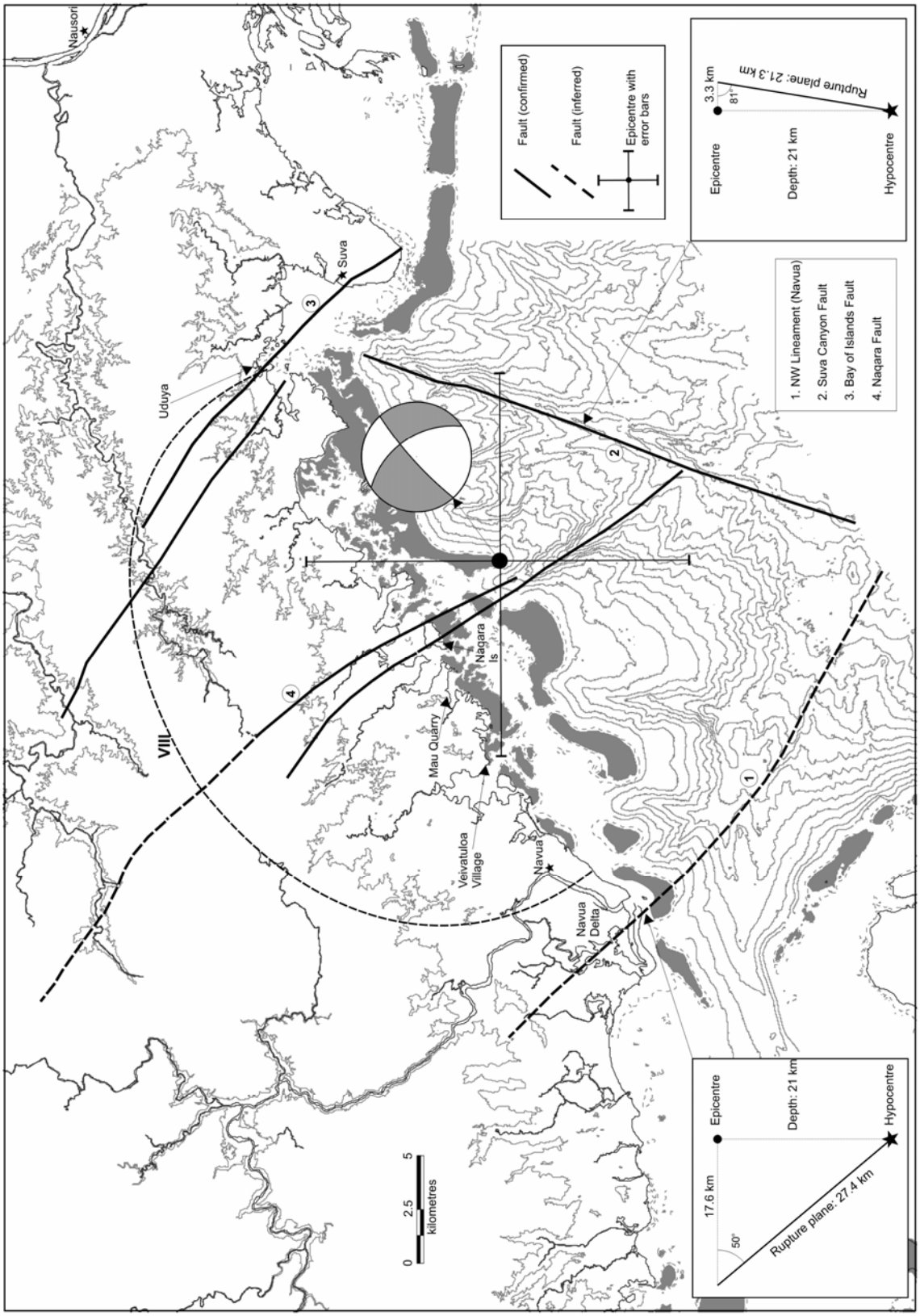

Figure 9.6: Four possible source structures of the 1953 Suva earthquake. Also shown are the isoseismal line of MM8, estimated epicentre with error (Houtz 1962a) and the focal mechanism (Hamburger et al 1990) of this earthquake.

structure.

The third potential choice of the source fault for the earthquake is the Bay of Islands Fault. The trace of this fault passes through Uduya Point, a small promontory at the head of the Bay of Islands 5 km to the west of Suva. Historical records and interviews with residents during the present study indicate that Uduya Point experienced large ground motions during the earthquake. A reinforced concrete house was almost totally destroyed (Figure 9.7a). The rear wall of this house (the western wall) collapsed altogether. The upper section of the house had moved a few centimetres relative to its foundation. The site also experienced extreme ground fissuring during the earthquake. A large ground fissure, about 30 m in length, 20 cm wide and 1.5 m deep, and approximately north–south trending occurred down a slope (Figure 9.7b). Ground fissures during earthquakes on level ground can typically be a manifestation of differential settlement and compaction, and tensional fissures perpendicular to slopes are often to due to gravity induced failures. The geometry of some fissures on Uduya relative to the slope of the area, such as the one shown in Figure 9.7b, suggests that the possibility of some of them being surface rupture effects along the Bay of Islands Fault cannot be discounted. Given that the Bay of Islands Fault may be associated with recent (Holocene) displacements (see Appendix 1), the occurrence of extreme ground fissuring at Uduya in 1953 suggests continued activity along the Bay of Islands Fault.

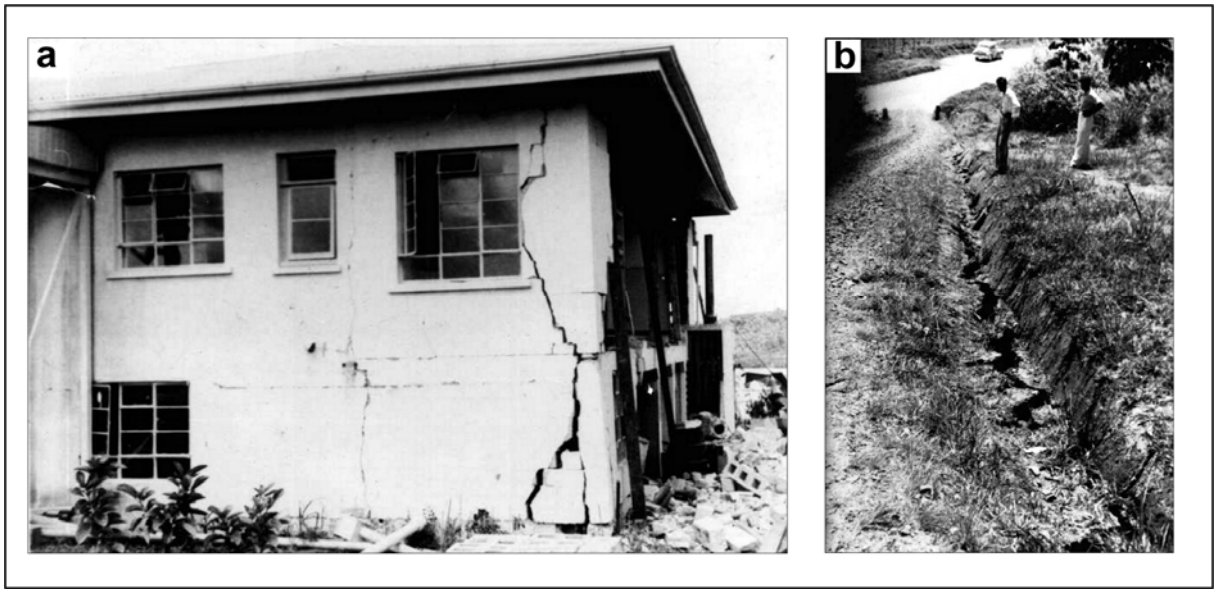

Figure 9.7: Possible near earthquake source effects at Uduya Point due to rupturing along the Bay of Islands Fault. (a) Severe damage of a reinforced concrete house. (b) Ground fissures possibly related to surface rupture (Photos used with permission of Mrs Sharon Light of Uduya Point).

The fourth possible candidate for the source structure is the Naqara Fault. This fault is chosen primarily because it occurs at the centre of the epicentral region of the earthquake. The epicentre given by Houtz (1962a) occurs very close to the offshore trace of this fault. The orientation of this fault is consistent with the NW fault plane solution of the earthquake focal mechanism. This fault is also the longest NW trending fault within the Muaivuso Fault/Lineament Zone. Indications of strong ground motions close to this structure during the earthquake are a large landslide (~1 million m^3) at Veivatuloa Village and ground fissures at Mau Quarry, both within 5 km of the Naqara Fault.

Presently it is difficult to select any one of these structures indisputably as the source structure of the 1953 earthquake. More corroborative evidence may become available from further onshore and offshore surveys in future. For the purpose of this study, the Suva Canyon Fault and the Naqara Fault were selected for further evaluations.

9.4 ESTIMATION OF MAXIMUM CREDIBLE EARTHQUAKES

9.4.1 Empirical Equations

The maximum credible earthquake defines the maximum earthquake potential of an earthquake source under a presumed tectonic setting. The maximum credible earthquakes of selected earthquake source structures identified in this study were estimated using the empirical relations between earthquake magnitude (M_w) and fault parameters of Wells & Coppersmith (1994) and Stirling et al. (2002). The relationships of Wells & Coppersmith (1994) are based on a worldwide database from both interplate and intraplate settings that included 421 historical earthquakes, with hypocentral depth less than 40 km and magnitude generally greater than 4.5. Wells & Coppersmith (1994) showed that the style of faulting did not greatly affect the earthquake magnitude. Their relationships for all slip types were therefore used in this study. Stirling et al. (2002) showed that the Wells & Coppersmith (1994) relationship underestimated the magnitudes of pre-instrumental crustal earthquakes and those derived from paleoseismic data. They used an extended and updated version of the Wells & Coppersmith (1994) database that included pre-instrumental data on large historical earthquakes from New Zealand, Japan and California to infer that the magnitude-fault parameter relationships of earthquakes vary depending on the size of the earthquake. Large earthquakes were inferred to have a different scaling relationship compared to smaller

earthquakes. The relationships of Stirling et al. (2002) based on instrumental data filtered to include only moderate to large earthquakes (M_w 6.1-8.1), were utilised in this study to estimate maximum credible earthquakes.

9.4.2 Fault parameters

Maximum magnitudes were estimated for faults that were considered the most likely sources of large ground motions at the sites of interest. Only potentially or tentatively active faults from each of the six priority fault/lineament zones were considered. The selected faults were either the longest fault or those that occurred closest to the site of interest relative to other faults within the containing fault/lineament zone. The surface rupture length and rupture area parameters were used in calculations. The longest uninterrupted surface length of a fault was assumed to represent the surface rupture length of the fault and was measured directly off the fault/lineament map. The confirmed trace and the inferred trace, where it only occurred beyond the ends of a confirmed trace, were used to define the total surface rupture lengths. Undifferentiated and projected lineaments were not used to add to the total surface rupture lengths. The rupture area can be calculated using the product of either the surface rupture length or the subsurface rupture length and the down dip rupture width. For the equations of Wells & Coppersmith (1994), the rupture area was calculated using the subsurface rupture length. It was shown by Wells & Coppersmith (1994) that the surface rupture is on average equal to 75% of the subsurface rupture length for earthquakes with magnitudes (M_w) between 5.5 to 8.0. This relationship was used to estimate the subsurface rupture length from the surface rupture length. For the equations of Stirling et al. (2002), the rupture area was calculated using the product of the surface rupture length and the down dip rupture width.

The down dip rupture width was constrained by the dip of fault planes, the seismogenic zone depth and the hypocentral depths of large earthquakes within the Fiji Platform. The best located microseismicity data indicates that the seismogenic depth in southeast Viti Levu is about 18 km. The majority of the micro-earthquakes occur at depths between 7 and 13 km (Hamburger et al., 1990). The best located hypocentres of the 1953 Suva Earthquake and the 1979 Taveuni earthquake are 21 km and 33 km respectively (Sykes et al., 1969; Everingham, 1983f). A seismogenic depth of 20 km was adopted to calculate the rupture area. Where the dip of a fault was not known, it was approximated as vertical. Focal mechanisms and field measurements indicate that most faults in Viti Levu have dips greater than 60 degrees.

Since there are uncertainties in the length, dip and seismogenic depth of faults, a sensitivity analysis of the maximum magnitude was carried by changing each of these parameters ± 20% while holding others constant. It was assumed that the true fault parameter value would fall within at least 20% of the estimated adopted value. Changes in the surface rupture length and seismogenic depth by 20% of the adopted values produced variations in magnitudes of only 0.1 magnitude units. Variation in fault dip by 20% resulted in changes in magnitude by 0.02 to 0.04 magnitude units. The variations in the maximum magnitude due to uncertainties in the fault parameter data are very small. They are in fact much smaller than the standard deviation inherent in the regression of the magnitude to fault parameter relationships used here. The calculations of MCEs and the sensitivity analysis are given in Appendix 12.

9.4.3 Maximum Credible Earthquakes

Table 9.3 summarises the parameters of faults considered to be the most likely sources of large ground motions at the sites of interest and includes the maximum magnitudes these faults are capable of producing. The entire known onshore length of the Mavuvu Fault/Lineament Zone was used in estimating the maximum credible earthquake as the whole structure is considered capable of rupturing along its entire length. The estimated maximum magnitude for the Mavuvu Fault/Lineament Zone ranges from M_w 7.5 to 7.6. The Sovi and Yalavou Faults within the Sovi Fault/Lineament Zone are considered to rupture as a single event. Using the combined length of these structures the estimated maximum credible earthquake ranges from M_w 6.8 to 7.1. The Naqara Fault, Nasivi Fault, Suva Canyon Fault and the Nakorotubu Fault are the longest faults in the other important fault/lineaments zones. The maximum credible earthquakes of these faults range from M_w 6.7 to 7.3. The maximum credible earthquake of the central active segment of the FFZ (Yadua Trough) ranges from M_w 7.4 to 7.5.

The estimated MCEs of source structures within the Fiji Platform are half an order of magnitude greater than the magnitudes of large historical earthquakes in the Fiji Platform over the last 150 years, which have been in the range M_w 6.6 to 7.0. Given the low rates of occurrence of large earthquakes within the Fiji Platform, it is reasonable to assume that the maximum historical earthquake would have a magnitude slightly lower than the maximum earthquake potential within the Platform. It is therefore plausible that the estimated maximum capability of the Mavuvu Fault/Lineament Zone of M_w 7.6 would be close to the upper limit

Table 9.3: Maximum Credible Earthquakes.

Earthquake source	SRL (km)	Fault dip	SSRL^ (km)	RW (km)	(Wells & Coppersmith 1994) [1](M_W)	(Wells & Coppersmith 1994) [2](M_W)	(Stirling et al 2002) [1](M_W)	(Stirling et al 2002) [2](M_W)	**Selected MCE (M_W)**
Mavuvu Fault/ Lineament Zone	127[&]	vertical	169	20	7.5	7.5	7.6	7.6	**7.6**
Naqara Fault	39*	70	52	21	6.9	7.0	7.2	7.2	**7.1**
Sovi/Yalavou Faults	37	vertical	49	20	6.9	7.0	7.1	7.2	**7.1**
Nasivi Fault	20	vertical	27	20	6.6	6.7	6.9	7.0	**6.8**
Suva Canyon Fault	25	75	33	21	6.7	6.9	7.0	7.1	**6.9**
Nakorotubu Fault	60[&]	vertical	80	20	7.1	7.2	7.3	7.3	**7.2**
FFZ	100	vertical	133	20	7.4	7.4	7.5	7.5	**7.5**

Abbreviations: SRL - surface rupture length, SSRL - subsurface rupture length, RW - rupture width, RA - rupture area

[&] Minimum length- continues offshore

* Combined onshore-offshore length

^ 1.33 SRL (Wells & Coppersmith 1994)

[1]using SRL

[2]using RA

of earthquakes within the Fiji Platform. The selected MCEs shown in Table 9.3 are an average of the results provided by all methods and reflect the best estimate of earthquake potential for each of the sources based on the currently known characteristics of the faults.

9.5 ESTIMATION OF GROUND MOTIONS

The final step in the deterministic procedure of seismic hazard analysis is to select the controlling maximum credible earthquake. This requires the estimation of ground shaking at the sites of interest, and the selection of the earthquake that produces the most severe level of shaking at the sites concerned. The level of ground motions is dependent upon the earthquake magnitude, mechanism of faulting, source to site distance, the location of the site with respect to the direction of fault rupture, and the site conditions. Figure 9.8 shows the relative locations of the fault sources and the sites of interest that were evaluated in this study.

Ground motion at a site is often expressed using amplitude parameters such as peak values of ground acceleration, velocity and displacement. The peak horizontal ground acceleration (PGA) is commonly used to quantify the seismic hazard of a site as it is related to the largest dynamic forces induced on rigid structures. The frequency content of earthquake ground motion, which is useful for the design of structures, is expressed using different types of ground motion spectra. The horizontal acceleration response spectra (S_a) indicates the potential effects of ground motion on structures of different natural frequencies. Generally, earthquake ground motions are complicated and it is necessary to use more than one parameter to adequately describe all aspects of earthquake ground motion characteristics.

In seismic hazard analysis, ground motion parameters are estimated using attenuation relationships. Attenuation relationships are in the form of equations and describe the attenuation of ground motion with distance from the earthquake source. The relationships are derived empirically from regression analysis of recorded strong ground motion data and express ground motion principally as functions of magnitude and source to site distance. More recently developed attenuation relationships have sourced larger strong ground motion data sets and are more sophisticated. They allow for the evaluation of other controlling/limiting factors such as source and site characteristics (Abrahamson & Shedlock, 1997). Attenuation relationships are typically categorised according different tectonic regions of the world. Those developed for shallow crustal interplate settings, deeper (subduction zone) interplate settings,

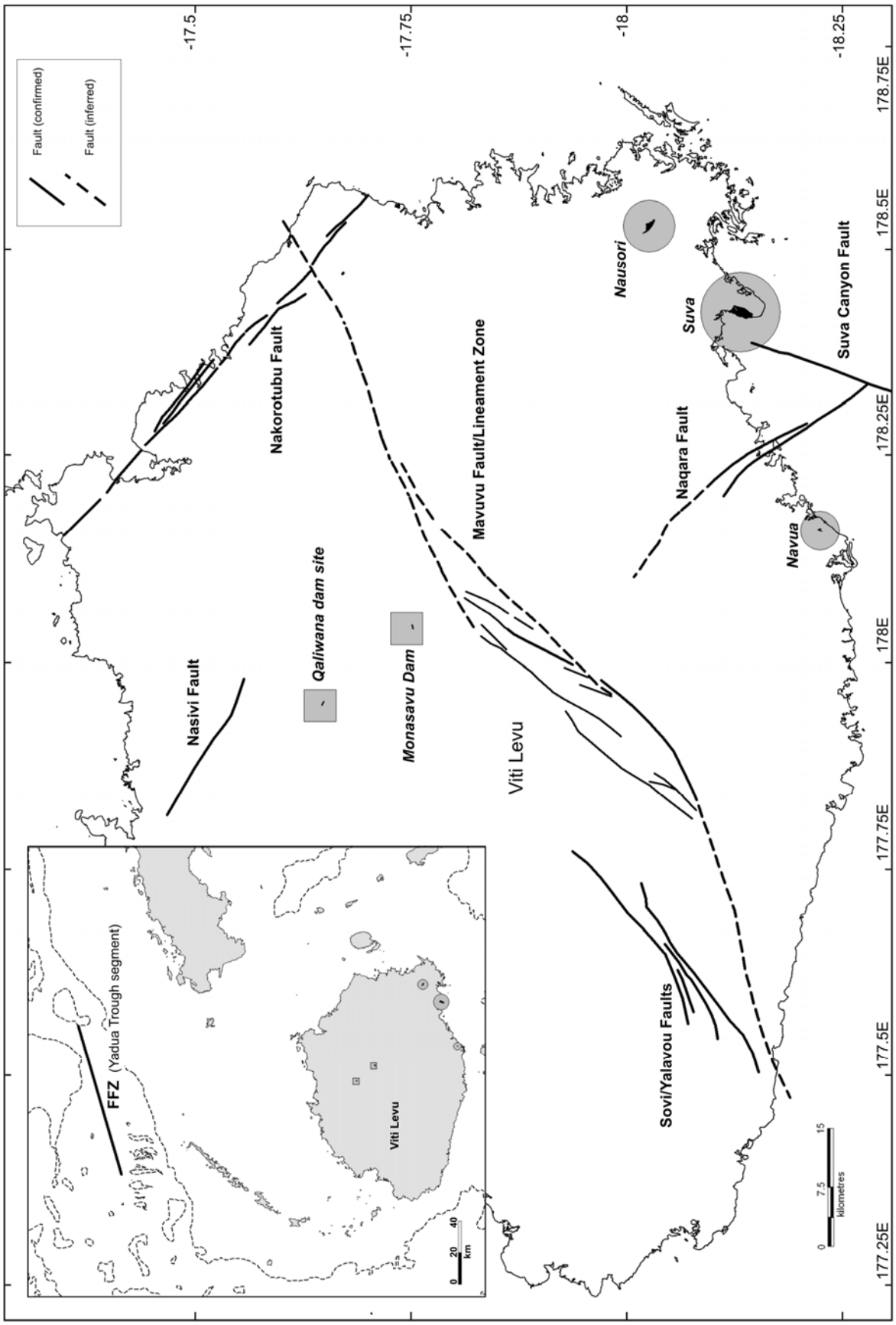

Figure 9.8: Map showing the faults and the sites evaluated in this study.

intraplate stable continent regions, and volcanic regions are commonly used in seismic hazard analysis (Abrahamson & Shedlock, 1997; Dowrick, 2003).

9.5.1 Selection of attenuation relationships

There are no significant instrumental records of strong ground motion data in Fiji, therefore a specific attenuation relation for Fiji is yet to be developed. Owing to this deficiency, attenuation models developed in other parts of world, but are also considered suitable for Fiji conditions, were selected for use in this study. The data on seismic source characteristics presented in this study however, can be used with attenuation models developed for Fiji when they become available in future.

In the absence of a local attenuation model for Fiji, recently updated attenuation relationships developed from shallow crustal earthquakes from active tectonic (interplate) regions of the world were considered for use in Fiji. Whilst in a diffused zone, Fiji remains actively engrossed in the interplate processes of the Pacific/Australian plate boundary zone (Chapter 8). Even though the main islands of Fiji occur up to a 100 km from active plate boundary elements, Fiji cannot be considered a stable continent of low attenuation as suggested by early investigators (e.g. Chase, 1971; Green & Cullen, 1973). It has a crustal thickness of about 20 km, much thinner than continental regions, and relatively low crustal velocities (Hamburger et al., 1990). The position of the Fiji Platform in the active back-arc region of the Tonga and Vanuatu subduction zone is overtly suggestive of an extensional setting. Low upper mantle velocities beneath the Fiji Platform are indicative of a ductile lithosphere with high thermal attenuation, quite similar to those in the neighbouring back arc-basins (Hamburger et al., 1988). There are currently no active volcanoes in Fiji and therefore allowances for high attenuation characteristics that are prevalent in active volcanic regions are not required (Dowrick, 2003).

The models of Abrahamson & Silva (1997), Sadigh et al. (1997), Campbell & Bozorgnia (2003) and Spudich et al. (1999) were used in this study. All four models are based on strong ground motion data from shallow earthquakes in active tectonic regions of the world whose focal depths are limited to 20 to 25 km. The attenuation relationships of Abrahamson & Silva (1997) feature the style of faulting factor, the hanging-wall effect and the site effect. The attenuation relationships of Sadigh et al. (1997) are based on data primarily from California,

from both tensional and compressional stress regimes. They incorporate the style of faulting and site factors. The model of Campbell & Bozorgnia (2003) also includes the style of faulting factor, site factor and the hanging-wall effect. The model of Spudich et al. (1999) was selected for use in this study due to the apparent setting of the Fiji Platform in an active region of back-arc extension, surrounded by spreading ridges with active magmatism. Extensional systems generally show smaller ground motion levels than those from other active tectonic regions (Spudich et al., 1999; Ambraseys & Douglas, 2003). The model of Spudich et al. (1999) is based on ground motion data from strike slip and normal faulting earthquakes collected from extensional regimes from around the world and allow for distinction between rocks sites and soils sites. All four models allow for the estimation of the horizontal PGA and the 5% damped horizontal acceleration or velocity response spectrum for various periods. The use of the different attenuations in this study is limited to estimating the expected level of ground motion parameters at the sites of interest from controlling seismic sources. A thorough comparison of the results between the various models is beyond the scope of this study. All four models used in this study are commonly used in seismic hazard analysis around the world.

9.5.2 Parameters for attenuation relationships

The parameters used in the various attenuation relationships can have different definitions. The applicability of attenuation relationships may also be valid for only a particular range of values of these parameters. These factors are dependent upon the characteristics of the original data used in regressions to derive the attenuation relations. In this study the source to site distance and magnitude parameters were measured to be consistent with the way they were defined in the attenuation relationship used. It was also ensured that the parameters used were within the range of applicability of the various attenuation relationships.

9.5.2.1 SOURCE TO SITE DISTANCE

The method of measurement of the source to site distance is often varied in attenuation relations (Figure 9.9). Epicentral and hypocentral distances are sometimes used. Other distances are measured from the highest energy release zone of the rupture plane, which is difficult to measure in most cases. The closest distance to the fault rupture plane (r_{rup}) is used in the model by Abrahamson & Silva (1997) and Sadigh et al. (1997). In the case of vertical

surface rupturing faults, this distance is the same as the closest horizontal distance to the surface trace of fault rupture. Spudich et al. (1999) used the r_{jb} distance, which is the closest horizontal distance to the vertical projection of the fault rupture plane. The closest distance to the zone of seismogenic energy release on a causative fault (r_{seis}) was used by Campbell & Bozorgnia (2003). By this definition, the closest distance is restricted to the rupture plane in basement rock only and does not take measurement to the rupture plane in overlying sediments. The average thickness of overlying sediments on Viti Levu can be taken as 20 to 30 m, except in alluvial plains where it can be up to 100 m thick. Sediment cover offshore can also be up to 100 m (Chapter 5). This range of thickness of the overburden does not make a significant difference to the value of r_{seis} compared to $r_{rup.}$ Therefore, r_{seis} is taken as the same value as r_{rup} in all cases, except for the distance between Suva and the Suva Canyon Fault due to the short distance involved here. The way each of these distances was measured is shown graphically in Figure 9.9. The values of r_{rup}, r_{jb} and r_{seis} for all combinations of source to site distances in this study are listed in Table 9.4. All models have an upper limit on the source to distance, outside which they do not remain applicable. These upper limits are 300 km for Abrahamson & Silva (1997), 100 km Sadigh et al. (1997), 60 km for Campbell & Bozorgnia (2003) and 100 km for Spudich et al. (1999). Models were not used where the source to site distances in this study exceeded the upper limit values.

9.5.2.2 MAGNITUDE

All attenuation relationships used in this study were derived using the moment magnitude scale. The MCEs for all faults were calculated in the moment magnitude scale and were used in the attenuation models as such. All attenuation relations were valid for the magnitude range of all the MCEs that were being evaluated in this study (M_w 6.8 to 7.6).

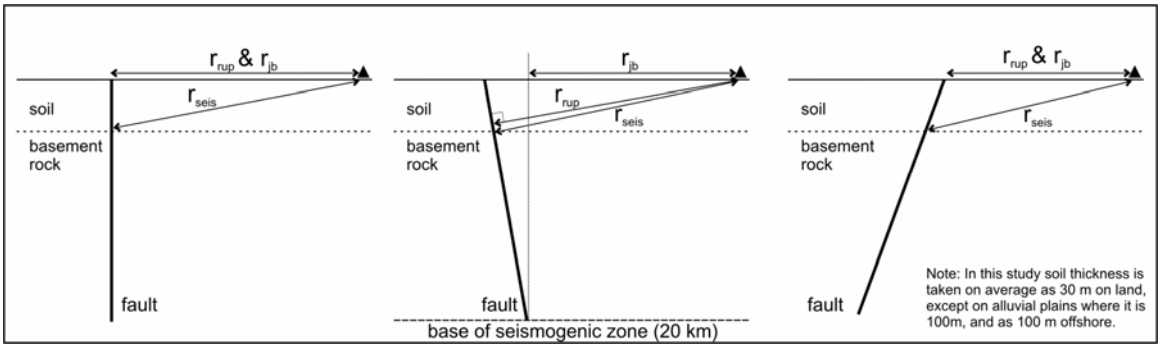

Figure 9.9: Various definitions of source to site distances used in this study, for vertical and dipping faults.

Table 9.4: Source to site distances.

Earthqauke source	Suva (km)			Nausori (km)			Navua (km)			Monasavu (km)			Qaliwana (km)		
	r_{rup}	r_{seis}	r_{jb}	r_{rup}	r_{seis}	r_{jb}	r_{rup}	r_{seis}	r_{jb}	r_{rup}	r_{seis}	r_{jb}	r_{rup}	r_{seis}	r_{jb}
Mavuvu Fault/ Lineament Zone	47	47	47	41	41	41	33	33	33	11	11	11	27	27	27
Naqara Fault	15	15	9	30	30	25	12	13	12	29	29	29	43	43	43
Sovi/Yalavou Faults	72	72	72	80	80	80	52	52	52	35	35	35	37	37	37
Nasivi Fault	79	79	79	79	79	79	76	76	76	23	23	23	11	11	11
Suva Canyon Fault	4	4.03	4	20	20	20	19	19	15	55	55	52	70	70	67
Nakorotubu Fault	51	51	51	37	37	37	72	72	72	41	41	41	39	39	39
FFZ	225	225	225	217	217	217	227	227	227	174	174	174	160	160	160

Different methods of distance measurement for r_{rup}, r_{seis} and r_{jb} are given graphically in Figure 9.9.

9.5.3 Local source and site factors

Local factors such as near source effects and site conditions can affect the level of seismic ground motion that will be experienced at a site. Near source effects are primarily dependent on the source to site distance and are most critical at short distances, usually a few kilometres. Site conditions can be critical even if the source is several hundred kilometres away. An assessment of local factors was undertaken by estimating the prevalent local site conditions at the five sites of interest and the potential near source effects of near source sites.

9.5.3.1 SOURCE MECHANISM AND GEOMETRY

For near-field faults, the type of faulting, their three dimensional geometry and rupture direction with respect to a selected site will affect the level of ground motion at that site (Reiter, 1990). Thrust and reverse faults induce the strongest ground motions relative to other types of faulting. Sites that are located on the hanging-wall of a thrust fault and normal faults experience the highest motions (Oglesby et al., 1998). Faults that dip towards a site, induce stronger ground motions at the site than those that dip away from the site or those that are vertical. As the velocity of rupture propagation almost equals the velocity of shear wave velocity, constructive interference of seismic wave fronts causes the largest motions to occur at a site in the direction of slip and rupture on a fault (Somerville et al., 1997).

The predominant style of faulting within the Fiji Platform appears to be oblique normal strike slip (Chapter 4). There is no evidence for large reverse/thrust faults within the Fiji Platform. The style of faulting factor was taken as strike slip for all the earthquake sources. As most faults are steeply dipping, the hanging wall factor is not considered significant for most faults. Owing to the near-field condition of the Suva site relative to the Suva Canyon Fault, the directivity effect and the hanging-wall factor are considered to be significant at this site.

9.5.3.2 SITE EFFECTS

The near surface geologic and soil condition of a site have considerable bearing on the level of earthquake ground motion and damage that will be experienced at that site. The effects of local site conditions on ground motion level can be more profound than the proximity to the earthquake source as was experienced in the Michoacan Earthquake in Mexico in 1985

(Reiter, 1990, Kramer 1996). Varying influence on earthquake motions by the nature and topography of underlying bedrock and the material properties and configuration of overlying soils can produce different surface ground motions. In addition to ground motion amplification due to site resonance, other site effects such as ground liquefaction, settlement, earthquake induced slope instability may all contributed significantly to damage during earthquakes (Dowrick, 2003). Elaborate classification of sites in terms of seismic response are based on the dynamic properties of soils, which are determined using information such as depth to bedrock, shear wave velocity, soil strength and natural period of vibration. In many cases rock sites have generally experienced lower levels of ground shaking and damage compared to soil sites. In attenuation relationships, the site condition is often crudely defined as either soil or rock.

In this study, the Suva, Qaliwana and Monsavu sites are classified as “rock” sites for the models of Abrahamson & Silva (1997) and Sadigh et al. (1997) and as “soft rock” sites for the model of Campbell & Bozorgnia (2003). The Qaliwana and Monasavu sites are, however, classified as “shallow soil” sites for the model of Spudich et al. (1999), as they are expected to have overlying residual soil cover of up to 20 m thick above bedrock. The Qaliwana and Monasavu sites are underlain by lavas, breccias (mostly pillows lavas) and basal volcanoclastic sediments of the late Miocene/Early Pliocene Ba Volcanic Group (Rodda, 1976). The bedrock at the Suva site is composed of marls, limestones and sandstones of the Medrausucu Group of Miocene/Pliocene age (Rodda, 1982). Past seismic microzonation work has divided the Suva area into four site classes of earthquake shaking susceptibility based on geology, topography, depth to bedrock and the Nakamura micro-tremor site response evaluation (Shorten et al., 2001) (see Appendix 11). The microzonation map, showing the four site classes, their characteristic resonant frequencies and estimated amplification factors are shown in Figure 9.10. The ground motion parameters estimated here for Suva using all attenuation models apply only to bedrock zone (class D) in the microzonation map. The response of other site classes will be different and are discussed further in the next section. The Nausori and Navua sites are classified as “soil” sites for the models of Abrahamson & Silva (1997), Sadigh et al. (1997) and Spudich et al. (1999) and as “firm soils” for the model of Campbell & Bozorgnia (2003). Nausori and Navua towns occur on the flood plains of the Rewa and Navua rivers respectively, and are underlain by a thick layer of soft and fine grained fluvial sediments. Seismic reflection and borehole data indicate that sediment thickness above bedrock at Nausori is between 70 to 100 m (Smith, 1997). Similarly,

boreholes in the Navua flood plain show that depth to bedrock is greater than 30 m, possibly up to 100 m is some places.

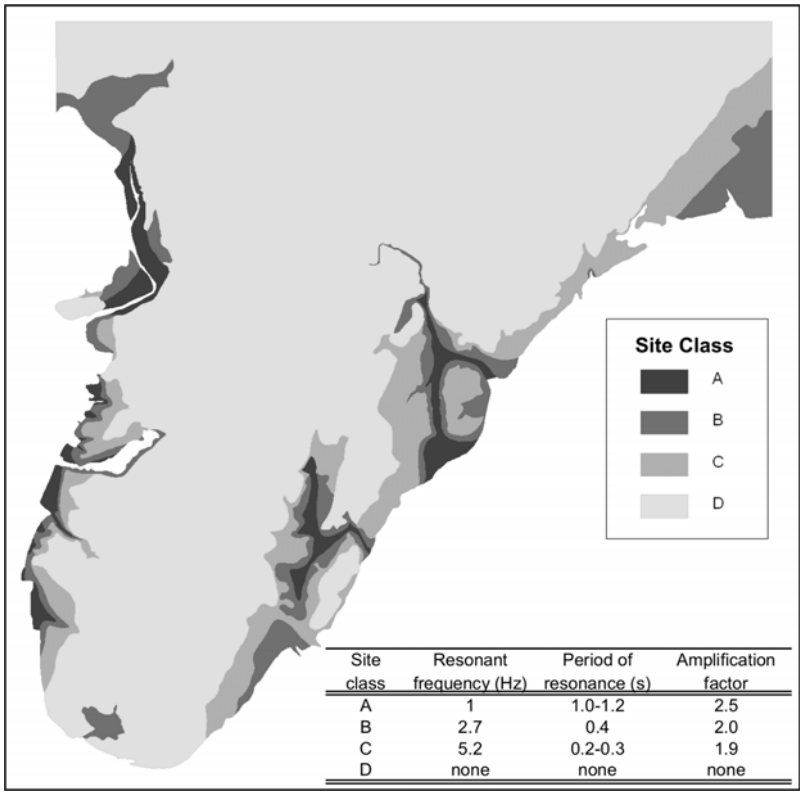

Site class	Resonant frequency (Hz)	Period of resonance (s)	Amplification factor
A	1	1.0-1.2	2.5
B	2.7	0.4	2.0
C	5.2	0.2-0.3	1.9
D	none	none	none

Figure 9.10: Seismic microzontation map of Suva (from Shorten et al. 2001).

9.5.4 Controlling maximum credible earthquakes

The estimated horizontal PGA at the five sites produced by all the six source structures using each of the four attenuation relationships are given in Table 9.5. All the horizontal PGA estimates are median values. The MCE of the source structure that produces the largest horizontal PGA value at a site was selected as the CMCE for that site. The CMCE PGA values are shown in bold in Table 9.5. The horizontal acceleration response spectra (S_a) for all sites were determined using the CMCEs and the spectral attenuation relationship of Abrahamson & Silva (1997). The calculated 5% damped horizontal acceleration response spectra for each site is shown in Figure 9.11. All CMCEs are from Viti Levu. The active Yadua Trough segment of the FFZ produces horizontal PGA of only 0.02g to 0.03g at all the sites. This is comparable to the low shaking intensity levels recorded in Viti Levu from large historical earthquakes from this source structure. The Suva Canyon Fault, Naqara Fault, Nasivi Fault and the Mavuvu Fault Lineament Zone are identified as controlling structures on Viti Levu. The maximum magnitude earthquakes these structures are capable of producing are

Table 9.5: Horizontal PGAs of MCE at Suva, Nausori, Navua, Monasavu and Qaliwana.

Source	Suva MCE PGA Value (g)				Nausori MCE PGA Value (g)				Navua MCE PGA Value (g)				Monasavu MCE PGA Value (g)				Qaliwana MCE PGA Value (g)			
	1	2	3	4	1	2	3	4	1	2	3	4	1	2	3	4	1	2	3	4
Mavuvu Fault/ Lineament Zone	0.12	0.12	0.12	0.1	0.13	0.15	0.16	0.15	0.15	0.18	0.2	0.19	**0.41**	**0.42**	**0.39**	**0.51**	0.19	0.22	0.21	0.23
Naqara Fault	0.27	0.29	0.25	0.32	0.14	0.15	0.16	0.18	**0.27**	**0.3**	**0.31**	**0.34**	0.14	0.16	0.14	0.15	0.1	0.1	0.1	0.1
Sovi/Yalavou Fault	0.06	0.05	~	0.05	0.06	0.05	~	0.05	0.09	0.09	0.09	0.09	0.12	0.13	0.12	0.13	0.11	0.12	0.11	0.12
Nasivi Fault	0.04	0.03	~	0.03	0.05	0.04	~	0.04	0.05	0.04	~	0.05	0.16	0.17	0.15	0.16	**0.32**	**0.33**	**0.28**	**0.3**
Suva Canyon Fault	**0.62**	**0.55**	**0.46**	**0.4**	**0.18**	**0.2**	**0.2**	**0.19**	0.19	0.2	0.21	0.25	0.07	0.06	0.06	0.07	0.05	0.03	0.05	0.06
Nakorotubu Fault	0.09	0.08	0.09	0.07	0.12	0.13	0.14	0.13	0.07	0.06	~	0.07	0.11	0.11	0.11	0.12	0.11	0.12	0.11	0.12
FFZ	0.02	~	~	~	0.03	~	~	~	0.03	~	~	~	0.03	~	~	~	0.03	~	~	~

Attenuation relationships used:
1 - Abrahamson & Silva (1997)
2 - Sadigh et al. (1997)
3 - Campbell & Bozorgnia (2002)
4 - Spudich et al. (1999)
~ source to site distances beyond model restrictions
Note: Values in bold represent CMCE PGAs

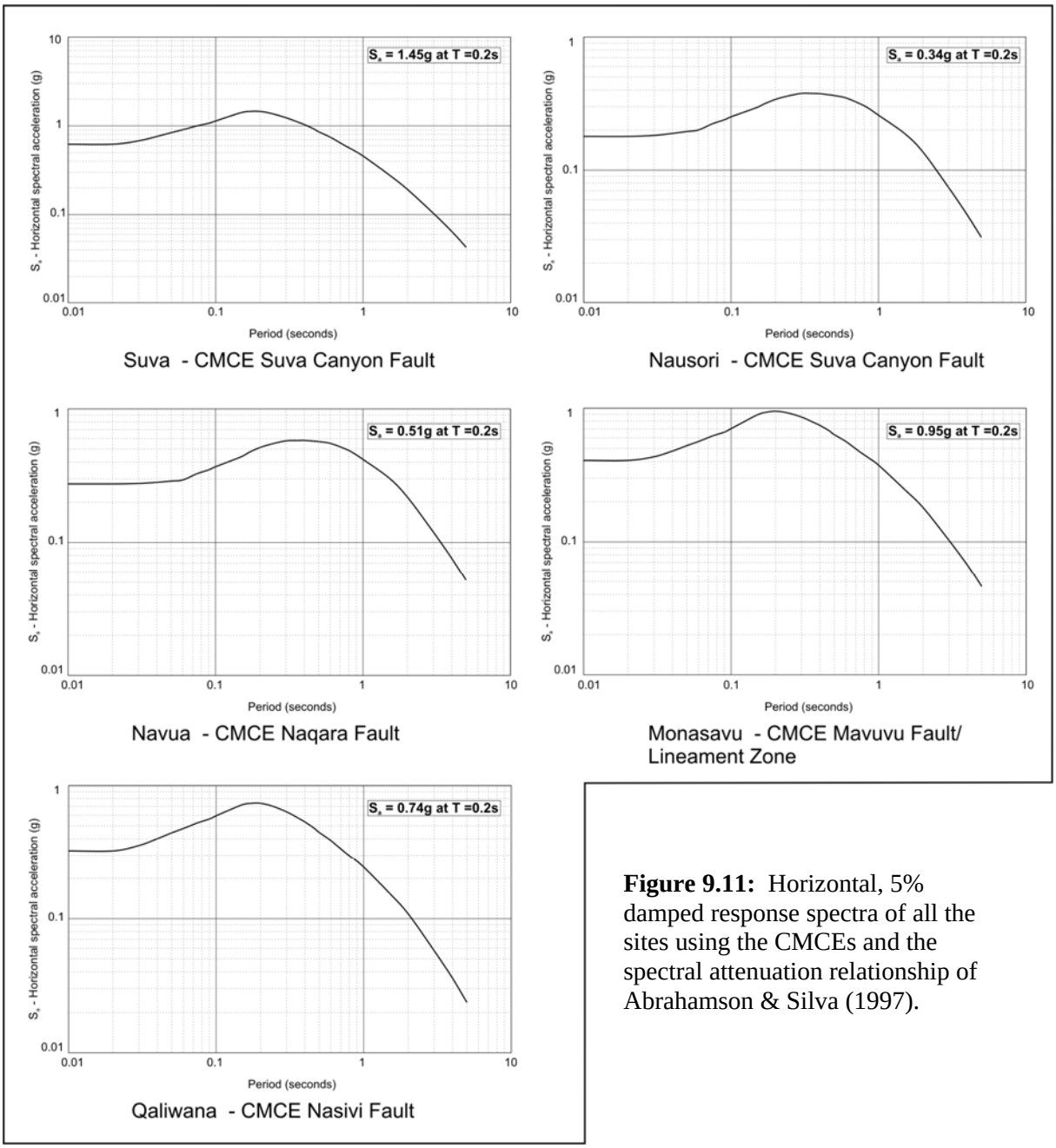

Figure 9.11: Horizontal, 5% damped response spectra of all the sites using the CMCEs and the spectral attenuation relationship of Abrahamson & Silva (1997).

likely to dominate the seismic hazard near at least one of the selected sites of interest. The CMCE horizontal PGA and S_a values provide a quantitative estimate of the highest potential level of seismic ground shaking hazard at the sites of interest that will be induced by these controlling structures. Full calculations of PGA and S_a are provided in Appendix 13.

The CMCE PGA value at Suva ranges from 0.4g to 0.6g and is produced by an earthquake of magnitude M_w 6.9 on the Suva Canyon Fault at a distance of 4 km from Suva City. The MCE on the Naqara Fault produces PGA values between 0.2g to 0.3g only in Suva. The high PGA value of the CMCE is attributed to the proximity of the Suva City to the Suva Canyon Fault.

The PGA value of 0.4g to 0.6g corresponds to rock sites only and it will be the level of motion expected in site class D of the microzonation map (Figure 9.10). These PGA values correspond to MM intensity levels of MMVII to MMIX according to the relationship of Wald (1999). Higher levels of acceleration are expected to occur at site classes A, B and C as they are expected to amplify the basement rock acceleration by factors given in Figure 9.10. The site class A, where soil depths are greater than 20 m above bedrock level and which has a natural period of vibration of 1.0 to 1.2 seconds, is likely to amplify ground motion at this period by a factor as high as 2.5 (Shorten et al., 2001). The spectral acceleration produced by the CMCE at a period of 1 second in bedrock at Suva is about 0.45g. Amplification in site class A is expected to yield surface accelerations just over 1g. Structures in Suva, especially multi-story buildings in the CBD area whose fundamental periods of vibration are equivalent to that of the site class on which they are built, are expected to be affected by site resonance. Given the high ground accelerations predicted for the site classes, ground deformation and failure of foundations are also considered to be a significant threat. A revised isoseismal map of the 1953 Suva earthquake produced by Rynn & Prasad in SPDRP (2002) shows that the highest levels of MM intensity in the Suva CBD area were MMVIII to MMX, especially in site classes A and B. The maximum ground motion intensity value predicted for the CMCE in Suva are expected to be higher than that produced by the 1953 historical event by one or two intensity units.

The hazard calculated for the Monasavu site is a horizontal PGA of 0.4g to 0.5g produced by a CMCE of M_w 7.6 on the Mavuvu Fault/Lineament Zone. The Mavuvu Fault/Lineament is identified as the most relevant seismic source structure to Monasavu Dam as it occurs only 11 km from the dam embankment. This structure was not previously identified in past seismic hazard evaluations of this dam. A probabilistic seismic hazard study on Monasavu Dam by Singh (1996) shows that a background zone of seismicity, which is the most proximal source zone to the site (depth 2 km), is the most significant contributor of the hazard at Monasavu and the 5% damped spectral acceleration of 0.44 g has a return period of 10 000 years. The horizontal PGA values at Nausori, Navua and Qaliwana range from 0.2g to 0.3g. The CMCE for Nausori is a magnitude M_w 6.9 event on the Suva Canyon Fault, for Navua a magnitude M_w 7.1 event on the Naqara Fault, and for Qaliwana a magnitude M_w 6.8 event on the Nasivi Fault. The level of shaking induced by these PGAs will be equivalent to shaking intensities of MMVI to MMVIII. For the Navua and Nausori sites, these intensities are comparable to those recorded during the 1953 Suva earthquake.

The 5% damped spectral acceleration at period equal to 0.2 seconds for all sites were compared to the results of a probabilistic seismic hazard analysis of Fiji by Jones (1998) (Table 9.6). Spectral accelerations similar to those calculated here using the deterministic approach have return periods between 50 years to over 1000 years in the probabilistic analysis. Based on comparisons with the probabilistic evaluation, the return period for the spectral acceleration calculated in the present study at Nausori would be between 50 and 150 years, at Navua between 150 and 450 years, and at Qaliwana between 450 and 1000 years. The return periods for comparable spectral acceleration at Suva and Monasavu are over 1000 years. Large returns periods at these two sites are due to the low rate of occurrence of large magnitude events in Viti Levu in the seismicity model used in the probabilistic analysis. Comparatively larger earthquake loading values at the Suva and Monasavu sites estimated in the present study are due to the closer proximity of the source structures of large earthquakes than was considered likely in the probabilistic analysis.

The deterministically derived values of the horizontal PGA and spectral acceleration for all the sites in this study can be taken as the basis for preliminary evaluation of the maximum design earthquake (MDE) for new critical structures such as tall buildings, wharfs, bridges, and lifeline facilities. The results can also be used as the basis for further evaluation of the safety and upgrade of existing critical structures at these sites. With modification to account for site-specific conditions, which may be required for all the sites other than Suva, the acceleration response spectra presented here can be used as the target acceleration response spectra for developing spectrally matched acceleration time histories. The seismic hazard estimates provided in this study can be generally taken as conservative values, as many uncertainties remain about the level of activity of proximal earthquake source structures.

Table 9.6: Deterministic and probabilistic estimates of horizontal, 5% damped spectral acceleration at T = 2 s in Viti Levu.

	Probabilitistic Seismic Hazard (Jones 1996)				This study
Site	50 yrs	150 yrs	450 yrs	1000 yrs	(Deterministic)
Suva	0.28	0.45	0.68	0.87	1.45
Navua	0.29	0.45	0.67	0.86	0.51
Viti Levu	0.2-0.3	0.4-0.5	0.6-0.7	0.8-0.9	0.34 (Nausori) 0.95 (Monasavu) 0.74 (Qaliwana)

All values are horizontal, 5% damped spectral acceleration (g) at T = 2 s.

9.6 SUMMARY AND CONCLUSIONS

This study presents the results of an unprecedented seismic hazard evaluation in Fiji using newly identified seismic source structures. The seismic hazard of the three main population centres in southeast Viti Levu; Suva City and Nausori and Navua Towns, as well as the sites of two critical structures at Qailwana and Monasavu in central Viti Levu were evaluated using a deterministic approach. Five seismotectonic source zones within 500 km of Viti Levu were first defined using seismicity distribution, focal mechanisms, regional bathymetry and the seismotectonic model of the Fiji Platform. These source zones are the Fiji Fracture Zone, the West Viti Levu Zone, the Peggy Ridge Zone, the Kadavu/Hunter Fracture Zone and the Fiji Platform. The Fiji Fracture Zone and the seismically active central region of the Fiji Platform were considered as the most relevant in terms of seismic hazards in Viti Levu. Faults were identified and characterised on Viti Levu by mapping lineaments on a high-resolution digital terrain model, in combination with regional geologic maps, field reconnaissance mapping and comprehensive review of literature. The activity of faults was classified using geology, geomorphology, epicentral distribution and structural relationships. Out the 12 fault/lineament zones, comprising a total of 47 individual fault strands, five faults and one fault/lineament zone as a whole, were selected for further quantitative analysis. These six structures, classified as potentially or tentatively active, were the Mavuvu Fault/Lineament Zone, Naqara Fault, Sovi/Yalavou Fault, Nasivi Fault, Suva Canyon Fault and the Nakorotubu Fault. The maximum magnitudes capable on these structures, as well as on the central active segment of the FFZ, determined using empirical relationships range from M_W 6.8 to 7.6. Their surface rupture lengths range from 20 to 127 km.

The data on the characteristics of these faults are admittedly very preliminary and much uncertainty remains on some of their parameters especially their level of activity. There is also uncertainty about local seismic wave attenuation characteristics and local site conditions. Nevertheless, the seismic source structures identified in this study are real, and their known parameters can be used to provide conservative estimates of ground motion parameters. Four attenuation relationships, developed using accelograms from shallow crustal active tectonic regions and extensional regions of the world, were used to estimate the horizontal peak ground acceleration (PGA) and the horizontal acceleration response spectra, in the absence of a specific attenuation relationship for Fiji. The PGA values estimated for Suva range from 0.4g to 0.6g, for Nausori from 0.18 g to 0.2g, for Navua from 0.27g to 0.32g, for Monasavu

from 0.39g to 0.42g, and for Qaliwana from 0.23g to 0.33g. The spectral accelerations at a period equal to 0.2 seconds are comparable to accelerations that have returns periods between 50 and over 1000 years based on a regional probabilistic seismic hazard study by Jones (1998).

The results of this deterministic study provide preliminary estimates of the upper bound maximum earthquake events that can be considered for the design and review of safety levels of critical structures at the sites evaluated. They provide the foundation for more elaborate studies in future and should be considered in site-specific engineering projects involving the design of port facilities, bridges, communication and other lifeline structures, schools, hospitals, and large public and residential buildings. The new data presented in this study can also be considered in any revisions or updates of building codes of the country.

CHAPTER 10

SYNTHESIS AND FUTURE WORK

10.1 INTRODUCTION

The overall aim of this research was to evaluate earthquake and tsunami hazards in southeast Viti Levu and propose a model to help improve our understanding of the seismotectonics of the Fiji region. In the beginning of this thesis some key problems were highlighted in conducting earthquake related hazard evaluations in Fiji. These problems ranged from the broader issue of the seismotectonic setting of the islands, to local ones, such as the difficulties associated with undertaking field work in a tropical setting and the need to extend the research to the offshore environment. With these challenges in mind, the overall aims of this research were addressed through a number of specifically developed objectives and utilising new data sets and methodologies not previously applied in Fiji. This chapter summarises the main outcomes from this research. It also offers some recommendations for future studies that could build on the findings obtained in this thesis. Finally, a discussion is provided on the implications of this research for the wider southwest Pacific region, where there are areas that face similar challenges in earthquake hazard research.

10.2 SUMMARY OF THE MAIN RESEARCH OUTCOMES

10.2.1 Onshore faults and fracture lineaments of southeast Viti Levu

The understanding of geological structures and associated tectonic deformation are important components for any seismotectonic evaluation. In Fiji, faults are incompletely mapped due to poor onshore bedrock exposures and this has contributed to the difficulty in interpreting the sources and causes of earthquakes. In this thesis, a detailed and comprehensive analysis of lineaments, as seen on remote sensing imagery, is presented as a viable approach to augment conventional field based study of geological structure, which is severely limited for large parts of Fiji.

The analysis of structural lineaments carried out in this research involves a multi-disciplinary

study that combines remote sensing imagery, geographical information systems and field mapping of scant outcrop exposures. Lineaments are mapped using different images of the surface and of the basement, and at regional and larger scales. Their validity is checked through strict statistical tests of spatial and orientation reproducibility. The lineament orientations are analysed in normalized plots of the least biased approach. Lineaments which correlate to mapped fractures are filtered from the reproducible data sets. Only these lineaments are then used for structural analysis.

The outcome of this procedure as applied in southeast Viti Levu shows that fractures present in bedrock are emphasized by topography, drainage, vegetation and magnetic contrast at depth and can be mapped as the most robust sets of lineaments using remote sensing images that portray such properties of the surface and the basement. Broad zones of surface lineaments mapped in southeast Viti Levu may represent upward diverging splay zones that merge downward into single planar discontinuities, represented by sparse uninterrupted magnetic lineaments at depth. It is also shown that fault correlated lineament sets provide a fuller coverage of regional fracture patterns within the study area, than was previously known. The mapping and analysis of lineaments using this approach can be used successfully in determining regional faulting patterns, which can provide the basis for further studies of tectonic deformation and seismic hazards.

10.2.2 Offshore morpho-structure and faults of southeast Viti Levu

In a seismically active coastal setting such as southeast Viti Levu, investigations must extend to the offshore area for a comprehensive evaluation of earthquake related hazards. Faults representing earthquake source structures may extend to the offshore area and need to be identified and characterised in conjunction with onshore source structures. High resolution nearshore multibeam mapping and seismic reflection profiling are used in this research to document the offshore morpho-structure and for locating offshore faults in southeast Viti Levu.

The southern offshore slope of Viti Levu is divided into six morphological units which are from west to east, the Western Slope, the Beqa Lagoon Slope, the Beqa Passage, the Eastern Slope and the Rewa Delta Foreslope. The Eastern Slope, between the Suva Peninsula and the Beqa Lagoon is the most structurally complex. Here linear submarine canyons that dissect this

slope represent the surface expressions of structural depressions in the underlying bedrock, caused by faults that down-throw toward the axes of the canyons. The trends of the submarine canyon faults project to the onshore and link to faults zones and structural lineaments, collectively defining a number of continuous onshore-offshore fault zones. The absolute lengths of the seismically active onshore-offshore faults can thus be used in the seismic hazard evaluations. The submarine canyons are inferred to have developed primarily by downslope erosional processes. The canyons are likely to have undergone several episodes of infilling and re-incisions, progressively entrenching along the fault-related zones of weakness, as a result of Quaternary global eustatic sea level changes.

10.2.3 Submarine landslide tsunami sources of southeast Viti Levu

Locally triggered tsunamis in seismically active regions pose a substantial hazard to the coastal population centres and infrastructure. Seismically induced submarine landslides are considered to be an important mechanism for local tsunami generation in Fiji. In this thesis, high resolution multibeam bathymetry data collected off the coast of southeast Viti Levu is used to identify and map submarine landslides, examine their possible triggering factors, evaluate their potential for generating tsunamis, and subsequently define a zone susceptible to tsunamigenic slope failures.

Submarine landslides in southeast Viti Levu are characteristically translational and they occur on the barrier reef fronts, canyon walls and heads, and in the mid slope areas. The slides are considered to undergo transformations to debris flows and/or turbidity currents as they lack bathymetric evidence for displaced debris masses at their base. Morphometric analysis and empirical modelling are used to show that reef edge and canyon head slides at the shelf break produce the largest initial tsunami amplitudes and they are interpreted to represent a significant local tsunami hazard. Instability at the reef fronts and at the canyon heads is inferred to be caused by high sedimentation rates and canyon undercutting, and tsunamigenic failures in these areas are primarily triggered by large earthquakes. A potential tsunami generating zone occurs at the top of the Eastern Slope of Viti Levu, within 5 km of the coastline, in which seismically triggered tsunamigenic failures may be initiated.

10.2.4 Tsunami hazard evaluation

Predictive numerical modelling of tsunami generation, propagation and inundation is now widely practised worldwide for tsunami hazard assessment and mitigation work. For this procedure to be credible, however, accurate data on tsunami source parameters, bathymetry and nearshore topography is required. Furthermore, the numerical model used for predictive simulations needs to be validated against real world case studies. In this thesis, a well constrained study is presented on the local tsunami hazard of Suva City, where almost all critical datasets are available for running predictive simulations, including the well documented historical 1953 Suva tsunami.

Using high resolution multibeam bathymetry, field mapping and historical data, the source of the 1953 Suva tsunami is identified as a 60 million cubic metre submarine landslide at the head of the Suva Canyon, 4 km WSW of Suva City. An incipient failure in this source area is indicative of another, potentially tsunamigenic failure. A test simulation of the 1953 event, using the Geowave numerical model, successfully reproduces a set of highly variable near-field coastal wave heights and arrival times observed in 1953. Using this model, a predictive simulation of a potentially worse case scenario, based on the incipient failure, shows a maximum vertical run up of at least 4 m and a maximum horizontal inundation level of at least 400 m at the Suva coast. The simulations show that high variability in tsunami impact over short coastal distances near Suva is attributable to the complex interplay of wave propagation with the barrier reef system, erratic lagoon bathymetry and irregularly shaped coastline. There are indications that the Suva Canyon head source area has produced tsunamigenic landslides in the past. A precursor to the 1953 event occurred sometime in the millennia prior to 1953, possibly as recently as 400 to 500 years before.

10.2.5 Seismotectonic model of the Fiji Platform

Present day seismicity is indicative of ongoing tectonic deformation within the Fiji Platform. The seismotectonics of the Fiji Platform, however, has remained poorly understood. Inadequate data on the structural framework of the Fiji Platform has been a major constraint for a comprehensive seismotectonic analysis of the region. New data on fault lineaments in southeast Viti Levu presented in this thesis, are used to interpret the structural framework, tectonic evolution and origin of seismicity in the area, which in turn have facilitated the

development of a new seismotectonic model for the entire Fiji Platform. Several fault/lineament zones are identified in southeast Viti Levu that combine to form a complex network of interlocking faults and intervening crustal fault blocks. It is postulated that the fault mesh progressively developed in the Neogene to Quaternary period as the brittle deformational response to the anticlockwise rotation of the Fiji Platform. Ongoing tectonic deformation in southeast Viti Levu is accommodated in a distributed manner through the fault mesh, which results in low magnitude earthquakes (<M4) along short linking faults of the mesh. Larger earthquakes (>M4) are interpreted to occur when linking faults, favourably aligned to the regional stress field, combine to form longer ruptures. Regional faults with similar orientations and distribution to those mapped in southeast Viti Levu occur throughout large parts of the Fiji Platform and these faults may also form fault mesh geometries locally, and similarly control tectonic deformation and seismicity. It is inferred that distributed deformation through a structural fault mesh is characteristic of the present day deformation within the Fiji Platform.

10.2.6 Seismic hazard evaluation of Viti Levu

Past seismic hazard evaluations in Fiji have been based entirely on seismicity data. Historical and instrumental records of seismicity, however, are incomplete in terms of quantifying the longer term seismic hazards. This thesis documents newly identified crustal fault seismic source structures on Viti Levu and evaluates the seismic hazard at five sites on Viti Levu using these source structures through a deterministic procedure. At present, there is insufficient data on fault properties (e.g. slip rates, displacement per events) for their application in a probabilistic study.

Five principal seismotectonic source zones in the Fiji region are first identified and evaluated. These include the Fiji Fracture Zone, the West Viti Levu Zone, the Peggy Ridge Zone, the Kadavu/Hunter Fracture Zone and the Fiji Platform. Twelve fault/lineament zones, composed of 47 recognised individual fault strands, are mapped on Viti Levu, out of which five faults and one fault/lineament zone are classified as sufficiently active for further evaluation. The six active structures are the Mavuvu Fault/Lineament Zone, the Naqara Fault, the Sovi/Yalavou Fault, the Nasivi Fault, the Suva Canyon Fault and the Nakorotubu Fault. The Maximum Credible Earthquakes of these six structures, as well as the central active segment of the Fiji Fracture Zone, calculated using empirical equations, range from M_w 6.8 to 7.6.

The controlling maximum credible earthquakes (CMCE) at each of the five sites are evaluated by estimating peak horizontal ground acceleration (PGA) using four recently updated attenuation relationships developed from earthquakes of shallow crustal active tectonic regions of the world. The CMCEs at the five sites are provided by the Suva Canyon Fault, the Naqara Fault, the Mavuvu Fault Lineament Zone, and the Nasivi Fault. The CMCE peak ground acceleration values for Suva City range from 0.4g to 0.6g, for Nausori Town from 0.18g to 0.2g, for Navua Town from 0.27g to 0.32g, for the Monasavu from 0.39g to 0.42g, and for Nadarivatu from 0.23g to 0.33g. The horizontal spectral accelerations at a period equal to 0.2 seconds, calculated using the CMCEs, are comparable to accelerations that have return periods between 50 and over 1000 years based on a previous regional probabilistic seismic hazard study (Jones 1998).

10.3 RECOMMENDATIONS FOR FUTURE WORK

The main outcomes of this research provide new information on the regional onshore-offshore geological structure, geomorphology, earthquake and tsunami sources and associated hazards in Viti Levu. At the same time a number of questions have arisen from this work. Based on the main findings of this research, outstanding problems and new questions, a number of follow up studies are outlined below that can build on this study.

1. Continued mapping of structures can be carried out as they become exposed at civil constructions sites, or from removal of regolith by natural processes such as landslides and erosion. These may provide further validation for lineaments mapped on remotely sensed images.

2. The preliminary work on canyon evolution presented in this study suggests an interplay between reef development on the marginal shelf, cycles of canyon infilling and incisions and Quaternary global eustatic sea level changes. Further seismic reflection profiling and sediment data from marine cores are likely to provide further insights into the complex active seabed processes operating in the offshore area of southeast Viti Levu during the Quaternary.

3. Morphological data indicate that some submarine landslides identified in southeast Viti Levu may be composite features. Offshore data sets such as seismic reflection and

acoustic backscatter imagery, when they become available in future, can be used to place further constraints on the characteristics of individual failures within the composite scars.

4. Radiocarbon dating, as well as other circumstantial evidence were used to try and constrain the age of the deposition of the older tsunami boulder field at the Suva Canyon head. The radiocarbon date, however, provides only an upper limit of the age of deposition. Exposure dating of the tsunami boulders, by the cosmogenic method (using the nuclides ^{3}He, ^{7}Be or ^{36}Cl), would provide a more direct age of deposition, and can be utilised in future. This will provide a better estimate of the time interval between the last two local tsunami events in the area.

5. Improved estimates of predicted tsunami inundation levels and flow velocities along the coast of Suva can be derived by incorporating the seawall, vegetation, and buildings in the computational grid to model their effects on the propagation of tsunami waves.

6. The results of the tsunami hazard analysis of Suva presented in this thesis can be used as the basis to implement a thorough tsunami risk analysis of the Suva Peninsula. Tsunami hazard parameters derived in this thesis, such as horizontal inundation levels, wave heights, and flow velocities, can be analysed with spatial building asset data for Suva (e.g. Buikoto et al. 2001) and the temporal population distribution data. The analysis can then be used to evaluate the likely impact on infrastructure/buildings and human losses and casualties, based on damage and loss functions (fragility curves). The results of the risk analysis will in turn provide the platform from which mitigation options can be worked out.

7. Some preliminary mitigating strategies with respect to tsunami hazard are suggested based on the initial modelling work done here. These can be further developed following the more detailed risk analysis work as suggested above. These include: 1) raising public awareness, 2) developing of preliminary evacuation and land use zoning maps, 2) designing of protective structures (e.g. mangrove barriers) at high impact sites such as Nasese and Lami, and 4) development of preliminary building codes (e.g. minimum floor levels) for the inundation zone on the Suva Peninsula.

8. A close-spaced sensitive network of broadband seismographs can be deployed throughout the Fiji Platform to record earthquake activity, which in turn can be used for comparisons to mapped locations of fault/lineament zones. The network should be configured to allow for the systematic accumulation of earthquake mechanism data. Geodetic observations of strain accumulation throughout the platform can be used to complement the seismicity data. These data sets will provide further tests for the active structural fault mesh model developed here.

9. Future studies can be aimed at improving the compiled database on faults identified on Viti Levu, especially those that have been selected as controlling earthquake source structures in this study. These structures should be targeted for paleoseismic investigations in future. It is likely that such work will provide new data that will allow for redefinition of the fault parameter values, activity classifications and subsequently alternative selections of controlling events.

10. It appears that the way forward for seismic hazard evaluations in Fiji, due to the poor outcrop exposures, is to collect high quality instrumental seismicity data and then compare emerging patterns of epicentres on a local scale to mapped fault/lineament data. Field studies then can be initiated with the specific objective of collecting fault data along those fault/lineaments that show correlations with epicentres. This process can be applied in offshore areas as well, where high resolution multibeam mapping and high-frequency seismic reflection surveys can be utilised to characterise fault parameters. A priority area can be the seismically active offshore region to the east of Viti Levu, where other source structures of potentially large earthquakes proximal to the developed area of southeast Viti Levu can be identified.

11. Further seismic hazard evaluation work needs to address local site conditions from the perspective of site response to seismic ground shaking and the liquefaction potential of materials. At present, critical parameters such as shear wave velocity data are not available from anywhere in Fiji and are crucial for evaluating the dynamic response of deep soils sites such as those which underlie Nausori and Navua Towns. A deployment of strong ground motion instruments is also justified as this will provide the grounds for deciphering and quantifying local attenuation characteristics.

12. The seismic hazard parameters presented in this study at the three population centres in southeast Viti Levu can be used for earthquake scenario based seismic risk analysis in GIS for estimating economic losses and casualties. This work would require the compilation of inventories of buildings, their replacement values and occupancy, and also the development of damage ratios and casualty functions.

10.4 FINAL COMMENTS

This study was undertaken to address seismic and tsunami hazards in Viti Levu and seismotectonics of the Fiji Platform, all of which hitherto remained poorly understood. From the work presented throughout this thesis, it is abundantly clear that new datasets and the application of new scientific methodologies are required to advance the knowledge base of hazards in the region. In summary, the advancement of understanding of seismic hazards was achieved through the application of several phases of study, which included:

1) The development of an innovative methodology of analysing fault lineaments using multiple remote sensing imagery.
2) The implementation of multibeam bathymetric mapping and high resolution marine seismic reflection profiling for identifying offshore faults.
3) The integration of onshore and offshore fault datasets to develop a combined structural framework for the region.
4) The interpretation of the available high quality seismicity data within the context of the structural framework to infer the seismotectonics of the region.
5) The use of new fault/lineament data for the characterisation of crustal fault earthquake source structures and their application in a deterministic seismic hazard analysis based on recently updated empirical earthquake scaling and attenuation relationships.

Similarly, an improvement in the understanding of tsunami hazards in southeast Viti Levu was achieved through a number of sequential studies that included:

1) The mapping and characterisation of submarine landslides using the multibeam bathymetric data.
2) The evaluation of the tsunamigenic potential of the submarine landslides using recently developed empirical models.

3) The analysis of inundation hazards through the review of historical tsunami data, utilisation of new bathymetric data, and the site-specific validation and application of a numerical tsunami simulation model.

Most of the developed and highly populated urban areas in island countries of the tectonically active southwest Pacific region are built around harbour cities vulnerable to seismic and associated tsunami hazards, quite similar to those of Suva City, in southeast Viti Levu. Other urban centres on islands of the Pacific face similar challenges in terms of assessing earthquake related hazards. New high-resolution satellite imagery and offshore data sets have now been acquired from around quite a number of these urban centres under the SOPAC/European Union Project: Reducing Vulnerabilities in Pacific ACP States. The research presented in this thesis provides a good example of how these high quality data sets, used in conjunction with new methodologies, can be utilised to improve the understanding of earthquake related hazards in built up coastal environments. The knowledge acquired can then be applied for better hazard management and for building safer coastal communities.

ACKNOWLEDGMENTS

The research presented in this thesis was made possible through the financial, scientific, logistical and motivational support from a number of organisations and people, whom I would like to acknowledge in the following paragraphs.

Firstly, I thank the New Zealand Agency for International Development - Ministry of Foreign Affairs and Trade, for providing me with a scholarship to undertake this study while based in New Zealand. The field component of this study benefited from a fellowship provided under the SOPAC/EU Project EDF 8: Reducing Vulnerability of Pacific ACP States. I also thank SOPAC for funding my attendance of the STAR meetings in 2004 and 2005. I was awarded a student travel grant by the New Zealand Ministry of Civil Defence & Emergency Management to attend the Natural Hazards Management Conference in 2004. I thank the Mason Trust for covering various research related expenses at the Department of Geological Sciences.

I am greatly indebted to my only supervisor in this project, Associate Professor Jarg Pettinga, for firstly willing to supervise this overseas-based project. Jarg not only provided scientific guidance as a supervisor, but was also an inspiring and motivating co-author. I thank him for introducing and guiding me through the challenge of publishing in international journals. Jarg was also a source of personal support, encouragement and a role model. I thank him for his effort in visiting me in Fiji and for helping Bina and I settle in on our arrival in Christchurch.

I thank Dr Russell Howorth, formerly of SOPAC, and Mr Bhaskar Rao in his role as the Director of the Fiji Mineral Resources Department (MRD), for securing my fellowship with SOPAC, and providing the early discussions on this project. I am grateful to my former manager at MRD, Mr Tevita Vuibau, and the present Director of MRD Mr Iferemi Dau, for their unwavering support in providing the logistics that made field work possible in Fiji.

Peter Rodda of MRD and Michael Bonte of SOPAC showed keen interest in the project and provided insightful discussions in the field and in many emails. I thank Robert Smith and his crew at SOPAC including, Simon, Peni, Ratu and Sekove, for their help in running the seismic reflection surveys. I also thank Robert for supplying me with the multibeam data and Quan Chung for processing the data. Many thanks to the gang at MRD, particularly Sakiusa, Donato, Moape and Manasa for accompanying me on numerous adventures in the bush or out to sea. Those with cool coconut drinks among our search for joints and faults will not be forgotten.

Don Wise and Phil Watts provided useful reviews and comments on early drafts of the work on lineaments and tsunami modelling respectively, and I appreciate the effective discussions provided by John Berrill that led to the seismic hazard assessment part of the project. I thank Joc Campbell for answering my numerous questions on structural geology throughout the project.

I am appreciative of the efficient IT support provided by John Southward. I thank Geraldine Murphy for proof reading the chapters of this thesis. To all the squash buddies – Henrik, Craig, Flo, Phil, Scot, Tennille and Jamie, thank you for the much needed Friday afternoon sessions. I thank everyone else at the Department of Geological Sciences for the enjoyable and memorable experience.

I am thankful to my parents for their continued encouragement through all these years. Finally, but not least, to my wife Bina, thank you for your support, understanding and tolerance in putting up with this "PhD" for the last three and a half years. Your companionship certainly made the experience a whole lot easier.

REFERENCES

Abrahamson, N.A. & Shedlock, K.M. 1997. Overview. *Seismological Research Letters* **68**, 9-23.

Abrahamson, N.A. & Silva, W.J. 1997. Empirical response spectral attenuation relations for shallow crustal earthquakes. *Seismological Research Letters* **68**, 94-127.

Anon 2004. *Fiji Nautical Almanac*. Hydrographic Office, Fiji Islands Maritime Safety Administration **F201**.

Ambraseys, N.N. & Douglas, J. 2003. Near-field horizontal and vertical earthquake ground motions. *Soil Dynamics and Earthquake Engineering* **23**, 1-18.

Armstrong, J. 1993. *Sesimic stratigraphy, sedimentology and holocene evolution of the Rewa estuary, Fiji*. Honours thesis, Department of Applied Geology, Queensland University of Technology, Brisbane.

Auzende, J.-M., Lafoy, Y. & Marsset, B. 1988. Recent geodynamic evolution of the North Fiji Basin (Southwest Pacific). *Geology* **16**, 925-929.

Auzende, J.-M., Pelletier, B. & Lafoy, Y. 1994. Twin active spreading ridges in the North Fiji Basin (Southwest Pacific). *Geology* **22**, 63-66.

Auzende, J.-M., Hey, R.N., Pelletier, B., Rouland, D., Lafoy, Y., Gracia, E. & Huchon, P. 1995a. Propagating rift west of the Fiji Archipelago (North Fiji Basin, SW Pacific*). Journal of Geophysical Research* **100**, 17,823-17,835.

Auzende, J.M., Pelletier, B. & Eissen, J.P. 1995b. The North Fiji Basin: Geology, structure and geodynamic evolution. *In*: Taylor, B. ed. *Backarc Basin: Tectonics and Magmatism*, Plenum Press, New York, 139-175.

Band, R.B. (comp.) 1967a, Geology of Korolevu Bay area, Viti Levu - Sheet **17**, 1:50 000 geological series, *Geological Survey of Fiji*.

Band, R.B. (comp.) 1967b, Geology of Navua River area, Viti Levu - Sheet **18**, 1:50 000 geological series, *Geological Survey of Fiji*.

Band, R.B. (comp.) 1967c, Geology of Mau area, Viti Levu - Sheet **19**, 1:50 000 geological series, *Geological Survey of Fiji*.

Band, R.B. 1968. The geology of southern Viti Levu and Mbengga. *Geological Survey of Fiji Bulletin* **15**, 49 p.

Begg, G. & Gray, D.R. 2002. Arc dynamics and tectonic history of Fiji based on stress and kinematic analysis of dikes and faults of the Tavua Volcano, Viti Levu Island, Fiji. *Tectonics* **21**, 14 p.

Berryman, K. 1979. Seismotectonic zoning study of the Fiji Islands. *New Zealand Geological Survey, Earth Deformation Section Report* **70**, 69 p.

Berryman, K. 1981. Retriangulation of Navua base net (across Suva-Beqa sesimic zone), Fiji Islands August 1980. *New Zealand Geological Survey, Earth Deformation Section Report* **20**.

Biukoto, L., Swamy, M., Shorten, G.G., Schmall, S. & Teakle, G. 2001. Welcome to the Pacific Cities CD Suva, Geographic Information System Hazards Dataset Version 1.0. *SOPAC Data Release Report* **5**.

Bohannon, R.G. & Gardner, J.V. 2004. Submarine landslides of San Pedro Escarpment, southwest of Long Beach, California. *Marine Geology* **203**, 261-268.

Bommer, J.J. 2002. Deterministic vs. probabilistic seismic hazard assessment: an exaggerated and obstructive dichotomy. *Journal of Earthquake Engineering* **6**, 43-73.

Borrero, J.C., Dolan, J.F. & Synolakis, C.E. 2001. Tsunamis within the eastern Santa Barbara Channel. *Geophysical Research Letters* **28**, 643-646.

Boyer, R. & McQueen, J. 1964. Comparison of mapped rocks fractures and airphoto linear features. *Photogrammetric Engineering and Remote Sensing* **30**, 630-635.

Braun, O.P.G. 1982. A structural analysis of Brazil, based on the study of major lineaments derived from remote sensing imagery. *Photogrammetria* **37**, 77-108.

British Admiralty (comp.) 1996, Beqa Passage and lagoon, 1:15 000, *Hydrographic Department*.

Brocher, T.M. 1985. On the formation of the Vitiaz Trench lineament and North Fiji Basin. In: *Investigations of the Northern Melanesian Borderland*, Circum-Pacific Council for Energy and Mineral Resources, Earth Science Series **3**, 13-33.

Brocher, T.M. & Holmes, R. 1985. The marine geology of sedimentary basins south of Viti Levu, Fiji. In: *Investigations of the Northern Melanesian Borderland*, Circum-Pacific Council for Energy and Mineral Resources, Earth Science Series **3**, 123-138.

Campbell, K.W. & Bozorgnia, Y. 2003. Updated near-source ground-motion (attenuation) relations for the horizontal and vertical components of peak ground acceleration and acceleration response spectra. *Bulletin of the Seismological Society of America* **93**, 314-331.

Carney, J.N. & Macfarlane, A. 1978. Lower to middle Miocene sediments on Maewo, New Hebrides, and their relevance to the development of the Outer Melanesian arc system. In: Coleman, P.J. ed., *Bulletin - Australian Society of Exploration Geophysicists* **9**, 123-130.

Cassie, R.A. 1978. *Palaeomagnetic studies in the Suva Marl*. B.Sc. (Hons), University of Sydney, Sydney.

Chase, C.G. 1971. Tectonic history of the Fiji plateau. *Geological Society of America Bulletin* **82**, 3087-3109.

Chen, Q., Kirby, J.T., Dalrymple, R.A., Kennedy, A.B. & Chawla, A. 2000. Boussinesq modelling of wave transformation, breaking, and runup II: 2D. *Journal of Waterway, Port, Coastal and Ocean Engineering* **126**, 48-56.

Cluff, L.S., Hansen, W.R., Taylor, C.L., Weaver, K.D., Brogan, G.E., McClure, F.E., Idriss, I.M. & Blayney, J.A. 1972 Site evaluation in seismically active regions; an interdisciplinary team approach. Proceedings, First International Conference on Microzonation, Seattle, Washington, 2, 957-987

Coleman, P.J. & Packham, G. 1976. The Melanesian Borderlands and India-Pacific plates' boundary. *Earth-Science Reviews* **12**, 197-233.

Colley, H. & Greenbaum, D. 1980. The mineral deposits and metallogenesis of the Fiji Platform. *Economic Geology* **75**, 6, 807-829.

Colley, H. & Hindle, W.H. 1984. Volcano-tectonic evolution of Fiji and adjoining marginal basins. In: Kokelaar, B.P. & Howells, M.F. eds. *Marginal basin geology. Volcanic and associated sedimentary and tectonic processes in modern and ancient marginal basins*, Blackwell Scientific Publications for the Geological Society, London, 151-162.

Cornell, C.A. 1968. Engineering seismic risk analysis. *Bulletin of the Seismological Society of America* **58**, 1583-1606.

Cortes, A.L., Maestro, A., Soriano, M.A. & Casas, A.M. 1998. Lineaments and fracturing in the Neogene rocks of the Almazan Basin, northern Spain. *Geological Magazine* **135**, 255-268.

Cortes, A.L., Soriano, M.A., Maestro, A. & Casas, A.M. 2003. The role of tectonic inheritance in the development of recent fracture systems, Duero Basin, Spain. *International Journal of Remote Sensing* **24**, 4325-4345.

Coulson, F.I.E., Richmond, R.N., Rodda, P. & Kroenke, L.W. 1975. The Structure of the Fiji Platform. *Fiji Mineral Resources Department Miscellaneous Report* **21**, 12 p.

Cronin, S., Ferland, M.A. & Terry, J.P. 2004. Nabukelevu volcano (Mt. Washington), Kadavu - a source of hitherto unknown volcanic hazard in Fiji. *Journal of Volcanology and Geothermal Research* **131**, 371-396.

Cronin, S.J., Bebbington, M. & Lai, C.D. 2001. A probabilistic assessment of eruption recurrence on Taveuni Volcano, Fiji. *Bulletin of Volcanology* **63**, 274-288.

Daly, R.A. 1936. Origin of submarine "canyons". *American Journal of Science* **31**, 401-420.

Day, S.J., Watts, P., Grilli, S.T. & Kirby, J.T. 2005. Mechanical models of the 1975 Kalapana, Hawaii earthquake and tsunami. *Marine Geology* **215**, 59-92.

De Lange, W.P., Moon, V.G. 2004. Estimating earthquake and landslide tsunami hazard for the New Zealand coast. *Bulletin of the New Zealand Society of Earthquake Engineering* **37**, 62-69.

Dickinson, W.R. 1967. Tectonic development of Fiji. *Tectonophysics* **4**, 543-553.

Dickinson, W.R. 1968. Singatoka dune sands, Viti Levu (Fiji). *Sedimentary Geology* **2**, 115-124.

Dickinson, W.R. 1972. Dissected erosion surfaces in northwest Viti Levu, Fiji. *Zeitschrift fur Geomorphologie NF* **16**, 256-267.

Dorwick, D. 2003 *Earthquake risk reduction*. John Wiley & Sons, West Sussex, 506 p.

Eguchi, T. 1984. Seismotectonics of the Fiji Plateau and Lau Basin. In: Carlson, R.L. & Kobayashi, K. eds. *Geodynamics in Back-arc Regions*, *Tectonophysics* **102**, 17-32.

Eichhubl, P., Greene, H.G. & Maher, N. 2002. Physiography of an active transpressive margin basin; high-resolution bathymetry of the Santa Barbara Basin, Southern California continental borderland. *Marine Geology* **184**, 95-120.

Ekstrom, G. & Dziewonski, A.M. 1988. Evidence of bias in estimations of earthquake size. *Nature* **332**, 319-323.

Evans, J.E. 1997. Sedimentology of the Navosa Group (Miocene-Pliocene), Southwest Viti Levu, Fiji, South Pacific. *The Compass* **73**, 60-83.

Everingham, I.B. 1983a. Reports of earthquakes felt in Fiji, 1850 - 1940. *Fiji Mineral Resources Department Report* **48**, 54 p.

Everingham, I.B. 1983b. Magnitude determinations for shallow earthquakes in the Fiji region, 1907-1960, and their implications. *Fiji Mineral Resources Department Note* **BP33/5**, 16 p.

Everingham, I.B. 1983c. The effects of the 16 December 1975 earthquake in Kadavu Passage, Fiji. *Fiji Mineral Resources Department Note* **BP33/7**, 19 p.

Everingham, I.B. 1983d. Focal mechanisms for 1982 earthquakes in Fiji. *Fiji Mineral Resources Department Note* **BP33/4**, 29 p.

Everingham, I.B. 1983e. Preliminary report on sesimic events in the Monasavu dam area. *Fiji Mineral Resources Department Note* **BP33/2**, 14 p.

Everingham, I.B. 1983f. Focal mechanisms for the 16 November 1979 earthquake near Taveuni, Fiji. *Fiji Mineral Resources Department Report* **49**, 8 p.

Everingham, I.B. 1986. A note earthquake risk zoning in Fiji. *Fiji Mineral Resources Department Note* **BP33/14**, 6 p.

Everingham, I.B. 1987. Tsunamis in Fiji. *Fiji Mineral Resources Department Report* **62**, 23 p.

Everingham, I.B. 1988. Catalogue of felt earthquake reports in Fiji, 1941 - 1981. *Fiji Mineral Resources Department Report* **64**, 22 p.

Ewart, A. & Bryan, W.B. 1972. Petrography and geochemistry of the igneous rocks from Eua, Tongan Islands. *Geological Society of America Bulletin* **83**, 3281-3298.

Falvey, D. 1975. Arc reversals, and a tectonic model for the North Fiji Basin. *Bulletin Australian Society for Exploration Geophysics* **6**, 47-49.

Falvey, D.A. 1978. Analysis of palaeomagnetic data from the New Hebrides. In: Coleman, P.J. ed., *Bulletin - Australian Society of Exploration Geophysicists* **9**, 117-123.

Fanning, M. 1986. Report on potassium-argon dating. *AMDEL Report* **G 6788/87**.

Farre, J.A., McGregor, B.A., Ryan, W.B.F. & Robb, J.M. 1983. Breaching the shelfbreak; passage from youthful to mature phase in submarine canyon evolution. In: Stanley, D.J. & Moore, G.T. eds. *The shelfbreak; cirtical interface on continental margins*, Special Publication - Society of Economic Paleontologists and Mineralogists **33**, 25-39.

Fisher, N.I. 1989. Smoothing a sample of circular data. *Journal of Structural Geology* **11**, 775-778.

Gazioglu, C., Gokasan, E., Algan, O., Yucel, Z., Tok, B. & Dogan, E. 2002. Morphologic features of the Marmara Sea from multi-beam data. *Marine Geology* **190**, 397-420.

Giardini, D. 1988. Frequency distribution and quantification of deep earthquakes. *Journal of Geophysical Research* **93**, 2095-2105.

Gill, J.B. 1970. Geochemistry of Viti Levu, Fiji and its evolution as an island arc. *Contributions to Mineralogy and Petrology* **27**, 179-203.

Gill, J.B. & Gorton, M. 1973. A proposed geological and geochemical history of Eastern Melanesia. In: Coleman, P.J. ed. *The Western Pacific - island arcs, marginal seas, geochemistry*, Western Australia University Press, 543-566.

Gill, J.B., Stork, A.L. & Whelan, P.M. 1984. Volcanism accompanying back-arc basin development in the south-west Pacific. *Tectonophysics* **102**, 207-224.

Gill, J.B. 1987. Early geochemical evolution of an oceanic island arc and backarc: Fiji and the South Fiji Basin. *The Journal of Geology* **95**, 589-615.

Gill, J.B. & Whelan, P. 1989a. Early rifting of an oceanic island arc (Fiji) produced shoshonitic to tholeiitic basalts. *Journal of Geophysical Research* **94**, 4561-4578.

Gill, J.B. & Whelan, P. 1989b. Postsubduction ocean island alkali basalts in Fiji. *Journal of Geophysical Research* **94**, 4579-4588.

Goldfinger, C., Kulm, L.D., McNeill, L.C. & Watts, P. 2000. Super-scale failure of the southern Oregon Cascadia margin. *Pure and Applied Geophysics* **157**, 1189-1226.

Gouldby, B., Chung, Q. & Smith, R. 2003. Multibeam survey of south coast of Viti Levu, Fiji, Naselei (Suva) to Momi (Nadi). SOPAC EU EDF 8 - *SOPAC Project: Reducing Vulnerabilty of Pacific ACP States.*

Green, D. & Cullen, D.J. 1973. The tectonic evolution of Fiji. In: Coleman, P.J. ed. *The Western Pacific - island arcs, marginal seas, geochemistry*, Western Australia University Press, 127-145.

Greene, H.G., Maher, N.M. & Paull, C.K. 2002. Physiography of the Monterey Bay National Marine Sanctuary and implications about continental margin development. Marine Geology 181, 55-82.

Greene, H.G. & Ward, S.N. 2003. Mass movement features along the central California margin and their modelled consequences for tsunami generation. In: Locat, J. & Mienert, J. eds. *Submarine mass movements and their consequences*, Ist International Symposium, Kluwer Academic Publishers **19**, 343-356.

Grilli, S.T. & Watts, P. 1999. Modeling of waves generated by a moving submerged body. Applications to underwater landslides. *Engineering Analysis with Boundary Elements* **23**, 645-656.

Grilli, S.T. & Watts, P. 2001 Modelling of tsunami generation by an underwater landslide in a 3D numerical wave tank. *Proceedings of the 11th Offshore and Polar Engineering Conference*, Stavanger, Norway, 3, 301-313.

Grilli, S.T., Vogelmann, S. & Watts, P. 2002. Development of a 3D numerical wave tank for modelling tsunami generation by underwater landslides. *Engineering Analysis with Boundary Elements* **26**, 301-313.

Grilli, S.T. & Watts, P. 2005. Tsunami generation by submarine mass failure Part I: Modeling, experimental validation, and sensitivity analysis. *Journal of Waterway, Port, Coastal and Ocean Engineering* **131**, 283-297.

Gunn, P.J., Mackey, T. & Meixner, A.J. 1998. Interpretation of the results of the Fiji airborne geophysical survey project. Report submitted by the Australian Geological Survey Organisation to AusAID as part of the *Fiji Airborne Geophysical Survey Project*, 36 p.

Hamburger, M.W. & Qiolevu, S.R. 1983. The Kadavu earthquake of July- August 1983. *Fiji Mineral Resources Department Note* **BP33/6**, 22 p.

Hamburger, M.W. & Everingham, I.B. 1986. Seismic and aseismic zones in the Fiji region. In: *Royal Society of New Zealand Bulletin* **24**, 439-453.

Hamburger, M.W. & Isacks, B.L. 1987. Deep earthquakes in the Southwest Pacific; a tectonic interpretation. *Journal of Geophysical Research* **92**, 13,841-13,854.

Hamburger, M.W. & Isacks, B.L. 1988. Diffuse back-arc deformation in the south-western Pacific. *Nature* **332**, 599-604.

Hamburger, M.W., Everingham, I.B., Isacks, B.L. & Barazangi, M. 1988. Active tectonism within the Fiji platform, southwest Pacific. *Geology* **16**, 237 -241.

Hamburger, M.W., Everingham, I.B., Isacks, B.L. & Barazangi, M. 1990. Seismicity and crustal structure of the Fiji Platform, southwest Pacific. *Journal of Geophysical Research* **95**, 2553-2573.

Hampton, M.A., Lee, H.J. & Locat, J. 1996. Submarine landslides. *Reviews of Geophysics* **34**, 33-59.

Hancock, P.L. 1985. Brittle microtectonics; principles and practice. *Journal of Structural Geology* **7**, 437-457.

Harris, R.A. & Day, S.M. 1993. Dynamics of fault interaction; parallel strike-slip faults. *Journal of Geophysical Research* **98**, 4461-4472.

Hathway, B. 1993. The Nadi Basin: Neogene strike-slip faulting and sedimentation in a fragmented arc, western Viti Levu, Fiji. *Journal of the Geological Society, London* **150**, 563-581.

Hathway, B. & Colley, H. 1994. Eocene to Miocene geology of the south-west Viti Levu, Fiji. In: Stevenson, A.J., Herzer, R.H. & Ballance, P.F. eds. *Contributions to the marine and on-land geology and resources of the Tonga -Lau-Fiji region*, SOPAC Technical Bulletin **8**, 153-169.

Hawkins, J.W. 1995. The geology of the Lau Basin. In: Taylor, B. ed. *Backarc Basin: Tectonics and Magmatism*, Plenum Press, New York, 63-138.

Herzer, R.H. 1979. Submarine slides and submarine canyons on the continental slope off Canterbury, New Zealand. *New Zealand Journal of Geology and Geophysics* **22**, 391-406.

Hindle, W.H. & Colley, H. 1981. An oceanic volcano in an island arc setting - Seatura Volcano, Fiji. *Geological Magazine* **118**, 1-14.

Hirst, J.A. 1965. Geology of east and north-east Viti Levu. *Geological Survey of Fiji Bulletin* **12**, 51 p.

Hirst, J.A. (comp.) 1966, Geology of Vunidawa area, Viti Levu - Sheet **13**, 1:50 000 geological series, Geological Survey of Fiji.

Hirst, J.A. (comp.) 1967, Geology of Nanduruloulou area, Viti Levu - Sheet **14**, 1:50 000 geological series, *Geological Survey of Fiji*.

Hodgson, J.H. 1958. *Direction of displacement in western Pacific earthquakes*. In: Contributions in geophysics (Gutenburg volume), Pergamon Press.

Holmes, R., Prasad, A. & Honza, E. 1985. Seismic profiles from the Fiji area. In: Lewis, K.B. ed. *A marine geological and geophysical survey of the northern Tonga Ridge and adjacent Lau Basin*, Ministry of Lands, Survey and Natural Resources of the Kingdom of Tonga, Report **N.1**, 37-41.

Holmes, R., Everingham, I.B. & Eden, R.A. 1987. Slides taken from a helicopter of the reef and coast, south Viti Levu: Reef and lagoon geology. *Fiji Mineral Resources Department Note* **BP23/28**, 22 p.

Houtz, R.E. 1959. Submarine canyons near Suva as possible fault lineations. *Fiji Geological Survey Department Report* **51**, 5 p.

Houtz, R.E. (comp.) 1960a, Geology of the Singatoka area, Viti Levu - Sheet **16**, 1:50 000 geological series, *Geological Survey of Fiji*.

Houtz, R.E. 1960b. Geology of Singatoka area, Viti Levu. *Geological Survey of Fiji Bulletin* **6**, 19 p.

Houtz, R.E. 1962a. The 1953 Suva earthquake and tsunami. *Bulletin of the Seismological Society of America* **52**, 1-12.

Houtz, R.E. 1962b. Note on minor damage caused by the Suva earthquake of June 1961. *Bulletin of the Seismological Society of America* **52**, 13 -16.

Houtz, R.E. (comp.) 1962c, Geology of Keiyasi, Viti Levu - Sheet **11**, 1:50 000 geological series, Geological Survey of Fiji.

Houtz, R.E. & Wellman, H.W. 1962. Turbidity current at Kadavu Passage, Fiji. *Geological Magazine* **99**, 57-62.

Hughes Clarke, J.E., Jarvis, P., Tiffin, D.L., Price, R.C. & Kroenke, L. 1993. Tectonic activity and plate boundaries along the northern flank of the Fiji Platform. *Geo-Marine Letters* **13**, 98-106.

Ibbotson, P. (comp.) 1960, Geology of Suva, Viti Levu - Sheet **20**, 1:50 000 geological series, *Geological Survey of Fiji.*

Ibbotson, P. & Coulson, F.I. 1967. Geology of Vanua Levu. *New Zealand Journal of Geology and Geophysics* **10**, 1180-1181.

Imamura, F., Gica, E., Takakashi, T. & Shuto, N. 1995. Numerical simulation of the 1992 Flores Tsunami: Interpretation of Tsunami Phenomena in Northeastern Flores Island and damage to Babi Island. *Pure and Applied Geophysics* **144**, 555-568.

Inokuchi, H., Yaskawa, K. & Rodda, P.U. 1992. Clockwise and anticlockwise rotation of Viti Levu, Fiji; in relation to the tectonic development of the North and the South Fiji Basin. *Geophysical Journal International* **110**, 225-237.

Ioualalen, M., Pelletier, B., Watts, P. & Grenier, M. 2006. Numerical modelling of the 26th November 1999 Vanuatu tsunami. *Journal of Geophysical Research* (submitted for publication).

Isacks, B., Sykes, L.R. & Oliver, J. 1969. Focal mechanisms of deep and shallow earthquakes in the Tonga-Kermadec region and the tectonics of island arcs. *Geological Society of America Bulletin* **80**, 1443-1469.

Isacks, B.L., Sykes, L.R. & Oliver, J. 1967. Spatial and temporal clustering of deep and shallow earthquakes in the Fiji-Tonga-Kermadec region. *Bulletin of the Seismological Society of America* **57**, 935 - 958.

Jackson, J. & Molnar, P. 1990. Active faulting and block rotations in the western Transverse Ranges, California. *Journal of Geophysical Research* **95**, 22,073-22,087.

James, A. & Falvey, D.A. 1978. Analysis of palaeomagnetic data from Viti Levu, Fiji. In: Coleman, P.J. ed., *Bulletin - Australian Society of Exploration Geophysicists* **9**, 115-117.

Jarvis, P., Hughes-Clarke, J., Tiffin, D., Tanahashi, M. & Kroenke, L. 1994. The western Fiji transform fault and its role in the dismemberment of the Fiji Platform. *Marine Geology* **116**, 57-68.

Johnson, H. 1994. Structure and petroleum geology of the Bligh Water and Bua Waters Basins, Fiji. In: Stevenson, A.J., Herzer, R.H. & Ballance, P.F. eds. Geology and Submarine Resources of the Tonga-Lau-Fiji Region, *SOPAC Technical Bulletin* **8**, 171-184.

Johnson, T. & Molnar, P. 1972. Focal Mechanisms and Plate Tectonics of the Southwest Pacific. *Journal of Geophysical Research* **77**, 5000-5032.

Jones, T. 1998. Probabilistic earthquake hazard assessment for Fiji. *Australian Geological Survey Organisation Record* **1997/46**.

Kennedy, A.B., Chen, Q., Kirby, J.T. & Dalrymple, R.A. 2000. Boussinesq modelling of wave transformation, breaking, and runup I: 1D. *Journal of Waterway, Port, Coastal and Ocean Engineering* **126**, 39-47.

Kineke, G.C., Woolfe, K.J., Kuehl, S.A., Milliman, J.D., Dellapenna, T.M. & Purdon, R. 2000. Sediment export from the Sepik River, Papua New Guinea; evidence for a divergent sediment plume. *Continental Shelf Research* **20**, 2239-2266.

Klaus, A. & Taylor, B. 1991. Submarine canyon development in the Izu-Bonin Forearc; a SeaMARC II and seismic survey of Aoga Shima Canyon. *Marine Geophysical Researches* **13**, 131-152.

Kramer, S.L. 1996 *Geotechnical earthquake engineering*. Prentice Hall, New Jersey, 653 p.

Krinitzsky, E.L. 1995. Deterministic versus probabilistic seismic hazard analysis for critical structures. *Engineering Geology* **40**, 1-7.

Krishna, R. 1983. Wave climatology of waters around Fiji. *Fiji Meteorological Service Technical Note* **19**, 4 p.

Kulikov, E.A., Rabinovich, A.B., Thomson, R.E. & Bornhold, B.D. 1996. The landslide tsunami of November 3, 1994, Skagway Harbor, Alaska. *Journal of Geophysical Research* **101**, 6609-6615.

Lafoy, Y., Auzende, J.-M., Ruellan, E., Huchon, P. & Honza, E. 1990. The 16 degrees 40'S triple junction in the North Fiji Basin (SW Pacific). *Marine Geophysical Researches* **12**, 285-296.

Lambeck, K. & Chappell, J. 2001. Sea level change through the last glacial cycle. *Science* **292**, 679-686.

Larue, B.M., Collot, J.Y. & Malahoff, A. 1980. A sedimentary structure southwest of Viti Levu, Fiji: The Baravi Basin. In: Symposium on petroleum potential in island arcs, small ocean basins, submerged margins and related areas, *UN ESCAP, CCOP/SOPAC Technical Bulletin* 3: 77-83.

Lettis, W.R., Wells, D.L. & Baldwin, J.N. 1997. Empirical observations regarding reverse earthquakes, blind thrust faults, and Quaternary deformation; are blind thrust faults truly blind?. *Bulletin of the Seismological Society of America* **87**, 1171-1198.

Lewis, K.B. & Barnes, P.M. 1999. Kaikoura Canyon, New Zealand; active conduit from near-shore sediment zones to trench-axis channel. *Marine Geology* **162**, 39-69.

Lewis, K., Garlick, R., Hill, R., McKay, J., Mitchell, J., Orpin, A. & Saunders, H. 2001, Underwater landscape evolution with NIWA's new Multibeam, *NIWA- Water & Atmosphere* **9**, 2, 24-25.

Little, T.A. & Roberts, A.P. 1997. Distribution and mechanism of Neogene to present-day vertical axis rotations, Pacific-Australian Plate boundary zone, South Island, New Zealand. *Journal of Geophysical Research* **102**, 20,447-20,468.

Locat, J., Lee, H.J., Locat, P. & Imran, J. 2004. Numerical analysis of the mobility of the Palos Verdes debris avalanche, California, and its implication for the generation of tsunamis. *Marine Geology* **203**, 269-280.

Luyendyk, B.P. 1991. A model for Neogene crustal rotations, transtension, and transpression in Southern California. *Geological Society of America Bulletin* **103**, 1528-1536.

Mabee, S.B., Hardcastle, K.C. & Wise, D.U. 1994. A method of collecting and analyzing lineaments for regional-scale fractured-bedrock aquifer studies. *Ground Water* **32**, 884-894.

Machette, M.N. 2000. Active, capable, and potentially active faults; a paleoseismic perspective. *Journal of Geodynamics* **29**, 387-392.

Maeda, Y., Miyata, T., Rodda, P., Sugimura, A., Matsumoto, E. & Matsushima, Y. 1986. Holocene sea level changes in Viti Levu and Vanua Levu, Fiji. In: Sugimura, A. ed. *Sea level changes and tectonics in the middle Pacific*, Report of the HIPAC Project in 1984 and 1985, Kobe University, 137-185.

Malahoff, A., Feden, R.H. & Fleming, H.S. 1982a. Magnetic anomalies and tectonic fabric of marginal basins north of New Zealand. *Journal of Geophysical Research* **87**, 4109-4125.

Malahoff, A., Hammond, S.R., Naughton, J.J., Keeling, D.L. & Richmond, R.N. 1982b. Geophysical evidence for post - Miocene rotation of the island of Viti Levu, Fiji, and its relationship to the tectonic development of the North Fiji Basin. *Earth and Planetary Science Letters* **57**, 398-414.

Mallick, D.I.J. & Habgood, F. 1987. Interpretation of SLAR imagery of the main islands of Fiji. *British Geological Survey Overseas Directorate Report* **MP/87/3**, 9 p.

Maltman, A. 1994. Introduction and Overview. In: Maltman, A. ed. *The Geologial Deformation of Sediments*, Chapman and Hall, 1-35.

Mandl, G. 1988 *Mechanic of tectonic faulting. Model and basic concepts*. Elsevier, Amsterdam, 407 p.

Martel, S.J. 2004. Mechanics of landslide initiation as a shear fracture phenomenon. *Marine Geology* 203, 319-339.

Mastronuzzi, G. & Sanso, P. 2000. Boulders transport by catastrophic waves along the Ionian coast of Apulia (southern Italy). *Marine Geology* 170, 93-103.

Matsuyama, M. & Yeh, H. 2003. Effects of tsunami at Sissano Lagoon, Papua New Guinea; submarine-landslide and tectonics origins. In: Yalciner, A.C., Pelinovsky, E., Okal, E.A. & Synolakis, C.E. eds. *Submarine landslides and tsunamis*, NATO Science Series. Series IV, Earth and Environmental Series, 21, 151-162.

McAdoo, B.G. & Watts, P. 2004. Tsunami hazard from submarine landslides on the Oregon continental slope. *Marine Geology* **203**, 235-245.

McGuire, R.K. 2001. Deterministic vs. probabilistic earthquake hazards and risks. *Soil Dynamics and Earthquake Engineering* **21**, 377-384.

McHugh, C.M.G., Ryan, W.B.F., Eittreim, S.L. & Reed, D. 1998. The influence of the San Gregorio Fault on the morphology of Monterey Canyon. *Marine Geology* **146**, 63-91.

Miyata, T., Maeda, Y., Matsumoto, E., Matsushima, Y., Rodda, P., Sugimura, A. & Kayanne, H. 1990. Evidence for a Holocene high sea-level stand, Vanua Levu, Fiji. *Quaternary Research* **33**, 352-359.

Morrison, R.J., Narayan, S.P. & Gangaiya, P. 2001. Trace element studies in Laucala Bay, Suva, Fiji. *Marine Pollution Bulletin* **42**, 397-404.

Mualchin, L. 2005. Seismic hazard analysis for critical infrastructures in California. Engineering Geology 79, 177-184.

Mulder, T. & Cochonat, P. 1996. Classification of offshore mass movements. *Journal of Sedimentary Research* **66**, 43-57.

Mullenbach, B.L., Nittrouer, C.A., Puig, P. & Orange, D.L. 2004. Sediment deposition in a modern submarine canyon; Eel Canyon, Northern California. *Marine Geology* **211**, 101-119.

Murty, T.S. 1979. Submarine slide-generated water waves in Kitimat Inlet, Bristish Columbia. *Journal of Geophysical Research* **84**, 7777-7779.

Musgrave, R.J. & Firth, J.V. 1999. Magnitude and timing of New Hebrides arc rotation: Paleomagnitic evidence from Nendo, Solomon Islands. *Journal of Geophysical Research* **104**, 2841-2853.

Narain, S., Pohler, S. & Smith, R. 2004 Stability of the Reef of Slope Basin west of the Rewa Delta (southern Viti Levu). Abstracts of Papers presented at the 21st SOPAC STAR Session (17-24 September 2004), Warwick Hotel, Fiji, *SOPAC Miscellaneous Report* **576**, 80 p

Naylor, M.A., Mandl, G. & Sijpesteijn, C.H.K. 1986. Fault geometries in basement-induced wrench faulting under different initial stress states. *Journal of Structural Geology* **8**, 737-752.

Nemec, W. 1988. The shape of the rose. *Sedimentary Geology* **59**, 149-152.

Nunn, P.D. 1988. Vatulele: A study in the geomorphological development of a Fiji island. *Fiji Mineral Resources Department Memoir* **2**, 99 p.

Nunn, P.D. 1990. Coastal geomorphology of the Beqa and Yanuca islands, South Pacific Ocean, and its significance for the tectonic history of the Vatulele-Beqa Ridge. *Pacific Science* **44**, 348-365.

Nunn, P.D. 1995. Lithospheric flexure in southeast Fiji consistent with the tectonic history of islands in the Yasayasa Moala. *Australian Journal of Earth Sciences* **42**, 377-389.

Nunn, P.D. 1998. *Pacific Island Landscapes*. Institute of Pacific Studies, The University of the South Pacific, 318 p.

Nunn, P.D. & Omura, A. 1999. Penultimate interglacial emerged reef around Kadavu Island, Southwest Pacific; implications for late Quaternary island-arc tectonics and sea-level history. *New Zealand Journal of Geology and Geophysics* **42**, 219-227.

Nur, A., Ron, H. & Scott, O. 1989. Mechanics of distributed fault and block rotation. In: Kissel, C. & Laj, C. eds. *Paleomagnetic rotations and continental deformation*, NATO ASI Series. Series C: Mathematical and Physical Sciences **254**, 209-228.

Oglesby, D.D., Archuleta, R.J. & Nielsen, S.B. 1998. Earthquakes on dipping faults; the effects of broken symmetry. *Science* **280**, 1055-1059.

Okada, Y. 1985. Surface deformation due to shear and tensile faults in a half-space. *Bulletin of the Seismological Society of America* **75**, 1135-1154.

O'Leary, D.W., Friedman, J.D. & Pohn, H.A. 1976. Lineament, linear, lineation; some proposed new standards for old terms. *Geological Society of America Bulletin* **87**, 1463-1469.

Parry, J.T. 1981. Ring ditch fortifications 2. *Bulletin of the Fiji Museum* **7**.

Parson, L.M., Pearce, J.A., Murton, B.J., Hodkinson, R.A., Bloomer, S., Ernewein, M., Huggett, Q.J., Miller, S., Johnson, L., Rodda, P. & Helu, S. 1990. Role of ridge jumps and ridge propagation in the tectonic evolution of the Lau back-arc basin, Southwest Pacific. *Geology* **18**, 470-473.

Pelletier, B. & Auzende, J.-M. 1996. Geometry and structure of the Vitiaz Trench lineament (SW Pacific). In: Auzende, J.M., & Collot, J.Y. eds. Seafloor Mapping in the West, Southwest and South Pacific: Results and Applications, *Marine Geophysical Researches* **18**, 305-335.

Pelletier, B., Calmant, S. & Pillet, R. 1998. Current tectonics of the Tonga - New Hebrides region. *Earth and Planetary Science Letters* **164**, 263 - 276.

Pelletier, B., Lagabrielle, Y., Benoit, M., Cabioch, G., Calmant, S., Garel, E. & Guivel, C. 2001. Newly identified segments of the Pacific-Australia plate boundary along the North Fiji transform zone. *Earth and Planetary Science Letters* **193**, 347 - 358.

Pickering, T.D. & Suda, Y. 2003. Report on the 2nd joint national fisheries university - University of the South Pacific fisheries and oceanography research cruise on board Koyo-Maru, Kadavu Passage, December 1997. Marines Studies Programme, *University of the South Pacific Technical Report* **2003/2**, 69 p.

Popescu, I., Lericolais, G., Panin, N., Normand, A., Dinu, C. & Le Drezen, E. 2004. The Danube submarine canyon (Black Sea); morphology and sedimentary processes. *Marine Geology* **206**, 249-265.

Pratson, L.F., Ryan, W.B.F., Mountain, G.S. & Twichell, D.C. 1994. Submarine canyon initiation by downslope-eroding sediment flows; evidence in late Cenozoic strata on the New Jersey continental slope. *Geological Society of America Bulletin* **106**, 395-412.

Pratson, L.F. & Coakley, B.J. 1996. A model for the headward erosion of submarine canyons induced by downslope-eroding sediment flows. *Geological Society of America Bulletin* **108**, 225-234.

Prichard, T.R. 1989. *Palaeomagnetism and tectonics of Fiji*. Masters Thesis, Department of Geology and Geophysics, University of Sydney, Sydney.

Prior, D.B. & Coleman, J.M. 1979. Submarine landslides; geometry and nomenclature. *Zeitschrift fuer Geomorphologie* **23**, 415-426.

Prior, D.B. & Coleman, J.M. 1984. *Submarine slope instability*. In: Brunsden, D. & Prior, D.B. eds. Slope Instability, John Wiley and Sons, New York, 419-455.

Rahiman, T.I.H., Fong, I. & Vuetibau, L. 2001. Preliminary assessment of earthquake damage west of Vatukoula, northern Viti Levu, Fiji. *Fiji Mineral Resources Department Note* **BP79/09**.

Rao, B. 1998. Mineral Resources Department: annual report for the year 1998. *Parliament of Fiji Paper* **43** of 2000, 30 p.

Reed, A.W. & Hames, I. 1967 *Myths and legends of Fiji and Rotuma*. A.H. & A.W. Reed, 251 p.

Reiter, L. 1990 *Earthquake Hazard Analysis: Issues and Insights*. Columbia University Press, New York, 254 p.

Rodda, P. 1967. Outline of the geology of Viti Levu. *New Zealand Journal of Geology and Geophysics* **10**, 260 -1273.

Rodda, P. (comp.) 1970, Geology of Namosi area, Viti Levu - Sheet **12**, 1:50 000 geological series, *Fiji Mineral Resources Department.*

Rodda, P. 1976. Geology of northern and central Viti Levu. *Fiji Mineral Resources Division Bulletin* **3**, 160 p.

Rodda, P. 1981. Fiji radiometric dates recalculated. *Fiji Mineral Resources Department Note* **BP1/35**, 9 p.

Rodda, P. 1982. Sedimentation in southwestern Viti Levu from the Late Miocene onwards. *Fiji Mineral Resources Department Note* **BP1/39**, 21 p.

Rodda, P. 1992. Geological observations around Kaba, Bau. *Fiji Mineral Resources Department Note* **BP1/102**, 6 p.

Rodda, P. 1993. Notes for geological excursion of the Suva area for the STAR/SOPAC meeting, 1993. *Fiji Mineral Resources Department Note* **BP1/106**, 8 p.

Rodda, P. 1994. Geology of Fiji. In: Stevenson, A.J., Herzer, R.H. & Ballance, P.F. eds. Contributions to the marine and on-land geology and resources of the Tonga -Lau-Fiji region, *SOPAC Technical Bulletin* **8**, 131-151.

Rodda, P. 2003. Stratigraphy - Suva Sheet. *Fiji Mineral Resources Department* (Based on MRD Note BP1/106; amended)

Rodda, P. & Band, R.B. (comps.) 1966, Geology of Viti Levu, map-scale 1:250 000, *Geological Survey of Fiji.*

Rodda, P. & Band, R.B. 1967. Geology of Viti Levu. *New Zealand Journal of Geology and Geophysics* **10,** 1179-1180.

Rodda, P. & Kroenke, L.W. 1984. Fiji: a fragmented arc. In: Kroenke, L.W. ed. Cainozoic tectonic development of the south-west Pacific, *UN ESCAP, CCOP/SOPAC Technical Bulletin* **6**, 65-85.

Rodda, P. & Lum, J. 1990. Geological evolution and mineral deposits of Fiji. In: von Stackelberg, U. & von Rad, U. eds. *Geological evolution and hydrothermal activity in the Lau and North Fiji Basins, south west Pacific Ocean*: *results of SONNE Cruise SO -35*, Geologisches Jahrbuch D 92, 37-66.

Rodda, P. & Nunn, P.D. 1990. Emerged microatolls off Government House, Suva. Fiji *Mineral Resources Department Note* **BP1/92**, 3 p.

Roy, D.W., Schmitt, L., Woussen, G. & DuBerger, R. 1993. Lineaments from airborne SAR images and the 1988 Saguenay earthquake, Quebec, Canada. *Photogrammetric Engineering and Remote Sensing* **59**, 1299-1305.

Roy, S. 1997. Coastal and nearshore geology of Savusvau Bay, Vanua Levu, Fiji. In: Sherwood, A., Howorth, R. & Rodda, P. eds. Coastal and environmental geoscience studies of the Southwest Pacific islands, *SOPAC Technical Bulletin* **9**, 193-205.

Sadigh, K., Chang, C.Y., Egan, J.A., Makdisi, F. & Youngs, R.R. 1997. Attenuation relationships for shallow crustal earthquakes based on California strong motion data. *Seismological Research Letters* **68**, 180-189.

Scholl, D.W., Buffington, E.C., Hopkins, D.M. & Rho Alpha, T. 1970. The structure and origin of the large submarine canyons of the Bering sea. *Marine Geology* **8**, 187-210.

Scholz, C.H. & Gupta, A. 2000. Fault interactions and seismic hazard. *Journal of Geodynamics* **29**, 459-467.

Schneider, W., Schmelzer, I. & Wurtz, J. 1995. Sedimentological interplay of siliclastic Rewa River input and organic carbonate production of the Suva Barrier Reef, Laucala Bay, Fiji. Marines Studies Programme, *University of the South Pacific Technical Report* **95/4**, 28 p.

Schwartz, D.P., Coppersmith, K.J. & Anonymous 1984. Fault behavior and characteristic earthquakes; examples from the Wasatch and San Andreas fault zones. *Journal of Geophysical Research* **89**, 5681-5698.

Setterfield, T.N., Eaton, P.C., Rose, W.J. & Sparks, S.J. 1991. The Tavua Caldera, Fiji: a complex shoshonitic caldera formed by concurrent faulting and downsagging. *Journal of the Geological Society, London* **148**, 115-127.

Shepard, F.P. & Dill, R.F. 1966 *Submarine Canyons and Other Sea Valleys*. Rand McNally, Chicago: 381.

Shepard, F.P. 1981. Submarine canyons; multiple causes and long-time persistence. *AAPG Bulletin* **65**, 1062-1077.

Shepherd, M.J. 1990. The evolution of a moderate energy coast in Holocene time, Pacific Harbour, Viti Levu, Fiji. *New Zealand Journal of Geology and Geophysics* **33**, 547-556.

Shorten, G.G. 1990. Structural geology of Suva Peninsula and Harbour and its implications for the Neogene tectonics of Fiji. *New Zealand Journal of Geology and Geophysics* **33**, 495-506.

Shorten, G.G. 1993a. The geological and tectonic setting for ground failure hazards in Suva Harbour and environs. *Fiji Mineral Resources Department Memoir* **3**, 105 p.

Shorten, G.G. 1993b. Stratigraphy, sedimentology and engineering aspects of Holocene organo-calcareous silts, Suva Harbour, Fiji. *Marine Geology* **110**, 275-302.

Shorten, G.G., Shapira, A., Regnier, M., Teakle, G., Biukoto, L., Swamy, M. & Vuetibau, L. 2001. Site-specific earthquake hazard determinations in capital cities in the South Pacific. *SOPAC Technical Report* **300**, 156 p.

Shuto, N. 1993. Tsunami intensity and disasters. In: Tinti, S. ed. *Tsunamis in the world*, Kluwer Academic Publishers 19, 1897-216.

Sibson, R.H. 1986. Earthquakes and lineament infrastructure. *Philosophical Transactions of the Royal Society of London, Series A: Mathematical and Physical Sciences* **317**, 63-79.

Siegal, B.S. 1977. Significance of operator variation and the angle of illumination in lineament analysis on synoptic images. *Modern Geology* **6**, 75-85.

Singh, A. 1996. *Seismic hazard assesment of a critical structure: the Monasavu Hydro-electric Dam, Fiji*. Masters thesis, RMIT, Melbourne.

Skiba, W. 1954. Letter from W. Skiba of the Fiji Geological Survey to H.W. Wellman of the N.Z. Geological Survey. 20 March 1954.

Smith, R. (comp.) 1992a, Lomaiviti, Fiji Bathymetric Map Series Sheet **5**, 1: 250 000, Fiji Mineral Resources Department.

Smith, R. (comp.) 1992b, Viwa, Fiji Bathymetric Map Series Sheet **4**, 1: 250 000, *Fiji Mineral Resources Department.*

Smith, R. 1997. Seismic investigation, proposed new Rewa Bridge site, Viti Levu, Fiji. *SOPAC Technical Report* **249**, 17 p.

Smith, R. & Raicebe, T. (comps.) 1984, Bathymetric map of Fiji, *Fiji Mineral Resources Department.*

Solomon, S. & Kruger, J. 1996. Vulnerability and adaptation, assesment coastal impact of sea level change, Suva and vicinity, Viti Levu, Fiji Islands. *SOPAC Technical Report* **242**, 84 p.

Somerville, P.G., Smith, N.F., Graves, R.W. & Abrahamson, N.A. 1997. Modification of empirical strong ground motion attenuation relations to include the amplitude and duration effects of rupture directivity. *Seismological Research Letters* **68**, 199-222.

South Pacific Disaster Reduction Programme (SPDRP) 2002. Suva Earthquake Risk Management Scenario Pilot Project (SERMP), Summary Report Part 1. *SOPAC Joint Contribution* **139**.

Spudich, P., Joyner, W.B., Lindh, A.G., Boore, D.M., Margaris, B.M. & Fletcher, J.B. 1999. SEA99; a revised ground motion prediction relation for use in extensional tectonic regimes. *Bulletin of the Seismological Society of America* **89**, 1156-1170.

Stirling, M., Rhoades, D. & Berryman, K. 2002. Comparison of earthquake scaling relations derived from data of the instrumental and preinstrumental era. *Bulletin of the Seismological Society of America* **92**, 812-830.

Stratford, J.M.C. & Rodda, P. 2000. Late Miocene to Pliocene paleogeography of Viti Levu, Fiji Islands. *Paleogeography, Palaeoclimatology, Paleoecology* **162**, 137 - 153.

Striem, H.L. & Miloh, T. 1976. Tsunamis induced by submarine slumpings off the coast of Israel. *International Hydrographic Review* **53**, 41-55.

Sugimura, A., Maeda, Y., Matsushima, Y., Rodda, P. & Matsumoto, E. 1988. Lobau lowland, Viti Levu, Fiji. In: Yonekura, N. ed. *Sea level changes and tectonics in the middle Pacific*, Report of the HIPAC Project in 1986 and 1987, University of Tokyo, 59-65.

Sykes, L.R., Isacks, B.L. & Oliver, J. 1969. Spatial distribution of deep and shallow earthquakes of small magnitudes in the Fiji-Tonga region. *Bulletin of the Seismological Society of America* **59**, 1093-1113.

Sylvester, A.G. 1988. Strike-slip faults. *Geological Society of America Bulletin* **100**, 1666-1703.

Synolakis, C.E., Yalciner, A.C., Borrero, J.C. & Plafker, G. 2002a. Modeling of the November 3, 1994 Skagway, Alaska tsunami. In: Ewing, L. & Wallendorf, L. eds. *Solutions to coastal disasters '02, conference proceedings*, American Society of Civil Engineers.

Synolakis, C.E., Bardet, J.-P., Borrero, J.C., Davies, H.L., Okal, E.A., Silver, E.A., Sweet, S. & Tappin, D.R. 2002b. The slump origin of the 1998 Papua New Guinea tsunami. *Proceedings - Royal Society. Mathematical, Physical and Engineering Sciences* **458**, 763-789.

Tappin, D.R. & Ballance, P.F. 1994. Contributions to the sedimentary geology of 'Eua Island, Kingdom of Tonga; reworking in an oceanic forearc. In: Stevenson, A.J., Herzer, R.H. & Ballance, P.F. eds. Contributions to the marine and on-land geology and resources of the Tonga -Lau-Fiji region, *SOPAC Technical Bulletin* **8**, 1-20.

Tappin, D.R., Watts, P., McMurtry, G.M., Lafoy, Y. & Matsumoto, T. 2001. The Sissano, Papua New Guinea tsunami of July 1998; offshore evidence on the source mechanism. *Marine Geology* **175**, 1-23.

Taylor, B., Zellmer, K., Martinez, F. & Goodliffe, A.M. 1996. Sea-floor spreading in the Lau back-arc basin. *Earth and Planetary Science Letters* **144**, 35-40.

Taylor, G.K., Gascoyne, J. & Colley, H. 2000. Rapid rotation of Fiji; paleomagnetic evidence and tectonic implications. *Journal of Geophysical Research* **105**, 5771-5781.

The Fiji Times & Herald. 1953a, *Earthquakes and tidal wave strike Suva area*, September 15.

The Fiji Times & Herald. 1953b, *Dramatic details of quake related for Sydney paper*, September 25.

The Fiji Times & Herald. 1953c, *Experts review causes and effect of 1953 earthquake*, October 7.

The Fiji Times & Herald. 1953d, *Cutter had terrifying experience*, September 16.

The Fiji Times & Herald. 1953e, *Felt quake while at sea in cutter - Mr G. Houng Lee's experience*, September 24.

The Fiji Times & Herald. 1953f, *Parents saw sons ride out wave in dinghy - Frightening experience in Makaluva Passage*, September 17.

Tinti, S., Armigliato, A., Manucci, A., Pagnoni, G., Zaniboni, F., Yalciner, A.C. & Altinok, Y. 2006. The generating mechanisms of the August 17, 1999 Izmit Bay (Turkey) Tsunami; regional (tectonic) and local (mass instabilities) causes. *Marine Geology* **225**, 311-330.

Titov, V.V. & Synolakis, C.E. 1997. Extreme inundation flow during the Hokkaido-Nansei-Oki tsunami. *Geophysical Research Letters* **24**, 1315-1318.

Twichell, D.C. & Roberts, D.G. 1982. Morphology, distribution, and development of submarine canyons on the United States Atlantic continental slope between Hudson and Baltimore canyons. *Geology* **10**, 408-412.

Usher, L. 1987. *Mainly about Fiji*. Sir Leonard Usher, Suva 111-113.

Verbeeten, A.C., Crawford, A.J., Eggins, S.M. & Maillet, P. 1995 Petrology, geochemistry and tectonic implications of magmatism in northern Hunter Ridge-Kadavu Island Group (Fiji). *Proceedings of the 1995 PACRIM Congress*, 599-603

Wald, D.J., Quitoriano, V., Heaton, T. & Kanamori, H. 1999. Relationships between peak ground acceleration, peak ground velocity, and modified mercalli intensity in California. *Earthquake Spectra* **15**, 557-564.

Walters, R.A., Barnes, P., Lewis, K., Goff, J.R. & Fleming, J. in press. Locally generated tsunami along the Kaikoura coastal margin: Part2: Submarine landslides. *New Zealand Journal of Marine and Freshwater Research.*

Watts, P. 1998. Wavemaker curves for tsunamis generated by underwater landslides. *Journal of Waterway, Port, Coastal and Ocean Engineering* **124**, 127-137.

Watts, P. 2000a. Tsunami features of solid block underwater landslides. *Journal of Waterway, Port, Coastal and Ocean Engineering* **126**, 144-152.

Watts, P. 2000b. The need for underwater landslide hazards prediction. *Science of tsunami hazards* **20**, 95-101.

Watts, P. 2004. Probabilistic predictions of landslide tsunamis off Southern California. *Marine Geology* **203**, 281-301.

Watts, P. & Grilli, S.T. 2003 Underwater landslide shape, motion, deformation, and tsunami generation. *Proceedings of the 13th Offshore and Polar Engineering Conference*, ISOPE03, Honolulu, Hawaii, 3, 364-371.

Watts, P., Grilli, S.T., Kirby, J.T., Fryer, G.J. & Tappin, D.R. 2003. Landslide tsunami case studies using a Boussinesq model and a fully nonlinear tsunami generation model. *Natural Hazards and Earth System Sciences* **3**, 391-402.

Watts, P., Grilli, S.T., Tappin, D.R. & Fryer, G.J. 2005. Tsunami generation by submarine mass failure Part II : Predictive equations and case studies. *Journal of Waterway, Port, Coastal and Ocean Engineering* **131**, 298-310.

Wei, G. & Kirby, J.T. 1995. Time-dependent numerical code for Boussinesq equations. *Journal of Waterway, Port, Coastal and Ocean Engineering* **121**, 251-261.

Wei, G., Kirby, J.T., Grilli, S.T. & Subramanya, R. 1995. A fully nonlinear Bousinesq model for free surface waves. Part 1: Highly nonlinear unsteady waves. *Journal of Fluid Mechanics* **294**, 71-92.

Wells, D.L. & Coppersmith, K.J. 1994. New empirical relationships among magnitude, rupture length, rupture width, rupture area, and surface displacement. *Bulletin of the Seismological Society of America* **84**, 974-1002.

Wever, T.F. & Fiedler, H.M. 1995. Variability of acoustic turbidity in Eckernfoerde Bay (Southwest Baltic Sea) related to the annual temperature cycle. *Marine Geology* **125**, 21-27.

Wharton, M.R., Hathway, B. & Colley, H. 1995. Volcanism associated with extension in an Oligocene-Miocene arc, south-western Viti Levu. In: Smellie, J.L. ed. *Volcanism associated with extension at consuming plate margins*, Geological Society, Special Publication **81**, 95-114.

Wheeler, R.L. & Wise, D.U. 1983. Linesmanship and the practice of linear geo-art; discussion and reply. *Geological Society of America Bulletin* **94**, 1377-1379.

Whelan, P.M., Gill, J.B., Kollman, E., Duncan, R.A. & Drake, R.E. 1985. Radiometric dating of magmatic stages in Fiji. In: Scholl, D.W. & Vallier, T.L eds. *Geology and offshore resources of Pacific island arcs - Tonga region*, Circum-Pacific Council for Energy and Mineral Resources Earth Science Series **2**, 415-440.

Whiticar, M.J. 2002. Diagenetic relationships of methanogenesis, nutrients, acoustic turbidity, pockmarks and freshwater seepages in Eckernfoerde Bay. *Marine Geology* **182**, 29-53.

Wise, D.U. 1982. Linesmanship and the practice of linear geo-art. *Geological Society of America Bulletin* **93**, 886-888.

Wise, D.U. & McCrory, T.A. 1982. A new method of fracture analysis; azimuth versus traverse distance plots. *Geological Society of America Bulletin* **93**, 889-897.

Wise, D.U., Funiciello, R., Parotto, M. & Salvini, F. 1985. Topographic lineament swarms; clues to their origin from domain analysis of Italy. *Geological Society of America Bulletin* **96**, 952-967.

Yalciner, A.C., Borrero, J.C., Kanoglu, U., Watts, P., Synolakis, C.E., Imamura, F. & Anonymous 1999. Field survey of 1999 Izmit tsunami and modeling effort of new tsunami generation mechanism. *Eos, Transactions, American Geophysical Union* **80**, 751.

Yalciner, A.C., Alpar, B., Altinok, Y., Ozbay, I. & Imamura, F. 2002. Tsunamis in the Sea of Marmara; historical documents for the past, models for the future. *Marine Geology* **190**, 445-463.

APPENDICES

APPENDIX 1: Active Faulting in the Bay of Islands area.

APPENDIX 2: Report on study of the Namosi Gorge area, central southeast Viti Levu.

APPENDIX 3: Radiocarbon Age Reports.

APPENDIX 4: Modified Mercalli (MM) Intensity Scale.

APPENDIX 5: Method for testing reproducibility in lineament analysis.

APPENDIX 6: Digital fly through over offshore southeast Viti Levu.

APPENDIX 7: Comparison of methods for calculating near field tsunami amplitudes.

APPENDIX 8: Near field tsunami amplitude calculations

APPENDIX 9: 1953 coastline of Suva CBD area.

APPENDIX 10: Simulation of the 1953 Suva tsunami.

APPENDIX 11: Past seismic hazard evaluations and related activities in Fiji.

APPENDIX 12: Calculation of Maximum Credible Earthquakes.

APPENDIX 13: Calculation of peak ground acceleration and the horizontal acceleration response spectra.

APPENDIX 1

ACTIVE FAULTING IN THE BAY OF ISLANDS AREA

Introduction

During the field component of this research project attempts were made to try and identify active faulting in southeast Viti Levu. This brief report summarises the main findings of onshore and onshore surveys that were done to characterise faulting in the Bay of Islands area.

Bay of Islands

The Bay of Islands, also known as Draunibota Harbour, is located 4 km to the northwest of Suva City in southeast Viti Levu (Figure 1). It is a narrow bay, approximately 1.5 km wide and 2 km long, bound on the east by a straight stretch of coastline between Kalekana and Suvavou Peninsula, and on the west by the Bilo Peninsula and the Lami Reef. Water depth in the middle of the bay reaches up to 15 m. Five small islands occur within the bay. Nukumaroriko (Mosquito island), Vuo island (Admiralty island), Labiko island (Snake island) and Vatutaya islet occur along a straight line following the eastern margin of the bay. Draunibota island (Cave island) occurs separately in the western side of the bay.

The bedrock in the area is composed of Late Miocene-Pliocene marine formations of the Medrausucu Group that dip gently (~10^{o}) to the southeast (Figure 2). The oldest formation is the shallow to moderately deep water Veisari Sandstone c. 400 m thick, which is exposed mainly at the head of the bay, and are found on the Uduya and Naqumu Peninsulas. The Veisari Sandstone is overlain by 10 to 50 m thick Lami Limestone, which consists of reef and large foraminiferal facies. Lami Limestone is exposed on Vatutaya and Labiko islands. The deepwater Suva Marl, 180 m thick, with thin (<0.5 m) interbedded tuff layers, overlies the Lami Limestone. Mosquito island is composed entirely of this formation. All three formations are exposed in Draunibota island.

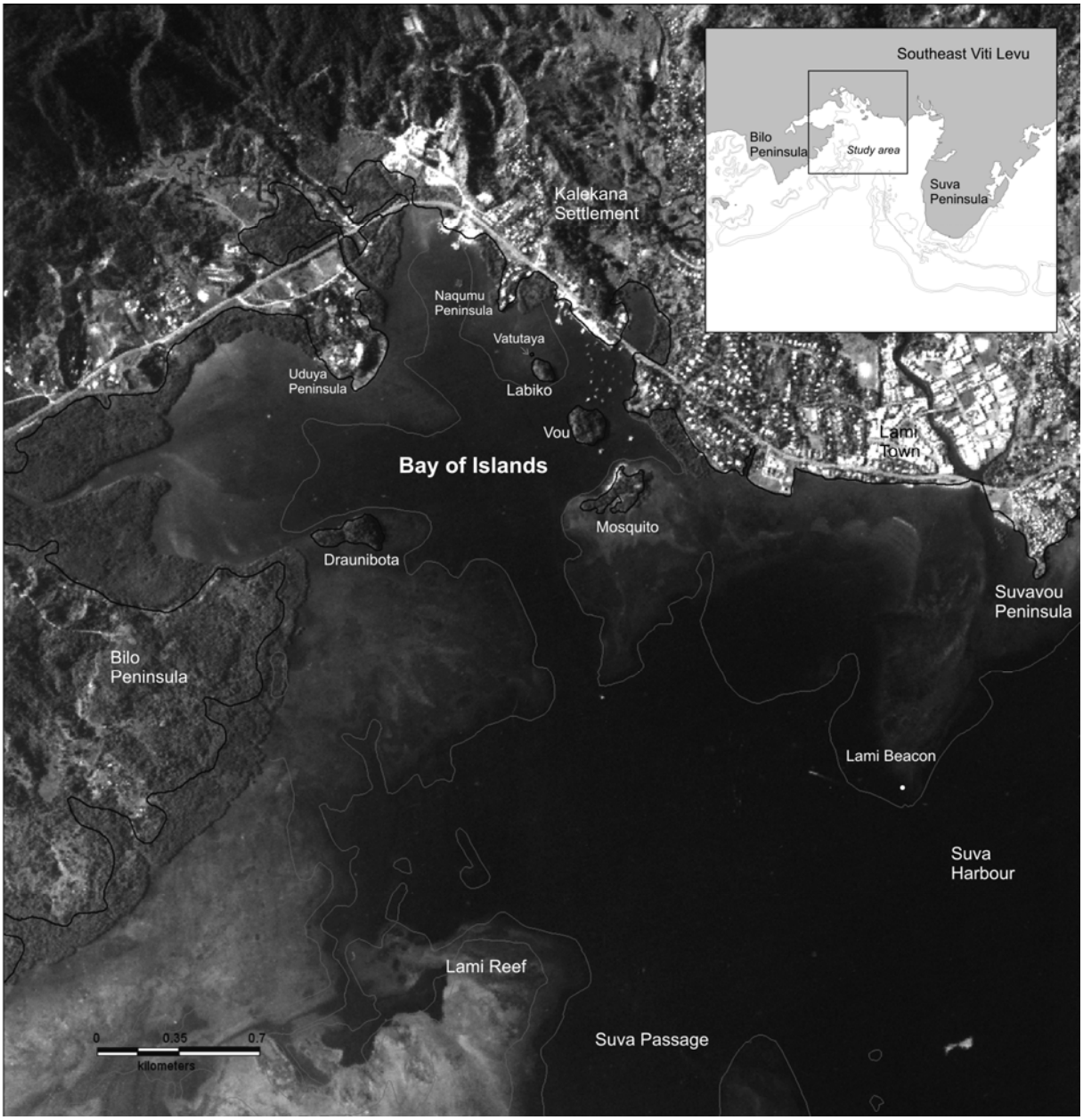

Figure 1: Locality map of the Bay of Islands.

Bay of Islands Fault Zone

The Bay of Islands fault zone is a prominent northwest trending structure in southeast Viti Levu (Section 9.3.2.2) that passes through the Bay of Islands. The fault zone exerts control of the overall shape of the bay and on the locations of the small peninsulas and islands that occur within it (Figure 2). The fault zone extends to the northwest of the bay as prominent lineaments on aerial photos. These lineaments have been verified by field mapping as a set of fractures controlling the northwest alignment of creeks on the hills behind the coastal

lowlands at the head of the bay (see Figure 4.14). This structure continues southeast of the bay, and was previously mapped near the Lami Beacon using seismic reflection profiling by Shorten (1993). Shorten refers to the structure at Lami Beacon as the Lami Beacon Fault.

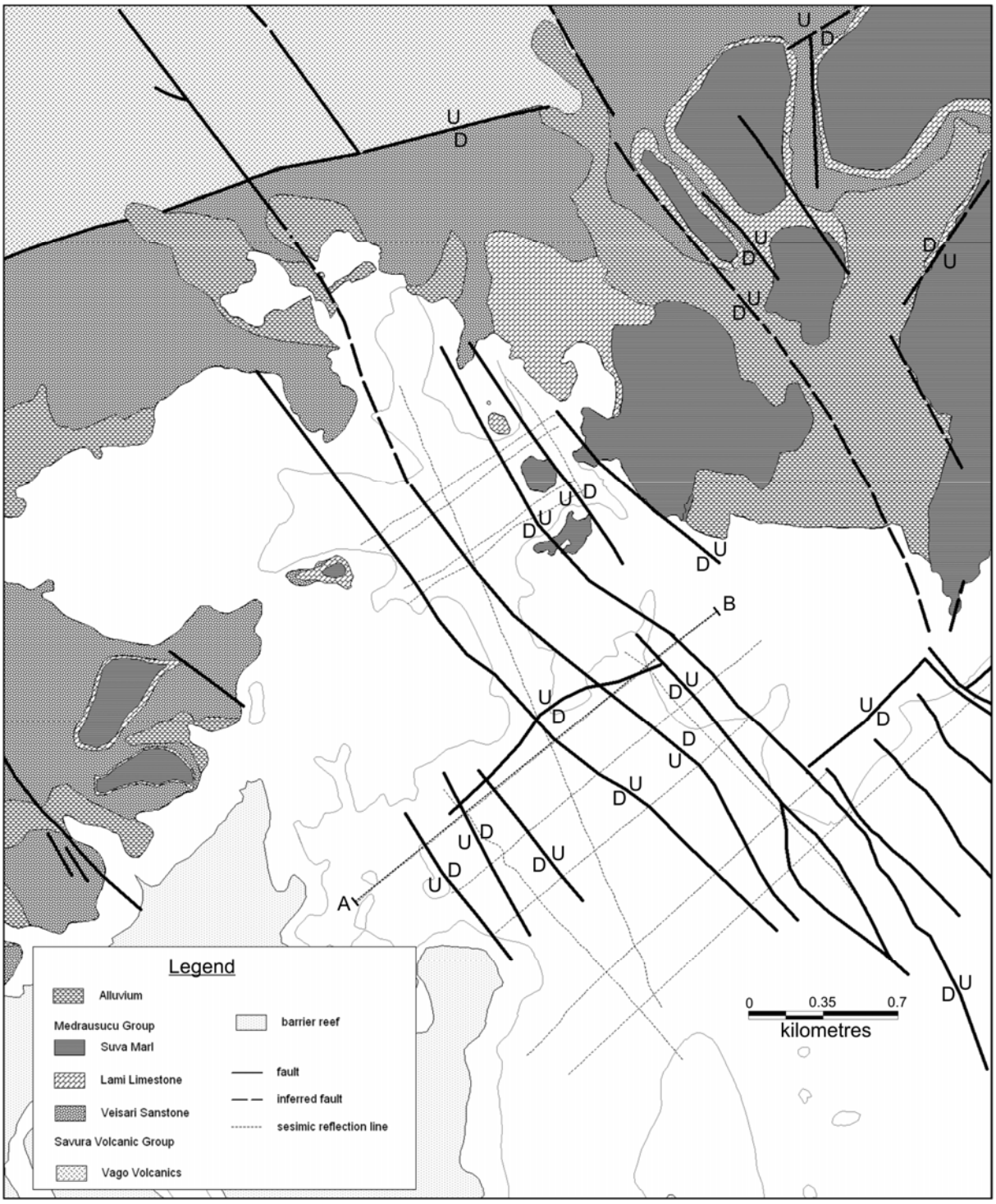

Figure 2: Geology of the Bay of Islands.

Outcrop exposures of the fault zone in the Bay of Islands area are restricted to the shoreline of

the bay and the islands and are only exposed at low tide. A zone of fracturing is mapped along the eastern edge of the bay, extending from Mosquito island to Naqumu point, passing through Vou, Labiko and Vatutaya islands. On Mosquito island and along the adjacent coast of Lami, steeply dipping and intense parallel jointing with NW strike occur in the Suva Marl. Fractures with this strike also occur along and control the western margin of Vou island (Figure 3a). Vou island appears to have a distinct tilt. The eastern coast is low laying and is lined with mangroves. It rises gently from eastern coast to the western coast, where it drops of steeply along a cliff. The cliff height increases from about 6 to 7 m to about 20 m from the southwest end to the northwest end of the island. The western coast has a narrow, 2 to 3 metre wide rock ledge (Figure 3a), beyond which the water becomes very deep, indicating a submarine cliff edge. A prominent set of vertical parallel joints, with strike directions of 290^{o}-300^{o} occur along the rock ledge along the entire western coast of the island. This joint set appears to control the cliff and the shape of the western coastline of the island. There are no apparent displacements across these fractures due to the massive nature of the Suva Marl at this location. Labiko island, composed of the Lami Limestone, has a similar morphological character as the Vou island.

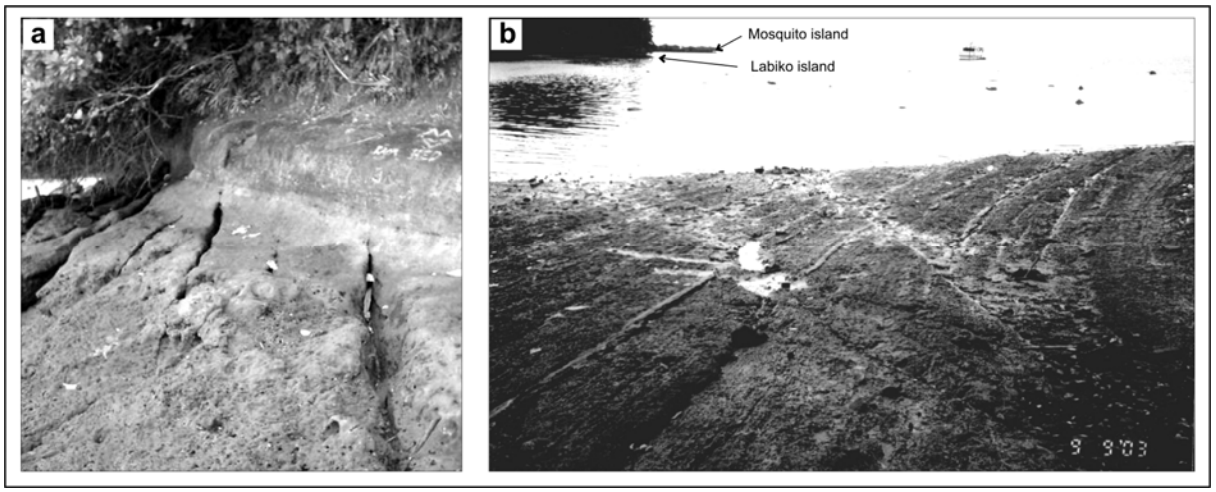

Figure 3: Outcrop exposures of the Bay of Islands Fault Zone. (a) Steeply dipping fracture sets along the western coast of Vou island. (b) Faults on the shore platform at Naqumu Point displacing strata of the Veisari Sandstone. (Photo view is to the southeast. Labiko and Mosquito islands can be seen in the background).

An excellent exposure of this fracture zone occurs on the wave cut cliff and shore platform at Naqumu Point (Figure 3b). The fracture zone is at least 20-m wide here, comprising of five northwest striking faults that clearly displace strata of the Veisari Sandstone. The faults dip steeply to the west and southwest. Slickenline lineations on the fault planes and relative

displacement of strata indicate oblique (dextral) normal movement of the faults. The Veisari Sandstone at this location dips steeply at 36^{o} to the ENE. The islands along the eastern side of the Bay of Islands and Naqumu Peninsula appear to be located on a fault bound structural block that has an overall tilted to the east.

Northwest trending joints occur along the eastern coast of Draunibota island. This eastern part of this island is topographically higher than the western part and it may represent a structural block tilted to the west.

Seismic Reflection Profiling

Seismic reflection data was acquired from within the Bay of Islands and along the southern projection of the Bay of Islands Fault Zone, between Lami Reef and the Lami Beacon. Detailed description of the method of acquisition of the dataset is presented in Section 5.2.2. Five profiles were collected from the Bay of Islands, seven from the area between Lami Beacon and Lami Reef, and one further line was done spanning the two areas (Figure 2). Individual seismic units can been identified from stratigraphic analysis of seismic profiles on the basis of their geometry, contact relationships, internal structure and reflection characteristics such as amplitude, continuity, frequency and configuration. The seismic profiles also image the near-surface expressions of the Bay of Islands Fault Zone and allowed for the mapping and extension of the fault zone to the offshore area.

Four primary seismic units are recognised in the seismic profiles (e.g. Figure 4). These are:

1. Underlaying bedrock with high amplitude parallel internal reflectors, equivalent to the onshore Late Miocene-Pliocene formations of the Medrausucu Group.

2. Broad isolated and buried reef mounds occur above the bedrock and are probably equivalent to the onshore Ucuna Limestone of Pliestocene age.

3. Up to 30 m thick lagoon fill sediments, with a clear internal reflector separating two sub-units occur above the bedrock. The top sub-unit (a), with low amplitude reflections, downlaps onto the internal reflector at the top of the lower, high amplitude sub-unit (b). The internal reflector correlates to a post glacial marine transgressive interface

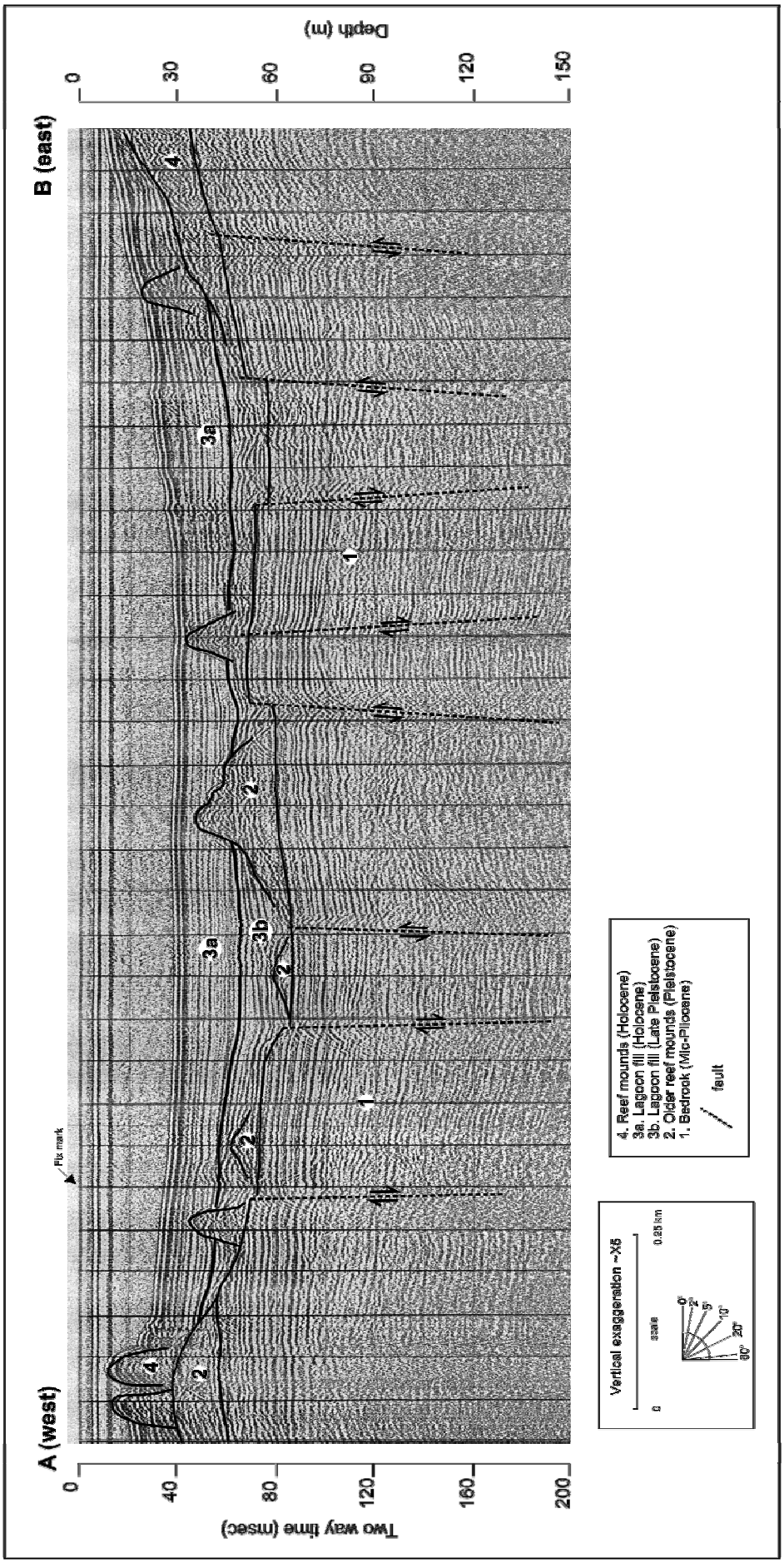

Figure 4: Interpreted seismic reflection profile across the Bay of Islands Fault Zone. Location of profile is shown in Figure 2.

logged in borehole data (Shorten 1993). This interface separates the underlaying late Pliestocene fluvio-deltaic sediments from Holocene lagoonal estuarine mud and has been dated at ~9 600 BP (Shorten, 1993).

4. Reef patches and pinnacles (Holocene) have developed above bedrock and the older reefs.

The seismic profiles clearly depicts the geometry of faulting of the Bay of Islands Fault Zone. The profiles show a number of faults offsetting reflectors within the underlaying rock (Suva Marl in Figure 4). The offsets are shown by abrupt terminations of reflectors, or by small monoclinal folds in the reflectors. The faults are often paired to form horst and graben features that range from 150 to 350 m wide and have downthrows up to 20 m. Displacements across the faults as seen in the underlaying bedrock also appear to affect the younger (Late Pleistocene to Holocene) overlaying lagoon fill seismic unit. The undulations in the internal reflector within this unit clearly appear to follow fault displacements in the underlaying bedrock. There also appears to be a correlation between the levels of reefs and faulting of bedrock. Older buried reefs occur on the downthrow side of bedrock (in grabens), while the reefs on the horsts are “alive” and at sea level. Some are still growing and have not reached sea level. It is possible that the reefs originally grew at the same level and were later downfaulted and were subsequently buried by sediments. No large offsetting fault can be interpreted in the seismic profiles. The Bay of Islands Fault Zone is composed of number of small offsetting faults that combine to control overall deformation in the area.

Emerged Tidal Notches

Emerged tidal notches occur on Draunibota island and Vatutaya island (Figure 5a,b). Geometrical characteristics of the notch profiles were measured following methods of Pirazzoli (1986). All measurements of heights were made to the sea level using stave and Brunton compass and the time of measurement were recorded. Heights were recalculated relative to Lowest Astronomical Tide (LAT) level (Fiji Datum) using tidal level predication method as in the Fiji Nautical Almanac (Anon, 2003, 2004). The LAT level in Fiji is 0.96 m below mean sea level (MSL). The spring tidal range in this area is about 1.3 m (Anon, 2004). Measurements of the notch profiles are shown in Figure 5c,d. Measurement error is ± 0.1 m.

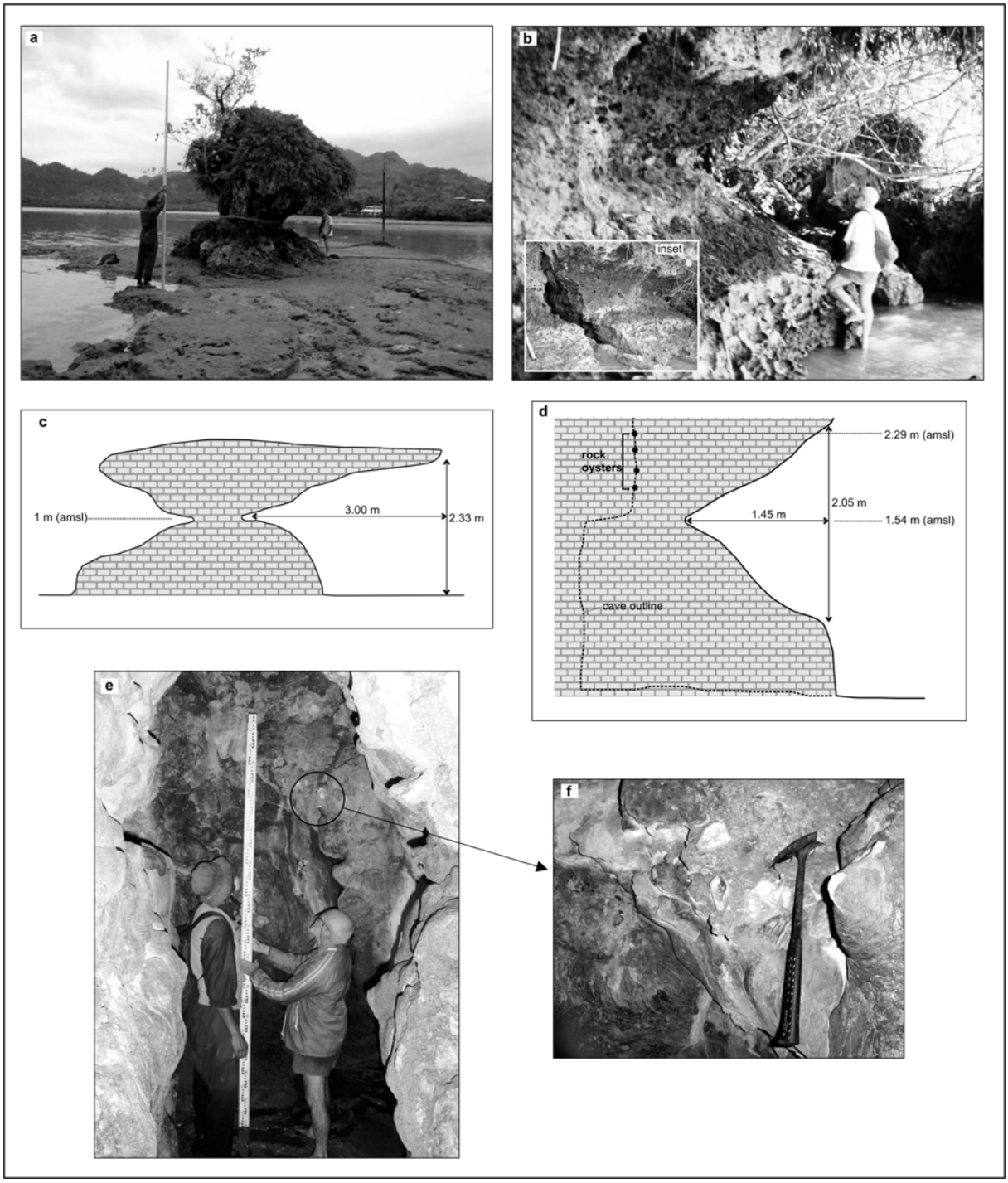

Figure 5: (a) Tidal notch at Vatuyata island. (b) Tidal notch at Draunibota island. (c) Notch profile and elevation, Vatutaya island. (d) Notch profile and location of rock oysters, Draunibota island. (e) Sea cave, Draunibota island (d) Fossilised rock oysters inside the sea cave.

In sheltered coasts the maximum retreat point of a notch occurs near MSL, the lower lip at mean low tide level, and the upper lip at mean high tide level (Pirazzoli, 1986) (Figure 6). The coasts of the Bay of Islands occur in a sheltered part of southeast Viti Levu, located at least 3.5 km inside the lagoon and protected by the barrier reefs. The geometry of notches at

Vatutaya and Draunibota can therefore be taken as indicative of sea level positions as described above.

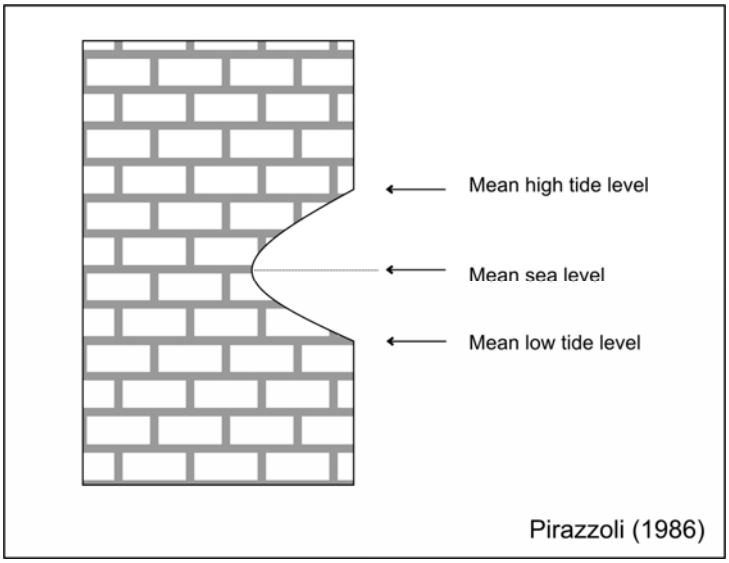

Figure 6: Tidal notch and its relation to sea level.

The tidal notch at Draunibota occurs in the Lami Limestone on the eastern coast of the island. The maximum retreat point of this notch occurs 1.54 m above present MSL, indicting the degree of emergence along this section of the coast (Figure 5d). A joint controlled cave occurs across this notch (Figure 5b inset). This cave is about 3 m in length and about 4 m high. Fossilised rock oysters were found on the walls of this cave (Figure 5e,f). The oysters occur only within a 1.20 m vertical zone, about 2 metres above the cave floor. The highest oyster was measured at 2.29 m above present MSL (Figure 5e). Rock oysters are filter feeders and have to be submerged for a period of time to survive. This means that they are inter tidal creatures. They cannot survive higher than the high tide mark, therefore their highest positions are indicative of the approximate high tide level. The position of the highest fossilized rock oyster at Draunibota occurs 0.75 m above the emerged tidal notch, and is well above the present high tide mark. The highest fossilised oyster was sampled and dated in this study by the radiocarbon method (WK15874), that yielded a conventional age of 4247 ± 34 yr BP (Libby half-life of 5568 yr) (see Appendix 3) and a calibrated age range of 4410-4160 BP* (2σ). The features mapped at Draunibota are clearly indicative of an emerged former shoreline position from the Mid-Holocene period.

Vatutuya island is mushroom shaped sea stack composed of the Lami Limestone (Figure 5a).

* Age calibrated using the OxCal v3.9 program and the South Pacific Regional mean delta-R of 43 ± 23 marine reservoir correction.

The maximum retreat point of the tidal notch on the island occurs 1.00 m above present MSL, indicating that the island has emerged by 1 m (Figure 5c). No datable material was found on the tidal notch on Vatutaya island.

Discussion

Emergence has clearly occurred at Vatutaya island and along the eastern coast of Draunibota island. The emergence can be attribute to tectonic uplift of the islands or a fall in sea level or a combination of both processes.

Mid-Holocene emerged shoreline features are known in other parts of southern Viti Levu and have been used to argue for the existence of a Mid-Holocene high sea level stand (e.g. Maeda et al., 1986; Sugimura et al., 1988; Shepherd, 1990; Nunn & Peltier, 2001). Quaternary fluctuations in sea level in the Pacific are largely attributable to glacio-eustactic changes. However, isostatic rebound from deglaciation of Antarctica, more local glacio-isostatic effects (e.g. New Zealand), hydro-isostatic deflections, large-scale climatic and gravity pertubations may also affect sea level (Clark et al., 1978; Hopley, 1987). Nunn & Peltier (2001) use Holocene paleo sea-level data from around southern Viti Levu to suggest that the post-glacial sea level reached its present level more than 6000 years BP and reached a maximum of 1.8 m at 3590-3360 years BP.

New data collected in this study in southwest Viti Levu further shows the existence of emerged Mid-Holocene features. Emerged beach rock occur almost along the entire southwest coast of Viti Levu, but only in some places along the southeast coast. Two samples of emerged beach rock, one of a clast and the other of cement, that occur 1.60 m above MSL, were collected from the coast at Vatoalailai in southwest Viti Levu for radiocarbon dating. The clasts provide the maximum age, and the cement the minimum age of the beachrock (Hopley, 1986). The acquired ages are given below (full reports are given in Appendix 3).

Beach rock clast (WK16093):
4157± 41 BP (conventional age), 4320-4040 BP* (calibrated age 2σ)
Beach rock clast (WK16094):
2323± 37 BP (conventional age), 1990-1800 BP* (calibrated age 2σ)

* Age calibrated using the OxCal v3.9 program and the South Pacific Regional mean delta-R of 38 ± 16 marine reservoir correction.

The elevation and maximum age of the beach rock is quite similar to the values obtained at Draunibota. Given the widespread and consistent nature of the data from southern Viti Levu, it is likely that there was a Mid-Holocene high sea level stand. The tidal notch at Draunibota is likely to have formed during this time. The tidal notch at Vatutaya is also possible a feature of the Mid-Holocene high sea level. Rodda and Nunn (1990) have mapped Mid-Holocene microatolls near Suva, that show emergence of 0.64 to 0.87 metres, similar to the level of emergence of Vatutaya island. These emerged microatolls occur 5 kilometres southeast of the Bay of Islands and on the same side of the Bay of Island Fault Zone as Vatutaya island.

Since the amount of emergence measured at Draunibota and Vatutaya are not the same, the Mid-Holocene high sea level stand alone cannot completely account for the measured levels of these features. It is reasonable to assume that with a higher sea level stand, tidal notches within a distance of less than a kilometre and in the same rock would have formed at the same level. It is explained here that the lower level of emerged features on the eastern side of the Bay of Islands Fault Zone is indicative of the effect tectonism associated with movement along the fault zone.

Fault block displacements associated with activity on the Bay of Islands Fault Zone is the most likely cause for the different levels of the emerged tidal notches. This occurred subsequent to the initial cutting of the notches by the Mid-Holocene high sea level stand 3000 to 4000 years BP (Figure 7). Several lines of evidence suggest that the Bay of Islands Fault Zone is still active. Tilts on the islands on the eastern side of the bay may have been the result of fault block tilting in the last few thousand years. The fracture zone that runs along the line of islands, extends to the Lami Beacon area. Tilting of basement blocks and displacement of harbour floor has occurred here as a result of movement on the fracture zone (Shorten 1993). The new seismic reflection data acquired across almost the entire width of the fault zone in this study also shows that Quaternary bay fill sediments, possibly as recent as the Holocene, are affected by fault displacements in the bedrock. Furthermore, during the 1953 Suva earthquake, a number of landslides and ground fissures occurred at Uduya point, possibly related to continued activity along the fault zone, as discussed in Section 9.3.2.4.

It is inferred from the level of the emerged shoreline features that a net displacement of 0.5 m has occurred across the Bay of Islands Fault Zone between Draunibota and Vatutaya in the last 3000 to 4000 years BP.

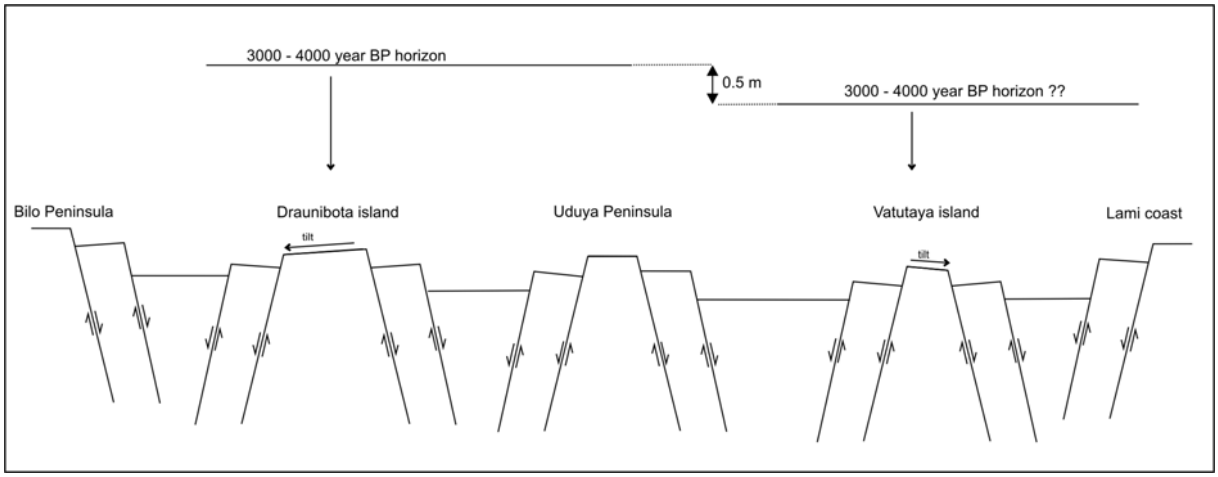

Figure 7: Diagrammatic representation of faulting across the Bay of Islands Fault Zone.

Conclusions

- The Bay of Islands Fault Zone is a prominent NE trending regional structure in southeast Viti Levu. Onshore and offshore mapping are used to trace the fault zone almost continuously from the Lami Beacon to the hills north of the Bay of Islands.
- The fault zone exerts control on the morphology of the bay and small islands that occur within it.
- Activity on the fault zone may be responsible for tilting of the islands within the bay and for displacements in Quaternary bay fill sediments.
- A net displacement of 0.5 m over a 1 km wide section of the fault zone is inferred to have occurred in the last 3000 to 4000 years BP.
- It can be drawn from the results of this study that the history of emergent features along the southeast coast of Viti Levu are more complex than has been previously assumed. The role of local vertical displacements caused by tectonic deformation along fault zones need to be carefully accounted for in studies of paleo sea levels in this area.

References

Anon 2003. *Fiji Nautical Almanac*. Hydrographic Office, Fiji Islands Maritime Safety Administration **F201**.

Anon 2004. *Fiji Nautical Almanac*. Hydrographic Office, Fiji Islands Maritime Safety Administration **F201**.

Clark, J.A., Farrell, W.E. & Peltier, W.R. 1978. Global changes in postglacial sea level; a numerical calculation. *Quaternary Research* **9**, 265-287.

Hopley, D. 1986. Beachrock as a sea level indicator. In: Van de Plassche, O. ed. *Sea-level research: a manual for the collection and evaluation of data*, Geo Books, 157-173.

Hopley, D. 1987. Holocene sea-level changes in Australasia and the southern Pacific. In: Devoy, R.J.N. ed. *Sea Surface Studies - A global review*, Croom Helm.

Maeda, Y., Miyata, T., Rodda, P., Sugimura, A., Matsumoto, E. & Matsushima, Y. 1986. Holocene sea level changes in Viti Levu and Vanua Levu, Fiji. In: Sugimura, A. ed. *Sea level changes and tectonics in the middle Pacific*, Report of the HIPAC Project in 1984 and 1985, Kobe University, 137-185.

Nunn, P.D. & Peltier, W.R. 2001. Far-Field test of the ICE - 4G Model of global isostatic response to deglaciation using empirical and theoretical Holocene seal level reconstructions for the Fiji Islands, Southwestern Pacific. *Quarternary Research* **55**, 203-214.

Pirazzoli, P.A. 1986. Marine notches. In: Van de Plassche, O. ed. *Sea-level research: a manual for the collection and evaluation of data*, Geo Books, 361-400.

Rodda, P. & Nunn, P.D. 1990. Emerged microatolls off Government House, Suva. *Fiji Mineral Resources Department Note* **BP1/92**, 3 p.

Shepherd, M.J. 1990. The evolution of a moderate energy coast in Holocene time, Pacific Harbour, Viti Levu, Fiji. *New Zealand Journal of Geology and Geophysics* **33**, 547-556.

Shorten, G.G. 1993. The geological and tectonic setting for ground failure hazards in Suva Harbour and environs. *Fiji Mineral Resources Department Memoir* **3**, 105 p.

Sugimura, A., Maeda, Y., Matsushima, Y., Rodda, P. & Matsumoto, E. 1988. Lobau lowland, Viti Levu, Fiji. In: Yonekura, N. ed. *Sea level changes and tectonics in the middle Pacific*, Report of the HIPAC Project in 1986 and 1987, University of Tokyo, 59-65.

APPENDIX 2

REPORT ON STUDY OF THE NAMOSI GORGE AREA, CENTRAL SOUTHEAST VITI LEVU.

Introduction

The Namosi Gorge is a peculiar geomorphological feature in central south east Viti Levu (Figure 1). It presently forms a wind gap between the Navua and Waidina river catchments. It has been speculated in previous studies (e.g. Terry et al., 2002; Band, 2003) that a paleo Navua-Waidina river once flowed through the Namosi Gorge. Disruption of flow of this paleo river is thought to have occurred at the Namosi Gorge, which led to southward flow the Navua river from Namuamua and which left Namosi Gorge dry. The occurrence of surficial lacustrine sediments reported by Band (2003) and Rodda (1976), east of the Namosi Gorge, is suggestive that ponding of the paleo–river system occurred during its disruption. The Namosi Gorge occurs within the Viti Levu Seismic Zone. The 1953 Suva earthquake caused numerous rock falls and landsliding in the upper Waidina River and Wainikoroiluva River areas (Figure 2). It is hypothesised that disruption of the paleo Navua–Waidina river may have similarly been caused by a large seismically triggered landslide. This report presents the results of mapping in the Namosi Gorge and upper Navua River area in order to understand the geological evolution of the area. The results of radiocarbon dating of samples collected in the area are also provided. Mapping was carried out with Michael Bonte of SOPAC in 2004.

General Physiography

The Namosi Gorge is a deep gorge within the Korobasagasaga Range. The Korobasagasaga Range is composed of pyroxene and hornblende andesite flows, volcanoclastics and intrusive rocks of the Late Miocene Namosi Andesite. The highest peaks along the Korobasasaga Range are between 800 m to 1000 m above MSL. The topography of the Korobasagasaga Range is controlled by poorly stratified andesitic volcanoclastics and series of ENE and NW fractures. The sub-horizontal Late Miocene Navua Mudstone, consisting of marine siltstones and fine grained sandstones, underlies the more gentle terrain in the west of the study area. Regionally, the boundary between the two basal formations is one of lateral gradation. In the

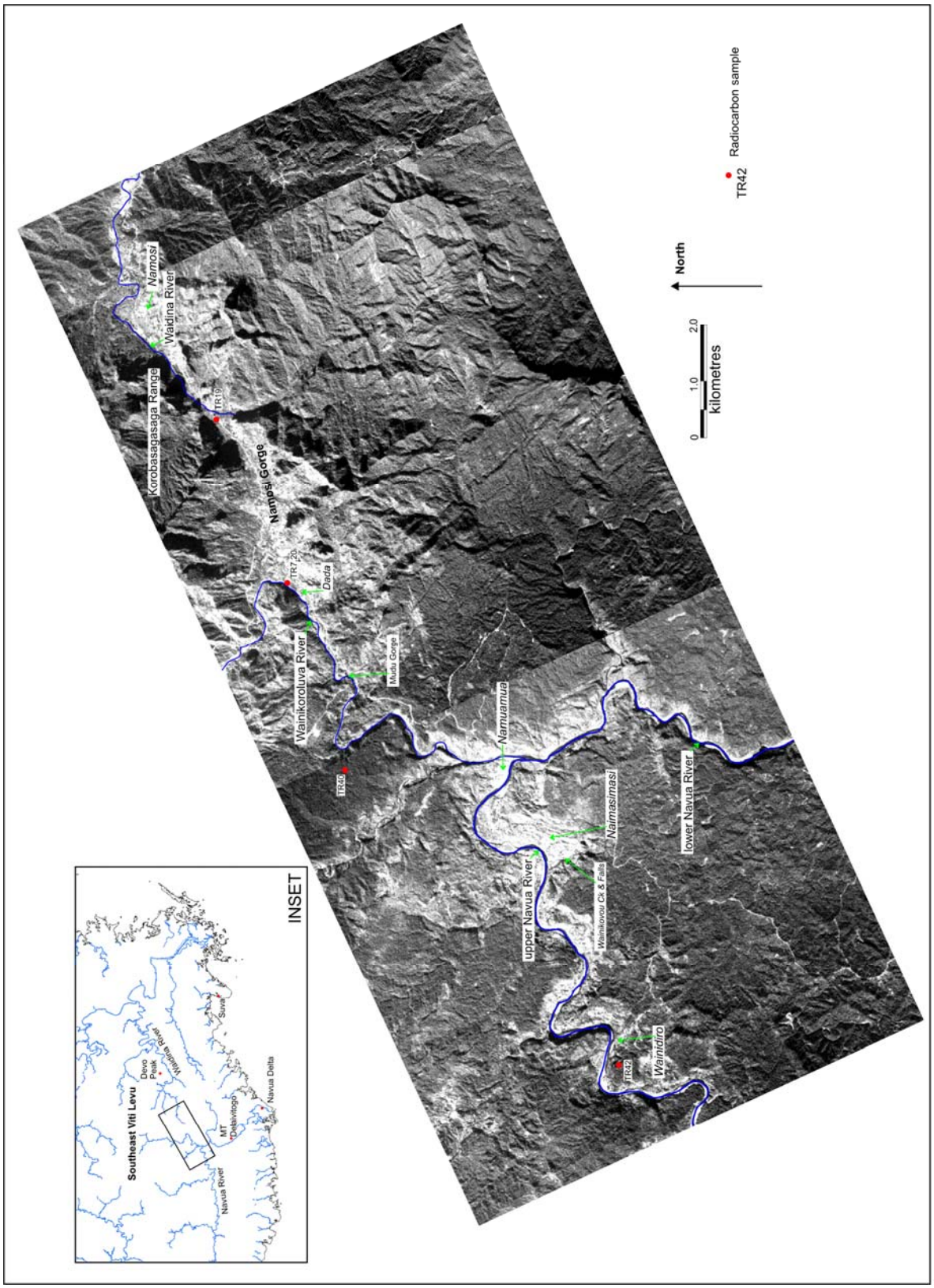

Figure 1: Locality map of the Namosi Gorge and upper Navua River area.

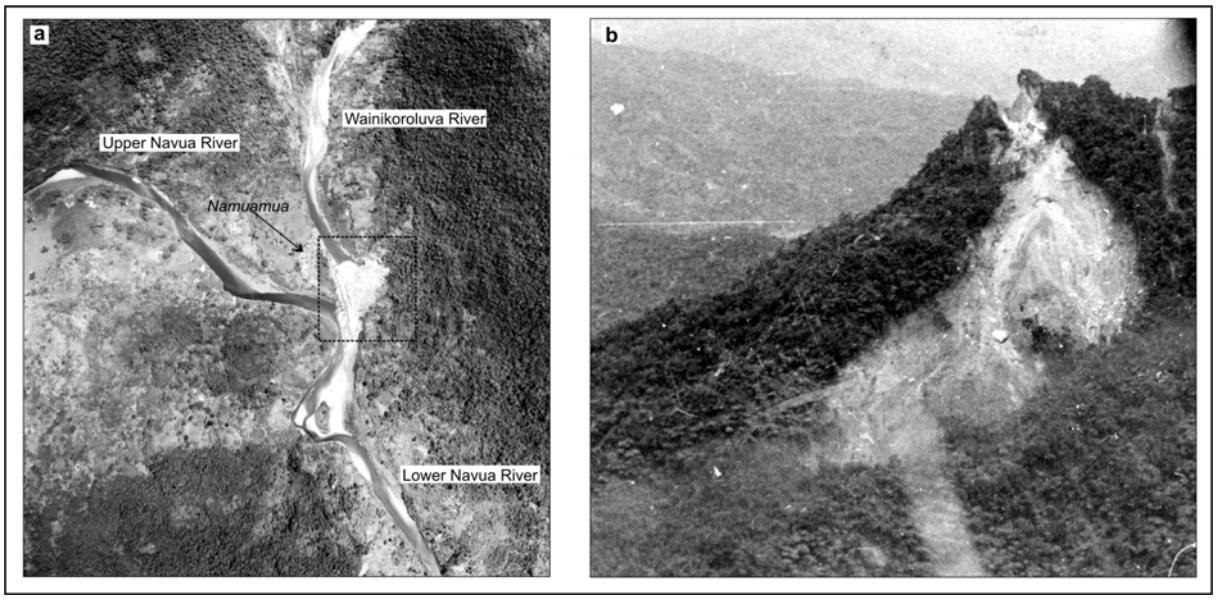

Figure 2: Landslides during the 1953 Suva earthquake (a) Lanslide partially blocking the Wainikoroluva River at Namuamua. Aerial photograph by Adastra Airways, September 1953 (b) Rock slide at the Devo Peak (660 m amsl). (Photo used with the permission of the Fiji Mineral Resources Department).

Wainikoroluva River, however, downstream from the Namosi Gorge, massive hornblende andesite appears to have intruded and tilted the Navua Mudstone.

The peaks immediately surrounding the Namosi gorge are 400 to 700 m AMSL. The gorge has a ENE trend and extends for 5.5 km from Namosi Village to a prominent bend in the Wainikoroluva River in the southwest, near Dada Settlement. The narrowest point in the gorge is in the middle section, which is about 200 m across, and is bound by vertical cliffs in the Namosi Andesite. It widens to a 700 to 900m wide valley at it two ends. At the Wainikoroluva end, the valley floor raises steeply (~6^o) from 80 to 90 m amsl at the river level to about 180 m amsl at the highest point in the valley. The valley floor to the north east of the highest point falls gradually (~2^o) to 70 m amsl at Namosi Village. The highest area in valley floor is formed by a distinct cross-valley plateau, about 250 m wide and 500 m long. This plateau forms the drainage divide between the Navua-Wainikoroluva catchment and the Waidina-Rewa catchment (Figure 3).

Stratigraphy of the Namosi Gorge area

Four main cover units are interpreted to occur above the basement Late Miocene rocks in the Namosi Gorge area. These are 1) basal landslide deposit, 2) lacustrine sediments, 3) fluvial

sediments and 4) surficial landslide/talus deposits. A general stratigraphic section of the Namosi Gorge area in given in Figure 4 and geological map is given in Figure 5. An outcrop exposure along the bank of the Wainikoroluva River, east of the Namosi Gorge, near Dada, reveals a 50 m vertical type section through the cover deposits of the Namosi Gorge area.

Figure 3: Cross valley plateau across the Namosi Gorge, looking NE from the Wainikoroluva River.

The basement rock is massive hornblende andesite flow of the Namosi Andesite. This is exposed at river level near Dada and further downstream at Mudu Gorge. The Navua Mudstone outcrops downstream of the Mudu Gorge. The massive andesite is overlain by a bouldery, poorly sorted breccia, composed of large angular andesitic agglomerate clasts ranging from 1 m to 15 m across. The boulders are set in a cobbly granular matrix (Figure 6). This deposit, about 20 m thick, is interpreted to be a basal landslide unit. This unit is overlain by a 20 m thick deposit of soft and finely laminated organic lacustrine mudstone (Figure 7). The mudstone is pale grey to black and consists of thin to finely laminated alternating layers of dark organic rich silt and paler or oxidised orange layers of inorganic fine sand. Organic material including leaves, twigs and logs are common within the deposit. Above the lacustrine unit is a 5 m thick fluvial feldspathic and quartz sand deposit that also contains coarse lenses of gravel. The gravel becomes predominant is some exposures. The base of this

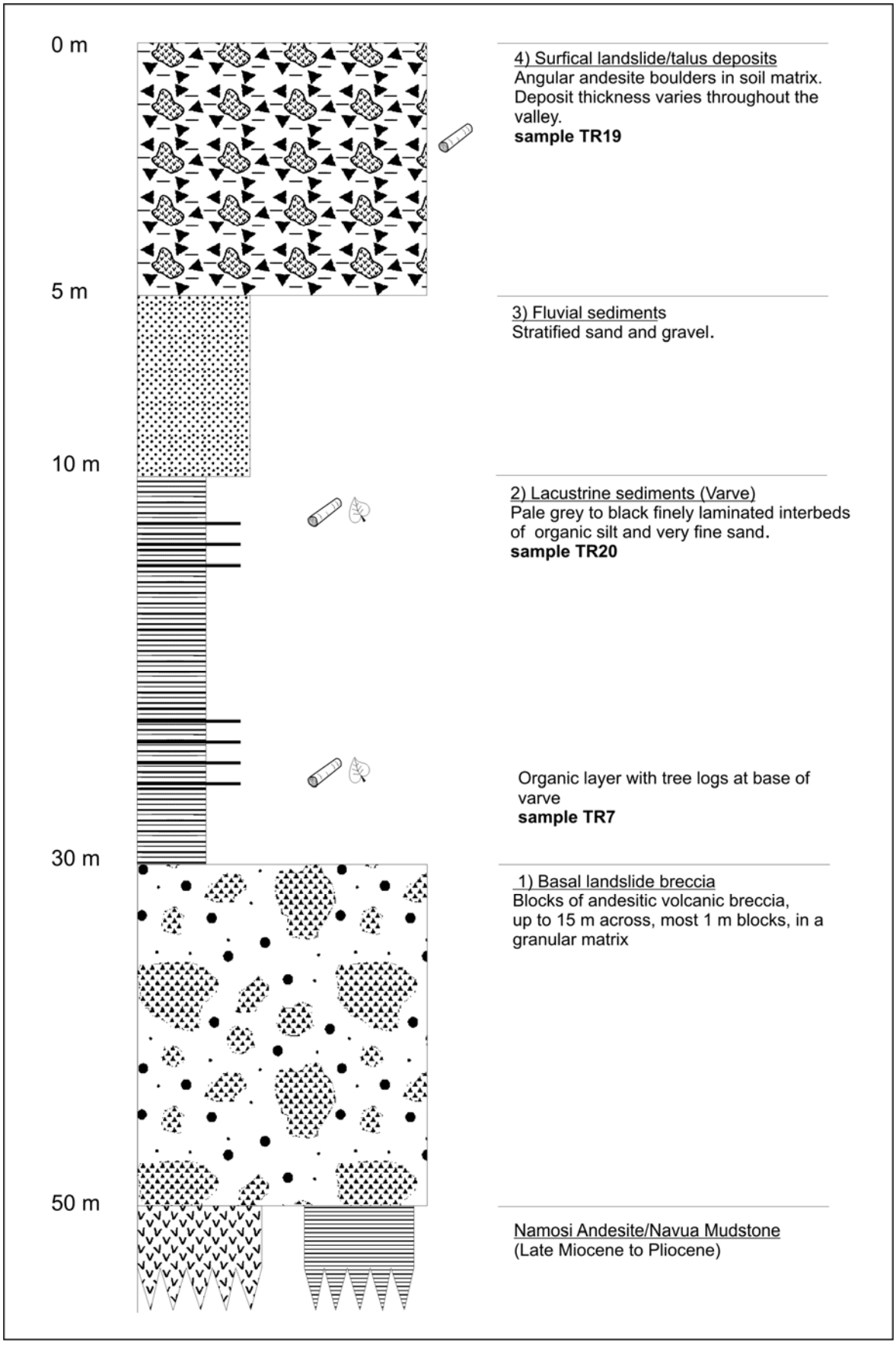

Figure 4: General stratigraphic section of cover units in the Namosi Gorge area.

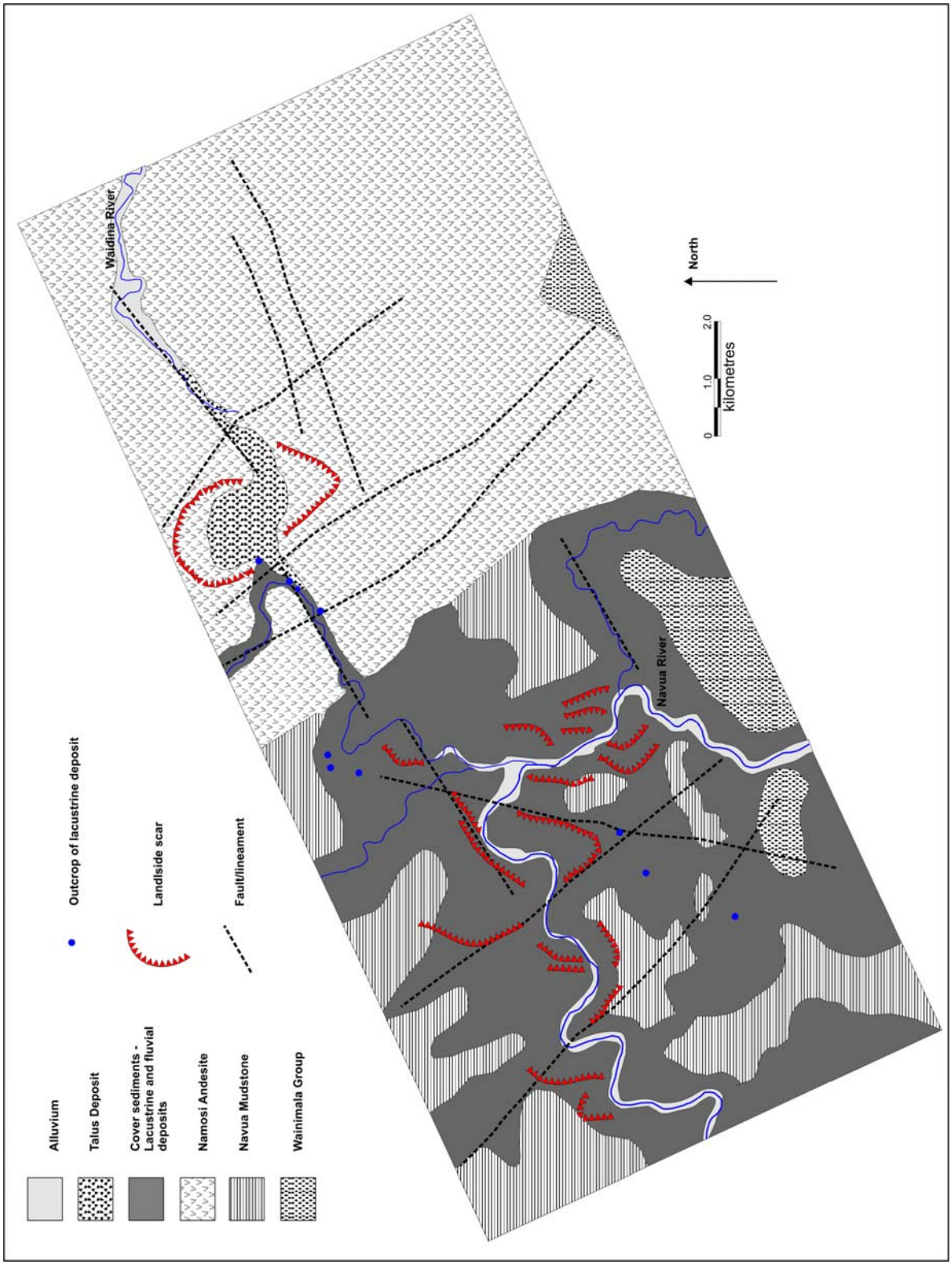

Figure 5: Geological map of the Namosi Gorge and upper Navua River area.

fluvial deposit occurs approximately 50 m above present river level. Above this is a surficial landslide/talus deposit of variable thickness that contains angular andesite boulders in soil matrix. This unit lies with an angular unconformity above the fluvial sediments.

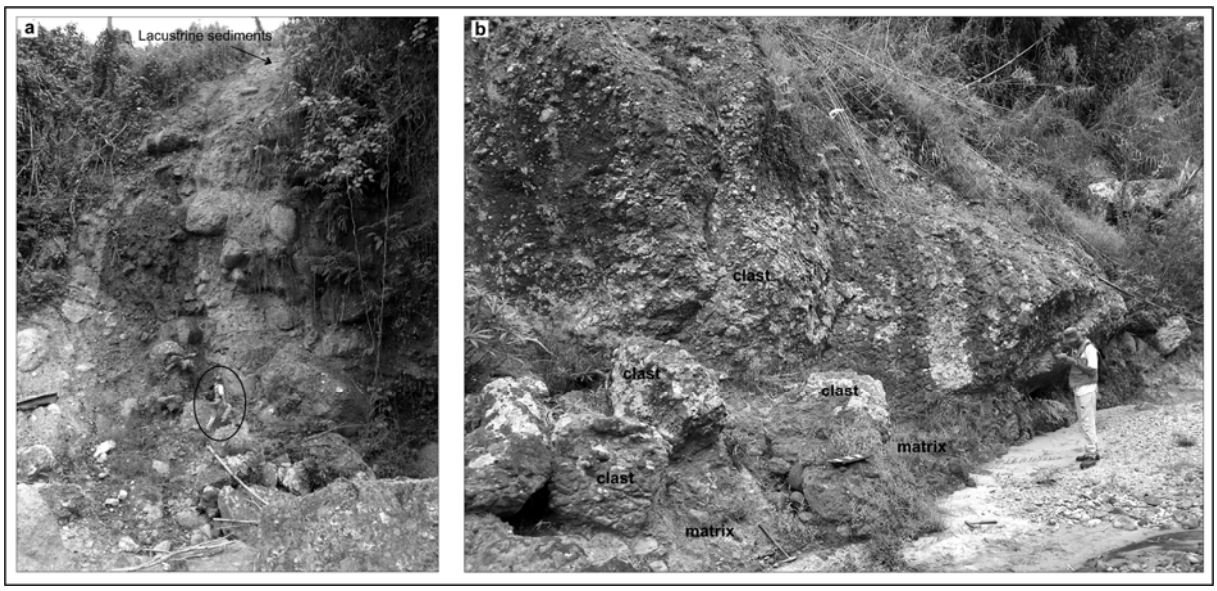

Figure 6: Basal landslide deposit. (a) Exposure at Dada showing 20 m thick landslide breccia overlain by lacustrine sediments. (b) Large angular clasts of andesitic breccia in a granular matrix.

Figure 7: Tilted lacustrine sediments overlain by fluvial gravels. Tape is 3 metre long. Inset shows convolute laminations within the lake sediments.

The occurrence of lake sediments has been confirmed in the field for seven kilometres west of the Namosi Gorge and has been found in the upper Navua River area. Liquefaction (convolute) structures are common in the lake sediments. In some sites the lake sediments are tilted by as much as 30 degrees. The fluvial sediments rests on top of the tilted lake sediments with a well-defined angular unconformity (Figure 7). The lake sediments and overlaying fluvial sediments form a distinct terrace level at 120 to 140 m amsl across the upper Navua River catchment. The terrace can be clearly seen on aerial photos and is suggestive of a drowned topography with isolated peaks of the Late Miocene Navua Mudstone surrounded by the flat terrace ground composed of the younger gravels and underlaying lacustrine sediments.

Mapping along creeks that dissect the floor of the Namosi Gorge reveals that the gorge is filled along its entire length by surficial landslide/talus material. The talus is composed of boulders of andesitic volcanic breccia derived from the adjacent surrounding ridges. The largest boulders are over 10 m across and would weigh several hundred tons (Figure 8). The boulders are embedded in a cobbly soil matrix that occasional contain tree logs.

Figure 8: Surficial landslide/talus deposit. The large boulders are about 10 m across, embedded in cobbly soil matrix.

Landslides in the Namosi Gorge and upper Navua River area

Examinations of aerial photographs of the Namosi Gorge have revealed that this area occurs at the intersection of a number of prominent structural lineaments. Some of these lineaments are active and form part of the Viti Levu Seismic Source Zone. The lineaments appear to control the location two large landslide head scarps that occur along ridges at the western end of the Namosi Gorge (Figure 5). These landslide scars occur of the steep valley walls north and south of the cross-valley plateau and are 1.5 and 1 km wide respectively.

Structural lineaments also appear to control the locations of large landslide along the upper Navua River (see Figure 1&5) between Waibogi and Naimasimasi villages. Numerous large landslides have modified the landscape along the Navua river in this area. Naimasimasi village is partially situated on a large landside, about 1.5 km wide. A number sharp ridges and gullies occur perpendicular to the slope above Naimasimasi village. These gullies have formed at the lower edge of back tilted slump blocks. River bank exposures across the base of the landslide reveal tilted intact blocks of mudstone, up to 20 m across, among broken or fragmented mudstone. The Naimasimasi landslide appears to be structurally control due zones of weakness in the bedrock caused by intersecting faults. A NW fault exposed at the Wanikavou Falls bounds the western margin of the Naimasimasi landslide. NNE trending faults exposed along the banks of Wainikavou creek are parallel to the trend of the landslide gullies and appear to control the headscarp of the slide.

Structural lineaments also control the head scarps of toppling blocks behind Wainidiro Village. Here a six NW trending tension cracks occur in the Navua Mudstone, behind an escarpment about 80 m above the Navua River level. The tension cracks form chasms in the ground, up to 50 m long, 15 m deep and 8 m wide (Figure 9). Travertine covers the lower walls of these chasms. Smaller elongate ditches and depressions parallel to the large chasms occur behind the escarpment. The deep-seated tension cracks separate large blocks of the Navua Mudstone that have toppled slightly towards the river.

Radiocarbon Dating

A number of samples were collected from the Namosi Gorge and upper Navua River area in an attempt to date the lacustrine and landslide deposits and the tension cracks by the

radiocarbon dating method. The locations of the dated samples are shown in Figure 1. The results are summarised in the table below. Full samples reports are given in Appendix 3.

Table 1: Results of radiocarbon dating in the Namosi Gap area.

sample no.	location	type	notes	Waikato sample no.	Conventional age (C^{14} yr BP)	Calibrated age* (cal yr BP) (1σ)
TR7	Wainikoroluva River - Dada	log	Base of lacustrine deposit	WK15873	42920 ± 781	-
TR19	Namosi Gorge - Waidina creek	log	Landslide deposit	WK16091	3687± 41	4090 - 3970
TR20	Wainikoroluva River - Dada	organic siltstone	Top of lacustrine deposit	WK15875	>50000	-
TR40	Nakavika Terrace	log	Lacustrine sediments	WK16095	>50000	-
TR42	Wainidiro	travertine	Tension fracture	WK16096	840 ± 35	485 - 415

Location of samples shown on Figure 1.
*Age calibrated using the OxCal v3.9 program and the South Pacific Regional mean delta-R of 43 ± 23 marine reservoir correction.

The stratigraphically inverted ages from TR7 and TR20 in the lacustrine deposit at the Dada exposure indicate contamination or redeposition. The possibilities are:

- The bottom sample (TR7) could be contaminated by younger material and is therefore too young. In this case the lake is older than 50 000 years BP. Contamination during sampling is unlikely, but contamination by CO_2 waters is a possibility, considering the high rainfall in the area. This could make the age look a lot younger than it is.

- The top sample (TR20) was from a piece of wood. It possible that it could have been transported and redeposited from an older site. In this case the age of the lake is 42 000 BP.

Since the sample from the lacustrine deposit at the Nakavika Terrace also yielded a date greater than 50 000 year, it is more likely that the lake sediments are greater than 50 000 years BP.

Discussion and Implications

The disruption of the paleo Navua-Waidina river has previously been attributed to gradual

tectonic uplift of the block east of the Namosi Gorge (Terry et al., 2002) and to river capture of the ancient headwaters of the Wadina River by the lower Navua River (Band, 2003). The existence of widespread landslides in the Namosi Gorge and upper Navua River area identified in this study allows for a new hypothesis that involves the disruption of the paleo Navua-Waidina River system by a landslide dam at the western end of the Namosi Gorge.

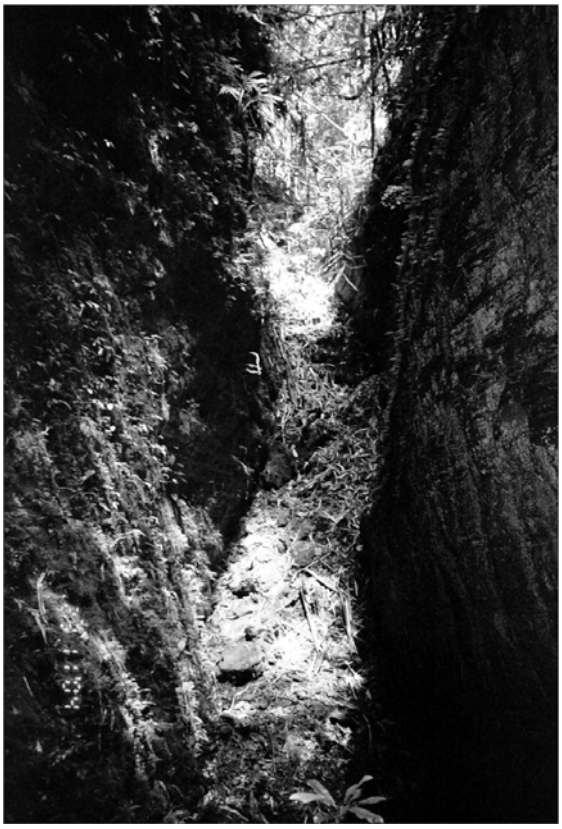

Figure 9: A 3 m wide chasm formed by a tension crack between toppling blocks of the Navua Mudstone at Wainidiro Village, upper Navua River.

The geological history of the study area as interpreted from the mapping of geomorphology and stratigraphy appears to be consistent with a large landsliding event in the Namosi Gorge, which caused widespread ponding west of the gorge for a number of thousands of years. The landslide(s) associated with the basal landslide deposit exposed along the Wainikoroluva River, underlaying the lake sediments, is most likely to be responsible for the ponding that led to deposition of the lake sediments. The event may have also been responsible for the disruption of the paleo Navua-Waidina drainage system. This landslide deposit contains large volcanic clasts which are similar to the Namosi Andesite bedrock that form the hills bounding

the western end of the Namosi Gorge. The two large slide scars mapped in this area (Figure 5) were probably the sources for this event. The cross valley plateau (Figure 3) lies directly in the run out path of the two slide scars and is inferred to be the landslide dam embankment. The valley at the western end of the Namosi Gorge is much higher (60 m) than the valley floor at eastern (Namosi Village) end. Deposition of landslide debris from the two slide scars may have locally increased the level of the valley floor at the western end of the gorge.

The level of the lake may have followed the present 160 m contour, as the top of lake deposit exposures range in heights from 140 to 160 m amsl. The inferred dam embankment height in the Namosi Gorge is 180 m. Overtopping of the lake may have occurred at the Mt Delaitogo area (Figure 1, inset). The present topography suggests that a narrow ridge, 160 to 200 m high, may have formed a drainage divide between the paleo Navua-Waidina river and the plaeo lower Navua river. Overflowing of the lake would have caused a water fall at the Delaitogo area into the paleo lower Navua River. Head ward erosion by the water fall would have caused slow breaching of the lake barrier at Delaitogo. The lake would have eventually drained flowing southward through the lower Navua River. Fluvial sediments above the lake deposits in the upper Navua River area reflect a change from lacustrine to a fluvial system. The occurrence of these fluvial deposits about 50 m above present river level, indicates that the Wainokoroluva and upper Navua River incised significantly during and following draining of the lake, probably to reach an equilibrium gradient with the base level of the lower Navua River. The deep gorge that cuts in bedrock along upper end of the lower Navua River and the Mudu Gorge in the Wainikoroluva River (Figure 10) may have formed as a consequence.

It is difficult to say with the available data what the exact age of the lake sediments is. It can only be inferred at present time that the ponding event occurred sometime before 40 000 years BP, probably in the Pleistocene period. Another dating technique, with a larger maximum limit for reliable age determinations, such as thermoluminescence and uranium series dating, will need to be applied for a more definite age of the lacustrine sediments.

The radiocarbon dates from the landslide deposit on the Namosi Gorge valley floor is too young to have been the responsible for the ponding event. The tension cracks in the upper Navua River area may also be very young. Based on the age of the travertine deposit, the fracture at Wainidiro opened as recently as 540 years ago. These two dates suggests that

Figure 10: The 30 m deep Mudu Gorge, Wainikoroluva River, cut in massive andesite.

several landsliding events may have occurred in the Namosi Gorge and upper Navua River area in the last few thousand years. Further mapping is required to identify and date these events. This will then provide a valuable database to compare with paleoseismic data and may increase our knowledge of recurrence intervals of large earthquakes of the Viti Levu Seismic Zone. For example, there is a well known Fijian legend from the Namosi area which describes an earthquake and flash flooding (Anonymous & Rodda, 1995). It is possible that the flooding would have happened after breaching of a landslide dam following a large earthquake. The age of this legend, possibly 400 to 500 years (Cronin et al. 2004, P. Geraghty pers comm. 2005), is similar to the age of the deep-seated tension crack at Wainidiro and to the inferred age of the older Suva Canyon head tsunami event (Section 7.7.2).

The understanding of landslides and ponding caused by temporary landslide dams in the area

also has implications for flooding risks for communities downstream along the lower Navua River, especially on the Navua Delta, 20 km to the south. The Navua Delta contains the Navua Town, extensive agricultural lands and is also growing in population due to the resettlement program of the Fiji Ministry of Agriculture. Sudden outburst of landslide dams are known worldwide for their long runout distances and destructive potential. The narrow Navua gorge is prone to blockages by major landsliding from the adjacent steep slopes. According to the flood legend and a reported event from the 1830s (Anonymous & Rodda, 1995), two temporary landslide dam outbursts may have happened in the Navua catchment area in the last 500 years.

Further studies of the continuous series of laminated Quaternary lake sediments identified in this study, which are rare in the humid tropics, will be very useful for several avenues of paleo-climatologic and paleo-environmental research. The lake deposit has the potential to provide an invaluable record of Quaternary climate changes in the region.

References

Anonymous & Rodda, P. 1995. A legend from Fiji: the flood. *Fiji Mineral Resources Department Note* **BP1/112**, 5 p.

Band, R.B. 2003. Geomorphological aspects of the Namosi Gap. *Fiji Mineral Resources Department Note* **BP30/39**, 2 p.

Cronin, S., Ferland, M.A. & Terry, J.P. 2004. Nabukelevu volcano (Mt. Washington), Kadavu - a source of hitherto unknown volcanic hazard in Fiji. *Journal of Volcanology and Geothermal Research* **131**, 371-396.

Rodda, P. 1976. Geology of northern and central Viti Levu. *Fiji Mineral Resources Division Bulletin* **3**,160 p.

Terry, J.P., Ollier, C. & Pain, C.F. 2002. Geomorphological evolution of the Navua River, Fiji. *Physical Geography* **23**, 418-426.

APPENDIX 3

RADIOCARBON AGE REPORTS

The full sample reports from the University of Waikato - Radiocarbon Dating Laboratory on samples collected and dated in this study are given in the following pages.

The University of Waikato

Radiocarbon Dating Laboratory

Private Bag 3105
Hamilton,
New Zealand.
Fax +64 7 838 4192
Ph +64 7 838 4278
email c14@waikato.ac.nz
Head: Dr Alan Hogg

Report on Radiocarbon Age Determination for Wk- 15873

Submitter	T Rahiman
Submitter's Code	TR7
Site & Location	Dada, Wainikoroluva River bank, Western Namosi Gap, Viti Levu, Fiji
Sample Material	Wood
Physical Pretreatment	Surfaces scraped clean. The wood was chopped up into small splinters and washed in ultrasonic bath.
Chemical Pretreatment	Sample was washed in hot 10% HCl, rinsed and treated with hot 1% NaOH. The NaOH insoluble fraction was treated with hot 10% HCl, filtered, rinsed and dried.

$d^{14}C$	-995.3 ± 0.4	‰
$\delta^{13}C$	-28.4 ± 0.2	‰
$D^{14}C$	-995.2 ± 0.4	‰
% Modern	0.5 ± 0.0	%
Result	**42,920 ± 781 BP**	

Comments

Alt Hogg

12/1/05

- Result is *Conventional Age or % Modern* as per Stuiver and Polach, 1977, Radiocarbon 19, 355-363. This is based on the Libby half-life of 5568 yr with correction for isotopic fractionation applied. This age is normally quoted in publications and must include the appropriate error term and Wk number.
- Quoted errors are 1 standard deviation due to counting statistics multiplied by an experimentally determined Laboratory Error Multiplier of 1 .
- The isotopic fractionation, $\delta^{13}C$, is expressed as ‰ wrt PDB.
- Results are reported as *% Modern* when the conventional age is younger than 200 yr BP.

The University of Waikato

Radiocarbon Dating Laboratory

Private Bag 3105
Hamilton,
New Zealand.
Fax +64 7 838 4192
Ph +64 7 838 4278
email c14@waikato.ac.nz
Head: Dr Alan Hogg

Report on Radiocarbon Age Determination for Wk- 15874

Submitter	T Rahiman
Submitter's Code	TR15
Site & Location	Draunibota Island, Suva, Fiji
Sample Material	Rock oyster
Physical Pretreatment	Surfaces drilled.
Chemical Pretreatment	Sample acid washed using 2 M dil. HCl for 100 seconds, rinsed and dried.

$d^{14}C$	-378.1 ± 2.6	‰
$\delta^{13}C$	1.1 ± 0.2	‰
$D^{14}C$	-410.6 ± 2.5	‰
% Modern	58.9 ± 0.2	%
Result	**4247 ± 34 BP**	

Comments

Ali Hogg
12/1/05

- Result is *Conventional Age or % Modern* as per Stuiver and Polach, 1977, Radiocarbon 19, 355-363. This is based on the Libby half-life of 5568 yr with correction for isotopic fractionation applied. This age is normally quoted in publications and must include the appropriate error term and Wk number.
- Quoted errors are 1 standard deviation due to counting statistics multiplied by an experimentally determined Laboratory Error Multiplier of 1 .
- The isotopic fractionation, $\delta^{13}C$, is expressed as ‰ wrt PDB.
- Results are reported as *% Modern* when the conventional age is younger than 200 yr BP.

The University of Waikato

Radiocarbon Dating Laboratory

Private Bag 3105
Hamilton,
New Zealand.
Fax +64 7 838 4192
Ph +64 7 838 4278
email c14@waikato.ac.nz
Head: Dr Alan Hogg

Report on Radiocarbon Age Determination for Wk- 15875

Submitter	T Rahiman
Submitter's Code	TR20
Site & Location	Dada - Wainikeroluva River Bank, Viti Levu, Fiji
Sample Material	Wood
Physical Pretreatment	Surfaces scraped clean. The wood was chopped up into small splinters.
Chemical Pretreatment	Sample was washed in hot 10% HCl, rinsed and treated with hot 1% NaOH. The NaOH insoluble fraction was treated with hot 10% HCl, filtered, rinsed and dried.

$d^{14}C$	-999.8 ± 0.4	‰
$\delta^{13}C$	-31.4 ± 0.2	‰
$D^{14}C$	-999.8 ± 0.4	‰
% Modern	0.0 ± 0.0	%

Result >50,000 BP

Comments

Alan Hogg
12/1/05

- Result is *Conventional Age or % Modern* as per Stuiver and Polach, 1977, Radiocarbon 19, 355-363. This is based on the Libby half-life of 5568 yr with correction for isotopic fractionation applied. This age is normally quoted in publications and must include the appropriate error term and Wk number.
- Quoted errors are 1 standard deviation due to counting statistics multiplied by an experimentally determined Laboratory Error Multiplier of 1 .
- The isotopic fractionation, $\delta^{13}C$, is expressed as ‰ wrt PDB.
- Results are reported as *% Modern* when the conventional age is younger than 200 yr BP.

The University of Waikato

Radiocarbon Dating Laboratory

Private Bag 3105
Hamilton,
New Zealand.
Fax +64 7 838 4192
Ph +64 7 838 4278
email c14@waikato.ac.nz
Head: Dr Alan Hogg

Report on Radiocarbon Age Determination for Wk- 15876

Submitter	T Rahiman
Submitter's Code	TR27
Site & Location	Waqanake reef flat, Suva, Fiji
Sample Material	Coral
Physical Pretreatment	Sample was crushed. Tested for recrystalisation: aragonite selected for dating.
Chemical Pretreatment	Sample was washed in 2M HCl for 200 seconds.

$d^{14}C$	-135.2 ± 3.3	‰
$\delta^{13}C$	-1.1 ± 0.2	‰
$D^{14}C$	-176.6 ± 3.1	‰
% Modern	82.3 ± 0.3	%
Result	**1561 ± 30 BP**	

Comments

AGHogg

12/1/05

- Result is *Conventional Age or % Modern* as per Stuiver and Polach, 1977, Radiocarbon 19, 355-363. This is based on the Libby half-life of 5568 yr with correction for isotopic fractionation applied. This age is normally quoted in publications and must include the appropriate error term and Wk number.
- Quoted errors are 1 standard deviation due to counting statistics multiplied by an experimentally determined Laboratory Error Multiplier of 1 .
- The isotopic fractionation, $\delta^{13}C$, is expressed as ‰ wrt PDB.
- Results are reported as *% Modern* when the conventional age is younger than 200 yr BP.

The University of Waikato

Radiocarbon Dating Laboratory

Private Bag 3105
Hamilton,
New Zealand.
Fax +64 7 838 4192
Ph +64 7 838 4278
email c14@waikato.ac.nz
Head: Dr Alan Hogg

Report on Radiocarbon Age Determination for Wk- 16091

Submitter	T Rahiman
Submitter's Code	TR19
Site & Location	Namosi Gap, SE Viti Levu, Fiji
Sample Material	Wood
Physical Pretreatment	Surfaces scraped clean. The wood was chopped up into small splinters.
Chemical Pretreatment	Sample was washed in hot 10% HCl, rinsed and treated with hot 1% NaOH. The NaOH insoluble fraction was treated with hot 10% HCl, filtered, rinsed and dried.

$d^{14}C$	-371.5 ± 3.2	‰
$\delta^{13}C$	-27.7 ± 0.2	‰
$D^{14}C$	-368.1 ± 3.2	‰
% Modern	63.2 ± 0.3	%
Result	**3687 ± 41 BP**	

Comments

AGHogg

15/2/05

- Result is *Conventional Age or % Modern* as per Stuiver and Polach, 1977, Radiocarbon 19, 355-363. This is based on the Libby half-life of 5568 yr with correction for isotopic fractionation applied. This age is normally quoted in publications and must include the appropriate error term and Wk number.
- Quoted errors are 1 standard deviation due to counting statistics multiplied by an experimentally determined Laboratory Error Multiplier of 1 .
- The isotopic fractionation, $\delta^{13}C$, is expressed as ‰ wrt PDB.
- Results are reported as *% Modern* when the conventional age is younger than 200 yr BP.

The University of Waikato

Radiocarbon Dating Laboratory

Private Bag 3105
Hamilton,
New Zealand.
Fax +64 7 838 4192
Ph +64 7 838 4278
email c14@waikato.ac.nz
Head: Dr Alan Hogg

Report on Radiocarbon Age Determination for Wk- 16093

Submitter	T Rahiman
Submitter's Code	TR38
Site & Location	Votualailai coast, S Viti Levu, Fiji
Sample Material	Beach rock clast (clam shell)
Physical Pretreatment	Surface removed. Tested for recrystalisation: aragonite.
Chemical Pretreatment	Sample was washed in 2M HCl for 120 seconds.

$d^{14}C$	-368.4 ± 3.2	‰
$\delta^{13}C$	3.2 ± 0.2	‰
$D^{14}C$	-404.0 ± 3.0	‰
% Modern	59.6 ± 0.3	%
Result	**4157 ± 41 BP**	

Comments

Alan Hogg
15/2/05

- Result is *Conventional Age or % Modern* as per Stuiver and Polach, 1977, Radiocarbon 19, 355-363. This is based on the Libby half-life of 5568 yr with correction for isotopic fractionation applied. This age is normally quoted in publications and must include the appropriate error term and Wk number.
- Quoted errors are 1 standard deviation due to counting statistics multiplied by an experimentally determined Laboratory Error Multiplier of 1 .
- The isotopic fractionation, $\delta^{13}C$, is expressed as ‰ wrt PDB.
- Results are reported as *% Modern* when the conventional age is younger than 200 yr BP.

The University of Waikato

Radiocarbon Dating Laboratory

Private Bag 3105
Hamilton,
New Zealand.
Fax +64 7 838 4192
Ph +64 7 838 4278
email c14@waikato.ac.nz
Head: Dr Alan Hogg

Report on Radiocarbon Age Determination for Wk- 16094

Submitter	T Rahiman
Submitter's Code	TR39
Site & Location	Votualailai coast, S Viti Levu, Fiji
Sample Material	Beach rock cement
Physical Pretreatment	Sample was crushed.
Chemical Pretreatment	None.

$d^{14}C$	-208.9 ± 3.6	‰
$\delta^{13}C$	1.6 ± 0.2	‰
$D^{14}C$	-251.1 ± 3.5	‰
% Modern	74.9 ± 0.3	%
Result	**2323 ± 37 BP**	

Comments

A G Hogg
15/2/05

- Result is *Conventional Age or % Modern* as per Stuiver and Polach, 1977, Radiocarbon 19, 355-363. This is based on the Libby half-life of 5568 yr with correction for isotopic fractionation applied. This age is normally quoted in publications and must include the appropriate error term and Wk number.
- Quoted errors are 1 standard deviation due to counting statistics multiplied by an experimentally determined Laboratory Error Multiplier of 1 .
- The isotopic fractionation, $\delta^{13}C$, is expressed as ‰ wrt PDB.
- Results are reported as *% Modern* when the conventional age is younger than 200 yr BP.

The University of Waikato

Radiocarbon Dating Laboratory

Private Bag 3105
Hamilton,
New Zealand.
Fax +64 7 838 4192
Ph +64 7 838 4278
email c14@waikato.ac.nz
Head: Dr Alan Hogg

Report on Radiocarbon Age Determination for Wk- 16095

Submitter	T Rahiman
Submitter's Code	TR40
Site & Location	Nakavika Terrace, Namosi, SE Viti Levu, Fiji
Sample Material	Wood
Physical Pretreatment	Surfaces scraped clean. The wood was chopped up into small splinters.
Chemical Pretreatment	Sample was washed in hot 10% HCl, rinsed and treated with hot 1% NaOH. The NaOH insoluble fraction was treated with hot 10% HCl, filtered, rinsed and dried.

$d^{14}C$	-1000.4 ± 0.5	‰
$\delta^{13}C$	-27.5 ± 0.2	‰
$D^{14}C$	-1000.4 ± 0.5	‰
% Modern	0.0 ± 0.1	%

Result **>50,000 BP**

Comments

A G Hogg

15/2/05

- Result is *Conventional Age or % Modern* as per Stuiver and Polach, 1977, Radiocarbon 19, 355-363. This is based on the Libby half-life of 5568 yr with correction for isotopic fractionation applied. This age is normally quoted in publications and must include the appropriate error term and Wk number.
- Quoted errors are 1 standard deviation due to counting statistics multiplied by an experimentally determined Laboratory Error Multiplier of 1 .
- The isotopic fractionation, $\delta^{13}C$, is expressed as ‰ wrt PDB.
- Results are reported as *% Modern* when the conventional age is younger than 200 yr BP.

The University of Waikato

Radiocarbon Dating Laboratory

Private Bag 3105
Hamilton,
New Zealand.
Fax +64 7 838 4192
Ph +64 7 838 4278
email c14@waikato.ac.nz
Head: Dr Alan Hogg

Report on Radiocarbon Age Determination for Wk- 16096

Submitter	T Rahiman
Submitter's Code	TR42
Site & Location	Wainidiro, SE Viti Levu, Fiji
Sample Material	Travertime
Physical Pretreatment	Surfaces removed.
Chemical Pretreatment	Sample was washed in 2M HCl for 120 seconds.

$d^{14}C$	-58.8 ± 4.1	‰
$\delta^{13}C$	-3.5 ± 0.2	‰
$D^{14}C$	-99.3 ± 3.9	‰
% Modern	90.1 ± 0.4	%
Result	**840 ± 35 BP**	

Comments

A Hogg
15/2/05

- Result is *Conventional Age or % Modern* as per Stuiver and Polach, 1977, Radiocarbon 19, 355-363. This is based on the Libby half-life of 5568 yr with correction for isotopic fractionation applied. This age is normally quoted in publications and must include the appropriate error term and Wk number.
- Quoted errors are 1 standard deviation due to counting statistics multiplied by an experimentally determined Laboratory Error Multiplier of 1 .
- The isotopic fractionation, $\delta^{13}C$, is expressed as ‰ wrt PDB.
- Results are reported as *% Modern* when the conventional age is younger than 200 yr BP.

APPENDIX 4

MODIFIED MERCALLI (MM) INTENSITY SCALE

The following is an abbreviated description of the 12 levels of Modified Mercalli intensity.

I. Not felt except by a very few under especially favourable conditions.

II. Felt only by a few persons at rest, especially on upper floors of buildings.

III. Felt quite noticeably by persons indoors, especially on upper floors of buildings. Many people do not recognize it as an earthquake. Standing motor cars may rock slightly. Vibrations similar to the passing of a truck. Duration estimated.

IV. Felt indoors by many, outdoors by few during the day. At night, some awakened. Dishes, windows, doors disturbed; walls make cracking sound. Sensation like heavy truck striking building. Standing motor cars rocked noticeably.

V. Felt by nearly everyone; many awakened. Some dishes, windows broken. Unstable objects overturned. Pendulum clocks may stop.

VI. Felt by all, many frightened. Some heavy furniture moved; a few instances of fallen plaster. Damage slight.

VII. Damage negligible in buildings of good design and construction; slight to moderate in well-built ordinary structures; considerable damage in poorly built or badly designed structures; some chimneys broken.

VIII. Damage slight in specially designed structures; considerable damage in ordinary substantial buildings with partial collapse. Damage great in poorly built structures. Fall of chimneys, factory stacks, columns, monuments, walls. Heavy furniture overturned.

IX. Damage considerable in specially designed structures; well-designed frame structures thrown out of plumb. Damage great in substantial buildings, with partial collapse. Buildings shifted off foundations.

X. Some well-built wooden structures destroyed; most masonry and frame structures destroyed with foundations. Rails bent.

XI. Few, if any (masonry) structures remain standing. Bridges destroyed. Rails bent greatly.

XII. Damage total. Lines of sight and level are distorted. Objects thrown into the air.

(adopted from USGS webpage URL: http://neic.usgs.gov/neis/general/mercalli.html)

APPENDIX 5

METHOD FOR TESTING REPRODUCIBILITY IN LINEAMENT ANALYSIS

In this study the two sets of lineament data were generated from mapping of lineaments on the digital terrain model (DTM), Side Looking Airborne Radar (SLAR) and the first vertical derivative of total magnetic intensity (1VD) images, in two trials separated by a period of 6 months. Below is an outline of the method used for testing the reproducibility of lineaments from the two data sets.

Multiple Trial Reproducibility Tests

The two lineament data sets for DTM, SLAR and 1VD images were checked for reproducibility by using specified criteria for spatial coincidence in GIS. In this study coincident lineaments were specified using same criteria as Mabee et al. (1994), that is as those that have azimuths within $\pm 5^{o}$ and the separation distances are within 1- 2 mm at the scale of mapping. So in this case the maximum separation distance for DEM, SLAR and the 1VD images, interpreted at the maximum scale of 1:150 000, was 300 m. The reproducibility tests were done in MapInfo GIS software using a combination of buffer analysis and querying techniques. The outline of the procedure is given below and illustrated in Figure 1a,b,c,d and e.

Lets take for example L1 and L2 as the two lineament maps for the same image. In this procedure a subset of L1 will be created in which all the lineaments are similar to L2 lineaments according to the criteria stated above. This subset of L1 represents all lineaments in L1 that are reproduced from L2.

Step 1: In the first step, buffer polygons are created around the L1 lineaments with 300 m radius. The buffer polygons are assigned the same attributes as the lines from which they were created using SQL Select query.

Step 2: The SQL Select is used to query for all polygons in the L1 buffer polygon map that

intersects lineaments in L2 map. The intersect operator selects polygons where there is at least one point common between the polygons in L1 and lineaments in L2. This means that all buffer polygons are selected that have *any part* of a lineament in L2 positioned *at the most* 300 m away. This satisfies the first criteria for spatial coincidence.

The result of this query is a table of selected polygons that have original attributes combined with that of the lineaments that meet the criteria. If a buffer polygon intersects more than one lineament from L2, then the buffer polygon is selected more than once, each time assigned with attributes of the L1 lineament and the L2 lineament it intersects.

Step 3: Two additional columns are added to the table of the selected polygons table from step 2. These two columns are named 'max line trend' and 'min line trend' and are updated with values of the selected L2 lineament azimuths added by 5 degrees and subtracted by 5 degrees respectively.

Step 4: The SQL Select is used to select all buffer polygons where the lineament trend associated with the buffer polygon less than 'max line trend' of the L2 lineament and greater than 'min line trend' of the L2 lineament.

The result of this query satisfies the second criteria for spatial coincidence and selects buffer polygons which correspond to *reproducible* L1 lineaments.

Step 5: The SQL Select is then used to select lineaments from L1 that occur within the selected buffer polygons of step 4. The selected L1 lineaments are *reproducible lineaments.*

Non reproducibly lineaments were removed from the database.

Reference

Mabee, S.B., Hardcastle, K.C. & Wise, D.U. 1994, A method of collecting and analyzing lineaments for regional-scale fractured-bedrock aquifer studies, *Ground* Water **32**, 6: 884-894.

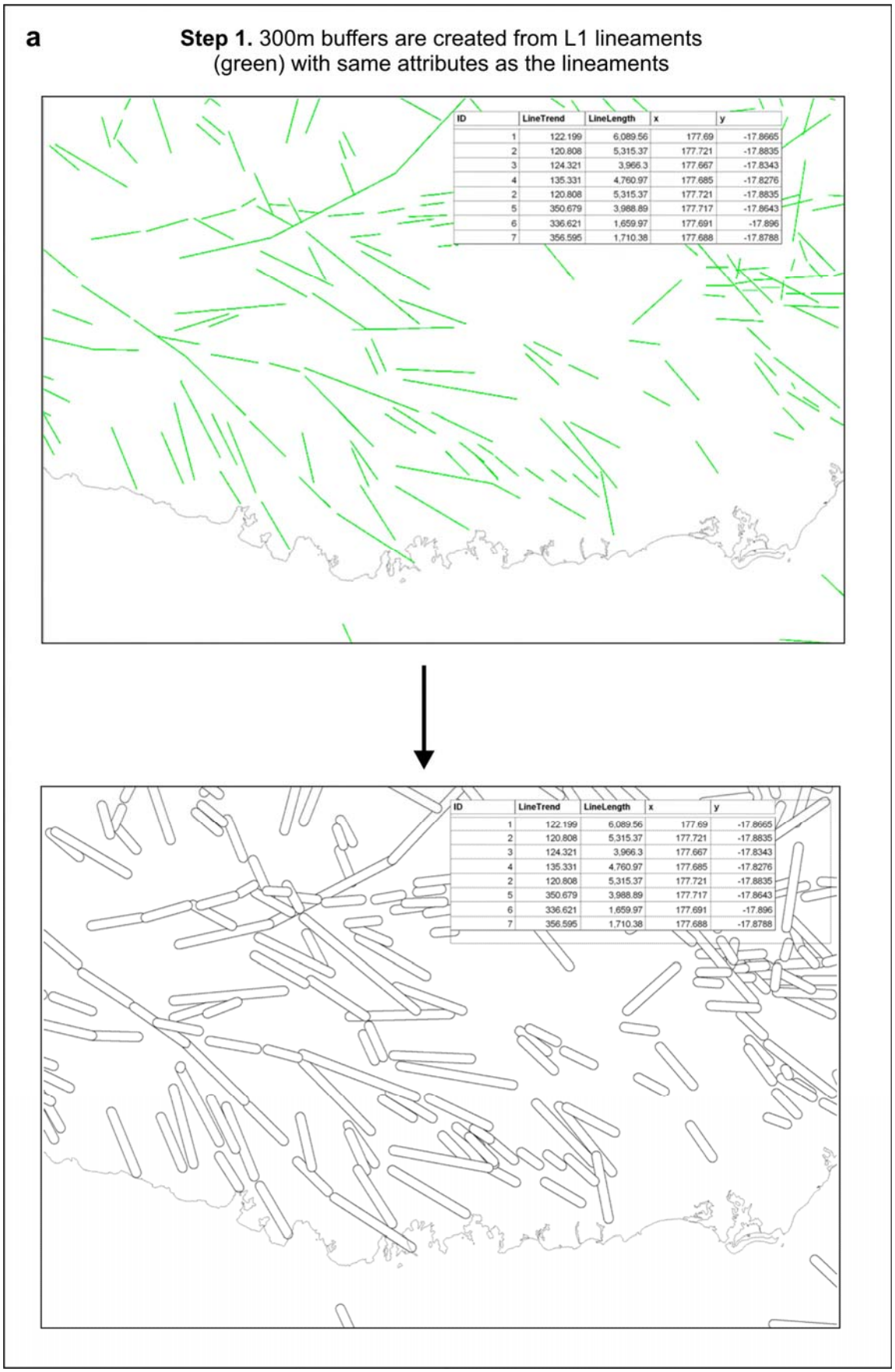

Figure 1 Illustrated are the main steps used in reproducibility test of multiple trial lineament data.

b **Step 2.** All buffer polygons which intersect the L2 lineaments (red) are selected. The attributes of the selected buffer polygons contain the data from the lineaments they intersect.

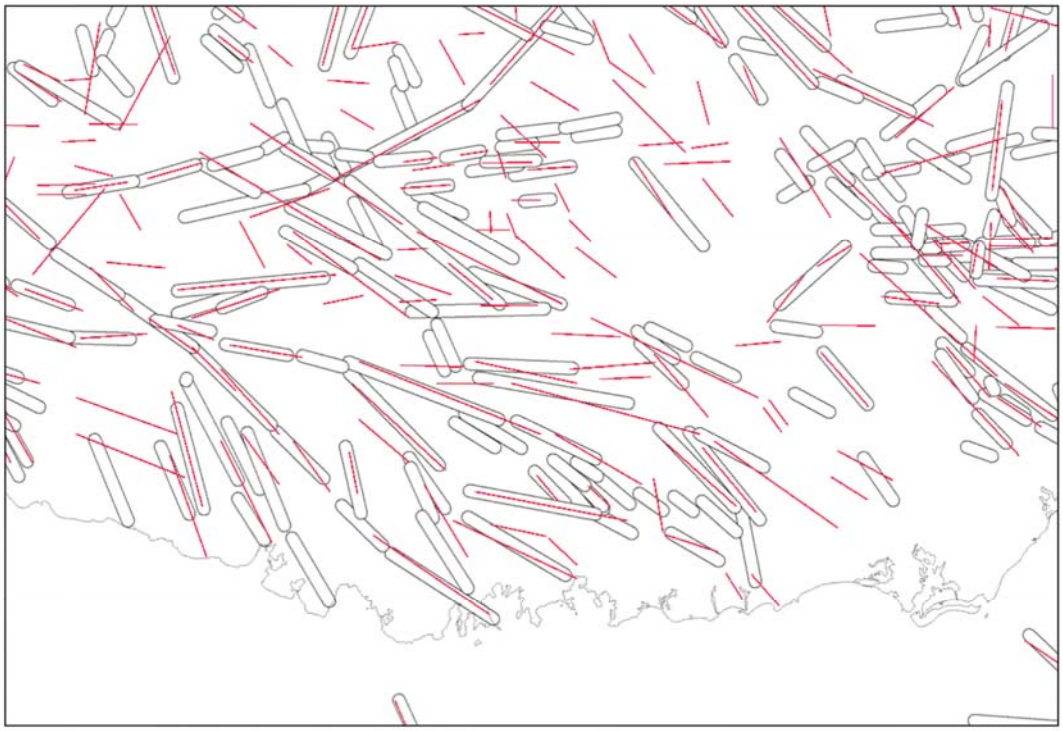

ID	LineTrend	LineLength	x	y	ID_2	LineTrend_2	LineLength_2	x_2	y_2	values_2
1	122.199	6,089.56	177.69	-17.8665	9	121.585	18,620.73	177.702	-17.8737	-58.4145
2	120.808	5,315.37	177.721	-17.8835	9	121.585	18,620.73	177.702	-17.8737	-58.4145
3	124.321	3,966.3	177.667	-17.8343	10	123.937	7,481.08	177.677	-17.8415	-56.0633
4	135.331	4,760.97	177.685	-17.8276	267	96.468	2,590.81	177.682	-17.8243	-83.532
2	120.808	5,315.37	177.721	-17.8835	9	121.585	18,620.73	177.702	-17.8737	-58.4145
2	120.808	5,315.37	177.721	-17.8835	269	25.425	1,408.01	177.712	-17.8552	25.425
5	350.679	3,988.89	177.717	-17.8643	9	121.585	18,620.73	177.702	-17.8737	-58.4145

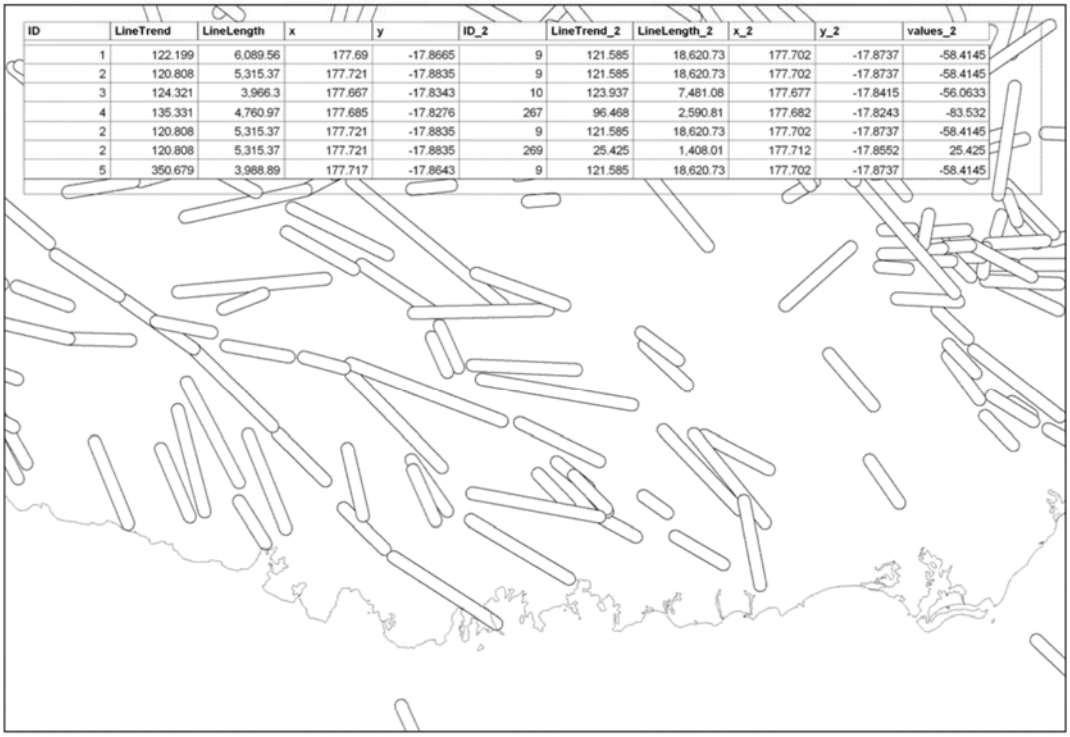

Figure 1 continued

c **Step 3.** Two additional columns are added to selected polygon table (”max line trend” and “min line trend”) updated with values of the selected lineament trends + 5 degrees and - 5 degrees respectively.

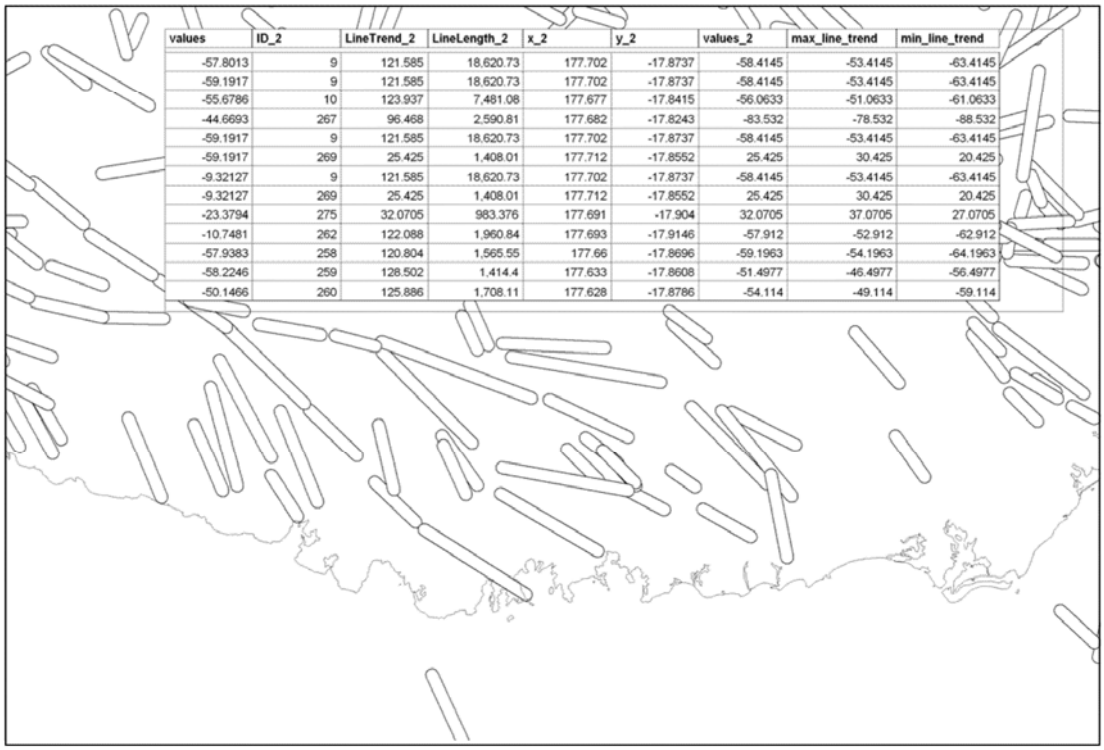

values	ID_2	LineTrend_2	LineLength_2	x_2	y_2	values_2	max_line_trend	min_line_trend
-57.8013	9	121.585	18,620.73	177.702	-17.8737	-58.4145	-53.4145	-63.4145
-59.1917	9	121.585	18,620.73	177.702	-17.8737	-58.4145	-53.4145	-63.4145
-55.6786	10	123.937	7,481.08	177.677	-17.8415	-56.0633	-51.0633	-61.0633
-44.6693	267	96.468	2,590.81	177.682	-17.8243	-83.532	-78.532	-88.532
-59.1917	9	121.585	18,620.73	177.702	-17.8737	-58.4145	-53.4145	-63.4145
-59.1917	269	25.425	1,408.01	177.712	-17.8552	25.425	30.425	20.425
-9.32127	9	121.585	18,620.73	177.702	-17.8737	-58.4145	-53.4145	-63.4145
-9.32127	269	25.425	1,408.01	177.712	-17.8552	25.425	30.425	20.425
-23.3794	275	32.0705	983.376	177.691	-17.904	32.0705	37.0705	27.0705
-10.7481	262	122.088	1,960.84	177.693	-17.9146	-57.912	-52.912	-62.912
-57.9383	258	120.804	1,565.55	177.66	-17.8696	-59.1963	-54.1963	-64.1963
-58.2246	259	128.502	1,414.4	177.633	-17.8608	-51.4977	-46.4977	-56.4977
-50.1466	260	125.886	1,708.11	177.628	-17.8786	-54.114	-49.114	-59.114

Figure 1 continued

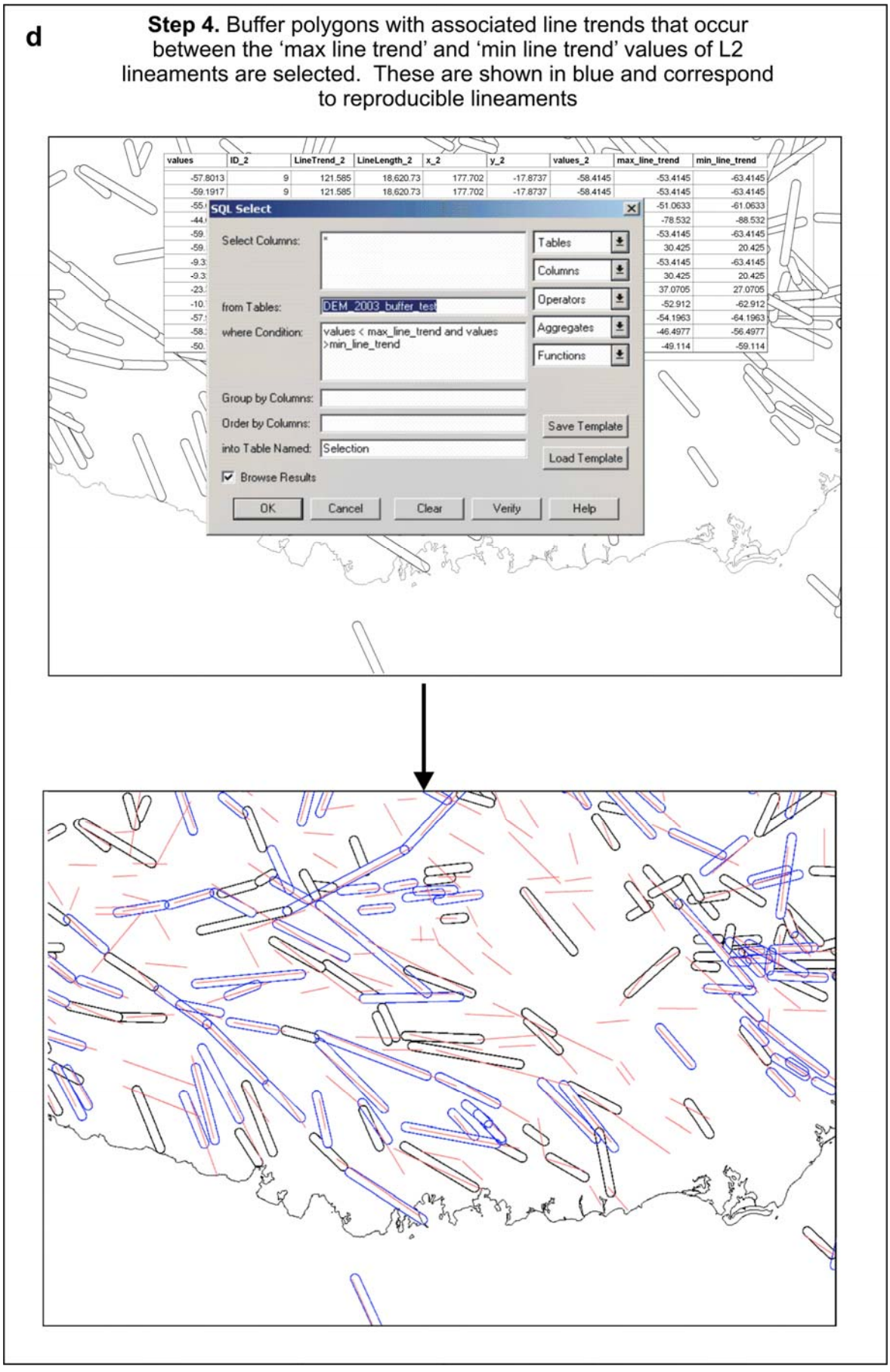

Figure 1 continued

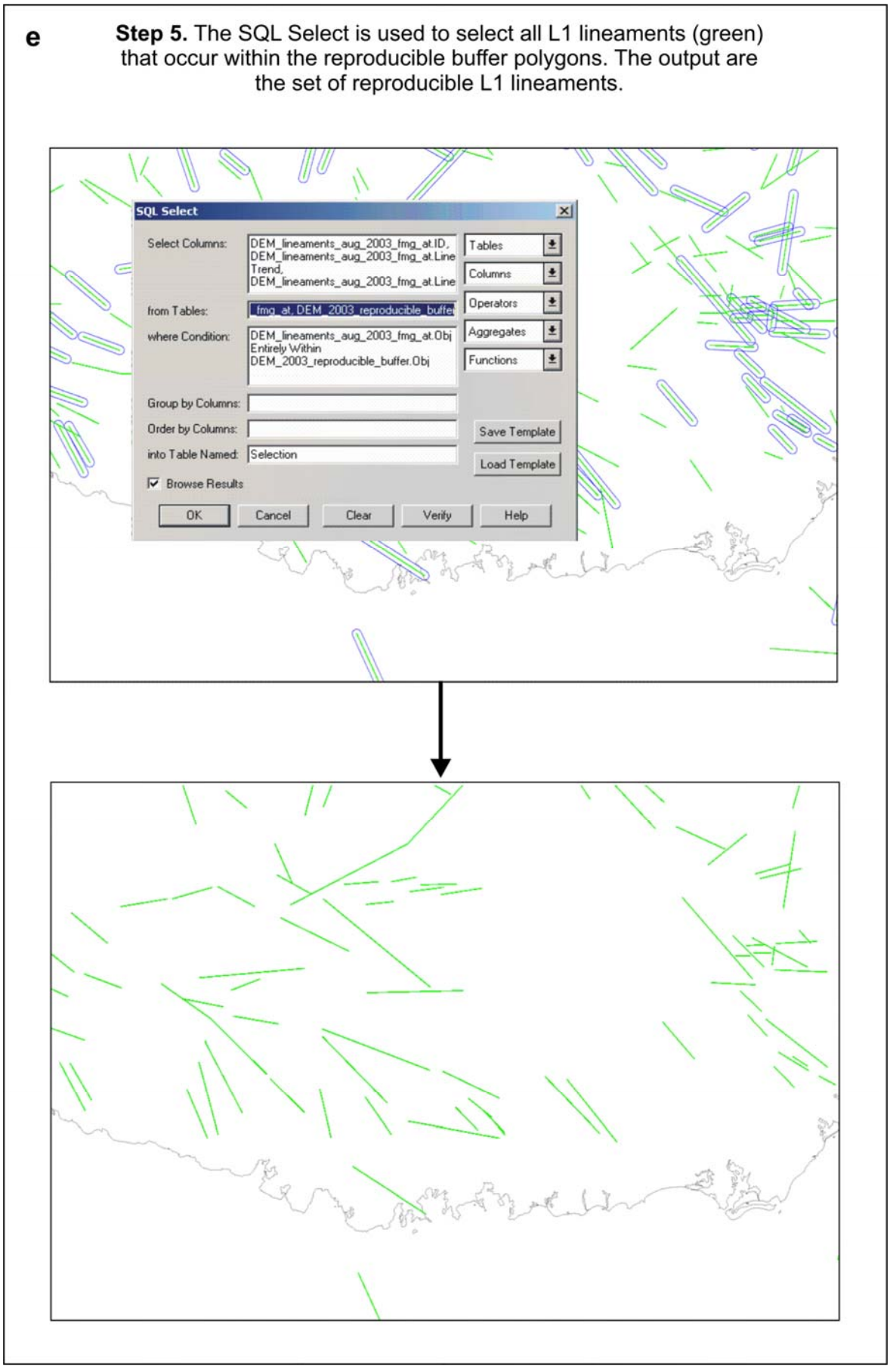

Figure 1 continued

APPENDIX 6

DIGITAL FLY THROUGH OVER OFFSHORE SOUTHEAST VITI LEVU

Digital animations files were created to show fly throughs over the offshore terrain of southeast Viti Levu. Four animation files can be found at the following folder location in the Data CD accompanying this thesis:

DataCD/Appendix 6/

These files can be opened with Windows Media Player, or other similar programs that read avi files. Below are descriptions of the avi files:

Eastern_slope_colour.avi - shows a fly through over 20 m resolution shaded relief image (colour) across the Eastern Slope of southern Viti Levu starting from the Beqa Passage and ending at the Rewa Delta Foreslope (flight path west to east).

Eastern_slope_grey.avi - shows a fly through over 20 m resolution image (grey scale) across the Eastern Slope of southern Viti Levu starting from the Beqa Passage and ending at the Rewa Delta Foreslope (flight path west to east).

Southern_slope_colour.avi - shows a fly through over 60 m resolution shaded relief image (colour) across the southern slopes of Viti Levu starting from the Western Slope, across the Beqa Lagoon and Eastern Slope, and ending at the Rewa Delta Foreslope (flight path west to east).

Southern_slope_grey.avi - shows a fly through over 60 m resolution shaded relief image (grey scale) across the southern slopes of Viti Levu starting from the Western Slope, across the Beqa Lagoon and Eastern Slope, and ending at the Rewa Delta Foreslope (flight path west to east).

Hint: The pause button can be used in Windows Media Player to view the slope as stills.

APPENDIX 7

COMPARISON OF METHODS FOR CALCULATING NEAR FIELD TSUNAMI AMPLITUDES

Calculations of tsunami amplitudes using the three methods described in Section 6.4 on this thesis were done using reef edge and canyon head slides from the offshore area of southeast Viti Levu. These values were then compared to the maximum wave observed during the 1953 Suva tsunami, of around 10 to 15 m (Houtz, 1962a).

The spreadsheet file (MS Excel file) with calculations can be found at the following file location in the Data CD accompanying this thesis:

DataCD/Appendix 7/tsunami amplitude method comparison.xls

A print out of this spreadsheet is given in the next page.

Appendix 7 Comparison of methods for calculating near field tsunami amplitude

Slide Number	Slide Parameters											
	length (m)	width (m)	thickness (m)	slope (deg)	slope (rads)	centre ls depth (m)	density of slide (kg/cubic metre)	density of sea water (kg/cubic metre)	Depth at end of slope (m)	Local water depth (m)	Drop in height (m)	Energy coeff.
1	4000	3600	25	15	0.261799	400	1900	1020	1000	1000	430	0.01
2	3500	1700	50	10	0.174533	400	1900	1020	850	850	370	0.01
3	2500	1700	40	10	0.174533	250	1900	1020	500	500	200	0.01
4	1500	2500	20	15	0.261799	200	1900	1020	350	350	150	0.01
14	1300	1300	35	15	0.261799	150	1900	1020	300	300	200	0.01
15	1300	1000	35	10	0.174533	120	1900	1020	250	250	100	0.01
16	1600	600	55	15	0.261799	125	1900	1020	300	300	130	0.01
17	2400	1500	50	12	0.20944	200	1900	1020	300	300	130	0.01
21	1200	1640	20	10	0.174533	150	1900	1020	300	300	130	0.01
22	800	500	25	10	0.174533	75	1900	1020	200	200	90	0.01
25	1740	1300	50	20	0.349066	200	1900	1020	600	600	250	0.01
26	1600	800	30	10	0.174533	125	1900	1020	300	300	130	0.01
27	1250	590	35	17	0.296706	130	1900	1020	300	300	130	0.01
28	850	690	30	20	0.349066	100	1900	1020	250	250	100	0.01
29	1000	770	50	15	0.261799	120	1900	1020	300	300	130	0.01
33	1700	1500	70	25	0.436332	200	1900	1020	400	400	175	0.01
34	1300	2100	50	20	0.349066	175	1900	1020	450	450	200	0.01
35	1400	2100	60	15	0.261799	200	1900	1020	400	400	175	0.01

Slide Number	Initial Tsunami Parameters			
	Method 1 3D equation from McAdoo & Watts (2004)		Method 2 Energy scaling equation of Bohannon & Gardner (2004)	Method 3 Solitary wave theory of Striem & Miloh (1976)
	Wavelength (m)	Amplitude (m)	Amplitude (m)	Amplitude (m)
1	**9622**	**3.88**	**8.61**	**37**
2	**10989**	**2.07**	**10.57**	**52**
3	**7342**	**2.74**	**5.87**	**41**
4	**4167**	**2.98**	**2.79**	**19**
14	**3359**	**4.66**	**3.96**	**29**
15	**3668**	**3.02**	**2.80**	**32**
16	**3402**	**6.40**	**4.44**	**50**
17	**5880**	**5.71**	**5.19**	**42**
21	**3940**	**1.62**	**2.32**	**19**
22	**2275**	**1.78**	**1.76**	**22**
25	**3904**	**8.01**	**6.13**	**43**
26	**4153**	**2.40**	**3.28**	**33**
27	**2885**	**3.67**	**3.13**	**31**
28	**1929**	**4.92**	**2.10**	**24**
29	**2635**	**5.13**	**3.35**	**35**
33	**3471**	**16.17**	**5.99**	**50**
34	**3156**	**10.52**	**4.74**	**37**
35	**4025**	**7.51**	**5.04**	**40**

APPENDIX 8

NEAR FIELD TSUNAMI AMPLITUDE CALCULATIONS

The spreadsheet file with the full calculations of the initial tsunami amplitudes using the method of McAdoo & Watts (2004) (Method 1) can be found at the following file location in the Data CD accompanying this thesis:

DataCD/Appendix 8/tsunami amplitude calculations.xls

A print out of this spreadsheet is given in the next page.

Appendix 8 Initial tsunami amplitude calculations using Method 1

Slide Number	Slide Parameters						Method 1 3D equation from McAdoo & Watts (2004)	
	length (m)	width (m)	thickness (m)	slope (deg)	slope (rads)	centre ls depth (m)	Wavelength (m)	Amplitude (m)
1	4000	3600	25	15	0.261799388	400	9622	3.88
2	3500	1700	50	10	0.174532925	400	10989	2.07
3	2500	1700	40	10	0.174532925	250	7342	2.74
4	1500	2500	20	15	0.261799388	200	4167	2.98
5	1400	730	20	15	0.261799388	300	4930	0.57
6	800	1500	25	15	0.261799388	150	2635	2.36
7	800	1220	30	30	0.523598776	150	1896	5.84
8	1120	1550	25	15	0.261799388	200	3600	2.08
9	1400	550	25	15	0.261799388	450	6038	0.28
10	670	850	50	30	0.523598776	650	3612	0.61
11	600	690	70	30	0.523598776	650	3418	0.65
12	1300	500	30	15	0.261799388	300	4751	0.57
13	760	1750	25	20	0.34906585	550	4278	0.47
14	1300	1300	35	15	0.261799388	150	3359	4.66
15	1300	1000	35	10	0.174532925	120	3668	3.02
16	1600	600	55	15	0.261799388	125	3402	6.40
17	2400	1500	50	12	0.20943951	200	5880	5.71
18	1800	1160	25	13	0.226892803	750	9481	0.22
19	3800	2000	40	15	0.261799388	900	14068	0.97
20	1400	810	40	10	0.174532925	550	8149	0.24
21	1200	1640	20	10	0.174532925	150	3940	1.62
22	800	500	25	10	0.174532925	75	2275	1.78
23	1100	900	45	30	0.523598776	650	4628	0.87
24	6300	1000	50	10	0.174532925	600	18056	1.02
25	1740	1300	50	20	0.34906585	200	3904	8.01
26	1600	800	30	10	0.174532925	125	4153	2.40
27	1250	590	35	17	0.296705973	130	2885	3.67
28	850	690	30	20	0.34906585	100	1929	4.92
29	1000	770	50	15	0.261799388	120	2635	5.13
30	960	680	20	10	0.174532925	225	4316	0.34
31	1170	530	25	5	0.087266463	275	7436	0.09
32	1200	2300	30	7	0.122173048	675	9977	0.16
33	1700	1500	70	25	0.436332313	200	3471	16.17
34	1300	2100	50	20	0.34906585	175	3156	10.52
35	1400	2100	60	15	0.261799388	200	4025	7.51
36	1540	520	50	10	0.174532925	200	5154	1.20

APPENDIX 9

1953 COASTLINE OF SUVA CBD AREA

The 1953 coastline of the Suva CBD area was determined from 1953 aerial photos. This coastline was used in the computational grid for the simulation of the 1953 Suva tsunami. On the next page, aerial photos from 1953 and 1998 show the amount of reclamation that has taken place in the Suva waterfront since 1953. Labelled on the 1998 photo are facilities that are located on the low-lying reclaimed area.

Appendix 9 Reclaimed waterfront of the Suva CBD area

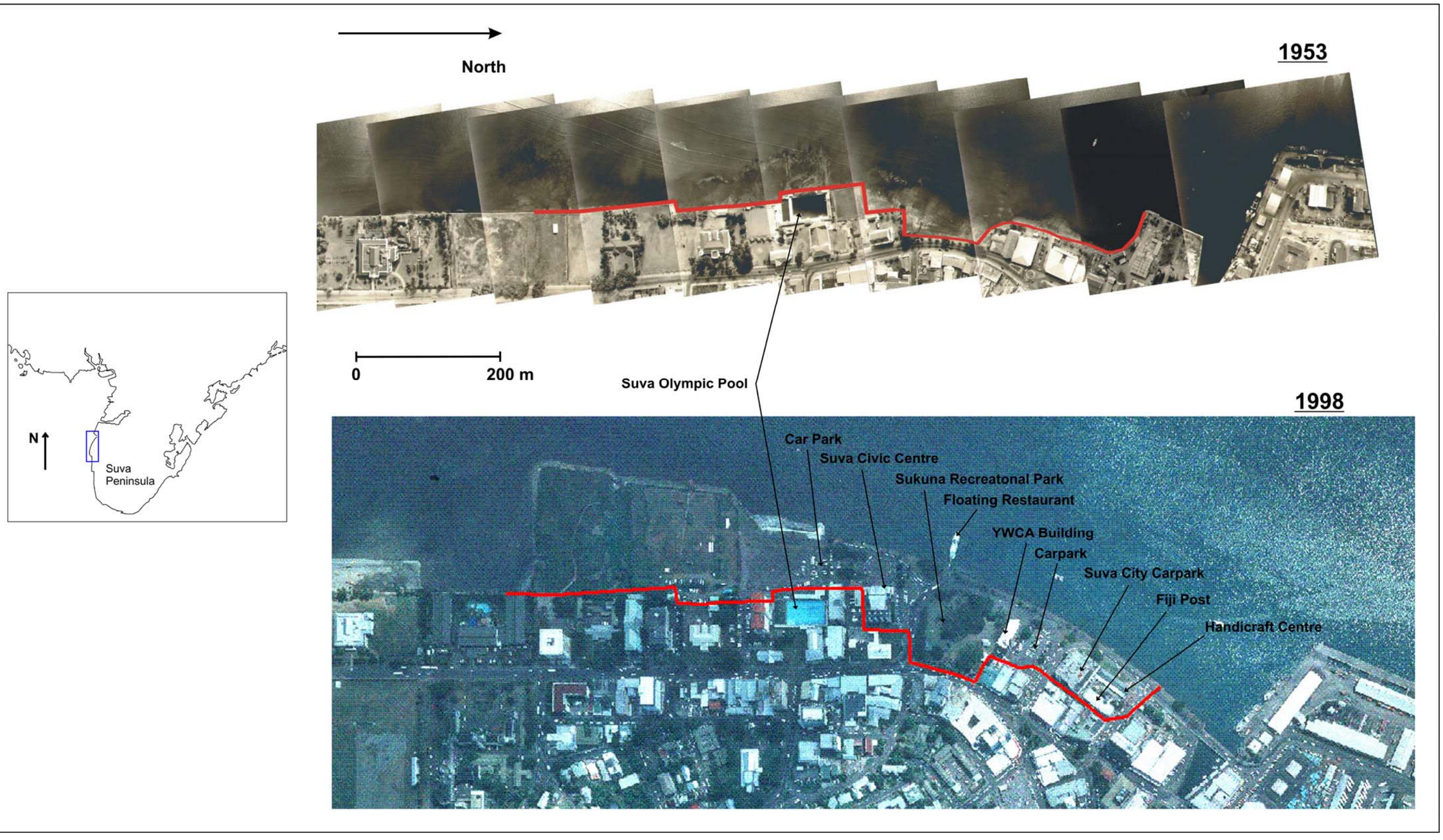

APPENDIX 10

SIMULATION OF THE 1953 SUVA TSUNAMI

The historical 1953 Suva tsunami was simulated using the Geowave model. The animation file created for this simulation can be found at the following file location in the Data CD accompanying this thesis:

DataCD/Appendix 10/suva_tsunami_1953.m1v

The Geowave model produced simulated sea surface elevation as grid files at 10-second (real time) intervals from tsunami initiation in the source area. The animation file was created by combining all the sea surface elevations files as movie frames. The animation file is in an mpeg file format that will run with Windows Media Player.

The simulation is presented in map view of the coast around Suva, between Muaivuso Village in the west and the Rewa Delta to the east. The black line shows the coastline. The thin light blue lines are the barrier reef edges. The blue areas of the sea are the wave depressions and the red areas are the wave crests. White areas of the sea represent the normal tide level. The animation file will run for about 20 seconds. This represents a real time of approximately 17 minutes after submarine landslide initiation. The real time values are given in the top left corner of the movie frame.

APPENDIX 11

PAST SEISMIC HAZARD EVALUATIONS AND RELATED ACTIVITIES IN FIJI

The specific terms “une une” for earthquake and “ua loka” for tsunami in the Fijian vocabulary indicate the occupants of Fiji have long experience of seismic activity. In the 1980s, a catalogue of historical earthquakes compiled from literature searches of Fiji's brief written history showed that significant strong and damaging earthquakes were felt in Fiji over the previous 130 years (Everingham, 1983a; Everingham, 1988).

The first seismograph to be installed in Fiji was in Suva in 1913 as part of the worldwide network (Draunidalo, 1990). The first reliable instrumental recordings of earthquakes in the Fiji region became available after 1918 and by the early 1930s recordings of earthquakes with magnitude greater than 6.0 in the Fiji region became routine with an improvement in the international seismograph network (Everingham, 1983a). Early earthquake hazard assessments in Fiji were made by Houtz (1959; 1961) who treated Fiji as a single zone of seismicity and estimated the frequency of a damaging earthquake in the zone at one every 40 years. In studies of the 1953 and 1961 earthquakes in southeast Viti Levu, Houtz (1962a; 1962b) recognised that the area between Navua and Nausori was susceptible to earthquakes emanating from an active zone near Naqara Passage.

The first local seismograph network in Fiji, comprising three stations was set up by the Lamont Geological Observatory, which operated from 1965 to 1969. Data from this network were used to define three seismic source zones located at: 1) north of Vanua Levu, extending east to the Tonga arc and west toward the Vanuatu arc, 2) east and northeast of Viti Levu and 3) southwest Viti Levu near Kadavu (Sykes et al., 1969; Draunidalo & Hamburger, 1984). In 1974, the seismic risk of Fiji was reviewed by the Suva City Building Bye-Laws Revisions Committee, and its recommendation that the Zone B of the New Zealand Basic Loads Code NZS4203 (1974) be adopted to cover all construction in Fiji (Power, 1978), was subsequently adopted for Suva.

A seismotectonic-zoning map of Fiji was produced by Berryman (1979) mainly from available epicentral data up to 1978 and late Quaternary uplift determined from raised coastal features. His map shows four zones. Zone 1, with maximum expected earthquake of magnitude 7.5, included an area north of Vanua Levu and an area south and southwest of Viti Levu including the area of the 1953 earthquake near Suva. Zone 2 covered much of Viti Levu and Vanua Levu, with maximum expected magnitude assigned as 7.0. Zone 3, to the southwest of Viti Levu and confined to an area of postulated seafloor spreading, was assigned maximum expected magnitude of 7.0. Zone 4 essentially covered the Lau Group, with maximum expected earthquake assigned as 5.5. Part of Berryman's seismotectonic zoning map is shown in Figure 1.

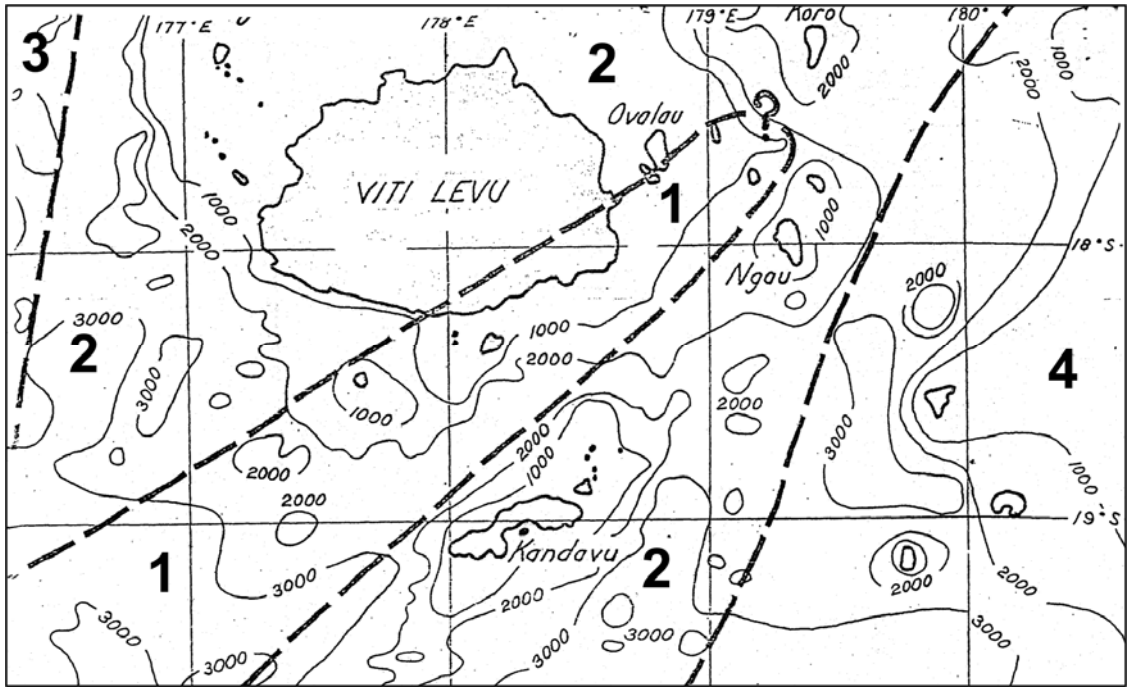

Figure 1: Seismotectonic zoning map of southern Fiji of Berryman (1979).

In 1979, the network of seismic stations in Fiji was extended to nine and later to seventeen (Figure 2). During the early to mid 1980s, using the magnitudes of earthquakes recorded teleseismically since 1918 and micro-seismicity data from the 1979 local network in Fiji, preliminary magnitude/frequency relationships were developed for Fiji (Everingham, 1983b, 1986a). The distribution of earthquakes from this period was used to derive a seismic zonation map of Fiji (Everingham, 1986a, b) (Figure 3). This map showed five zones of concentrated seismicity, which included: 1) the northeastern zone, 2) the northern zone, 3) the western zone, 4) Kadavu zone, 5) the southeast Viti Levu zone and a sixth, ill-defined zone

was through Koro and extended to the south of Kadavu. The frequencies of earthquake intensities recorded within these zones over a 100 year period were used for comparisons with zones of seismicity in Australia and New Zealand. Recommendations were made for the adoption of building standards in Fiji based on comparable zones in Australia and New Zealand (Everingham, 1986b).

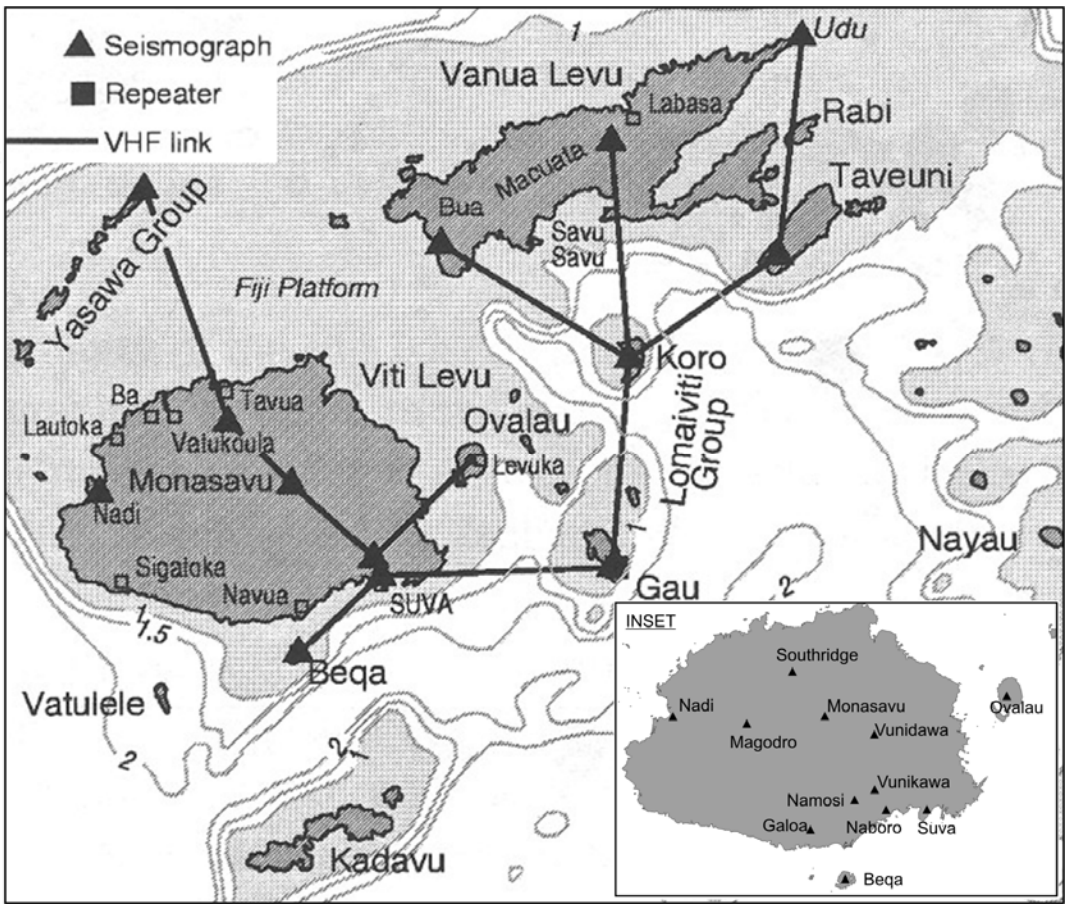

Figure 2: Fiji Seismograph Network in 1993 (after Jones 1998). Inset shows dense network of stations in Viti Levu in the early to mid 1980s.

Benchmarks in southeastern Viti Levu initially triangulated by McCaw (1916) were retriangulated by Berryman (1981) to determine if there was significant horizontal deformation taking place in this seismically active area. The retriangulation survey found that there were large changes in common angles of the base net and that significant strain was accumulating in the northern part of the base network. Strain rates of the order of 0.6 μrad/year had accumulated over a period 1909 to 1980, with total strain accumulation of about 40 μrad. The strains rates were found to be similar to those areas in New Zealand and California that were undergoing active deformation (e.g. Bibby, 1976; Pearson, 1994). The results of this work indicated that southeast Viti Levu was an area of significant tectonic strain

accumulation and that moderate to large earthquakes here were not isolated events, but reflected progressive crustal deformation in the area.

In the late 1980s geological studies on the Suva Peninsula and Harbour revealed that seismicity in the area was related to recent faulting on the NW trend (Shorten, 1993).

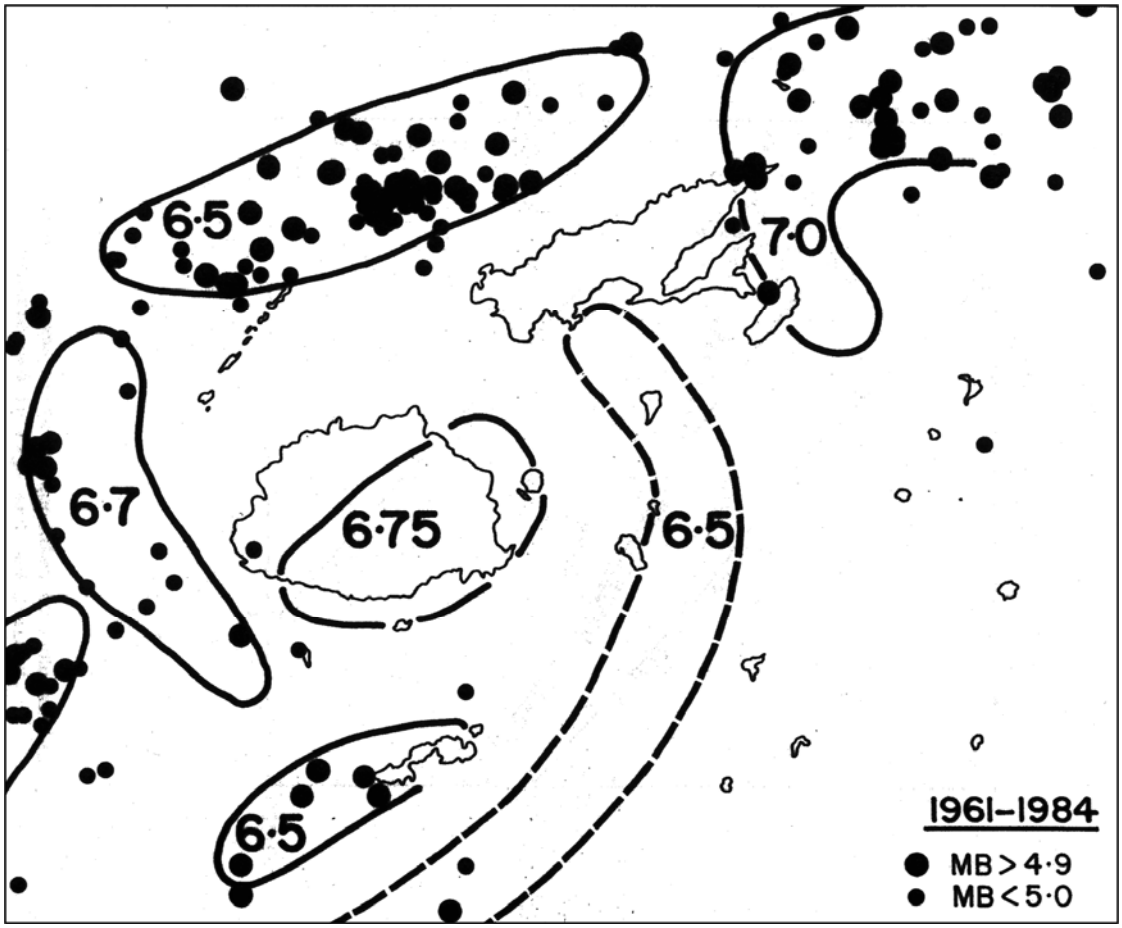

Figure 3: Earthquake zone map of Everingham (1986a), with the magnitude of the largest recorded earthquake shown in each zone.

In 1989 a probabilistic hazard study for Fiji was initiated by the Mineral Resources Department (Jones, 1998). The aim of this study was to produce probabilistic earthquake hazard maps which could be used in the 1990 draft National Building Code of Fiji, for design of special structures, for planning, for emergency management and for risk management. The study used 3200 shallow earthquakes, compiled from early teleseismic and the early local network catalogues, but mostly recorded from the period of 11 years from 1979 through the Fiji Seismograph Network. Macroseismic data from 16 shallow earthquakes were used to establish a relation for the attenuation of Modified Mercalli Intensity in Fiji. Seismicity

parameters for nine earthquake source zones covering all parts of Fiji were defined. The nine earthquake source zones are shown in Figure 4. In the absence of instrumental records of strong ground motion from Fiji, the Modified Katayama relation for the attenuation of strong ground shaking developed for New Zealand was used. Probabilistic earthquake hazard maps were prepared for return periods of 50, 150, 450 and 1000 showing contours of elastic, 5% damped, horizontal spectral acceleration for Katayama ground condition Type 3 at period T=0.2 seconds. A large area of Fiji, including almost all of Viti Levu including Suva, lies between 0.5g and 0.7g in the map for a 450-year return period (Figure 5). This map was recommended as the basis for the Zone Factor map to replace the Preliminary Earthquake Risk Zoning Map in the draft 1990 National Building Code of Fiji. The zone factor map of Jones (1998) has since been adopted in the building code. Regulatory authorities in Fiji, with the approval of the Fiji Government in 2002, are now implementing the code.

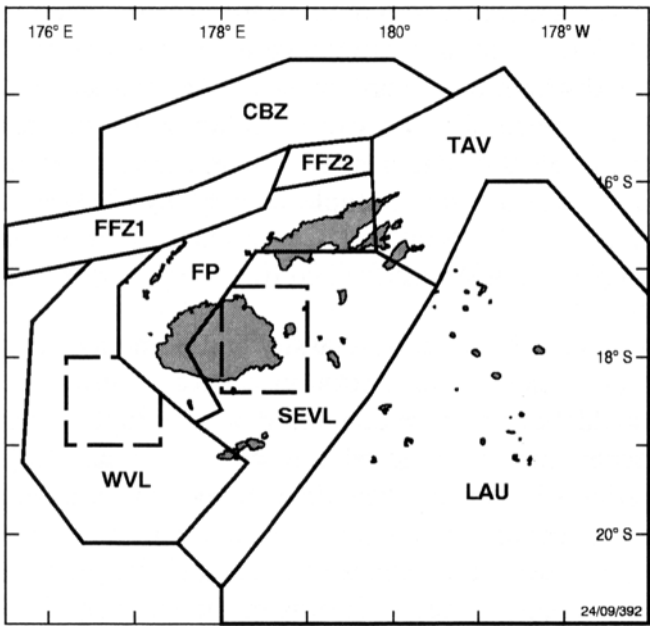

Figure 4: Earthquake source zones for Fiji defined by Jones (1998).

Singh (1996) carried out a probabilistic seismic hazard study of the Monasavu Dam in central Viti Levu. He divided the area within 200 km of the dam site into five area source zones and calculated their activity rates, b values and maximum magnitudes. These areas coincided with the source area selected in previous studies, namely the FFZ, southeast Viti Levu, Taveuni-Vanua Levu region, West of Viti Levu, Lau Basin, and a background seismicity area to represent the seismicity of the whole region. A sensitivity analysis was carried out using a number of different attenuation relationships from the US, Australia and New Zealand.

Californian relationships developed for crustal earthquakes in the early part of the last decade and the decade before were used to calculate ground motion parameters at Monasavu as a function of the return period. Hazard computational programs GMRes and EZ-FRISK were used for calculations. The maximum magnitude earthquakes for all sources were taken as M_W 7.5. The results indicate that spectral acceleration at the Monasavu Dam has a 20% probability of exceeding 0.2g during the lifetime of the dam (100 years).

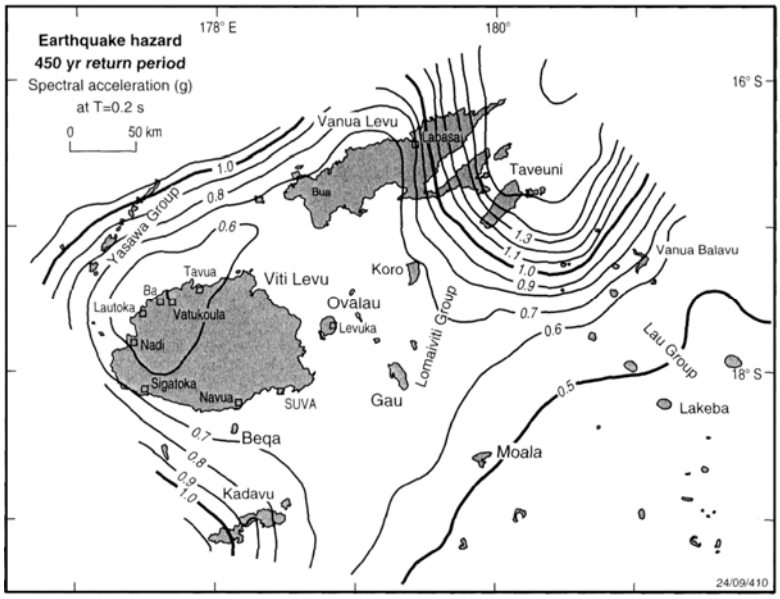

Figure 5: Earthquake hazard map of Fiji for a return period of 450 years (from Jones 1990)

Under the Suva Earthquake Risk Management Scenario Pilot Project (SERMP), work on seismic microzonation in the greater Suva area was carried out by the Mineral Resources Department (MRD) in collaboration with the Institute of Geological and Nuclear Sciences (IGNS) of New Zealand in 1997 (Hull et al., 1997; Singh et al., 1998). The purpose of this survey was to characterise soil and rock of the area with respect to dominant frequency response. Preliminary ground-shaking hazard zones were determined using geological data of the surface and subsurface (Hull et al., 1997). The Nakamura microtremor method (Nakamura, 1989) was used for site response characterisation. Four principal zones of earthquake shaking response were defined in Suva based on both the geological data and the Nakamura site response evaluations. Site resonance was observed in areas where Holocene-age sediment exceeds about 10 m depth (class A and B). There was no resonance over bedrock sites (Class D), or where sediment thickness was less than 10 m (Class C) (Singh et al., 1998). Further work in the SERMP project addressed the potential risk posed by

earthquake and tsunami hazards in Suva (SPDRP 2002a,b,c).

Further microzonation work in Suva was carried out under the project: Earthquake Microzoning in Capital Cities in the South Pacific, that involved collaboration of the Geophysical Institute of Israel, the Institut de Recherche pour le Development (IRD) and the South Pacific Applied Geoscience Commission (SOPAC) (Shorten et al., 2001). This project produced a revised and more accurate microzonation map. The data of the MRD/IGNS project was re-analysed and with additional work that included calculation of the analytical site response function and application of the SvE method of determining the uniform hazard response spectrum (Shapira & van Eck, 1993), the acceleration response curves, preliminary characteristic resonant frequencies and amplification factors were produced for each of the four zones in Suva. This study concluded that significant parts of Suva could be prone to effects of amplification of earthquake shaking due to resonance and could also suffer from the effects of liquefaction and settlement.

The completeness, coverage and accuracy of instrumental records of seismicity in the last 10 years have suffered mainly as a result of the ageing and depletion of instruments in the local seismograph network and through the loss of trained professionals from the Seismology Section of the Fiji Mineral Resources Department. There is now a significant gap in the record of accurate microseismicity data. Reliance on such data therefore, to further improve the understanding of earthquake hazard in Fiji seems unreasonable in the near future until new good quality local network data becomes available. There are still no records of instrumentally recorded strong ground motion data for developing local attenuation relationships or measured shear velocity data for characterisation of local site response. The use of many critical parameters in seismic hazard evaluations in the past studies have been theoretically estimated or adopted from studies elsewhere.

Past seismic hazard studies in Fiji have not considered individual earthquake source structures, data on which are critical for evaluating the long term hazard of an area. Information on faults in seismically active areas of Fiji is generally very poor and paleoseismic data on fault sources are non-existent. Sparse surface exposures and past field surveys lacking the motive to seek information on faults are the primary reasons for the scarcity in fault data. The deficiency in knowledge on seismic source structures and their potential for generating large earthquakes in Fiji needs to be redressed through highly

focussed surveys aimed at identifying and characterising active faults, both onshore and offshore, and incorporating them in seismic hazard evaluations. Chapters 4 and 9 of this thesis attempt to confront this issue in Viti Levu in order to the improve the knowledge base of earthquake source structures and their capability in this area. The metholodology presented in those chapters can be favourably applied in future seismic hazard evaluations in other regions of Fiji.

References

Berryman, K. 1979. Seismotectonic zoning study of the Fiji Islands. *New Zealand Geological Survey, Earth Deformation Section Report* **70**: 69 pp.

Berryman, K. 1981. Retriangulation of Navua base net (across Suva-Beqa sesimic zone), Fiji Islands August 1980. *New Zealand Geological Survey, Earth Deformation Section Report*: 20 pp.

Bibby, H.M. 1976. Crustal strain across the Marlborough faults, New Zealand. *New Zealand Journal of Geology and Geophysics* **19**, 407-425.

Draunidalo, K. 1990. Seismological status report in the Fiji region. *Bulletin of the International Institute of Seismology and Earthquake Engineering* **24**, 41-57.

Draunidalo, K.B. & Hamburger, M.W. 1984. Seismicity of Fiji, 1965-1969. *Fiji Mineral Resources Department Note* **BP30/14**: 8 pp.

Everingham, I.B. 1983a. Reports of earthquakes felt in Fiji, 1850 - 1940. *Fiji Mineral Resources Department Report* **48**: 54 pp.

Everingham, I.B. 1983b. Magnitude determinations for shallow earthquakes in the Fiji region, 1907-1960, and their implications. *Fiji Mineral Resources Department Note* **BP33/5**: 16 pp.

Everingham, I.B. 1986a. Magnitude determinations for shallow earthquakes in the Fiji region, 1961-1983. *Fiji Mineral Resources Department Note* **BP33/12**: 20 pp.

Everingham, I.B. 1986b. A note earthquake risk zoning in Fiji. *Fiji Mineral Resources Department Note* **BP33/14**: 6 pp.

Everingham, I.B. 1988. Catalogue of felt earthquake reports in Fiji, 1941 - 1981. *Fiji Mineral Resources Department Report* **64**: 22 pp.

Houtz, R.E. 1959. Earthquake risk, Colony of Fiji. *Fiji Geological Survey Short Report* **75**: 2 pp.

Houtz, R.E. 1961. Revised earthquake risk, Fiji area. *Geological Survey Department of Fiji Note* **93**: 3 pp.

Houtz, R.E. 1962a. The 1953 Suva earthquake and tsunami. *Bulletin of the Seismological Society of America* **52**, 1-12.

Houtz, R.E. 1962b. Note on minor damage caused by the Suva earthquake of June 1961. *Bulletin of the Seismological Society of America* **52**, 13 -16.

Hull, A., Hengesh, J., Heron, D. & Rynn, J. 1997. Earthquake ground shaking in Suva: Notes to accompany maps, Suva Earthquake Risk Management Scenario Pilot Project. *Institute of Geological and Nuclear Science Client Report* **43698D**.

Jones, T. 1998. Probabilistic earthquake hazard assessment for Fiji. *Australian Geological Survey Organisation Record* **1997/46.**

McCaw, G.T. 1916. Report of trigonometrical survey of Viti Levu. Government of Fiji

Nakamura, Y. 1989. A method for dynamic characteristics estimation of subsurface using microtremor on the ground surface. *Quarterly Report of Railways Technical Research Institute* **30**, 25-33.

Pearson, C. 1994. Geodetic strain determinations from the Okarito and Godley-Tekapo regions, central South Island, New Zealand. *New Zealand Journal of Geology and Geophysics* **37**, 309-318.

Power, C.A. 1978. Earthquake risk in Fiji and the problems of earthquake engineering. *Transactions and proceedings of the Fiji Society (for years 1978 to 1980)* **14**, 44 - 58.

Shapira, A. & van Eck, T. 1993. Synthetic uniform hazard site specific response spectrum. *Natural Hazards* **8**, 201-215.

Shorten, G.G. 1993. The geological and tectonic setting for ground failure hazards in Suva Harbour and environs. *Fiji Mineral Resources Department Memoir* **3**:105 pp.

Shorten, G.G., Shapira, A., Regnier, M., Teakle, G., Biukoto, L., Swamy, M. & Vuetibau, L. 2001. Site-specific earthquake hazard determinations in capital cities in the South Pacific. *SOPAC Technical Report* **300**:156 pp.

Singh, A. 1996.*Seismic hazard assesment of a critical structure: the Monasavu Hydro-electric Dam, Fiji*. Masters thesis, RMIT, Melbourne.

Singh, A., Stephenson, B. & Hull, A. 1998. Assessment for amplification of earthquake shaking by soft soils in Suva. *Fiji Mineral Resources Department Report* **71**:38 pp.

South Pacific Disaster Reduction Programme (SPDRP) 2002a. Suva Earthquake Risk Management Scenario Pilot Project (SERMP), Summary Report Part 1. *SOPAC Joint Contribution* **139**.

South Pacific Disaster Reduction Programme (SPDRP) 2002b. Suva Earthquake Risk Management Scenario Pilot Project (SERMP), Recommendations Part 2. *SOPAC Joint Contribution* **139**.

South Pacific Disaster Reduction Programme (SPDRP) 2002c. Suva Earthquake Risk Management Scenario Pilot Project (SERMP), Methodology Part 3. *SOPAC Joint Contribution* **139**.

Sykes, L.R., Isacks, B.L. & Oliver, J. 1969. Spatial distribution of deep and shallow earthquakes of small magnitudes in the Fiji-Tonga region. *Bulletin of the Seismological Society of America* **59**, 1093-1113.

APPENDIX 12

CALCULATION OF MAXIMUM CREDIBLE EARTHQUAKES

Described below are the formulas of Wells & Coppersmith (1994) and Stirling et al. (2002) used for the calculation of Maximum Credible Earthquakes (MCE). The spreadsheet file with calculations can be found at the following folder location in the Data CD accompanying this thesis:

DataCD/Appendix 12/MCE.xls

A print out of this spreadsheet is given in the next page. The spreadsheet also shows the results of a sensitivity analysis on the value of the MCE by varying the fault parameters by ± 20%.

Equations of Wells & Coppersmith (1994):

For all fault types -

Using SRL: $M_w = 5.08 + 1.16 \log (SRL)$

Using RA: $M_w = 4.07 + 0.98 \log (RA)$

SRL – Surface Rupture Length, RA – Rupture Area.
Note: RA = SSRL * RW (where SSRL – Subsurface Rupture Length (1.33 SRL), RW – Rupture Width).

Equations of Stirling et al. (2002):

Using SRL: $M_w = 5.88 + 0.8 \log (SRL)$

Using RA: $M_w = 5.09 + 0.73 \log (RA)$

SRL – Surface Rupture Length, RA – Rupture Area.

Note: RA = SRL * RW (where RW – Rupture Width).

References

Stirling, M., Rhoades, D. & Berryman, K. 2002. Comparison of earthquake scaling relations derived from data of the instrumental and preinstrumental era. *Bulletin of the Seismological Society of America* **92**, 812-830.

Wells, D.L. & Coppersmith, K.J. 1994. New empirical relationships among magnitude, rupture length, rupture width, rupture area, and surface displacement. *Bulletin of the Seismological Society of America* **84**, 974-1002.

Calculations of Maximum Credible Earthquakes

Fault Parameters	SRL			RW			Fault Dip			Selected MCE (average value)
Fault zone	SRL (km)	Max +20 SRL (km)	Min -20 SRL (km)	Width of rupture (km)	Min width - 20	Max width +20	dip -20	dip -20 width	dip	
Mavuvu Fault/Lineament Zone	127	152	102	20	16	24	70	21	vertical	**7.55**
Naqara Fault	39	47	31	21	17	25	55	24	70	**7.09**
Sovi/Yalavou Faults	37	44	30	20	16	24	70	21	vertical	**7.06**
Nasivi Fault	20	24	16	20	16	24	70	21	vertical	**6.81**
Suva Canyon Fault	25	30	20	21	17	24	60	23	75	**6.91**
Nakorotubu Fault	60	72	48	20	16	24	70	21	vertical	**7.25**
FFZ	100	120	80	20	16	24	70	21	vertical	**7.45**

(Wells & Coppersmith, 1994) All Faults	Using SRL			Using RA				RA				SSRL
	MAX MCE	MIN MCE	MCE	MAX MCE	MIN MCE	MCE	RA -20 dip	RA (km^2)	Min RA (km^2)	Max RA (km^2)	RA -20 dip	SSRL
Mavuvu Fault/Lineament Zone	7.61	7.41	7.52	7.61	7.43	7.53	7.55	3387	2709	4064	3556	169
Naqara Fault	7.02	6.81	6.93	7.12	6.96	7.05	7.10	1092	884	1300	1248	52
Sovi/Yalavou Faults	6.99	6.79	6.90	7.08	6.91	7.00	7.03	987	789	1184	1036	49
Nasivi Fault	6.68	6.48	6.59	6.82	6.65	6.74	6.76	533	427	640	560	27
Suva Canyon Fault	6.79	6.59	6.70	6.92	6.77	6.86	6.90	700	567	800	767	33
Nakorotubu Fault	7.23	7.03	7.14	7.29	7.12	7.21	7.23	1600	1280	1920	1680	80
FFZ	7.49	7.29	7.40	7.51	7.33	7.43	7.45	2667	2133	3200	2800	133

(Stirling et al., 2002)	Using SRL			Using RA				RA			
	MAX MCE	MIN MCE	MCE	MAX MCE	MIN MCE	MCE	RA -20 dip	RA (km^2)	Min RA (km^2)	Max RA (km^2)	RA -20 dip
Mavuvu Fault/Lineament Zone	7.63	7.49	7.56	7.63	7.50	7.58	7.59	2540	2032	3048	2667
Naqara Fault	7.22	7.07	7.15	7.27	7.15	7.22	7.26	819	663	975	936
Sovi/Yalavou Faults	7.19	7.06	7.13	7.24	7.11	7.18	7.20	740	592	888	777
Nasivi Fault	6.98	6.84	6.92	7.05	6.92	6.99	7.00	400	320	480	420
Suva Canyon Fault	7.06	6.92	7.00	7.12	7.01	7.08	7.10	525	425	600	575
Nakorotubu Fault	7.37	7.22	7.30	7.40	7.27	7.34	7.35	1200	960	1440	1260
FFZ	7.54	7.40	7.48	7.56	7.43	7.50	7.52	2000	1600	2400	2100

Note: Measured fault parameters and calculated MCEs in black represent the actual values used in this study. The sensitivity analysis on the MCE by varying fault parameters are shown in red (+ 20% of fault parameter) and blue (-20% of fault parameter). The values in green represent the effect of lowering the fault dip by 20%, on the rupture width and the MCE.

APPENDIX 13

CALCULATION OF PEAK GROUND ACCELERATION AND THE HORIZONTAL ACCELERATION RESPONSE SPECTRA

Described below are the attenuation relationships that were used in this thesis for calculating the peak horizontal ground acceleration (PGA) and the horizontal acceleration response spectra (S_a).

PGA calculations

The spreadsheet file with PGA calculations can be found at the following folder location in the Data CD accompanying this thesis:

DataCD/Appendix 13/PGA/PGA.xls

The models of Abrahamson & Silva (1997), Sadigh et al. (1997), Campbell & Bozorgnia (2003) and Spudich et al. (1999) were used to estimate PGA in this study.

Within the PGA.xls file the calculations using these models are presented in separate sheets as follows:

Sheet 1: Abrahamson & Silva (1997) method
Sheet 2: Sadigh et al. (1997) method
Sheet 3: Campbell & Bozorgnia (2003) method
Sheet 4: Spudich et al. (1999) method

The equations used in these models are presented below, and the printouts of the separate spreadsheets are given in subsequent pages.

ATTENUATION EQUATIONS OF ABRAHAMSON & SILVA (1997):

$$\ln S_a(g) = f_1 (M, r_{rup}) + F f_3(M) + HW f_4(M, r_{rup}) + S f_5(\text{pga}_{\text{rock}})$$

where $S_a(g)$ is the spectral acceleration (or *PGA* at period = 0.01s) in g, M is the moment magnitude, r_{rup} is the closest distance to the fault rupture plane, F is the fault type (1 for reverse, 0.5 for reverse/oblique, and 0 for otherwise), HW is the dummy variable for hanging wall sites (1 for sites over the hanging wall, 0 for other wise), and S is a dummy variable for the site class (0 for rock or shallow soil, 1 for deep soil).

The function $f_1(M, r_{rup})$ is the basic functional form of the attenuation for strike-slip events recorded at rock sites. For $f_1(M, r_{rup})$, the following is used:

For $M \leq c_1$

$$f_1(M, r_{rup}) = a_1 + a_2(M-c_1) + a_{12} (8.5-M)^n + [a_3 + a_{13}(M-c_1)] \ln R$$

For $M \geq c_1$

$$f_1(M, r_{rup}) = a_1 + a_4(M-c_1) + a_{12} (8.5-M)^n + [a_3 + a_{13}(M-c_1)] \ln R$$

where:

$$R = (r_{rup}^2 + c_4^2)^{0.5}$$

Style of faulting factor:

$$f_3(M) = \begin{cases} a_5 & \text{for } M \leq 5.8 \\ a_5 + ((a_6 - a_5)/(c_1 - 5.8)) & \text{for } 5.8 < M < c_1 \\ a_6 & \text{for } M \geq c_1 \end{cases}$$

Hanging wall effect:

$$f_4(M, r_{rup}) = f_{HW}(M)\, f_{HW}(r_{rup})$$

where:

$$f_{HW}(M) = \begin{cases} 0 & \text{for } M \leq 5.5 \\ M-5.5 & \text{for } 5.5 < M < 6.5 \\ 1 & \text{for } M \geq 6.5 \end{cases}$$

$$f_{HW}(r_{rup}) = \begin{cases} 0 & \text{for } r_{rup} < 4 \\ a_9\,((r_{rup} - 4)/4) & \text{for } 4 < r_{rup} < 8 \\ a_9 & \text{for } 8 < r_{rup} < 18 \\ a_9\,(1 - ((r_{rup} - 18)/7) & \text{for } 18 < r_{rup} < 24 \\ 0 & \text{for } r_{rup} > 25 \end{cases}$$

Site response:

$$f_5(\text{pga}_{\text{rock}}) = a_{10} + a_{11} \ln (\text{pga}_{\text{rock}} + c_5)$$

where:

pga_{rock} is the expected peak acceleration on rock in g by the median attenuation relationship with $S = 0$.

The values for the various regression coefficients (a) and (c) are given in the spreadsheet file.

ATTENUATION EQUATIONS OF SADIGH ET AL. (1997):

For rock sites (and strike slip faults):

$$\ln (\gamma) = C_1 + C_2 M + C_3 (8.5M)^{2.5} + C_4 \ln (r_{rup} + \exp(C_5 + C_6 M) + C_7 \ln (r_{rup} + 2)$$

where γ is the spectral acceleration (or PGA) in g, M is the moment magnitude and r_{rup} is the minimum distance to the rupture surface.

For deep soil sites (and strike slip faults):

$$\ln(\gamma) = C_1 + C_2 M - C_3 \ln(r_{rup} + C_4 e^{C_5 M}) + C_6 + C_7 (8.5\text{-}M)^{2.5}$$

The values for the various regression coefficients (C) are given in the spreadsheet file.

ATTENUATION EQUATIONS OF CAMPBELL & BOZORGNIA (2003):

$$\ln Y = c_1 + f_1(M_w) + c_4 \ln(f_2(M_w, r_{seis}, S))^{0.5} + f_3(F) + f_4(S) + f_5(HW, F, M_w, r_{seis})$$

where the magnitude characteristics are given by:

$$f_1(M_w) = c_2 M_w + c_3(8.5 - M_w)^2$$

the distance scaling characteristics are given by:

$$f_2(M_w, r_{seis}, S) = r_{seis}^2 + g(S)^2 (\exp[c_8 M_w + c_9(8.5 - M_w)^2])^2$$

the near-source effect of local site conditions is given by:

$$g(S) = c_5 + c_6(S_{VFS}) + (S_{SR}) + c_7 S_{FR}$$

the effect of faulting mechanism is given by:

$$f_3(F) = c_{10} F_{RV} + c_{11} F_{TH}$$

the far-source effect of local site conditions is given by:

$$f_4(S) = c_{12} S_{VFS} + c_{13} S_{SR} + c_{14} S_{FR}$$

and the effect of the hanging wall (HW) is given by:

$$f_5(HW, F, M_w, r_{seis}) = HW f_3(F) f_{HW}(M_w) f_{HW}(r_{seis})$$

where:

$$HW = \begin{cases} S_{VFS} + S_{SR}\,0 & \text{for } r_{jb} \geq 5 \text{ km} \\ S_{FR}\,(5 - r_{jb})/5 & \text{otherwise } \delta > 70^{o} \end{cases}$$

$$f_{HW}(M_w) = \begin{cases} 0 & \text{for } M_w < 5.5 \\ M_w - 5.5 & \text{for } 5.5 \leq M_w \leq 6.5 \\ 1 & \text{for } M_w > 6.5 \end{cases}$$

and

$$f_{HW}(r_{seis}) = \begin{cases} c_{15}(r_{seis}/8) & \text{for } r_{seis} < 8 \text{ km} \\ c_{15} & \text{for } r_{seis} \geq 8 \text{ km} \end{cases}$$

In the previous equations, Y is either average horizontal component of PGA or 5% damped spectral acceleration in g; M_w is the moment magnitude; r_{seis} is the closest distance to seismogenic rupture in kilometres; r_{jb} is the closest distance to the surface projection of fault rupture in kilometres; δ is fault dip in degrees; S_{VFS} = 1 for very firm soil, S_{SR} = 1 for soft rock, S_{FR} = 1 for firm rock, and $S_{VFS} = S_{SR} = S_{FR} = 0$ for firm soil, and F_{RV} = 1 for reverse faulting, F_{TH} = 1 for thrust faulting, and $F_{RV} = F_{TH} = 0$ for strike slip and normal faulting. The values for the various regression coefficients (c) are given in the spreadsheet file.

ATTENUATION EQUATIONS OF SPUDICH ET AL. (1999):

$$\log_{10}(Z) = b_1 + b_2\,(M - 6) + b_3\,(M - 6)^2 + b_5 \log_{10} D + b_6 T$$

where Z is the PGA (g) at 5% damping and M is the moment magnitude.

$$D = (r_{jb}^2 + h^2)^{0.5}$$

r_{jb} is the Joyner-Boore distance (see Section 9.5.2.1), T is 0 for rock site and is 1 for soil site. The values for the various regression coefficients (b) and h are given in the spreadsheet file.

Spectral Acceleration Calculation

The spreadsheet files with S_a calculations for all five sites can be found at the following folder location in the Data CD accompanying this thesis:

DataCD/Appendix 13/SA

Prints out of the various S_a spreadsheets are given in the pages following the PGA spreadsheets.

The horizontal acceleration response spectra (S_a) for all sites were determined using the selected Controlling Maximum Credible Earthquakes and the spectral attenuation relationship of Abrahamson & Silva (1997) based on the equations described in the previous section. The full least of regression coefficients for periods between 0.01 to 5 seconds are given in the spreadsheets files.

References

Abrahamson, N.A. & Silva, W.J. 1997. Empirical response spectral attenuation relations for shallow crustal earthquakes. *Seismological Research Letters* **68**, 94-127.

Campbell, K.W. & Bozorgnia, Y. 2003. Updated near-source ground-motion (attenuation) relations for the horizontal and vertical components of peak ground acceleration and acceleration response spectra. *Bulletin of the Seismological Society of America* **93**, 314-331.

Sadigh, K., Chang, C.Y., Egan, J.A., Makdisi, F. & Youngs, R.R. 1997. Attenuation relationships for shallow crustal earthquakes based on California strong motion data. *Seismological Research Letters* **68**, 180-189.

Spudich, P., Joyner, W.B., Lindh, A.G., Boore, D.M., Margaris, B.M. & Fletcher, J.B. 1999. SEA99; a revised ground motion prediction relation for use in extensional tectonic regimes. *Bulletin of the Seismological Society of America* **89**, 1156-1170.

PGAs from Abrahamson & Silva (1997) model

	M	r_{rup}	F	HW	S	PGA	$ln(S_a)$	$f_1(M,r_{rup})$	$f_3(M)$	$f_4(M,r_{rup})$	$f_{HW}(M)$	$f_{HW}(r_{rup})$	$f_5 pga_{(rock)}$	R	$pga_{(rock)}$	$ln(S_a)$	$f_1(M,r_{rup})$	$f_3(M)$	$f_4(M,r_{rup})$	$f_{HW}(M)$	$f_{HW}(r_{rup})$	R
Mavuvu Fault/lineament Zone																						
Suva	7.6	47	0	0	0	0.12	-2.16	-2.16	0.26	0.00	1.00	0.00	0.03	47.33	0.12	-2.16	-2.16	0.26	0.00	1.00	0.00	47.33
Nausori	7.6	41	0	0	1	0.13	-2.03	-2.04	0.26	0.00	1.00	0.00	0.00	41.38	0.13	-2.04	-2.04	0.26	0.00	1.00	0.00	41.38
Navua	7.6	33	0	0	1	0.15	-1.87	-1.84	0.26	0.00	1.00	0.00	-0.03	33.47	0.16	-1.84	-1.84	0.26	0.00	1.00	0.00	33.47
Monasavu	7.6	11	0	0	0	0.41	-0.90	-0.90	0.26	0.37	1.00	0.37	-0.23	12.34	0.41	-0.90	-0.90	0.26	0.37	1.00	0.37	12.34
Qaliwana	7.6	27	0	0	0	0.19	-1.65	-1.65	0.26	0.00	1.00	0.00	-0.07	27.57	0.19	-1.65	-1.65	0.26	0.00	1.00	0.00	27.57
Naqara Fault																						
Suva	7.1	15	0	0	0	0.27	-1.31	-1.31	0.26	0.37	1.00	0.37	-0.14	16.01	0.27	-1.31	-1.31	0.26	0.37	1.00	0.37	16.01
Nausori	7.1	30	0	0	1	0.14	-1.98	-1.97	0.26	0.00	1.00	0.00	-0.01	30.52	0.14	-1.97	-1.97	0.26	0.00	1.00	0.00	30.52
Navua	7.1	12	0	0	1	0.27	-1.29	-1.11	0.26	0.37	1.00	0.37	-0.18	13.24	0.33	-1.11	-1.11	0.26	0.37	1.00	0.37	13.24
Monasavu	7.1	29	0	0	0	0.14	-1.93	-1.93	0.26	0.00	1.00	0.00	-0.02	29.54	0.14	-1.93	-1.93	0.26	0.00	1.00	0.00	29.54
Qaliwana	7.1	43	0	0	0	0.10	-2.33	-2.33	0.26	0.00	1.00	0.00	0.06	43.36	0.10	-2.33	-2.33	0.26	0.00	1.00	0.00	43.36
Sovi/Yalavou Fault																						
Suva	7.1	72	0	0	0	0.06	-2.85	-2.85	0.26	0.00	1.00	0.00	0.14	72.22	0.06	-2.85	-2.85	0.26	0.00	1.00	0.00	72.22
Nausori	7.1	80	0	0	1	0.06	-2.80	-2.96	0.26	0.00	1.00	0.00	0.16	80.20	0.05	-2.96	-2.96	0.26	0.00	1.00	0.00	80.20
Navua	7.1	52	0	0	1	0.09	-2.43	-2.52	0.26	0.00	1.00	0.00	0.09	52.30	0.08	-2.52	-2.52	0.26	0.00	1.00	0.00	52.30
Monasavu	7.1	35	0	0	0	0.12	-2.12	-2.12	0.26	0.00	1.00	0.00	0.02	35.45	0.12	-2.12	-2.12	0.26	0.00	1.00	0.00	35.45
Qaliwana	7.1	37	0	0	0	0.11	-2.18	-2.18	0.26	0.00	1.00	0.00	0.03	37.42	0.11	-2.18	-2.18	0.26	0.00	1.00	0.00	37.42
Nasivi Fault																						
Suva	6.8	79	0	0	0	0.04	-3.13	-3.13	0.26	0.00	1.00	0.00	0.18	79.20	0.04	-3.13	-3.13	0.26	0.00	1.00	0.00	79.20
Nausori	6.8	79	0	0	1	0.05	-2.94	-3.13	0.26	0.00	1.00	0.00	0.18	79.20	0.04	-3.13	-3.13	0.26	0.00	1.00	0.00	79.20
Navua	6.8	76	0	0	1	0.05	-2.91	-3.08	0.26	0.00	1.00	0.00	0.18	76.21	0.05	-3.08	-3.08	0.26	0.00	1.00	0.00	76.21
Monasavu	6.8	23	0	0	0	0.16	-1.83	-1.83	0.26	0.11	1.00	0.11	-0.04	23.67	0.16	-1.83	-1.83	0.26	0.11	1.00	0.11	23.67
Qaliwana	6.8	11	0	0	0	0.32	-1.12	-1.12	0.26	0.37	1.00	0.37	-0.18	12.34	0.32	-1.12	-1.12	0.26	0.37	1.00	0.37	12.34
Suva Canyon Fault																						
Suva	6.9	4	0	0	0	0.62	-0.48	-0.48	0.26	0.00	1.00	0.00	-0.32	6.88	0.62	-0.48	-0.48	0.26	0.00	1.00	0.00	6.88
Nausori	6.9	20	0	0	1	0.18	-1.72	-1.65	0.26	0.26	1.00	0.26	-0.07	20.77	0.19	-1.65	-1.65	0.26	0.26	1.00	0.26	20.77
Navua	6.9	19	0	0	1	0.19	-1.68	-1.60	0.26	0.32	1.00	0.32	-0.08	19.81	0.20	-1.60	-1.60	0.26	0.32	1.00	0.32	19.81
Monasavu	6.9	55	0	0	0	0.07	-2.69	-2.69	0.26	0.00	1.00	0.00	0.12	55.28	0.07	-2.69	-2.69	0.26	0.00	1.00	0.00	55.28
Qaliwana	6.9	70	0	0	0	0.05	-2.94	-2.94	0.26	0.00	1.00	0.00	0.16	70.22	0.05	-2.94	-2.94	0.26	0.00	1.00	0.00	70.22
Nakorotubu Fault																						
Suva	7.2	51	0	0	0	0.09	-2.45	-2.45	0.26	0.00	1.00	0.00	0.08	51.31	0.09	-2.45	-2.45	0.26	0.00	1.00	0.00	51.31
Nausori	7.2	37	0	0	1	0.12	-2.11	-2.13	0.26	0.00	1.00	0.00	0.02	37.42	0.12	-2.13	-2.13	0.26	0.00	1.00	0.00	37.42
Navua	7.2	72	0	0	1	0.07	-2.66	-2.79	0.26	0.00	1.00	0.00	0.13	72.22	0.06	-2.79	-2.79	0.26	0.00	1.00	0.00	72.22
Monasavu	7.2	41	0	0	0	0.11	-2.23	-2.23	0.26	0.00	1.00	0.00	0.04	41.38	0.11	-2.23	-2.23	0.26	0.00	1.00	0.00	41.38
Qaliwana	7.2	39	0	0	0	0.11	-2.18	-2.18	0.26	0.00	1.00	0.00	0.03	39.40	0.11	-2.18	-2.18	0.26	0.00	1.00	0.00	39.40
FFZ																						
Suva	7.5	225	0	0	0	0.02	-3.71	-3.71	0.26	0.00	1.00	0.00	0.25	225.07	0.02	-3.71	-3.71	0.26	0.00	1.00	0.00	225.07
Nausori	7.5	217	0	0	1	0.03	-3.42	-3.67	0.26	0.00	1.00	0.00	0.25	217.07	0.03	-3.67	-3.67	0.26	0.00	1.00	0.00	217.07
Navua	7.5	227	0	0	1	0.03	-3.46	-3.72	0.26	0.00	1.00	0.00	0.25	227.07	0.02	-3.72	-3.72	0.26	0.00	1.00	0.00	227.07
Monasavu	7.5	174	0	0	0	0.03	-3.46	-3.46	0.26	0.00	1.00	0.00	0.22	174.09	0.03	-3.46	-3.46	0.26	0.00	1.00	0.00	174.09
Qaliwana	7.5	160	0	0	0	0.03	-3.38	-3.38	0.26	0.00	1.00	0.00	0.22	160.10	0.03	-3.38	-3.38	0.26	0.00	1.00	0.00	160.10

period	c4	a1	a2	a3	a4	a5	a6	a9	a10	a11	a12	a13	c1	c5	n
0.01	5.600	1.640	0.512	-1.1450	-0.144	0.610	0.260	0.370	-0.417	-0.230	0.0000	0.17	6.4	0.03	2

PGAs from Sadigh et al. (1997) model

	Rocks sites	*M*	r_{rup}	*PGA*	ln (γ)
Mavuvu Fault/lineament Zone					
	Suva	7.6	47	**0.12**	-2.12
	Monasavu	7.6	11	**0.42**	-0.86
	Qaliwana	7.6	27	**0.22**	-1.51
Naqara Fault	Suva	7.1	15	**0.29**	-1.23
	Monasavu	7.1	29	**0.16**	-1.86
	Qaliwana	7.1	43	**0.10**	-2.34
Sovi/Yalavou Fault					
	Suva	7.1	72	**0.05**	-3.08
	Monasavu	7.1	35	**0.13**	-2.08
	Qaliwana	7.1	37	**0.12**	-2.15
Nasivi Fault	Suva	6.8	79	**0.03**	-3.48
	Monasavu	6.8	23	**0.17**	-1.78
	Qaliwana	6.8	11	**0.33**	-1.12
Suva Canyon Fault	Suva	6.9	4	**0.55**	-0.60
	Monasavu	6.9	57	**0.06**	-2.88
	Qaliwana	6.9	78	**0.03**	-3.37
Nakorotubu Fault	Suva	7.2	51	**0.08**	-2.50
	Monasavu	7.2	41	**0.11**	-2.21
	Qaliwana	7.2	39	**0.12**	-2.15
FFZ	Suva	7.5	225	**0.01**	-4.67
	Monasavu	7.5	174	**0.01**	-4.21
	Qaliwana	7.5	160	**0.02**	-4.06

	Soils sites	*M*	r_{rup}	*PGA*	ln (γ)
Mavuvu Fault/lineament Zone					
	Nausori	7.6	41	**0.15**	-1.90
	Navua	7.6	33	**0.18**	-1.70
Naqara Fault	Nausori	7.1	30	**0.15**	-1.88
	Navua	7.1	12	**0.30**	-1.20
Sovi Fault	Nausori	7.1	80	**0.05**	-2.98
	Navua	7.1	52	**0.09**	-2.45
Nasivi Fault	Nausori	6.8	79	**0.04**	-3.20
	Navua	6.8	76	**0.04**	-3.14
Suva Canyon Fault	Nausori	6.9	20	**0.20**	-1.63
	Navua	6.9	19	**0.20**	-1.59
Nakorotubu Fault	Nausori	7.2	37	**0.13**	-2.02
	Navua	7.2	72	**0.06**	-2.77
FFZ	Nausori	7.5	217	**0.02**	-4.05
	Navua	7.5	227	**0.02**	-4.11

Rock sites, strike slip faults, M>6.5

C_1	C_2	C_3	C_4	C_5	C_6	C_7
-1.274	1.1	0	-2.1	-0.48451	0.524	0

Deep soil sites, strike slip faults, M>6.5

C_1	C_2	C_3	C_4	C_5	C_6	C_7
-2.17	1	1.7	0.3825	0.5882	0	0

PGAs from Campbell & Bozorgnia (2002) model

	M_w	r_{seis}	r_{jb}	F_{RV}	F_{TH}	S_{VFS}	S_{SR}	S_{FR}	PGA	ln(Y)	$f_1(M_w)$	$f_2(M_w, r_{seis}, S)$	$g(S)$	$f_3(F)$	$f_4(S)$	$f_5(HW,F,M_w,r_{seis})$	HW	$f_{HW}(M_w)$	$f_{HW}(r_{seis})$
Mavuvu Fault/Lineament Zone																			
Suva	7.6	**47**	47	0	0	0	1	0	**0.12**	-2.09	6.20	2364.99	0.04	0	-0.14	0	0	1	0.37
Nausori	7.6	**41**	41	0	0	0	0	0	**0.16**	-1.83	6.20	1883.33	0.04	0	0.00	0	0	1	0.37
Navua	7.6	**33**	33	0	0	0	0	0	**0.20**	-1.63	6.20	1291.33	0.04	0	0.00	0	0	1	0.37
Monasavu	7.6	**11**	11	0	0	0	1	0	**0.39**	-0.95	6.20	276.99	0.04	0	-0.14	0	0	1	0.37
Qaliwana	7.6	**27**	27	0	0	0	1	0	**0.21**	-1.57	6.20	884.99	0.04	0	-0.14	0	0	1	0.37
Naqara Fault																			
Suva	7.1	**15**	9	0	0	0	1	0	**0.25**	-1.37	5.84	303.41	0.04	0	-0.14	0	0	1	0.37
Nausori	7.1	**30**	25	0	0	0	0	0	**0.16**	-1.86	5.84	1001.71	0.04	0	0.00	0	0	1	0.37
Navua	7.1	**13**	12	0	0	0	0	0	**0.31**	-1.17	5.84	270.71	0.04	0	0.00	0	0	1	0.37
Monasavu	7.1	**29**	29	0	0	0	1	0	**0.14**	-1.96	5.84	919.41	0.04	0	-0.14	0	0	1	0.37
Qaliwana	7.1	**43**	43	0	0	0	1	0	**0.10**	-2.35	5.84	1927.41	0.04	0	-0.14	0	0	1	0.37
Sovi/Yalavou Fault																			
Suva	7.1	**72**	72	0	0	0	1	0	**0.06**	-2.88	5.84	5262.41	0.04	0	-0.14	0	0	1	0.37
Nausori	7.1	**80**	80	0	0	0	0	0	**0.06**	-2.85	5.84	6501.71	0.04	0	0.00	0	0	1	0.37
Navua	7.1	**52**	52	0	0	0	0	0	**0.09**	-2.41	5.84	2805.71	0.04	0	0.00	0	0	1	0.37
Monasavu	7.1	**35**	35	0	0	0	1	0	**0.12**	-2.14	5.84	1303.41	0.04	0	-0.14	0	0	1	0.37
Qaliwana	7.1	**37**	37	0	0	0	1	0	**0.11**	-2.20	5.84	1447.41	0.04	0	-0.14	0	0	1	0.37
Nasivi Fault																			
Suva	6.8	**79**	79	0	0	0	1	0	**0.04**	-3.19	5.63	6293.75	0.04	0	-0.14	0	0	1	0.37
Nausori	6.8	**79**	79	0	0	0	0	0	**0.05**	-3.05	5.63	6309.43	0.04	0	0.00	0	0	1	0.37
Navua	6.8	**76**	76	0	0	0	0	0	**0.05**	-3.01	5.63	5844.43	0.04	0	0.00	0	0	1	0.37
Monasavu	6.8	**23**	23	0	0	0	1	0	**0.15**	-1.92	5.63	581.75	0.04	0	-0.14	0	0	1	0.37
Qaliwana	6.8	**11**	11	0	0	0	1	0	**0.28**	-1.28	5.63	173.75	0.04	0	-0.14	0	0	1	0.37
Suva Canyon Fault																			
Suva	6.9	**4.03**	4	0	0	0	1	0	**0.46**	-0.78	5.69	76.36	0.04	0	-0.14	0	0	1	0.19
Nausori	6.9	**20**	20	0	0	0	0	0	**0.20**	-1.61	5.69	477.98	0.04	0	0.00	0	0	1	0.37
Navua	6.9	**19**	15	0	0	0	0	0	**0.21**	-1.57	5.69	438.98	0.04	0	0.00	0	0	1	0.37
Monasavu	6.9	**55**	52	0	0	0	1	0	**0.06**	-2.74	5.69	3085.12	0.04	0	-0.14	0	0	1	0.37
Qaliwana	6.9	**70**	67	0	0	0	1	0	**0.05**	-2.99	5.69	4960.12	0.04	0	-0.14	0	0	1	0.37
Nakorotubu Fault																			
Suva	7.2	**51**	51	0	0	0	1	0	**0.09**	-2.45	5.91	2690.73	0.04	0	-0.14	0	0	1	0.37
Nausori	7.2	**37**	37	0	0	0	0	0	**0.14**	-2.00	5.91	1485.39	0.04	0	0.00	0	0	1	0.37
Navua	7.2	**72**	72	0	0	0	0	0	**0.07**	-2.68	5.91	5300.39	0.04	0	0.00	0	0	1	0.37
Monasavu	7.2	**41**	41	0	0	0	1	0	**0.11**	-2.23	5.91	1770.73	0.04	0	-0.14	0	0	1	0.37
Qaliwana	7.2	**39**	39	0	0	0	1	0	**0.11**	-2.18	5.91	1610.73	0.04	0	-0.14	0	0	1	0.37
FFZ																			
Suva	7.5	**225**	225	0	0	0	1	0	**0.02**	-3.79	6.13	50760.58	0.04	0	-0.14	0	0	1	0.37
Nausori	7.5	**217**	217	0	0	0	0	0	**0.03**	-3.62	6.13	47264.85	0.04	0	0.00	0	0	1	0.37
Navua	7.5	**227**	227	0	0	0	0	0	**0.03**	-3.66	6.13	51704.85	0.04	0	0.00	0	0	1	0.37
Monasavu	7.5	**174**	174	0	0	0	1	0	**0.03**	-3.52	6.13	30411.58	0.04	0	-0.14	0	0	1	0.37
Qaliwana	7.5	**160**	160	0	0	0	1	0	**0.03**	-3.43	6.13	25735.58	0.04	0	-0.14	0	0	1	0.37

PGA	c1	c2	c3	c4	c5	c6	c7	c8	c9	c10	c11	c12	c13	c14	c15	c16	c17
corrected	-4.033	0.81	0.04	-1.1	0.04	-0	-0	0.766	0.034	0.343	0.351	-0.123	-0.138	-0.289	0.37	0.92	0.219

PGAs from Spudich et al. (1999) model

		M	r_{jb}	*PGA*	$\log_{10}(Z)$	*D*	*T*
Mavuvu Fault/Lineament Zone							
	Suva	7.6	47	**0.10**	-0.99	47.56	0
	Nausori	7.6	41	**0.15**	-0.81	41.64	1
	Navua	7.6	33	**0.19**	-0.72	33.79	1
	Monasavu	7.6	11	**0.51**	-0.29	13.19	1
	Qaliwana	7.6	27	**0.23**	-0.63	27.96	1
Naqara Fault							
	Suva	7.1	9	**0.32**	-0.49	11.57	0
	Nausori	7.1	25	**0.18**	-0.75	26.04	1
	Navua	7.1	12	**0.34**	-0.47	14.03	1
	Monasavu	7.1	29	**0.15**	-0.81	29.90	1
	Qaliwana	7.1	43	**0.10**	-0.98	43.61	1
Sovi/Yalavou Fault							
	Suva	7.1	72	**0.05**	-1.33	72.37	0
	Nausori	7.1	80	**0.05**	-1.26	80.33	1
	Navua	7.1	52	**0.09**	-1.07	52.51	1
	Monasavu	7.1	35	**0.13**	-0.89	35.75	1
	Qaliwana	7.1	37	**0.12**	-0.92	37.71	1
Nasivi Fault							
	Suva	6.8	79	**0.03**	-1.46	79.33	0
	Nausori	6.8	79	**0.04**	-1.35	79.33	1
	Navua	6.8	76	**0.05**	-1.33	76.35	1
	Monasavu	6.8	23	**0.16**	-0.80	24.12	1
	Qaliwana	6.8	11	**0.30**	-0.53	13.19	1
Suva Canyon Fault							
	Suva	6.9	4	**0.40**	-0.40	8.30	0
	Nausori	6.9	20	**0.19**	-0.72	21.28	1
	Navua	6.9	15	**0.25**	-0.61	16.67	1
	Monasavu	6.9	52	**0.07**	-1.13	52.51	1
	Qaliwana	6.9	67	**0.06**	-1.24	67.39	1
Nakorotubu Fault							
	Suva	7.2	51	**0.07**	-1.14	51.52	0
	Nausori	7.2	37	**0.13**	-0.89	37.71	1
	Navua	7.2	72	**0.07**	-1.19	72.37	1
	Monasavu	7.2	41	**0.12**	-0.93	41.64	1
	Qaliwana	7.2	39	**0.12**	-0.91	39.67	1
FFZ							
	Suva	7.5	225	**0.02**	-1.73	225.12	0
	Nausori	7.5	217	**0.03**	-1.60	217.12	1
	Navua	7.5	227	**0.02**	-1.62	227.12	1
	Monasavu	7.5	174	**0.03**	-1.50	174.15	1
	Qaliwana	7.5	160	**0.03**	-1.46	160.17	1

b1	b2	b3	b5	b6	h(km)
0.299	0.299	0	-1.052	0.112	7.27

Spectral acceleration calculation for Suva using Abrahamson & Silva (1997) model

CMCE	M	r_{rup}	F	HW	S	PGA
Suva Canyon Fault	6.9	4	0	0	0	0.62

S_a	$ln(S_a)$	$f_1(M,r_{rup})$	$f_3(M)$	$f_4(M,r_{rup})$	$f_{HW}(M)$	$f_{HW}(r_{rup})$	$f_5 pga_{(rock)}$	R	$pga_{(rock)}$	$ln(S_a)$	$f_1(M,r_{rup})$	$f_3(M)$	$f_4(M,r_{rup})$	$f_{HW}(M)$	$f_{HW}(r_{rup})$	R
0.04	-3.15	-3.15	-0.20	0.00	1.00	0.00	0.56	5.32	0.04	-3.15	-3.15	-0.20	0.00	1.00	0.00	5.32
0.06	-2.74	-2.74	-0.20	0.00	1.00	0.00	0.55	5.32	0.06	-2.74	-2.74	-0.20	0.00	1.00	0.00	5.32
0.10	-2.27	-2.27	-0.16	0.00	1.00	0.00	0.55	5.32	0.10	-2.27	-2.27	-0.16	0.00	1.00	0.00	5.32
0.19	-1.65	-1.65	-0.09	0.00	1.00	0.00	0.55	5.32	0.19	-1.65	-1.65	-0.09	0.00	1.00	0.00	5.32
0.28	-1.27	-1.27	-0.05	0.00	1.00	0.00	0.55	5.35	0.28	-1.27	-1.27	-0.05	0.00	1.00	0.00	5.35
0.46	-0.78	-0.78	0.01	0.00	1.00	0.00	0.42	5.45	0.46	-0.78	-0.78	0.01	0.00	1.00	0.00	5.45
0.54	-0.62	-0.62	0.04	0.00	1.00	0.00	0.39	5.52	0.54	-0.62	-0.62	0.04	0.00	1.00	0.00	5.52
0.60	-0.51	-0.51	0.06	0.00	1.00	0.00	0.34	5.59	0.60	-0.51	-0.51	0.06	0.00	1.00	0.00	5.59
0.74	-0.30	-0.30	0.09	0.00	1.00	0.00	0.22	5.74	0.74	-0.30	-0.30	0.09	0.00	1.00	0.00	5.74
0.86	-0.15	-0.15	0.12	0.00	1.00	0.00	0.10	5.87	0.86	-0.15	-0.15	0.12	0.00	1.00	0.00	5.87
0.93	-0.07	-0.07	0.13	0.00	1.00	0.00	0.03	5.93	0.93	-0.07	-0.07	0.13	0.00	1.00	0.00	5.93
1.03	0.03	0.03	0.15	0.00	1.00	0.00	-0.07	6.04	1.03	0.03	0.03	0.15	0.00	1.00	0.00	6.04
1.10	0.10	0.10	0.17	0.00	1.00	0.00	-0.14	6.11	1.10	0.10	0.10	0.17	0.00	1.00	0.00	6.11
1.23	0.21	0.21	0.20	0.00	1.00	0.00	-0.26	6.25	1.23	0.21	0.21	0.20	0.00	1.00	0.00	6.25
1.37	0.32	0.32	0.23	0.00	1.00	0.00	-0.43	6.38	1.37	0.32	0.32	0.23	0.00	1.00	0.00	6.38
1.45	0.37	0.37	0.26	0.00	1.00	0.00	-0.54	6.48	1.45	0.37	0.37	0.26	0.00	1.00	0.00	6.48
1.45	0.37	0.37	0.26	0.00	1.00	0.00	-0.63	6.55	1.45	0.37	0.37	0.26	0.00	1.00	0.00	6.55
1.41	0.34	0.34	0.26	0.00	1.00	0.00	-0.68	6.62	1.41	0.34	0.34	0.26	0.00	1.00	0.00	6.62
1.26	0.23	0.23	0.26	0.00	1.00	0.00	-0.66	6.71	1.26	0.23	0.23	0.26	0.00	1.00	0.00	6.71
1.14	0.13	0.13	0.26	0.00	1.00	0.00	-0.64	6.80	1.14	0.13	0.13	0.26	0.00	1.00	0.00	6.80
1.07	0.07	0.07	0.26	0.00	1.00	0.00	-0.64	6.83	1.07	0.07	0.07	0.26	0.00	1.00	0.00	6.83
1.00	0.00	0.00	0.26	0.00	1.00	0.00	-0.64	6.87	1.00	0.00	0.00	0.26	0.00	1.00	0.00	6.87
0.90	-0.10	-0.10	0.26	0.00	1.00	0.00	-0.65	6.88	0.90	-0.10	-0.10	0.26	0.00	1.00	0.00	6.88
0.84	-0.17	-0.17	0.26	0.00	1.00	0.00	-0.58	6.88	0.84	-0.17	-0.17	0.26	0.00	1.00	0.00	6.88
0.76	-0.27	-0.27	0.26	0.00	1.00	0.00	-0.50	6.88	0.76	-0.27	-0.27	0.26	0.00	1.00	0.00	6.88
0.68	-0.39	-0.39	0.26	0.00	1.00	0.00	-0.39	6.88	0.68	-0.39	-0.39	0.26	0.00	1.00	0.00	6.88
0.62	-0.48	-0.48	0.26	0.00	1.00	0.00	-0.32	6.88	0.62	-0.48	-0.48	0.26	0.00	1.00	0.00	6.88
0.62	-0.48	-0.48	0.26	0.00	1.00	0.00	-0.32	6.88	0.62	-0.48	-0.48	0.26	0.00	1.00	0.00	6.88

period (seconds)	c4	a1	a2	a3	a4	a5	a6	a9	a10	a11	a12	a13	c1	c5	n
5	3.500	-1.460	0.512	-0.7250	-0.144	0.400	-0.200	0.000	0.664	0.040	-0.2150	0.17	6.4	0.03	2
4	3.500	-1.100	0.512	-0.7250	-0.144	0.400	-0.200	0.039	0.640	0.040	-0.1956	0.17	6.4	0.03	2
3	3.500	-0.690	0.512	-0.7250	-0.144	0.400	-0.156	0.089	0.630	0.040	-0.1726	0.17	6.4	0.03	2
2	3.500	-0.150	0.512	-0.7250	-0.144	0.400	-0.094	0.160	0.610	0.040	-0.1400	0.17	6.4	0.03	2
1.5	3.550	0.260	0.512	-0.7721	-0.144	0.438	-0.049	0.210	0.600	0.040	-0.1200	0.17	6.4	0.03	2
1	3.700	0.828	0.512	-0.8383	-0.144	0.490	0.013	0.281	0.423	0.000	-0.1020	0.17	6.4	0.03	2
0.85	3.810	1.020	0.512	-0.8648	-0.144	0.512	0.038	0.309	0.370	-0.028	-0.0927	0.17	6.4	0.03	2
0.75	3.900	1.160	0.512	-0.8852	-0.144	0.528	0.057	0.331	0.320	-0.050	-0.0862	0.17	6.4	0.03	2
0.6	4.120	1.428	0.512	-0.9218	-0.144	0.557	0.091	0.370	0.194	-0.089	-0.0740	0.17	6.4	0.03	2
0.5	4.300	1.615	0.512	-0.9515	-0.144	0.581	0.119	0.370	0.085	-0.121	-0.0635	0.17	6.4	0.03	2
0.46	4.380	1.717	0.512	-0.9652	-0.144	0.592	0.132	0.370	0.020	-0.136	-0.0594	0.17	6.4	0.03	2
0.4	4.520	1.860	0.512	-0.9880	-0.144	0.610	0.154	0.370	-0.065	-0.160	-0.0518	0.17	6.4	0.03	2
0.36	4.620	1.955	0.512	-1.0052	-0.144	0.610	0.170	0.370	-0.123	-0.173	-0.0460	0.17	6.4	0.03	2
0.3	4.800	2.114	0.512	-1.0350	-0.144	0.610	0.198	0.370	-0.219	-0.195	-0.0360	0.17	6.4	0.03	2
0.24	4.970	2.293	0.512	-1.0790	-0.144	0.610	0.232	0.370	-0.350	-0.223	-0.0238	0.17	6.4	0.03	2
0.2	5.100	2.406	0.512	-1.1150	-0.144	0.610	0.260	0.370	-0.445	-0.245	-0.0138	0.17	6.4	0.03	2
0.17	5.190	2.430	0.512	-1.1350	-0.144	0.610	0.260	0.370	-0.522	-0.265	-0.0040	0.17	6.4	0.03	2
0.15	5.270	2.407	0.512	-1.1450	-0.144	0.610	0.260	0.370	-0.577	-0.280	0.0050	0.17	6.4	0.03	2
0.12	5.390	2.272	0.512	-1.1450	-0.144	0.610	0.260	0.370	-0.591	-0.280	0.0180	0.17	6.4	0.03	2
0.1	5.500	2.160	0.512	-1.1450	-0.144	0.610	0.260	0.370	-0.598	-0.280	0.0280	0.17	6.4	0.03	2
0.09	5.540	2.100	0.512	-1.1450	-0.144	0.610	0.260	0.370	-0.609	-0.280	0.0300	0.17	6.4	0.03	2
0.075	5.580	2.037	0.512	-1.1450	-0.144	0.610	0.260	0.370	-0.628	-0.280	0.0300	0.17	6.4	0.03	2
0.06	5.600	1.940	0.512	-1.1450	-0.144	0.610	0.260	0.370	-0.665	-0.280	0.0300	0.17	6.4	0.03	2
0.05	5.600	1.870	0.512	-1.1450	-0.144	0.610	0.260	0.370	-0.620	-0.267	0.0280	0.17	6.4	0.03	2
0.04	5.600	1.780	0.512	-1.1450	-0.144	0.610	0.260	0.370	-0.555	-0.251	0.0245	0.17	6.4	0.03	2
0.03	5.600	1.690	0.512	-1.1450	-0.144	0.610	0.260	0.370	-0.470	-0.230	0.0143	0.17	6.4	0.03	2
0.02	5.600	1.640	0.512	-1.1450	-0.144	0.610	0.260	0.370	-0.417	-0.230	0.0000	0.17	6.4	0.03	2
0.01	5.600	1.640	0.512	-1.1450	-0.144	0.610	0.260	0.370	-0.417	-0.230	0.0000	0.17	6.4	0.03	2

Spectral acceleration calculation for Nausori using Abrahamson & Silva (1997) model

CMCE	M	r_{rup}	F	HW	S	PGA
Suva Canyon Fault	6.9	20	0	0	1	0.18

Sa	$ln(S_a)$	$f_1(M,r_{rup})$	$f_3(M)$	$f_4(M,r_{rup})$	$f_{HW}(M)$	$f_{HW}(r_{rup})$	$f_5 pga_{(rock)}$	R	$pga_{(rock)}$	$ln(S_a)$	$f_1(M,r_{rup})$	$f_3(M)$	$f_4(M,r_{rup})$	$f_{HW}(M)$	$f_{HW}(r_{rup})$	R
0.03	-3.47	-4.01	-0.20	0.00	1.00	0.00	0.54	20.30	0.02	-4.01	-4.01	-0.20	0.00	1.00	0.00	20.30
0.05	-3.07	-3.60	-0.20	0.03	1.00	0.03	0.53	20.30	0.03	-3.60	-3.60	-0.20	0.03	1.00	0.03	20.30
0.07	-2.61	-3.13	-0.16	0.06	1.00	0.06	0.53	20.30	0.04	-3.13	-3.13	-0.16	0.06	1.00	0.06	20.30
0.14	-1.99	-2.51	-0.09	0.11	1.00	0.11	0.52	20.30	0.08	-2.51	-2.51	-0.09	0.11	1.00	0.11	20.30
0.19	-1.67	-2.19	-0.05	0.15	1.00	0.15	0.52	20.31	0.11	-2.19	-2.19	-0.05	0.15	1.00	0.15	20.31
0.26	-1.35	-1.77	0.01	0.20	1.00	0.20	0.42	20.34	0.17	-1.77	-1.77	0.01	0.20	1.00	0.20	20.34
0.29	-1.23	-1.64	0.04	0.22	1.00	0.22	0.41	20.36	0.19	-1.64	-1.64	0.04	0.22	1.00	0.22	20.36
0.32	-1.15	-1.54	0.06	0.24	1.00	0.24	0.39	20.38	0.21	-1.54	-1.54	0.06	0.24	1.00	0.24	20.38
0.35	-1.05	-1.36	0.09	0.26	1.00	0.26	0.31	20.42	0.26	-1.36	-1.36	0.09	0.26	1.00	0.26	20.42
0.36	-1.01	-1.23	0.12	0.26	1.00	0.26	0.22	20.46	0.29	-1.23	-1.23	0.12	0.26	1.00	0.26	20.46
0.37	-1.00	-1.16	0.13	0.26	1.00	0.26	0.17	20.47	0.31	-1.16	-1.16	0.13	0.26	1.00	0.26	20.47
0.38	-0.98	-1.07	0.15	0.26	1.00	0.26	0.09	20.50	0.34	-1.07	-1.07	0.15	0.26	1.00	0.26	20.50
0.38	-0.98	-1.02	0.17	0.26	1.00	0.26	0.04	20.53	0.36	-1.02	-1.02	0.17	0.26	1.00	0.26	20.53
0.38	-0.98	-0.92	0.20	0.26	1.00	0.26	-0.05	20.57	0.40	-0.92	-0.92	0.20	0.26	1.00	0.26	20.57
0.36	-1.02	-0.85	0.23	0.26	1.00	0.26	-0.18	20.61	0.43	-0.85	-0.85	0.23	0.26	1.00	0.26	20.61
0.34	-1.08	-0.82	0.26	0.26	1.00	0.26	-0.26	20.64	0.44	-0.82	-0.82	0.26	0.26	1.00	0.26	20.64
0.32	-1.15	-0.83	0.26	0.26	1.00	0.26	-0.32	20.66	0.44	-0.83	-0.83	0.26	0.26	1.00	0.26	20.66
0.30	-1.22	-0.86	0.26	0.26	1.00	0.26	-0.35	20.68	0.42	-0.86	-0.86	0.26	0.26	1.00	0.26	20.68
0.27	-1.31	-0.97	0.26	0.26	1.00	0.26	-0.34	20.71	0.38	-0.97	-0.97	0.26	0.26	1.00	0.26	20.71
0.25	-1.38	-1.05	0.26	0.26	1.00	0.26	-0.33	20.74	0.35	-1.05	-1.05	0.26	0.26	1.00	0.26	20.74
0.24	-1.43	-1.11	0.26	0.26	1.00	0.26	-0.32	20.75	0.33	-1.11	-1.11	0.26	0.26	1.00	0.26	20.75
0.22	-1.50	-1.17	0.26	0.26	1.00	0.26	-0.33	20.76	0.31	-1.17	-1.17	0.26	0.26	1.00	0.26	20.76
0.20	-1.61	-1.27	0.26	0.26	1.00	0.26	-0.34	20.77	0.28	-1.27	-1.27	0.26	0.26	1.00	0.26	20.77
0.19	-1.64	-1.35	0.26	0.26	1.00	0.26	-0.29	20.77	0.26	-1.35	-1.35	0.26	0.26	1.00	0.26	20.77
0.19	-1.67	-1.44	0.26	0.26	1.00	0.26	-0.22	20.77	0.24	-1.44	-1.44	0.26	0.26	1.00	0.26	20.77
0.18	-1.70	-1.56	0.26	0.26	1.00	0.26	-0.14	20.77	0.21	-1.56	-1.56	0.26	0.26	1.00	0.26	20.77
0.18	-1.72	-1.65	0.26	0.26	1.00	0.26	-0.07	20.77	0.19	-1.65	-1.65	0.26	0.26	1.00	0.26	20.77
0.18	-1.72	-1.65	0.26	0.26	1.00	0.26	-0.07	20.77	0.19	-1.65	-1.65	0.26	0.26	1.00	0.26	20.77

period (seconds)	c4	a1	a2	a3	a4	a5	a6	a9	a10	a11	a12	a13	c1	c5	n
5	3.500	-1.460	0.512	-0.7250	-0.144	0.400	-0.200	0.000	0.664	0.040	-0.2150	0.17	6.4	0.03	2
4	3.500	-1.100	0.512	-0.7250	-0.144	0.400	-0.200	0.039	0.640	0.040	-0.1956	0.17	6.4	0.03	2
3	3.500	-0.690	0.512	-0.7250	-0.144	0.400	-0.156	0.089	0.630	0.040	-0.1726	0.17	6.4	0.03	2
2	3.500	-0.150	0.512	-0.7250	-0.144	0.400	-0.094	0.160	0.610	0.040	-0.1400	0.17	6.4	0.03	2
1.5	3.550	0.260	0.512	-0.7721	-0.144	0.438	-0.049	0.210	0.600	0.040	-0.1200	0.17	6.4	0.03	2
1	3.700	0.828	0.512	-0.8383	-0.144	0.490	0.013	0.281	0.423	0.000	-0.1020	0.17	6.4	0.03	2
0.85	3.810	1.020	0.512	-0.8648	-0.144	0.512	0.038	0.309	0.370	-0.028	-0.0927	0.17	6.4	0.03	2
0.75	3.900	1.160	0.512	-0.8852	-0.144	0.528	0.057	0.331	0.320	-0.050	-0.0862	0.17	6.4	0.03	2
0.6	4.120	1.428	0.512	-0.9218	-0.144	0.557	0.091	0.370	0.194	-0.089	-0.0740	0.17	6.4	0.03	2
0.5	4.300	1.615	0.512	-0.9515	-0.144	0.581	0.119	0.370	0.085	-0.121	-0.0635	0.17	6.4	0.03	2
0.46	4.380	1.717	0.512	-0.9652	-0.144	0.592	0.132	0.370	0.020	-0.136	-0.0594	0.17	6.4	0.03	2
0.4	4.520	1.860	0.512	-0.9880	-0.144	0.610	0.154	0.370	-0.065	-0.160	-0.0518	0.17	6.4	0.03	2
0.36	4.620	1.955	0.512	-1.0052	-0.144	0.610	0.170	0.370	-0.123	-0.173	-0.0460	0.17	6.4	0.03	2
0.3	4.800	2.114	0.512	-1.0350	-0.144	0.610	0.198	0.370	-0.219	-0.195	-0.0360	0.17	6.4	0.03	2
0.24	4.970	2.293	0.512	-1.0790	-0.144	0.610	0.232	0.370	-0.350	-0.223	-0.0238	0.17	6.4	0.03	2
0.2	5.100	2.406	0.512	-1.1150	-0.144	0.610	0.260	0.370	-0.445	-0.245	-0.0138	0.17	6.4	0.03	2
0.17	5.190	2.430	0.512	-1.1350	-0.144	0.610	0.260	0.370	-0.522	-0.265	-0.0040	0.17	6.4	0.03	2
0.15	5.270	2.407	0.512	-1.1450	-0.144	0.610	0.260	0.370	-0.577	-0.280	0.0050	0.17	6.4	0.03	2
0.12	5.390	2.272	0.512	-1.1450	-0.144	0.610	0.260	0.370	-0.591	-0.280	0.0180	0.17	6.4	0.03	2
0.1	5.500	2.160	0.512	-1.1450	-0.144	0.610	0.260	0.370	-0.598	-0.280	0.0280	0.17	6.4	0.03	2
0.09	5.540	2.100	0.512	-1.1450	-0.144	0.610	0.260	0.370	-0.609	-0.280	0.0300	0.17	6.4	0.03	2
0.075	5.580	2.037	0.512	-1.1450	-0.144	0.610	0.260	0.370	-0.628	-0.280	0.0300	0.17	6.4	0.03	2
0.06	5.600	1.940	0.512	-1.1450	-0.144	0.610	0.260	0.370	-0.665	-0.280	0.0300	0.17	6.4	0.03	2
0.05	5.600	1.870	0.512	-1.1450	-0.144	0.610	0.260	0.370	-0.620	-0.267	0.0280	0.17	6.4	0.03	2
0.04	5.600	1.780	0.512	-1.1450	-0.144	0.610	0.260	0.370	-0.555	-0.251	0.0245	0.17	6.4	0.03	2
0.03	5.600	1.690	0.512	-1.1450	-0.144	0.610	0.260	0.370	-0.470	-0.230	0.0143	0.17	6.4	0.03	2
0.02	5.600	1.640	0.512	-1.1450	-0.144	0.610	0.260	0.370	-0.417	-0.230	0.0000	0.17	6.4	0.03	2
0.01	5.600	1.640	0.512	-1.1450	-0.144	0.610	0.260	0.370	-0.417	-0.230	0.0000	0.17	6.4	0.03	2

Spectral acceleration calculation for Navua using Abrahamson & Silva (1997) model

CMCE	M	r_{rup}	F	HW	S	PGA
Naqara Fault	7.1	12	0	0	1	0.27

Sa	$ln(S_a)$	$f_1(M,r_{rup})$	$f_3(M)$	$f_4(M,r_{rup})$	$f_{HW}(M)$	$f_{HW}(r_{rup})$	$f_5 pga_{(rock)}$	R	$pga_{(rock)}$	$ln(S_a)$	$f_1(M,r_{rup})$	$f_3(M)$	$f_4(M,r_{rup})$	$f_{HW}(M)$	$f_{HW}(r_{rup})$	R
0.05	-2.96	-3.51	-0.20	0.00	1.00	0.00	0.55	12.50	0.03	-3.51	-3.51	-0.20	0.00	1.00	0.00	12.50
0.08	-2.58	-3.11	-0.20	0.04	1.00	0.04	0.54	12.50	0.04	-3.11	-3.11	-0.20	0.04	1.00	0.04	12.50
0.12	-2.12	-2.66	-0.16	0.09	1.00	0.09	0.54	12.50	0.07	-2.66	-2.66	-0.16	0.09	1.00	0.09	12.50
0.22	-1.52	-2.06	-0.09	0.16	1.00	0.16	0.54	12.50	0.13	-2.06	-2.06	-0.09	0.16	1.00	0.16	12.50
0.30	-1.19	-1.73	-0.05	0.21	1.00	0.21	0.54	12.51	0.18	-1.73	-1.73	-0.05	0.21	1.00	0.21	12.51
0.42	-0.87	-1.29	0.01	0.28	1.00	0.28	0.42	12.56	0.27	-1.29	-1.29	0.01	0.28	1.00	0.28	12.56
0.47	-0.75	-1.15	0.04	0.31	1.00	0.31	0.40	12.59	0.32	-1.15	-1.15	0.04	0.31	1.00	0.31	12.59
0.50	-0.68	-1.05	0.06	0.33	1.00	0.33	0.37	12.62	0.35	-1.05	-1.05	0.06	0.33	1.00	0.33	12.62
0.55	-0.59	-0.86	0.09	0.37	1.00	0.37	0.26	12.69	0.42	-0.86	-0.86	0.09	0.37	1.00	0.37	12.69
0.57	-0.56	-0.73	0.12	0.37	1.00	0.37	0.17	12.75	0.48	-0.73	-0.73	0.12	0.37	1.00	0.37	12.75
0.57	-0.55	-0.66	0.13	0.37	1.00	0.37	0.10	12.77	0.52	-0.66	-0.66	0.13	0.37	1.00	0.37	12.77
0.58	-0.54	-0.56	0.15	0.37	1.00	0.37	0.02	12.82	0.57	-0.56	-0.56	0.15	0.37	1.00	0.37	12.82
0.58	-0.54	-0.50	0.17	0.37	1.00	0.37	-0.04	12.86	0.61	-0.50	-0.50	0.17	0.37	1.00	0.37	12.86
0.58	-0.55	-0.40	0.20	0.37	1.00	0.37	-0.15	12.92	0.67	-0.40	-0.40	0.20	0.37	1.00	0.37	12.92
0.55	-0.60	-0.32	0.23	0.37	1.00	0.37	-0.29	12.99	0.73	-0.32	-0.32	0.23	0.37	1.00	0.37	12.99
0.51	-0.67	-0.28	0.26	0.37	1.00	0.37	-0.39	13.04	0.76	-0.28	-0.28	0.26	0.37	1.00	0.37	13.04
0.47	-0.75	-0.29	0.26	0.37	1.00	0.37	-0.46	13.07	0.75	-0.29	-0.29	0.26	0.37	1.00	0.37	13.07
0.44	-0.82	-0.32	0.26	0.37	1.00	0.37	-0.50	13.11	0.72	-0.32	-0.32	0.26	0.37	1.00	0.37	13.11
0.40	-0.92	-0.44	0.26	0.37	1.00	0.37	-0.48	13.15	0.65	-0.44	-0.44	0.26	0.37	1.00	0.37	13.15
0.37	-1.00	-0.53	0.26	0.37	1.00	0.37	-0.46	13.20	0.59	-0.53	-0.53	0.26	0.37	1.00	0.37	13.20
0.35	-1.05	-0.59	0.26	0.37	1.00	0.37	-0.46	13.22	0.55	-0.59	-0.59	0.26	0.37	1.00	0.37	13.22
0.33	-1.12	-0.65	0.26	0.37	1.00	0.37	-0.46	13.23	0.52	-0.65	-0.65	0.26	0.37	1.00	0.37	13.23
0.29	-1.22	-0.75	0.26	0.37	1.00	0.37	-0.47	13.24	0.47	-0.75	-0.75	0.26	0.37	1.00	0.37	13.24
0.29	-1.24	-0.83	0.26	0.37	1.00	0.37	-0.42	13.24	0.44	-0.83	-0.83	0.26	0.37	1.00	0.37	13.24
0.28	-1.26	-0.92	0.26	0.37	1.00	0.37	-0.34	13.24	0.40	-0.92	-0.92	0.26	0.37	1.00	0.37	13.24
0.28	-1.28	-1.03	0.26	0.37	1.00	0.37	-0.25	13.24	0.36	-1.03	-1.03	0.26	0.37	1.00	0.37	13.24
0.27	-1.29	-1.11	0.26	0.37	1.00	0.37	-0.18	13.24	0.33	-1.11	-1.11	0.26	0.37	1.00	0.37	13.24
0.27	-1.29	-1.11	0.26	0.37	1.00	0.37	-0.18	13.24	0.33	-1.11	-1.11	0.26	0.37	1.00	0.37	13.24

period (seconds)	c4	a1	a2	a3	a4	a5	a6	a9	a10	a11	a12	a13	c1	c5	n
5	3.500	-1.460	0.512	-0.7250	-0.144	0.400	-0.200	0.000	0.664	0.040	-0.2150	0.17	6.4	0.03	2
4	3.500	-1.100	0.512	-0.7250	-0.144	0.400	-0.200	0.039	0.640	0.040	-0.1956	0.17	6.4	0.03	2
3	3.500	-0.690	0.512	-0.7250	-0.144	0.400	-0.156	0.089	0.630	0.040	-0.1726	0.17	6.4	0.03	2
2	3.500	-0.150	0.512	-0.7250	-0.144	0.400	-0.094	0.160	0.610	0.040	-0.1400	0.17	6.4	0.03	2
1.5	3.550	0.260	0.512	-0.7721	-0.144	0.438	-0.049	0.210	0.600	0.040	-0.1200	0.17	6.4	0.03	2
1	3.700	0.828	0.512	-0.8383	-0.144	0.490	0.013	0.281	0.423	0.000	-0.1020	0.17	6.4	0.03	2
0.85	3.810	1.020	0.512	-0.8648	-0.144	0.512	0.038	0.309	0.370	-0.028	-0.0927	0.17	6.4	0.03	2
0.75	3.900	1.160	0.512	-0.8852	-0.144	0.528	0.057	0.331	0.320	-0.050	-0.0862	0.17	6.4	0.03	2
0.6	4.120	1.428	0.512	-0.9218	-0.144	0.557	0.091	0.370	0.194	-0.089	-0.0740	0.17	6.4	0.03	2
0.5	4.300	1.615	0.512	-0.9515	-0.144	0.581	0.119	0.370	0.085	-0.121	-0.0635	0.17	6.4	0.03	2
0.46	4.380	1.717	0.512	-0.9652	-0.144	0.592	0.132	0.370	0.020	-0.136	-0.0594	0.17	6.4	0.03	2
0.4	4.520	1.860	0.512	-0.9880	-0.144	0.610	0.154	0.370	-0.065	-0.160	-0.0518	0.17	6.4	0.03	2
0.36	4.620	1.955	0.512	-1.0052	-0.144	0.610	0.170	0.370	-0.123	-0.173	-0.0460	0.17	6.4	0.03	2
0.3	4.800	2.114	0.512	-1.0350	-0.144	0.610	0.198	0.370	-0.219	-0.195	-0.0360	0.17	6.4	0.03	2
0.24	4.970	2.293	0.512	-1.0790	-0.144	0.610	0.232	0.370	-0.350	-0.223	-0.0238	0.17	6.4	0.03	2
0.2	5.100	2.406	0.512	-1.1150	-0.144	0.610	0.260	0.370	-0.445	-0.245	-0.0138	0.17	6.4	0.03	2
0.17	5.190	2.430	0.512	-1.1350	-0.144	0.610	0.260	0.370	-0.522	-0.265	-0.0040	0.17	6.4	0.03	2
0.15	5.270	2.407	0.512	-1.1450	-0.144	0.610	0.260	0.370	-0.577	-0.280	0.0050	0.17	6.4	0.03	2
0.12	5.390	2.272	0.512	-1.1450	-0.144	0.610	0.260	0.370	-0.591	-0.280	0.0180	0.17	6.4	0.03	2
0.1	5.500	2.160	0.512	-1.1450	-0.144	0.610	0.260	0.370	-0.598	-0.280	0.0280	0.17	6.4	0.03	2
0.09	5.540	2.100	0.512	-1.1450	-0.144	0.610	0.260	0.370	-0.609	-0.280	0.0300	0.17	6.4	0.03	2
0.075	5.580	2.037	0.512	-1.1450	-0.144	0.610	0.260	0.370	-0.628	-0.280	0.0300	0.17	6.4	0.03	2
0.06	5.600	1.940	0.512	-1.1450	-0.144	0.610	0.260	0.370	-0.665	-0.280	0.0300	0.17	6.4	0.03	2
0.05	5.600	1.870	0.512	-1.1450	-0.144	0.610	0.260	0.370	-0.620	-0.267	0.0280	0.17	6.4	0.03	2
0.04	5.600	1.780	0.512	-1.1450	-0.144	0.610	0.260	0.370	-0.555	-0.251	0.0245	0.17	6.4	0.03	2
0.03	5.600	1.690	0.512	-1.1450	-0.144	0.610	0.260	0.370	-0.470	-0.230	0.0143	0.17	6.4	0.03	2
0.02	5.600	1.640	0.512	-1.1450	-0.144	0.610	0.260	0.370	-0.417	-0.230	0.0000	0.17	6.4	0.03	2
0.01	5.600	1.640	0.512	-1.1450	-0.144	0.610	0.260	0.370	-0.417	-0.230	0.0000	0.17	6.4	0.03	2

Spectral acceleration calculation for Monasavu using Abrahamson & Silva (1997) model

CMCE	M	r_{rup}	F	HW	S	PGA
Mavuvu F/L Zone	7.6	11	0	0	0	0.41

S_a	$ln(S_a)$	$f_1(M,r_{rup})$	$f_3(M)$	$f_4(M,r_{rup})$	$f_{HW}(M)$	$f_{HW}(r_{rup})$	$f_5 pga_{(rock)}$	R	$pga_{(rock)}$	$ln(S_a)$	$f_1(M,r_{rup})$	$f_3(M)$	$f_4(M,r_{rup})$	$f_{HW}(M)$	$f_{HW}(r_{rup})$	R
0.05	-3.08	-3.08	-0.20	0.00	1.00	0.00	0.56	11.54	0.05	-3.08	-3.08	-0.20	0.00	1.00	0.00	11.54
0.07	-2.71	-2.71	-0.20	0.04	1.00	0.04	0.55	11.54	0.07	-2.71	-2.71	-0.20	0.04	1.00	0.04	11.54
0.10	-2.28	-2.28	-0.16	0.09	1.00	0.09	0.55	11.54	0.10	-2.28	-2.28	-0.16	0.09	1.00	0.09	11.54
0.18	-1.71	-1.71	-0.09	0.16	1.00	0.16	0.55	11.54	0.18	-1.71	-1.71	-0.09	0.16	1.00	0.16	11.54
0.25	-1.40	-1.40	-0.05	0.21	1.00	0.21	0.55	11.56	0.25	-1.40	-1.40	-0.05	0.21	1.00	0.21	11.56
0.37	-0.98	-0.98	0.01	0.28	1.00	0.28	0.42	11.61	0.37	-0.98	-0.98	0.01	0.28	1.00	0.28	11.61
0.43	-0.85	-0.85	0.04	0.31	1.00	0.31	0.39	11.64	0.43	-0.85	-0.85	0.04	0.31	1.00	0.31	11.64
0.47	-0.76	-0.76	0.06	0.33	1.00	0.33	0.35	11.67	0.47	-0.76	-0.76	0.06	0.33	1.00	0.33	11.67
0.56	-0.57	-0.57	0.09	0.37	1.00	0.37	0.24	11.75	0.56	-0.57	-0.57	0.09	0.37	1.00	0.37	11.75
0.63	-0.45	-0.45	0.12	0.37	1.00	0.37	0.13	11.81	0.63	-0.45	-0.45	0.12	0.37	1.00	0.37	11.81
0.68	-0.39	-0.39	0.13	0.37	1.00	0.37	0.07	11.84	0.68	-0.39	-0.39	0.13	0.37	1.00	0.37	11.84
0.74	-0.30	-0.30	0.15	0.37	1.00	0.37	-0.02	11.89	0.74	-0.30	-0.30	0.15	0.37	1.00	0.37	11.89
0.79	-0.24	-0.24	0.17	0.37	1.00	0.37	-0.09	11.93	0.79	-0.24	-0.24	0.17	0.37	1.00	0.37	11.93
0.86	-0.15	-0.15	0.20	0.37	1.00	0.37	-0.20	12.00	0.86	-0.15	-0.15	0.20	0.37	1.00	0.37	12.00
0.92	-0.08	-0.08	0.23	0.37	1.00	0.37	-0.34	12.07	0.92	-0.08	-0.08	0.23	0.37	1.00	0.37	12.07
0.95	-0.05	-0.05	0.26	0.37	1.00	0.37	-0.44	12.12	0.95	-0.05	-0.05	0.26	0.37	1.00	0.37	12.12
0.93	-0.07	-0.07	0.26	0.37	1.00	0.37	-0.51	12.16	0.93	-0.07	-0.07	0.26	0.37	1.00	0.37	12.16
0.89	-0.12	-0.12	0.26	0.37	1.00	0.37	-0.55	12.20	0.89	-0.12	-0.12	0.26	0.37	1.00	0.37	12.20
0.78	-0.24	-0.24	0.26	0.37	1.00	0.37	-0.53	12.25	0.78	-0.24	-0.24	0.26	0.37	1.00	0.37	12.25
0.70	-0.35	-0.35	0.26	0.37	1.00	0.37	-0.51	12.30	0.70	-0.35	-0.35	0.26	0.37	1.00	0.37	12.30
0.66	-0.41	-0.41	0.26	0.37	1.00	0.37	-0.51	12.32	0.66	-0.41	-0.41	0.26	0.37	1.00	0.37	12.32
0.62	-0.48	-0.48	0.26	0.37	1.00	0.37	-0.51	12.33	0.62	-0.48	-0.48	0.26	0.37	1.00	0.37	12.33
0.56	-0.57	-0.57	0.26	0.37	1.00	0.37	-0.52	12.34	0.56	-0.57	-0.57	0.26	0.37	1.00	0.37	12.34
0.52	-0.64	-0.64	0.26	0.37	1.00	0.37	-0.46	12.34	0.52	-0.64	-0.64	0.26	0.37	1.00	0.37	12.34
0.48	-0.74	-0.74	0.26	0.37	1.00	0.37	-0.39	12.34	0.48	-0.74	-0.74	0.26	0.37	1.00	0.37	12.34
0.43	-0.84	-0.84	0.26	0.37	1.00	0.37	-0.29	12.34	0.43	-0.84	-0.84	0.26	0.37	1.00	0.37	12.34
0.41	-0.90	-0.90	0.26	0.37	1.00	0.37	-0.23	12.34	0.41	-0.90	-0.90	0.26	0.37	1.00	0.37	12.34
0.41	-0.90	-0.90	0.26	0.37	1.00	0.37	-0.23	12.34	0.41	-0.90	-0.90	0.26	0.37	1.00	0.37	12.34

period (seconds)	c4	a1	a2	a3	a4	a5	a6	a9	a10	a11	a12	a13	c1	c5	n
5	3.500	-1.460	0.512	-0.7250	-0.144	0.400	-0.200	0.000	0.664	0.040	-0.2150	0.17	6.4	0.03	2
4	3.500	-1.100	0.512	-0.7250	-0.144	0.400	-0.200	0.039	0.640	0.040	-0.1956	0.17	6.4	0.03	2
3	3.500	-0.690	0.512	-0.7250	-0.144	0.400	-0.156	0.089	0.630	0.040	-0.1726	0.17	6.4	0.03	2
2	3.500	-0.150	0.512	-0.7250	-0.144	0.400	-0.094	0.160	0.610	0.040	-0.1400	0.17	6.4	0.03	2
1.5	3.550	0.260	0.512	-0.7721	-0.144	0.438	-0.049	0.210	0.600	0.040	-0.1200	0.17	6.4	0.03	2
1	3.700	0.828	0.512	-0.8383	-0.144	0.490	0.013	0.281	0.423	0.000	-0.1020	0.17	6.4	0.03	2
0.85	3.810	1.020	0.512	-0.8648	-0.144	0.512	0.038	0.309	0.370	-0.028	-0.0927	0.17	6.4	0.03	2
0.75	3.900	1.160	0.512	-0.8852	-0.144	0.528	0.057	0.331	0.320	-0.050	-0.0862	0.17	6.4	0.03	2
0.6	4.120	1.428	0.512	-0.9218	-0.144	0.557	0.091	0.370	0.194	-0.089	-0.0740	0.17	6.4	0.03	2
0.5	4.300	1.615	0.512	-0.9515	-0.144	0.581	0.119	0.370	0.085	-0.121	-0.0635	0.17	6.4	0.03	2
0.46	4.380	1.717	0.512	-0.9652	-0.144	0.592	0.132	0.370	0.020	-0.136	-0.0594	0.17	6.4	0.03	2
0.4	4.520	1.860	0.512	-0.9880	-0.144	0.610	0.154	0.370	-0.065	-0.160	-0.0518	0.17	6.4	0.03	2
0.36	4.620	1.955	0.512	-1.0052	-0.144	0.610	0.170	0.370	-0.123	-0.173	-0.0460	0.17	6.4	0.03	2
0.3	4.800	2.114	0.512	-1.0350	-0.144	0.610	0.198	0.370	-0.219	-0.195	-0.0360	0.17	6.4	0.03	2
0.24	4.970	2.293	0.512	-1.0790	-0.144	0.610	0.232	0.370	-0.350	-0.223	-0.0238	0.17	6.4	0.03	2
0.2	5.100	2.406	0.512	-1.1150	-0.144	0.610	0.260	0.370	-0.445	-0.245	-0.0138	0.17	6.4	0.03	2
0.17	5.190	2.430	0.512	-1.1350	-0.144	0.610	0.260	0.370	-0.522	-0.265	-0.0040	0.17	6.4	0.03	2
0.15	5.270	2.407	0.512	-1.1450	-0.144	0.610	0.260	0.370	-0.577	-0.280	0.0050	0.17	6.4	0.03	2
0.12	5.390	2.272	0.512	-1.1450	-0.144	0.610	0.260	0.370	-0.591	-0.280	0.0180	0.17	6.4	0.03	2
0.1	5.500	2.160	0.512	-1.1450	-0.144	0.610	0.260	0.370	-0.598	-0.280	0.0280	0.17	6.4	0.03	2
0.09	5.540	2.100	0.512	-1.1450	-0.144	0.610	0.260	0.370	-0.609	-0.280	0.0300	0.17	6.4	0.03	2
0.075	5.580	2.037	0.512	-1.1450	-0.144	0.610	0.260	0.370	-0.628	-0.280	0.0300	0.17	6.4	0.03	2
0.06	5.600	1.940	0.512	-1.1450	-0.144	0.610	0.260	0.370	-0.665	-0.280	0.0300	0.17	6.4	0.03	2
0.05	5.600	1.870	0.512	-1.1450	-0.144	0.610	0.260	0.370	-0.620	-0.267	0.0280	0.17	6.4	0.03	2
0.04	5.600	1.780	0.512	-1.1450	-0.144	0.610	0.260	0.370	-0.555	-0.251	0.0245	0.17	6.4	0.03	2
0.03	5.600	1.690	0.512	-1.1450	-0.144	0.610	0.260	0.370	-0.470	-0.230	0.0143	0.17	6.4	0.03	2
0.02	5.600	1.640	0.512	-1.1450	-0.144	0.610	0.260	0.370	-0.417	-0.230	0.0000	0.17	6.4	0.03	2
0.01	5.600	1.640	0.512	-1.1450	-0.144	0.610	0.260	0.370	-0.417	-0.230	0.0000	0.17	6.4	0.03	2

Spectral acceleration calculation for Qaliwana using Abrahamson & Silva (1997) model

CMCE	M	r_{rup}	F	HW	S	PGA
Nasivi Fault	6.8	11	0	0	0	0.32

S_a	$ln(S_a)$	$f_1(M,r_{rup})$	$f_3(M)$	$f_4(M,r_{rup})$	$f_{HW}(M)$	$f_{HW}(r_{rup})$	$f_5 pga_{(rock)}$	R	$pga_{(rock)}$	$ln(S_a)$	$f_1(M,r_{rup})$	$f_3(M)$	$f_4(M,r_{rup})$	$f_{HW}(M)$	$f_{HW}(r_{rup})$	R
0.02	-3.75	-3.75	-0.20	0.00	1.00	0.00	0.55	11.54	0.02	-3.75	-3.75	-0.20	0.00	1.00	0.00	11.54
0.04	-3.33	-3.33	-0.20	0.04	1.00	0.04	0.53	11.54	0.04	-3.33	-3.33	-0.20	0.04	1.00	0.04	11.54
0.06	-2.85	-2.85	-0.16	0.09	1.00	0.09	0.53	11.54	0.06	-2.85	-2.85	-0.16	0.09	1.00	0.09	11.54
0.11	-2.22	-2.22	-0.09	0.16	1.00	0.16	0.53	11.54	0.11	-2.22	-2.22	-0.09	0.16	1.00	0.16	11.54
0.15	-1.87	-1.87	-0.05	0.21	1.00	0.21	0.53	11.56	0.15	-1.87	-1.87	-0.05	0.21	1.00	0.21	11.56
0.24	-1.41	-1.41	0.01	0.28	1.00	0.28	0.42	11.61	0.24	-1.41	-1.41	0.01	0.28	1.00	0.28	11.61
0.28	-1.26	-1.26	0.04	0.31	1.00	0.31	0.40	11.64	0.28	-1.26	-1.26	0.04	0.31	1.00	0.31	11.64
0.32	-1.15	-1.15	0.06	0.33	1.00	0.33	0.37	11.67	0.32	-1.15	-1.15	0.06	0.33	1.00	0.33	11.67
0.39	-0.95	-0.95	0.09	0.37	1.00	0.37	0.27	11.75	0.39	-0.95	-0.95	0.09	0.37	1.00	0.37	11.75
0.45	-0.81	-0.81	0.12	0.37	1.00	0.37	0.17	11.81	0.45	-0.81	-0.81	0.12	0.37	1.00	0.37	11.81
0.48	-0.73	-0.73	0.13	0.37	1.00	0.37	0.11	11.84	0.48	-0.73	-0.73	0.13	0.37	1.00	0.37	11.84
0.54	-0.63	-0.63	0.15	0.37	1.00	0.37	0.03	11.89	0.54	-0.63	-0.63	0.15	0.37	1.00	0.37	11.89
0.57	-0.56	-0.56	0.17	0.37	1.00	0.37	-0.04	11.93	0.57	-0.56	-0.56	0.17	0.37	1.00	0.37	11.93
0.64	-0.45	-0.45	0.20	0.37	1.00	0.37	-0.14	12.00	0.64	-0.45	-0.45	0.20	0.37	1.00	0.37	12.00
0.70	-0.35	-0.35	0.23	0.37	1.00	0.37	-0.28	12.07	0.70	-0.35	-0.35	0.23	0.37	1.00	0.37	12.07
0.74	-0.30	-0.30	0.26	0.37	1.00	0.37	-0.38	12.12	0.74	-0.30	-0.30	0.26	0.37	1.00	0.37	12.12
0.74	-0.30	-0.30	0.26	0.37	1.00	0.37	-0.45	12.16	0.74	-0.30	-0.30	0.26	0.37	1.00	0.37	12.16
0.72	-0.33	-0.33	0.26	0.37	1.00	0.37	-0.50	12.20	0.72	-0.33	-0.33	0.26	0.37	1.00	0.37	12.20
0.65	-0.43	-0.43	0.26	0.37	1.00	0.37	-0.48	12.25	0.65	-0.43	-0.43	0.26	0.37	1.00	0.37	12.25
0.59	-0.52	-0.52	0.26	0.37	1.00	0.37	-0.47	12.30	0.59	-0.52	-0.52	0.26	0.37	1.00	0.37	12.30
0.56	-0.58	-0.58	0.26	0.37	1.00	0.37	-0.46	12.32	0.56	-0.58	-0.58	0.26	0.37	1.00	0.37	12.32
0.53	-0.64	-0.64	0.26	0.37	1.00	0.37	-0.46	12.33	0.53	-0.64	-0.64	0.26	0.37	1.00	0.37	12.33
0.48	-0.74	-0.74	0.26	0.37	1.00	0.37	-0.48	12.34	0.48	-0.74	-0.74	0.26	0.37	1.00	0.37	12.34
0.44	-0.81	-0.81	0.26	0.37	1.00	0.37	-0.42	12.34	0.44	-0.81	-0.81	0.26	0.37	1.00	0.37	12.34
0.40	-0.91	-0.91	0.26	0.37	1.00	0.37	-0.34	12.34	0.40	-0.91	-0.91	0.26	0.37	1.00	0.37	12.34
0.36	-1.03	-1.03	0.26	0.37	1.00	0.37	-0.25	12.34	0.36	-1.03	-1.03	0.26	0.37	1.00	0.37	12.34
0.32	-1.12	-1.12	0.26	0.37	1.00	0.37	-0.18	12.34	0.32	-1.12	-1.12	0.26	0.37	1.00	0.37	12.34
0.32	-1.12	-1.12	0.26	0.37	1.00	0.37	-0.18	12.34	0.32	-1.12	-1.12	0.26	0.37	1.00	0.37	12.34

period	c4	a1	a2	a3	a4	a5	a6	a9	a10	a11	a12	a13	c1	c5	n
5	3.500	-1.460	0.512	-0.7250	-0.144	0.400	-0.200	0.000	0.664	0.040	-0.2150	0.17	6.4	0.03	2
4	3.500	-1.100	0.512	-0.7250	-0.144	0.400	-0.200	0.039	0.640	0.040	-0.1956	0.17	6.4	0.03	2
3	3.500	-0.690	0.512	-0.7250	-0.144	0.400	-0.156	0.089	0.630	0.040	-0.1726	0.17	6.4	0.03	2
2	3.500	-0.150	0.512	-0.7250	-0.144	0.400	-0.094	0.160	0.610	0.040	-0.1400	0.17	6.4	0.03	2
1.5	3.550	0.260	0.512	-0.7721	-0.144	0.438	-0.049	0.210	0.600	0.040	-0.1200	0.17	6.4	0.03	2
1	3.700	0.828	0.512	-0.8383	-0.144	0.490	0.013	0.281	0.423	0.000	-0.1020	0.17	6.4	0.03	2
0.85	3.810	1.020	0.512	-0.8648	-0.144	0.512	0.038	0.309	0.370	-0.028	-0.0927	0.17	6.4	0.03	2
0.75	3.900	1.160	0.512	-0.8852	-0.144	0.528	0.057	0.331	0.320	-0.050	-0.0862	0.17	6.4	0.03	2
0.6	4.120	1.428	0.512	-0.9218	-0.144	0.557	0.091	0.370	0.194	-0.089	-0.0740	0.17	6.4	0.03	2
0.5	4.300	1.615	0.512	-0.9515	-0.144	0.581	0.119	0.370	0.085	-0.121	-0.0635	0.17	6.4	0.03	2
0.46	4.380	1.717	0.512	-0.9652	-0.144	0.592	0.132	0.370	0.020	-0.136	-0.0594	0.17	6.4	0.03	2
0.4	4.520	1.860	0.512	-0.9880	-0.144	0.610	0.154	0.370	-0.065	-0.160	-0.0518	0.17	6.4	0.03	2
0.36	4.620	1.955	0.512	-1.0052	-0.144	0.610	0.170	0.370	-0.123	-0.173	-0.0460	0.17	6.4	0.03	2
0.3	4.800	2.114	0.512	-1.0350	-0.144	0.610	0.198	0.370	-0.219	-0.195	-0.0360	0.17	6.4	0.03	2
0.24	4.970	2.293	0.512	-1.0790	-0.144	0.610	0.232	0.370	-0.350	-0.223	-0.0238	0.17	6.4	0.03	2
0.2	5.100	2.406	0.512	-1.1150	-0.144	0.610	0.260	0.370	-0.445	-0.245	-0.0138	0.17	6.4	0.03	2
0.17	5.190	2.430	0.512	-1.1350	-0.144	0.610	0.260	0.370	-0.522	-0.265	-0.0040	0.17	6.4	0.03	2
0.15	5.270	2.407	0.512	-1.1450	-0.144	0.610	0.260	0.370	-0.577	-0.280	0.0050	0.17	6.4	0.03	2
0.12	5.390	2.272	0.512	-1.1450	-0.144	0.610	0.260	0.370	-0.591	-0.280	0.0180	0.17	6.4	0.03	2
0.1	5.500	2.160	0.512	-1.1450	-0.144	0.610	0.260	0.370	-0.598	-0.280	0.0280	0.17	6.4	0.03	2
0.09	5.540	2.100	0.512	-1.1450	-0.144	0.610	0.260	0.370	-0.609	-0.280	0.0300	0.17	6.4	0.03	2
0.075	5.580	2.037	0.512	-1.1450	-0.144	0.610	0.260	0.370	-0.628	-0.280	0.0300	0.17	6.4	0.03	2
0.06	5.600	1.940	0.512	-1.1450	-0.144	0.610	0.260	0.370	-0.665	-0.280	0.0300	0.17	6.4	0.03	2
0.05	5.600	1.870	0.512	-1.1450	-0.144	0.610	0.260	0.370	-0.620	-0.267	0.0280	0.17	6.4	0.03	2
0.04	5.600	1.780	0.512	-1.1450	-0.144	0.610	0.260	0.370	-0.555	-0.251	0.0245	0.17	6.4	0.03	2
0.03	5.600	1.690	0.512	-1.1450	-0.144	0.610	0.260	0.370	-0.470	-0.230	0.0143	0.17	6.4	0.03	2
0.02	5.600	1.640	0.512	-1.1450	-0.144	0.610	0.260	0.370	-0.417	-0.230	0.0000	0.17	6.4	0.03	2
0.01	5.600	1.640	0.512	-1.1450	-0.144	0.610	0.260	0.370	-0.417	-0.230	0.0000	0.17	6.4	0.03	2